AFOSR Scientific Report
AFOSR TR-71-0922

UNSTEADY COMBUSTION IN GASEOUS PROPELLANT ROCKET MOTORS

by
DONALD R. HARDESTY

PRINCETON UNIVERSITY
DEPARTMENT OF
AEROSPACE AND MECHANICAL SCIENCES

December 1970

Grant No. AF 69-1649/Project No. 9711-01

Research sponsored by Air Force Office of Scientific Research, Office of Aerospace Research, United States Air Force

UNCLASSIFIED

Security Classification

DOCUMENT CONTROL DATA - R & D

(Security classification of title, body of abstract and indexing annotation must be entered when the overall report is classified)

1. ORIGINATING ACTIVITY (Corporate author) PRINCETON UNIVERSITY DEPARTMENT OF AEROSPACE & MECHANICAL SCIENCES PRINCETON, NEW JERSEY 08540	2a. REPORT SECURITY CLASSIFICATION UNCLASSIFIED 2b. GROUP

3. REPORT TITLE

UNSTEADY COMBUSTION IN GASEOUS PROPELLANT ROCKET MOTORS

4. DESCRIPTIVE NOTES (Type of report and inclusive dates)

Scientific Interim

5. AUTHOR(S) (First name, middle initial, last name)

DONALD R HARDESTY

6. REPORT DATE	7a. TOTAL NO. OF PAGES	7b. NO. OF REFS
December 1970	373	154

8a. CONTRACT OR GRANT NO	9a. ORIGINATOR'S REPORT NUMBER(S)
AFOSR-1649-69 b. PROJECT NO. 9711-01 c. 61102F d. 681308	TECHNICAL REPORT NO. T-965 9b. OTHER REPORT NO(S) (Any other numbers that may be assigned this report) AFOSR-TR-71-0922

10. DISTRIBUTION STATEMENT

1. ~~This document has been approved for public release and sale;~~ ~~its distribution is unlimited.~~ Approved for public release; distribution unlimited.

11. SUPPLEMENTARY NOTES	12. SPONSORING MILITARY ACTIVITY
TECH, OTHER	AF Office of Scientific Research (NAE) 1400 Wilson Boulevard Arlington, Virginia 22209

13. ABSTRACT

Diagnostic experiments of the gas rocket combustion zone led to a formulation of a model of the overall burning process which supplied the appropriate combustion zone boundary condition to the Crocco-Mitchell analysis of the chamber wave dynamics. The analysis is valid for the case where the small mean chamber Mach number serves as a measure of the steady level of combustion as well as the mean nozzle outflow. Overall reaction rate data from turbulent flow reactor studies was used to calculate the energy release rate due to chemical kinetics and to identify a characteristic combustion time. Perturbation in the mean combustion zone thermodynamic and gasdynamic properties were linearly coupled to the pressure perturbation. The important consequence of a phase lag between oscillations in temperature, combustion volume, and pressure was noted. A single nonlinear ordinary integro-differential equation governing the amplitude of the pressure oscillation was derived. The linear and nonlinear system response was predicted for the H2/O2/N2 and CH4/Air systems for several particular cases. Comparison of theoretical predictions and stability limit and shock wave amplitude data for H2/O2/N2 and CH4/O2/N2 systems showed excellent agreement and confirmed the importance of finite overall chemical kinetic rates in the coupling process. The new theoretical predictions of the important stabilizing influences of unchoked propellant injection and preheating of the unburned propellants were confirmed experimentally.

DD FORM 1 NOV 65 1473

UNCLASSIFIED

Security Classification

14 KEY WORDS	LINK A		LINK B		LINK C	
	ROLE	WT	ROLE	WT	ROLE	WT
COMBUSTION INSTABILITY						
GASEOUS ROCKET MOTOR						
GASEOUS PROPELLANTS						
LONGITUDINAL COMBUSTION INSTABILITY						
HARMONICS IN COMBUSTION INSTABILITY						
HYDROGEN-OXYGEN-NITROGEN PROPELLANTS						
METHANE-OXYGEN-NITROGEN PROPELLANTS						
CARBON MONOXIDE-OXYGEN-NITROGEN PROPELLANTS						
UNCHOKED PROPELLANT INJECTION						
CHEMICAL KINETIC EFFECTS IN COMBUSTION INSTABILITY						

AIR FORCE OFFICE OF SCIENTIFIC RESEARCH

AFOSR REPORT NO. TR-71-0922

UNSTEADY COMBUSTION
IN
GASEOUS PROPELLANT ROCKET MOTORS

By

Donald R. Hardesty

AMS Report T-965

AFOSR Grant 69-1649

December 1970

Approved by: Irvin Glassman

Irvin Glassman
Professor of Aerospace Sciences
Principal Investigator

Guggenheim Laboratories for the Aerospace Propulsion Sciences
Department of Aerospace and Mechanical Sciences

Princeton University
Princeton, New Jersey

ABSTRACT

This research work was directed toward the development of a consistent experimental and theoretical description of the phenomenon of intrinsic unstable combustion in the gas rocket. A determination was achieved of the contribution of gas phase rate processes, (in particular, chemical kinetics), to the coupling of a finite-dimensional unsteady turbulent combustion zone and finite amplitude (linear and nonlinear) longitudinal mode pressure oscillations.

Experiments with the $CO(H_2O)/O_2/N_2$ propellant system confirmed the critical importance of the mean combustion temperature in determining the onset of nonsteady burning. As previously observed in the $H_2/O_2/N_2$ and $CH_4/O_2/N_2$ systems, the spontaneous transition from a regime of steady combustion located about the stoichiometric mixture ratio to a regime of nonsteady combustion characterized by finite amplitude, constant frequency, longitudinal mode pressure oscillations occurs at approximately fixed combustion temperatures independent of the relative dilution of the combustible mixture. Subsequent investigation in which trace amounts of CH_4 (which is known to have an inhibiting effect on the overall rate of reaction in the $CO(H_2O)/O_2$ system) were added to $CO(H_2O)/O_2/N_2$ mixtures showed conclusively the dominant influence of the propellant chemistry on the linear and nonlinear system response.

Diagnostic experiments (temperature profiles and direct and high-speed schlieren photography) showed that the combustion zone is characterized by the existence of distributed high intensity turbulent reaction zones centered at each injection port and extending axially 1 to 4 cm into the combustion chamber. Reaction is completed with the attainment of the equilibrium adiabatic combustion temperature within the mixing zone of the high velocity expanding jet. Combustion is maintained in the initially sonic underexpanded jet by virtue of the recirculation of hot product gases and the intense mixing of products and reactants. No intrinsic

fluid dynamic jet unsteadiness was observed. During sustained nonlinear oscillations the overall turbulent combustion zone volume is unsteady and undergoes large amplitude oscillations in size at precisely the same frequency as the pressure oscillation. The shock wave passage nearly corresponds to the observed minimum in the volume oscillation.

These data led to a formulation of a model of the overall burning process which supplied the appropriate combustion zone boundary condition to the Crocco-Mitchell analysis of the chamber wave dynamics. The analysis is valid for the case where the small mean chamber Mach number serves as a measure of the steady level of combustion as well as the mean nozzle outflow. Overall reaction rate data from turbulent flow reactor studies was used to calculate the energy release rate due to chemical kinetics and to identify a characteristic combustion time. Perturbation in the mean combustion zone thermodynamic and gasdynamic properties were linearly coupled to the pressure perturbation. The important consequence of a phase lag between oscillations in temperature, combustion volume, and pressure was noted. A single nonlinear ordinary integro-differential equation governing the amplitude of the pressure oscillation was derived. The linear and nonlinear system response was predicted for the $H_2/O_2/N_2$ and CH_4/Air systems for several particular cases. A strong system resonance was predicted to occur for ratios of the combustion time to the period of oscillation of the order of 0.1 to 1.0. Comparison of theoretical predictions and stability limit and shock wave amplitude data for $H_2/O_2/N_2$ and $CH_4/O_2/N_2$ systems showed excellent agreement and confirmed the importance of finite overall chemical kinetic rates in the coupling process. The similarity between experimental results for the CH_4/Air and $CO(H_2O)$/Air systems was explained on basis of available overall kinetic rate data and the theoretical results. The new theoretical predictions of the important stabilizing influences of unchoked propellant injection and preheating of the unburned propellants were confirmed experimentally.

ACKNOWLEDGMENTS

The author would like to take this opportunity to acknowledge the debt of gratitude owed to Professor Irvin Glassman. Professor Glassman provided support and direction for the research effort. His enthusiasm and encouragement during the author's graduate program served as a continuing inspiration. The author would also like to express his sincere appreciation for the guidance lent by Professor Luigi Crocco, particularly with reference to the analytical work. Many stimulating and fruitful discussions with Professor William A. Sirignano also contributed materially to the final product.

The general assistance of the entire staff of the Guggenheim Laboratories including Messrs. Cooper, Warshaw, Drobnek, Edwards, Gadsby, Morris, Crosby, Beach, Lakacauskis, Mathis, and Kline is gratefully acknowledged.

The author was most fortunate to have the able assistance of Mr. Joseph Sivo during the course of the experimental work. Mr. Sivo's technical prowess in the design, fabrication and operation of test equipment was indispensable. Mr. Andy Tamasi assisted with the equipment design and manufacture. The late Mr. Anthony Bozowski also made important contributions to the experimental program. Mr. Tony Poli lent valuable assistance in the design of various components of the apparatus.

A special note of appreciation must go to Mr. Steve Marquardt of the Instrumentation Group. Mr. Marquardt's talents and patience proved to be of paramount importance in the actual performance of experiments and the recording and reduction of data.

Special thanks also go to Mr. Don Neiler for his continuing assistance over the years in the preparation of slides, figures, and photographs and for advice regarding various aspects of the photographic work.

Numerous discussions with fellow graduate students including Mr. Frederick Dryer, Professor James Tien, and Dr. C. T. Bowman proved helpful.

The labors of Mrs. Daisy Guest in completing the prodigous task of typing the manuscript are gratefully acknowledged. Miss Dorothy Morris and Miss Claire Hartmann also contributed to the final typing. Thanks go to Mr. Tony Poli, Mr. Michael Freeman, and Mr. Joseph Vergara for their assistance in the preparation of the figures appearing in the text.

The research program was supported by the Office of Aerospace Research, Air Force Office of Scientific Research under AFOSR Grant No. 69-1649.

The thesis is designated No. T-965 in the records of the Department of Aerospace and Mechanical Sciences.

TABLE OF CONTENTS

LIST OF TABLES

LIST OF FIGURES

LIST OF FIGURES

LIST OF FIGURES

LIST OF FIGURES

LIST OF FIGURES

LIST OF FIGURES

NOMENCLATURE

a, c	=	sound speed
c_p, c_v	=	specific heats at constant pressure and constant volume
d_{port}	=	injection port diameter
f	=	wave amplitude parameter
f_i	=	mole fraction of i th species
h	=	enthalpy
k	=	pre-exponential factor in empirical overall rate law
$\hat{k}$	=	k/MW_{O_2} (referred to as pre-exp in several figures)
k_t	=	turbulent eddy conductivity
l, l_c	=	axial dimension (characteristic length) of combustion zone
m	=	oscillation mode order (1 = fundamental, 2 = second harmonic, 3= third harmonic, etcetera)
m, n	=	reaction order with respect to oxidizer and fuel
$\dot{m}$, $\dot{m}_{tot}$	=	total mass flux per unit area per unit time
n_h, n_{holes}	=	number of holes in showerhead injector
p	=	pressure in combustion chamber
p_{inj}	=	ratio of mixing chamber pressure to combustion chamber pressure
$\triangle p$	=	dimensionless wave amplitude at injector
q	=	heat of combustion per unit mass of fuel
$\dot{q}$, r	=	volumetric energy release rate due to finite-rate kinetics (cal/sec cm^3)
s	=	entropy
t	=	time
u	=	gas velocity
x	=	axial coordinate referenced to injector face
x	=	axial coordinate divided by injector port diameter
A, B, C, D, E, F	=	dimensionless coefficients appearing in equations for stability characteristics
A	=	area
A_{ch}	=	cross-sectional area of combustion chamber
A_{eff}	=	effective cross-sectional area of combustion chamber (A_{ch}/n_h)
E, E_a, E_{act}	=	overall activation energy (kcal/gmmole)
H	=	E/RT_b

K	=	standard rate constant appearing in overall rate law
L, L_c	=	length of combustion chamber
	=	terms appearing in linear stability limit equation
M	=	mean chamber Mach number based on adiabatic burned gas conditions; a small parameter for gas rocket
M_{inj}	=	mean injection Mach number based on total cross-sectional area of injection ports
MW_i	=	molecular weight of i th species
R, $\mathcal{R}$	=	gas constant, universal gas constant
S	=	flame surface area
S_l, S_t	=	laminar and turbulent flame speeds
T	=	temperature
T_b	=	adiabatic combustion temperature
T_{lim}	=	adiabatic combustion temperature at stability limit
V, V_c	=	combustion zone volume
X_i	=	molar concentration of i th species
α	=	jet expansion (half) angle
α, β, ξ	=	dimensionless coefficients appearing in combustion zone boundary condition
γ	=	ratio of specific heats
δ	=	axial extent of unburned gas zone of combusting jet
ϵ	=	eddy viscosity; amplitude parameter; ratio of averaged property to burned gas property
ϵ_{TP}	=	phase angle of oscillation in mean combustion temperature with respect to pressure oscillation
ϵ_{VP}	=	phase angle of oscillation of combustion volume with respect to pressure oscillation
ζ	=	mass ratio of N_2 to O_2 in initial oxidizer mixture
η	=	amplitude ratio of oscillation in combustion temperature to oscillation in pressure
θ	=	dimensionless time
θ_i	=	ratio of unburned to burned gas temperatures
λ	=	wave length
μ	=	stoichiometric mixture ratio of oxidizer mass fraction to fuel mass fraction
ν	=	kinematic viscosity
ρ	=	density
ρ_i	=	$X_i \cdot MW_i$
∇_i	=	mass fraction of i th species

Σ = response function coupling perturbation in the combustion time to perturbations in the mean combustion temperature and pressure

Σ_T = response function coupling perturbations in characteristic combustion time and mean combustion temperature

Σ_p = response function coupling perturbations in characteristic combustion time and pressure

γ, γ_j = dimensionless combustion temperature, $\frac{T_c - \bar{T}_i}{\bar{T}_b - \bar{T}_i}$

γ_c, γ_{comb} = characteristic combustion time; essentially a measure of mean rate of heat release

γ_{per}, γ_{wave} = period of oscillation, ½ period of oscillation

$\gamma_{res,u}$ = residence time of propellant gases in unburned zone

$\gamma_{mix,j}$ = characteristic mixing time or local eddy stay time within expanding turbulent jet

$\bar{\Phi}$ = equivalence ratio of initial propellant mixture ($\bar{\Phi} > 1$ corresponds to oxidizer-rich mixture)

$(\bar{\Phi}_{lim})_l$ = equivalence ratio at lower (closest to $\bar{\Phi} = 1$) stability limit

$(\bar{\Phi}_{lim})_u$ = equivalence ratio at upper (furthest from $\bar{\Phi} = 1$) stability limit

ψ = response function coupling oscillation of mass injection flux to pressure oscillation

ω = angular frequency

Subscripts

ave - average value (over combustion zone volume)

b - burned gas property at adiabatic combustion temperature

c, comb - combustion zone property (volume averaged)

crit, lim, lower, upper - critical values of property at linear stability limit

f - fuel

i, o, u - unburned gas property at injection port (x = 0)

j - property within expanding jet

L, n - property evaluated at nozzle end (x = 1)

mix - mixing chamber property

O_2, ox - oxygen, oxidizer

prod - products

r, recir - recirculation zone property

1, 2, 3	=	perturbation quantities of order M, M^2, M^3

Superscripts

*	-	dimensional quantity
_	-	steady-state quantity
'	-	denotes perturbation of quantity from steady-state
o	-	quantity evaluated at injector end (x = 0)

CHAPTER I: INTRODUCTION

The steady-state operation of solid and liquid propellant rocket combustion chambers is characterized by high levels of temperature, pressure, and turbulent multiphase mixing. Random fluctuations in the nominally steady chamber conditions lead to extraordinary levels of noise generation and are collectively termed rough combustion. Frequently superimposed on this tolerable level of disorganized fluctuations are cyclic gas and wave motions which may impose detrimental loads on the programmed functioning of the motor. Such undesirable effects range from substantial increases in the noise output, unanticipated deviations in the system output in terms of specific impulse and thermal loads on the chamber walls, structural vibrations and loss of control, to total system failure. It is conventional to refer synonymously to these periodic phenomena as unstable, nonsteady, unsteady, or oscillatory combustion. The basic feature common to all of the observed organized motions is the existence of a measurable, well-defined frequency. In view of the close relationship between the observed frequency of the oscillations and the mechanisms by which the oscillations are sustained it is conventional to distinguish among frequency ranges according to the mechanism of coupling of the waves and the motor system.

Low frequency or chugging oscillations with frequencies below 200 Hz were first observed in liquid propellant rocket motors in the early 1940's. Characterized by in-phase oscillations of the chamber pressure at all axial locations and supported by properly phased oscillations in the propellant mass injection flux, this mode of oscillation is experimentally and theoretically well understood (1-11)[1]. Successful elimination of combustion chamber and propellant feed line coupling has been achieved by suitable injector and feed line design. Subsequently, pressure oscillations having frequencies in this range were observed in solid propellant rocket motors with the advent of

---

[1] Numbers in parentheses indicate references, listed beginning page 318.

geometrically larger motors operating at lower steady-state pressures. Recent experimental and theoretical efforts (12, 13) indicate that the mechanisms of coupling between the nonacoustic pressure and temperature waves and the burning propellant are complicated by lag effects in the solid phase. Theoretical developments (14) indicate that to a close degree of approximation the pressure oscillations take the form of standing waves.

A second class of pressure oscillations in liquid propellant motors with frequencies in the range of 200 to 1000 Hz is generally denoted. This type of oscillatory behavior is characterized by mixture ratio oscillations which induce fluctuations in the burned gas entropy or density and the chamber pressure. Crocco and Cheng (3) and Berman (7) have attributed such oscillations to the nonsteady injection and burning of the propellants. As in the case of low frequency chugging this type of unstable combustion is effectively eliminated by appropriate injector design and propellant feed line manifolding.

It is important to distinguish between the aforementioned types of combustion instability and unsteady combustion wherein high frequency or acoustic pressure oscillations are supported in solid, liquid, and gaseous propellant rocket motors. This report will be restricted to an experimental and analytical treatment of a particular type of acoustic wave motion observed in a gaseous propellant motor. The designation <u>acoustic</u> is preferred over the usual classification of <u>high frequency</u>. This follows from the observation that pressure oscillations of this type manifest frequencies which depend critically on the combustion chamber geometry and the sound speed of the burned gases and can generally be associated with one of the principal acoustic modes of the chamber cavity with sealed ends. Thus distinctions are drawn among acoustic oscillations on the basis of the characteristic dimension of the combustion chamber associated with the wave motion rather than on the basis of frequency. In fact acoustic mode oscillations are observed to span the frequency range from 100 to 50,000 Hz. Despite this broad range of frequency the mechanism for sustaining acoustic oscillations is attributed to the com-

plex interaction of the pressure waves with the energy and/or mass sources in the combustion process. It should be noted that the term acoustic is a compromise in diction in view of the connotation of vanishing amplitude, continuous, linear waves. While the acoustic oscillations discussed in the report typically assume these characteristics close to intrinsic or natural stability limits, large amplitude, nonlinear, and often discontinuous waves are encountered upon sufficient departure from the limiting conditions. Furthermore, in some systems it is possible to excite high amplitude nonlinear oscillations by artificially disturbing otherwise intrinisically steady combustion chamber operation. In both situations the characteristic frequency of the excited oscillation invariably lies sufficiently close to a natural mode of the chamber so that the term acoustic is appropriate in the limited sense of denoting the frequency. As noted the distinction among the various acoustic oscillations observed in rocket motors can be made on the basis of the particular mode excited. The low frequency (100 to 1000 Hz) end of the scale is generally attributed to longitudinal or axial wave motion. Higher frequency or screaming (1000 to 50,000 Hz) is associated with oscillations in planes normal to the chamber axis and which are termed radial, tangential, and spinning.

From an historical standpoint the initial interest of the liquid propellant rocket designers was primarily with the longitudinal mode oscillations. A great deal of theoretical and experimental effort (1, 3, 15, 16, 17, 18) was expended toward their description and elimination. With the subsequent trend toward the development of low aspect ratio (chamber length/chamber diameter) combustion chambers and the use of high combustion pressures interest shifted to the higher frequency transverse modes (19, 20). On the other hand, the early encounters with combustion instability in solid propellant systems generally involved the higher frequency transverse modes (21, 23, 24). The appearance of these high frequency modes was inhibited with the advent of the addition of metallic additives to the solid propellants. The transverse modes were found to be strongly damped by the presence of con-

densed phase metal oxide particles in the product gases. The subsequent trend toward the development of larger solid propellant rocket motors and the use of lower combustion pressures has focussed attention on the lower frequency longitudinal modes and the L* instability.

The recognition of the fundamental and practical significance of the problems presented by the phenomena of acoustic oscillations in solid and liquid propellant combustion chambers has inspired extensive experimental and analytical programs in these areas at Princeton. The specific program to which this report is devoted is closely associated with the liquid propellant rocket instability program. While attention is therefore directed to the liquid rocket studies it has been suggested that certain aspects of the work may bear a closer relationship with nonsteady combustion in a solid propellant system.

Theoretical description of the phenomenon of acoustic mode nonsteady combustion in a liquid propellant rocket motor was initially undertaken by Crocco (1). Quantitative estimates of longitudinal mode stability characteristics were achieved through the linearization of the conservation equations for one-dimensional compressible flow in a high aspect ratio combustion chamber. Because of the dearth of experimental information concerning the physics of the complex combustion processes occurring in the combustion chamber, the interaction of the combustion process and the pressure waves was expressed through heuristic arguments in which a pressure sensitive time lag influenced the instantaneous rate of mass addition to the chamber gases. This pioneering effort summarized by Crocco and Cheng (3) provided the basic guidelines for a systematic experimental investigation of the phenomena of unstable combustion in liquid motors. The subsequent correlations drawn between the experimental results and theoretical predictions described in (18) confirmed the significant role of a time delay mechanism in the coupling between the combustion process and the pressure oscillations. The immediate consequence of this interim comparison of theory and experiment was the generation of parallel theoretical and experimental investigations. The experi-

ments had defined the intrinsic longitudinal mode motor stability limits[1] and the mean wave amplitudes as a function of the chamber geometry and the propellant equivalence ratio[2]. The growth of low amplitude sinusoidal oscillations into large amplitude nonlinear (occasionally shock-type) pressure waves occurred as the regime of unstable burning was traversed. Theoretically it was necessary to treat the full nonlinear problem in order to account for the existence of finite amplitude pressure waves. The new investigations carried out by Sirignano (26, 27) retained the sensitive time lag model to describe the combustion source terms and resulted in quantitative correlations between the time lag model and the wave shape and amplitude of axial mode oscillations. Experimentally a better understanding of the complex processes of nonsteady combustion in a liquid propellant combustion chamber was needed. It was necessary to improve the physical combustion model employed in the theoretical analysis and, hopefully, to distinguish those processes which determine the response or coupling (in particular the time lag and its sensitivity to the physical and chemical properties of the combustion gases) of the combustion process to the pressure oscillations. The original experiments of Crocco, Harrje, and Grey (18) indicated the possible importance of gas phase rate processes in the coupling process. This inference was drawn from the observation that the experimentally determined sensitive time lag was in the range that one might expect if the gas phase (chemistry) was controlling. Thus among the new experimental investigations, the program of studying longitudinal mode combustion instability in a simplified rocket motor using premixed gaseous propellants was initiated[3].

---

[1] A stability limit is a boundary demarcating a zone of steady combustion and a regime of spontaneous or intrinsic, combustion-driven oscillations. A point in the unstable regime is characterized by oscillations having approximately constant peak-to-peak amplitude and steady frequency.

[2] The equivalence ratio is defined as the oxidizer to fuel mixture ratio divided by the stoichiometric mixture ratio.

[3] Initial experimental results obtained with such a device at Purdue (58) indicated that in many ways the instability characteristics observed in the gaseous system were similar to those encountered in the liquid motors.

The gaseous propellant rocket motor or gas rocket was designed as a research tool to accomplish a specific goal. In brief, the system provides for the control of those parameters observed to be of significance in determining the longitudinal mode stability characteristics of liquid propellant systems. A combustion zone is established at one end of a high aspect ratio combustion chamber by the injection of premixed energetic gaseous propellants. The combustion chamber geometry including the chamber length, the injection pattern, and the nozzle shape is easily varied. By adjustment of the propellant mass flow rate and the nozzle contraction ratio a range of propellant equivalence ratios, combustion pressures and mean flow Mach numbers can be achieved. It was originally hoped that by eliminating liquid phase phenomena an explicit determination could be made of the influence of gas phase rate processes (in particular chemical kinetics) on the phenomena of axial mode unstable combustion.

It should be emphasized that despite certain similarities between system operation and the observed stability characteristics in liquid and gaseous propellant systems the study of the stability characteristics of the gas rocket must not be taken as an end in itself. Knowledge of the system's stability characteristics is useful only insofar as this knowledge can be integrated with a satisfactory physical and analytical description of the coupling between the gas phase combustion process and the oscillating pressure waves. In this regard the gas rocket conceptually provides the simplest form of a dynamically coupled combustion zone and combustion chamber flow field. As such it presents a system amenable to a analytical treatment. Ideally one would hope to combine a realistic description of the combustion zone with an analysis of the combustion chamber dynamics and, after including an appropriate description of the nonsteady nozzle behavior, determine the stability characteristics of the system as a function of the principal system variables. It is only after the establishment of a realistic and consistent analytical and experimental argument that useful information from the gas rocket investigations can be extracted.

Following an initial series of experiments by Pelmas (28), Bertrand (29), and Schob (30), Bowman (32) in 1966 completed an extensive catalogue of the stability characteristics of the gas rocket. These investigations included a description of the motor stability limits as a function of the combustion chamber, injector, and nozzle geometries, the steady state combustion pressure, the mean flow Mach number, and the propellant equivalence ratio or combustion zone temperature. The waveform of the combustion pressure oscillation was observed to be distinctly nonlinear and generally assumed the form of a steep-fronted shock wave propagating axially at approximately the fundamental longitudinal mode frequency. The systematic appearance of regimes of harmonic mode oscillations in the form of two or three propagating shock waves was noted. Comparison of these experimental results with an analytical model formulated by Sirignano and Crocco (26) was attempted. In view of the fact that the theory represented a first attempt in the application of a simplified zero time lag combustion zone boundary condition to a nonlinear analysis of the combustion chamber dynamics, the tentative agreement between theory and experiment on certain points was encouraging. A more complete discussion of these experimental and analytical results is offered in Chapter II. Suffice it to say at this point that significant quantitative and qualitative discrepancies among theory, accumulated experimental data, and published kinetics data were apparent. In addition certain anomalies in the experimental results were totally puzzling.

The present work represents a logical sequel to the preceding investigations and is keyed to the development of a consistent theoretical model which accurately predicts the experimental observations. In this regard, special effort is devoted to characterizing the role played by gas-phase rate processes - specifically chemical kinetics - and a finite-dimensioned flame zone in the coupling between the combustion zone energy release and the nonlinear longitudinal mode oscillations. In view of the definitive nature of this work a particular effort is made to place the previous and the present researches (at Princeton and elsewhere) in the proper perspective especially with regard to the fundamental

bearing of gas rocket investigations on the more practical problems of nonsteady combustion in liquid and solid propellant systems. To this end a critical examination of several related investigations is undertaken in Chapter II. Chapter III presents a description of the basic gas rocket system. Certain important changes in the basic system were necessitated in the course of the experimental work. Several of these are discussed in Chapter III.

It was felt that most of the discrepancies between the Sirignano-Crocco analysis and the experimental results could be attributed to the simplifications in the theoretical model necessitated by a virtually complete lack of experimental information about the structure of the gas rocket combustion zone. These discrepancies are discussed in Chapters II, IV, and V. Furthermore, the predicted critical dependence of the system stability characteristics on the propellant chemistry (the activation energy) had not been confirmed experimentally. Chapter IV details the results of a lengthy series of experiments performed with the $CO(H_2O)/O_2/N_2$ propellant system to which minute traces of CH_4 were added in order to accurately test this prediction. The inhibiting effect of the CH_4 molecule in the CO/O_2 reaction, expressed as an increase in the one-step or overall reaction activation energy is manifest in a marked shift of the stability limits in qualitative accord with the theoretical prediction of the original Sirignano-Crocco model. A discussion follows of four separate experiments designed to improve the understanding of the combustion zone distribution under steady and nonsteady conditions and thereby facilitate the formulation of a more realistic combustion zone model. Radial steady state combustion zone temperatures were measured with "wall mounted" thermocouples. Axial profiles of the steady state combustion zone temperature as a function of the propellant equivalence ratio and the injector configuration were obtained using traversing uncooled and water cooled thermocouple probes. Direct photographs of the combustion of H_2 and air under stable conditions were obtained employing a specially designed combustion chamber section with quartz windows. A description follows of a

series of experiments employing instantaneous spark schlieren and shadowgraph photography of the combustion zone under steady and nonsteady operating conditions. A brief discussion of the schlieren system and a second redesigned windowed chamber section is included.

Chapter IV concludes with the results of a series of experiments employing techniques of high speed schlieren photography to observe the combustion zone under steady and nonsteady operating conditions. A discussion of the system to allow remote operation of the high speed Hycam framing camera and the correlation of the photographs with the transient pressure record is included.

Chapter V presents the details of a more realistic model for longitudinal mode combustion instability in the gaseous propellant rocket motor. A nonlinear analysis (originally due to Crocco and Mitchell (33, 34) and reformulated by Crocco) of the wave dynamics in the combustion chamber for the case of low mean flow Mach number is performed. The important contribution of the diagnostic experiments in the formulation of the combustion zone boundary condition is discussed. An initial model, partially motivated by the comparison of Bowman's experimental results with the original Sirignano-Crocco model and with kinetics data, in which the combustion zone is assumed to take the form of extended noninteracting cone-shaped flamelets is outlined. The influence of the experimental work and initial numerical results from the first model on the formulation of the alternative combustion model is pointed out. Emphasis on the physical aspects of the "real" system is shown to lead naturally to a distributed combustion model which can be postulated independently or derived by appropriate spacial averaging of a one-dimensional recirculation-stabilized combustion zone. Unsteady effects arise due to the sensitivity to the oscillating pressure of the burning rate, the injection mass flux (in the case of unchoked propellant injection flux), and the overall combustion zone geometry or burning zone volume. The development and solution of the ordinary non-linear integro-differential equation governing the form of the dimensionless pressure wave for the linear and nonlinear system response are discussed. Additional particulars

of the numerical techniques and the digital computer programs are contained in the Appendices.

Two additional experiments designed to test the important new predictions of the analytical model are described. The results are shown not only to corroborate the theoretical predictions but also to serve to explain an otherwise anomalous experimental observation.

Chapter VI presents a general summary of the experimental and analytical results. Relevant conclusions are discussed. The inappropriateness of comparing the results of Tsuji and Takeno (and perhaps those of the Purdue investigators) to results obtained at Princeton is indicated. The existence of two modes or operational regimes for a gaseous propellant rocket-type system is noted. The relevance of gas rocket data to practical liquid systems is discussed. The possibility of relaxing the quasi-steady treatments of the gas phase reaction zone in theoretical analyses of liquid and solid propellant rocket combustion instability is suggested.

CHAPTER II: Nonsteady Combustion of Premixed Gaseous Propellants

A critical discussion of researches relevant to the investigations discussed in this report.

A. Early Investigations

The development of the gaseous propellant rocket motor at Princeton was motivated by the expressed desire to improve the understanding of the influence of gas phase rate processes on the phenomena of unstable combustion in liquid propellant rocket motors. Somewhat similar devices were constructed at Purdue University and at the University of Tokyo with more or less the same goal in mind. Previous experimental and analytical researches pertaining to these three systems form the necessary context in which the present work should be considered. These will be critically reviewed in the paragraphs to follow.

The study of nonsteady combustion in systems utilizing premixed gaseous reactants is certainly not a recent development. Indeed, the well known temporal and spacial Rayleigh criteria (35) for the support of oscillations by the periodic addition of heat were formulated in the mid 19th century. Excellent reviews of basic research work on combustion supported acoustic oscillations including those prior to World War II are to be found in (41, 48). During the early 1950's Kaskan and Markstein independently performed basic experimental studies of nonsteady flame propagation (36, 37, 38, 39, 40). These works are summarized by Markstein (41) and represent the first systematic attempts to study the physics of the coupled interaction between pressure waves and a zone of gas phase combustion. While the observations made by these investigators are not directly applicable to the gas rocket studies, they succeeded in delineating certain mechanisms of pressure wave amplification by flame systems which have been applied by investigators in the propulsion fields. Markstein and Kaskan concluded that the fluctuation of the total burning surface or flame area in response to applied fields of varying pressure is an important coupling mechanism. For low amplitude sinusoidal pressure waves they observed that this source of coupling may

dominate the expected amplification due to increased burning rate in response to the pressure and temperature variations. Kaskan concluded that this is especially true in the case of higher frequency oscillations ($\sim$ 4000 Hz) where the oscillation period becomes of the order of the expected chemical reaction times in near stoichiometric flames. A completly theoretical analysis of the generation of acoustic waves at a thin planar flame front whenever there occurs a change in the burning velocity, the heat release per unit mass, the specific heat ratio of the gases, upstream entropy variation, or the interaction of a thin flame front with a pressure or velocity wave was presented by Chu (43). The ability of a steady premixed laminar propane-air flame (established at one end of a long thin tube at atmospheric pressure) to drive or damp artificially impressed longitudinal mode acoustic oscillations was studied analytically and experimentally by Blackshear (44, 45). Blackshear analytically treated the flame as a pressure-velocity discontinuity and used the conservation equations of mass and momentum to develop a simplified wave equation. The assumptions of a nonsteady, short, flame zone and low Mach number of the combustion product gases allowed predictions from the wave equation analysis of the effects of flame area change, mixture ratio, unburned and burned gas density ratio, and the impressed wave amplitude on the driving characteristics of the flame. The generation of pressure waves by virtue of momentum fluctuations (velocity fluctuations) was emphasized. The use of energy conservation relationships was avoided and a step change in temperature and density across a zero thickness flame was considered. Blackshear's analysis also supported the conclusion that fluctuations in the flame area can be critically important in determining the ability of a flame to drive standing waves. The omission of the possibility of coupling through the influence of the pressure waves on the burning rate represents a serious shortcoming of this early work.

B. Studies of Putnam and Merk

The first systematic observations of spontaneous combustion supported oscillations in a premixed gaseous propellant combustor

were reported by Putnam, et al. (46, 47, 48, 49, 50). Schematics of the devices employed in these investigations are shown in Figure II-1. Putnam referred to these system geometries as "rocket shaped". This term is appropriate only in the sense that combustion is concentrated at the upstream end of the cylindrical burner. He also applied the term "low duty" in describing the operating characteristics. Again the appropriateness of this term lies in the fact that the systems were generally operated at atmospheric pressure with no aft end nozzle. While use was made of energetic premixed gaseous reactants such as hydrogen and air, the total mass flux was on the order of 0.2 gms/sec or about two orders of magnitude lower than that used in the gas rocket studies discussed in this report. In addition the injection Mach number was approximately 0.03. Putnam reported the effects of the system geometry (the relative lengths of the plenum and combustion chambers) and the percent theoretical air on the frequency of acoustic longitudinal mode standing wave (organ pipe) pressure oscillations sustained in the plenum and combustion chambers. By virtue of the small pressure drop across the injector ports the injection mass flux was strongly coupled to the pressure variations in the combustion chamber. Invoking the Rayleigh criterion (for the driving of periodic oscillations) that requires an oscillating component of the heat release rate to be properly phased with the pressure fluctuation at the point of heat release, Putnam argued that energy is periodically input to the standing wave system due to the coupled interaction of the combustion chamber, the plenum chamber, and the injection ports. For the "short port" system of Figure II-1a, Putnam suggested that pressure fluctuations originating in the combustion chamber pass upstream, reflect from the end of the mixing chamber, return to the ports, and produce a surge of premixed reactants into the combustion chamber. This additional slug of unburned propellant is then consumed after an appropriate time lag (the nature of which is not specified). For a proper match of the characteristic frequencies of the plenum and combustion chambers and the right time delay between injection and consumption of the extra globule of reactants a system resonance will

FIGURE II-1

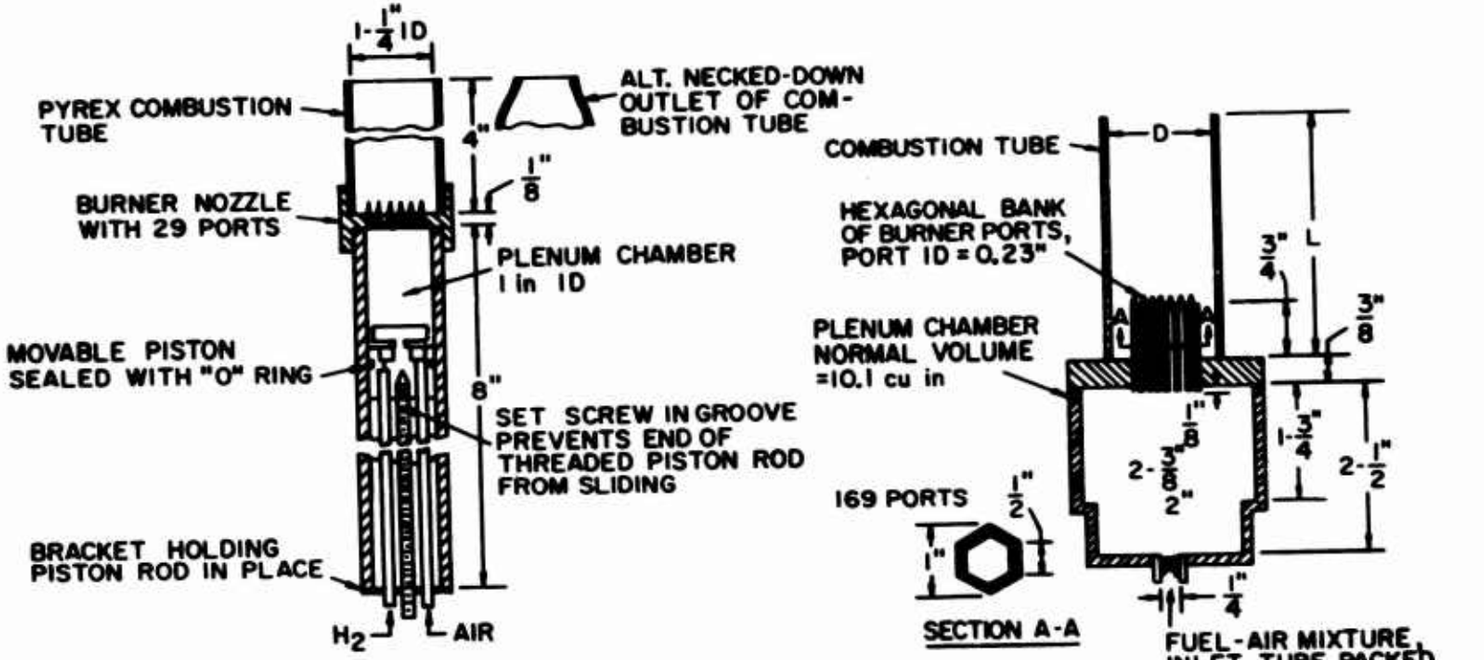

ROCKET SHAPED COMBUSTION CHAMBERS USED BY PUTNAM

REF.- PUTNAM AND DENNIS, JOUR. ACOUS. SOC., 28, 2, 1956

occur and standing waves will be driven, the final amplitude depending on the system losses (which were not specified). A similar coupling mechanism was postulated for the system in Figure II-1b where the size of the plenum chamber is sufficiently large to produce a mismatch between the characteristic acoustic frequencies of the two chambers.[1] Putnam suggested that the mass injection flux varies in response to pressure fluctuations in the combustion chamber by virtue of the sensitivity of the mass of gas in the long column of unburned gases in the extended injector tubes to the pressure changes. The important action of a time delay mechanism between injection and consumption of the extra reactant mass (accumulated in the tubes during the higher pressure portion of the combustion chamber pressure cycle and subsequently dumped into the combustion chamber during the low pressure phase of the cycle) was emphasized. Putnam logically argued that only by virtue of the time lag between the oscillating component of the flow rate (which is always oppositely phased to the pressure fluctuation for a zero inertia gas system) and the oscillating component of the energy release can standing waves be driven. It should be emphasized that Putnam's arguments are essentially qualitative. No formal analytical structure was proposed to model the system. While the physical reasoning is persuasive no diagnostics of the system were performed other than measurements of the mixture ratio, the blowoff limits, and the supported frequencies. The basic observations revealed the presence under certain conditions of low amplitude, linear, standing longitudinal mode waves. It is of interest that preferred frequency ranges depending on geometry were observed with the regimes of sustained oscillations falling at and around the stoichiometric mixture ratio. For the ethane-air system second harmonic standing wave oscillations prevailed at the stoichimetric mixture ratio with the fundamental mode "limits" falling at off-stoichiometric mixtures. A lower combustion chamber

---

[1] The characteristic frequency of the plenum chamber filled with cold unburned reactants and the combustion chamber filled with hot combustion products.

length limit[1] for the appearance of nonsteady combustion was postulated.

A comprehensive theoretical analysis of the nonsteady combustion of premixed gases in systems analagous to those studied experimentally by Putnam was carried out by Merk (51-56). A detailed review by Putnam of this work is found in (41). The analyses represent a significant contribution toward the understanding of mechanisms by which acoustic oscillations in simplified flow-combustion systems are coupled to the energy release in a premixed gaseous reactant flame zone. Merk (52) considered the system shown in Figure II-2.

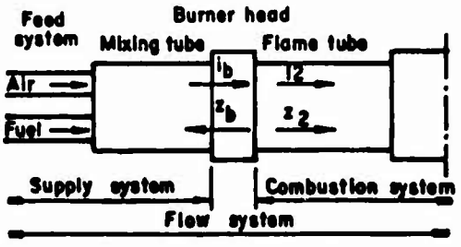

Figure II-2. Combustor analyzed by Merk

The standard principles of linearized dynamic stability analysis were applied to the conservation equations of mass, momentum, and energy for the system. The conventional acoustics treatment of the system components by means of lumped element electrical circuit analogues allowed a determination of the linear stability characteristics. Quantitative comparison of the theory with experimental data was precluded by the introduction of several undetermined parameters in the analysis and the inability to calculate a priori the necessary acoustic impedances and admittances for various components of the system. The analyses showed qualitative agreement with Putnam's results.

Merk considered the case where the plenum or mixing chamber and the combustion chamber are acoustic resonators closely coupled through the low pressure drop ports in the burner head. One-di-

---

[1] That is, a characteristic chamber length below which, stable combustion prevails for all propellant equivalence ratios.

mensional flow with low Mach number was assumed with friction and heat conduction neglected. Laminar premixed flames are anchored at each injection port and have a characteristic length which is short compared to the characteristic chamber lengths. Merk wrote the conservation equations valid across the injector in order to relate the uniform properties in regions 1 and 2 of Figure II-3.

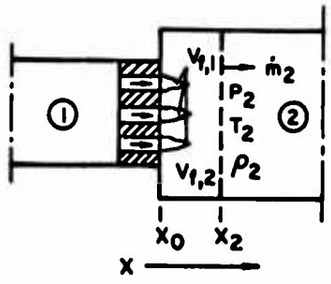

Figure II-3. Flow system near the burner ports

The nonsteady effect of the fluctuation in the flame volumes, V_{fi}, was included in the conservation equations. Oscillations upstream (region 1) of the flames were shown to be isentropic. Merk demonstrated the nonisentropicity of the downstream oscillations but also showed that in the limiting case of low mean flow Mach number these are unimportant. The heat release fluctuations at the flames were coupled to the acoustic standing wave oscillations in 1 and 2 through the sensitivity of the heat release rate to the fluctuations in density, flame speed, and the flame area. The sensitivity of the flame speed to fluctuations in the particle velocity and the pressure upstream of the flames was accounted for by linearized transfer functions. Following the approach of Crocco and Cheng (3) used in the treatment of combustion instability in a liquid propellant system, a time lag was introduced to account for the delay between injection of the premixed gases and their consumption in the thin flame front. All perturbation quantities were taken to be of order Mach number and proportional to $e^{i\omega t}$. As will be demonstrated in this report this is not quite correct for the case of low mean flow Mach number and led Merk to the incorrect conclusion that the only pressure sensitive energy source of importance in the heat release-pressure oscillation coupling is the fluctuation in flame area. Nevertheless, the theoretical analyses of Merk

viewed together with the experimental results of Putnam provide a firm foundation for understanding the nonsteady operation of the "low duty" gaseous propellant combustor. The emphasis placed by Putnam and Merk on the importance of the acoustic and fluid dynamic interaction of the propellant mass injection flux and the upstream flow and downstream combustion systems in determining the overall stability characteristics of the combustor is well substantiated by their results.

C. Gas Rocket Experiments: Zucrow, Osborn, et al. at Purdue

As was noted earlier, the development of the gas rocket as a viable research tool for the determination of the influence of gas phase processes (within the combustion chamber) on the phenomenon of unstable combustion occurred independently at Purdue University's (57-71) Jet Propulsion Center, the University of Tokyo (72-76) and at the Guggenheim Laboratories at Princeton (26-32). These researches have been motivated by interest in the practical problems of nonsteady combustion in liquid propellant rocket motors. Thus the combustors were developed with an eye toward simulating the geometry and the critical parameters observed (1, 3, 5, 6, 7, 18, 19) to influence the appearance of acoustic oscillations in the liquid systems. It is of interest to reiterate and to contrast the principal experimental and analytical results obtained in these three programs and to comment on the systems themselves. As will be shown in this report the steady and nonsteady operating characteristics of the system employed by Tsuji and Takeno at the University of Tokyo differs markedly from that used at Princeton principally due to the failure of those investigators to uncouple the mass injection flux of unburned propellant from the pressure fluctuations in the combustion chamber by suitable injector design. As a result of the extensive diagnostic program carried out by Tsuji and Takeno further doubt is cast on the appropriateness of comparing the longitudinal mode stability characteristics of either their motor or the Purdue system to those observed with the Princeton system.

The studies of nonsteady combustion in a gaseous propellant system by Osborn, Zucrow et al. at Purdue have been primarily

experimental. Both longitudinal mode and transverse mode oscillations have been examined. Here only those experiments related to the investigation of longitudinal mode acoustic[1] waves will be discussed. Zucrow and Osborn (58) studied the influence of the combustion chamber length, the mean combustion pressure, the nozzle geometry, and the equivalence ratio of methane, ethane, superheated propane, and ethylene on the longitudinal mode stability characteristics of the system shown in Figure II-4a. In contrast to the low amplitude standing acoustic waves monitored by Putnam in his low duty system, Zucrow and Osborn observed, during nonsteady combustion, finite amplitude sinusoidal or nonlinear shock-type waves propagating axially at approximately the fundamental acoustic frequency of the combustion chamber (with closed ends). Under certain conditions (e.g., higher mean chamber pressure) there was observed a shift from the fundamental longitudinal mode to a transverse mode. Larger amplitude, higher frequency shock-type waves were supported at higher mean chamber pressure (an increase in $\bar{P}_c$ from 52 to 130 psia produced a shock amplitude increase from 20 to 35 psi although the dimensionless amplitude actually decreased from 0.39 to 0.27). An increase in the length of the convergent nozzle for fixed contraction ratio effected a shift from the shock type wave form to a nonlinear continuous waveform. Subsequently, Osborn and Bonnell (64) reported the maximum amplitude of longitudinal mode oscillations supported by ethylene, ethane, and methane in air as a function of the chamber length. Osborn and Derr (66) using a somewhat different system than that shown in Figure 4a determined a so-called lower critical combustion chamber length below which no oscillations are sustained. Zucrow, et al.(61) correlated the oscillation in the (ethylene-air) combustion zone luminosity with the fluctuation in combustion pressure. The results of these investigations are summarized in Figure II-4b, c, d, e.

---

[1] "Acoustic" in the sense indicated in Chapter I. The frequency can be associated with wave motion determined by the combustion chamber geometry and the sound speed of the hot combustion products.

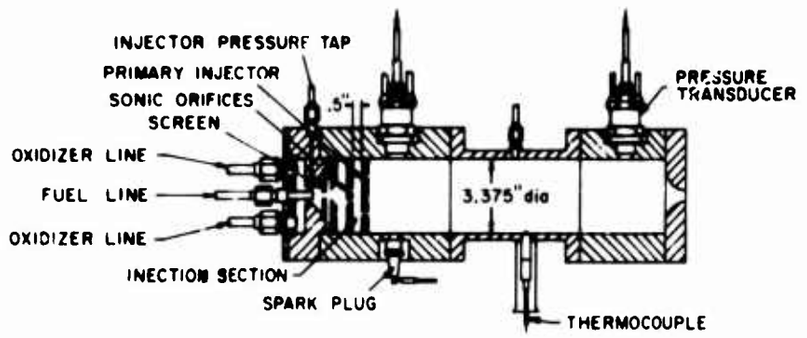

a) PURDUE GAS ROCKET FOR LONGITUDINAL MODE STUDIES (REF. a)

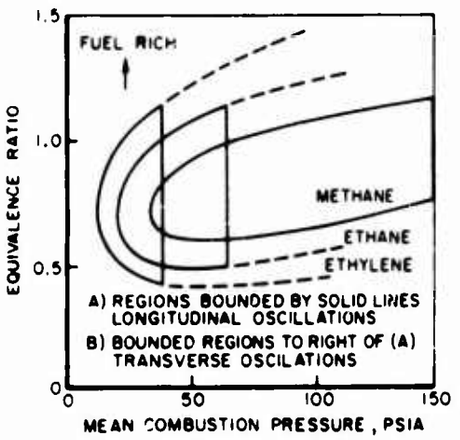

b) STABILITY LIMITS FOR LONGITUDINAL AND TRANSVERSE MODES (REF. a)

CHAMBER LENGTH in	TYPE OF OSCILLATION	FREQUENCY OF THE OSCILLATIONS cps	AMPLITUDE OF THE OSCILLATIONS psi
28.0	SHOCK (L)*	570	22
22.3	SHOCK (L)	685	22
16.3	SHOCK (L)	948	17
12.6	SINUSOIDAL (L)	1219	4

VALUES FOR THE VARIABLES:
EQUIVALENCE RATIO, .2 ± 0.08 (FUEL RICH)
PROPANE LINE PRESSURE DROP, 158 ± 8 psi
AIR LINE PRESSURE DROP 150 ± 10 psi
MEAN COMBUSTION PRESSURE, 45 psia ± 2 psi

* L INDICATES A LONGITUDINAL MODE OF OSCILLATION

c) TYPICAL RESULTS FOR SUPERHEATED PROPANE + AIR (REF. a)

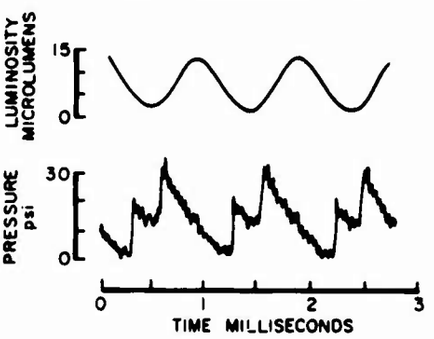

d) OSCILLOGRAMS FOR ETHYLENE + AIR (REF. b)

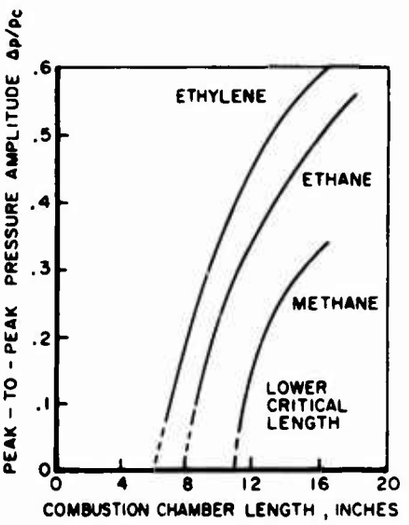

e) AMPLITUDE OF LONGITUDINAL MODE OSCILLATIONS vs CHAMBER LENGTH (REF. c)

REF. a: ZUCROW AND OSBORN, JET PROP., 28, OCT. 1958
REF. b: ZUCROW et. al., ARS JOUR., 30, AUG. 1960
REF. c: OSBORN AND BONNELL, ARS JOUR., 31, OCT. 1961

FIGURE II-4

SUMMARY OF LONGITUDINAL MODE COMBUSTION INSTABILITY DATA FROM PURDUE GAS ROCKET

Essentially no systematic analytical formulation of the coupled system-pressure oscillation instability phenomena was offered. The work of Goede (69) is insufficient and open to criticism on several grounds (e.g., the "system" was not analyzed and no mechanisms for energy removal were included). A qualitative argument for the mechanism of coupling between finite waves propagating axially in a high aspect ratio combustion chamber and a pressure sensitive combustion zone was proffered by Zucrow and Osborn (58). The postulated mechanism follows closely the concepts introduced by Crocco (3) and developed at some length by Smith and Sprenger (25). Zucrow and Osborn envisioned a finite amplitude pressure wave passing through a gas phase combustion zone characterized by a pressure-temperature sensitive burning rate. In response to the increased pressure-temperature field following the wave (after a delay of approximately 10^{-4} seconds due to the inertia of the finite rate kinetics and corresponding to the observed lag in the luminosity traces) the burning rate accelerates and pumps energy into the travelling wave system thereby sustaining the wave. The inverse dependence of the wave amplitude on the oscillation frequency for frequencies close to that observed at the lower critical chamber length followed from the condition that more propellant is available for driving if the positive portion of the pressure cycle is temporally extended (assuming system losses to be unchanged for small changes in the chamber length).

Specific criticisms of this argument were offered by Crocco (59). While certain of these remarks must be modified by our most recent theoretical and experimental work, Crocco made the important point that the critical factor determining whether an oscillation will be supported by a pressure sensitive combustion zone is the "balance between the excess energy" (released during one cycle in response to increased pressure) "and the excess energy absorbed by dissipative processes and by the nozzle". The basic point to be made in reference to the Purdue work is simply that, in lieu of diagnostic experiments (which would, for example, discern whether the apparent fluctuation in combustion zone luminosity was "real".

or merely due to a fluctuation in the axial location of the combustion zone), little gain in physical understanding from a series of empirical measurements of motor stability characteristics can be achieved unless a systematic consistent analytical formulation of the complete problem is achieved. As pointed out earlier the accumulation of experimental data in the form of stability characteristics of a gas rocket should not be considered an end in itself. Only as these observations are shown to relate directly to phenomena occurring in practical liquid or solid propellant systems, or to be consistent with a realistic model thus allowing definite conclusions to be drawn about what is and what is not important can they be considered useful. As will be indicated, the failure to achieve either of these goals and the subsequent results of studies by Tsuji and Takeno employing a similar gas rocket system casts doubt as to the appropriate coupling mechanism active in the Purdue experiments.[1]

D. Theoretical Model of Gas Rocket Instability: Culick

It is appropriate to review the theoretical work of Culick (79, 80) at this point in view of the fact that he made explicit comparison of his results with the experimental results of the Purdue group. Culick determined for the general three-dimensional case the stability of a cylindrical combustion chamber with regard to the support of acoustic standing wave oscillations by energy release. A linearized treatment of the equations of conservation of mass, momentum, and energy for the case of low mean flow Mach number allowed the derivation of a single inhomogeneous wave equation applicable to liquid or gaseous propellant motors. The effects of

---

[1] In this regard the observation of Osborn and Derr (66) that an apparently longitudinal mode acoustic oscillation (referred to by the authors as an "air whistle") was sustained in the absence of combustion is interesting. The measured frequency of this oscillation was sensitive to the chamber length and was of the same order of magnitude as that characteristic of oscillations observed during nonsteady combustion of ethylene and air. The possibility that the mechanism by which the "air whistle" was sustained may indeed play a significant role in the support of combustion oscillations was acknowledged but not investigated.

energy release due to combustion and of the steady mean flow were concentrated in the inhomogeneous term. The nozzle boundary condition was specified in terms of an admittance function $A = \gamma \frac{u'_n}{p'_n}$ where p'_n is the dimensionless pressure perturbation and u_n the dimensionless velocity perturbation, both at the nozzle end. A separate detailed calculation of the admittance function was performed. By setting the perturbations in pressure proportional to $e^{i\omega t}$, Culick could have determined the stability criteria for each mode (distinguished by appropriate wave number k where a is the burned gas sound speed) by equating the imaginary part of the complex frequency ($ak = \omega + i\lambda$) to zero following standard stability analysis procedures. Instead an expression for λ the amplification coefficient in terms of parameters corresponding to the energy release, the mean flow, and the nozzle damping was derived which is valid near $\lambda = 0$. The effect of changes in the important driving and damping terms could then be determined. Stability of a given mode is indicated for $\lambda > 0$.

The system stability could be examined for various postulated combustion-pressure wave coupling models. Of particular interest with regard to the present work is the stability analysis (79) for the case where the energy source term incorporates the gross features of a gas phase combustion zone. The qualitative results of that analysis were tentatively compared to the experimental data obtained in the Purdue work. Culick artificially separated the volumetric energy release rate term characterizing the combustion zone into two terms, a pure rate term ($\sim$ 1/sec) and a coupled energy release per unit volume term. The mean rate term was written as $\bar{W}_c = B\bar{p}^m e^{-E/\bar{R}\bar{T}}$ (1/sec), where $B\bar{p}^m$ represents the frequency factor, $\bar{p}$ the mean chamber pressure, E the activation energy, and $\bar{T}$ the mean combustion chamber temperature. The perturbation in this mean rate corresponding to the dimensionless pressure perturbation is thus $W'_c = \bar{W}_c\left(m + \frac{\gamma-1}{\gamma}\frac{E}{\bar{R}\bar{T}}\right)p'$ where the isentropic relationship was used to relate p' to T' the perturbations in pressure and T. Following the reasoning of Pickford and Peoples (78), Culick set $\bar{Q}W'_c$ equal to the perturbation in the volumetric

energy release rate (cal/cm^3 sec) where $\bar{Q}$ is defined to be the average available energy per unit volume added to the wave during the positive portion of the transient pressure cycle. $\bar{Q} = \Delta \frac{\pi}{\omega} q \dot{m}_{tot} f$ where π/ω is ½ the oscillation period, Δ the ratio of the available energy to the total energy released, q the heat of combustion for a given mixture, $\dot{m}_{tot}$ the total propellant mass flux, and f is a combustion distribution function so defined that $\int_{vol} f dV = 1$ where the integration is over the <u>entire</u> chamber volume. Thus the final form for the perturbation in the volumetric energy release rate was written as

$$\bar{Q} W_c' = \Delta \frac{\pi}{\omega} q \dot{m}_{tot} \bar{W}_c \left(m + \frac{\gamma-1}{\gamma} \frac{E}{R\bar{T}}\right) f e^{-i\varepsilon} p'$$

where the arbitrary factor $e^{-i\varepsilon}$ allows for a phase lag ε between the pressure perturbation and the combustion response. Culick derived a single parameter, I_c, the magnitude of which determines the system stability.

$$I_c = \frac{2}{\gamma-1}\left(\frac{\omega L_c}{\bar{a}}\right)\left(\frac{\pi R_c^2}{A_t L_c}\right)\left(\frac{\bar{a}^2 c^*}{\gamma q \bar{W}_c}\right)\frac{D_n}{F_n} \quad \begin{cases} > 1 & \text{STABLE} \\ < 1 & \text{UNSTABLE} \end{cases}$$

where

$\frac{\omega L_c}{\bar{a}}$ = dimensionless frequency dependent on geometry

$\frac{\pi R_c^2}{A_t L_c}$ = geometry factor, R and L are the chamber radius and length respectively, the nozzle throat area

c^* = $(f(\gamma) R \bar{T})^{\frac{1}{2}}$ the characteristic velocity

$\frac{\bar{a}^2 c^*}{\gamma q \bar{W}_c}$ = factor depending on the propellant chemistry, mixture ratio, and chamber pressure

γ = $\Delta \pi \left(m + \frac{\gamma-1}{\gamma}\right) \frac{E}{R\bar{T}}$

$\frac{D_n}{F_n}$ = factor accounting for all damping effects due to nozzle geometry and Mach number at the nozzle entrance (the mean flow) and the distribution of combustion

While Culick emphasized (80) the importance of the combustion distribution (F_n) and hence the injection configuration in determining the ultimate system stability, he also offered (79) certain conclusions regarding the influence on the stability characteristics of the geometry, the mean flow Mach number, and the mean chamber temperature and pressure. By simply noting the effect on the magnitude of I_c of a change in each parameter (all others held constant), the change could be classified as "stabilizing" (I_c increasing in magnitude) or destabilizing (vice versa). Thus, increasing the nozzle length (D_n increases) or increasing the mean chamber Mach number were seen to have stabilizing effects by virtue of the corresponding increase in nozzle damping and convection by the mean flow of energy through the nozzle. For a given axial mode (ω fixed) increasing the chamber length was observed to be destabilizing. Furthermore the lower modes should be the least stable. Finally Culick examined the effect of variations in the term $\bar{a}^2 c^*/\gamma q \bar{W}_c \sim \bar{T}^{\frac{3}{2}}/(m+\frac{\gamma-1}{\gamma}\frac{E}{R\bar{T}})q\bar{W}_c$ and concluded that increasing the heat of combustion q of the propellant is destabilizing. Thus ethylene should be "more unstable" than methane. Furthermore in view of the exponential dependence on the parameter $E/R\bar{T}$ of the term $\bar{W}_c$ an increase in the combustion temperature $\bar{T}$ is destabilizing. (Implicit in the argument is the conclusion that increasing the activation energy E is stabilizing due to the same exponential dependence). While Culick has indicated the incorrectness of the isentropic relationship between the pressure and temperature perturbations in a zone of combustion (24), it is the feeling of this author that the conclusions regarding the effects of the mean chamber Mach number and the parameter $E/R\bar{T}$ are also incorrect for the case of longitudinal mode acoustic oscillations in a gaseous propellant rocket motor having a low mean flow Mach number. Culick's qualitative results cannot be compared properly to the longitudinal mode gas rocket results (Purdue). Justification for these remarks will follow a discussion of results obtained with the Princeton system. The point is simply that the gas rocket combustion zone has a characteristic length which

is much less than the overall chamber length (in the case of longitudinal mode oscillations). This concentration of combustion has important consequences in the description of the coupling between the combustion zone energy release and the pressure waves.

E. Gas Rocket Experiments and Theory: Tsuji and Takeno, Tokyo

Tsuji and Takeno (73-77) have completed a series of experimental and analytical studies on longitudinal mode acoustic oscillations supported in a rocket motor employing premixed gaseous propellants of similar design to that originally used in the Purdue work. They have pursued a course of investigation quite similar to that followed by Bowman (32) and completed in this report. The motivation for their work was to study the basic phenomena of nonsteady combustion in a system substantially simpler than a liquid propellant rocket motor. Premixed city gas of approximate composition - 37% H_2, 24% CH_4, 6.2% CO, 4% C_2H_4, 4% C_3H_6, 9% CO_2, 2.8% O_2, and 13% N_2 - and air were used as propellants in all of their investigations. The initial experiments discussed in (73) determined the longitudinal mode stability characteristics of the system shown in Figure II-5a as a function of the mean chamber pressure ($\bar{P}_c$), the propellant equivalence ratio, ($\phi = \frac{1}{\bar{\Omega}}$) and the motor geometry including the chamber length (L_c) and the nozzle geometry. With regard to the injector section geometry it is noted that a choked orifice was located upstream of the primary showerhead injector. This orifice was designed to suppress low frequency combustion pressure oscillations and to inhibit the upstream propagation of combustion in the event of flashback through the primary injector. This design produced an "injection section" (2 cm long, approximately 37 cm^2 in cross section or a volume of about 74 cm^3) upstream of the primary injection orifices. Subsequent modification of the system to allow monitoring of the transient pressure in the injection section required an injection section length of 4 cm (148 cm^3 volume) to accommodate the transducer. Comparison of this injection system with that in the Purdue motor shows that a similar configuration was used by Zucrow, Osborn, et al. in their longitudinal mode studies. In the Purdue system

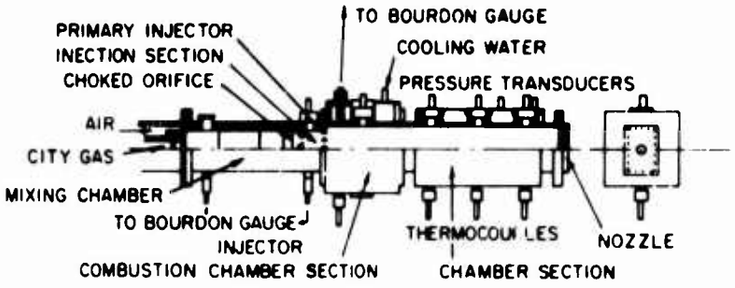

a) UNIV. OF TOKYO GAS ROCKET
FOR LONGITUDINAL MODE STUDIES

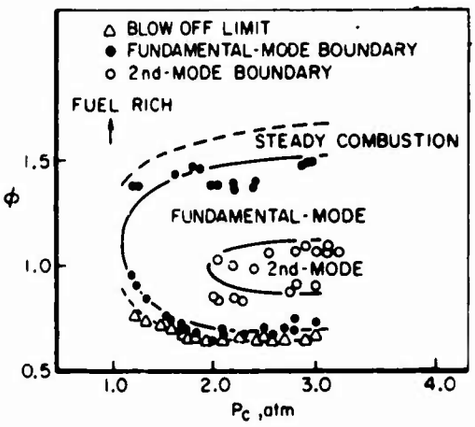

b) REGIONS OF INSTABILITY
FOR CHAMBER LENGTH, L_c = 39.3 cm

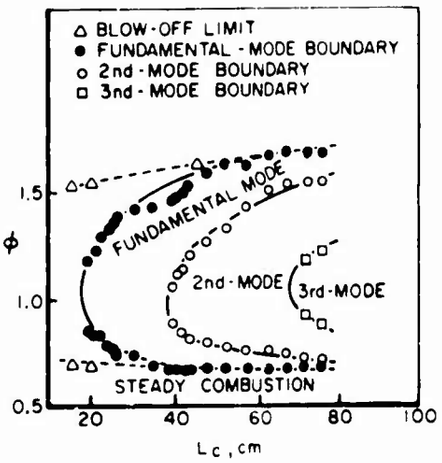

d) REGIONS OF INSTABILITY
FOR MEAN CHAMBER PRESSURE, P_c = 2.9 atm

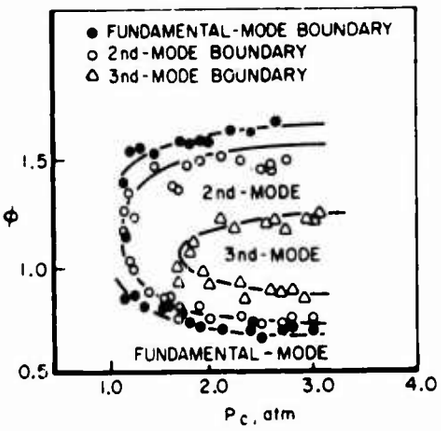

c) REGIONS OF INSTABILITY
FOR CHAMBER LENGTH, L_c = 75.3 cm

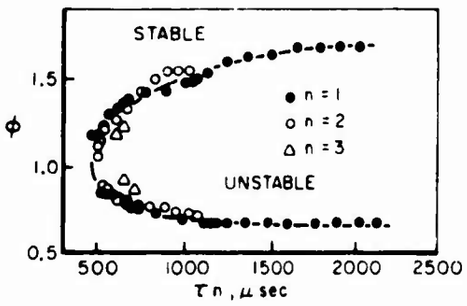

e) CROSSPLOT OF PERIOD OF OSCILLATION (τ_n) vs ϕ
OBSERVED AT STABILITY LIMITS SHOWN
IN (d), FOR P_c = 2.9 atm

REF. : TSUJI AND TAKENO, 10th SYMP. ON COMB., p 1327, 1955.

SUMMARY OF LONGITUDINAL MODE COMBUSTION
INSTABILITY DATA FROM UNIV. OF TOKYO GAS ROCKET

FIGURE II-5

the "injection section" volume was cylindrical (1.32 cm long and a volume of 44 cm^3).

Initially a determination of the stability limits as a function of the propellant equivalence ratio, the mean chamber pressure, and the chamber length was made. As indicated in Figure II-5b, c, d these experiments determined narrow regions of longitudinal mode oscillations located about the stoichiometric mixture ratio. No transverse oscillations were reported. The observation of three axial acoustic modes, the fundamental and the 2nd and 3rd harmonics, was noted. A lower and upper critical chamber length for each mode (inferred for the 3rd harmonic) was noted. Examination of the transient combustion pressure records indicated the sustained pressure waves to be predominantly low amplitude, continuous, standing waves. This implies an in-phase (or precisely 180° out of phase - depending on axial location with respect to the pressure nodes) oscillation of pressure at all axial positions in the chamber with pressure antinodes located at the injector and nozzle ends. Upon further scrutiny these pressure records showed the low amplitude discontinuous shock waves (when supported) to be superimposed on the sinusoidal standing wave oscillation. The axial propagation of the shock waves occurred at the acoustic frequency corresponding to the sustained standing mode harmonic. Confirmation of this point is indicated in (75) where the point is emphasized that the excited oscillation remains essentially the continuous acoustic standing wave oscillation. In the case of the higher harmonics reflection of the shock waves at the velocity nodes (pressure antinodes) of the standing waves was observed. The amplitude of the waves increased with increasing mean chamber pressure and combustion gas temperature with the maximum amplitude supported at the stoichiometric mixture ratio. Tsuji and Takeno report wave amplitudes of 3 to 5 psi corresponding to mean chamber pressures of 1 to 2.5 atm ($\Delta p/\bar{p}_c \sim 0.1$).

A determination of the steady frequency of each mode showed primary dependence on the chamber length and the mean combustion temperature. The correlation of the measured periods of oscilla-

tion at the stability limits with the appropriate equivalence ratio for a mean combustion pressure of 2 atm is shown in Figure II-5e, where the data points represent combinations of equivalence ratio, chamber length, and mode order. Tsuji and Takeno made an important inference on the basis of these data. They concluded that the existence for each equivalence ratio (ϕ) of a lower "critical" period (τ_{crit}) of oscillation corresponding to the observed lower "critical" lengths (L_{crit}) at each ϕ is indicative of the existence of a "critical combustion time lag." They suggested that this characteristic combustion zone response time included both a mechanical or fluid dynamic time lag and a chemical time lag corresponding to that time necessary for the combustion zone to sense, respond to, and feed back energy into the pressure wave. This total lag should be determined by the propellant chemistry, the mean chamber pressure, and the injection velocity. Support of oscillations should arise only when the oscillation period exceeds the critical time. Further development of this model followed a second series of optical investigations. It should be noted that the effect of the injection velocity was included in their model. The primary injection velocity during the experiments was estimated to be 1.2×10^4 cm/sec (injection Mach number, $M_{inj} = 0.3$).

Having completed a determination of the phenomenological aspects of nonsteady combustion in their gas rocket, Takeno then performed a series of experiments designed to obtain information about the combustion zone. These studies were directed towards establishing a firm physical foundation, i.e., a better understanding of the "real world" interaction of the combustion zone and the pressure waves, upon which an analytical model could be constructed. To this end Takeno first determined the influence on the motor stability characteristics of the injection geometry (the length of the injection section) and the premixed propellant injection Mach number. While lengthening the injection section from 2 to 4 cm had no effect on the critical oscillation periods, Takeno did find that a low amplitude oscillation of the injection section pressure

accompanied oscillations in the combustion chamber pressure. He observed that the frequency of this upstream oscillation was identical to that in the combustion chamber although the amplitude was of the order of 0.2 times the chamber pressure oscillation amplitude. However, in view of the insensitivity of the stability characteristics to changes in the injection section length, Takeno concluded that no wave amplification mechanism was associated with the coupling of waves upstream and downstream of the primary injector. A determination of the influence of the injection Mach number was made by simply varying the hole size in the showerhead type injector. It is important to keep in mind that in all of these tests the pressure drop across the injector was extremely low and of the same order as the amplitude of the standing wave oscillation in the combustion chamber (1 to 5 psi). An increase of the injection Mach number from 0.29 to 0.37 had a destabilizing influence in the sense that the regions of nonsteady burning expanded and the critical oscillation period at each decreased. Subsequent investigation of the axial distribution of the mean temperature in the combustion zone during nonsteady burning coupled with direct photographs of the combustion zone under steady burning conditions showed that combustion occurs through turbulent flames surrounding each injected stream of propellant with the peak temperature located approximately 3 to 4 cm from the injector face. Takeno pointed out that for $M_{inj} = 0.29$, $\bar{p}_c = 3$ atm neither the temperature maximum nor the temperature distribution were comparable at the fuel rich and fuel lean stability boundaries. For example, a 400° K difference was reported between the combustion temperatures at the fuel rich and fuel lean boundaries between the fundamental mode and the stable combustion regime. He concluded that the combustion zone temperature is <u>not</u> a critical ingredient in the coupling mechanism between combustion process and the pressure waves.

A series of high speed Schlieren photographs of the combustion zone under steady and nonsteady conditions completed the experimental work and facilitated certain fundamental conclusions regarding the nature of the flame zone-pressure wave interaction.

These tests were accomplished using a radically modified injection scheme. The 20 hole short port length showerhead injector having a total flow area of 1 cm^2 (for M_{inj} = 0.29) was replaced by a "two-dimensional" injector machined to provide injection through four slots (0.1 cm x 5 cm) having a total flow area of 2 cm^2 (M_{inj} = 0.19). Essentially the same transient combustion pressure waveform was observed with this design as was found in the earlier work (a standing wave with a low amplitude superimposed propagating pulse). The schlieren photographs revealed an oscillation of the dense core zone of the low velocity streams of cold unburned premixed gases. This oscillation, which appeared as a periodic axial extension and contraction of the propellant stream, was observed to have the same frequency as the simultaneously measured transient combustion pressure waveform but was seen to be almost precisely 180^o out of phase with the pressure oscillation. Upon closer examination of the photographs Takeno observed that dark islands of apparently unburned propellant are shed from the ends of the gas streams during that phase of the cycle when the streams are lengthening. Referring to this phenomenon as that of "flame tip breaking" Takeno succeeded in correlating the visually observed disappearance of the unburned islands after an appropriate "ignition delay" of one-quarter of the period of the pressure cycle with the appearance at the injector end of the nonlinear propagating pulse. Thus he discerned the mechanism of coupling between the turbulent flame zones and the pressure oscillation to be a complex fluid mechanical-chemical interaction. The sensitivity of the propellant injection mass flux to the nonsteady chamber pressure (essentially a linear effect) by virtue of the negligible pressure drop across the showerhead injector produces oscillations in the propellant injection velocity which are 180^o out of phase with the pressure fluctuations. The highly nonlinear effects of flame tip breaking and subsequent ignition of the shed islands of unburned gas occur after a chemical time delay or ignition lag. The propellant chemistry and the combustion chamber environment determine the ignition time lag. Takeno concludes that this is the important characteristic time which must lie in the right range (3) in order

that the heat release due to the delayed ignition be properly phased with the standing wave pressure oscillation. According to Takeno the nonlinear pressure pulse which on occasion assumes a shock wave form has no effect of the standing wave oscillations per se. The important influence is the heat release corresponding to the delayed ignition. The pulse merely acts as a signal of that release. From the photographs and the pressure traces Takeno determined that this critical time, τ_{CRIT}, is approximately 500 μsec which compares favorably with critical times discerned from the stability limit data Figure II-5e.

Takeno completed his investigations by developing (77) an analytical model of the phenomena to provide quantitative as well as qualitative explanation of the observed experimental results. The results obtained from the detailed combustion zone diagnostics were used as a basis for the physical structuring of the model. Following Culick's approach a linearized analysis of the conservation equations of mass, momentum, and energy yields a simplified one-dimensional wave equation with a heat source due to chemical reaction. The equation was developed for the case of low mean flow Mach number such that the free stream velocity is of the order of perturbation quantities and was written

$$\frac{\partial^2 p'}{\partial t^2} = \frac{\partial^2 p'}{\partial x^2} + \frac{\partial q'}{\partial t}$$

where p' and q' are the perturbations in the dimensionless pressure and the heat release rate. Takeno dispensed with the observed highly structured flame zone and treated the simplified configuration shown in Figure II-6 where a uniform low Mach number flow of combustion products at the mean combustion temperature proceeds from the injector face to the nozzle entrance. The influence

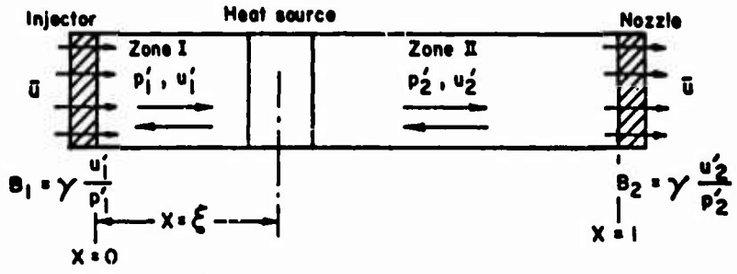

Figure II-6. System analyzed by Takeno

of heat release due to combustion is concentrated in a thin one-dimensional heat source zone located at nondimensional axial position ξ, such that $q' = Q_\xi(t)\delta(x-\xi)$. The method of solution is to obtain separately the simplified wave equation $\partial^2 p'/\partial t^2 = \partial^2 p'/\partial x^2$ for the standing isentropic waves in regions I and II. The injector and nozzle boundary conditions appear as arbitrary admittance functions $B_{I,II} = \gamma u'/p'$ where u' is the perturbation in the mean flow velocity. No attempt at calculating these admittance functions was made. They remain as adjustable parameters. Two matching conditions (a jump condition on velocity $u'_{II} - u'_I = Q_\xi(t)/\gamma$ and a statement of pressure continuity $p'_I = p'_{II}$) at the heat source interface are obtained by integrating the inhomogeneous wave equation $\frac{\partial^2 p'}{\partial t^2} = \frac{\partial^2 p'}{\partial x^2} + \frac{\partial}{\partial t}\left[Q_\xi(t)\delta(x-\xi)\right]$ (valid in the heat source region) across the heat source. The characteristic equation governing the form of the complex frequency $s = \alpha + i\beta$ is obtained in the standard fashion. Of particular interest is the form assumed for the heat source function. Based on the flame zone observations Takeno assumed that, in response to a harmonic pressure function of the form $p'(x,t) = \sigma(x)\, e^{st}$, the heat release rate can be written as $q' = -A\sigma_I(0)\, e^{+s(t-\tau)}\delta(x-\xi)$. Recall that the photographs indicated that the flames oscillated in response to a fluctuation in flow velocity at $x = 0$. The flow velocity fluctuation appeared to be approximately 180° out of phase with the pressure fluctuation. The term $-\sigma_I(0)$ accounts for this observation. Furthermore the increase in the heat release rate (the ignition) was deemed to occur τ μsec after the pressure minimum. τ was observed to be approximately one-quarter of the period of the pressure oscillation. Thus the lag effect is accounted for by the factor $e^{-s\tau}$. (A) is an arbitrary parameter termed the interaction index. Takeno points out that the choice of q' is solely dependent on the combustion model adopted. Appropriate expressions for a chemical kinetic Arrhenius rate law and a velocity dependent rate law are indicated. Numerical analysis of the final characteristic equation allowed the amplification coefficient α and the frequency β to be determined parametrically in terms of the location of the heat source ξ, the time lag τ, and the mode order n

for arbitrary values of the injector and nozzle admittance functions and the interaction index. For details of the calculations and the results refer to (77).

In order to arrive at an acceptable correlation between theory and experiment Takeno made several arbitrary assumptions. The interaction index was set equal to 0.5. The dimensional time lag required by the analysis to compute τ , was set equal to three-quarters of the lower critical oscillation period τ_{CRIT} despite the observations detailed in (76) that $\tau \sim 1/4\,\tau_{CRIT}$. Significantly the choice of $\tau = 1/4\,\tau_{CRIT}$ yields very poor correlation between theory and experiment for A = 0.5. This point was not discussed by Takeno.

Since prediction of the system stability behavior by this analysis requires the use of experimental data (the form of β' , ζ etc.) it would seem that a better procedure would have been to preserve (A) as a single datum fit parameter and restrict $\tau = 1/4\,\tau_{CRIT}$ in accordance with the experimental data. This would eliminate one arbitrary parameter (namely τ) from the analysis. It should be noted that the comparison between theory and experiment was made for the case of finite driving due to the heat source but where damping effects are neglected (both admittance functions set equal to zero). Out of context this would seem to be an invalid procedure for determining the stability of the hypothetical gas rocket system since the important consideration determining the linear stability limit must be the relative balance between the rate of energy addition by combustion and the rate of energy removal by dissipative processes. Justification for the technique follows from the fact that Takeno obtained an expression for the amplification coefficient and identified the stability limit with the (lower length) zero of the amplification coefficient. By determining the relative magnitudes of the amplification coefficient for the various modes Takeno determined which mode is the most likely to be sustained for various combinations of the parameters.

F. Gas Rocket Experiment and Theory: Princeton University

It is appropriate to complete this review with an account of previous researches at Princeton devoted to the study of longitudinal

mode combustion instability in a gaseous propellant rocket motor. While the program bears some resemblance to those at Purdue and at the University of Tokyo the basic systems, approaches, and results can be contrasted. As indicated in the first chapter there has been a systematic emphasis on the deductive approach as opposed to the inductive one followed in the other programs. Each phase of the work has evidenced the feedback between theory and experiment. Qualitative and quantitative predictions have been derived from analyses of the nonsteady combustion phenomena in the gas rocket and have served to guide the experimental investigations. Insight gained from the experimental observations has been applied to the development of more realistic analytical models. The ultimate goal has been the achievement of a realistic description of the coupled gas phase combustion zone and pressure wave phenomena which accurately portrays the experimental observations.

It has been noted that the gas rocket was developed at Princeton as a research tool to allow a determination of the influence of gas phase chemical rate processes on the phenomena of longitudinal mode combustion instability. As indicated in the first chapter, the system derived from the liquid propellant rocket instability program where substantial success had been achieved in correlating experimental results by means of Crocco's sensitive time lag model (1, 3, 15, 18, 19). Of interest was the possibility that gas phase chemical kinetics influences the time lag deduced from the liquid propellant system data. Since the observations of Zucrow and Osborn (58) demonstrated certain similarities between longitudinal mode instability observed in gaseous and liquid rocket motors, it was felt that the phenomena observed in the gas rocket should also exhibit the "time lag behavior" and, furthermore, that this time lag should naturally derive from gas phase chemical rate processes.

The initial experimental work of Pelmas (29) was designed to explore this thesis and to obtain fundamental information about the stability characteristics of the gas rocket. The system used by Pelmas essentially corresponds to that discussed in Chapter III. For the CH_4 and oxygen-enriched air (40% O_2 and 60% N_2, molar basis)

propellant system, the characteristics of longitudinal mode acoustic instability were determined as a function of the propellant equivalence ratio, the combustion chamber length, and the injector configuration. The principal results of that work are indicated in Figure II-7a, b from (29). In agreement with the Purdue work, Pelmas observed a lower critical chamber length limit and a failure of the regimes of oscillation to close with increasing chamber length. In contrast to the Purdue results with CH_4+ Air where a single region of nonsteady combustion including the stoichiometric mixture ratio was observed, Pelmas found two regimes of longitudinal mode oscillations offset symmetrically (with respect to the adiabatic flame temperature) from the stoichiometric mixture ratio. The insensitivity of the stability characteristics to changes in the chamber length (for lengths greater than the lower critical length) was surprising. This result together with the observation that the appearance of higher harmonic mode oscillations was primarily a function of the equivalence ratio (Figure II-6b) seemed to indicate that finite rate chemical kinetics must not influence the time lag coupling mechanism between the combustion zone and the pressure oscillations. It should be noted that this conclusion followed from the consideration that the gas phase combustion process must present a finite, pressure sensitive time lag of sufficient magnitude in order for the burning rate to positively couple with the pressure oscillations. In view of the experimental results and the feeling that gas phase kinetics should present short characteristic times compared to the oscillation periods observed in these experiments, an alternative driving mechanism for the oscillations was sought. Thus followed the theoretical work of Bortzmeyer (28), and the experimental investigations of Schob (31) and Bertrand (30) designed to examine the postulate that the longitudinal mode acoustic oscillations are driven by an oscillation in the rate of heat transfer to the primary injector plate wherein time lag effects are produced by the inertia of the heat transport and convection processes. A discussion by Bowman of this model and the experimental results is found in (32). In short, the insensitivity of the system stability characteristics

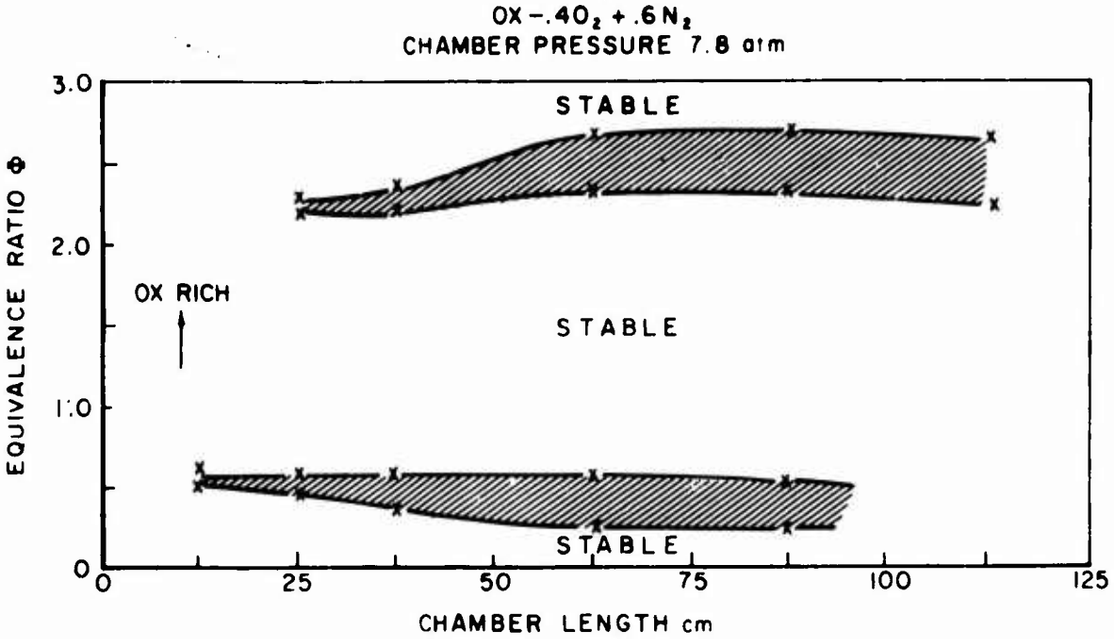

a) INSTABILITY REGIONS FOR METHANE-OXYGEN ENRICHED AIR USING POROUS INJECTOR

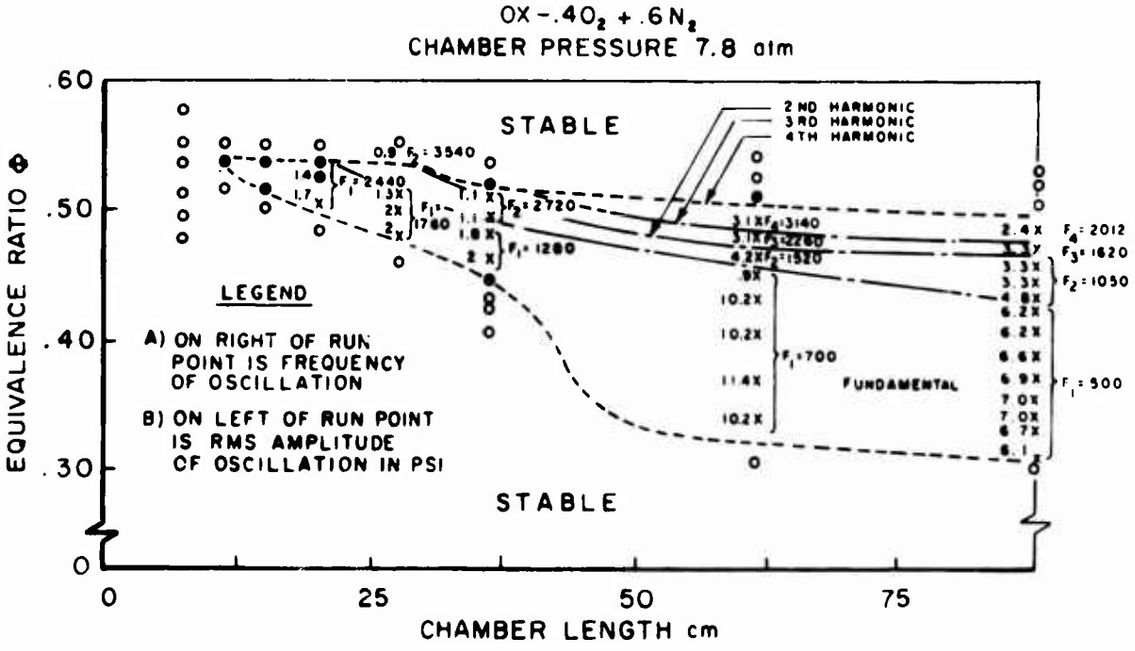

b) INSTABILITY REGIONS FOR METHANE-OXYGEN ENRICHED AIR USING POROUS INJECTOR

REF.: PELMAS et. al., AERO. ENGR. REPT. 589, PRINCETON, 1961

SUMMARY OF LONGITUDINAL MODE COMBUSTION INSTABILITY DATA FOR PRINCETON GAS ROCKET FROM PELMAS

FIGURE II-7

to the theoretically predicted important heat transfer rate to the injector led to the conclusion that this scheme was also inappropriate. These results and the confirmed sensitivity of the onset of pressure oscillations to the equivalence ratio, hence the combustion temperature, led to the speculation that the time lag model itself was not applicable to the gaseous propellant rocket motor. That is, if the gas phase chemistry is indeed important in the coupling of the energy release and the pressure waves as argued qualitatively by Zucrow and Osborn (58, 60, 61, 64) then these rate processes should respond (in a linear sense) with no lag to the variation in chamber pressure. Such reasoning led Sirignano and Crocco (26, 27) to a detailed nonlinear analysis of longitudinal mode acoustic instability for a simplified premixed gas rocket. As noted earlier the theoretical results obtained from that analysis served to guide the experimental work of Bowman (32, 33) and some of the initial aspects of the present work.

Sirignano and Crocco made explicit use of the observed characteristics of nonsteady combustion in the Princeton gas rocket. The experiments of Pelmas (29) had revealed that under favorable conditions of motor geometry and propellant equivalence ratio, low, constant amplitude shock waves oscillate axially at fixed frequency corresponding approximately to the acoustic frequencies (Pelmas observed the fundamental and three higher harmonic modes as shown in Figure II-6b) of the combustion chamber filled with hot products. For a simple form of the energy release rate law the criteria for the existence of (explicity assumed) periodic shock type waves were determined. By considering the combustion zone to be concentrated (zero thickness) at the injector end and the nozzle length to be short compared to the chamber length the nonlinear one-dimensional analysis of the shock wave propagation in the combustion chamber was uncoupled from the description of the combustion zone energy release and the nozzle damping. These were introduced separately to obtain the appropriate boundary conditions on the perturbation in the particle velocity at the ends of the combustion chamber. By assumption the strength of the propagating shock wave was determined by the first order imbalance

between the combustion zone and nozzle admittances. The nozzle boundary condition was based on the assumption of quasisteady flow in a short length nozzle. The approximation of fixed nozzle entrance Mach number was made. A simplified one dimensional combustion zone was analyzed for the case where the ratio of the characteristic combustion time to the wave travel time is small (negligible). The effect of propellant chemistry - chemical kinetics - was emphasized in a simple volumetric energy release rate law wherein no time lag effects appear. For a combustion zone length (ℓ^*)[1] which is small compared to the overall chamber length (L_c^*), the energy and mass conservation equations were combined and integrated over the combustion zone length to yield

$$(\rho u)_{x=\ell} = -\frac{\ell}{\gamma}\frac{dp}{dt} + \frac{\gamma-1}{\gamma}\int_0^\ell r\,dx \qquad \text{[II-1]}$$

The momentum equation was replaced by the approximation of (spacially) uniform pressure across the short combustion zone and the above equation was written neglecting heat transfer to the injector and energy ($\dot{m}_{in}^* C_p^* T_u^*$) convected into the combustion zone by the unburned gases. The equation applies for the case of constant mean burning rate and all terms are dimensionless. For the case of small perturbations two expressions follow

$$\bar{u}_{x=\ell} = \frac{\gamma-1}{\gamma}\int_0^\ell \bar{r}\,dx \qquad \text{[II-2]}$$

$$(\rho u)'_{x=\ell} = -\frac{\ell}{\gamma}\frac{dp'}{dt} + \frac{\gamma-1}{\gamma}\int_0^\ell r'\,dx \qquad \text{[II-3]}$$

where $(\rho u)'_{x=\ell}$ represents the perturbation in the rate of energy release or the input power to the wave at $x=\ell$. It is of interest to note that the authors concluded from this perturbation relation that increasing the length of the combustion zone (e.g., by reducing the chamber pressure) leads to larger power input to the wave and should therefore be destabilizing. As will be shown in

---

[1] Starred ( )* quantities are dimensional. Thermodynamic quantities are nondimensionalized by the steady state burned gas values (T_b^*, p_b^*, ρ_b^*) particle velocity by the burned gas sound speed (a_b^*), and energy release rate by $p_b^* a_b^*$, x^* and ℓ^* by L_c^* , and t^* by L_c^*/a_b^*.

the following paragraphs this statement is incorrect for the gas rocket. Finally, perturbations in the energy release rate were coupled to perturbations in temperature and pressure in a linear fashion and the isentropic relationship was used to express perturbations in pressure in terms of temperature perturbations. For the case where $\lambda = \ell^*/L_c^* \ll 1$, the steady state energy release rate term $\bar{r}$ was taken to be an appropriate mean value for the combustion zone. Thus general expressions for two important parameters governing the wave amplitude and the waveform were determined. Sirignano and Crocco then specialized the results for the case where the energy release rate is simply written as $r = e^{-E^*/\bar{R}^*T^*}$. They found that the stability limit criterion could be expressed in terms of a critical value for the Arrhenius parameter

$$\left[\frac{E^*}{\bar{R}^*T^*}\right]_{CRIT} = \frac{3\gamma - 1}{2(\gamma-1)} \qquad \text{at the stability limit}$$

$$\frac{E^*/\bar{R}^*T^*}{[E^*/\bar{R}^*T^*]_{CRIT}} \begin{cases} > 1 & \text{unstable} \\ < 1 & \text{stable} \end{cases}$$

Furthermore the finite amplitude of the discontinuous fundamental mode wave was found to be proportional to the parameter

$$\Delta p \sim \frac{\epsilon}{\lambda} F(\bar{u}, \gamma) \sim \left[(\gamma-1)\frac{E^*}{\bar{R}^*T^*} - \frac{3\gamma-1}{2}\right] \cdot F(\bar{u}, \gamma)$$

The pressure waveform was observed to take the form of a shock discontinuity followed by an exponential decay. Thus for a choice of E^* and γ the theory predicts that unstable combustion will occur for mean combustion temperatures <u>below</u> a critical value T^*_{CRIT}. Thus, depending upon the critical value of T^*_{CRIT} and the functional relationship between the mean combustion zone temperature and the equivalence ratio for a given propellant system either a single zone of nonsteady combustion surrounding the stoichiometric mixture ratio or two zones offset from the stoichiometric ratio are predicted. The theory indicates that both the effect of nozzle

damping and energy addition are directly proportional to the mean flow Mach number ($\bar{u}$ in this case). Thus for a fixed combustion zone temperature the shock strength is proportional to the mean flow Mach number ($\epsilon \sim F(\bar{u})$). Alternatively for fixed Mach number the shock strength increases monotonically with decreasing combustion temperature ($\epsilon \sim E^*/R^*T^*$).

Certain results of the analysis seemed to be in qualitative agreement with the experimental data collected by Pelmas, Schob, and Bertrand and by Zucrow and Osborn at Purdue. To that extent the theory effectively provided direction to the detailed experimental work of Bowman (32). However, before outlining the important results of that work and the correlations with the theoretical predictions several additional comments on the Sirignano-Crocco analysis and a simple extension of their one-dimensional combustion zone description are included.

With regard to the simplified combustion zone analysis and the use of the isentropic relationship to link pressure and temperature perturbations, it must be recognized that the complete analysis represented a first attack at the description of the observed real world nonlinearity of the longitudinal mode combustion instability phenomena in a premixed gas rocket. (Actually the treatment of the chamber gas dynamics is not restricted to a gas rocket system and other combustion zone models, in principle, could be applied provided the basic assumptions with regard to the short extent of that zone compared to the chamber length are not violated.) For the specific case of a gas phase flame zone the theory presents the first systematic analysis demonstrating that nonlinear instability can be supported by a combustion zone whose characteristic response time to pressure and temperature fluctuations is short compared to the wave travel time. In view of these considerations, and since negligible experimental information was available at the time to facilitate a more realistic description of the combustion zone, the simple one-dimensional treatment seemed appropriate.

It was noted earlier that the conclusions of the authors regarding the effects of spreading the combustion zone (increasing $\ell = \ell^*/L_c^*$ but still maintaining $\ell^*/L_c^* << 1$) are incorrect for

the premixed gas rocket. Consideration of this point leads to an interesting extension of the Sirignano-Crocco boundary condition.

Recall that the expression for the dimensionless perturbation in the energy release rate or the power input to the wave at can be written as

$$(\rho u)' \cong \frac{\gamma-1}{\gamma} \int_0^{\ell} r' dx \qquad \text{[II-4]}$$

where the term $-\frac{\ell}{\gamma}\frac{dp'}{dt} = -\frac{\ell}{\gamma}\bar{u}\frac{dp'}{dx}$ is of higher order for a short flame zone where ℓ, $\bar{u}\ dp'/dx$ are all small. The key point to be demonstrated is that the remaining term $\frac{\gamma-1}{\gamma}\int_0^{\ell} r' dx$ is in fact independent of the combustion zone length in the context of the analysis. That this is the case can be shown by taking into account the principles of operation of the gas rocket.

The above expression is written in dimensional terms as

$$(\rho^* u^*)' = \frac{\gamma-1}{\gamma} \int_0^{\ell^*} r^*(x^*,t^*)\, dx^* \qquad \text{[II-5]}$$

where the starred quantities represent dimensional quantities. For the simple rate law used by Sirignano and Crocco the steady state volumetric energy release rate is

$$\bar{r}^*(x^*) = B^* e^{-E^*/\bar{R}^* T^*(x^*)} \qquad \text{[II-6]}$$

where the pre-exponential factor (B) is a constant. Written in this form the rate law is temperature explicit and can be simply expressed as

$$r^*(x^*,t^*) = \bar{r}^*(x^*) + r^*(x^*,t^*)'$$

where

$$r^*(x^*,t^*)' = \frac{d\bar{r}^*(x^*)}{d\bar{T}^*(x^*)} \Delta T^*(x^*,t^*)$$

is the perturbation in the volumetric energy release rate due to a temperature perturbation, $\Delta T^*(x^*,t^*)$ whence

$$r^*(x^*,t^*) = \frac{E^*}{\bar{R}^* \bar{T}^*(x^*)^2} e^{-E^*/\bar{R}^*\bar{T}^*(x^*)} \left[T^*(x^*,t^*) - \bar{T}^*(x^*)\right]$$

Since $T^*(x^*,t^*) = \bar{T}^*(x^*) + \Delta T^*(x^*,t^*)$ the expression for the dimen-

sional perturbation in the volumetric energy release rate becomes

$$r^*(x^*,t^*)' = \frac{E^*}{\bar{R}^*\bar{T}^*(x^*)} e^{-\frac{E^*}{\bar{R}^*\bar{T}^*(x^*)}} \left[\frac{T^*(x^*,t^*)}{\bar{T}^*(x^*)} - 1 \right] \qquad [II-7]$$

It is convenient to replace $\bar{T}^*(x^*)$ by an appropriate mean value in the combustion zone (following the authors). An appropriate space mean definition of $\bar{T}^*(x^*)$ is indicated by Bowman (32) and is simply

$$e^{-\frac{E^*}{\bar{R}^*\bar{T}^*_{mean}}} = \frac{1}{\ell^*} \int_0^{\ell^*} e^{-\frac{E^*}{\bar{R}^*\bar{T}^*(x^*)}} dx^*$$

For a linear profile in temperature (with axial position) the spacial average becomes a simple average over the temperature profile. For the propellant systems of interest and for the above <u>simple</u> rate law (where the maximum rate is achieved at $\bar{T}^* = T_b^*$ rather than at some lower temperature) the ratio $\bar{T}^*_{mean}/T_b^*$ = (0.90 to 0.95) according to Bowman (32). A reasonable approximation for our purposes here is simply to set $\bar{T}^*_{mean} = T_b^*$ = adiabatic flame temperature. Thus in terms of mean values

$$r^{*\prime} = \frac{E^*}{\bar{R}^*\bar{T}_b^*} e^{-\frac{E^*}{\bar{R}^*\bar{T}_b^*}} \left[T - 1 \right]$$

and

$$(p^*u^*)' \sim \frac{\gamma-1}{\gamma} \int_0^{\ell^*} r^{*\prime} dx^*$$

$$(p^*u^*)' \sim \frac{\gamma-1}{\gamma} \frac{E^*}{\bar{R}^*T_b^*} \left[e^{-\frac{E^*}{\bar{R}^*T_b^*}} \cdot \ell^* \right] \cdot \left[T - 1 \right] \qquad [II-8]$$

The key point is simply that

$$\int_0^{\ell^*} e^{-E^*/\bar{R}^*T_b^*} dx^* = \ell^* e^{-\frac{E^*}{\bar{R}^*T_b^*}} = \dot{m}^*_{TOT} \cdot \beta T_{f,i} \cdot g^* \qquad [II-9]$$

where $\dot{m}^*_{TOT}$ is the total mass flux[1] of combustible in $gms/cm^2\,sec$

[1] In general, $\dot{m}_{TOT}{}^*$ should be interpreted as the mean mass flux (per unit area) of propellant.

which by suitable injection design (choked flow) can be maintained constant and independent of the pressure oscillations, q^* is the heat of combustion of the fuel in $\frac{cal}{gm}$, $\nabla_{f,i}$ is the constant mass fraction of fuel in the total mass flow rate of propellant, and $\beta = 1$ for fuel lean mixtures or $\beta = \Phi$ for fuel rich initial mixtures (Φ is the equivalence ratio; $\Phi > 1$ → ox-rich).

Thus the dimensional power input to the wave by combustion becomes

$$(p^* u^*)' \sim \frac{\gamma - 1}{\gamma} \frac{E^*}{\bar{R}^* T_b} \left[\frac{\bar{C}_p^* (T_b^* - T_u^*)}{T_b^*} \right] \dot{m}_{TOT}^* T^{*\prime} \frac{cal}{cm^2 sec} \qquad [II\text{-}10]$$

Expressing the perturbation in temperature in terms of the pressure perturbation by the factor η ($\eta = \frac{\gamma - 1}{\gamma}$ in the Sirignano-Crocco analysis)

$$T^{*\prime} = \eta \frac{p^{*\prime}}{p_b^*} T_b^*$$

which for isentropic coupling is

$$T^{*\prime} = \frac{\gamma - 1}{\gamma} \frac{MW_b^*}{\rho_b^* \bar{R}^*} p^{*\prime} = \frac{p^{*\prime}}{\bar{C}_p^* \rho_b^*}$$

The power input becomes

$$(p^* u^*)' \sim \frac{\gamma - 1}{\gamma} \frac{E^*}{\bar{R}^* T_b^*} \left[1 - \frac{T_u^*}{T_b^*} \right] \bar{u}_b^* p^{*\prime} \qquad [II\text{-}11]$$

where

$$\dot{m}_{TOT}^* = \rho_b^* \bar{u}_b^*$$

In terms of dimensionless quantities used by Sirignano and Crocco (both sides of II-11 are divided by $p_b^* a_b^*$)

$$(pu)' \sim \frac{\gamma - 1}{\gamma} \frac{E^*}{\bar{R}^* T_b^*} \left[1 - \frac{T_u}{T_b} \right] M_b \cdot p' \qquad [II\text{-}12]$$

The term $(1 - T_u/T_b)$ shows the influence of the propellant heat of combustion. For larger q^*, that is, higher T_b^*, $(1 - T_u/T_b)$

increases. For the propellant systems discussed in this report the dominant factor is the ratio $E^*/\bar{R}^* T_b^*$. Expressions II-11,12 and 13 demonstrate quite clearly the importance of the Arrhenius factor $E^*/\bar{R}^* T_b^*$ and the total propellant mass flux, $\dot{m}_{TOT}^*$, or, alternatively, the linear velocity of the burned gases ($\bar{u}_b^*$) at the end of the combustion zone in determining the coupling between perturbations in the thermodynamic variables and the combustion zone response. For a gas phase combustion zone wherein the instantaneous energy release rate follows a simplified Arrhenius type law the power input to the wave in response to a fluctuation in temperature and pressure will be larger at lower combustion temperature and higher mean propellant burning rate (which must be proportional to the mean mass flux). The effect of the length of the combustion zone disappears since the power input depends on the integrated effect of energy release at the end of the short zone.

M_b is the Mach number of the burned gases at $x^* = \ell^*$ and thus serves as a measure of the "level" of combustion in the premixed gas rocket. For the adiabatic system and a quasi-steady, short nozzle the mean combustion chamber Mach number also serves as a measure of the power removed form the wave due to convection through the nozzle. That is, for the gas rocket case of low mean flow Mach number,

$$u = \bar{u} + u' = M_b + u'$$

$$\rho = 1 + \rho'$$

$$a = 1 + a'$$

$$\rho u = \bar{\rho}\bar{u} + (\rho u)' = M_b + (\rho u)'$$

$$(\rho u)' = u' + M_b \rho'$$

For the short nozzle, at the nozzle entrance

$$u_n' = M a_n'$$

$$(\rho u)_n' = M (a' + \rho')_n$$

$$M_n = M_b = M$$

and $a' = \frac{\gamma-1}{2\gamma} p'$ for isentropic waves at nozzle.
Thus,

$$(\rho u)'_n = \frac{3\gamma-1}{2\gamma} M p'_n$$

represents the power removed from the wave at the nozzle. The difference between the power input by the combustion zone and removed by the nozzle serves as a measure of the rate of energy input to the wave and for a given p' is simply,

$$\Delta(\rho u)' = \left[\frac{\gamma-1}{\gamma}\frac{E^*}{\bar{R}^* T_b^*}\left(1 - \frac{T_u}{T_b}\right) - \frac{3\gamma-1}{2\gamma}\right] M \cdot p' \qquad \text{[II-13]}$$

As Sirignano and Crocco pointed out this difference serves as a measure of the wave amplitude in the case of nonlinear oscillations. From this relationship which can be compared to that derived by Sirignano and Crocco for the amplitude parameter ϵ [1], the importance of the Arrhenius factor $E/\bar{R}^* T_b^*$ and the Mach number of the burned gases in determining the net power input to the waves is again apparent. The appearance of the factor $(1 - T_u/T_b)$ which did not appear in the expression for ϵ indicates that an increase in the ratio of the unburned to burned gas temperature should decrease the rate of energy addition to the waves for a given perturbation in pressure and thus be stabilizing. This prediction originally appeared as a result of the analytical work presented in Chapter V. This term in fact arises due to the heat of combustion term $q^* = \frac{\bar{c}_p^*}{\sqrt{\gamma_i \beta}}(T_b^* - T_u^*)$. The influence of higher q^* is manifest in an increase in this factor. Clearly the factor $E^*/\bar{R}^* T_b^*$ dominates.

An important consequence of II-13 is that the net power input to the waves is linearly dependent on the mean chamber Mach number originally shown by Sirignano and Crocco. However, the statement is correct for the premixed gas rocket only in the limited sense that the mean chamber Mach number serves as a dimensionless meas-

---

[1] Sirignano and Crocco obtained the amplitude parameter (for the simplified Arrhenius rate law) as

$$\epsilon = \bar{u}_b \left[(\gamma-1)\frac{E^*}{\bar{R}^* T_b^*} - \frac{3\gamma-1}{2}\right]$$

sure of the mean propellant burning rate. This point will be discussed further when Bowman's results are considered.

From the standpoint of combustion modeling for the gas rocket, the preceding discussion has bearing on the analysis performed by Culick (79) and discussed earlier. Culick preserved the exponential dependence of the mean rate of reaction on the mean temperature in the Arrhenius factor. He was led to conclude that the exponential factor dominated the linear term $E^*/\bar{R}^* T_b^*$ (see page 25). The point is simply that for the gas rocket having a short combustion zone length compared to the chamber length[1] the appropriate "combustion zone" averaging is a spacial or volumetric one over the axial reaction coordinate. Such averaging will always result in the simple step

$$\int_0^{\ell^*} \bar{r}^*(x^*)\, dx^* \sim \dot{m}_{TOT}^* \cdot \beta\, \tau_{f,i} \cdot q^* \qquad \text{[II-14]}$$

and, following the preceding developments, in a simplified expression for the "driving" terms of the form II-10,11,12,13 where the linear term in the Arrhenius factor prevails.

The Sirignano-Crocco theory served to guide much of the extensive experimental investigation of the gas rocket stability characteristics completed by Bowman (32). Basically the work represents a detailed description of the stability limits, the wave amplitude, and the waveform of the pressure oscillations as a function of the equivalence ratio (or combustion zone temperature), the combustion chamber and nozzle geometries, the injector configuration, the mean chamber pressure, and the mean flow Mach number. While certain qualitative agreements between theory and experiment were encouraging, Bowman observed significant quantitative and the qualitative discrepancies among the theory, the accumulated experimental data, and published kinetics data. Most of these were

---

[1] The "length" of the combustion zone for the high pressure (1 to 20 atm) premixed gas rocket is observed ((32), (76), and the present report) to be of the order of 1 to 3 cm. The ratio of ℓ^*/L_c^* is thus primarily dependent on L_c^* and always small for sustained longitudinal mode oscillations.

attributed to the simplifications in the theoretical model necessitated by a virtually complete lack of experimental information about the structure of the combustion zone. Thus the experimental work of Bowman and his systematic evaluation of the data in light of the predictions of the Sirignano-Crocco theory provide the immediate background for the present work. It should be noted that some of the qualitative reasoning offered by Bowman in connection with comparisons between theory and experiment is incomplete or inaccurate in light of the experience and knowledge gained in the course of the present work. Indeed, one of the objectives of this work is to "set the record straight" regarding the observed phenomena of nonsteady combustion in the premixed gas rocket. It would be premature to begin that task at this point. Detailed discussion towards that end is reserved for Chapters IV-VI.

Using essentially the same system as that studied by Pelmas, Bowman defined the longitudinal mode stability characteristics for the $H_2/O_2/N_2$ system. Of particular significance is the fact that all of the H_2 + Air data were obtained under the condition of choked primary injection of the premixed propellant into the combustion chamber. In contrast to the system of Tsuji and Takeno (and apparently that of the Purdue investigators), the propellant mass injection flux was positively decoupled from the transient downstream combustion chamber conditions.[1] Each datum point was secured under the conditions of constant mass injection flux (although important but unreported systematic variations in this total flux often occurred from point to point).

For the H_2 + Air system Bowman defined the system stability limits as a function of the propellant equivalence ratio, the chamber length, and the mean chamber pressure. Subsequently experiments were carried out to determine the effects (of the injector and nozzle configuration) on the location of the stability limits. As Pelmas had reported earlier (29) Bowman observed two distinct regimes in the equivalence ratio, Φ, chamber length, L_c,

---

[1] A complete description of the gas rocket system is given in Chapter III.

plane of longitudinal mode instability each offset from the stoichiometric mixture ratio such that the (lower) stability limits (closest to $\Phi = 1$) are characterized by mixtures having approximately the same adiabatic flame temperature. The majority of the measurements were confined to equivalence ratios greater than one in view of the very narrow regime of nonsteady combustion for $\Phi < 1$. The typical pattern of observed limits for $\Phi > 1$ are indicated in Figure II-9a. Essentially the same dependence of the stability limits on Φ and L_c was observed for a variety of multiholed showerhead and impinging injectors and for 3 different nozzle geometries. Bowman noted that as the number of injection ports increased (for the same total flow area) the stability limits shift to lower combustion temperatures. The singular behavior of the system with an unchoked low pressure drop porous plug injector was noted. Despite the fact that such an injector was expected to provide a nearly one-dimensional flame zone (as assumed in the Sirignano-Crocco theory) no regimes of combustion instability were observed over the entire operating range of equivalence ratio, chamber length, and chamber pressure.

For chamber lengths below 50 cm instability in the form of a single low amplitude shock wave followed by a steep decay of pressure and propagating at approximately the frequency corresponding to the longitudinal acoustic mode of the chamber filled with hot products was observed as shown in Figure II-8. As the equivalence ratio was traversed across the regime of nonsteady combustion the dimensionless shock strength was observed to increase rapidly near the lower stability boundary, to maximize, and eventually to decrease slowly for further increase in the equivalence ratio (see Figure II-10).[1] As indicated in Figure II-10 larger amplitude shock waves were supported at higher mean chamber pressures, longer chamber lengths, and higher mean chamber

---

[1] During the course of the experimental work discussed in this present work low amplitude propagating continuous waves have been observed near the stability limits. In no case have low amplitude standing waves been observed as reported in the work of Tsuji and Takeno.

Mach number.[1] For sufficiently long chambers Bowman observed the systematic appearance of higher "harmonic" modes. The term "harmonic" is adapted from the terminology of acoustics to indicate the phenomenon of the simultaneous appearance of 2 or 3 finite amplitude shock waves each propagating axially at approximately the frequency corresponding to the longitudinal acoustic mode of the combustion chamber. As indicated in Figure II-8 the apparent frequencies presented by such harmonic mode phenomena and sensed by transient pressure transducers situated at various axial locations in the combustion chamber correspond to the second or third harmonics of the fundamental acoustic mode. As indicated in Figure II-9a, Bowman observed the regimes of higher harmonics (a better term for the Princeton gas rocket phenomenon is "multiple shock propagation") to appear with increasing order as the chamber length or mean chamber pressure is increased or the equivalence ratio decreased toward the lower stability limit.

Bowman also performed a series of experiments designed to test the theoretically predicted importance of the Arrhenius parameter, $E^*/\bar{R}^* T_b^*$. In this regard it should be recalled that the Sirignano-Crocco theory indicated that the stability limit for a given propellant system should be characterized by a fixed critical value of the Arrhenius parameter $\left(E^*/\bar{R}^* T_b^*\right)_{CRIT}$. Results obtained by Sawyer (128) with an adiabatic flow reactor indicate that the one-step activation energy of the H_2/O_2 reaction is a constant independent of N_2 concentration over the range of equivlence ratios relevant to the gas rocket studies. By adding controlled amounts of N_2 to the H_2 + Air system and thereby depressing the profile of mean combustion temperature versus equivalence ratio, Bowman experimentally confirmed the theoretically predicted shift of the stability limit toward the stoichiometric ratio (to

---

[1] These results will be discussed in Chapter V and VI. For the moment note that the substantial importance of increases in the total mean mass burning rate which accompanied increases in p_c, L_c, M was not recognized by Bowman in the original discussion of these data.

maintain $T^*_{limit} = T^*_{CRIT}$) with increasing diluent concentration. These results are shown in Figure II-9b. The experimentally measured temperatures at the stability limits were observed to be constant within the allowable experimental error. A similar experiment was carried out using the $CH_4/O_2/N_2$ system with similar results. For the CH_4 + Air system a single regime of nonsteady combustion located around the stoichiometric mixture ratio was observed at lower chamber lengths in agreement with the results of Zucrow and Osborn.

With regard to the numerical results derived from the Sirignano-Crocco analysis it is noted from estimates of the magnitude of $E^*/\bar{R}^*T^*_{CRIT}$ that one would predict for H_2 or CH_4 + Air systems unstable combustion at all equivalence ratios. Recall that the theory expressed $E^*/\bar{R}^*T^*_{CRIT} = \frac{3\gamma-1}{2(\gamma-1)}$. For $\gamma = 1.25$ and activation energies commensurate with those reported for H_2/O_2 (or hydrocarbon $/O_2$) systems, i.e., 30 to 60 kcal/mole, estimates of T^*_{CRIT} fall in the range of 2700°K to 5500°K. That is, critical temperatures are predicted to be in excess of the maximum theoretical adiabatic combustion temperatures (Θ(2400°K)) for these systems. In view of this quantitative discrepancy Bowman advanced several qualitative arguments based on physical reasoning and a comparison of theory, experiment, and kinetics data.[1] The activation energies derived from the Sirignano-Crocco limit criterion and measured combustion zone temperatures at the stability limits seemed to be about one half the selected published values. It was reasoned that perhaps a simple turbulent flame combustion zone rate law wherein the Arrhenius factor appears as $e^{-E^*/2\bar{R}^*T^*}$ would be a more appropriate expression to use in the analysis. Indeed, this factor of two argument provided part of the motivation for Crocco's initial approach to the model developed in the present work.

---

[1] The arguments presented by Bowman must be viewed with some caution. They are in part based on results obtained from an experiment with the $CO/O_2/N_2/H_2$ system. These results were not repeatable. Furthermore the adiabatic flame temperatures for the CO/Air reaction used to estimate T^*_{CRIT} in the numerical calculations based on those results are low by some 35% due to a programming error.

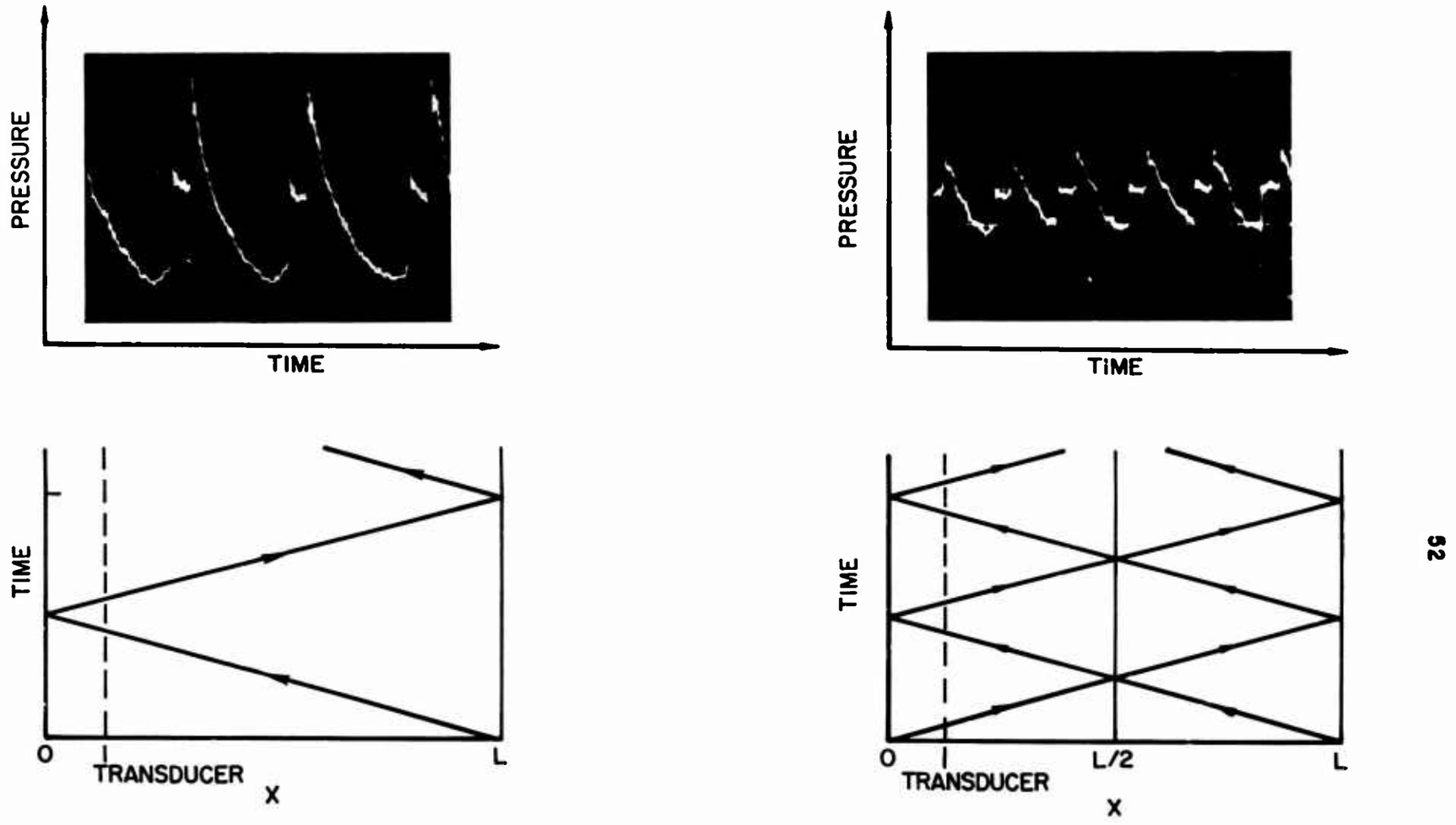

a. FUNDAMENTAL MODE (1 SHOCK WAVE)

b. SECOND HARMONIC MODE (2 SHOCK WAVES)

REF. : BOWMAN, C.T., TECHNICAL REPORT 784, Pprinceton, 1967

FIGURE II-8

PRESSURE-TIME HISTORY AND x-t DIAGRAM FOR SHOCK-TYPE INSTABILITIES

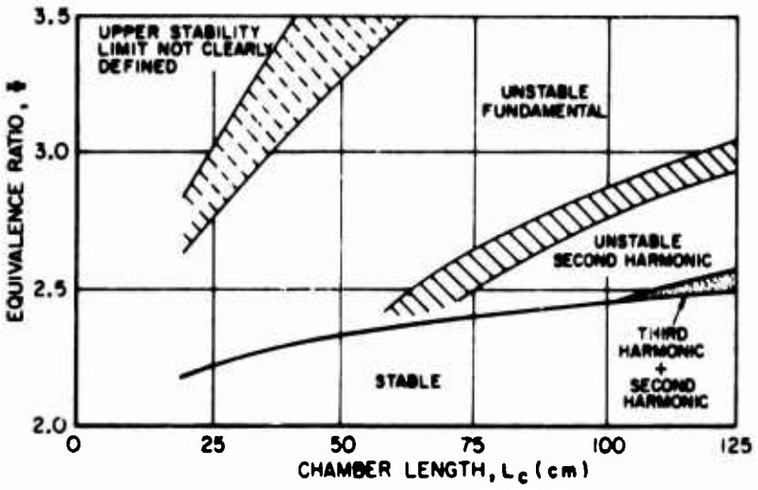

REGIONS OF HARMONIC MODE INSTABILITY IN THE Φ-L_c PLANE FOR H_2-AIR:

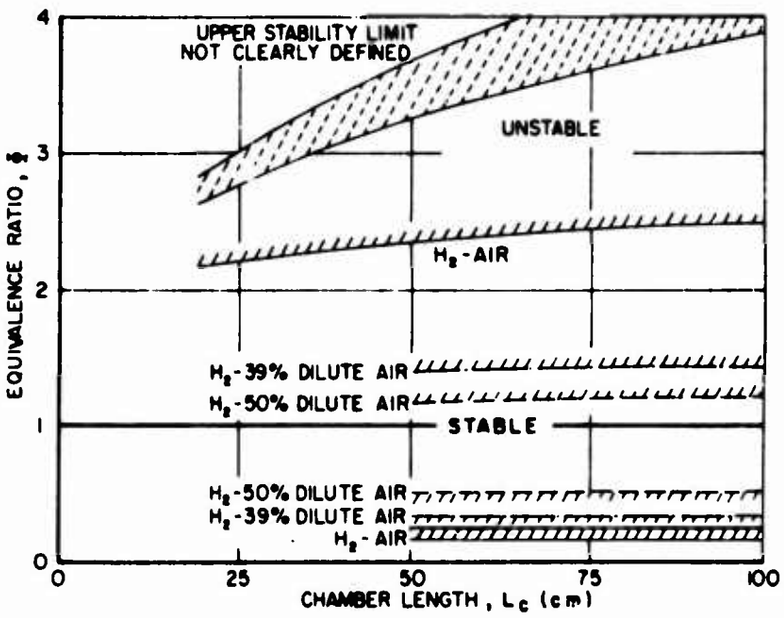

REGIONS OF UNSTABLE COMBUSTION IN THE Φ-L PLANE FOR H_2-AIR AND H_2-DILUTE AIR

REF.: BOWMAN, C.T., TECHNICAL REPORT 784, PRINCETON, 1967

REGIMES OF UNSTABLE COMBUSTION FOR $H_2/O_2/N_2$ SYSTEM
$\bar{P}_c$ = 7.8 atm, CHOKED 31-HOLE SHOWERHEAD INJECTION

FIGURE II-9

FIGURE II-10

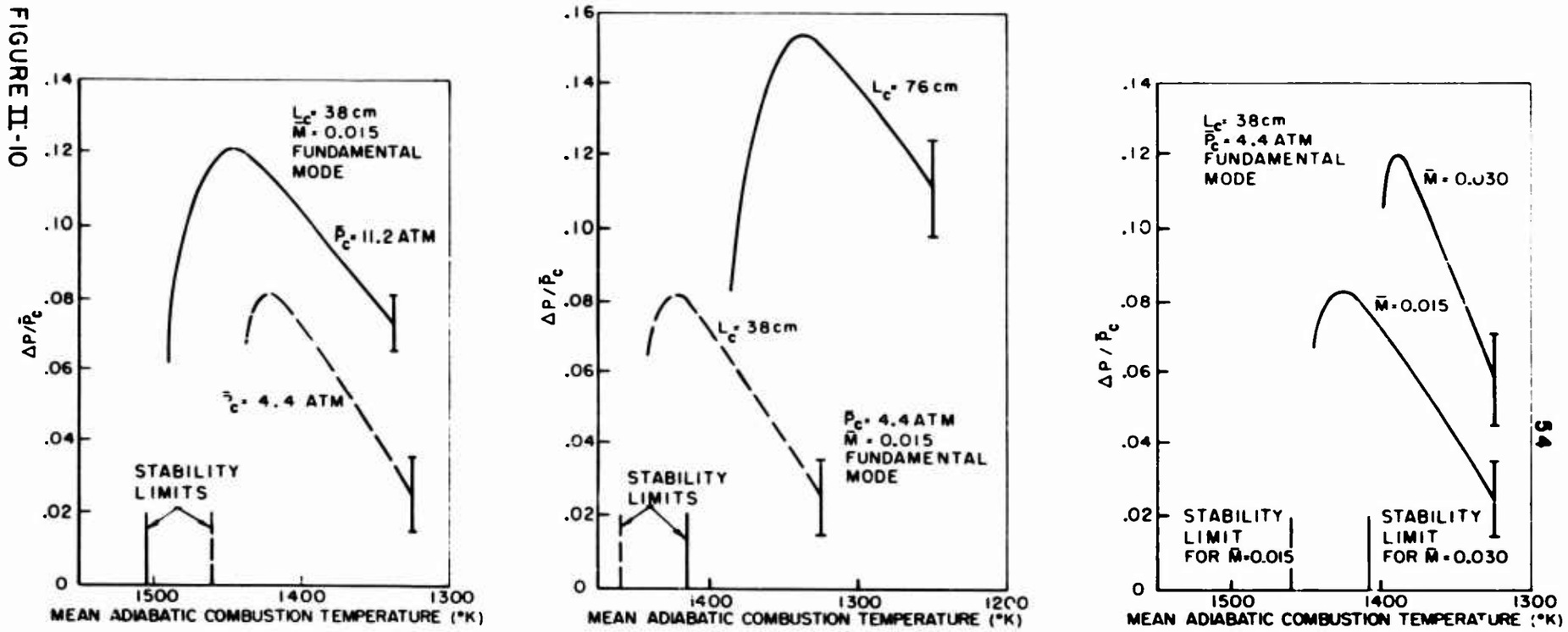

REF.: BOWMAN, C.T., TECHNICAL REPORT 784, PRINCETON, 1967

VARIATION OF $\Delta P/\bar{P}_c$ WITH COMBUSTION TEMPERATURE FOR H_2/AIR AS FUNCTION OF $\bar{P}_c$, L_c, AND $\bar{M}$

Chapter III: The Princeton Gas Rocket

As noted in the first two chapters the past years have encompassed an extensive program at Princeton of experimental research devoted to increasing our understanding of the contribution of gas phase rate processes to the complex phenomenon of nonsteady combustion in a rocket motor. This effort has resulted in the development and refinement of the gaseous propellant rocket motor or "gas rocket" as the principal research tool. As such it is important that a general description of the basic components and subsystems of the gas rocket be included at this point. Discussions of the apparatus pertinent to earlier researches are to be found in (29, 30, 31, 32). Because of the nature of this present research program it was necessary to make substantial modifications and additions within each subsystem. This chapter will not attempt to describe the specialized configurations of hardware and diagnostic equipment utilized in the various researches discussed in this report. Such comments will be reserved for Chapter IV at which time detailed discussion of the experiments and techniques will be entertained.

Essentially the gas rocket system consists of three integrated subsystems: the rocket motor, the propellant flow control and metering system, and the system of diagnostic equipment providing the capability of monitoring and recording steady state and transient phenomena. Conceptually the system was originally designed to simulate on a reduced scale a conventional rocket motor employing gaseous propellants. To this end the parameters found to be of significance in influencing longitudinal mode nonsteady combustion characteristics of large scale practical motors can be easily controlled and monitored in the gas rocket system. These variables include: geometric parameters - chamber length, injector and nozzle configuration; propellant parameters - chemical composition of fuel and oxidizer, mixture ratio; system parameters - total propellant mass flow rate, mean chamber pressure, mean chamber Mach number.

A. The Rocket Motor

The original rocket motor subsystem has five integral components including the impinging injector and associated manifolding, the mixing chamber, the primary injector, the combustion chamber, and the nozzle. A schematic of the basic system is shown in Figure III-1 and a photograph of the motor appears in Figure III-2.

A.1 The Impinging Injector

Initial mixing of the principal components of fuel and oxidizer is accomplished by passage through the impinging injector secured to the upstream end of the mixing chamber. The injector manifolding provides four pairs of like-on-unlike injection ports. Essentially this component has remained unchanged throughout the course of gas rocket experimentation.

A.2 The Mixing Chamber

After initial mixing the principal components of fuel and oxidizer pass through the mixing chamber where final mixing is achieved by passage through a packed bed of stainless steel balls. The admission of a third gas to the system is provided for by a radial inlet just downstream of the impinging injector face. Bowman (32) determined the degree of mixture homogeneity following propellant flow through the mixing chamber. Chromatographic analysis of gas samples taken downstream of the mixing chamber for several different mixtures of fuel and oxidizer indicated satisfactory mixing of the propellants. It should be noted that the assumption of completely mixed propellants prior to combustion is implicit in the experimental and analytical work discussed in this report.

Ideally the mixing chamber is isolated from processes occurring downstream in the combustion chamber by suitable choice of the primary injector. The presence of high pressure, low velocity, premixed propellant gases in the mixing chamber during operation admits the possibility of combustion occurring in the mixing chamber via "flashback" of the combustion through or around the injection plate or due to spontaneous ignition arising from heat transfer through the hot primary injector.

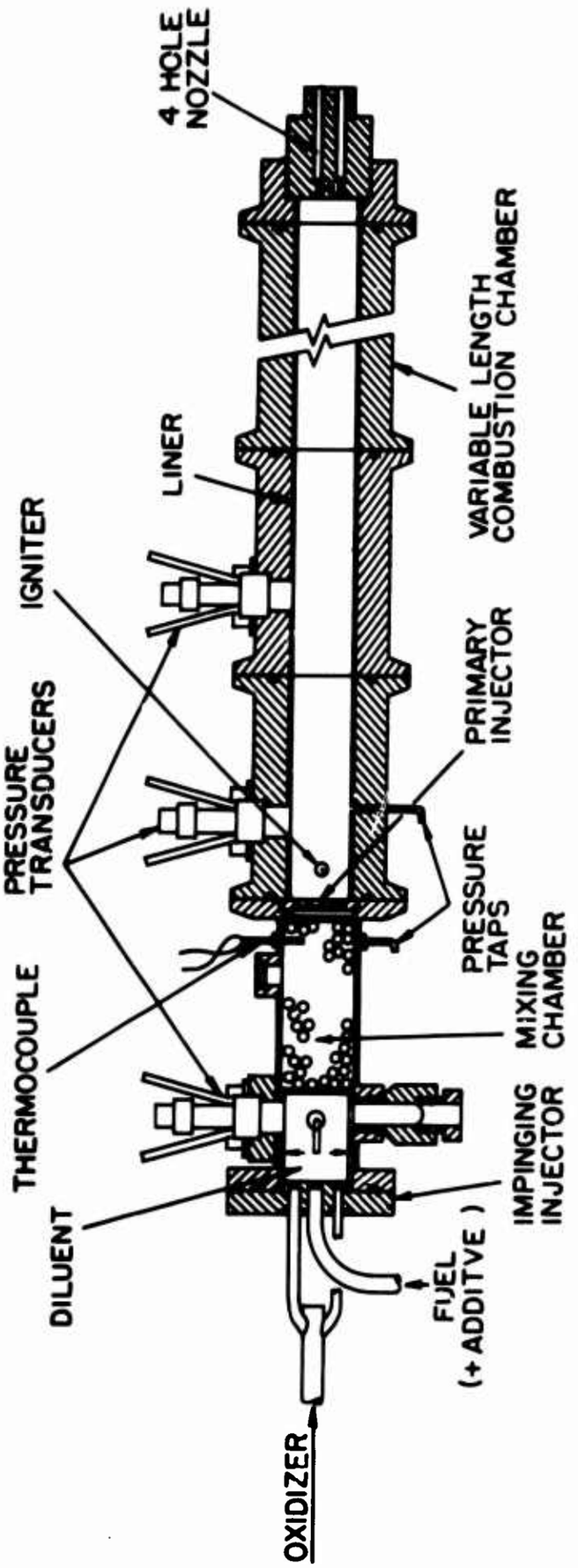

SCHEMATIC OF BASIC GAS ROCKET SYSTEM

FIGURE III-1

GAS ROCKET MOUNTED ON TEST STAND

FIGURE III-2

Either circumstance is undesirable and can produce substantial damage to the mixing chamber. To limit the extent of damage due to combustion in the mixing chamber a rapid response "safety circuit" (see Webb and Knauer (83)) was incorporated in the system. Radiation emitted from the combusting propellants is sensed through plexiglass windows by two photocells mounted at 90 degrees to the mixing chamber axis. The electrical output signal from the photocells activates a solenoid which bootstraps to a pressure actuated valve in the oxidizer flow line and produces shutdown of the oxidizer flow. Subsequent shutdown of the remaining propellant flow(s) is accomplished manually. A schematic of the safety circuit is shown in Figure III-3. A secondary backup safety device, a high pressure burst disk, is also fitted to the mixing chamber.

Provision is made for monitoring the steady-state static pressure in the mixing chamber through a pressure tap installed at approximately 3 cm from the downstream end of the section. In the course of the present work a second tap was added at the same axial position at 90 degrees from the pressure tap to allow for monitoring of the static temperature of gases in the mixing chamber. In addition, the mixing chamber section was modified to allow installation of a pressure transducer to record the transient static pressure in the mixing chamber.

A.3 The Primary Injector

Admission of completely mixed gases from the mixing chamber into the combustion chamber is accomplished by fitting a primary injector into the downstream end of the mixing chamber. An O-ring seal between the mixing chamber and the injector provides a positive seal against leakage of propellants around the injector. Injectors used in conjunction with the windowed chamber sections will be discussed in Chapter IV. For all experiments other than those involving optical investigations of the combustion zone the primary injector configuration is basically that of a circular metal disk 0.635 to 0.685 cm in thickness. In the course of the experimental program a variety of injection

FIGURE III-3

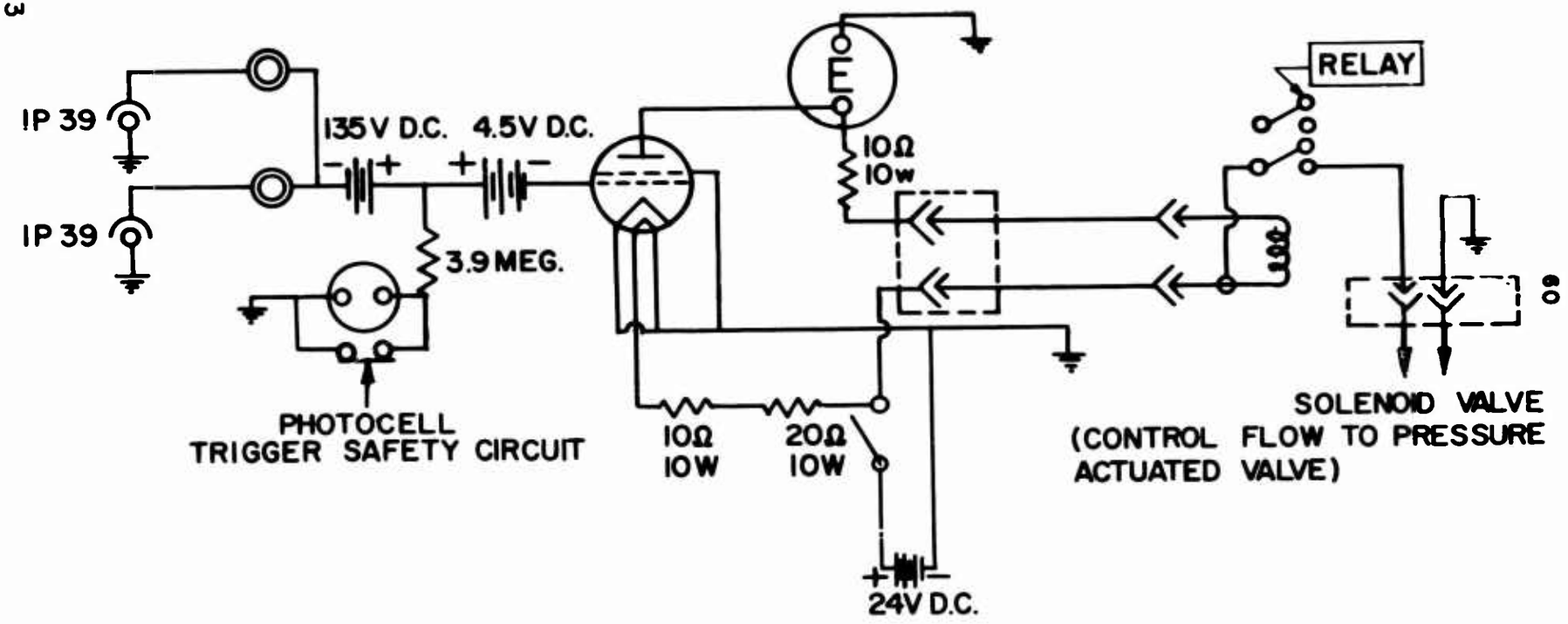

FLASHBACK SHUTDOWN SYSTEM

(WIRING SCHEMATIC)

JPR 1089a

configurations has been employed. Three basic subgroups can be distinguished: the porous plug; the multiholed showerhead, and; the multiholed impinging injector. Only the porous plug and the multiholed showerhead injectors have been used in the present investigations. Typical representatives of these injectors are shown in Figure III-4.

The porous plug injectors are machined from sintered steel plates and have a mean pore size of five microns. Porous plug injectors introduce a low pressure drop between the mixing and combustion chambers at total mass flow rates characteristic of gas rocket operation. Hence, they do not provide for complete isolation of the upstream flow conditions from phenomena occurring in the combustion chamber. Despite this limitation it was originally felt that the plugs should provide for nearly one dimensional injection of propellant into the combustion chamber. Thus an experimental approximation to the analytically tractable one dimensional combustion zone should be effected. Unfortunately, this condition is not realized in practice. The porous plugs have substantial radial deviations in porosity resulting in localized regions of mass flow concentration which vary in size and location from one plug to the next. Indication of this characteristic is seen in the nonuniform darkening and erosion of the plug surface which results from oxidation by the hot combustion chamber gases. Confirmation of the nonuniformity of porosity was obtained when radial velocity profiles (cold nitrogen flow) were scanned using a hot wire probe. In spite of these properties self-consistent repeatable data have been obtained when porous plug injectors are used.

The multiholed showerhead injectors are machined from copper bar stock and typically have a symmetrical array of small injection ports machined perpendicular to the injector face. By countersinking the upstream side of the orifices it is expected that the discharge coefficient of each port will approach unity. Calculations based on one-dimensional isentropic flow through the showerhead injectors using experimentally measured static

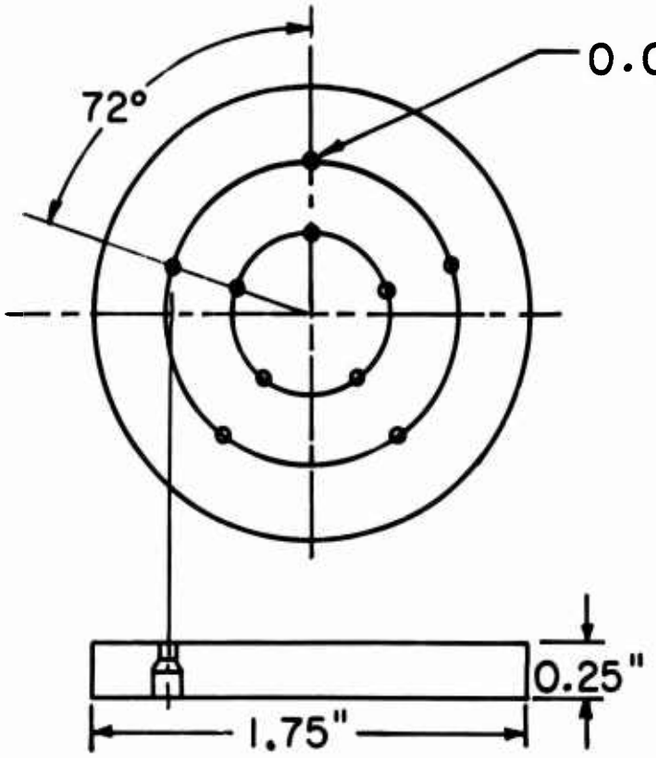

SCHEMATIC OF 10-HOLE SHOWERHEAD INJECTOR

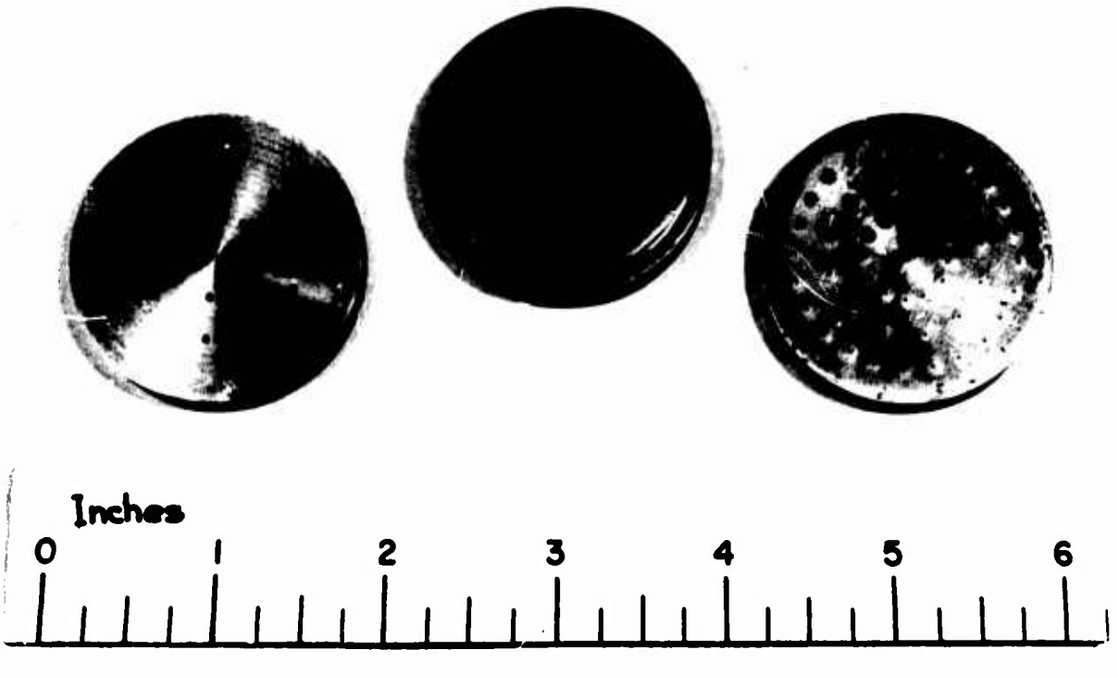

SHOWERHEAD INJECTORS

FIGURE III-4

temperatures and pressures in the mixing and combustion chambers (under cold flow conditions) indicate that the assumption of unity discharge coefficient is acceptable. The showerhead injectors can provide for isolation of propellant flow rate from transient combustion chamber phenomena by suitable choice of injector port size and the number of ports, that is the total flow area. By providing for direct choked injection of propellants into the combustion chamber the capability exists of decoupling the mass injection rate and transient combustion chamber phenomena associated with nonsteady combustion. Most of the experimental results presented in (32) were obtained under conditions of choked flow showerhead injection. Injectors having approximately the same total flow area and differing in the number (10, 31, 49), port diameter (0.094 to 0.035 cm), and distribution of injection ports were employed. The type of injector and relevant injection parameters are discussed in Chapter IV in connection with detailed discussions of the experiments.

A.4 The Combustion Chamber

The combustion chamber is a variable length (from 10 to 200 cm) composite of individual cylindrical copper sections each 12.5 cm in length and having an inside diameter of 3.8 cm and wall thickness of 1.9 cm. The generally high aspect ratio of the combustion chamber for all but the shortest chamber lengths serves to inhibit the appearance of radial and transverse modes of pressure oscillation. Each section is fitted with a stainless steel liner of 0.080 cm thickness to reduce heat losses. For short periods of operation (steady-state operation of less than 30 seconds) the structural integrity of the combustion chamber is insured by virtue of the high thermal capacity of the copper walls. Spray cooling of the external surfaces of the chamber with water facilitates extended operating periods. Several chamber sections have been modified to accomodate transient pressure transducers, ignition spark plugs, steady-state pressure taps, and statically

mounted thermocouples. One chamber section was modified to allow placement of the nozzle at 90 degrees to the axis of the combustion chamber when using the axially traversing thermocouple probe. The chamber sections especially designed for optical studies of the combustion zone are discussed in Chapter IV.

A.5 The Exhaust Nozzle

The exhaust nozzle is fitted at the downstream end of the variable length combustion chamber. Three different nozzles have been used in earlier research efforts including two water-cooled, converging-diverging nozzles having identical convergence angles but differing in throat area, and an uncooled four hole tungsten nozzle shown in Figure III-5. All experiments in this report were performed with the tungsten "plug" nozzle. It should be noted that the tungsten nozzle approximates in total flow area the smaller throat area converging-diverging nozzle and is designed to provide choked exhaust flow to the atmosphere. The nozzle presents an effective contraction ratio (total chamber cross sectional area/total area of the nozzle ports) of 46 to the combustion chamber gases and provides a physical approximation to the analytical assumption of a short or zero length nozzle boundary condition. A discussion of the influence of the nozzle geometry and the related mean chamber Mach number (controlled in a one-dimensional sense by the chokes nozzle contraction ratio) on the motor stability characteristics is presented by Bowman (32).

B. Propellant Flow Control System

The propellant flow control system provides the capability of simultaneously regulating, monitoring, and recording the mass flow rate to the rocket motor of four different gases. A schematic of the flow control system is shown in Figure III-6, and a photograph of the system control panel is shown in Figure III-7. Essentially the four systems are identical with final mixture homogeneity being attained upon admission of the gases to the mixing chamber.

PHOTOGRAPH OF PLUG NOZZLE

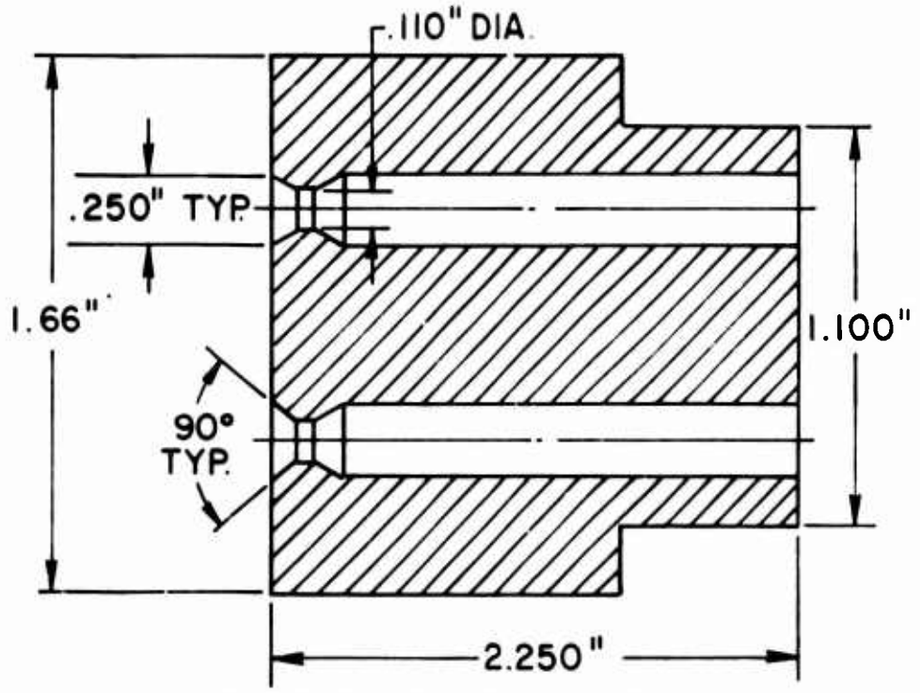

SCHEMATIC OF PLUG NOZZLE

FIGURE III-5

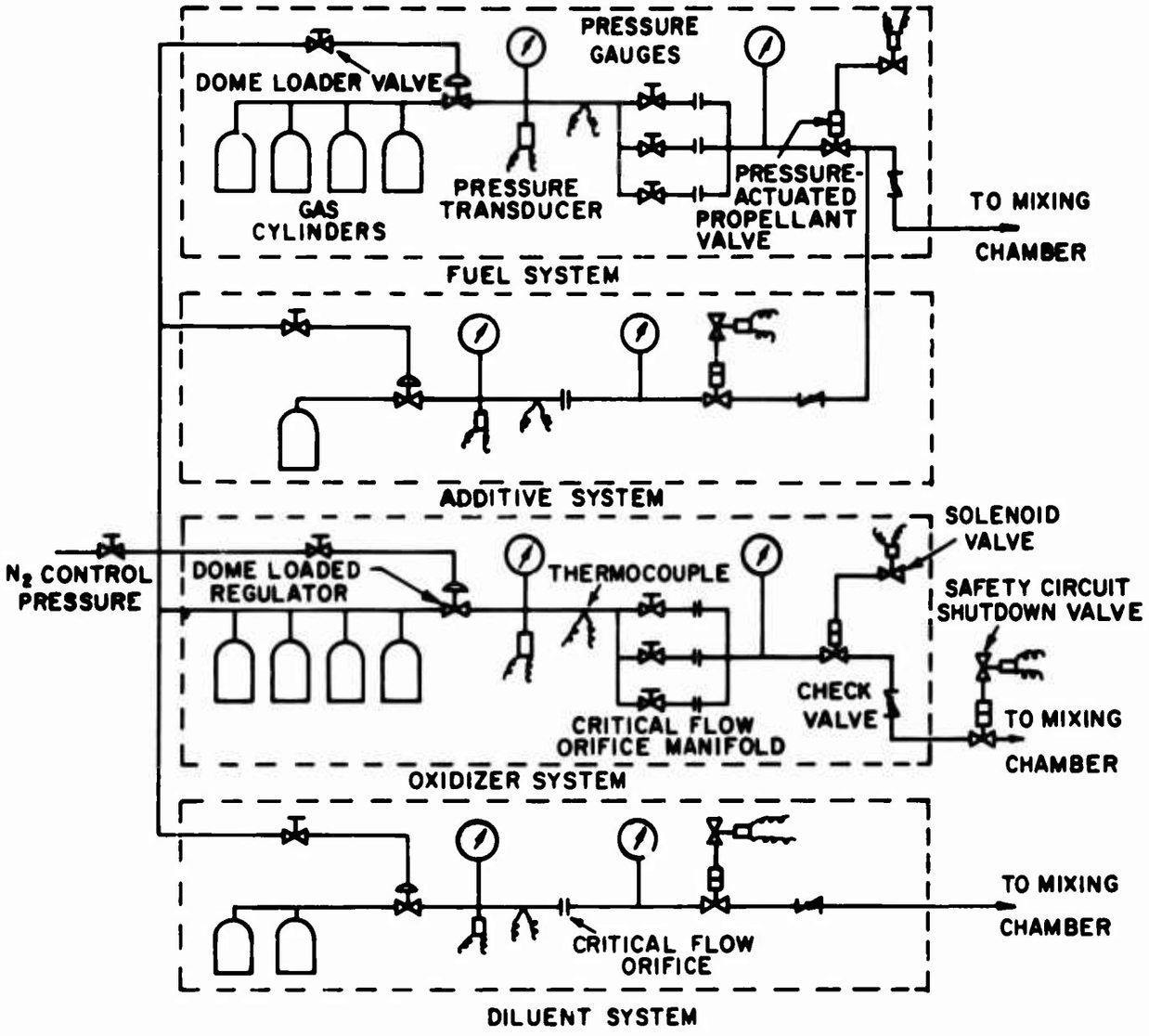

FLOW SCHEMATIC OF PROPELLANT FEED SYSTEM

FIGURE III-6

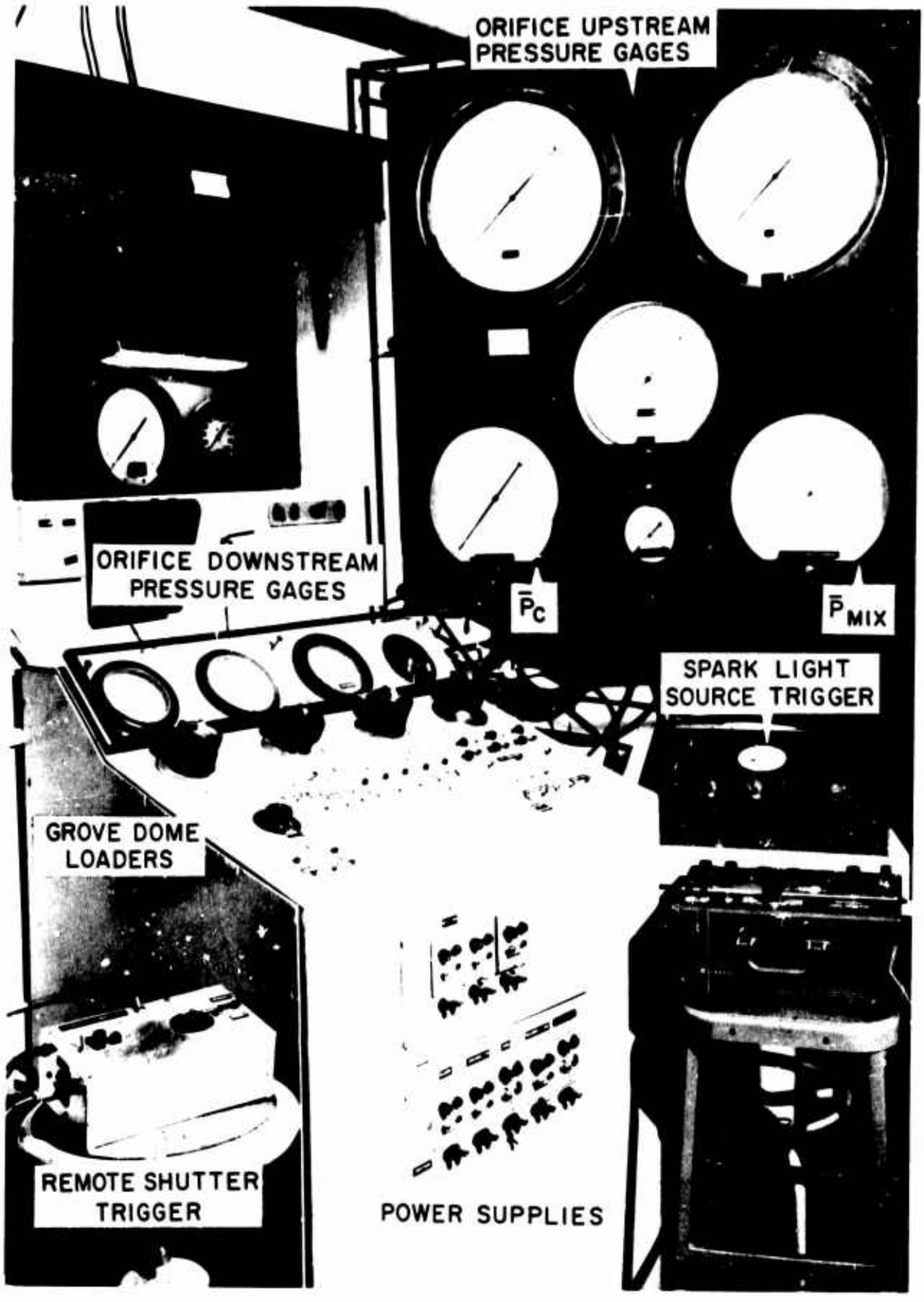

FLOW CONTROL PANEL

FIGURE III-7

With the exception of nitrogen and air obtained from in-house high pressure storage banks all gases were stored at ambient temperature in bottled sources. The system does not provide the capability of utilizing vaporized propellants which condense at ambient temperature although in principle this is feasible. An auxiliary heat exchanger was added to the oxidizer system to allow the temperature of the unburned propellants to be controlled prior to injection into the combustion chamber. This addition is discussed more completely in Chapter IV.

Gas mass flow rates are controlled manually through the action of control-pressure (nitrogen) actuated Grove dome regulators. In each gas system the regulator allows the gas pressure to be controlled upstream of a calibrated critical flow orifice. For specific details of the calibration procedure for these orifices see(32). A range of calibrated orifices is available including a series of micro-orifices machined in the course of the present work to provide a fine control capability on gases (hydrogen and methane) used as additives in the series of experiments in which carbon monoxide served as the fuel. A nitrogen purge system allows all gas lines to be flushed with nitrogen following operation of the system.

During operation of the system the stagnation pressures of the propellants upstream of the critical flow orifices are monitored visually on the bank of high pressure Bourdon tube gages at the control panel. The outputs of temperature compensated Statham (pg-731) strain gage pressure transducers and unshielded copper-constantan thermocouples upstream of each orifice are recorded on Leeds and Northrup and Bristol recording potentionmeters. From these recorded outputs the mass flow rate of each gas is accurately registered for subsequent analysis. The static gas pressure downstream of each orifice is also monitored at the control panel to insure choked operation of the critical flow orifices.

As noted in section A.2 the oxidizer line is equipped with a pressure actuated valve to terminate the flow of oxidizer to the mixing chamber in the event of combustion occurring in the mixing chamber.

C. Basic Instrumentation and Diagnostic Equipment

The basic instrumentation and diagnostic equipment provides the capability of monitoring and recording steady state and transient static pressure in the combustion chamber and steady-state static pressure in the mixing chamber. The mixing chamber was modified to allow the temperature and the transient static pressure of the unburned gases in the mixing chamber to be recorded. One combustion chamber section was previously modified to allow placement of thermocouples at various axial and radial locations in the combustion chamber.

Steady-state static pressure of gases in the combustion chamber is sensed through a pressure tap in the chamber wall located approximately 8 cm from the injector face by a high pressure Bourdon tube gage mounted at the control panel. The output signal from a Flader PSHD pressure transducer senses the combustion pressure and is recorded on a Leeds and Northrup recording potentiometer. The steady-state static pressure of gases in the mixing chamber is also displayed on a control panel gage. Frequency and amplitude characteristics of the transient static combustion chamber pressure can be sensed at several axial locations in the combustion chamber by high frequency Dynisco PT49CF pressure transducers. These transducers are temperature compensated, water-cooled, resistance-bonded strain gage devices each having a diaphragm diameter of 1.75 cm and are mounted flush with the inner wall of the combustion chamber. A Dynisco transducer also serves to sense the transient static pressure of gases in the mixing chamber. The outputs from the Dynisco transducers are amplified by Jones-Porter (model 12AC) decade amplifiers and recorded on a 7 track FM carrier magnetic tape recorder-Ampex model S3561. For comparison purposes including a determination of the inherent noise level of the tape deck system, several experiments were performed in which the Dynisco signals were recorded on the Honeywell Model 7600 7 track magnetic tape recorder.

The temperature of the unburned premixed gases is monitored by an unshielded copper constantan thermocouple positioned

approximately 2 cm upstream of the primary injector. Provision is made for recording the gas temperature at various axial and radial positions in the combustion chamber. This was originally accomplished by mounting unshielded Pt-Pt10%Rh and Pt-Pt13%Rh thermocouples through ports located in the chamber wall. Subsequently an axially traversing thermocouple probe system employing Pt6%Rh - Pt30%Rh thermocouples was designed to facilitate the measurement of continuous temperature profiles in the combustion chamber. Both uncooled and water-cooled probes were employed. All thermocouple outputs were referenced to 273.2 ^{o}K and recorded on Leeds and Northrup recording potentiometers. A complete discussion of the thermocouple systems and measurements is to be found in Chapter IV.

Optical observations of the combustion zone were facilitated by the design of two windowed chamber sections. A discussion of the schlieren and direct photographic systems and associated combustion chamber designs is reserved for Chapter IV.

Comments on the operation of the system, experimental techniques, and data reduction appear together with the discussion of each particular experimental investigation in Chapter IV.

D. Instrumentation Calibration

As noted, the critical flow orifices utilized in these experiments were calibrated using a standard water displacement technique described by Bowman (32). A recheck of all calibrations was performed at the time of the initial calibration of the new microorifices. Agreement with previous calibration curves was found to be within 1% over the range of flow rates employed. Because of the minute size of the small orifices a periodic check of their calibration curves was instituted. Essentially no change was observed in their calibrations over the period of use.

All pressure gages and transducers were periodically calibrated using a static dead weight tester. The Dynisco pressure transducers were examined for response and rise time at several

bridge excitation voltages by standard shock tube tests. The transducers used in these experiments evidence rise times on the order of $1 - 2 \cdot 10^{-5}$ seconds for incident shock amplitudes of approximately 10 psia. The measured sensitivity and frequency response of the transducers (32,84), indicates constant sensitivity over the range of operating pressure with the slope directly proportional to the bridge excitation voltage and a flat output to within 10% from 20 Hz to 6 kHz with a natural resonant frequency at 25 to 30 kHz. The maximum peak to peak amplitudes and frequencies of transient pressure phenomena encountered in the experimental program are of the order of 10 psi and 1000 cps. Hence, the Dynisco transducers are satisfactory for determining amplitude, frequency, and wave shape of longitudinal instabilities produced in the gas rocket system. In the course of experimentation an improvement in Dynisco signal to system noise ratio was achieved by operating the transducers at 15 volts bridge excitation rather than at the rated 10 volts.

Calibrations of the Pt6%Rh-Pt30%Rh thermocouples used in the axial temperature profile measurements were supplied by the manufacturers. Standard published calibrations were used for all other thermocouple outputs.

E. Propellant Gases

The gaseous reactants and diluents used in the present experiments are summarized in Table I. The gases were stored at room temperature and were used without purification. Premixing of fuels was accomplished through the propellant flow control system.

F. Experimental Procedure

As noted in the preceding paragraphs, the basic gas rocket system was designed so as to facilitate the rapid accumulation of data on the longitudinal mode stability characteristics of several different propellant systems over a wide range of equivalence ratios, geometric configurations, and mean thermodynamic conditions. Because of the relative simplicity of the

Table I: Propellant Gases and Composition

Principal Components	Supplier	Grade	Typical Composition (Vol %)
Air	In House Compressor		N_2 78 O_2 20.8 Ar 0.93 CO_2 660 ppm
Oxygen	Air Products	Extra Dry	O_2 99.5 Ar 0.45 N_2 0.05 Dew Point $-76^{\circ}F$
Nitrogen	Air Reduction	Liquid	N_2 99.8 O_2 0.2 Dew Point $-76^{\circ}F$
Hydrogen	General Dynamics	Electro-lytic	H_2 99.8 O_2 0.2
Methane	Matheson	CP	CH_4 99.05 C_2H_6 0.12 CO_2 0.20 N_2 0.60 C_3H_8 0.03
		Commercial	CH_4 93.63 C_2H_6 3.58 C_3H_8 1.02 CO_2 0.70 N_2 0.47 HC 0.60
Carbon Monoxide	Matheson	CP	CO 99.5 O_2 950 ppm CO_2 700 ppm Ar 50 ppm CH_4 43 ppm HC 30 ppm $Fe(CO)_5$ None det. H_2O 1 to 150 ppm *

* The H_2O content of the CP grade CO was supplied according to our specifications.

system and the ease with which stability testing could be carried out, the results of these experiments are numerous and repeatable. The capability of exerting a fine control on the propellant equivalence ratio and the total mass flow allows a high degree of accuracy in determining the precise location of the onset of nonsteady burning-the stability limit-as well as the nonlinear instability characteristics of the system.

While the complexity of the system and of the diagnostic techniques employed increased considerably in the course of the present work, the data remain fundamentally repeatable and systematic. Irrespective of the diagnostics involved the basic operational procedure of the gas rocket system has remained unchanged. A typical experiment designed to obtain instability data would proceed as follows: Initially a determination of the desired mean values of the experimental variables is made. Having determined the appropriate geometric parameters a calculation is made of the mass flow rate of each propellant required to achieve the desired equivalence ratio and mean chamber pressure (see Section III.G). The mass flow determinations fix the stagnation pressures which must be maintained in the propellant systems upstream of the critical flow orifices during the data acquisition portion of the experiment. Immediately prior to each experiment the gas rocket system is sealed and checked for leaks by pressurizing the motor with N_2 diluent. With the desired final upstream stagnation pressures in each propellant line noted at the control panel gages, the experiment is initiated by presetting a flow of oxidizer and diluent, energizing the spark igniter, and gradually increasing the fuel flow rate until ignition occurs. By maintaining a moderate flow rate of oxidizer and diluent during the ignition sequence, the tendency of the combustion to flashback through the primary injector is suppressed. The ignition at reduced total mass flow rate eliminates the possibility of a damaging explosive or "hard" ignition transient and facilitates ignition in cases where the desired final equivalence ratio is

beyond the system ignition limits (yet within the system flammability limits). Following ignition the spark is extinguished and the propellant flow rates smoothly increased to the desired final magnitudes. Generally 5 to 10 seconds are allowed for the suppression of starting transients and for the system to achieve steady mean conditions (mass flow rate and chamber pressure). Data are recorded during the ensuing 10 to 20 second interval. During this phase the Dynisco outputs of transient combustion pressure at one or more axial locations in the combustion chamber are recorded on magnetic tape. The steady state combustion pressure and the orifice upstream stagnation pressures and temperatures are recorded on the strip charts to allow accurate determination of the propellant equivalence ratio. In addition the steady state pressures in the mixing chamber and at locations downstream of each critical flow orifice are recorded manually at the control panel in order to verify that the condition of choking of the orifices and of the primary injector (showerhead injection) is achieved. The experiment is terminated by sequentially cutting the flows of fuel, oxidizer, and diluent.

It should be emphasized that nonsteady combustion in the gas rocket arises as an intrinsic instability of the coupled combustion zone energy release and the gas dynamic flow field in the combustion chamber. Under certain well-defined "preferred" combinations of the various system parameters constant amplitude, nonlinear, shock-type waves are sustained at fixed frequencies. This behavior is to be contrasted to the nonlinear instabilities observed in liquid propellant rocket motors which may be triggered by bombing or pulsing a nominally steady combustion process. To emphasize this point, Figure III-8 shows typical Flader transducer outputs corresponding to the mean static pressure records in two experiments conducted at fixed system geometry and total mass flux and bracketing (in equivalence ratio) the H_2 + Air system stability limit. In Figure III-9 typical Dynisco transducer outputs of transient static combustion pressure obtained simultaneously at three different

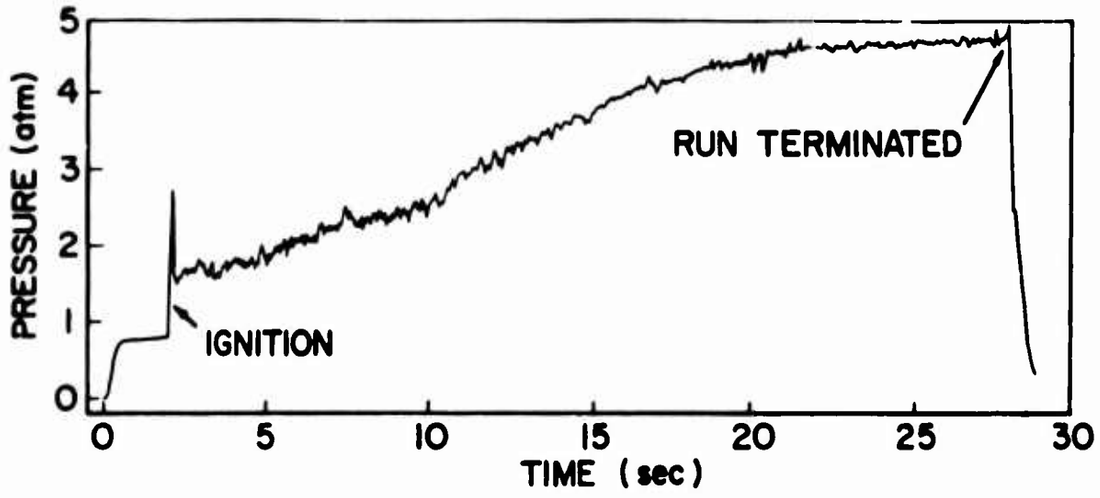

a) STABLE COMBUSTION : Φ = 2.25, $\bar{P}c$ = 4.6 atm

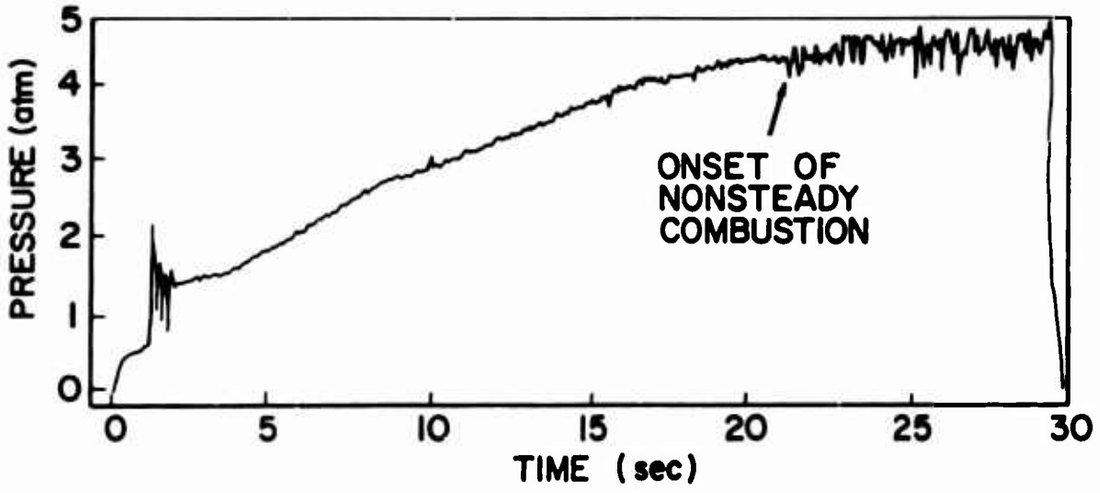

b) UNSTABLE COMBUSTION : Φ = 2.45, $\bar{P}c$ = 4.5 atm

TYPICAL HISTORY OF MEAN COMBUSTION PRESSURE VS TIME FOR STEADY AND NONSTEADY COMBUSTION OF H_2 + AIR, 10 HOLE SHOWERHEAD INJECTOR L_c = 104 cm, 4 HOLE NOZZLE

FIGURE III-8

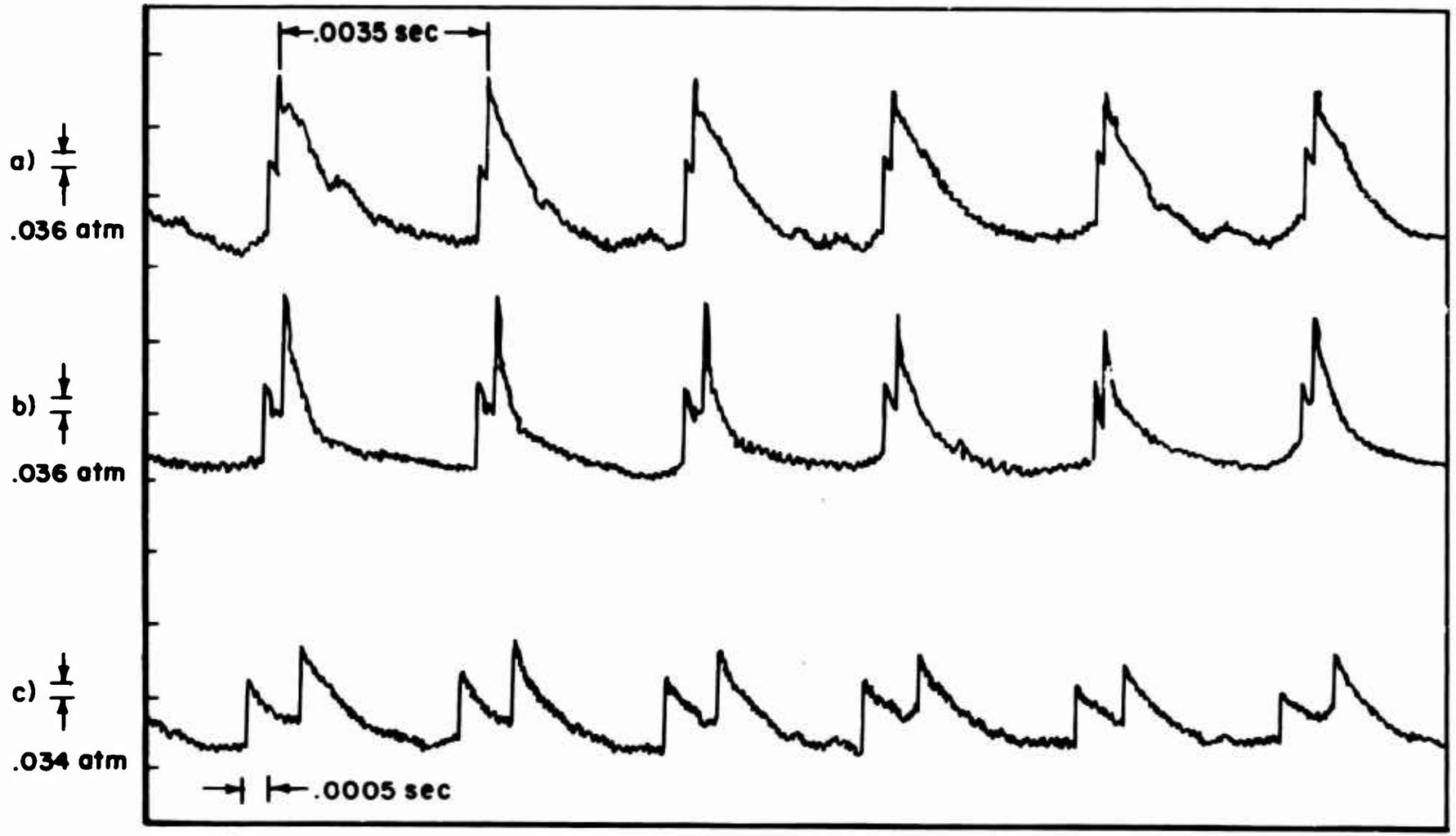

FIGURE III-9

TYPICAL HISTORY OF TRANSIENT PRESSURE VS TIME FOR NONSTEADY COMBUSTION OF H_2 + AIR , Φ = 2.80 , $\bar{P}_c$ = 4.2 atm , 31 HOLE SHOWERHEAD INJECTOR , 4 HOLE NOZZLE , L_c = 105 cm

TRANSDUCERS LOCATED AT (a) 4.5 cm , (b) 9.5 cm , (c) 30 cm FROM INJECTOR FACE

MEAN $\frac{\Delta P_{SHOCK}}{\bar{P}_c}$ = .06 , FREQUENCY = 298 cps , FUNDAMENTAL MODE

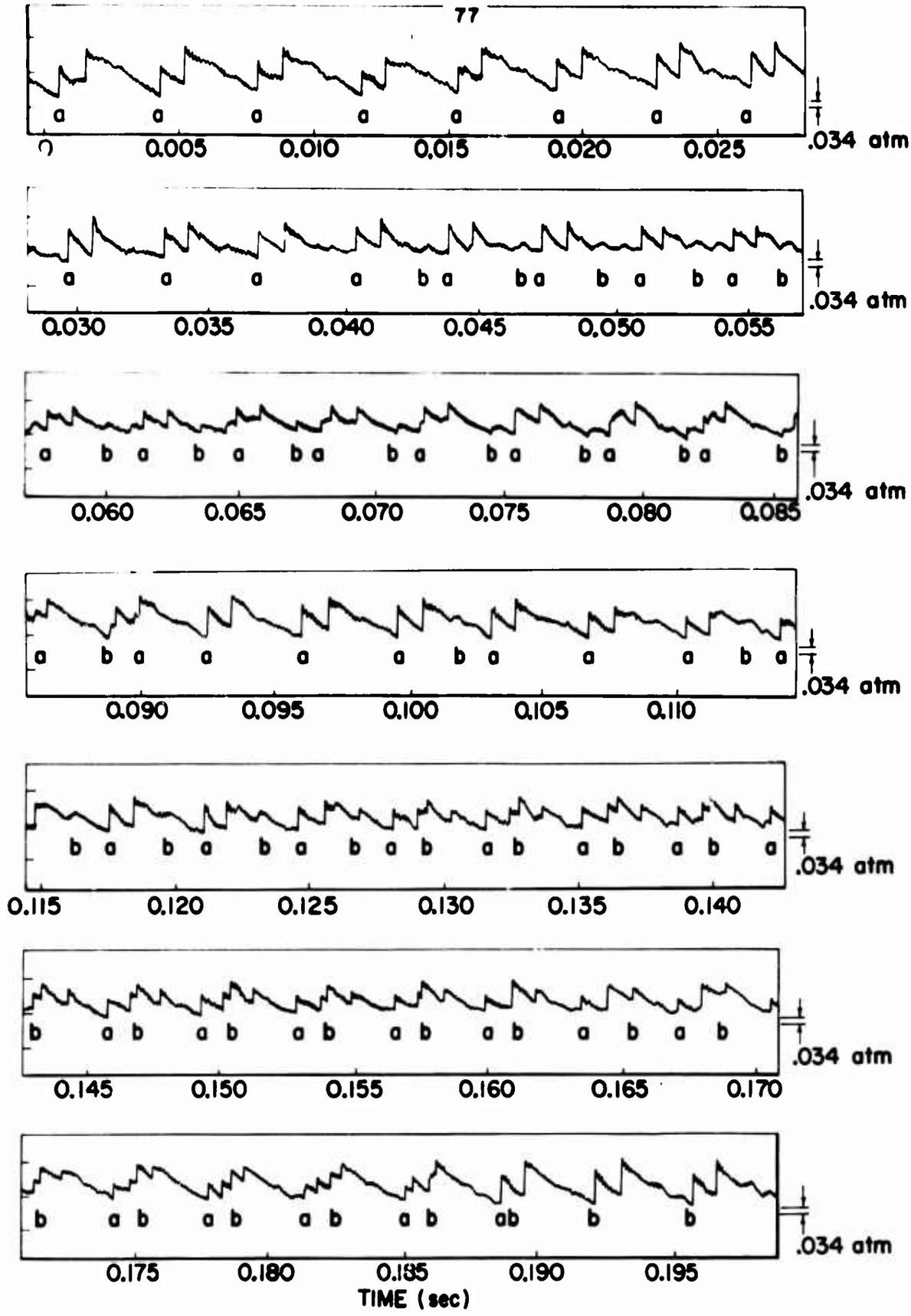

PRESSURE VS TIME HISTORY SHOWING TRANSITION FROM FUNDAMENTAL TO SECOND HARMONIC MODE

FIGURE III-10

axial locations in the combustion chamber during nonsteady combustion of H_2 + Air are reproduced. The data of Figure III-9 indicate the typically steady nonlinear waveform, amplitude, and frequency observed at propellant equivalence ratios within the regime of fundamental mode nonsteady combustion. Figure III-10 is a typical transient pressure record observed at conditions close to the stability limit of the fundamental mode. As indicated in the pressure trace, near the boundaries of nonsteady combustion the spontaneous transition between the fundamental and second harmonic modes is evidenced by the appearance of one or more shock waves oscillating (generally slightly out of phase) at approximately the fundamental acoustic frequency of the combustion chamber filled with burned products. As mentioned in Chapter II, regimes of thermodynamic and geometric parameters have been defined wherein two or three shock waves are sustained at constant frequency and amplitude (see Figures II-8, 10).

G. Range of Experimental Variables

Table II summarizes the basic system parameters and appropriate orders of magnitude. It should be noted with regard to the range of experimental parameters that the steady-state operating conditions of the gas rocket can be calculated by applying a one-dimensional analysis to a nonadiabatic duct with choked mass efflux and influx (in the case of showerhead injection). Thus while the system in principle provides the capability of controlling the propellant equivalence ratio and total mass flux, the chamber length and nozzle contraction ratio, and the combustion chamber pressure and mean flow Mach number, in practice it is not possible to independently vary these parameters. In short, changes in any one of these variables necessarily introduce adjustments in one or more of the remaining variables. While most of the system instability data have been presented (29, 30, 31, 32) as a function of two parameters one should bear in mind that in the course of the experimental work

Table II: Experimental Variables

A. Geometric Variables	Nominal Dimension
1. Combustion Chamber	
Length, L_c	5 to 180 cm
Internal diameter, d_c	3.4 cm
Internal cross section, A_c	9.1 cm^2
2. Nozzle (4 hole) Contraction Ratio, A_c/A_t	46
3. Primary Injector	
10 Hole Showerhead	
Port diameter, d_{port}	0.085 cm
Port flow area, A_{port}	0.006 cm^2
Total Flow area, A_{tot}	0.060 cm^2
31 Hole Showerhead	
Port diameter	0.052 cm
Port flow area	0.0021 cm^2
Total flow area	0.065 cm^2
49 Hole Showerhead	
Port diameter	0.037 cm
Port flow area	0.0011 cm^2
Total flow area	0.055 cm^2
Porous Plug	
Mean pore size	5 microns

B. Thermodynamic Variables	Nominal Operating Range For H_2 + Air System
1. Combustion Chamber Pressure, $\bar{P}_c$	2.4 to 11.4 atm
2. Total Mass Flow Rate, $\dot{m}_{tot}$	10 to 35 gms/sec
3. Ratio of Mixing Chamber Pressure To Combustion Chamber Pressure $\bar{P}_{mix}/\bar{P}_c$	
10 and 31 Hole Showerhead Inj.	2.5
49 Hole Showerhead Inj.	3.3
Porous Plug Injector	1.20 to 1.60

Table II: continued

4. Unburned Premixed Gas Properties	
Stagnation Temperature, $\overline{T}_{mix}$	280 to 300 ^{o}K
Injection Mach Number	
Showerhead injectors	1.0 (underexpanded)
Porous plug injectors	0.3 to 0.8
Injection Velocity	
Showerhead injectors	3.6×10^{4} cm/sec
Porous plug injectors	$3 \text{ to } 7 \times 10^{3}$ cm/sec
Injection Reynolds Number	
Showerhead injectors (based on port diameter)	$6 \text{ to } 8 \times 10^{6}$
Mixing Chamber Flow Velocity, $\overline{V}_{mix}$	100 cm/sec
Propellant Equivalence Ratio,	0.2 to 4.0
5. Burned Gas Properties	
Adiabatic Combustion Temperature T_b (Figures IV-2, 9 and D-4)	900 to 2440^{o}K
Adiabatic Combustion Temperature At Stability Limit, T_{lim}	1400^{o}K
Velocity of Burned Gases, $\overline{V}_b$	$0.5 \text{ to } 1.5 \times 10^{3}$ cm/sec
Mach Number of Burned Gases, M_b	0.01 to 0.02
Mean Axial Temperature Gradient	-5 ^{o}K/cm
C. Nonsteady Combustion Parameters	
1. Frequency of Pressure Oscillation, f	150 to 2000 Hz
2. Characteristic Time of Oscillation At Stability Limit, $2 \cdot L_c / n \cdot \overline{c}_b$	$2.5 \times 10^{-4} \text{ to } 10^{-3}$ sec
3. Dimensionless Shock Wave Amplitude, $\Delta P_{shock} / \overline{P}_c$	0 to 0.20

additional parameters have simultaneously undergone (often significant) changes. For example, a typical "two parameter" experiment was carried out to determine the stability limit of the H_2 + Air system as a function of the propellant equivalence ratio and the chamber length at a nominal combustion pressure of 7.8 atm. A 10 to 20 % increase in the total mass flux at fixed equivalence ratio was necessary due to heat losses in order to maintain fixed combustion pressure as the chamber length was increased from 20 to 100 cm. As indicated in Chapter II, Bowman carried out an experiment designed to determine the influence of the mean chamber Mach number at fixed combustion pressure on the H_2 + Air system stability characteristics. A Mach number change by a factor of two was achieved by halving the nozzle contraction ratio. However, an unreported 100% increase in the total propellant flow rate was required to maintain a nominal pressure of 7.8 atm. The mass flow rate adjustments typically accompanying experiments in which a "single" parameter in the H_2 + Air system was varied are summarized in Table III.

Table III: Mass Flow Rate Changes In Typical Gas Rocket Experiments With H_2 + Air

Parameters Held Constant	Parameter Varied and Range	Mass Flow Rate Adjustment
(I) M_b (Nozzle $\frac{A_c}{A_t}$ = 46)		
$\bar{P}_c$ = 7.8 atm		
(i) L_c = 19 cm	Φ = 2.0 to 3.0	(+5%) 21 gms/sec ⇝ 22 gms/sec
(ii) L_c = 76 cm	Φ = 2.0 to 3.0	(+12%) 25 gms/sec ⇝ 28 gms/sec
(II) M_b (A_c/A_t = 46)		
$\bar{P}_c$ = 7.8 atm		
(i) Φ = 2.50	L_c = 19 cm to 104 cm	(+8%) 21.3 gms/sec ⇝ 25 gms/sec
(ii) Φ = 2.92	L_c = 19 cm to 104 cm	(+20%) 22.5 gms/sec ⇝ 27 gms/sec
(III) M_b (A_c/A_t = 46)		
L_c = 104 cm		
Φ = 2.57	$\bar{P}c$ = 4.4 atm to 7.8 atm	(+67%) 15 gms/sec ⇝ 24.5 gms/sec
(IV) L_c = 104 cm		
$\bar{P}_c$ = 4.4 atm	A_c/A_t = 46 to 23	
Φ = 2.43	M_b = 0.015 to 0.030	(+100%) 14.1 gms/sec ⇝ 28 gms/sec

Chapter IV: Experimental Investigations

At the outset of the present work it was felt that despite a relative abundance of experimental data due to Pelmas, Schob and Bowman (29, 31, 32) regarding the stability characteristics of the gas rocket, there existed an incomplete understanding of the underlying factors contributing to the observed phenomena. The first section of this chapter presents the details and principal results of a series of experiments designed to provide a critical test of the thesis that the chemical reactivity of the premixed gaseous propellants is an important parameter in determining the stability characteristics of the gas rocket. The remainder of the chapter is devoted to discussion of diagnostic experiments designed to obtain both quantitative and qualitative information regarding the structure of the H_2/Air combustion zone under steady and nonsteady conditions. These experiments include (1) the measurement of radial and axial temperature profiles in the combustion zone as a function of the propellant equivalence ratio, the mean chamber pressure, and the injection configuration, (2) direct photographic observation of the combustion zone, and (3) the application of techniques of instantaneous and high speed shadow and schlieren photography to the observation of the combustion zone.

During the course of much of the experimental work a parallel theoretical effort was pursued with the ultimate goal being the development of a consistent theoretical and experimental description of the gas rocket instability phenomena. The experiments described in the following sections were designed to provide a firmer physical basis upon which to construct a realistic analytical model which accurately predicts the experimentally observed stability characteristics. The measure of success that has been achieved in this effort as discussed in Chapters V and VI is in large part due to the results of these experiments.

A. Experiments With The Carbon Monoxide, Oxygen, Nitrogen System

A.1 Discussion of Earlier Work of Bowman

The results of the original Sirignano-Crocco (henceforth, the S-C model) combustion model appropriately suggested certain directions to the experimental investigations. It will be recalled that the theory predicted the existence of a critical value at the stability limit of the Arrhenius exponent E/RT in the gas phase burning rate law. In addition the theory expressed the nonlinear shock amplitude as a monatonic function of E/RT for values of E/RT in excess of the critical value. Two points should be emphasized. First, the special role played by the Arrhenius parameter and the specific heat ratio of the combustion products in the theoretical results was due to the expression of the dimensionless gas phase burning rate in the simple form $r = e^{-E/RT}$. Hence, all of the "kinetics" were concentrated in the exponential. Secondly, the use of a more realistic expression for r in the S-C theory (e.g., allowing for a concentration dependence in the preexponential factor) led to the prediction of nonsteady burning at all mixture ratios (27). That the simple expression for the burning rate is unrealistic is clear, however, the lack of any experimental data regarding the gas rocket combustion process precluded expression of a more detailed model.

In light of the simplicity of the combustion model, as discussed in Chapters I and II, the qualitative agreement between the theory and Bowman's "dilute air" experimental work was encouraging. The existence of a critical temperature at the stability limit for the $H_2/O_2/N_2$ and the $CH_4/O_2/N_2$ systems was experimentally verified by examining the stability characteristics of the N_2 diluted reactions (Figure II-9). Since the theory allowed a prediction of the critical value of the Arrhenius parameter at the stability limit in terms of the specific heat ratio of the product gases, determination of the existence of a critical temperature at the limit allowed a calculation of the cor-

responding propellant activation energy (E_{lim})[1]. Quantitative comparisons between E_{lim} and published values of E showed poor agreement.

It is most important to recognize that the experimental evidence of the strong temperature sensitivity of the nonsteady burning characteristics in the gas rocket does not in itself lead to the conclusion that chemical kinetics is an important factor in the coupling of the combustion zone energy release and the pressure oscillations. The theoretical prediction of a critical value of the Arrhenius parameter and the experimental verification of the existence of a T_{crit} for the H_2/O_2 and CH_4/O_2 systems led Bowman to attempt a series of experiments wherein the reactant activation energy of the CO/O_2 reaction is modified (with negligible thermal effect) by the addition of trace amounts of a catalyst. According to the theory a change in the activation energy of limit mixtures should be manifest in a corresponding shift of the equivalence ratio (combustion temperature) at the stability limit to maintain fixed ratio $(E/RT)_{crit}$. Again it should be emphasized that this reasoning follows from (a) the lumping of kinetics effects in the parameter $e^{-E/RT}$ in the combustion model, and (b) from the inference that modification of reaction kinetics would necessarily modify the overall activation energy of the reaction.

To achieve this goal, Bowman performed a series of experi-

---

[1] The term "activation energy" as applied in this work and in the S-C model is to be considered as the so called "overall activation energy" of the gas phase fuel-oxygen reaction. The activation energy corresponds to the parameter typically arising from flame, flow reactor, and stirred reactor studies as an empirical data fit parameter from a plot of log r vs. 1/T. While of no fundamental significance in terms of representing a single elementary reaction step for the reactions considered here, as pointed out in this and succeeding chapters, there is substantial agreement in the literature regarding the existence of characteristic overall activation energies for the H_2/O_2, CH_4/O_2, and CO/O_2 (wet) combustion reactions. One can make persuasive arguments to show that the observed overall activation energies derive from the progression of the fuel-oxygen reactions through sequences of interrelated intermediate reaction steps.

ments with the $CO/O_2/N_2$ system. The well-documented (86, 87, 90, 91, 92, 99) sensitivity of the CO/O_2 reaction rate to trace amounts of water vapor and hydrogen suggested that the reaction kinetics characterizing the combustion of CO/O_2 in the gas rocket could be modified by adding H_2 to the reaction. Accordingly, Bowman performed a few tests in which H_2 was admitted to the oxidizer-rich mixtures of CO and Air. The details of these tests are found in (32). While the basic idea behind the experiments was a good one, the experimental results are inconclusive in view of: (1) the experimental results were the outcome of a single series of experiments which were not repeatable either by Bowman or this author; no transient pressure data were recorded; (2) the H_2 mass fraction admitted to the overall reaction was poorly controlled and estimated on the basis of the difference in mixing chamber pressure with and without H_2; (3) the water vapor content of the CO reactant was not controlled and was of the order of 150 to 200 ppm; (4) the rather circuitous arguments employed by Bowman to effect a numerical comparison between theory, experiment, and published kinetics data are not justified in view of the simplicity of the guiding model and the tenuous nature of the experimental results; (5) the theoretical adiabatic combustion temperatures at the reported stability limits computed by Bowman are low by $350^{\circ}K$ for the $CO/Air/H_2$ system and by $390^{\circ}K$ for the CO/Air system.

The inability of Bowman to substantiate the indications of the original tests with the $CO/O_2/N_2/H_2$ system provided a logical starting point for the present work. The initial experiments discussed here were also motivated by the S-C model and hence were approached from the standpoint of utilizing H_2 additive to effect a change in the gas phase burning rate of $CO/O_2/N_2$ mixtures by modifying the overall activation energy appearing in the Arrhenius parameter.

A.2 Reaction Mechanism of the CO/O_2 System With and Without Hydrogen

The CO/O_2 reaction has been studied extensively by kineticists over a wide range of pressures and temperatures utilizing diverse experimental techniques. Table IV presents a summary of

the best available overall rate data for the CO/O_2 reaction with H_2 or H_2O present in the initial mixtures. These data have been combined with the reported experimental conditions in each investigation to obtain a numerical evaluation of $d f_{co}/dt$ as a function of 1/T where f_{co} = the mole fraction of CO. This dependency is plotted in Figure IV-1. With respect to these data the following points are noted: (1) All of the experiments were performed with initially wet CO/O_2 mixtures; (2) There is unanimous agreement on the first order dependency of the oxidation rate of CO with respect to the CO concentration; (3) With the exception of Friedman and Cyphers the dependency of the rate of oxidation of CO on the O_2 concentration is small; (4) Most of the overall activation energies reported fall in the range of 20 to 30 kcal/mole; (5) The effect of H_2O on the reaction rate is expressed through the concentration terms in the pre-exponential factors. The activation energy is not influenced by varying amounts of H_2 or H_2O in the initial mixtures.

The sensitivity of the CO/O_2 reaction rate to the presence of hydrogen is discussed by all of these investigators. Others, including Shuler, Hoare and Walsh, Burgoyne and Hirsch, and Brokaw (88, 90, 96, 91) to name a few, have also reported on this point. There is general agreement that the CO/O_2 rate is accelerated regardless of whether the hydrogen is introduced to the system via the H_2O or the H_2 molecule, although Friedman and Nugent (87) point out that H_2 seems to have a more pronounced catalytic effect. These observations have led to the presently accepted (85) reaction mechanism for the combustion of CO/O_2 + (H_2 or H_2O)mixtures. The system is characterized by the consumption of CO by the low activation energy, exothermic step

$$CO + OH \xrightarrow{k_f} CO_2 + H \qquad k_f = 7.1 \times 10^{12}\, e^{\frac{-7.7}{RT}}$$

where the reverse reaction is slow. The reaction proceeds through the propagation of radicals by the thermoneutral chain

TABLE IV: SUMMARY OF OVERALL REACTION RATE DATA FOR CO COMBUSTION

OVERALL CONSUMPTION RATE OF CO EXPRESSED AS: $\frac{d[CO]}{dt} = k[CO]^a[H_2O]^b[O_2]^c e^{-E/RT}$ $\frac{\text{moles}}{\text{cm}^3 \text{ sec}}$

where $[A] = \frac{\text{moles A}}{\text{cm}^3 \text{ sec}}$, $E = \frac{\text{kcal}}{\text{mole}}$

*	INVESTIGATOR	REF	TECHNIQUE	TEMP ($^\circ$K)	P (ATM)	k	a	b	c	E
A	SAWYER & NEMETH	106	MASS SPEC. SAMPLING OF HC AFTERBURNING ZONE	1800-2000	1	2×10^{11}	1	.5	.25	24.6
B	FRIEDMAN & CYPHERS	92	BURNING VEL. MEAS. OF $CO-O_2-N_2-H_2O$ FLAME	2010	.08-.13	5.3×10^9	1	1	0	20.0
C	FENIMORE & JONES (1)	99	SAMPLING LEAN HC FLAME AFTERBURNING ZONE	1700-2000	1	1.2×10^{12}	1	0 1	1 0	24
D	FRIEDMAN & NUGENT	87	TEMP. MEAS. & SAMPLING LEAN $CO-O_2$ (H_2,H_2O) FL	1600-1800	.04	-	1	0	.5	20
E	SOBOLEV	89	BURNING VEL. & SAMPL. CO (H_2O)-O_2-N_2 FLAME	1900-2400	1	9.5×10^7	1	.2	0	30
F	SOBOLEV	89	SAMPLING $CO-O_2-N_2-H_2O$ FLAME AFTERBURNING ZN	1900-2400	1	2.7×10^5	1	0	0	27
G	HOTTEL, et al	95	STIRRED REACTOR	1280-1535	.25-1	8×10^{10}	1	.3	.5	16
H	WILLIAMS & HOTTEL	110	STIRRED REACTOR	1450-1750	.6	1.8×10^{13}	1	.5	.5	25
I	KOZLOV (2)	100	LAMINAR FLOW REACTOR	970-1370	1	$\frac{1.04 \times 10^{12}}{T^{2.5}}$	1	.25	.5	32
	KYDD & FOSS	108	STIRRED REACTOR	1000-1400	1-2	-	1	0	0	38

* Capital letters refer to curve designation in Figure

1 Fenimore & Jones find (b=0, c=1) when $[H_2O]$ is large, (b=1, c=0) for $[H_2O]$ small

2 Kozlov expresses rate law in terms of mole fractions of CO, O_2, H_2O, hence $T^{-2.5}$ appears as factor in k .

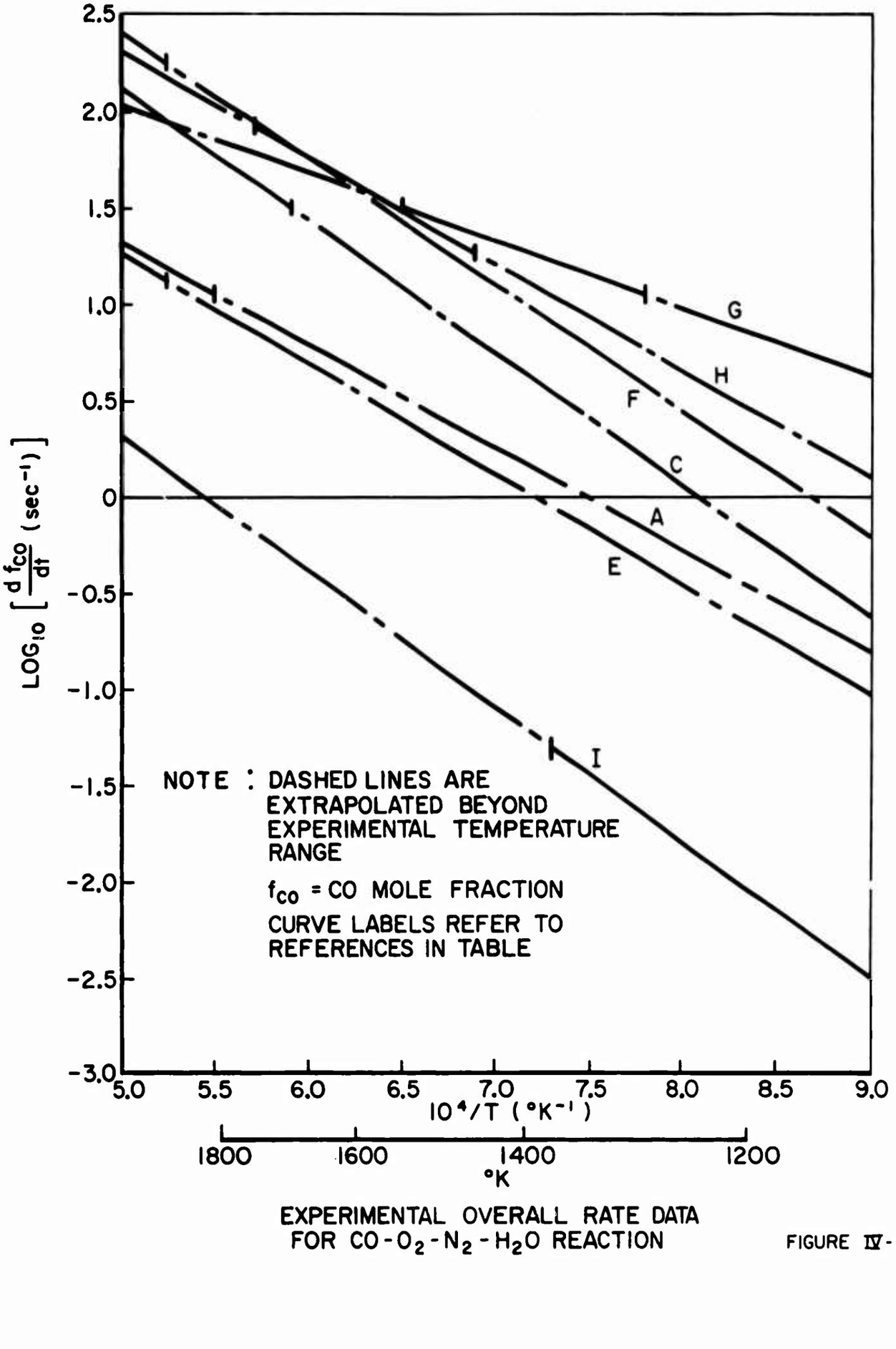

EXPERIMENTAL OVERALL RATE DATA FOR $CO-O_2-N_2-H_2O$ REACTION

FIGURE IV-1

branching reactions

$$H + O_2 \rightleftharpoons OH + O$$
$$O + H_2 \rightleftharpoons OH + H$$
$$O + H_2O \rightleftharpoons OH + OH$$

with the principal evolution of heat via the three body chain terminating recombination reactions such as

$$H + O_2 + M \longrightarrow HO_2 + M$$
$$O + O + M \longrightarrow O_2 + M$$
$$H + OH + M \longrightarrow H_2O + M$$

where the most likely third body is H_2O. Brokaw (91) makes the point that traces of water vapor of the order of 20 ppm seem sufficient to produce domination by the hydrogenous species of the kinetics of the CO/O_2 conversion where characteristic reaction times are of the order of 0.1 to 1 millisecond. This mechanism which relies heavily on the presence of active OH and H radicals is responsible for the acceleration of the otherwise slow CO/O_2 reaction. The kinetics of the dry CO/O_2 reaction necessarily involves the slow initiation step

$$CO + O_2 \underset{k_b}{\overset{k_f}{\rightleftharpoons}} CO_2 + O$$

$$k_f = 2.5 \times 10^{12} e^{-\frac{48,000}{RT}}$$

$$k_b = 1.7 \times 10^{13} e^{-\frac{53,000}{RT}} \quad \frac{cm^3}{mole\ sec}$$

(rate constants from shock tube induction time studies according to Brokaw). The overall reaction of the dry CO/O_2 system should therefore be dominated by this slow step and thus one might speculate that the characteristic overall activation energy of the dry CO/O_2 reaction (no H atoms present) should be of the order of 50 kcal/mole.

In light of the above information the following points are pertinent to the $CO/O_2/N_2$ + (H_2 or H_2O) experiments in the gas rocket: (1) The overall activation energy of the dry CO/O_2 reaction is estimated to be of the order of twice that of the CO/O_2 + (H_2 or H_2O) system; (2) Increasing the initial water vapor or H_2 concentration in a nominally wet CO/O_2 reaction increases the reaction rate through the concentration dependence

of the preexponential factor in the rate law but does not affect the overall activation energy; (3) There is a minimum concentration of H_2 or H_2O, estimated by Brokaw at 20 ppm, necessary to produce sufficient numbers of active free radicals to achieve wet CO/O_2 kinetics; (4) Experiments designed to determine the influence of the activation energy on the CO/O_2 system stability characteristics must allow for comparison of data for the dry and wet systems; (5) Comparison of stability characteristics for systems with increasing H_2 concentration should allow determination of the influence of the preexponential factor not specifically treated in the S-C model.

A.3 Initial Experiments With $CO/O_2/N_2$ System; H_2 Addition

In order to determine the influence of H_2 addition on the stability characteristics of the CO/O_2 system several changes in the gas rocket system were required. The precise control of the mole fraction of H_2O and H_2 in the initial reactant mixture was required. To this end a fourth gas "flow control" system (labelled "additive" in Figure III-6 was installed to allow accurate independent control and monitoring of the mass flow rate of H_2 additive. A series of micro-orifices was machined and calibrated by the water displacement technique to provide the capability of maintaining steady H_2 flows over the range of 1.3×10^{-3} to 0.1 gms/sec. The addition of the system allowed a fine control of H_2 mole fraction in the premixed reactants down to 0.005. The H_2O content of the Matheson CP grade CO was maintained at less than 1 ppm by the manufacturer. In the course of these experiments oxidizers with varying relative molar proportions of O_2 and N_2 were used. Air, (30% O_2 + 70% N_2), and (40% O_2 + 60% N_2) mixtures were used.

The addition of the fourth gas system and susceptability to blowoff of the CO/Oxidizer combustion in the gas rocket complicated the experimental procedure. It was impossible to produce ignition of the dry CO/Oxidizer mixtures with small H_2 flows using the additive system. In order to achieve repeatable ignition a fifth gas system (not shown in the flow control schematic)

was used to admit "ignition H_2" to the combustion chamber. The O_2 and N_2 flow rates were controlled separately to provide a combustible H_2/Oxidizer mixture in the chamber. Ignition was achieved by setting the additive H_2 flow rate at the desired final level and the ignition H_2 at a convenient level. The flow rate of N_2 at ignition was maintained at about 1/3 of the final value to discourage flashback. With the above conditions established the spark was actuated and the O_2 flow rate increased to ignition. The CO, O_2, and N_2 flow rates were then slowly increased to the desired experimental values at which time the H_2 ignition flow and the spark were terminated. Approximately 20 seconds were allowed prior to recording data to allow the system to clear of excess H_2.

Despite numerous attempts to carry out these experiments under a variety of experimental conditions (L_c = 50 to 100 cm, $\bar{P}_c$ = 4.4 to 7.8 atm, Φ = 0.4 to 5.0) with choked flow showerhead injection, it was impossible to maintain combustion in the absence of H_2 additive. This was precisely the same behavior observed by Bowman and this author in earlier experiments with the cruder flow control system. For large mole fractions of H_2 (0.07 to 0.10) and the (40% O_2 + 60% N_2) oxidizer nonsteady burning was occasionally observed at very lean ($\Phi > 5$) mixture ratios. However, these results were not systematic or repeatable. With decreasing H_2 mole fraction the equivalence ratio at the blowoff limits of the system rapidly collapse about the stoichiometric mixture ratio with stable combustion persisting out to the blowoff limits.

A.4 Alternative Approach to the Study of the Stability Characteristics of the $CO/O_2/N_2$ System: The Influence of CH_4 on the CO/O_2 Reaction

The inability to sustain combustion in the absence of H_2 additive and the narrow range of Φ wherein combustion could be maintained with H_2 additive with the showerhead injectors led to the decision to replace the choked flow showerhead injector with a porous plug injector. In the course of earlier

experiments with the $CH_4/O_2/N_2$ system (which also is characterized by a rather narrow range of Φ over which combustion can be maintained in the gas rocket when using showerhead injection), porous plug injection had been observed to substantially widen the blowoff limits and to generally improve the flame-stabilization and ignition characteristics of the system. Furthermore a comparison of stability limit data for the CH_4 + (40% O_2 + 60% N_2) system with porous plug (Pelmas (29)) injection and with showerhead (Bowman (32) and the present work) injection shows reasonably good agreement between the two systems. A series of preliminary investigations confirmed the improved flameholding characteristics of the porous injectors with the CO system.

It was decided to dispense with the attempt to decrease the overall activation energy (to increase the gas phase burning rate) by the addition of H_2 to a dry $CO/O_2/N_2$ system in light of (a) Brokaw's estimation that an H_2O mole fraction of 20 ppm is sufficient to produce wet CO/O_2 kinetics, (b) the numerous experimental kinetics results showing that the effect of changes in the H_2O or H_2 concentration in the initial mixtures on the overall CO consumption rate is a higher order (compared to changes in the Arrhenius factor) effect due to modifications in the concentration terms of the preexponential factor, and (c) the uncertainty of the actual concentration of hydrogenous species in the unburned premixed gases due to the presence of trace hydrocarbon impurities in the H_2O-free CO and the necessity to use a separate H_2 ignition system.

The alternative approach of reducing the rate of the initially wet CO/O_2 system by means of addition to the unburned gases of controlled small amounts of an inhibitor methane was selected. Again recourse to the volume of fundamental kinetics studies of the wet CO/O_2 reaction proved helpful. It is worth noting that the relative abundance of basic experimental data regarding the kinetics of the wet CO/O_2 reaction is due principally to the practical interest in hydrocarbon combustion reactions and the well substantiated observations of the crucial role played by the

oxidation of CO in those reactions (in particular the oxidation of CH_4 at high temperatures). There is substantial agreement with regard to the overall kinetic rates and reaction mechanisms among the various investigators who have examined the CH_4/O_2 oxidation reaction in the temperature range of 600 to 2500 ^oK. It is well established that the reaction path from CH_4 to CO_2 proceeds through the long lived CO intermediate.

The early investigations of the wet CO/O_2 reaction and the CH_4/O_2 reaction by Hoare and Walsh (90, 97) using low temperature 600 to 800 ^oK static bomb explosion limit techniques and Burgoyne and Hirsch (96), who employed a laminar isothermal flow reactor technique in the temperature range of 1200 to 1300 ^oK, first demonstrated that the wet CO/O_2 reaction is strongly inhibited by the presence in the initial reactant mixture of small amounts of CH_4. This observation has repeatedly been substantiated and the conclusions of Hoare and Walsh and Burgoyne and Hirsch regarding the inhibition of the CO reaction by hydrocarbons amplified and refined by the following investigators: Laffitte, Cusin, and James (93) and Vanpee and Grard (104) using low temperature (600 to 700^oK) static bomb explosion limit techniques; Friedman and Cyphers (92), Sobolev (89), and Koslov (100) who examined the rate of CO oxidation in the afterburning zone of hydrocarbon flames and in lean $CO/O_2/N_2$ flames in the temperature range of 1600 to 2400^oK; Kydd and Foss (108) and Williams, Hottel, and Morgan (110) using stirred reactor techniques at 1400 to 1800^oK.

It is the consensus of these investigators that the inhibition of the wet CO/O_2 reaction by small[1] amounts of CH_4 arises from the interruption of the chain reaction mechanism responsible for the fast CO to CO_2 oxidation due to the removal of H and O atoms and hydroxyl radicals by reaction with the CH_4 molecule and its combustion intermediates such as formaldehyde (H_2CO). The inhibiting effect can be formally expressed as follows (Fristrom and Westenberg (85)). The oxidation of CO in the wet

---

[1] Small in the sense that the addition of CH_4 does not alter the thermal balance of the reaction system. There is negligible variation in the adiabatic combustion temperature.

system proceeds principally through the low activation energy step

$$CO + OH \longrightarrow CO_2 + H$$

as discussed earlier, while a high concentration of active intermediates is sustained by the equilibrated branching reactions

$$H + O_2 \rightleftharpoons OH + O$$
$$O + H_2 \rightleftharpoons OH + H$$
$$O + H_2O \rightleftharpoons OH + OH$$

The oxidation of CH_4 proceeds principally through such low activation energy steps as

$$CH_4 + H \rightleftharpoons CH_3 + H_2$$
$$CH_4 + OH \rightleftharpoons H_2O + CH_3$$

with the latter reaction prevailing in H_2 lean systems such as those considered in the present case. At least some important fraction of the methyl radicals thus formed are consumed according to

$$CH_3 + O_2 \rightleftharpoons H_3COO \rightleftharpoons H_2CO + OH$$

with the formaldehyde species leading to partial chain termination through

$$H_2CO + OH \rightleftharpoons HCO + H_2O$$
$$HCO + OH \rightleftharpoons CO + H_2O$$

the latter reaction being exothermic and probably rapid.

In view of the apparent action of CH_4 and H_2CO as sinks for the free radicals necessary for the propagation of the CO reaction and the measured strong retarding effect of additions of CH_4 and H_2CO on the CO (wet) rate of combustion it is clear that the effective overall activation energy (which results from the complex interaction of the elementary reaction steps) of the CO reaction in the presence of such additives is increased.

A.5 Range of Experimental Variables in $CO/O_2/N_2$ + CH_4 Studies

Despite the relative agreement between the stability characteristics of the CH_4/O_2 system with showerhead and porous plug injection it has been noted that the H_2/Air system showed markedly different stability characteristics when porous injectors were substituted for the choked showerhead injectors. It was decided at the outset of the present investigations to expand the studies to allow a verification of the existence of a critical temperature for the $CO(H_2O)/O_2/N_2$ system with porous plug injection at the stability limits as observed in the H_2/Air and the $CH_4/O_2/N_2$ systems.

The propellant gases used were CP grade CO with water vapor content adjusted by the supplier to 100 to 200 ppm, O_2, N_2, and CP grade CH_4 with typical compositions as indicated in Table I, Chapter III, page 72 . It is noted that the CP grade CO typically contained trace hydrocarbon impurities including CH_4. These mole fractions are well below those reported in the literature to produce inhibition of the CO/O_2 reaction and can be considered merely to contribute to the initial "wetness" of the CO. The mass flow rates of each reactant were controlled separately with premixing occurring in the mixing chamber. The micro-orifices used in the original study were recalibrated to provide a fine control on the CH_4 additive mass flow rate. The mass flow rate of CH_4 additive was accurately controlled to 0.1% of the mass flow rate of CO. This allowed the mole fraction of CH_4 in total moles

$$f_{CH_4} = \frac{\text{moles/sec}_{CH4}}{\text{moles/sec}_{CO+O_2+N_2+CH_4}}$$

to be varied from $f_{CH_4} \geq 0.00035$ where the lower limit is 20 to 30 times the mole fraction of CH_4 arising due to impurities in the CO.

The complete range of gas rocket system variables (chamber length, nozzle configuration, chamber pressure, and total propellant mass flow) was not explored in detail in the course of

this work. The data reported in the following paragraphs correspond to the following experimental conditions:

injector = porous plug
chamber length = 104 cm
typical ratio of $\bar{P}_{mix}/\bar{P}_c$ = 1.2
typical injection Mach number = 0.5
nozzle = 4 hole plug nozzle with effective A_c/A_t = 46
total propellant flow rate, for $\bar{P}_c$ = 4.4 atm
$\dot{m}_{tot}$ = 11 gms/sec
$\bar{P}_c$ = 7.8 atm
$\dot{m}_{tot}$ = 23 gms/sec
Dynisco pressure transducer located at 18 cm from injector

Independent checks of the system stability characteristics as observed under these conditions were made to insure that the observations were not a unique function of the above system conditions.

It was possible to make a systematic determination of the stability characteristics of the wet $CO/O_2/N_2$ system including the stability limit and pressure waveform, amplitude, and frequency in the absence of CH_4 inhibitor and as a function of the mole fraction of CH_4 in total moles of fuel

$$M_{CH_4} = \frac{\text{moles } CH_4}{\text{moles CO} + \text{moles } CH_4}$$

A.6 Influence of the Combustion Temperature (T_b) On the Stability Characteristics of the Wet $CO/O_2/N_2$ System

In the absence of CH_4 inhibitor and under the conditions enumerated above, a series of experiments was carried out to determine the influence of the combustion temperature on the stability characteristics of the $CO(H_2O)/O_2/N_2$ system. There is general agreement among kineticists that the CO consumption rate is independent of the concentration of N_2 diluent. Thus, the addition of increasing amounts on N_2 to the CO/O_2 reaction for fixed ratio of O_2 to CO should produce a strong

effect on the CO reaction rate solely through the dependence of the rate on the combustion temperature. According to the S-C predictions the decrease in combustion temperature, T_b, with increasing N_2 concentration should cause a shift of the stability limits toward the stoichiometric mixture ratio. The dependence of the stability characteristics of the CO/O_2 system on the propellant equivalence ratio was determined for the $CO(H_2O)/(.5O_2 + .5N_2)_{molar}$ system under three different conditions of dilution, 0 %, 20 %, and 60 %, where

$$\% \text{ dilution} = \frac{\text{diluent flow rate}}{\text{diluent + oxidizer flow rate}_{molar}} \times 100$$

The equivalent % dilutions on a mass basis are 0, 19, and 58 %.

The unburned gas mole fractions in total moles and the theoretical, equilibrium, adiabatic combustion temperatures (T_b) of the mixtures studied are summarized in Figure IV-2. It should be pointed out that the experiments were restricted to near stoichiometric and oxidizer rich mixtures. The results of these experiments are shown in Figure IV-3. For reference purposes the curves of constant T_b as a function of Φ and % dilution are shown. Under each condition of dilution unstable combustion is observed to be sustained over a narrow range of equivalence ratios. The shift toward the stoichiometric mixture ratio of both the upper and lower stability limits with increasing dilution and the relatively fixed magnitude (independent of the % dilution) of T_b corresponding to the lower limit offer strong support for the importance of the combustion temperature of the CO/O_2 system as a fundamental parameter in determining the stability characteristics of the system. In this regard it is noted that the range of T_b over which nonsteady burning is observed decreases with increasing dilution. This decrease (as will be obvious following the discussions of Chapter V) is due to the fact that the gradient of the T_b vs Φ curve in the vicinity of the stability limit becomes steeper as the % dilution increases (see Figure IV-2).

REACTANT MOLE FRACTIONS IN UNBURNED GAS MIXTURE									
	0 % Dilution			20 % Dilution			60 % Dilution		
Φ	CO	O_2	N_2	CO	O_2	N_2	CO	O_2	N_2
0.9	.526	.237	.237	.470	.212	.318	.308	.138	.554
1.0	.500	.250	.250	.445	.222	.334	.286	.142	.572
1.5	.400	.300	.300	.348	.261	.390	.210	.158	.632
2.0	.333	.333	.333	.286	.286	.428	.167	.167	.667
2.5	.286	.357	.357	.242	.303	.455	.138	.172	.690
3.0	.250	.375	.375	.211	.316	.475	.118	.176	.706
3.5	.222	.389	.389	.186	.326	.488	.103	.180	.719

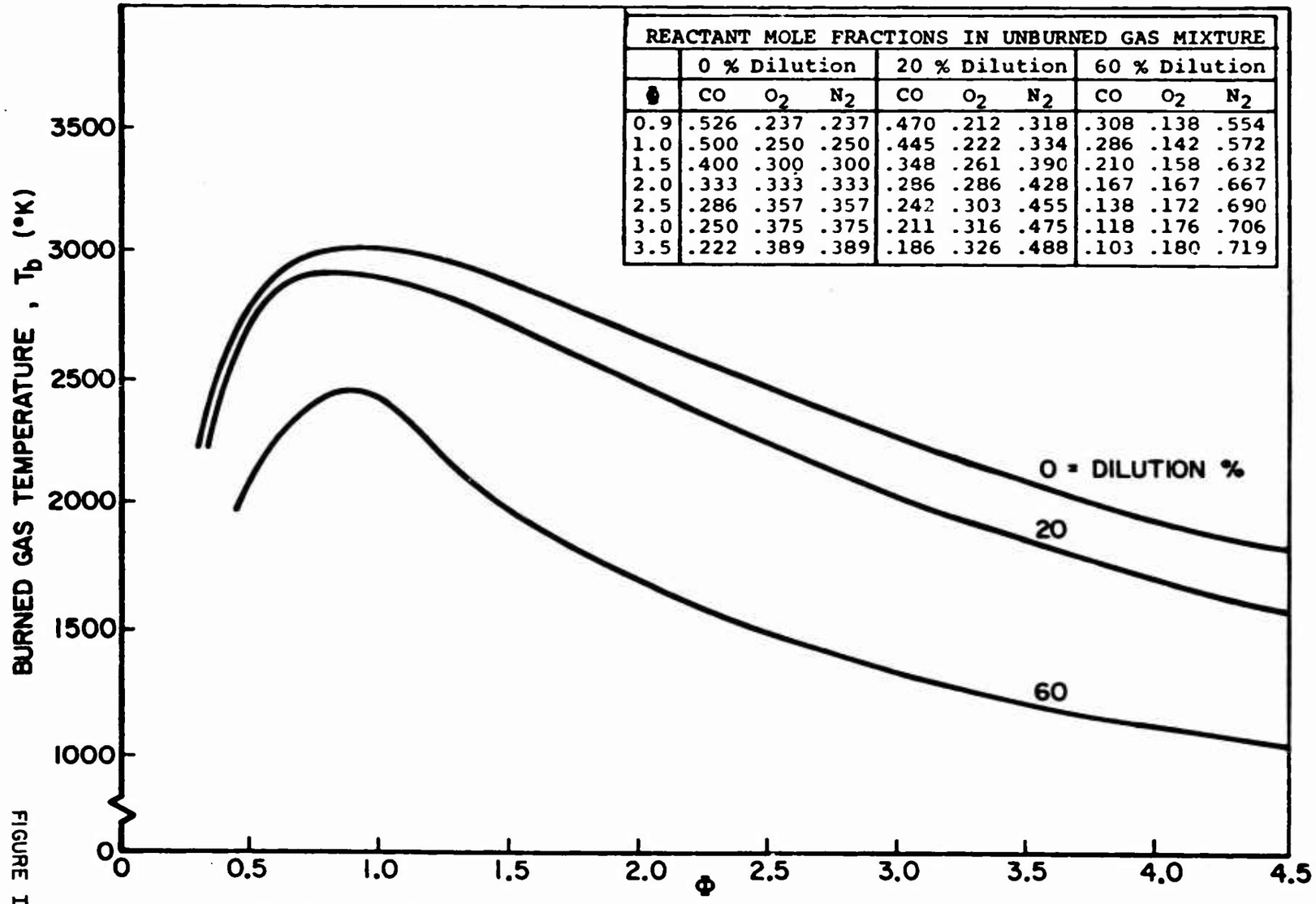

FIGURE IV - 2

THEORETICAL EQUILIBRIUM ADIABATIC BURNED GAS TEMPERATURE (T_b) AND INITIAL MIXTURE COMPOSITION AS A FUNCTION OF EQUIVALENCE RATIO Φ, $CO+[.5O_2+.5N_2]$ MIXTURES, $\bar{P}_c$ = 7.8 atm, $T_{UNBURNED\ GAS}$ = 300°K, 0 TO 60% DILUTION

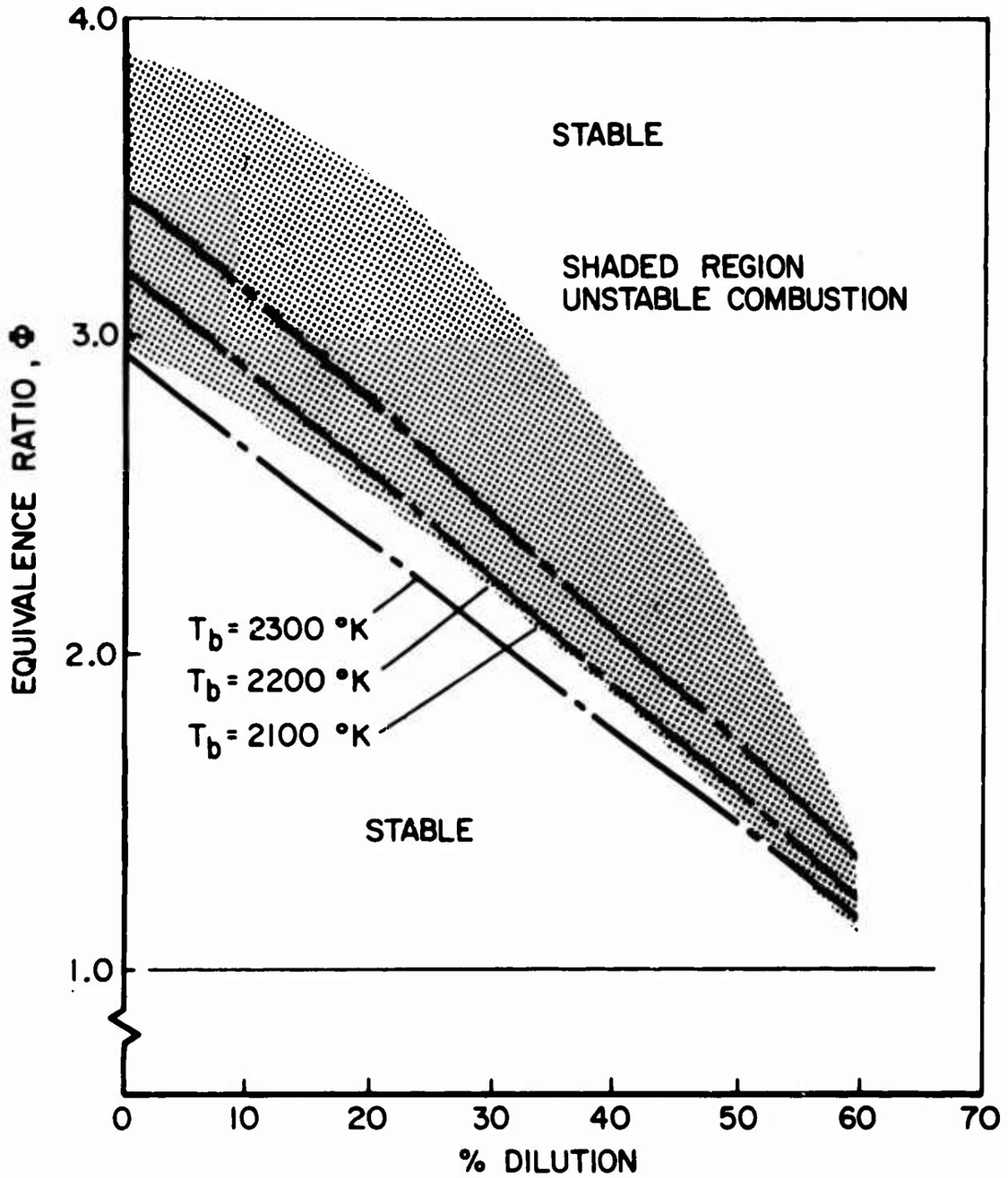

REGIME OF UNSTABLE COMBUSTION FOR CO + [.5O_2 + .5N_2] AS FUNCTION OF EQUIVALENCE RATIO, Φ, AND % DILUTION FOR P_c = 7.8 atm, L_c = 104 cm, POROUS PLUG INJECTOR

FIGURE IV - 3

The data strengthen the conviction that despite the radical differences between the showerhead and porous plug injection schemes in the gas rocket substantially the same coupling mechanism between the combustion process and the gas dynamic flow field is operative during nonsteady combustion in the $CO/O_2/N_2$ system as in the $H_2/O_2/N_2$ and $CH_4/O_2/N_2$ systems.

As in previous experimental instability studies of other propellant systems a systematic increase of the dimensionless pressure wave amplitude $\Delta p/\bar{p}_c$ to a maximum followed by decrease with increasing Φ (decreasing T_b) beyond the lower stability limit is observed. In Figure IV-4 the observed $\Delta p/\bar{p}_c$ shown as a function of Φ for the 20% dilution system. Of particular interest is the observation that near the lower and upper stability limits the sustained waveform is continuous. Indeed the systematic growth of wave amplitude and the shift from linear continuous travelling waves to nonlinear continuous travelling waves and ultimately to nonlinear discontinuous propagating shock waves with increasing Φ near the lower limit is clearly shown by the data. It should be pointed out that one of the contributing factors to these observations was an order of magnitude increase in the signal to noise ratio of the output playback of the Honeywell tape deck used in these experiments compared to the previously used Ampex system. Subsequent experiments with the H_2 + Air system using the Honeywell system showed conclusively that the same systematic transition with increasing Φ (although over a narrower range of Φ) from stable combustion through a regime of linear continuous waves near the lower stability limit to the condition of sustained nonlinear shock type waves occurred.

A.7 Influence of CH_4 Inhibitor On the Stability Characteristics of The Wet $CO/O_2/N_2$ System

The inhibiting influence of CH_4 in the combustion of CO $(H_2O)/O_2$ mixtures has been discussed. It was pointed out that based on the present understanding of the kinetics of the CO $(H_2O)/O_2$ reaction this influence should be manifest by an

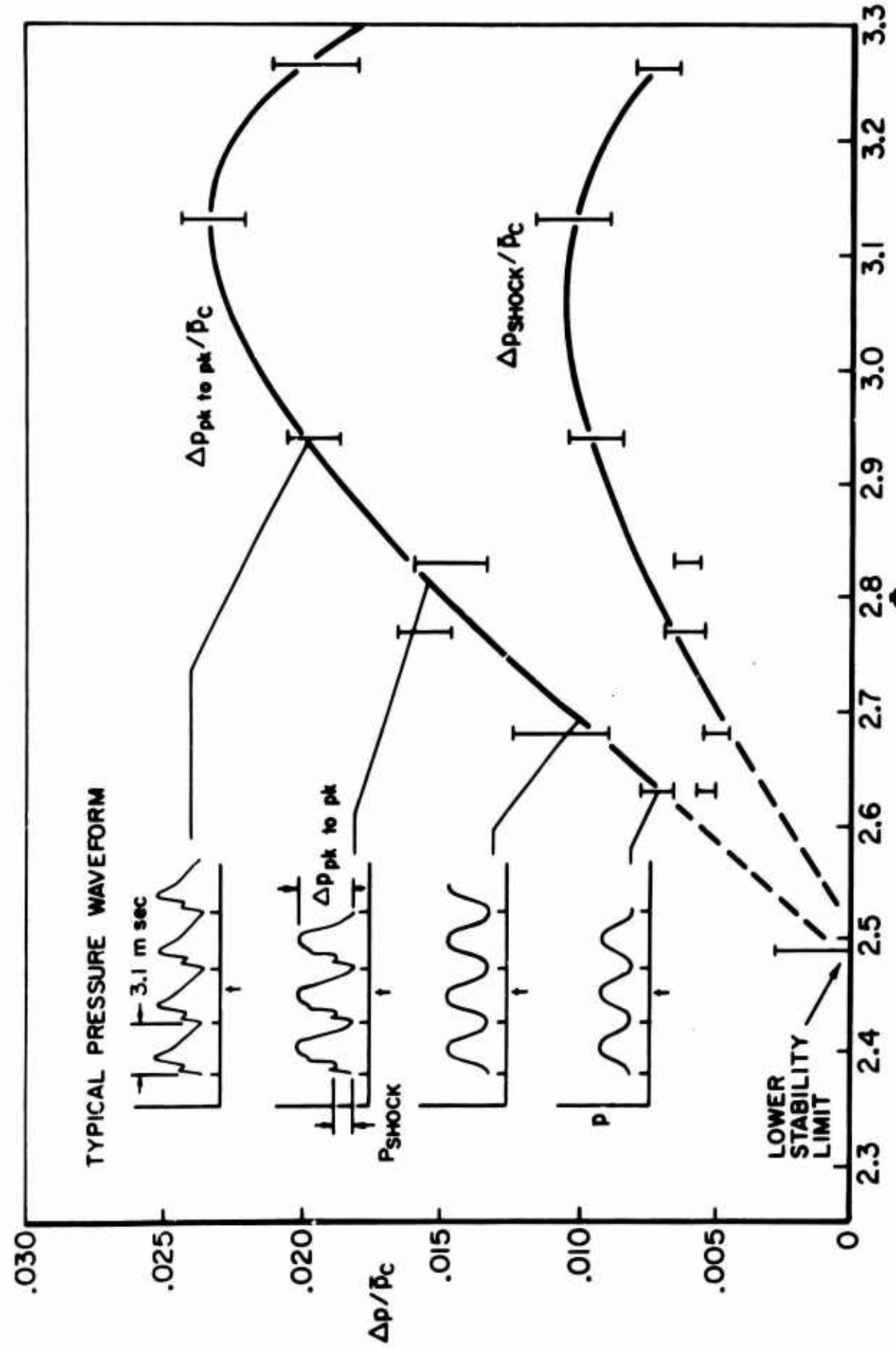

VARIATION OF WAVE AMPLITUDE $\Delta p/\bar{P}_c$ AND WAVE FORM WITH EQUIVALENCE RATIO (Φ)
FOR $CO + (.5O_2 + .5N_2) + 20\%$ N_2 DILUTION, $\bar{P}_c = 7.8$ atm
$L_c = 104$ cm, POROUS PLUG INJECTOR

FIGURE IV - 4

increase in the overall activation energy of the reaction and effectively as a decrease in the overall kinetic combustion rate. In terms of the S-C model the addition of trace amounts of CH_4 to the reaction should lead to a systematic shift of the stability limit toward the stoichiometric mixture ratio, that is to higher combustion temperature in order to satisfy the criterion $(E/RT)_{lim}$ = constant or constant burning rate.

Initially theoretical calculations of the adiabatic combustion temperature for $(CO + m_{CH_4} CH_4)/(0.5\ O_2 + 0.5\ N_2)$ mixtures under varying conditions of dilution were carried out for several values of $m_{CH_4} = \frac{\text{moles } CH_4}{\text{moles } CO + \text{moles } CH_4}$. The objective of the experiments was to vary the kinetic combustion rate of CO by changing the activation energy independent of T_b. It was important to determine the sensitivity of the $CO/O_2/N_2$ combustion temperature to small amounts of the energetic CH_4 species. Figure IV-5 shows T_b as a function of Φ for $CO/(0.5\ O_2 + 0.5\ N_2)$ mixtures for 0 and 20% dilution and several values of m_{CH_4} used in the course of the experimental work. For reference purposes the % increase in T_b for selected values of Φ near the experimentally observed stability limits of the CH_4-free system are shown in the insert. For the range of Φ, % dilution, and mole fraction of CH_4 (in total fuel) examined the combustion temperature variations are less than 1% for $m_{CH_4} < 0.008$.

The experiments were carried out under the conditions noted in section A.5. The stability characteristics of the system were determined with no dilution at $\bar{P}_c$ = 4.4 and 7.8 atm for $0 \leq m_{CH_4} \leq 0.045$ and for 20% N_2 dilution at $\bar{P}_c$ = 7.8 atm for $0 \leq m_{CH_4} \leq 0.0045$.

The principal results of these experiments are shown in Figures IV-6 and IV-7. Both systems exhibit the marked shift of the lower stability limit(Φ_{lim}) towards the stoichiometric mixture ratio for addition of small amounts of CH_4 inhibitor ($m_{CH_4} \simeq 0.005$). Φ_{lim} for the 20% dilute mixtures is more sharply defined with and without CH_4 additive in the sense that the transition from low amplitude continuous waveform observed at the onset (in terms of Φ) of the nonsteady combustion regime

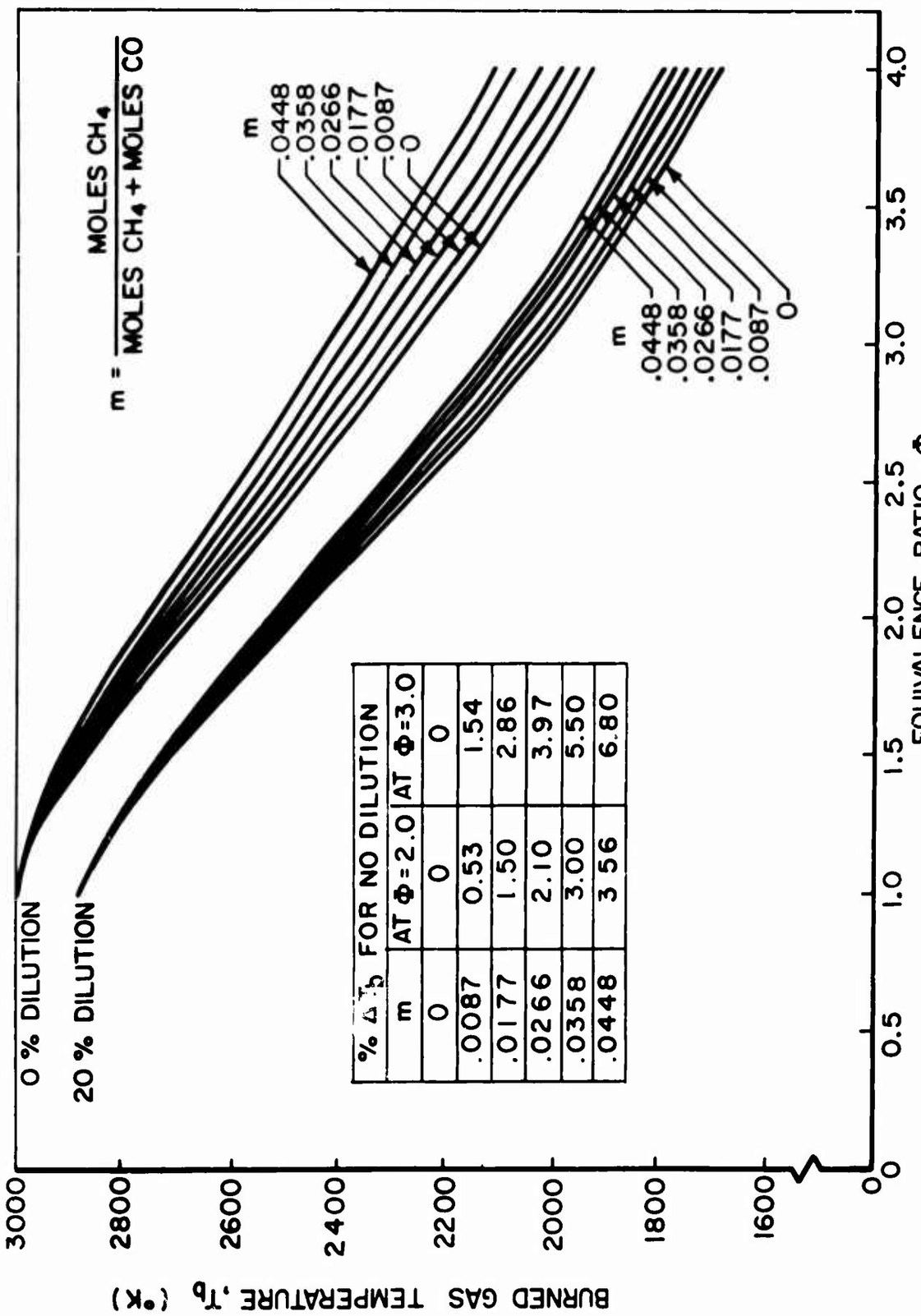

% Δ Tb FOR NO DILUTION		
m	AT Φ=2.0	AT Φ=3.0
0	0	0
.0087	0.53	1.54
.0177	1.50	2.86
.0266	2.10	3.97
.0358	3.00	5.50
.0448	3 56	6.80

THEORETICAL EQUILIBRIUM ADIABATIC BURNED GAS TEMPERATURE, T_b, AS A FUNCTION OF EQUIVALENCE RATIO, Φ, FOR CO+[.5O_2+.5N_2], 0 AND 20% DILUTION WITH CH_4 ADDITIVE, $\bar{P}_c$ = 7.8 atm, T_u = 300 °K

FIGURE IV - 5

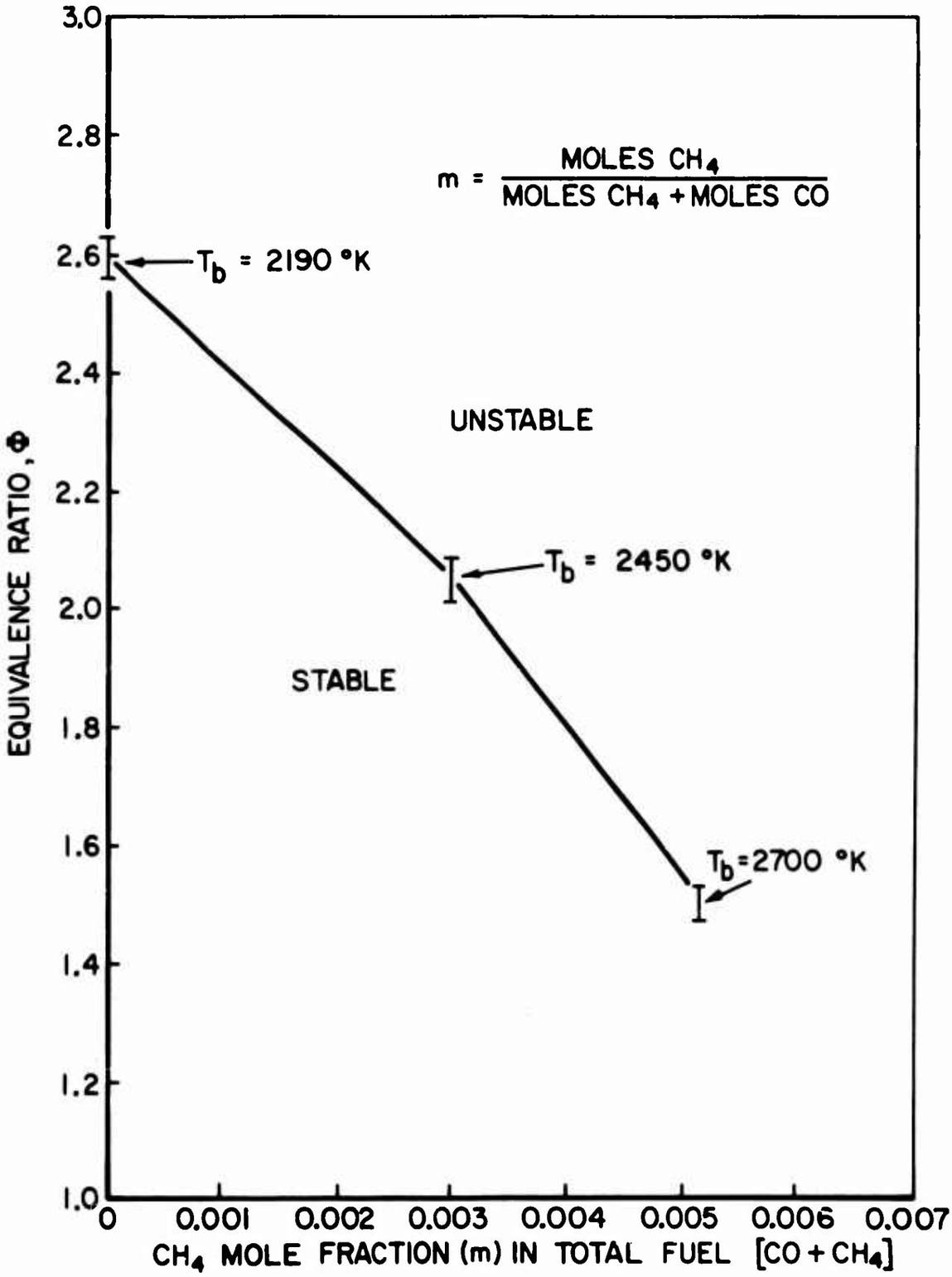

SHIFT OF LOWER STABILITY LIMIT (Φ_{LIM}) WITH ADDITION CH_4 TO $CO + [.5O_2 + .5N_2] + 20\%$ N_2 DILUTION
$L_c = 104$ cm, $\bar{P}_c = 7.8$ atm

FIGURE IV-6

FIGURE IV-7

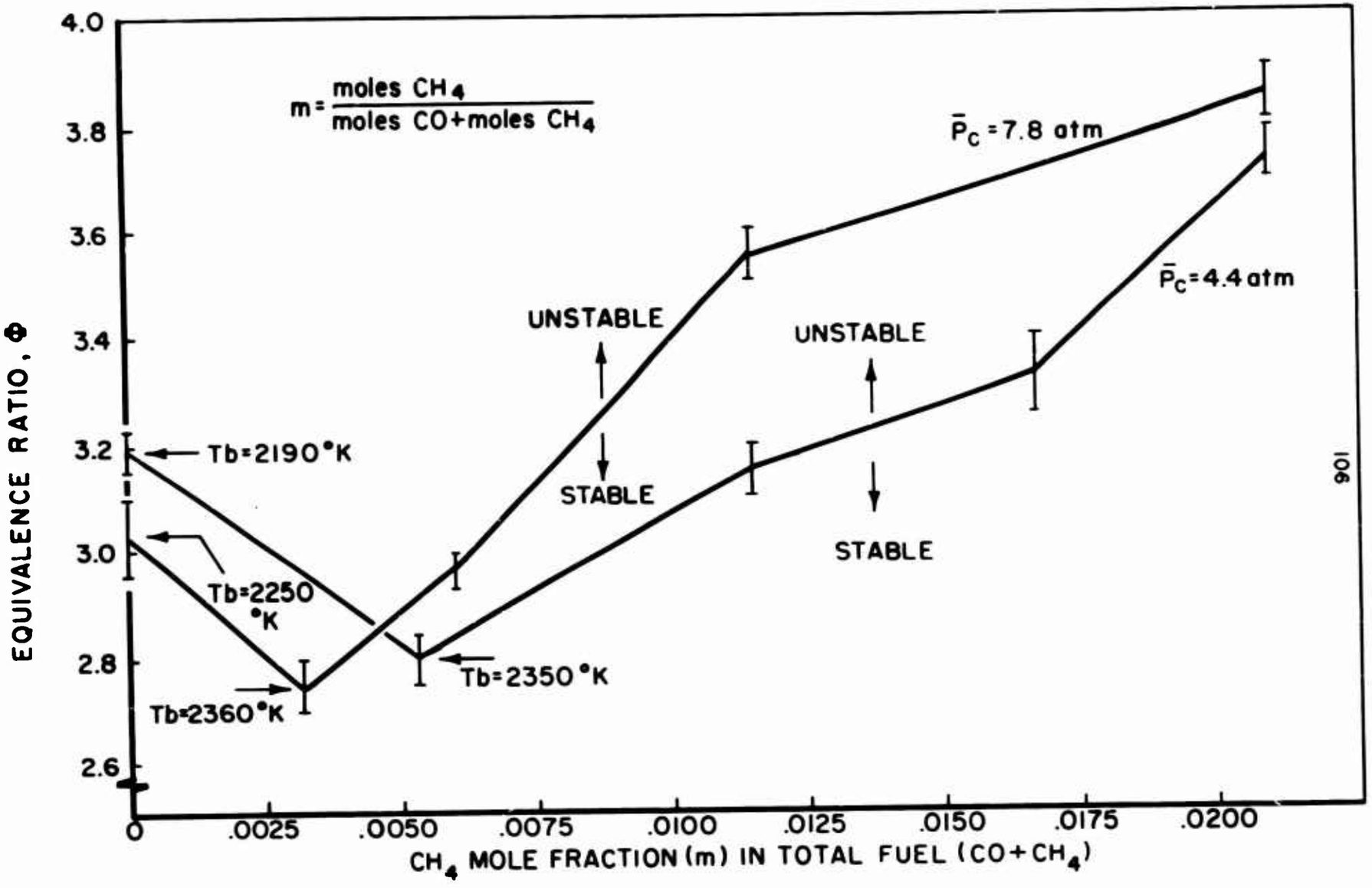

SHIFT OF LOWER STABILITY LIMIT (Φ_{LIM}) WITH ADDITION OF CH_4 TO $CO+(.5O_2+.5N_2)$, Lc=104 cm

to discontinuous shock type waves occurs over a narrower range of Φ . The effect in terms of stability limit shift of equivalent CH_4 mole fractions is observed to be greater in the dilute system where the addition of $m_{CH_4} \simeq .005$ results in a 23% increase in T_{lim}. A shift in mode order at the limit was observed to occur as well. In the absence of CH_4 the onset of nonsteady burning occurred at $\Phi \simeq 2.6$ or T_{lim} 2190°K with the appearance of a single (fundamental mode) wave with a mean frequency of 325 ± Hz. The addition of $m_{CH_4} \simeq 0.003$ resulted in a shift of the limit to $\Phi \simeq 2.05$, $T_{lim} = 2450$°K, and a shift to the second harmonic mode with a mean frequency of 610 ± Hz. The addition of $m_{CH_4} \simeq .005$ produced a shift of the limit to $\Phi \simeq 1.5$, $T_{lim} = 2700$ °K and resulted in the appearance of both the second (mean frequency 690 ± 10 Hz) and third (mean frequency 1035 ± 20 Hz) harmonic modes.

The investigations with the 20% dilute system were restricted to near limit mixtures with comparatively smaller m_{CH_4}. The experiments with the undiluted system were extended to higher Φ within the regime of nonsteady combustion and to higher m_{CH_4}. The dependence of the stability characteristics of the undiluted system for $\bar{P}_c = 4.4$ and 7.8 atm ($\dot{m}_{tot}$ differing by a factor of two) on the m_{CH_4} are essentially identical. The addition of $m_{CH_4} \simeq .005$ produced a measureable shift in Φ_{lim} to lower Φ and higher T_b. The curve of Φ_{lim} vs m_{CH_4} is observed to minimize in the vicinity of $m_{CH_4} = 0.0025$ to 0.005 and further addition of CH_4 produces a corresponding shift of Φ_{lim} away from the stoichiometric mixture ratio. Furthermore, investigations of the wave amplitude ($\frac{\Delta P_{shock}}{\bar{P}_c}$ and $\frac{\Delta P_{pk\pm pk}}{\bar{P}_c}$) within the regime of nonsteady burning at constant Φ showed that the amplitude underwent a systematic increase in magnitude with addition of small amounts of CH_4 and was followed by a decrease (ultimately to zero with the resumption of stable combustion) for larger amounts of CH_4. There was no observed change in mode order at the limit for this system with increasing m_{CH_4}.

At this juncture the following comments are pertinent:

(1) The experimentally observed shift of the regime of nonsteady combustion to higher combustion temperatures with the ad-

dition of trace amounts of CH_4 coupled with the observed strong temperature dependence of the CH_4 - free system stability limits (the existence of a T_{lim}) provide positive confirmation of the contention that gas phase chemical kinetics plays a crucial role in the coupling between the combustion zone energy release and the gas dynamic flow field. The qualitative predictions of the S-C theory regarding the dependence of the stability characteristics on E/RT, the data in the literature regarding the dependence of the CO/O_2 kinetics on the presence of small amounts of CH_4, and the observed experimental data are in mutual agreement.

(2) The addition of CH_4 to the undiluted $CO\ (H_2O)/(.5O_2+SN_2)$ system is observed to influence the linear (limit) and the non-linear (wave amplitude) stability characteristics.

(3) The observed stabilizing tendency of the addition of larger amounts of CH_4 to the undiluted system most likely results from the counteracting thermal effect of increasing combustion temperature with increasing m_{CH_4}. Depending upon the inhibiting effect of the CH_4 additive, increasing m_{CH_4} should eventually lead to the observed behavior. Schematically

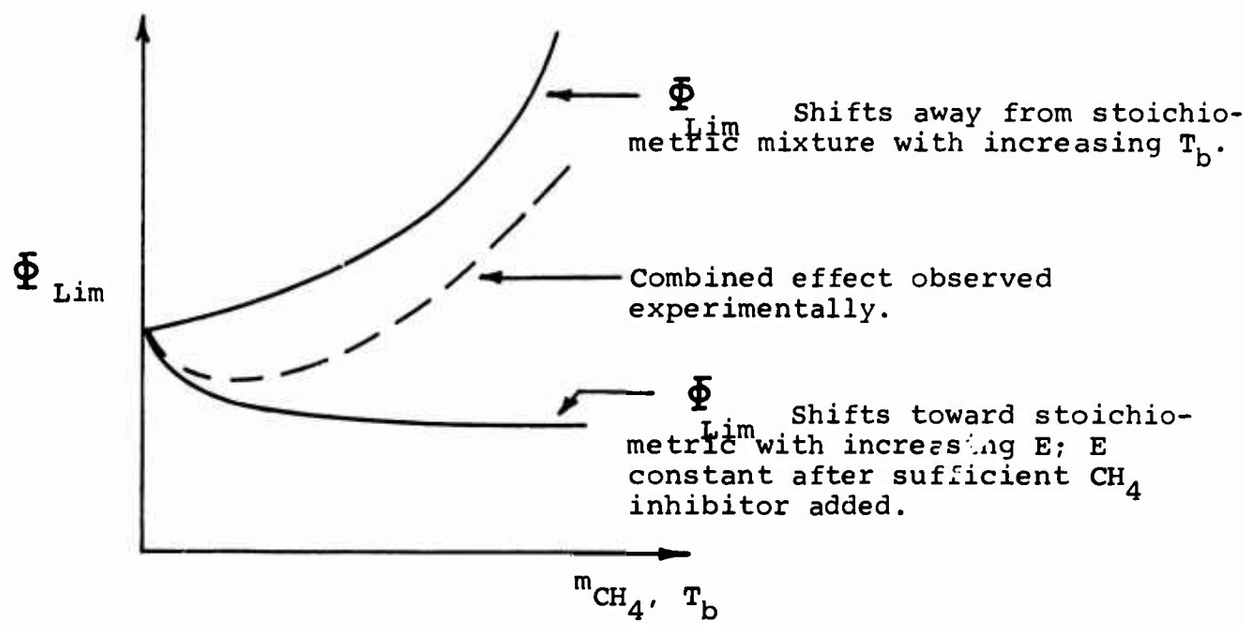

Figure IV-8

B. Combustion Zone Diagnostics: Measurement Of Mean Gas Temperature In The Combustion Zone

The systematic measurement of local mean temperatures in the combustion zone was felt to be a logical first step in the examination of the distribution of combustion during steady and non-steady burning. These investigations initiated the series of diagnostic experiments designed to obtain an understanding of the structure of the combustion zone and thereby to facilitate the development of a more realistic model of the complete non-steady problem.

Knowledge of the distribution of mean gas temperature in the combustion zone is important from the standpoints of developing a physical model of the (mean) combustion process and of properly matching the modeled combustion process to an analysis of the wave dynamics in the combustion chamber. With respect to the second point, the overall extent or mean axial dimension of the combustion zone becomes an important parameter that must be determined before realistic coupling of the combustion process and the chamber dynamics can be achieved. As will be shown in the following chapter the overall mean length of the combustion zone relative to the average particle velocity in the combustion zone and relative to the overall chamber length has important consequences on the analytical treatment of the complete problem. It might be added that it was equally important to determine whether any significant changes in the combustion zone structure accompany the spontaneous transition from stable to unstable combustion.

In the course of previous investigations (Schob (31) and Bowman (32)) attempts were made to determine "axial profiles" of the mean gas temperature in the combustion zone. These investigations typically involved the placement of 4 to 6 "wall mounted" unshielded, uncoated Pt-Pt 13% Rh thermocouples at intervals along the center line of the combustion chamber just downstream from the injector. Bowman (32) reports the results of experiments with the H_2 + Air system, $\bar{p}_c$ = 7.8 atm, and under various primary injection configurations. An experimental determination of the importance of radiation losses from the un-

shielded thermocouples showed the negligible importance of this source of error. In view of the high heat transfer coefficient of the combustion gases and the observation that measured peak combustion zone temperatures were within 40°K of the theoretical adiabatic combustion temperature conduction losses also were assumed small. The results of Bowman are considered only tentative for the following reasons: First, the physical size of the thermocouple wires (0.025 cm diam) with large bead size (0.06 cm) and the fact that the wires were not coated should contribute to the catalytic recombination of reaction intermediates in the H_2/O_2 reaction at the wire surface. That both factors are important in thermocouple measurements of temperatures in H_2 + Air flames is well known (Kaskan (94), Cookson (102)). As Bowman noted, the only reliable temperature measurements under the above conditions are those in the post flame product gases. Second, the inference of axial mean static temperature profiles using the above technique (even in the absence of catalytic effects) necessitates that several conditions be satisfied. The combustion zone must be sufficiently one-dimensional (Bowman felt that the high turbulence levels in the combustion chamber should produce such a zone) so that the radial location (i.e., the centerline in his work) investigated is representative of the entire combustion chamber cross-section. There must be no downstream or wake effect of each thermocouple element on the gas dynamic field sensed by succeeding thermocouples. Finally, the local gas mean flow kinetic energy must be negligible compared to the translational energy so that measured stagnation temperatures correspond to effective local static temperatures. Bowman argued this point on the basis that the mean combustion zone Mach number equaled the mean downstream combustion chamber Mach number.

The diagnostic studies of the gas rocket combustion zone discussed in the following paragraphs were restricted to the H_2 + Air or H_2 + "dilute" Air systems. The $H_2/O_2/N_2$ system was selected since the system was the easiest to work with in terms of ignition and flashback characteristics and since the experimental stability characteristics of the system were more completely and pre-

cisely defined than those of the $CH_4/O_2/N_2$ and $CO/O_2/N_2$ systems. It should be noted that the combustion distribution over the entire range of $\bar{\Phi}$ could not be probed due to the temperature limitations of the thermocouples. For reference purposes the variation of for the H_2 + Air system (T_u = 298°K and $\bar{P}_c$ = 4.4 to 7.8 atm) is shown in Figure IV-9. For the H_2 + Air system is independent of $\bar{P}_c$ over the range of interest.

B.1 Measurement of Radial Temperature Profiles

The first indication that the previous measurements of axial mean static temperature profiles may be subject to substantial error resulted from an initial series of experiments designed to measure the local static temperature at fixed axial location and at several radial positions in the combustion zone. These measurements were made by inserting three Pt-Pt 13% RH thermocouples through the chamber wall at approximately 2.5 cm from the injector face and positioning them along a single radius at the motor center line, 0.63 cm from the centerline, and 0.63 cm from the chamber wall. The "radial temperature profiles" were determined for the H_2 + Air system, L_c = 104 cm, 4 hole plug nozzle, $\bar{P}_c$ = 7.8 atm, $\dot{m}_{tot}$ = 25 gms/sec for a variety of choked flow showerhead (10, 31, 49 hole) and porous plug injection configurations. The results of these measurements also must be viewed as tentative in the sense that the wire and bead diameters were large (0.025 cm and 0.06 cm) and the thermocouples were uncoated.

Figure IV-10 summarizes the results of these experiments. The uncorrected measured mean local temperatures at the three radial positions are recorded in terms of $\bar{\Phi}$ for 4 injection configurations. The radial position of the symmetrical injection port arrays is noted for each injector. The dashed curves distinguish data obtained in separate experiments.

There is an obvious failure of the data to support the concept of a more or less uniform one-dimensional combustion zone with a unique axial dimension over the chamber cross-section even for the porous plug injector. It was observed that this nonuniformity is not simply related to radial position and $\bar{\Phi}$ but is

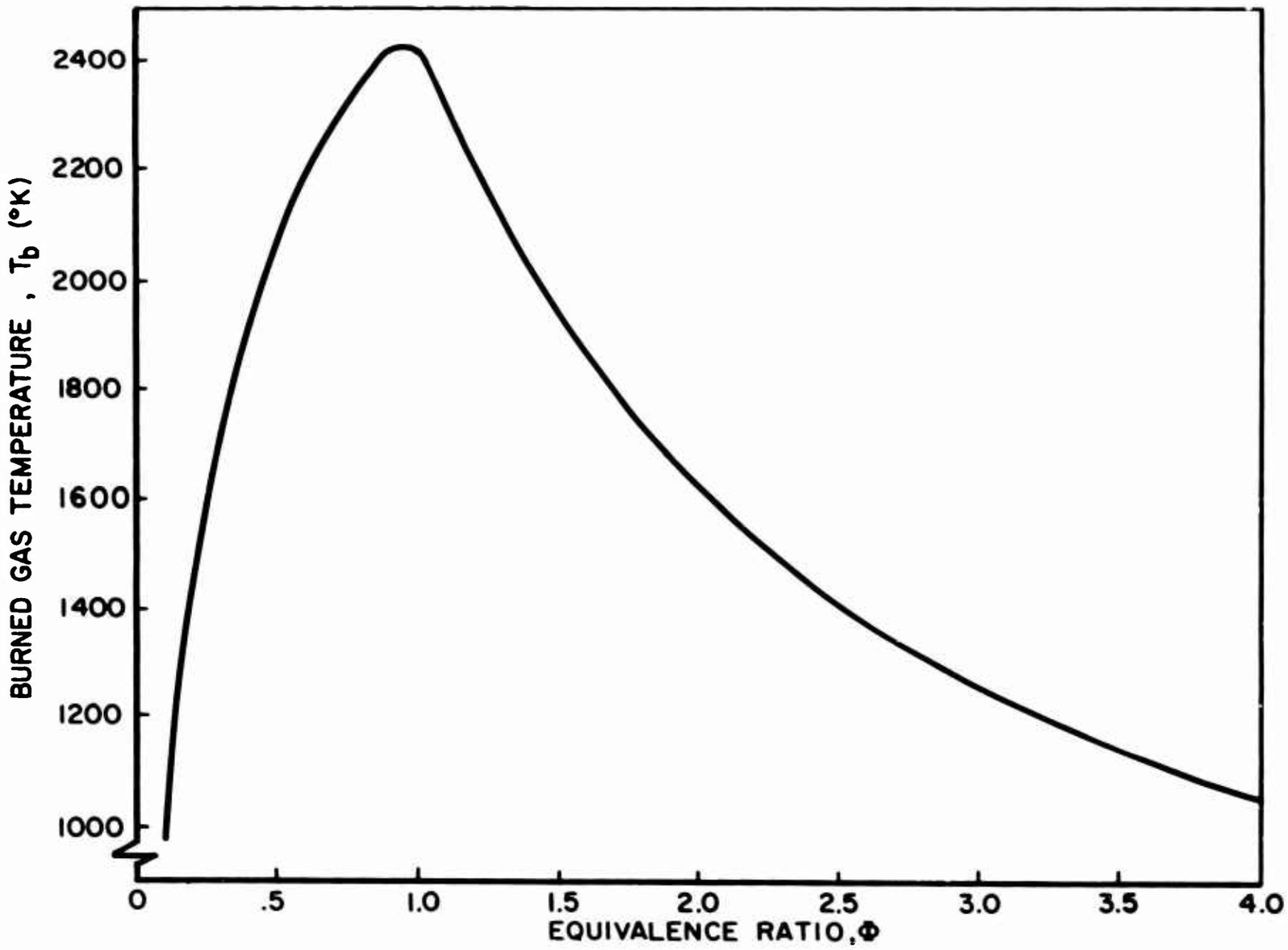

FIGURE IV-9

THEORETICAL ADIABATIC COMBUSTION TEMPERATURE AS A FUNCTION OF EQUIVALENCE RATIO FOR H_2 + AIR , $\bar{P}_c$ = 4.4 to 7.8 atm, T_u = 298 °K

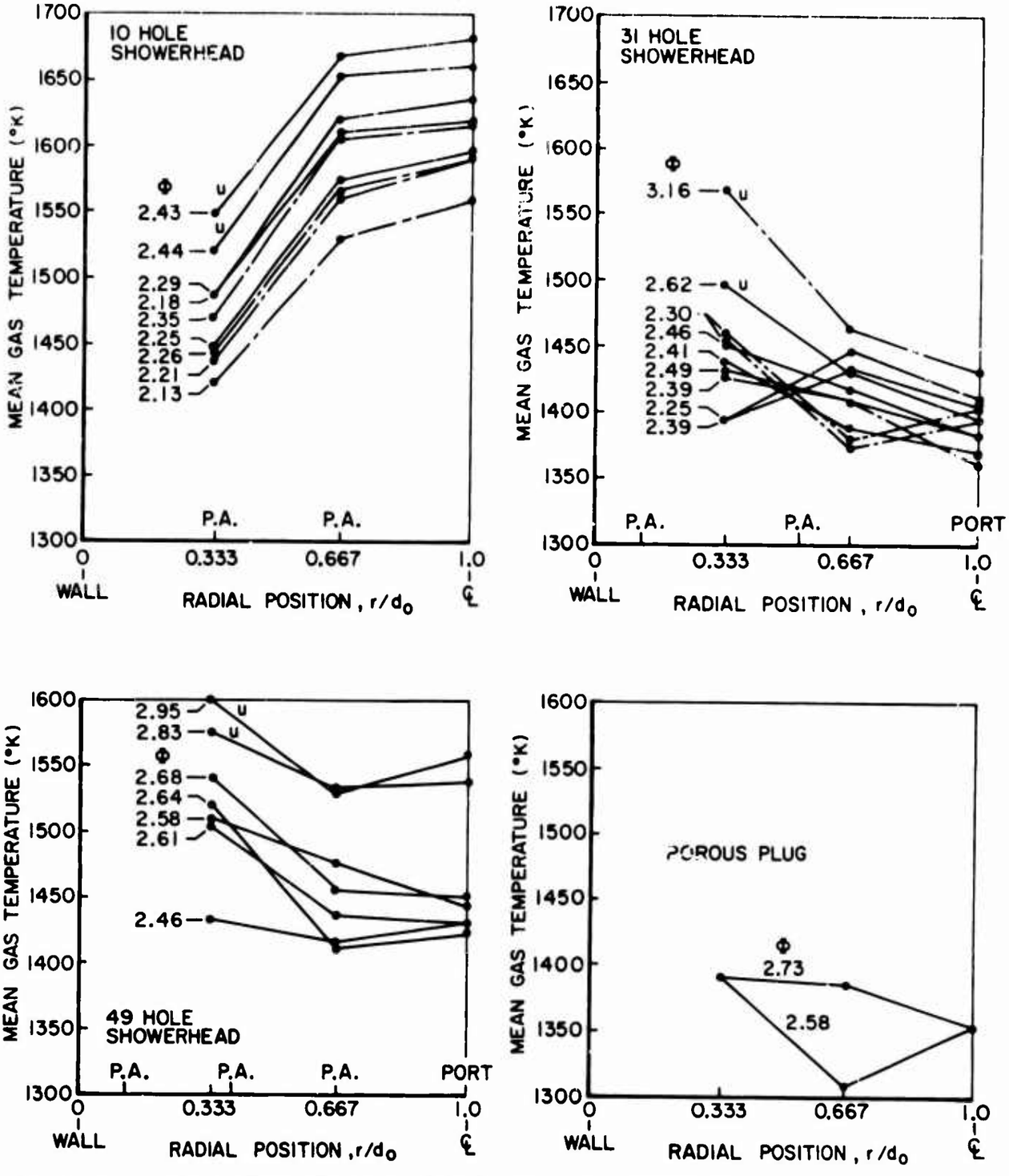

NOTE : u - INDICATES FUNDAMENTAL MODE OSCILLATION SUSTAINED
P.A.- INDICATES RADIAL LOCATION OF SYMMETRIC INJECTION PORT ARRAY (SEE FIG.)
PORT- INDICATES INJECTION PORT LOCATED ON CENTER LINE

MEASURED RADIAL PROFILES OF MEAN GAS TEMPERATURE(°K)
H_2 + AIR, $\bar{P}_c$ = 7.8 atm, Lc = 104 cm, 4 HOLE NOZZLE

FIGURE IV-10

sensitive to the position relative to the radial array of the injection ports and to apparent changes in the structure of the combustion zone with changes in Φ and with the appearance of nonsteady burning. For fixed radial position there is a general trend to the indication of higher temperature with increasing Φ (decreasing T_b) and furthermore measured temperatures generally increase to magnitudes in excess of T_b. The data for the 49 hole showerhead experiments systematically indicate temperatures in excess of the T_b.

The measurement of temperatures in excess of the theoretical maxima was felt to be an indication of catalytic heating accompanying the recombination of reaction intermediates at the thermocouple junction. This underscored the necessity for using coated thermocouples when probing the gas rocket H_2 + Air combustion zone and also demonstrated the inaccuracy inherent in earlier axial temperature profile measurements. In the experiments $\dot{m}_{tot}$ remained essentially fixed with Φ variations achieved by varying the low H_2 mass flow rate. The increase in measured temperature with increasing Φ and with the onset of nonsteady burning was felt to be an indication of structural changes (radially and axially) in the combustion distribution occurring as the mixture was leaned.

Finally, it was not known what effect the radial proximity of the injection ports and thermocouple position had on the measured temperatures. The centerline thermocouple in the case of 31 and 49 hole showerhead injection was directly opposite a central injection port whereas in the case of the 10 hole showerhead the centerline thermocouple was located at 0.64 cm radially from the nearest port axis. In fact all of the data for the 10 hole showerhead injector correspond to zones located approximately equidistant from the injection port axes.

B.2 Combustion Zone Diagnostics: Measurement of Axial Temperature Profiles

The determination of axial profiles of the mean gas temperature in the combustion zone and the axial "extent" of the com-

bustion zone was the goal of the second series of diagnostic experiments. The results from the radial temperature profile measurements reinforced the belief that previously obtained "axial temperature profiles" in the combustion zone were highly suspect. In particular, the necessity to eliminate the possibility of catalytic effects due to the presence of large diameter uncoated Pt wire at the thermocouple junction had been demonstrated. Furthermore, the indication of the nonuniformity of the combustion zone perpendicular to the combustion chamber axis illustrated the need for axial temperature data at more than one radial position.

In order to remove the limitations accompanying previous attempts at these measurements several steps were taken. An axially traversing thermocouple probe and drive assembly similar to that already in use on the Princeton flow reactor (128) were designed. This enabled the measurement of a continuous temperature distribution over a 15 to 20 cm interval downstream from the injector face. Such a scheme also eliminated the unacceptable necessity of placing several thermocouples in close proximity along the combustion chamber axis. Figure IV-11 shows a photograph of the probe, drive assembly, and the modified gas rocket configuration employed during these experiments. To permit axial probe alignment a single combustion chamber section was modified to allow placement of the 4-hole tungsten nozzle at 90° to the chamber axis. A water-cooled end plate allowed the 0.63 cm (.25 in) diameter thermocouple probe to be traversed continuously. A positive pressure seal was provided around the probe shaft by an O-ring in the end plate. The probe traverse rate was variable but for the experiments discussed here was maintained at 0.317 cm/sec or several orders of magnitude lower than the mean flow velocity in the chamber.

In order to minimize the possibility of catalytic effects and to reduce conduction losses quartz coated thermocouples were constructed of .005 in Pt 6% Rh/Pt 30% Rh wire stretched between .020 in support wires of the same materials which also served as the cold junction lead wires. The quartz coating was applied to the .005 in wire by immersing the thermocouple in a bunsen flame

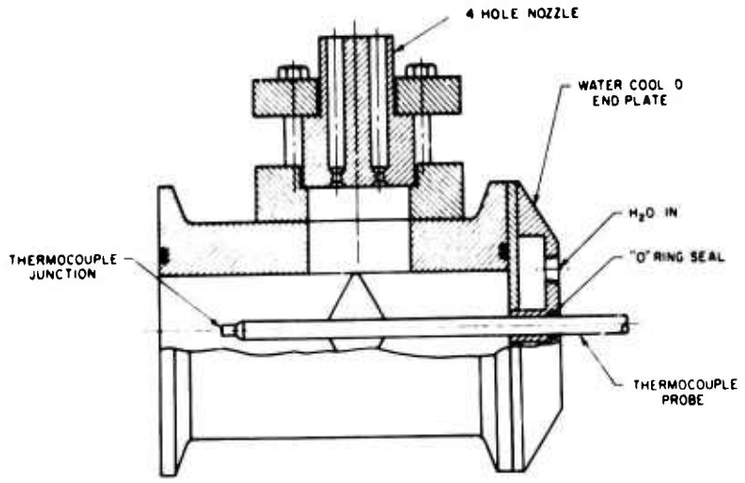

a) PROBE - CHAMBER CONFIGURATION

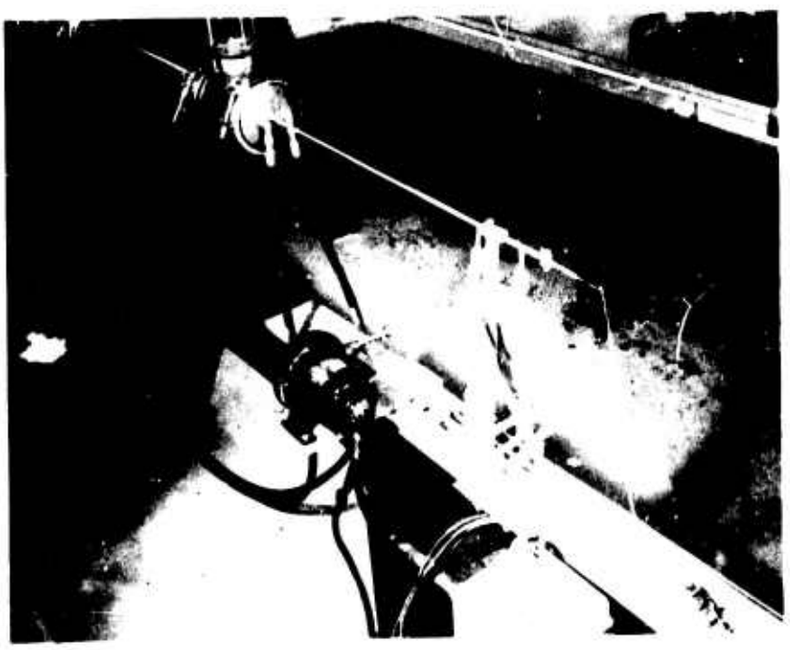

b) THERMOCOUPLE PROBE DRIVE

FIGURE IV-11

in which small quantities of hexamethyl-disiloxane had been burned (94, 128). It was not possible to coat the larger support wires. Both water-cooled and uncooled thermocouple probes were used. A sketch of the probe tip and thermocouple junction is shown in Figure IV-11a.

In addition to conduction losses[1] which were significant only with the H_2O-cooled probe, the principal source of error in the measurement of axial temperature profiles lies in the uncertainty of the thermocouple junction location relative to the chamber axis and to the injector face (assuming no disturbance of the combustion zone due to the probe). Note that measurements were made only during the inward traverse of the probe[2] and preliminary experiments indicated that the H_2 + Air system stability characteristics were insensitive to probe location in the chamber. Microswitches at the probe drive motor shaft and at the end of the drive mechanism provided an indication of probe location during the traverse. The total uncertainty in the axial thermocouple location is estimated at $\pm$ 0.2 cm and includes an allowance for probe expansion in the case of uncooled probes.

The uncertainty in the radial position of the thermocouple is higher for several experiments where an injection port was located at the chamber centerline (31 hole showerhead injector). No systematic temperature measurements could be obtained along the motor center line and within 3 cm of the injector for such an injection configuration because of distortion or breakage of the thermocouple wires presumably due to excessive drag forces arising from the high velocity field associated with the injection port flow. This observation in itself is important and will be commented on later. Repeatable profiles of temperature in such cases could only be secured by offsetting the thermocouple junction with respect to the axes of the injection ports. Temperature measurements with the 10 hole showerhead and porous plug injector were made along the motor centerline. Temperature measurements with the 31 hole showerhead injector were made by bending the support wires so as to place the thermocouple junction ap-

---

[1] Radiation losses are considered small as discussed earlier (page 110).

[2] In order to minimize distortion of the combustion zone due to the presence of the probe.

proximately midway between the motor centerline and the first circle of injection ports (i.e., at approximately 0.432 cm off the centerline).

Axial temperature profiles were measured with the 10 hole showerhead injector at $\bar{P}_c$ = 4.4 atm, 31 hole showerhead injector at $\bar{P}_c$ = 4.4 and 7.8 atm and the porous plug injector at $\bar{P}_c$ = 4.4 atm. All experiments were carried out with L_c = 38 cm and the 4 hole nozzle offset at 90° to the chamber axis. Temperature profiles were obtained for $\Phi > 1.7$. With reference to Figure II-9, the onset of nonsteady burning occurs at approximately $\Phi = 2.3$ to 2.4 for the 10 and 31 hole showerhead injectors.

Figures IV-12 to IV-17 summarize the results of these experiments. Typical (raw data) temperature profiles obtained with the 10 hole and 31 hole showerhead injectors for $\bar{P}_c$ = 4.4 atm ($\dot{m}_{tot}$ = 14 gms/sec) and uncooled probe are shown in Figures IV-12 and IV-13. Figure IV-13a shows the sharp discontinuity in the temperature traces at two different Φ's for the case of 31 hole showerhead injection where the thermocouple junction was placed initially on the motor centerline. Examination of the probe tip following such traces revealed that the support wires had been bent off axis. Generally a failure of the .005 in wire resulted. For those runs where the thermocouple remained intact the axial location of the abrupt discontinuity was remarkably repeatable. Figure IV-13b is typical of temperature traces obtained with the support wires initially bent and the thermocouple junction located off the motor centerline (referred to as off-axis profiles). Figure IV-14 summarizes the mean profiles obtained with the 10 hole showerhead injector. All profiles were obtained along the centerline of the combustion chamber. Figures IV-15 and IV-16 summarize the results obtained with the 31 hole showerhead injector with the off-axis sensing junction for $\bar{P}_c$ = 4.4 atm and $\bar{P}_c$ = 7.8 atm. Figure IV-17 presents the results for the case of porous plug injection.

The data represent (smoothed) uncorrected mean gas temperatures. The importance of conduction losses in the apparent local temperature sensed by the water-cooled probe is evident in

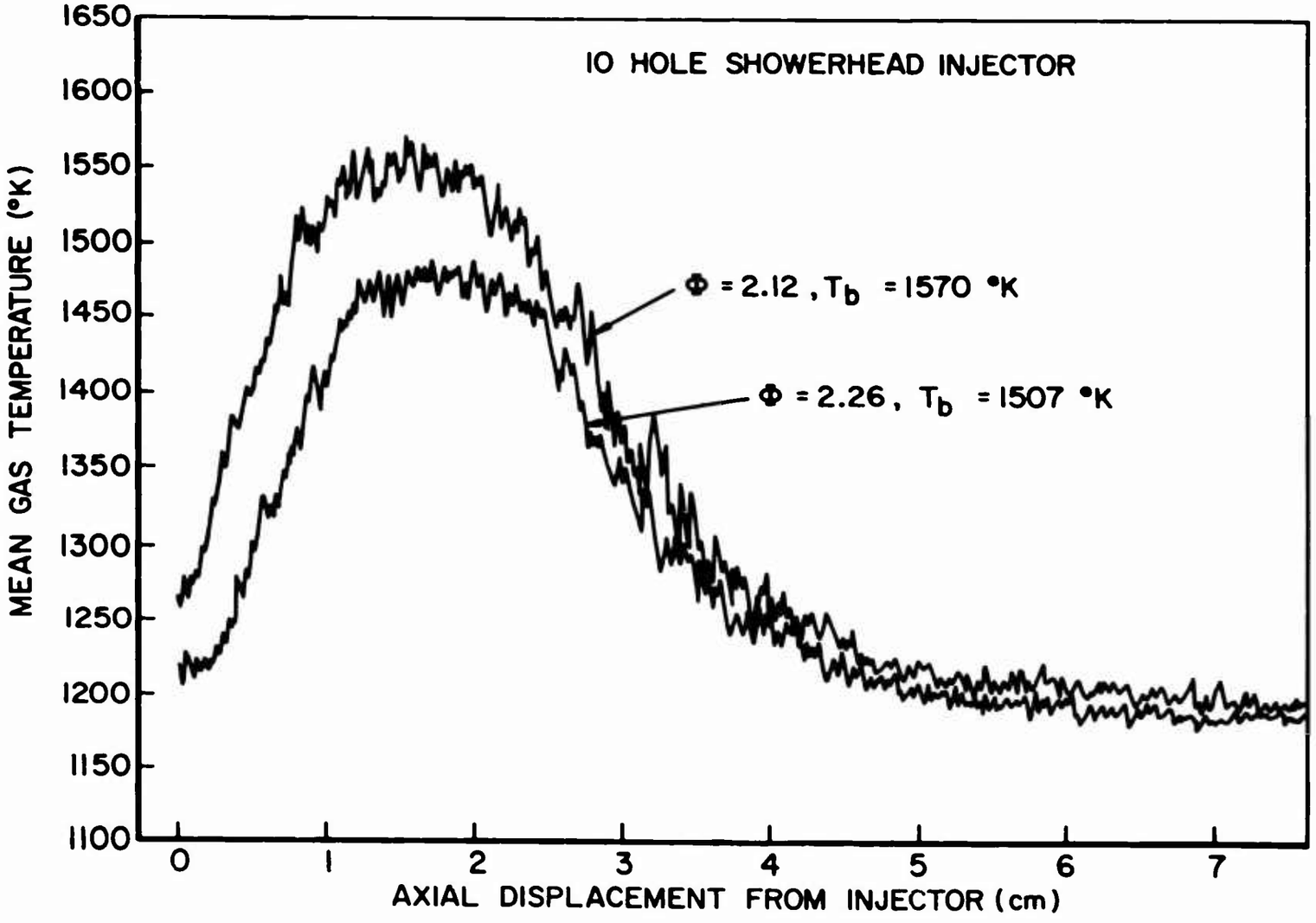

TYPICAL AXIAL TEMPERATURE PROFILE FOR H_2 + AIR,
4 HOLE PLUG NOZZLE, UNCOOLED PROBE, $\bar{P}_c$ = 4.4 atm, L_c = 38 cm

FIGURE IV-12

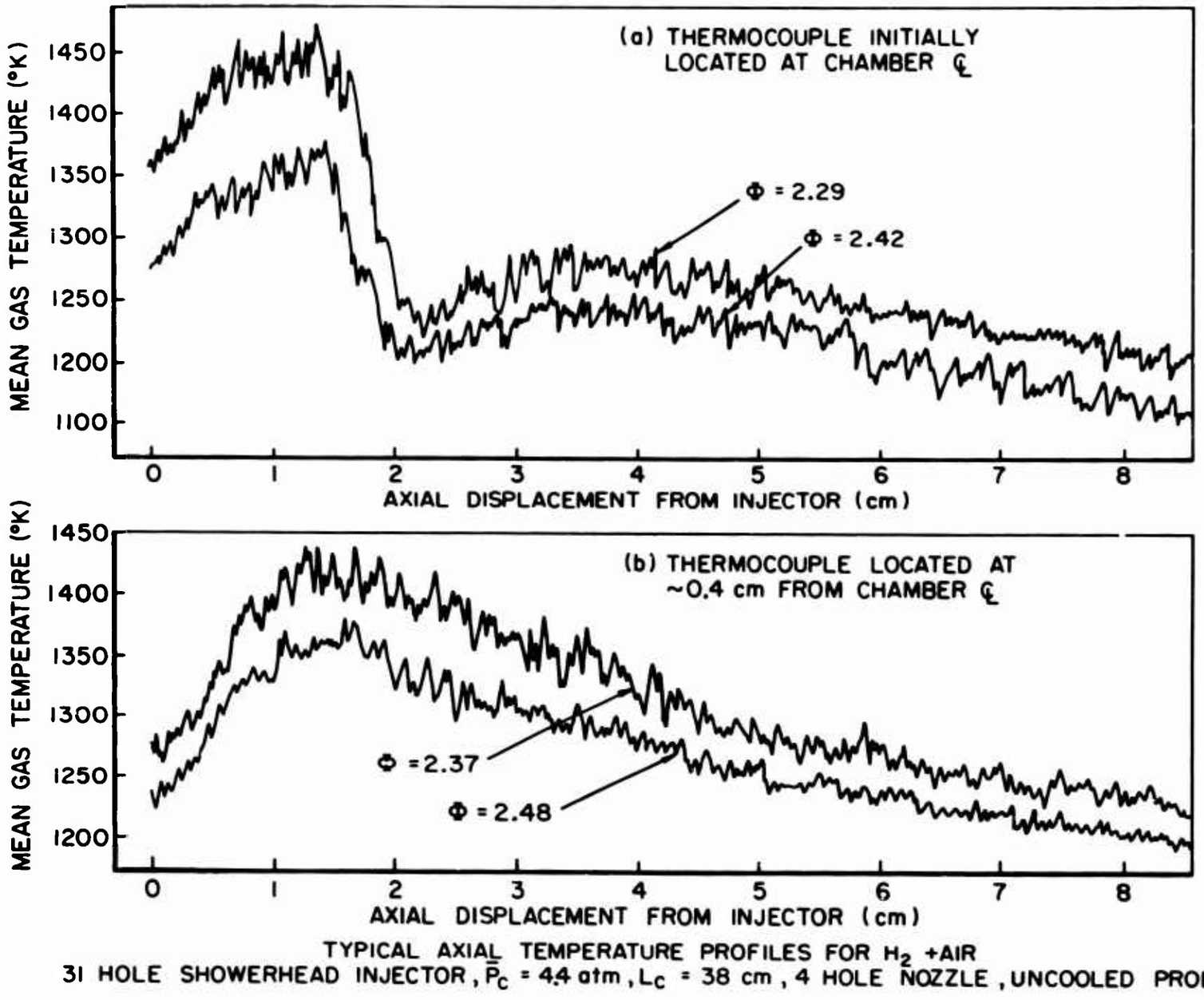

FIGURE IV-13

TYPICAL AXIAL TEMPERATURE PROFILES FOR H_2 +AIR
31 HOLE SHOWERHEAD INJECTOR, $\bar{P}_C$ = 4.4 atm, L_C = 38 cm, 4 HOLE NOZZLE, UNCOOLED PROBE

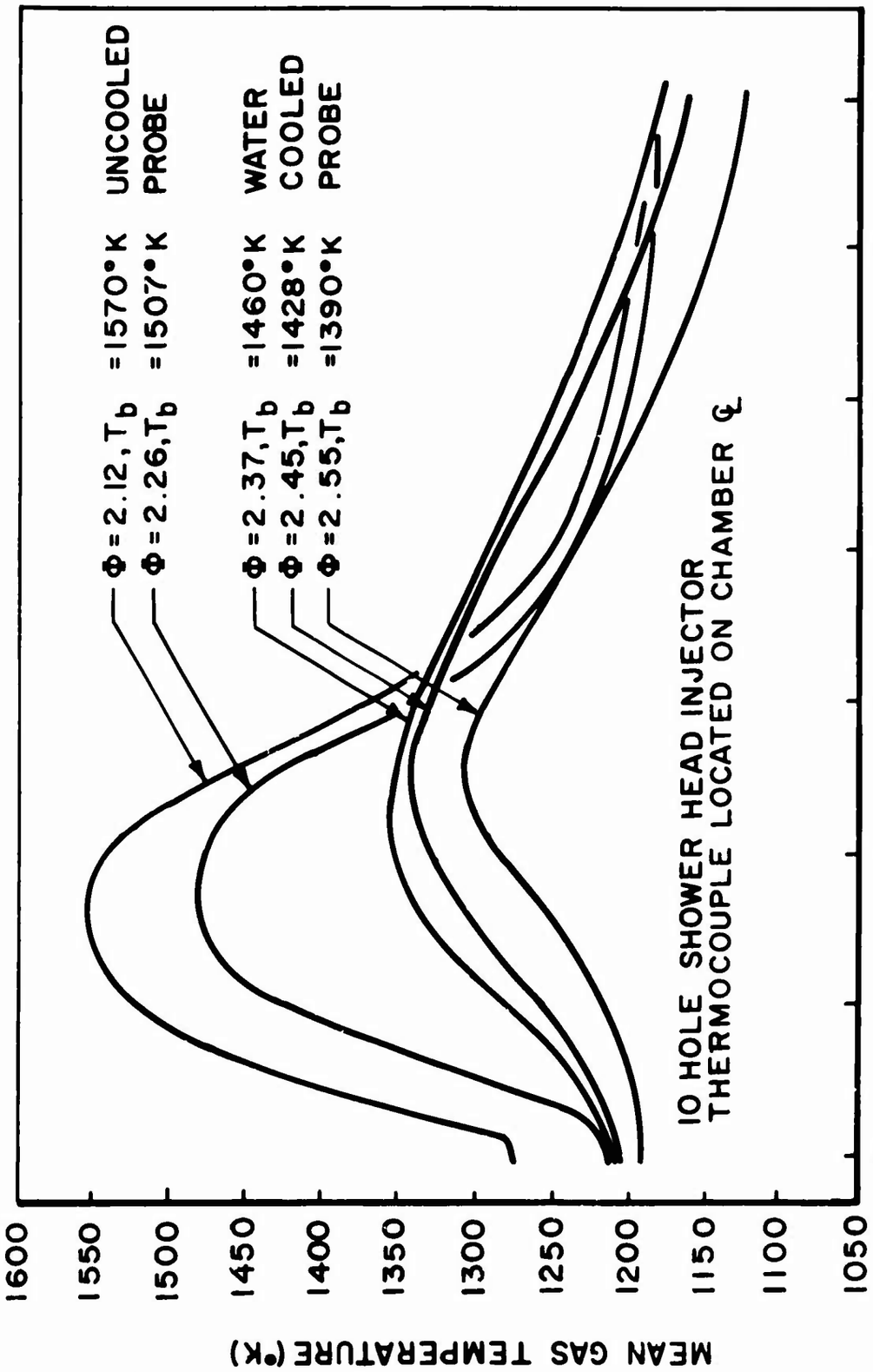

AXIAL PROFILES OF MEAN GAS TEMPERATURE (°K)
H_2 + AIR, $\bar{P}_c$ = 4.4 ATM, L_c = 38 cm, 4 HOLE PLUG NOZZLE

FIGURE IV-14

FIGURE IV-15

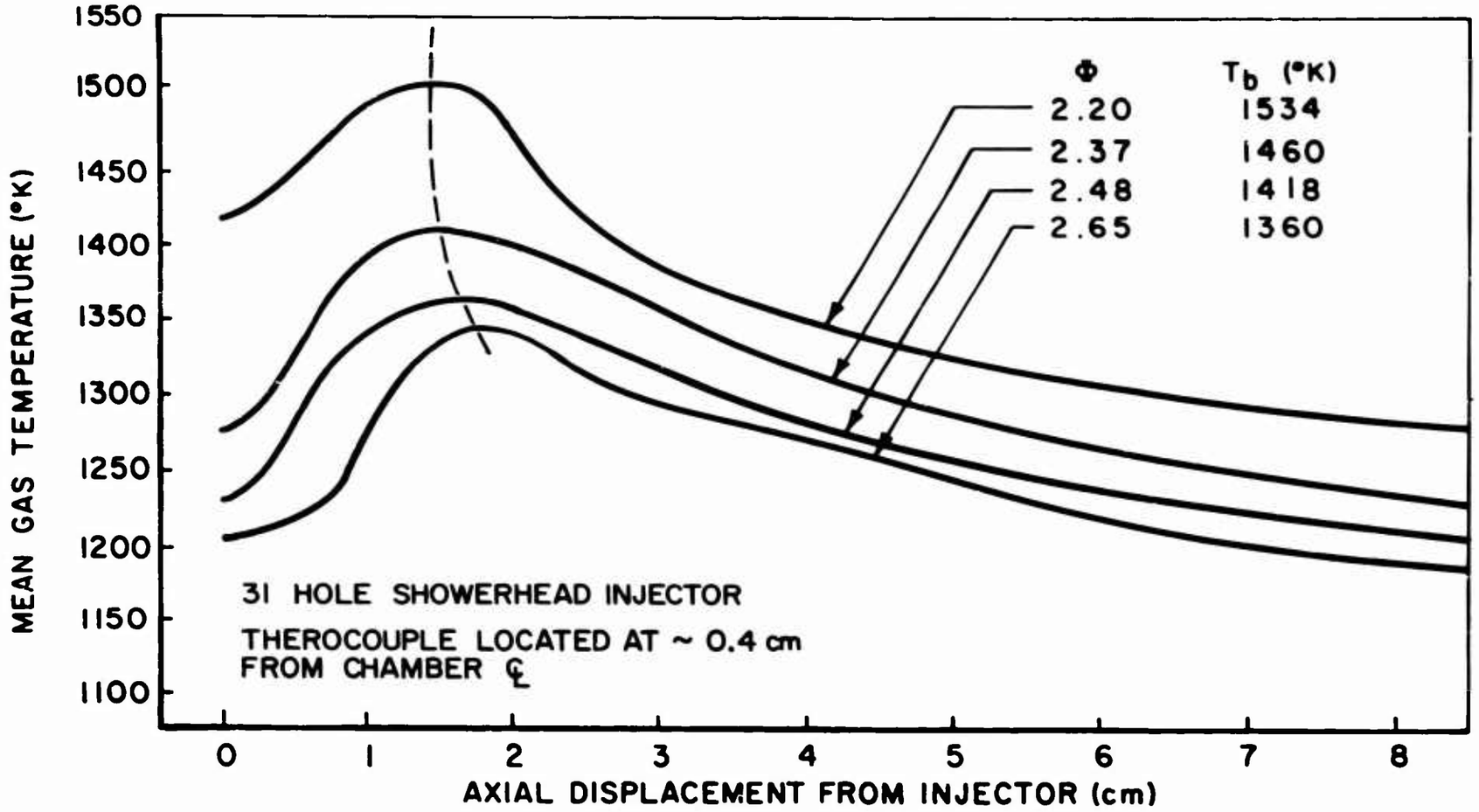

AXIAL PROFILES OF MEAN GAS TEMPERATURE (°K)
H_2 + AIR , $\bar{P}_c$ = 4.4 atm , L_c = 38 cm, 4 HOLE PLUG NOZZLE, UNCOOLED PROBE

JP 13 R 4182 70

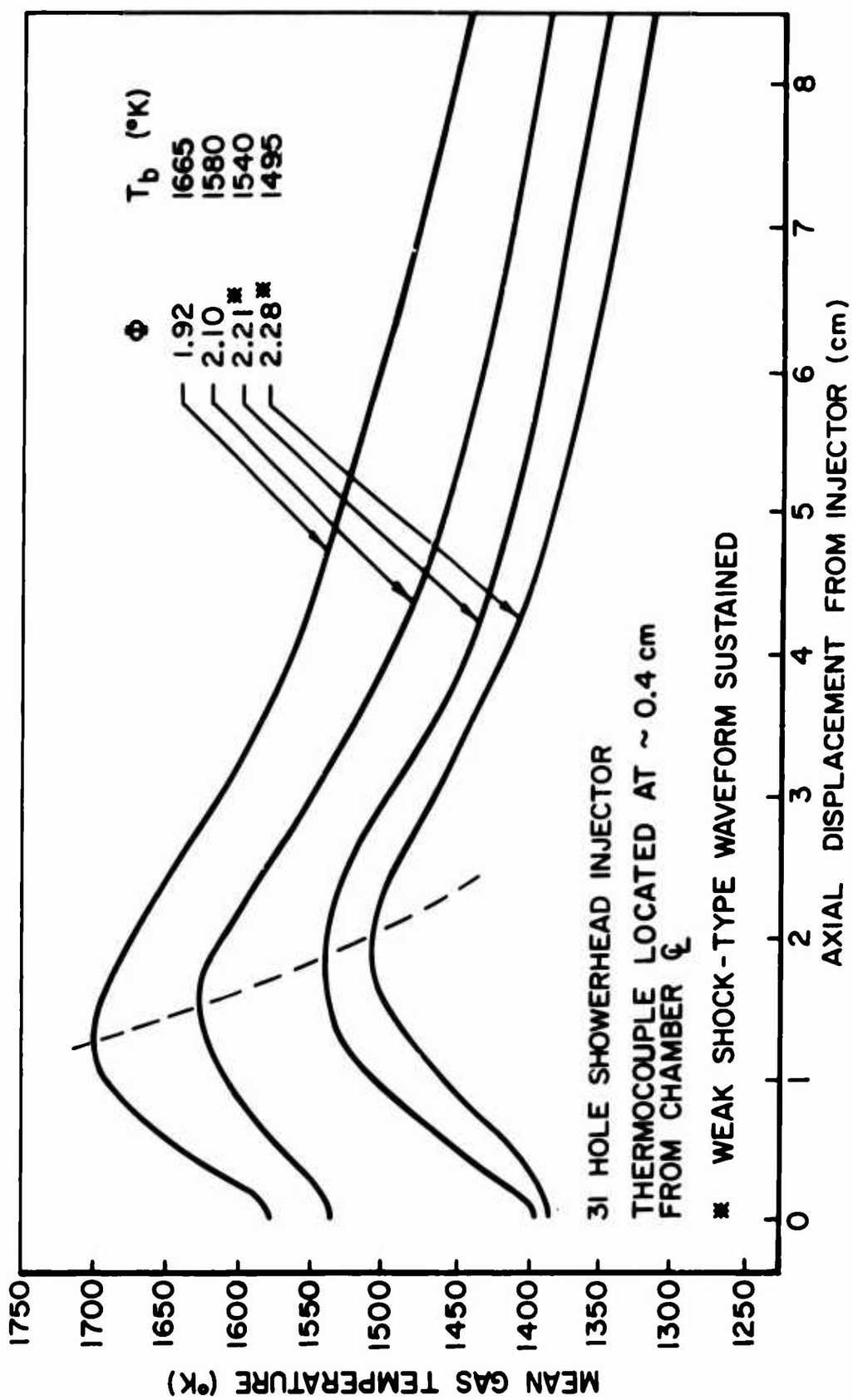

AXIAL PROFILES OF MEAN GAS TEMPERATURE (°K)
H_2 + AIR, $\bar{P}_c$ = 7.8 atm, L_c = 38 cm, 4 HOLE PLUG NOZZLE, UNCOOLED PROBE

FIGURE IV-16

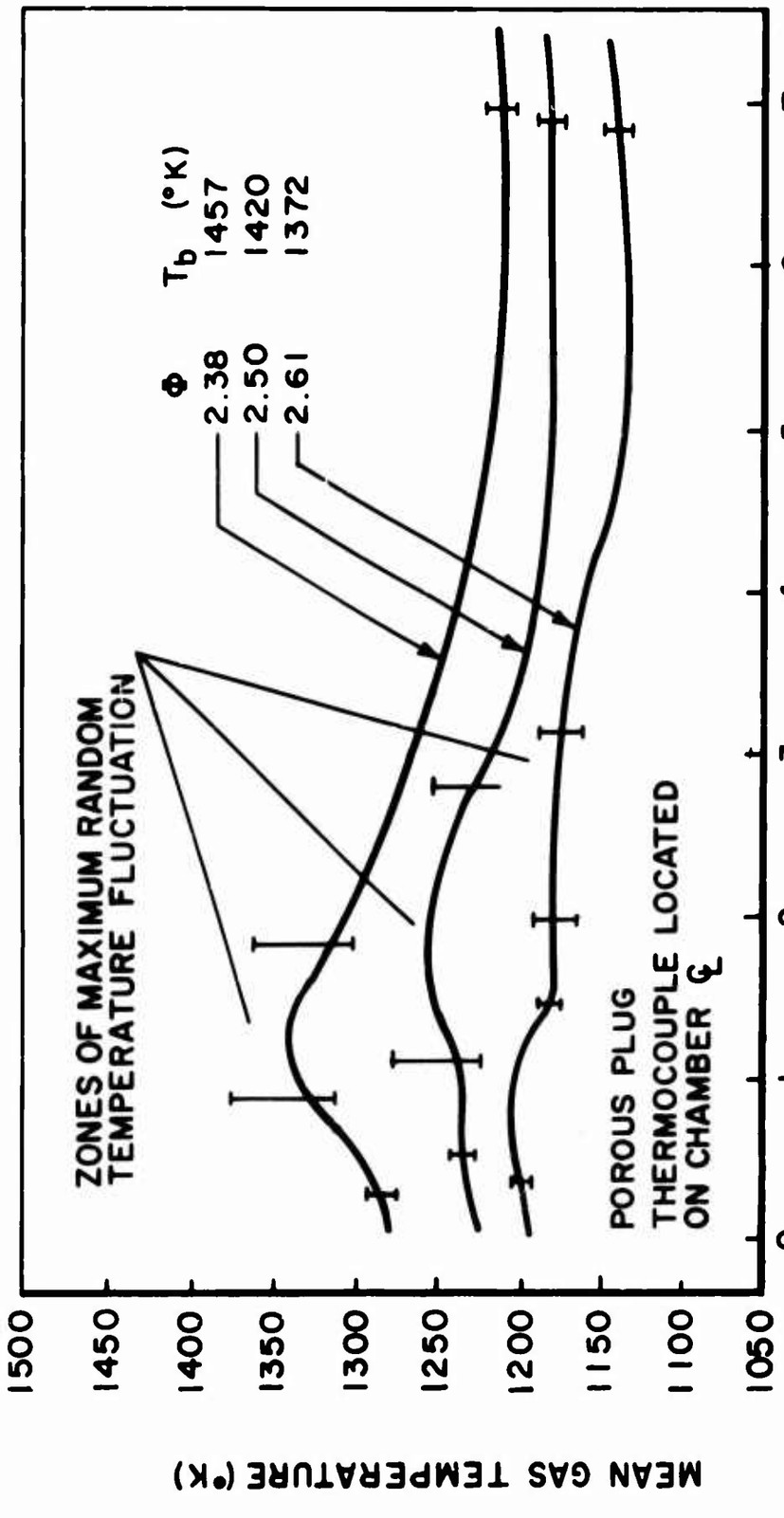

AXIAL PROFILES OF MEAN GAS TEMPERATURE (°K)
H_2 + AIR, POROUS PLUG INJECTOR, $\bar{P}_c$ = 4.4 ATM,
Lc = 38 cm, 4 HOLE PLUG NOZZLE, WATER COOLED PROBE

FIGURE IV - 17

data obtained with the 10 hole showerhead injector. In general the maxiumum of the random fluctuations in temperature for the 4.4 atm experiments were of the order of 3% of the mean local gas temperature. Larger amplitude fluctuations up to 7% of the mean temperature were observed in the 7.8 atm experiments.

Several trends in the temperature data obtained with the showerhead injectors were noted. With increasing Φ the overall temperature profiles are depressed (as expected) in contrast to the results obtained with the uncoated thermocouples in the radial profile measurements. All traces exhibit the characteristic humped shape with the broadened peaks ($\bar{P}_c$ = 4.4 atm) located at 1 to 1.5 cm from the injector face for the 31 hole showerhead injector and at 1.5 to 2 cm from the injector for the 10 hole showerhead injector. In general the temperature maxima are 0 to 5% lower than the theoretical adiabatic combustion temperature. The absolute magnitudes of the random fluctuations in temperature in the vicinity of the temperature maxima are on the order of twice those observed downstream. There is a measureable shift in the maxima away from the injector for both the 10 and 31 hole injectors with decreasing Φ for fixed $\dot{m}_{tot}$ and $\bar{\rho}_c$. A comparison of the 31 hole showerhead temperature profiles obtained at Φ = 2.20 for $\bar{\rho}_c$ = 4.4 and 7.8 atm shows that a similar shift in the maximum temperature zone occurs with increasing $\bar{\rho}_c$ and $\dot{m}_{tot}$.

In terms of our present understanding of the combustion process, the negative results obtained with the centerline traverses (Figure IV-13a) in the case of the 31 hole showerhead injector are important. Beyond the 3.5 cm point the temperature profiles are similar to those obtained with the off axis probe. Between 2 and 3.5 cm the temperature is observed to decrease as the injector is approached, followed reproducibly by an abrupt rise to a temperature typical of the maximum observed in the off-axis traverses. These results were felt to be indicative of the persistence of localized high velocity (perhaps slightly lower temperature) regimes at locations downstream from the injector previously envisioned to be filled with burned gas products at approximately the adiabatic combustion temperature. The physical

bending of the .020 in diameter support wires could only arise from the existence of extremely high drag forces associated with a high velocity port flow. Because of this phenomenon it was not possible to obtain temperature data along the chamber centerline with the 31 hole showerhead injector. The lower temperatures sensed along the centerline (ignoring the fact that the local Mach number may not be low in this region) indicate that along the port axes combustion is not complete in these regions. When these results were contrasted with the substantially smoother profiles recorded for off-axis profiles (in the case of both 10 and 31 hole injection) the following inferences were drawn regarding the measured temperature profiles: (1) For the case of choked showerhead injection the combustion zone seems to be characterized by the existence of regimes of cooler high velocity (mixing and combusting) gases which persist 2 to 3 cm into the combustion chamber and which are surrounded by zones of high temperature gases; (2) It was not clear whether the broadened temperature peaks found in the off-axis traverses and located at 1 to 3 cm from the injector and the observation that the random noise on the thermocouple output generally doubled or tripled in this region were indicative of a reaction zone; (3) The gradual temperature decay 2 to 3 cm downstream of the peak temperature is due to the nonadiabaticity of the gas rocket. The axial temperature gradient downstream from the combustion zone due to heat loss is estimated to be 5 to 10^{o}K/cm; (4) The cause of the steeper decays in the temperature profiles just upstream and downstream of the maxima was not immediately evident. It was recognized that the decrease may be an accurate record of a temperature profile in the zone arising due to the complex interaction of turbulent mass and energy transport in a nonadiabatic system or may simply be the result of the increasing importance of thermocouple losses due to radiation and heat conduction in regions of diminished effective heat transfer coefficient; (5) No unusual changes in the measured temperature profiles were observed as the stability limit was crossed.

The profiles obtained with porous plug injection are typically quite flat becoming more so as the propellant mixture is leaned. As indicated in Figure IV-17 the profiles are characterized by a region in which the amplitude of the random signal increases markedly and (depending on the Φ) where somewhat higher mean temperatures are recorded. It is not clear whether this region arises due to a concentration of combustion in the zone or due to a complex turbulent exchanges. For the porous injector used in these experiments it is observed that the displacement of this zone from the injector increases with increasing Φ (decreasing T_b) at constant $\dot{m}_{tot}$. Such behavior is to be expected if the reaction is kinetically controlled. However, the wide variation of porosity across the face of the plug plus the variation among individual plugs prevents any definite statement regarding the temperature distribution in the porous plug combustion zone.

On the basis of these temperature data it was difficult to draw really substantive conclusions regarding the nature of the gas rocket combustion zone. The presence of strong radial and axial inhomogeneities in the combustion zone was evident. The concepts of a relatively thin flame sheet or of a more or less uniformly distributed combustion zone in a low mean flow Mach number field were not supported by the temperature data. While the temperature profiles ultimately obtained are certainly not representative of profiles through a distributed combustion zone, the location of the temperature maxima in the off-axis profiles (for the showerhead injectors) serve as valid indicators of the extent or maximum length of the combustion zone. On the basis of the temperature data it can be argued that the length of the combustion zone increases with decreasing combustion temperature (mixture strength) and increasing total mass flux (increasing $\bar{\rho}_e$). Furthermore for fixed Φ and $\bar{\rho}_e$ the extent (ℓ) of the combustion zone increases in accordance with

$$\ell_{\text{porous plug}} < \ell_{31 \text{ hole}} < \ell_{10 \text{ hole}}.$$

Finally, an important observation follows on the basis of the close approach of the maximum measured temperatures to the adiabatic

combustion temperatures, namely, that the combustion efficiency is 100% with respect to the deficient species. Product gases leaving the combustion zone for $\phi > 1$ must consist only of H_2O and excess air oxidizer.

Because of apparent inhomogeneities in the velocity and thermal fields of the combustion zone it was clear that further temperature measurements could add little information.

C. Combustion Zone Diagnostics: Direct Photographic Observation of the H_2 + Air Combustion Zone During Steady Combustion

The radial and axial measurements of the combustion zone temperature indicated the need for more explicit information about the combustion zone structure. The temperature data had shown that the concept of a completely one-dimensional combustion zone was not valid for the case of showerhead injection. It seemed that the most useful information would be direct photographic records of the combustion zone under conditions of steady and nonsteady burning. The following paragraphs describe the series of experiments designed to obtain direct photographs of the gas rocket combustion zone.

C.1 Modification Of The Gas Rocket System

To facilitate direct observation of the combustion zone the design and fabrication of a new quartz windowed combustion chamber section was necessary. A schematic and photograph of the chamber section with a showerhead injector in place are shown in Figure IV-18. The original design provided for a single 1.9 cm thick quartz window to be positioned at the injector so as to allow observation of a 1.3 cm wide region extending from the injector face to 6.4 cm downstream. As indicated by the axial temperature profile measurements this would allow the significant axial and radial features of the combustion zone to be examined at pressures up to 7.8 atm. The windows were flush mounted with the chamber wall to minimize distortion of the internal chamber cross section at the injector and were cushioned in a removable window

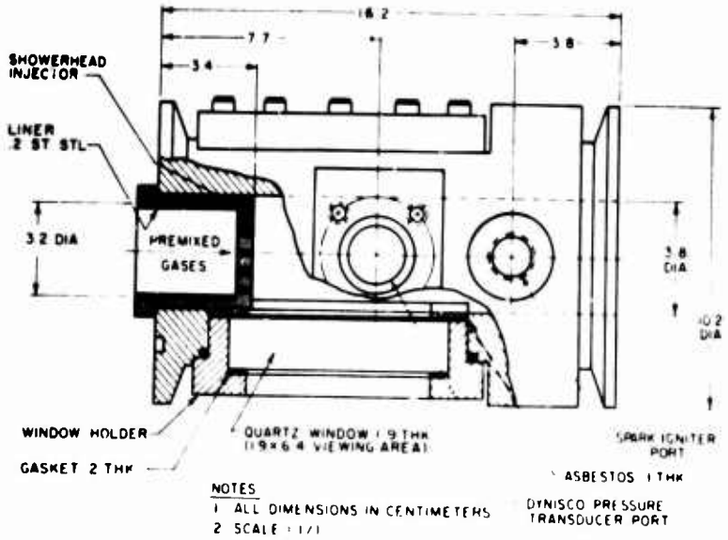

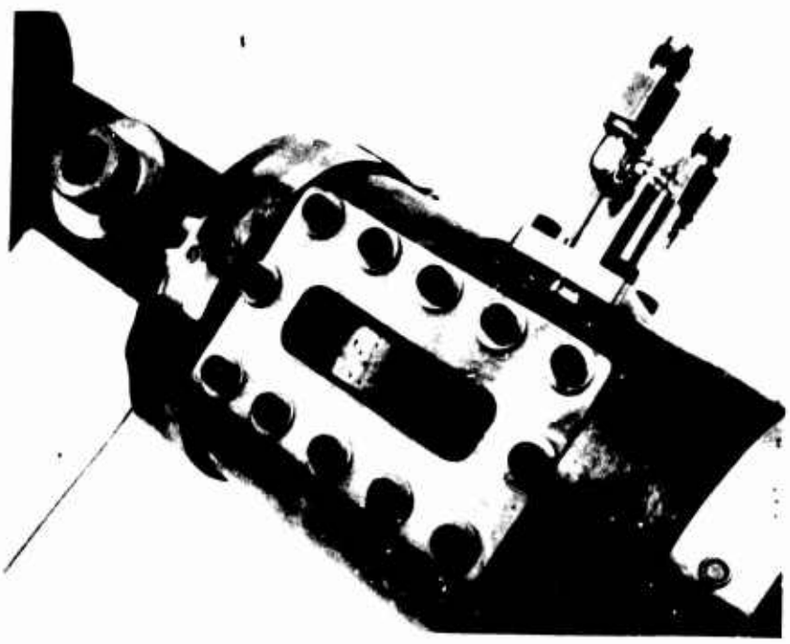

COMBUSTION CHAMBER SECTION USED FOR DIRECT PHOTOGRAPHS

FIGURE IV-18

holder by an asbestos gasket. The chamber section was machined to accommodate a spark igniter and a single Dynisco pressure transducer at 4.3 cm from the injector. Showerhead injectors were machined so as to permit choked injection of the unburned premixed gases. It was necessary to insert a 0.076 cm stainless steel liner in the injector cavity to reduce heat transfer to the mixing chamber gases. In the absence of the liner ignition of the low velocity gases in the mixing chamber occurred due to heat feedback during the 20 to 40 second period of operation.

C.2 Choice Of Propellant System

The H_2 + Air system was selected for the initial series of experiments. Basically the same reasoning applied here as did in the decision to use H_2 + Air in the temperature measurements, i.e., ignitability, wide blowoff limits, and the abundance of experimental stability limit data for showerhead injection. In particular, the relative case of ignition of the H_2 + Air system was important. In view of the extremes of temperature and pressure encountered in the combustion zone especially during the ignition and flow buildup portion of the experiment, the thermal limitations of the quartz windows, and the fact that it was necessary to dispense with the external spray cooling of the combustion chamber during the optical work the requirements of controlled low ignition transient and minimum run time were important.

C.3 Experimental Technique

It is well known that the H_2 + Air flame is essentially nonluminous in the visible region of the spectrum (Gaydon (150)). It was hoped that this characteristic could be used to advantage. By adding controlled amounts of NaCl to the premixed gases issuing from a single injection port the contribution to the overall combustion process of individual injection port flows could, in principle, be examined during steady and nonsteady combustion. By carrying out the experiments over a range of $\bar{P}_c$, $\dot{m}_{tot}$ and Φ, it was hoped to substantiate the trends (regarding the combustion distribution as a function of these parameters) indicated by the

temperature measurements.

It was recognized that the reduced thermal emission from the NaCl additive in the range of Φ of interest could be a limiting factor. Most of the Na line-reversal work reported in the literature is confined to combustion temperatures in excess of 2000°K (151) with sensitive experiments reported down to 1700°K. Fristrom and Westenberg (85) have recently noted that no appreciable emission of the Na doublet occurs at temperatures below 1700°K.

A series of preliminary investigations were carried out in order to (a) determine a reliable ignition and operation sequence, (b) establish the allowable range of Φ , $\bar{P}_c$ and run time in terms of minimizing window deterioration, (c) establish a reliable means of seeding a single injection port flow with NaCl, and (d) determing the allowable range of Φ (combustion temperature) in terms of providing sufficient luminosity for photographic purposes. The results of these investigations were disappointing. In order to achieve sufficient Na D-line emission it was necessary to restrict operation to $\Phi < 1.60$, that is to H_2 + Air mixtures having $T_b > 1875°K$. Furthermore operation with these mixtures invariably led to severe and unacceptable window deterioration at chamber pressures in excess of 4 atm and run times in excess of 15 seconds. Despite numerous attempts at Na-seeding the flow to individual ports it was impossible to selectively seed the combustion process associated with individual port flows. The basic difficulty encountered here was the necessity to use an in house source of high pressure air which contained sufficient Na impurities to mask specially imposed additive effects.

Thus prior to actual data runs several of the immediate objectives were voided. The critical temperature (T_{lim}) associated with the lower stability limit of the H_2 + Air system is of the order of 1450°K. That is, mixtures where $\Phi < 2.40$ with $T_b > 1450°K$ do not support unstable combustion. Therefore the minimum temperature limitation imposed by the necessity to obtain sufficient luminosity from the Na impurities precluded the application of the technique of direct photography to the examination of the nonsteady combustion zone of H_2 + Air. The requirement that

$\Phi < 1.6$ for photographic purposes also prevented the examination of the Φ regime immediately adjacent to the nonsteady regime. With operation restricted to the high temperature regime and the necessity to minimize window deterioration experiments were restricted to $\bar{P}_c$ = 2 to 4 atm. For the lower $\dot{m}_{tot}$ required run times could be maintained at less than 15 seconds by presetting the upstream stagnation pressures in the H_2 + Air system at the desired operating points. The conditions of choked mass injection flux was maintained.

All photographs of the H_2 + Air combustion zone were obtained with a Graflex Speed Graphic 4 in x 5 in camera using a Polaroid Land Film Holder. The camera was equipped with a 135 mm f4/7 lens. Two #3 Ednalite close-up lenses were added to provide an enlarged image. With the 3 lens array the depth of field in the photographs is approximately 0.5 cm. Polaroid (ASA) 3000 film was used. Remote shutter operation was controlled manually.

C.4 Direct Photographs Of H_2 + Air Combustion

Direct photographs of the steady combustion of H_2 + Air were obtained under the following gas rocket system conditions:

Φ = 1.2 to 1.6

$\bar{P}_c$ = 2 to 4 atm

$\dot{m}_{tot}$ = 8 to 10 gms/sec

L_c = 20.5 cm

4 hole plug nozzle

Choked showerhead injection (10 and 11 holes)

$\bar{P}_{mix}/\bar{P}_c \geq 2$

Exposure times were varied from 0.02 to 0.5 seconds. Thus in terms of the estimated gas residence times (maximum) the photographs yield time-mean records of the combustion process.

Typical direct photographs of the H_2 + Air combustion zone under the above conditions (0.5 sec exposure time) are shown in Figure IV-20a, b. For reference the injection configuration per-

tinent to the photographs is shown in Figure IV-19 below. The camera was focussed on the plane of the port designated by the arrow. The photograph of Figure IV-20a corresponds to the 11 hole arrangement shown while IV-20b corresponds to a 10 hole configuration obtained by sealing the port located directly behind the "arrowed" port in the line of sight.

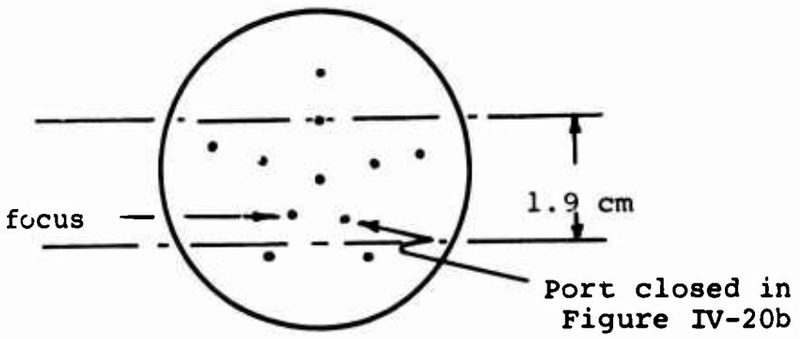

Figure IV-19

In view of the extreme sensitivity of the Na D-line emission intensity to temperature it is clear that the luminous zones observed in the photographs correspond to the high temperature regions of the combustion zone.

The complete set of photographs indicate that the combustion zone is characterized by the existence of turbulent combustion zones (referred to on the basis of the photographs as flames or turbulent flamelets) centered at each injection port of the choked flow showerhead injector and extending axially into the combustion zone. Each "flame" has the dark inner core zone with the surrounding luminous mantel characteristic of turbulent jet flames. In view of the characteristic jet Reynolds number of 6×10^6 based on the port diameter and the broadened zone of luminosity it would seem that the appropriate turbulence regime is that of small scale high intensity turbulence.

The photographs indicate no interaction between adjacent

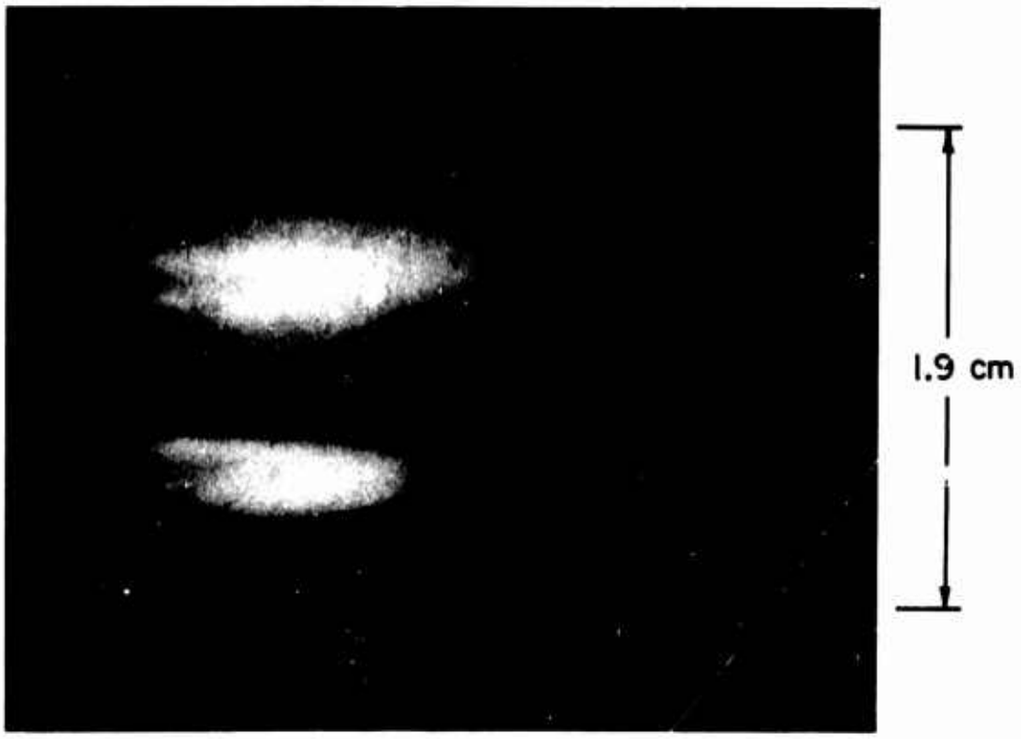

a) 11 HOLE SHOWERHEAD, $\Phi = 1.5$, $\bar{P}_c = 2$ atm

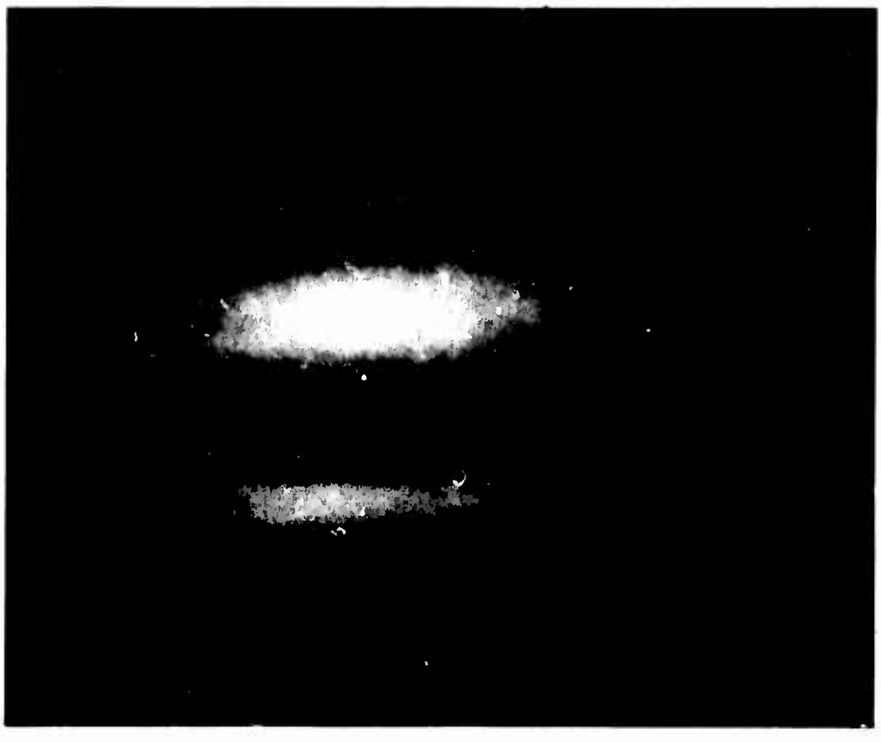

d) 10 HOLE SHOWERHEAD, $\Phi = 1.3$, $\bar{P}_c = 3.5$ atm

TYPICAL DIRECT PHOTOGRAPHS OF STEADY H_2 + AIR COMBUSTION

FIGURE IV-20

flamelets in the absence of sustained shock wave instability. The transparency of the zones surrounding the flames coupled with the temperature measurements indicates that these regions are filled with recirculating combustion products which have been slightly cooled through turbulent energy exchanges with the nonadiabatic chamber walls. Indeed this observation provides a partial explanation for the measurement of combustion temperature maxima somewhat below the adiabatic combustion temperature in the axial profile experiments.

In view of the fact that the photographs depict combustion of H_2 + Air at slightly lower Φ (higher T_b) and reduced $\dot{m}_{tot}$ as compared to the axial temperature measurements at $\bar{P}_c = 4.4$ atm it is not surprising that the axial extent of the luminous zones as measured in the photographs of the (10 hole showerhead) combustion zone, i.e., approximately 1.3 cm, is slightly less than the corresponding length of 1.5 cm (at $\Phi = 2.12$) determined from the temperature profiles. Therefore despite the relatively narrow range of parameters examined in these investigations it is felt that the photographs provide reliable indications of the principal features of the steady gas rocket combustion zone over the entire spectrum of operating conditions. Furthermore the extension of the dark zones of the turbulent flamelets approximately midway into the combustion zone supports the explanation (page 126) offerred for the unusual temperature profiles obtained with centerline traverses for the 31 hole showerhead injector. The dark zone must correspond to cool unburned premixed propellant. The temperature profiles indicate that while the velocity of the unburned propellant must decay from the sonic value at the injector port outlet (not precisely so for the case of underexpanded injection as will be discussed later), the velocity is still high at the end of the dark zone.

C.5 Implications Of Initial Diagnostic Experiments

In the Sirignano-Crocco model the combustion zone was assumed to be of zero length. This assumption facilitated the application of the combustion zone boundary condition to the analysis

of the wave equation in the combustion chamber at (dimensionless axial position) x = 0. In any analytical formulation of the completely coupled nonsteady combustion process it is somewhat simpler to treat the process as being concentrated in length relative to the overall chamber length ($\ell_c \ll L_c$) and concentrated in time (residence time of the propellant gases in the combustion zone τ_{res}) relative to the overall period of oscillation of "acoustic" waves in the combustion chamber ($\tau_{res} \ll \tau_{period}$). If indeed the first condition is satisfied then at any instant of time during the nonsteady process, although a pressure distribution over the entire chamber exists, the pressure may be considered constant over the combustion zone. On an instantaneous basis the momentum balance across the combustion zone may be replaced by the statement $P_c = P = p(t)$) and not $P_c = P(x, t)$. If the second condition is also satisfied then the approximation of combustion at constant pressure is valid for each elemental volume of propellant injected into the combustion zone, despite the fact that pressure is varying with time.

The direct photographs and the temperature profiles provided direct evidence that the approximation of a spacially concentrated combustion zone is a good one for the typical gas rocket conditions during steady and nonsteady combustion. Recall that mean axial temperature profiles were obtained during nonsteady combustion and showed essentially no change in the combustion distribution. Combustion zone lengths as determined by the temperature profile measurements are approximately 1 to 3 cm whereas overall combustion chamber lengths range between 12 and 150 cm. It should be remembered that the overall combustion lengths observed in the direct photographs are slightly shorter than those estimated from the temperature profiles and correspond to lower $\dot{m}_{tot}$. Such lower $\dot{m}_{tot}$ combustion is generally associated with shorter L_c for fixed $\bar{P}_c$ as indicated in Chapter III. That is, due to a small change in ℓ_c with changing $\dot{m}_{tot}$, ℓ_c/L_c undergoes a slightly different change with variations in L_c than would be expected on the basis of L_c variations alone.

The experimental data offer less concrete evidence as to the validity of the temporally concentrated combustion approximation. Initial estimates of the residence time of the propellant gases in the combustion zone and based on simple one dimensional considerations (flow area set equal to the total combustion chamber cross section, constant velocity and $\tau_{res} = l_c / \dot{m}_{tot} \cdot \bar{\rho}_b \cdot A_c$) indicated that $\tau_{res} / \tau_{per} = O(1 \text{ to } 1)$. In view of the diagnostic experiments discussed thus far this calculation seems dubious. Depending upon the mean velocity field throughout the combustion zone a range of residence times from $\tau_{res} / \tau_{per} << 1$ to $\tau_{res} / \tau_{per} = O(1)$ is conceivable. In Chapter V an estimate of the order of magnitude to be expected for this ratio is made on more reasonable grounds.

The direct photographs seemed to support the initial turbulent flame model of the combustion zone boundary condition. For the case of showerhead[1] injection the photographs supported the hypothesis that the gas rocket combustion zone can be described in terms of an array of identical, extended, noninteracting, cone-shaped, turbulent flamelets wherein high intensity small scale turbulence acts to increase the local gas transport processes (thereby thickening the flame front).

A principal shortcoming of the work up to this point was a failure to provide much information about the nonsteady burning process. While the axial temperature profile measurements had indicated no radical change in the temperature distribution with the onset of unstable combustion, direct photography could shed no light on the phenomena for the reasons noted earlier. An attempt at using the $CH_4/O_2/N_2$ system where $T_{lim} \cong 2400^{\circ}K$ in connection with direct photo-

---

[1] All measurements and discussion of nonsteady burning of H_2 + Air properly are restricted to showerhead type injectors. Implicit in these discussions is the assumption that the basic mechanisms of combustion in the gas rocket are identical with porous plug and showerhead injection. This is not a moot point. Specific arguments in support of this contention are presented in Chapters V and VI.

graphic observation of the combustion zone proved unsuccessful principally due to the sensitivity of the system to blowoff and the rapid deterioration of the window surfaces during the ignition phase of the experiment.

As noted the experiments had influenced the formulation of a new combustion model which involved several assumptions concerning the combustion zone structure. Some of these assumptions relied on the estimates ℓ_c and γ_{res} made on the basis of the temperature measurements while others remained simply as hypotheses. In particular the model emphasized the important sensitivity to the pressure oscillation of the thermodynamic properties and the volume of the (dark zone) of unburned premixed propellant within the turbulent flame cone. Implicit in the analysis was the assumption that fluid dynamic phenomena such as jet instabilities, vortex shedding, and jet interaction do not influence the nonsteady burning process. In order to obtain specific information regarding these points and to study the nonsteady burning process an experimental program of instantaneous and high speed schlieren and shadow photography of the H_2 + Air combustion zone during steady and nonsteady combustion was initiated.

D. Combustion Zone Diagnostics: Schlieren and Shadowgraph Studies of the H_2 + Air Combustion Zone

The following paragraphs describe the series of experiments designed to obtain instantaneous and high speed schlieren and shadow photographs of the H_2 + Air combustion zone during conditions of stable and unstable combustion. The experiments facilitated an examination of several of the critical assumptions regarding the combustion process during steady and non-steady combustion made in the original turbulent flame model. Chronologically these experiments were carried out simultaneously with the analytical study of the turbulent flame combustion model and were completed during the development of the new combustion model described in Chapter V. As will be shown the experimental observations played a crucial role in the development of this new model.

D.1 Modification of the Gas Rocket System

Substantial system modifications were required to allow schlieren photography of the combustion zone. These modifications included the design and fabrication of (a) a new "windowed" combustion chamber section and related components, (b) a schlieren system and associated optical components, and (c) a remote controlling and recording system to allow remote operation of light sources, cameras, and the correlation of photographic records and mean and transient $p_c(t)$ traces

(a) Combustion Chamber Section Design

The original windowed combustion chamber design (Figure IV-18) used in the direct photography experiments was unsatisfactory for the schlieren work. The rapid deterioration of the quartz windows (melting, inadequate support, impingement of particles from the chamber liner) and the necessity of using high grade schlieren quality quartz windows in the new studies made it imperative that a combustion chamber section be fabricated to allow protection of the exposed window surfaces. In particular it was necessary to insure complete protection of the expensive thick pressure bearing windows. A schematic of the section

designed to achieve these ends is shown in Figure IV-21. The design encorporates a double window configuration on each side, positioned so as to allow observation of a 2.5 cm x 7.6 cm zone extending from the injector face. The windows are schlieren quality (Corning Supra-sil 2) quartz. The thin inner window is separated from the outer load bearing window by a rectangular channel bounded on three sides by porous metal (5 micron pore size) "purge plates". Nitrogen"window purge" is admitted to the annulus behind the porous plates, flows with negligible pressure drop through the plates and the channel between the windows, and is directed downstream across the inner face of the thin window by means of the channel cut in the copper spacer at the injector end of the window assembly. To prevent condensation of H_2O product gas on the inner surface of the thin windows it was necessary to preheat the N_2 purge. To allow preheating a simple heat exchanger was provided in the N_2 purge line. The exchanger was fabricated from a section of stainless steel tubing filled with copper pellets and wrapped with 4.6 m of (A-1), .091 cm diameter Kanthal resistance wire. By controlling (Variac) voltage across the heater N_2 purge temperatures up to 500°K at the inlet to the chamber section could be achieved. The N_2 purge flow rate was regulated through the diluent system.

To eliminate the possibility of ignition of the relatively stagnant premixed gases in the volume upstream of the face of the choked showerhead injector, a coolant coil and manifold were designed to couple the chamber section to the mixing chamber. Both H_2O and N_2 coolant were used in the course of the experiments. The coolant manifold and coil are also shown in Figure IV-21. The typical "optical" array of the showerhead injection ports designed to preserve the basic hole spacing of the 10 hole showerhead injector and to facilitate the observation of individual port flow without intervening jets along the optical axis is visible through the chamber section windows in the photograph. Figure IV-22a,b shows exploded views of the window holder assembly and the windowed section injector and coolant manifolding assembly.

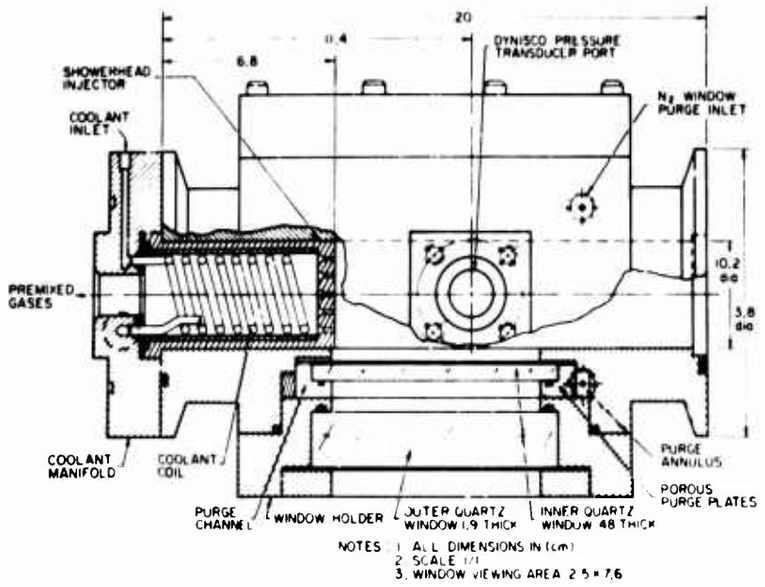

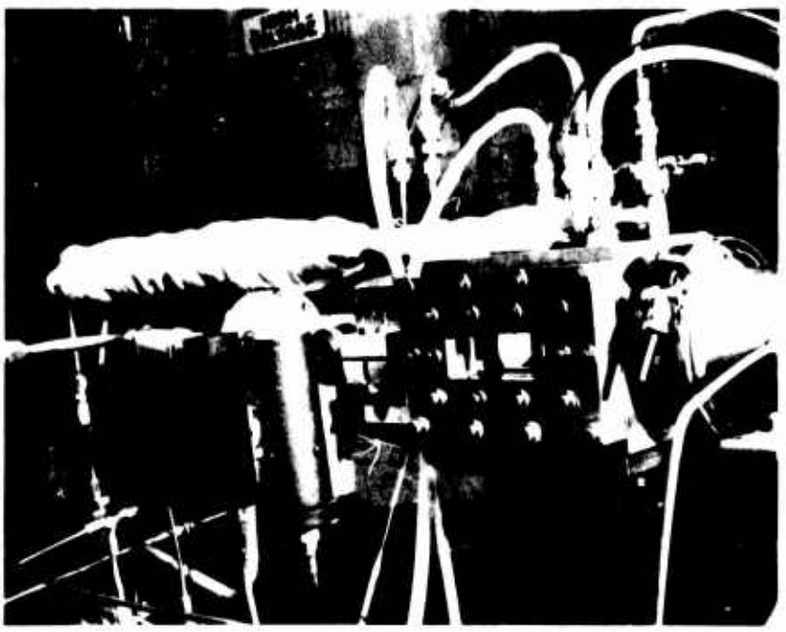

COMBUSTION CHAMBER SECTION USED FOR SCHLIEREN STUDIES

FIGURE IV-21

(a) CHAMBER SECTION, INJECTOR, COOLANT MANIFOLD

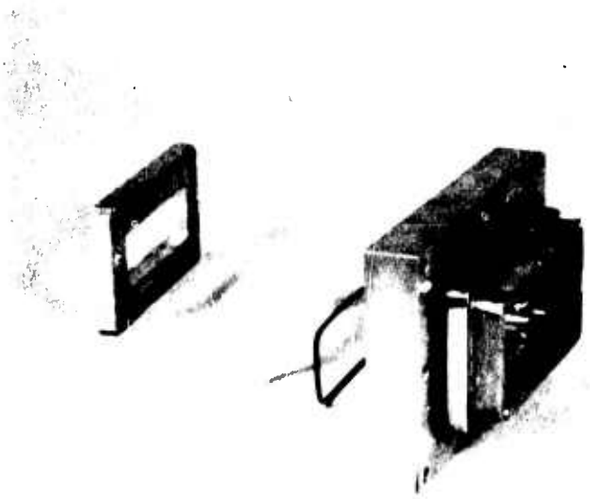

(b) WINDOW HOLDER

FIGURE IV-22

Prior to the optical studies the stability characteristics of the system with the new windowed section and injection configuration were determined. The influence of heated and unheated N_2 purge flows up to 10% of the total mass flux of propellant was determined and a successful ignition and experimental procedure determined (see page 149).

(b) Schlieren System

A schematic of the schlieren system designed for these studies is shown in Figure IV-23a and an overall view of the experimental arrangement is shown in Figure IV-23b. The system was designed to allow instantaneous spark photography as well as high-speed cine photography using a Hycam 16mm framing camera. A folded Z configuration provided for parallel beam illumination of the test section and minimum distortion due to aberrations (coma). A 0.3 mw He-Ne laser facilitated system alinement. The principal features of the system components are noted in Table V.

High-speed schlieren photography was accomplished by introducing an Osram 100W/2 continuous Hg-arc lamp at the source position and an achromat lens in the beam 31 cm beyond the knife edge to form a small inverted image of the test section on the entrance stop of the Hycam. To allow variable magnification (depending on the focal length of the achromat used) the Hycam position along the optic axis was adjustable by means of a lathe tool bed camera mount.

Instantaneous spark schlieren photography was facilitated by replacing the continuous source with a high voltage spark electrode source, removing the achromat and Hycam, and imaging the test section directly on 4 x 5 Polaroid film mounted in a shutter-holder at 3 m from the knife edge. A fixed magnification of 1.8 applies to the spark schlieren photographs.

(c) Remote Control Circuits

In view of the safety restrictions prohibiting presence of personnel in the test cell during system operation, remote control of the Hycam, the 4x5 shutter, and the spark light source was required. Schematics of the circuits designed for these

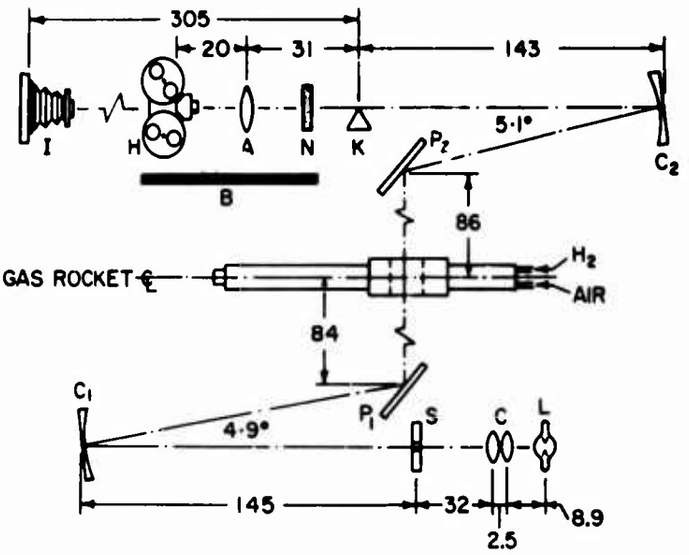

a) SCHLIEREN SYSTEM SCHEMATIC

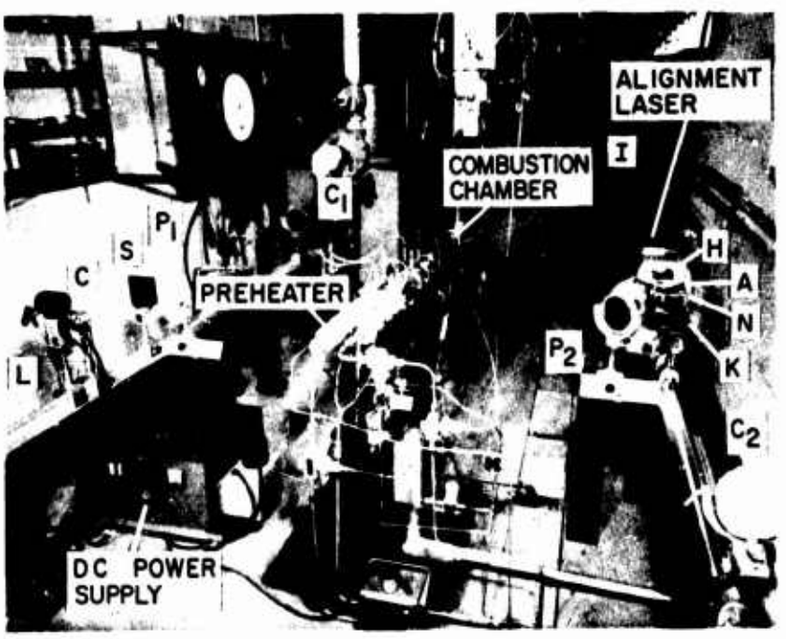

b) EXPERIMENTAL ARRANGEMENT FOR SCHLIEREN STUDIES

FIGURE IV-23

TABLE V: SCHLIEREN SYSTEM COMPONENTS

SYMBOL*	COMPONENT	SOURCE	SPECIFICATION
A	Projection Lens	Laboratory Optical " " Edmunds Scientific	f/6, 15.3 cm f.l. f/30, 76 cm f.l. f/5.6, 21.6 cm f.l.
B	Camera blast shield	In House	1.3 cm plexiglass
C	Condensing Lens	Laboratory Optical	f/3.3, 2 f/6, 2.5 cm diam condensing lens
C_1, C_2	Concave Schlieren Mirrors	Laboratory Optical	f/13.8, 144cm f.l., first surface
H	Hycam 16mm Camera	In House	Model K20S4E, 400ft 1000 cps T.L. gener Event synchronizer
I	4 x 5 Polaroid Film Holder and Shutter	In House	
K	Knife Edge	In House	
L	Continuous Light Source DC Power Supply	Osram In House	HBO 100W/2, DC air cooled Hg-arc Lamp 100v, 10 amp
	Spark Electrode High Voltage Power Supply	In House Spellman	 0-20 kw
N	Neutral Density Filter	Kodak	0.1 to 0.6
P_1, P_2	Plane Mirrors	Laboratory Optical	10.4 cm diameter first surface
S	Pin Hole	In House	circular, 0.16cm diameter

*Symbols correspond to labels in Figure IV-23

purposes are shown in Figure IV-24. Photographs of the H_2 + Air combustion zone during steady and nonsteady conditions have been obtained. The remote operation of the optical systems once the desired experimental conditions were attained is described in the following paragraphs.

Remote operation of the system for instantaneous photography relied on the nonluminosity of the H_2 + Air combustion zone at $\phi > 2.0$. With experimental conditions achieved, the 4 x 5 shutter solenoid was actuated at the control panel exposing the film to the test section. A second control panel switch applied a triggering voltage to the spark electrode and allowed a controlled breakdown at preset voltage. Following spark discharge the shutter was closed and the experiment terminated. For discharge voltages of the order of 9 to 12 kv, exposure times of the order of 5 to 20 μsec are achieved. An N_2 bleed across the spark electrode discouraged premature breakdown due to the buildup of H_2O vapor in the test cell during a series of experiments. An RCA LS600 photodiode was mounted at the base of the condenser lens and sensed the spark discharge. The 1 to 2 volt output from the photodiode was recorded on the Ampex tape for subsequent correlation of transient pressure and the photographs. Polaroid PN-55 (ASA50) and P52 (ASA 400) films were used.

For high-speed cine photography the arc lamp blower was disconnected immediately prior to the experiment. Lamp vibration induced by the blower mounted on the housing produced unacceptable light intensity fluctuations. With the desired experimental conditions achieved, 24 volts DC power was applied to the Hycam camera. The two NE2J timing lights in the Hycam were wired so as to (1) provide 1000 marks per second on the film and (2) to simultaneously provide a zero time reference on the film and on the magnetic tape for subsequent correlation of the image sequence and the transient pressure. To achieve the latter a relay was connected in parallel with the power line to the camera as shown in Figure IV-24a. Upon actuating the Hycam the relay closed the second timing light circuit and a 250 V photographic battery powered the light. The "event" feature of the Hycam opened the circuit at a preselected (constant speed) film footage. This

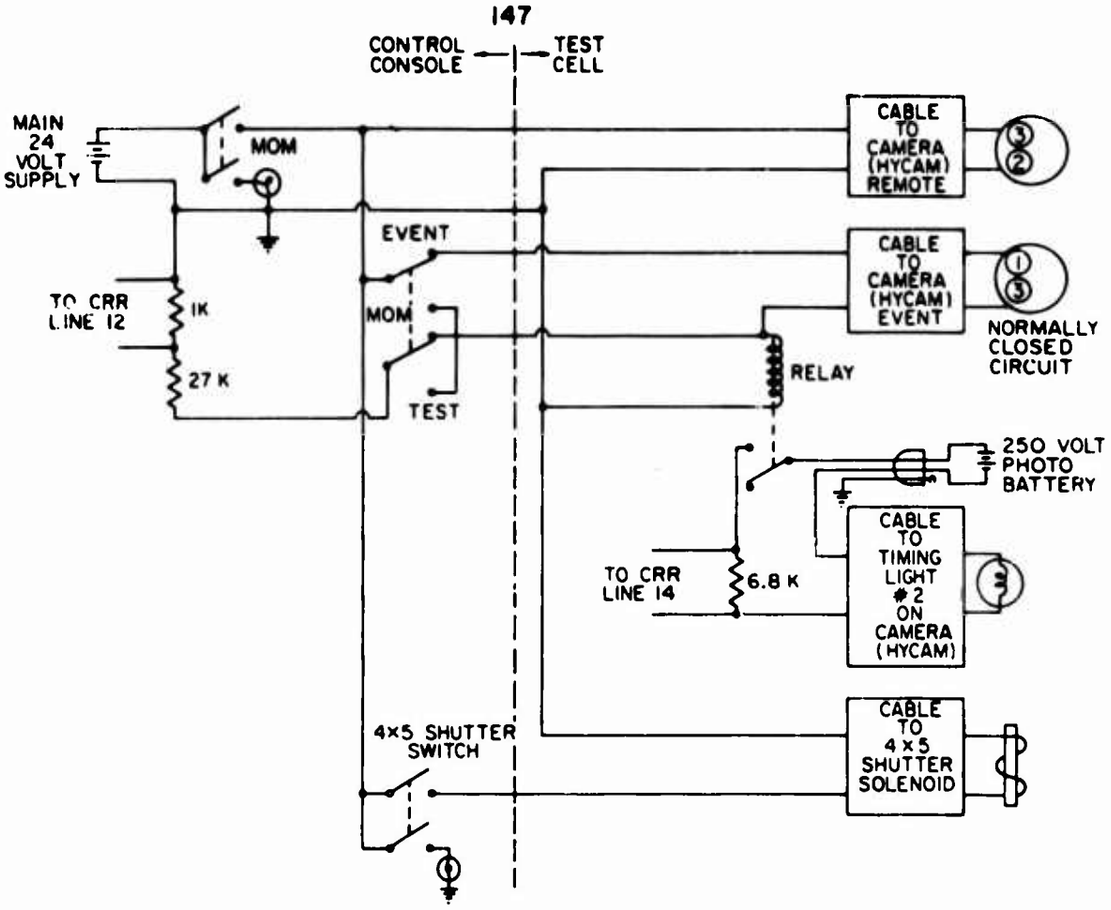

REMOTE CONTROL CIRCUITS FOR HYCAM CAMERA AND 4x5 SHUTTER

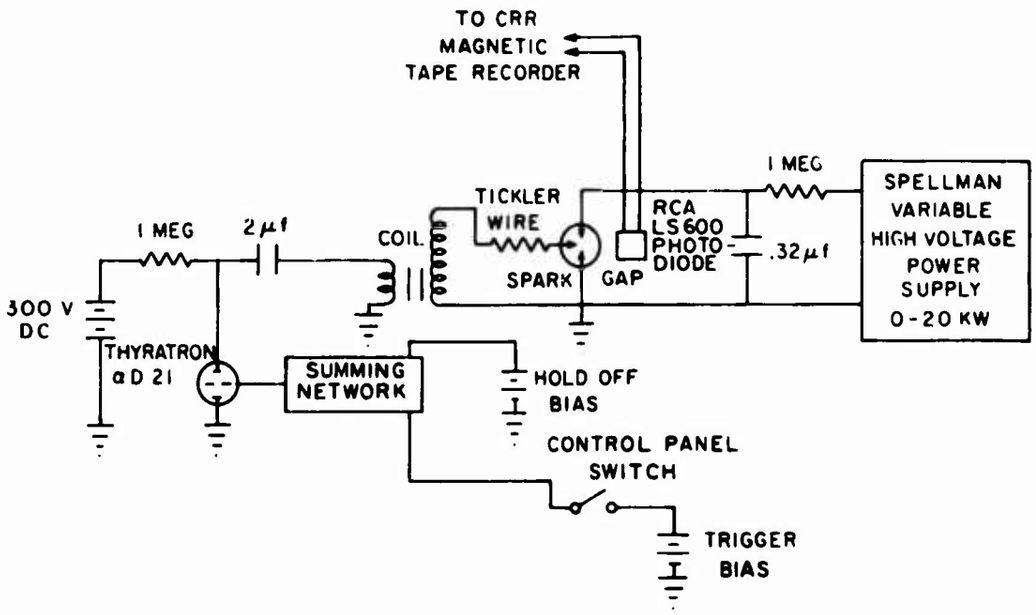

TRIGGER CIRCUIT FOR HIGH VOLTAGE SPARK LIGHT SOURCE

FIGURE IV-24

"zero" reference point was recorded by monitoring the voltage drop across the 6.8Kohm resistor in the timing light circuit. At framing rates of 5000 frames per second a maximum undertainty of 30 μsec is estimated in the correlation of film and pressure trace due principally to the finite luminosity decay time of the timing light. Dupont 932A film developed to a negative (ASA 125) was used. Much greater detail in the photographs was realized by subsequent processing to positives of selected sequences. Exposure times ranged from 10 to 100 μsec.

D.2 Preliminary Investigations

Preliminary experiments were carried out to determine a repeatable ignition and operation sequence and to examine the system stability characteristics with the new windowed chamber section and the modified showerhead injection port alignment. Initially a series of experiments with a conventional combustion chamber configuration showed that the H_2 + Air system stability characteristics (stability limits and nonlinear shock amplitude) were essentially similar for choked showerhead injection with the asymmetric "optical" 9-port configuration and the previously used 10-hole array. A shift in the precise location of the stability limits in the $\Phi - L_c$ plane was observed for 9-hole injection with mean port size of d_{port} = .057 cm compared to a similar injector with mean port size of d_{port} = .092 cm. Both injectors were used in the course of the optical work. The larger port injector supported nonsteady burning in a narrow range of $2.05 \leq \Phi \leq 2.20$. The smaller port injector evidenced nonsteady burning for $\Phi \geq 2.45$.

The influence on the system stability characteristics of N_2 window purge flows up to 10% of the total propellant mass flux was also determined in a preliminary study. A slight decrease in equivalence ratio at the stability limit (Φ_{lim}) was observed with the addition of small N_2 flows, but the overall stability characteristics were unchanged. The frequency of the sustained pressure oscillation at the limit was independent of the N_2 mass

flux.[1] This indicated that the wave travel time (i.e., the mean combustion chamber temperature and Mach number) was essentially constant at $\bar{\Phi}_{lim}$.

The influence on the operating characteristics of the gas rocket of significant distortion in the combustion chamber geometry in the vicinity of the injector was noted during these preliminary tests. With the small inner windows removed from the configuration shown in Figure IV-21 it was impossible to stabilize (in the sense of flameholding) combustion of the H_2 + Air propellant at the injector (independently of N_2 purge flow) over the entire range of equivalence ratio ($\bar{\Phi} > 1$) investigated. This observation, although a bi-product of preliminary testing lends important support to the final combustion model developed in Chapter V. It represents a clear indication of the strong recirculation of burned product gases to the base of the propellant jets.

In the course of the optical studies two experimental procedures were used. Initially spark schlieren and shadow photographs of the stable combustion of H_2 + Air were obtained. The experiments were carried out at $\bar{P}_c$ = 4.4 atm and used the standard procedure discussed in Chapter III. Total run times on the order of 30 to 40 seconds were required. To provide adequate protection of the windows for these long runs and to eliminate H_2O condensation a 30 minute window preheat preceded each series of experiments. Using this technique with preheated N_2 mass flows of 8 to 10% of $\dot{m}_{tot}$ virtually complete window protection was achieved. This procedure proved completely satisfactory for obtaining shadowgraph photographs of the combustion zone due to the inherent low sensitivity of the shadowgraph system. The distortion introduced in the image by the purge flow in the more sensitive schlieren observations proved excessive for high speed cine photographic observation of the nonsteady combustion zone (a series of spark schlieren photographs of steady combustion with

---

[1] This behavior is to be expected in light of the combustion model developed in Chapter V . Earlier work had shown that the addition of N_2 diluent to the premixed propellants upstream of the combustion chamber produced a shift in $\bar{\Phi}_{LIM}$ toward the stoichiometric ratio. It is of interest to note that addition of N_2 directly into the combustion chamber produces a similar reduction in $\bar{\Phi}_{LIM}$.

N_2 purge flow was obtained). In order to obtain satisfactory resolution of the nonsteady combustion zone an abbreviated experimental procedure similar to that used in the direct photographic work was used. For these experiments the N_2 purge was used to preheat the windows for 30 minutes prior to each experiment. The experimental ignition sequence was initiated with the termination of the N_2 purge flow. Total run times were minimized by presetting the air mass flow rate at the desired final value and increasing the H_2 flow rapidly to the desired final magnitude.

D.3 Results of Spark Schlieren and Shadowgraph Investigations

Spark schlieren and shadow photographs of the steady combustion H_2 + Air have been obtained under the following conditions:

$1.70 \leq \phi \leq 3.00$
$\bar{P}_c = 4.4 \quad 0.7$ atm
$\dot{m}_{tot} = 13 \pm 2$ gms/sec
$L_c = 104$cm
4 hole plug nozzle
N_2 window purge: 400 to 500 ^{o}K, 8 to 10% of $\dot{m}_{TOT}$
choked showerhead injection
$\bar{P}_{mix}/\bar{P}_c = 2.1$ to 3.2, corresponding to two 9 hole showerhead injectors having mean port diameters of (I) 0.092 cm and (II) 0.056 cm (schematic of port configuration is shown in Figure IV-25)

A series of cold air flow schlieren and shadow photographs with and without N_2 purge flow were obtained prior to the series of combustion experiments. These initial photographic studies were aimed at determining the basic structure and degree of steadiness of the gas jets issuing from the showerhead injector ports as a function of $\dot{m}_{tot}$, $\bar{P}_{mix}/\bar{P}_c$, and d_{port} in the absence of combustion. The oscillatory behavior of axisymmetric, choked, underexpanded jets expanding into unconfined quiescent atmospheres is well documented (145, 146, 147). High velocity air jets are typically observed to "emit discrete frequency screeches which are superimposed on broadband noise" (146) in the frequency range of 5000 to 10,000 Hz (145). Such phenomena as eddy and vortex shedding, sound wave emission, and shock structure oscillation along the jet axis and rotation about the axis are observed (146).

Figure IV-25 presents typical photographs obtained of the cold air flow jet structure. A complete series of schlieren and shadow photographs of the air jet structure over the range of total air mass flow rates typical of the combustion experiments and of ratios of $\bar{P}_{mix}/\bar{P}_c$ for both injectors verified the inherent uniformity and steadiness of the underexpanded jets. The characteristic three-zone structure (regions of supersonic flow, a system of standing shock waves, and a diffuse turbulent outer mixing zone) of the underexpanded choked air jet is visible in all photographs. The shock structure remained fixed in location and configuration over several individual photographs taken under identical flow conditions. A subsequent observation of the cold air jets by high speed cine photography substantiated the conclusion of the inherent steadiness of the showerhead injector jets in the absence of combustion.

For the cold flow case at fixed mass flow and choked showerhead injection the mean chamber pressure and Mach number (M) are functions of the nozzle throat area (A_t). The photographs shown are typical of the results obtained with the 4 hole plug nozzle. At fixed total mass flow but with combustion the jet underexpandedness, $\bar{P}_{mix}/\bar{P}_c$ decreases substantially due to the increase in the stagnation temperature and static pressure and the attendant decrease in stagnation pressure across the combustion zone. A series of cold flow shadowgraphs for fixed total mass flux but decreasing underexpandedness (achieved by reducing the nozzle throat area) are shown in Figure IV-26 and demonstrate the pronounced effect of decreasing $\bar{P}_{mix}/\bar{P}_c$ on the jet shock structure. The third photograph corresponds to $(\bar{P}_{mix}/\bar{P}_c)$ cold = $(\bar{P}_{mix}/\bar{P}_c)$ with combustion. In the absence of combustion viscous dissipation restricts the supersonic portion of the jet to 0.7 cm (7.7 d_{port}) for $\bar{P}_{mix}/\bar{P}_c$ = 4.03 and to $\sim$ 0.5 cm (5.5 d_{port}) for $\bar{P}_{mix}/\bar{P}_c$ = 2.15. Comparison of Figures IV-25 and IV-26 shows that the supersonic portion of the jet in the case of the smaller total flow area injector is about the same length (in absolute terms) for the same $\bar{P}_{mix}/\bar{P}_c$ (=0.7 cm) but is longer relative to port diameter (12 d_{port}).

I) d_{PORT} = .092 cm, $\bar{P}_{MIX}/\bar{P}_C$ = 3.2

2.54 cm (1 in)

a) SCHLIEREN HORIZ KE

b) SCHLIEREN VERT KE

c) SHADOWGRAPH

II) d_{PORT} = .057 cm, $\bar{P}_{MIX}/\bar{P}_C$ = 4.5

2.54 cm (1 in)

a) SCHLIEREN HORIZ KE

b) SHADOWGRAPH

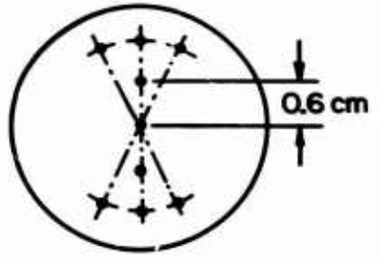

9 HOLE SHOWERHEAD INJECTOR

FIGURE IV-25

TYPICAL SPARK SHLIEREN AND SHADOW PHOTOGRAPHS OF COLD AIR FLOW

(a) $\bar{P}_{MIX}/\bar{P}_C = 4.0$ (b) $\bar{P}_{MIX}/\bar{P}_C = 2.8$ (c) $\bar{P}_{MIX}/\bar{P}_C = 2.2$

SPARK SHADOWGRAPHS OF COLD AIR FLOW SHOWING JET STRUCTURE AS FUNCTION OF $\bar{P}_{MIX}/\bar{P}_C$

$d_{PORT} = .092$ cm, $\dot{m}_{TOT} = 16.5$ gms/sec, $\bar{P}_{MIX} = 11.6$ atm.

FIGURE IV-26

Initially a series of spark schlieren photographs of the steady combustion of H_2 + Air were obtained for showerhead injector (I) (d_{port} = 0.092 cm, $\bar{P}_{mix}/\bar{P}_c$ = 2.1) under the conditions noted on page 150. Typical horizontal knife edge schlieren photographs of the combustion zone as a function of Φ are shown in Figure IV-27. Typical shadowgraphs at Φ = 1.95 for the two injectors are shown in Figure IV-28. A series of shadowgraphs (injector II) spanning the range of Φ of interest in terms of the nonsteady burning characteristics evidenced by the conventional injection configurations is shown in Figure IV-29. The shadowgraph at Φ = 2.80 was obtained during sustained low amplitude shock-type instability.

There is some difficulty in extracting information from these spark photographs. These data were obtained, as noted earlier, simultaneously with the analytical studies of the turbulent flame model of the gas rocket combustion process. Several tentative observations were made on the basis of these schlieren and shadowgraph results which are consistent with earlier diagnostic results from the temperature measurements and the direct photographs and which had a direct bearing on the analytical work. The schlieren sequence supports the earlier observation that the combustion zone increases in length with increasing Φ or decreasing T_b. As Φ increases from 1.70 to 2.80 the apparent length of the combustion zone increases from approximately 1.5 cm to 4.2 cm. The supersonic region of the underexpanded combusting jet flows is quite well shown considering the integrated path length effect (with hot N_2 window purge) in the optics. In view of the repeatability of the shock structure evidenced by the shadowgraphs it seemed that the underexpanded zone of the jet remains steady during steady combustion. The region of cold high velocity unburned premixed propellant gases extends into the combustion zone. For the same total mass flux and underexpandedness the supersonic region is attenuated by about 20% (from its cold flow length) in the case of the combusting jet. This attenuation seems to be quite reasonable in view of the higher levels of turbulent mixing and viscous shear in the case of the combusting

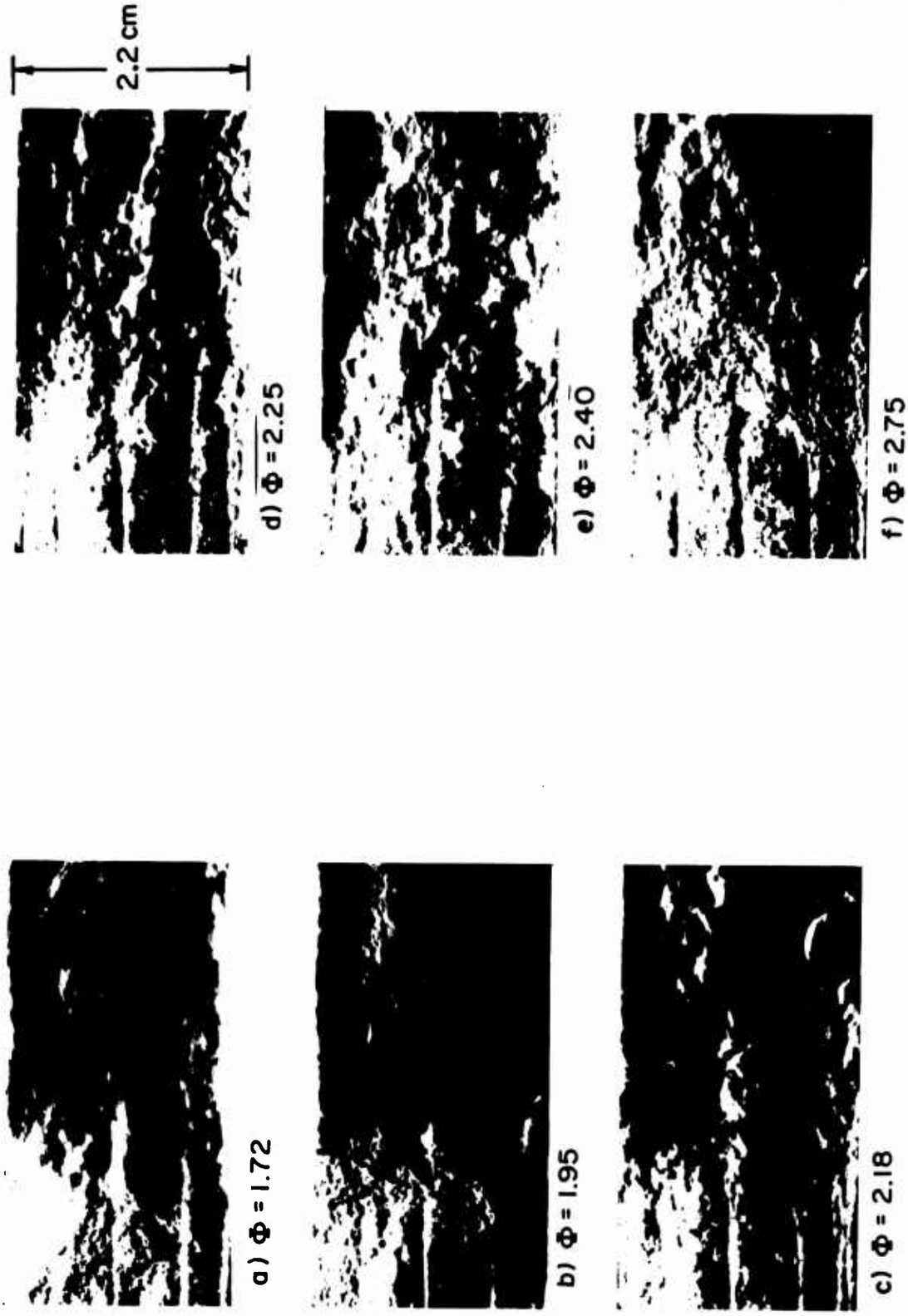

SPARK SCHLIEREN PHOTOGRAPHS OF STEADY H_2 + AIR COMBUSTION
d_{PORT} = .092 cm, L_c = 104 cm, $\bar{P}_c$ = 4.4 atm, $\bar{P}_{MIX} / \bar{P}_c$ = 2.1, $\dot{m}_{TOT}$ = 15 ± .5 gms/sec

FIGURE IV-27

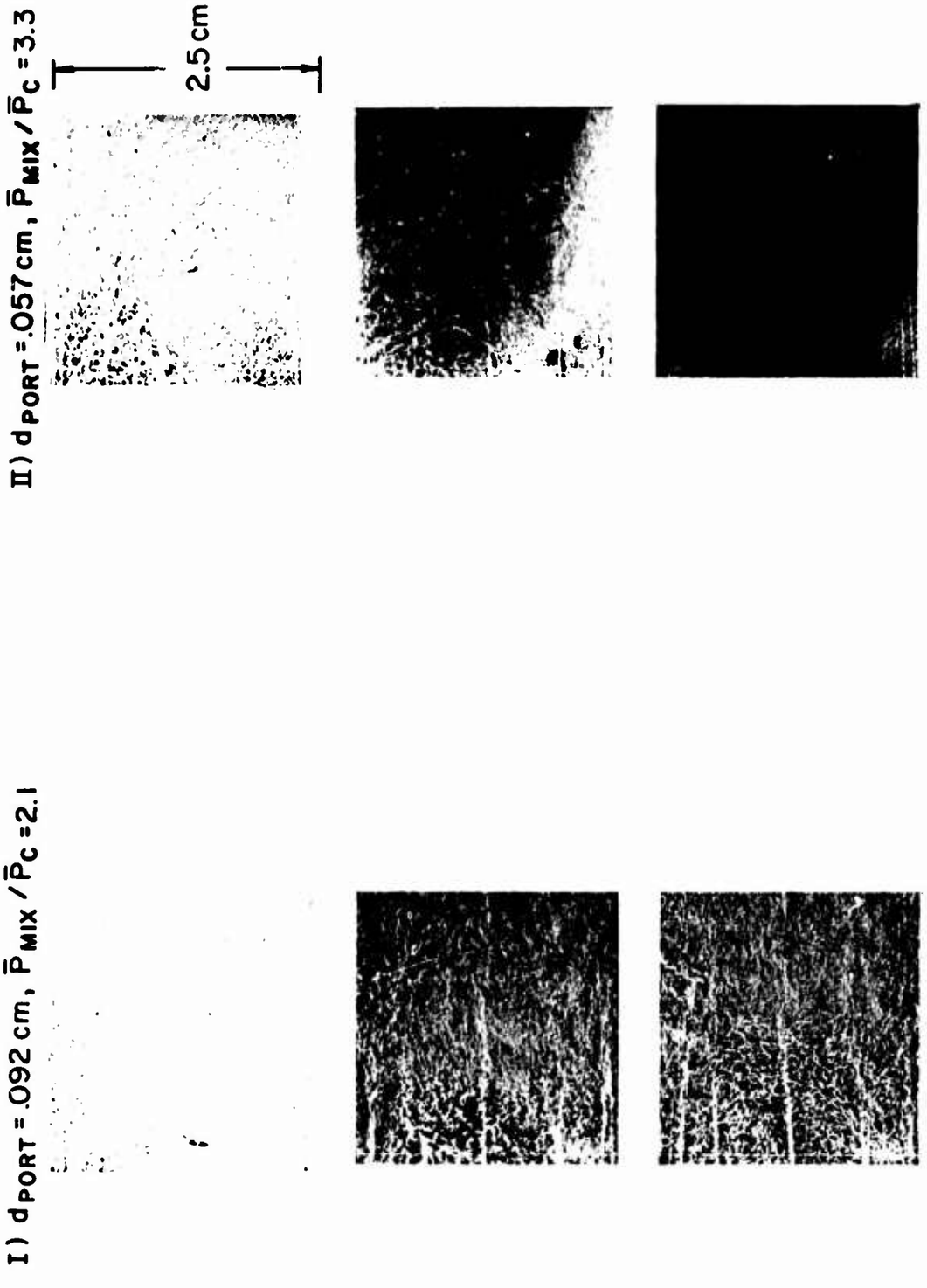

TYPICAL SPARK SHADOWGRAPHS OF STEADY H_2 + AIR COMBUSTION
Φ = 1.95, $\bar{P}_C$ = 4.4 atm, $\dot{m}_{TOT}$ = 14.5 gm/sec, L_C = 104 cm

FIGURE IV-28

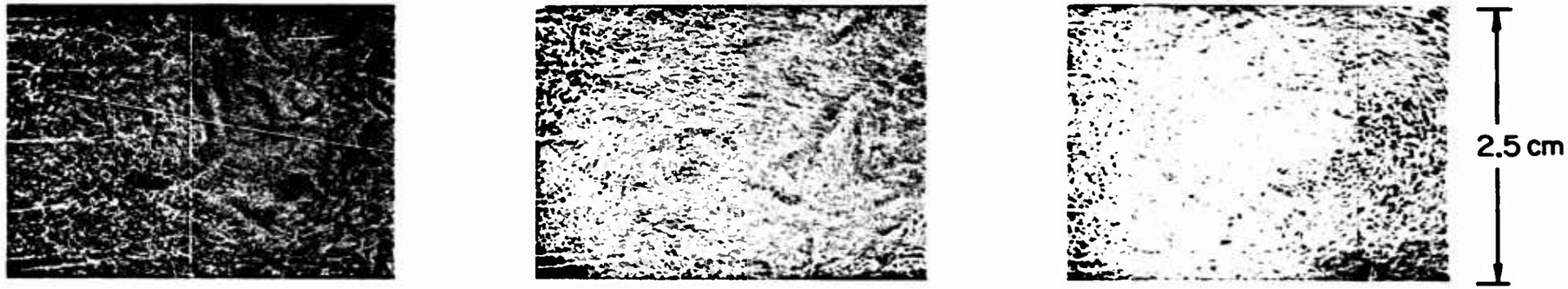

(a) $\Phi = 1.95$ (b) $\Phi = 2.40$ (c) $\Phi = 2.80$

SPARK SHADOWGRAPHS OF STEADY H_2 + AIR COMBUSTION

$d_{PORT} = .057$ cm, $L_C = 104$ cm, $\bar{P}_C = 4.4$ atm, $\bar{P}_{MIX}/\bar{P}_C = 3.3$

$m_{TOT} = 15 \pm .5$ gms/sec

FIGURE IV-29

jet. Indeed, the photographs indicate that the actual burning zone commences quite close to the base of the jet (especially with increasing $\bar{\Phi}$) and extends axially, surrounding the underexpanded zone. As shown in Figure IV-28 the length of the underexpanded region of the jet is independent of the $\bar{P}_{mix}/\bar{P}_c$ at fixed $\bar{\Phi}$ (1.95) and $\dot{m}_{tot}$. At $\bar{\Phi}$ = 1.95 the underexpanded zone extends approximately (0.5 to 0.7 cm) into the combustion chamber. The length of this zone is appreciably shortened as the mean T_b is decreased ($\bar{\Phi}$ increased) as shown in Figure IV-29. Note that $\dot{m}_{tot}$ was increased slightly to maintain fixed $\bar{P}_c$ over the entire range of .

It is of interest to compare the observations of the combustion zone at $\bar{\Phi}$ = 1.95 and $\bar{P}_{mix}/\bar{P}_c$ = 2.1, $\dot{m}_{tot}$ = 14.5 gms/sec with the direct photographs obtained earlier at $\bar{\Phi}$ = 1.60 and $\bar{P}_{mix}/\bar{P}_c$ = 2.0 and $\dot{m}_{tot}$ = 8 gms/sec. It will be recalled that the inner dark zone observed in the direct photographs extended approximately 0.4 to 0.5 cm from the injector port with the overall flamelet length being 1.3 cm. In view of the slight difference between the mean conditions of the combustion process in the two experiments it seems reasonable to conclude that the inner dark zone observed in the direct photographs corresponds to the steady underexpanded portion of the propellant jet visible in the shadowgraphs.

These observations reflected directly on the theoretical analysis of the turbulent flame model of the combustion process. The basic assumption crucial to the development of the turbulent flame combustion model, namely, that the combustion process is coupled to the pressure oscillation through the sensitivity (indeed isentropic response) of the unburned premixed propellant gases within the cone volume seemed to be highly suspect. Furthermore the postulated relative thinness and overall conical geometry of the turbulent flame zone seemed to be unrealistic. In particular the applicability of the concept of a turbulent flame speed appropriate to the combustion zone visualized in these schlieren, shadowgraph, and direct photographs seemed dubious.

D.4 Results of Schlieren 16mm Cine Photography of Steady and Nonsteady Combustion of H_2 + Air

The experimental procedure used to obtain 16mm schlieren records of the combustion of H_2 + Air is described in section D.2. High speed schlieren photographs of the steady and non-steady combustion of H_2 + Air have been obtained with and without N_2 purge during the filming under the following conditions:

$1.8 \leq \Phi \leq 2.7$
$\overline{P}_c = 3.1 \pm 0.3$ atm
$L_c = 104$ cm
4 hole plug nozzle
choked showerhead injection
$\overline{P}_{mix}/\overline{P}_c = 2.8$, corresponding to 9-hole showerhead injector (I1) having mean port diameter of 0.056 cm

In Figure IV-30 a typical 16mm schlieren sequence (5000 frames/sec, 20 usec exposure time, horizontal knife edge) depicts the steady combustion of H_2 + Air at $\Phi = 2.4$, slightly below the onset of nonsteady burning (with Φ). Figures IV-31a,b and IV-32a to f show 16mm schlieren sequences of the nonsteady combustion zone of H_2 + Air at $\Phi \simeq 2.6$ during sustained shock-type instability. The two sequences shown were separated in time by 0.130 sec during the experiment. A single nonlinear shock-type wave was observed to oscillate at the fundamental frequency of f = 267 $\pm$ 10 cps with a steady $\Delta P_{shock}/\overline{P}_c = 0.03$. The overall peak to peak wave amplitude as sensed by the Dynisco transducers located at 4.6 cm from the injector face was $\Delta P_{pk\ t\ pk}/\overline{P}c = 0.06$. The approximate time of passage of the shock wave relative to the film sequence is designated by (s ⟶). Under these observed conditions the period of oscillation is approximately 3.75 msec and the mean shock velocity is 5.6×10^4 cm/sec which also represents the mean sound speed in the combustion chamber. The mean sound speed in the vicinity of the injector is somewhat higher and is estimated to be (Θ(7.3 cm/sec)) corresponding to a mean temperature near the injector of 1325°K or 50°K below the adiabatic combustion temperature for the mixture.

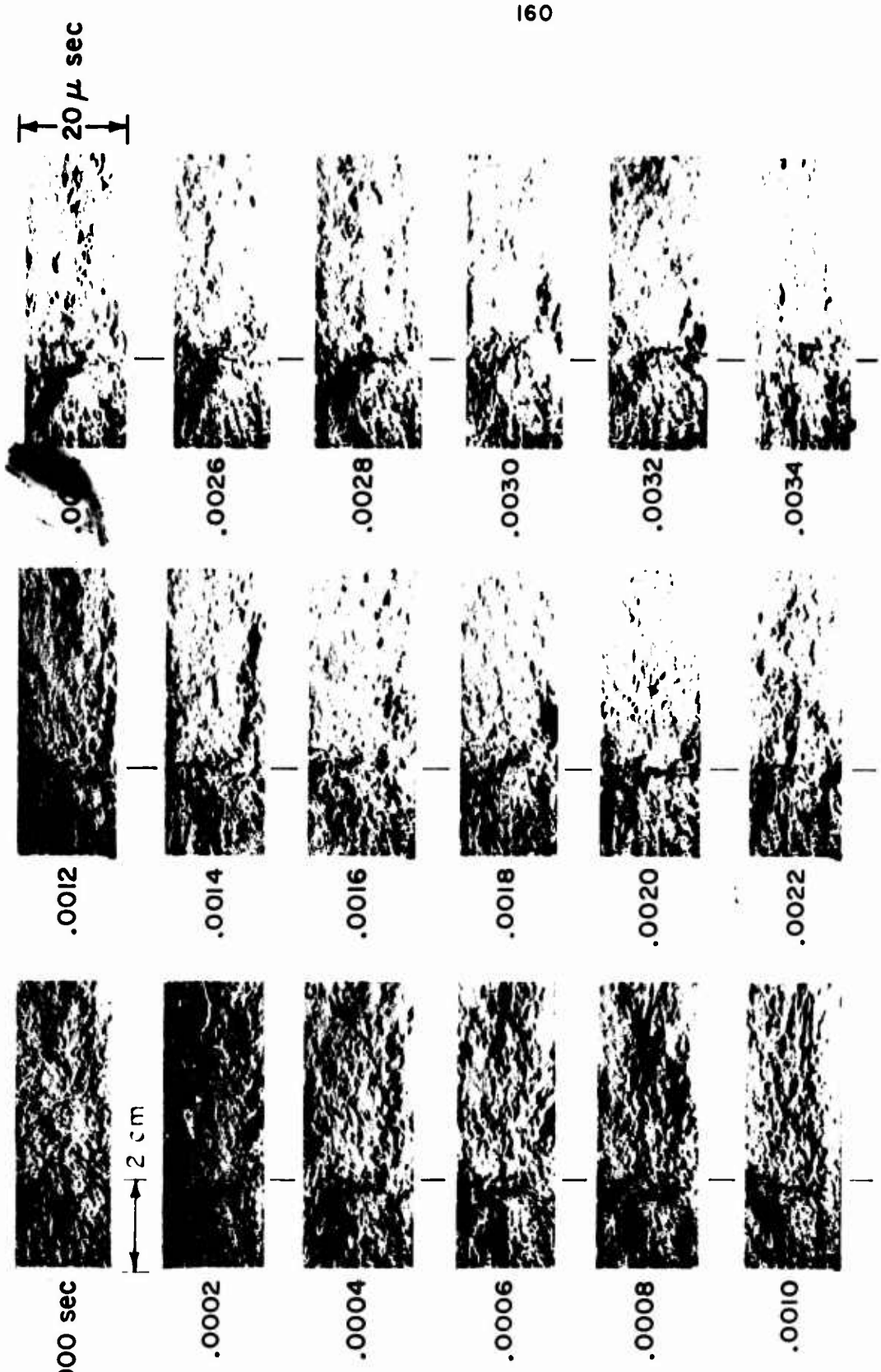

HIGH SPEED SCHLIEREN PHOTOGRAPHS OF STEADY COMBUSTION OF H_2 + AIR

$\Phi = 2.40$, $\bar{P}_c = 3.2$ atm, $\bar{P}_{MIX} / \bar{P}_c = 2.8$, $L_c = 104$ cm

FIGURE IV - 30

Thus the midpoint of the Dynisco transducer and the x = 2 cm point in the chamber are separated in time by an estimated 35 usec corresponding to the time for an acoustic pulse to travel the interval. This correction is included in the data shown.

The information obtained from the high speed schlieren sequences was important to the overall understanding of the gas rocket instability phenomena and represents a key element in the development of a consistent theoretical and physical combustion model. The high speed schlieren films obtained at $2.20 \leq \Phi \leq 2.40$ confirmed the steadiness of both the underexpanded region of the unburned propellant jets as well as the larger surrounding zone of mixing and reacting gases in the absence of sustained pressure oscillations.

With regard to the structure of the combustion zone as shown in the high speed photographs on a frame by frame basis the following points are noted: The underexpanded regions of the three central jets (see Figure 49 for the injector port configuration) are visible in most of the frames as dark streaks parallel to the axial coordinate. The injector face is at the left hand border of the image. Combustion and jet expansion predominate in the 1.5 to 3 cm zone extending from the injector face. This region is clearly distinguished from the somewhat cooler more uniform (velocity, composition, and temperature) downstream zone of product gases. The axial extent of the underexpanded regions of the propellant jets and the overall combustion and mixing zone as observed in the high speed schlieren photographs is consistent with similar measurement of these zones in earlier diagnostic work (the individual frames of the high speed photographs show a 2.4cm x 6.4 cm area of the test section). The marked difference in the schlieren image between the 16mm frames and the spark schlieren photographs is in part due to the lower contrast, lower speed film used in the high speed photographs. The major factor is the additional distortion introduced by the N_2 purge flow in the spark schlieren studies. Several 16mm high speed schlieren records of the combustion zone with

N_2 purge evidenced precisely the same oscillatory behavior in the combustion zone gases when viewed continuously at 8 frames/sec playback. The oscillation is not shown as clearly on a frame by frame basis as in the experiments with no N_2 purge flow during the filming.

On the basis of high speed schlieren sequences such as those shown in Figures IV-31,32 during sustained fundamental mode shock type instability the following observations were made: The finite dimensioned combustion zone volume is itself nonsteady in the presence of sustained shock type instability and oscillates in size at the precise frequency of the pressure oscillation. The "magnitude" of the observable volume oscillation diminishes with decreasing shock wave amplitude and is absent during steady combustion. The combustion zone oscillation is not in phase with the pressure oscillation. The passage of the shock wave follows by ½ to 1/3 of the period of oscillation the occurrence of the maximum extension of the combustion zone. There is no evidence that the small (in comparison to the overall combustion zone volume) zones of unburned underexpanded propellant gases play a significant role in the nonsteady burning process. There is no evidence that unsuspected nonlinear fluid dynamic-chemical interactions such as flame tip breaking and subsequent properly phased ignition of these displaced volumes of propellants as observed by Tsuji and Takeno are active in the nonsteady combustion zone response.

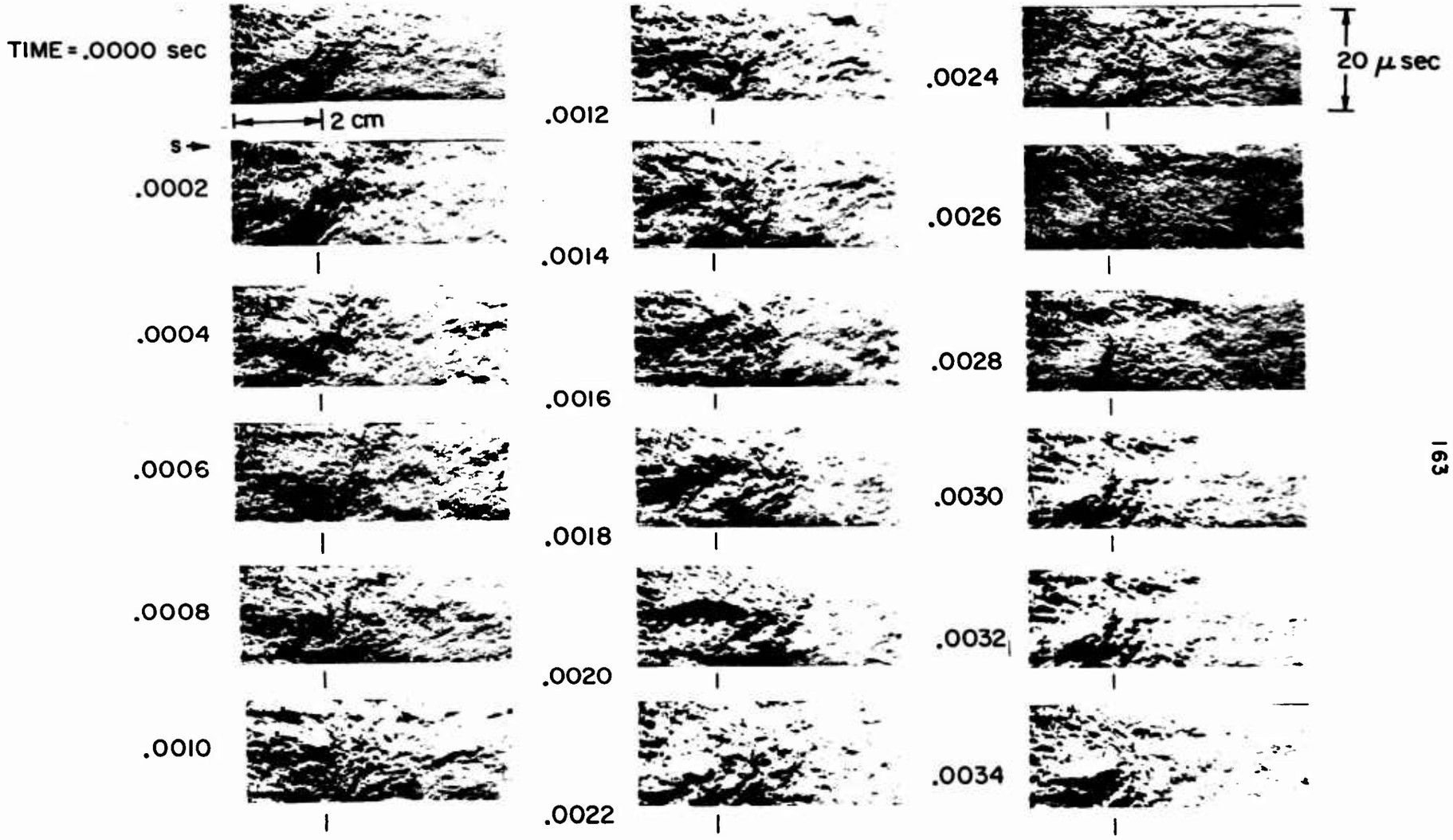

HIGH SPEED SCHLIEREN PHOTOGRAPHS OF UNSTABLE COMBUSTION H_2 + AIR

Φ = 2.62, $\bar{P}_c$ = 3.1 atm, $\bar{P}_{MIX}/\bar{P}_c$ = 2.8, L_c = 104 cm, 9 HOLE SHOWERHEAD

ΔP SHOCK / $\bar{P}_c$ = 0.08, f = 267 ± 10 cps, FUNDAMENTAL MODE

(SEQUENCE 1)

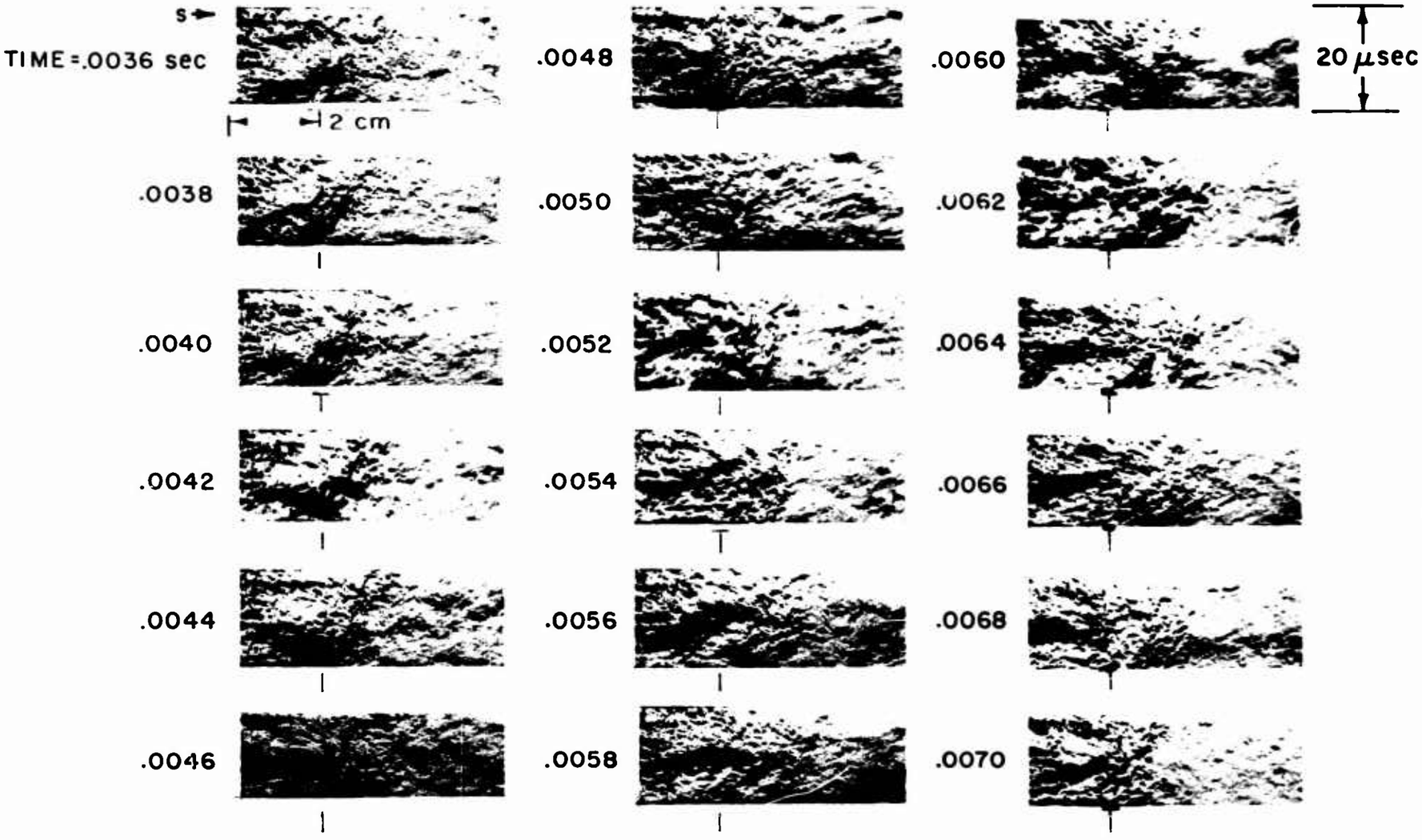

(SEQUENCE I, continued)

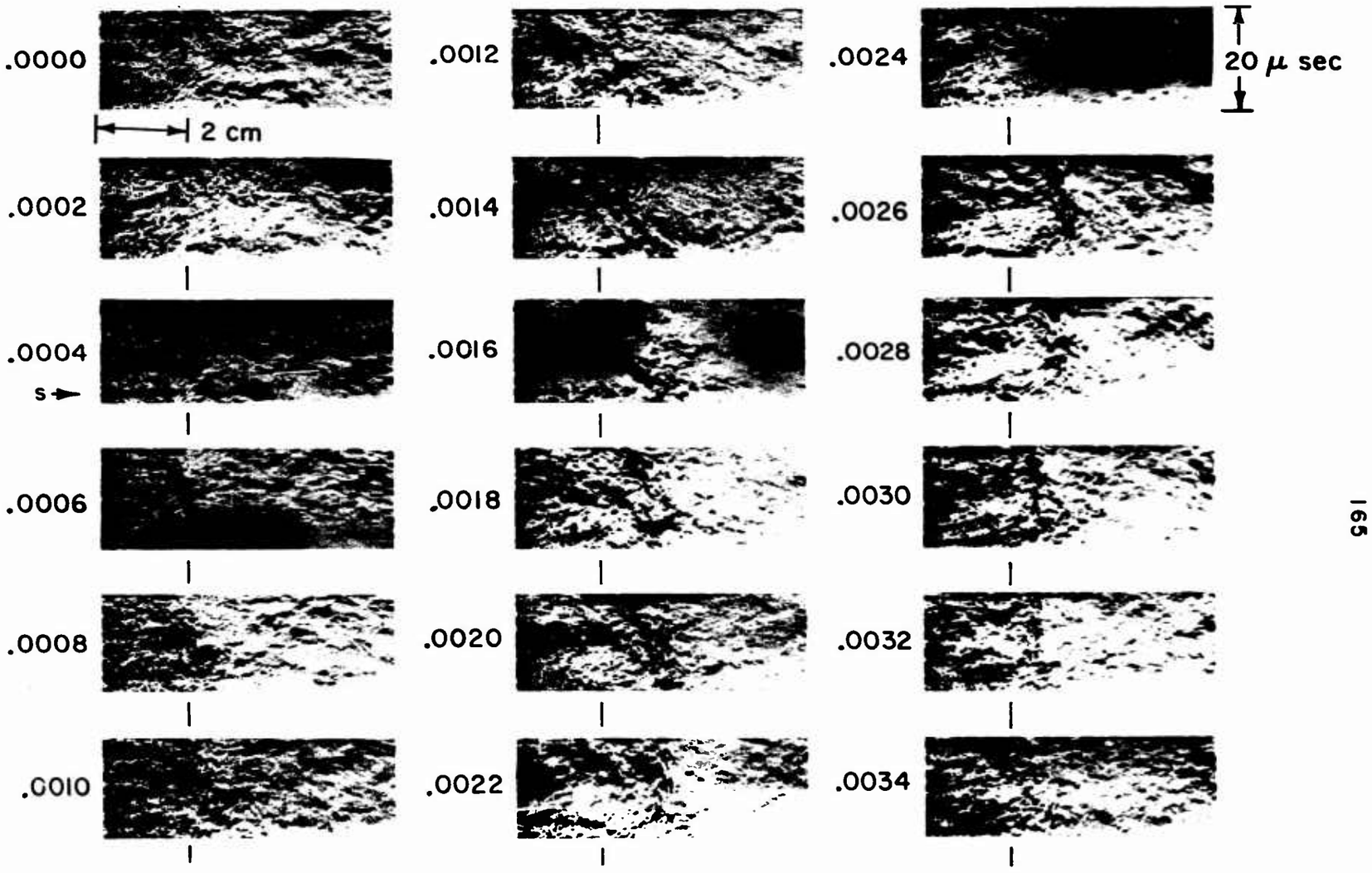

HIGH SPEED SCHLIEREN PHOTOGRAPHS OF UNSTABLE COMBUSTION H_2 + AIR

Φ = 2.62, $\bar{P}_c$ = 3.1 atm, $\bar{P}_{MIX}/\bar{P}_c$ = 2.8, L_c = 104 cm, 9 HOLE SHOWERHEAD
ΔP SHOCK/$\bar{P}_c$ = 0.08, f = 267 ± 10 cps, FUNDAMENTAL MODE
(SEQUENCE 2)

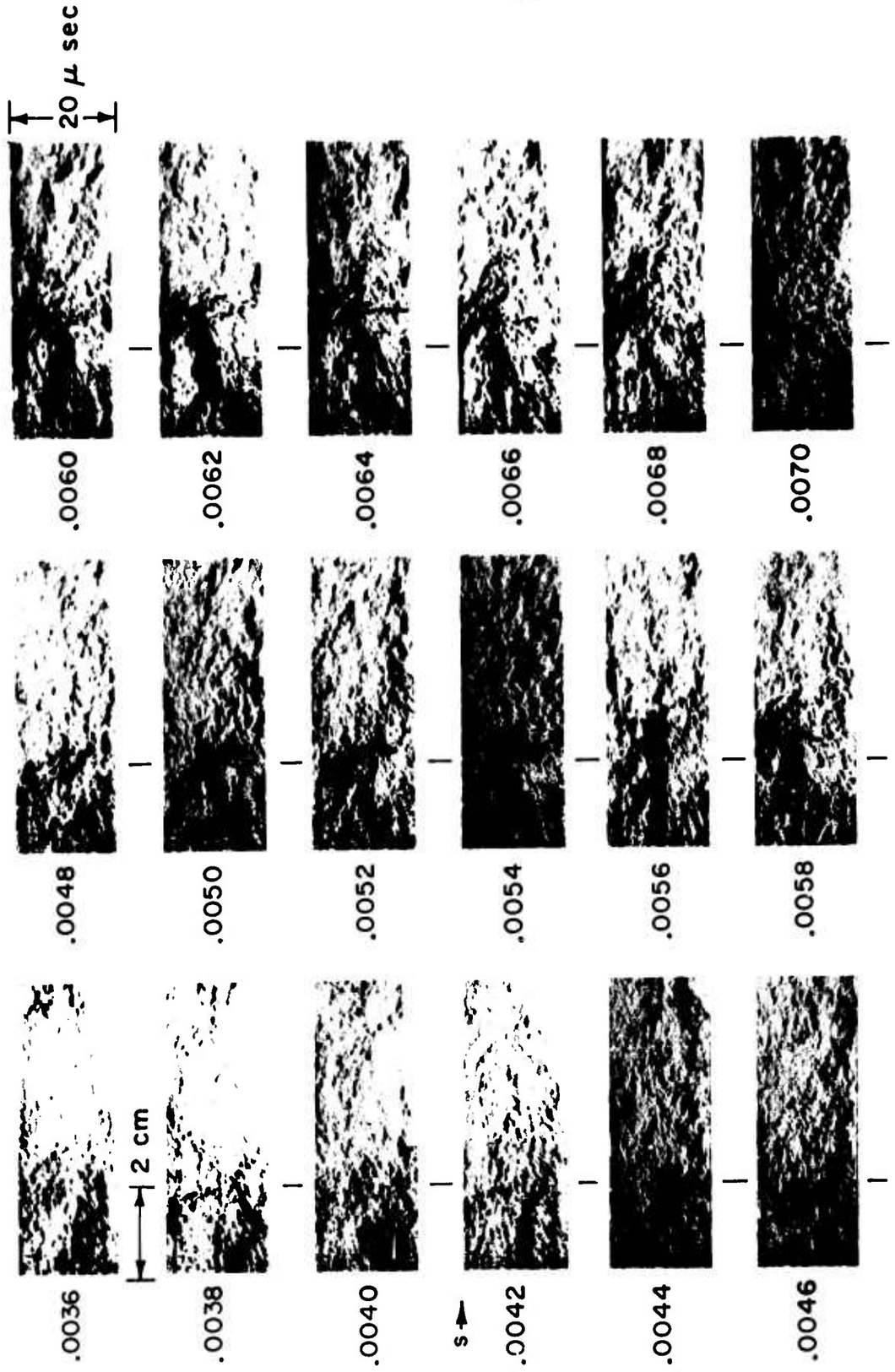

(SEQUENCE 2, continued)

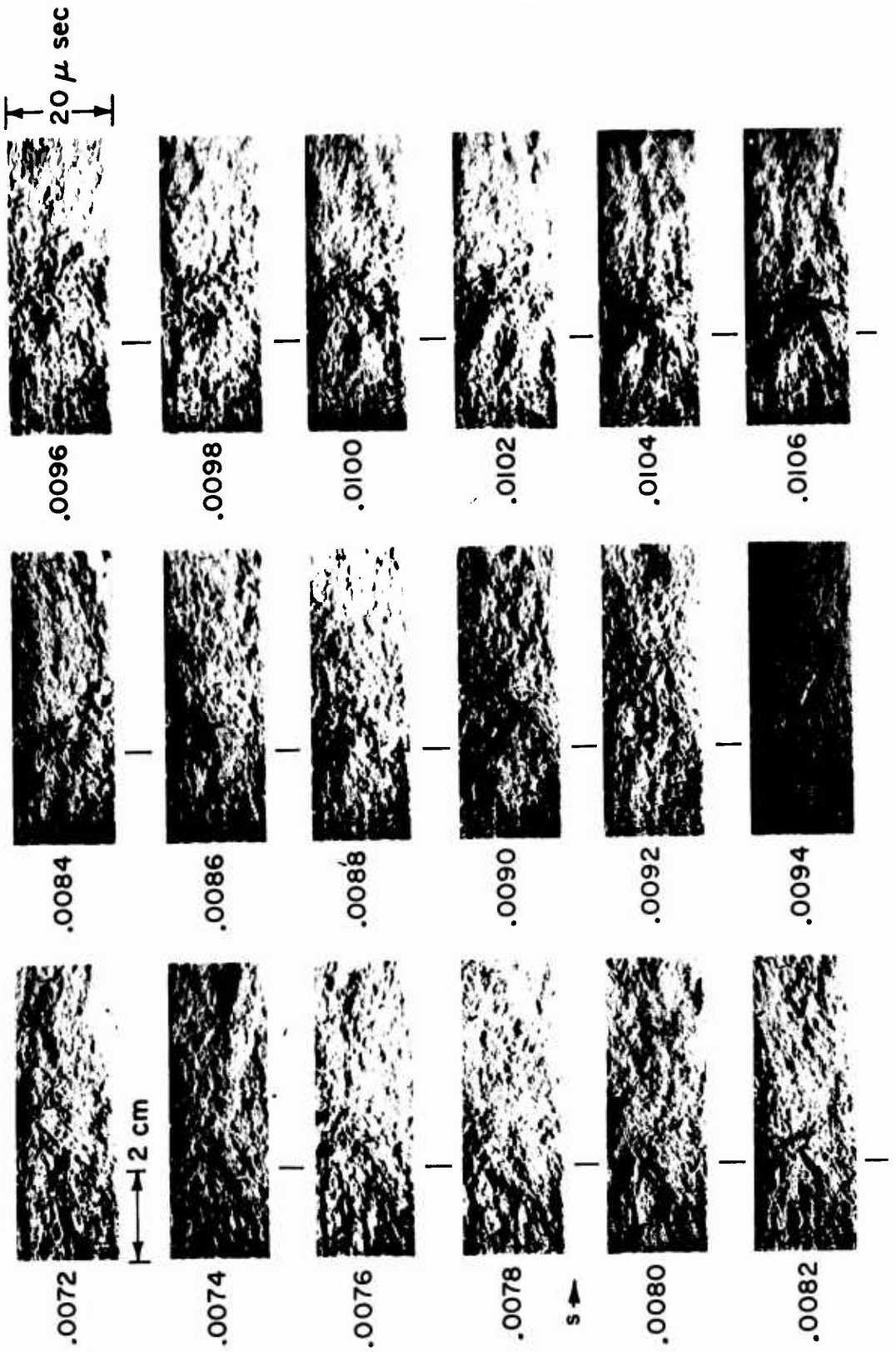

(SEQUENCE 2, continued)

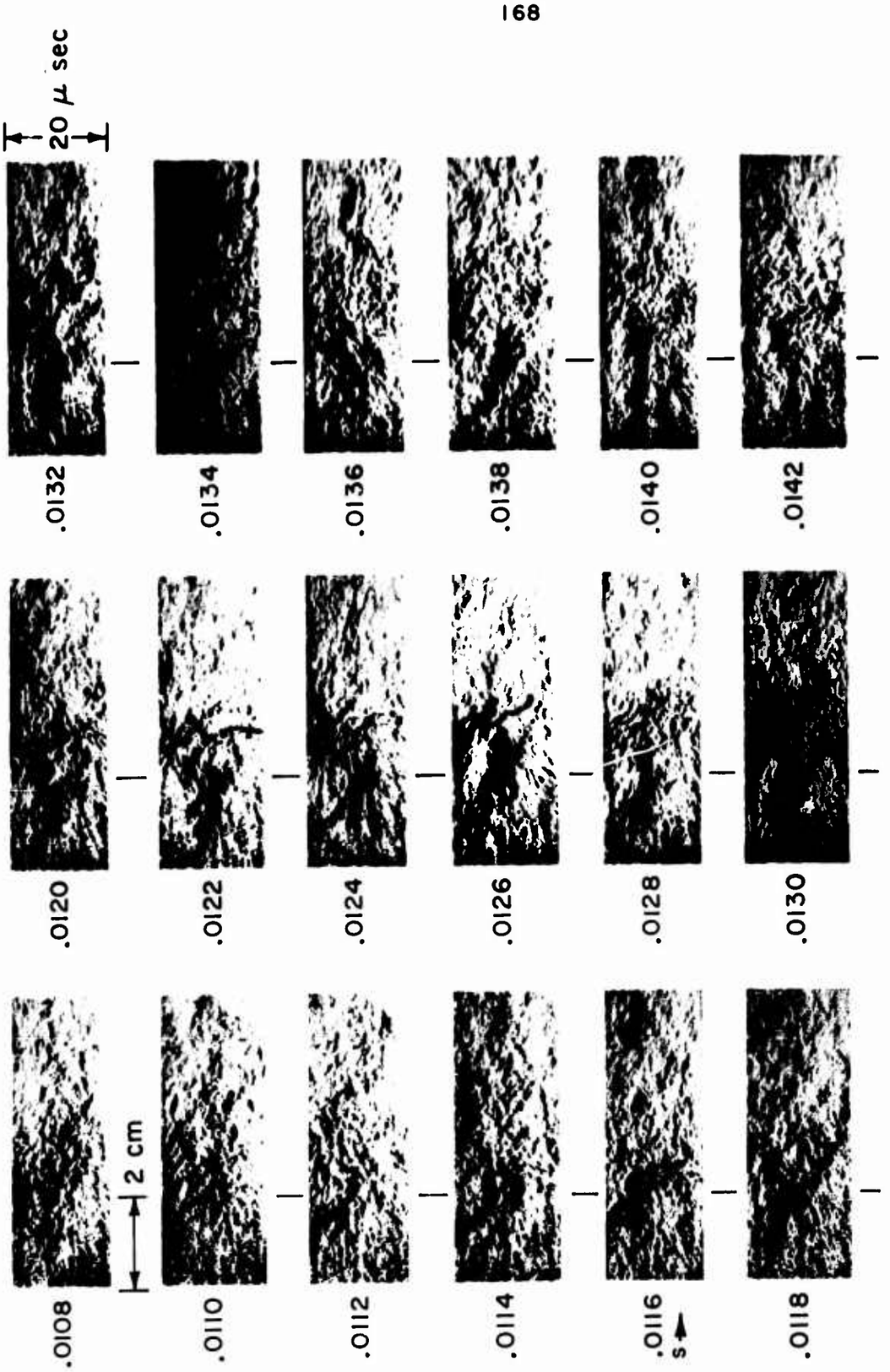

(SEQUENCE 2, continued)

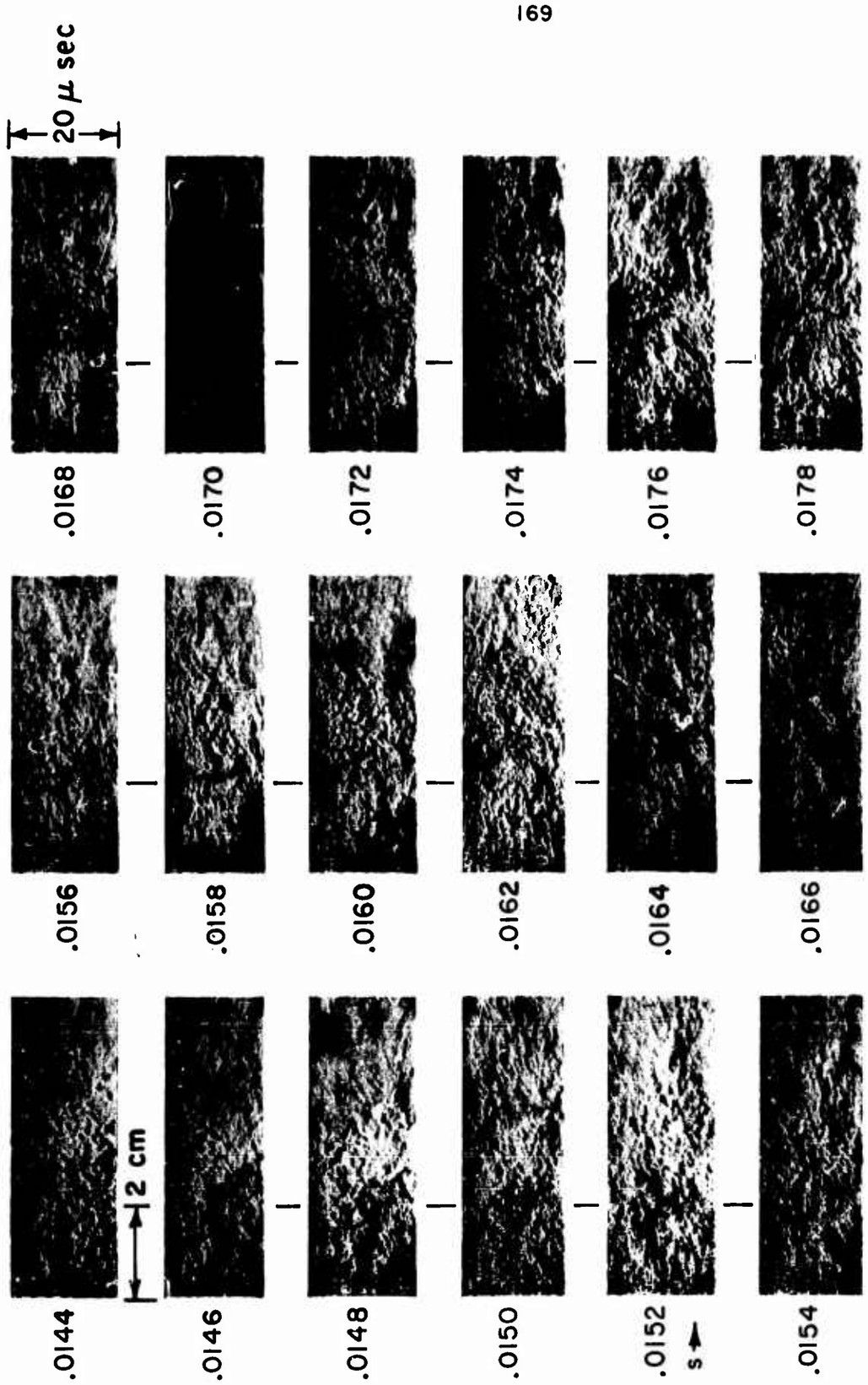

(SEQUENCE 2, continued)

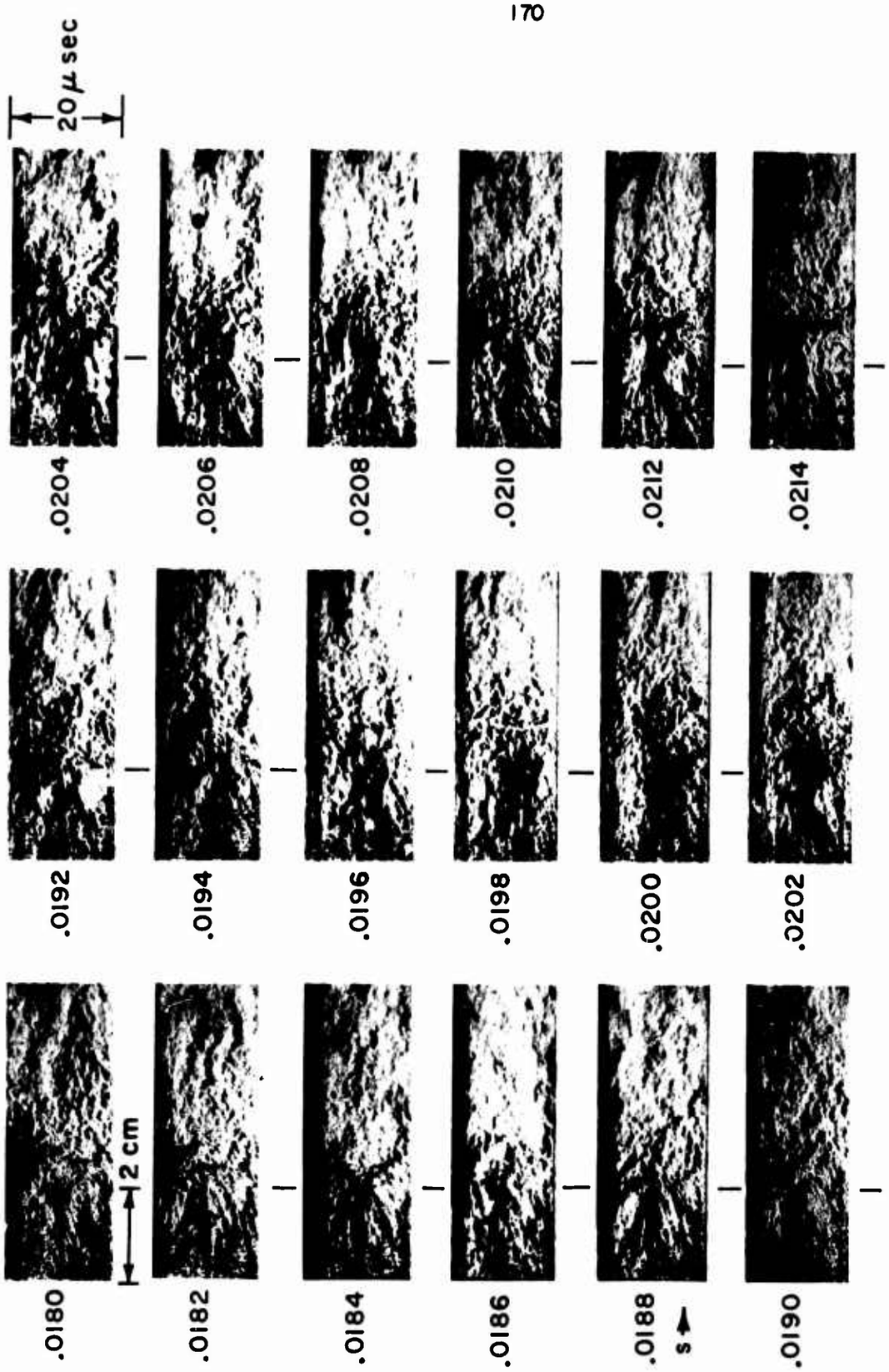

(SEQUENCE 2, continued)

CHAPTER V: A Combustion Model For The Premixed Gas Rocket

A. Introduction

In the preceding chapters emphasis has been placed on the necessity for developing a realistic analytical model of the coupled nonsteady burning process in the gas rocket. To this end a systematic interaction between theory and experiment has occurred in the course of this work. The predictions of the original Sirignano-Crocco theory aided in defining certain avenues of experimental work including the investigation of the stability characteristics of the CO $(H_2O)/O_2/N_2/CH_4$ system reported in Chapter IV. The quantitative disagreement between the experimental results of Bowman and the original theory do not negate the significance of the experimental work in terms of approaching the longer range goal. The stability limit data of Bowman with the $H_2/O_2/N_2$ system (choked showerhead injection), of Bowman, Pelmas, and this author with the $CH_4/O_2/N_2$ system (choked showerhead and unchoked porous plug injection), and the data (Chapter IV) from the CO work (porous plug injection) conclusively demonstrate the fundamental importance of the combustion temperature (and by inference the gas phase reaction kinetics) in determining the onset of nonsteady burning. The data obtained with the $CO(H_2O)/O_2/N_2$ system with CH_4 additive likewise demonstrate the important influence of the reactant chemistry at essentially fixed combustion temperature on the nonsteady burning characteristics of the system. The comparison (Chapter VI and Appendix D) of the stability limit data of the CO $(H_2O)/O_2/N_2$ and $CH_4/O_2/N_2$ systems in light of the currently available overall reaction rate data for these systems and the model developed in this chapter strongly supports the inference of a dominant role played by chemical kinetics in the coupling of the combustion process and the pressure oscillations.

In light of these results and the inadequacy of the original S-C model the series of diagnostic experiments described in the preceding chapter was carried out in order to improve the understanding of the structure of the combustion zone during

steady and nonsteady combustion. The data from the early temperature profile measurements and the direct photographs together with Bowman's suggestion of a factor of two difference between published and calculated (on the basis of experimental results and the original S-C model) activation energies for the H_2 + Air and $CH_4/O_2/N_2$ systems led to the formulation (originally due to Crocco) of a turbulent flame model of the combustion process. This model was developed in detail in the course of the present work and in fact provided the original impetus for the experimental examination of the importance in the coupling process of the propellant injection Mach number and the ratio of unburned to burned gas temperatures. These experiments are discussed in Section G of this chapter. The important elements of the turbulent flame model and its principal shortcomings are noted in Sections C and D.

The final series of schlieren and shadowgraph observations of the combustion zone were instrumental in the formulation of an improved turbulent combustion model of the nonsteady burning process in the gas rocket. Certain additional and equally important considerations contributed to the development of the final model. These factors are discussed in Section D. The steady-state model of the combustion process is discussed in Section E. The development of the appropriate combustion zone boundary condition used in the complete analysis of the nonsteady problem is completed in Section F.2. Solutions to the equations governing the linear and nonlinear system response are presented in Sections F.3 and F.4.

In order to provide a measure of cohesion to the subsequent developments, Section B is reserved for a general overview of the analytical problem and an outline of the important results of the Mitchell-Crocco nonlinear analysis of longitudinal mode pressure oscillations in a rocket motor. The results of their analysis have been applied in the present turbulent combustion models.

B. Analysis of the Wave Dynamics in the Combustion Chamber

The last ten years have seen the development of sophisticated analytical techniques for the treatment of nonlinear longitudinal mode combustion oscillations in liquid and solid propellant rocket

motors. The important contributions of Mitchell, Sirignano, and Crocco (21, 26, 27, 34, 35, 81, 82) have led to the formulation of a nonlinear analysis of the wave dynamics in the combustion chamber which provides a realistic and quite general framework for the consideration of longitudinal mode combustion instability in the gaseous propellant rocket motor.

A complete description of the nonlinear instability problem necessarily involves an analytical expression of:

(1) The wave dynamics in the combustion chamber

(2) The nonsteady behavior of the gas dynamic flow field in the nozzle

(3) The combustion process and the nonsteady coupling of the burning rate and the pressure oscillations.

The early diagnostic studies of the H_2 + Air combustion zone (the measurement of axial temperature profiles and the direct photographic observations) demonstrated that insofar as the wave dynamics of the gas rocket are concerned the combustion zone may be considered as short compared to the overall chamber length. Similarly the 4 hole plug nozzle provides a physically realistic approximation to the "short nozzle" which was originally analyzed by Crocco (3). These observations provide the necessary justification for the separate analytical treatment of the nonsteady processes in the combustion zone, the nozzle, and the combustion chamber. In view of the low mean flow Mach number (.005 to .02) of the product gases in the combustion chamber of the gas rocket the recent analysis of Mitchell and Crocco (34) becomes appropriate. In their "concentrated combustion model" the analysis of the wave dynamics in the combustion chamber is carried out independently of the combustion and nozzle conditions, the latter appearing as boundary conditions to the wave equation in the free stream. The analysis is valid for the case of low mean flow Mach number where the steady-state Mach number serves as a measure of the level of combustion in the chamber and of the mean outflow through the nozzle. The particular utility of the analysis lies in the fact that the combustion modelling aspects are divorced from the treatment of the chamber dynamics thus facilitating the examination of (in the present case) several turbulent combustion models. The

combustion model determines the functional form of the perturbation in particle velocity at the injector end of the motor and thus serves as the appropriate combustion zone boundary condition for the wave analysis. Similarly the short or quasi-steady nozzle condition allows a simple expression of the nozzle end boundary condition on the particle velocity. Finally, the necessary time (initial) condition is replaced by a cyclic condition on the nonsteady thermodynamic and gasdynamic variables.

Once a satisfactory description of the combustion zone response to the pressure waves is achieved the coupled problem can be readily solved. For the three turbulent combustion models examined in the course of this work the analysis ultimately leads to the formulation of an ordinary, nonlinear, integro-differential equation governing the form of the dimensionless pressure perturbation (over one period of oscillation). The attraction of the entire approach is the fact that one may simultaneously solve the linearized form of the final equation to obtain the linear system response and the full nonlinear form of the equation by numerical techniques to obtain the nonlinear response. Thus a determination of the system stability limits as well as finite wave amplitude and waveform within the regime of nonlinear instability can be made. The influence on the stability characteristics of the motor of the important system variables including the propellant chemistry and equivalence ratio, the combustion temperature and pressure, the mean flow Mach number and the chamber length is easily calculated.

For the sake of completeness the Mitchell-Crocco analysis of the wave dynamics in the combustion chamber for the case of concentrated combustion is reviewed in Appendix A. The principal constraints on the analysis appear in the assumptions. These are acceptable in terms of the characteristics of the gas rocket. The assumptions include:

(1) One dimensional flow in a uniform cross-sectional area chamber

(2) The length of the convergent section of the nozzle is short compared to the overall chamber length such that the Mach number at the nozzle entrance remains fixed during nonsteady operation

(3) The chamber flow is homentropic through second order in the wave amplitude. That is, the mean flow and the oscillations are considered isentropic. With regard to the mean flow, the analysis does not prohibit entropy oscillations at the combustion zone boundary. For the general case of nonsteady burning, product gases leave the combustion zone with differing entropies (for the gas rocket combustion zone the nonisentropicity lies mainly in the density waves) on the time scale of the pressure oscillations. However, the entropy wavelength is determined by the mean flow velocity. For the gas rocket the entropy wavelength is ($\lambda_s = U_b \cdot \tau_{per}$) and is ($\mathcal{O}$(.1 to 1 cm)). For the turbulent conditions of the mean flow it is likely that these waves will be strongly damped. With regard to the pressure waves the low amplitude oscillations characteristic of nonsteady gas rocket operation ($\Delta p/\bar{p}_c$ = ($\mathcal{O}$(0 to 0.20)) are nearly isentropic since

$$\frac{\Delta s}{c_v} = \mathcal{O}\left[\frac{\gamma^2-1}{12\gamma^2}\left(\frac{\Delta p}{\bar{p}_c}\right)^3\right]$$

(4) Implicit in the one dimensional homentropic flow assumptions is the assumption of adiabatic flow. In view of the measured axial temperature gradient ($\mathcal{O}$(-5 ^{o}K/cm)) in the gas rocket the adiabatic condition is an approximation the accuracy of which decreases at longer chamber lengths. The dispersive effect of a radial temperature profile on the plane propagating waves is ignored. In principle the analysis could be generalized to account for the negative axial gradient in the mean temperature (and, hence, in the flow velocity). For the gas rocket where the gradients are small compared to the mean values the existence of a finite axial gradient in the mean temperature leads to corrective terms in the first order equations. The influence of a corresponding axial gradient in the mean velocity appears only to second order. It can readily be shown that these corrective terms are negligible for short overall chamber lengths and increase in magnitude as displacement from the injector increases. The principal influence of a finite temperature gradient is to modify the wave travel time and to reduce the instantaneous power loss at the nozzle (that is to destabilize the system due to the decrease in nozzle entrance Mach number which is proportional to $\bar{T}^{-2}$).

(5) The product gases in the chamber are assumed to be uniform in composition and calorically perfect.

Under the above assumptions Mitchell combined the conservation equations of mass and momentum in the combustion chamber (no energy addition or removal along the chamber axis) to obtain the Riemann form of the equations,

$$\frac{\partial}{\partial t}\left(u + \frac{2}{\gamma-1}a\right) + (u+a)\frac{\partial}{\partial x}\left(u + \frac{2}{\gamma-1}a\right) = 0$$

$$\frac{\partial}{\partial t}\left(u - \frac{2}{\gamma-1}a\right) + (u-a)\frac{\partial}{\partial x}\left(u - \frac{2}{\gamma-1}a\right) = 0 \qquad \text{(V-1)}$$

Crucial to the analysis is the expansion technique used to express the thermodynamic and gas dynamic variables. The expansion parameter is set equal to the steady-state Mach number (a small parameter in the gas rocket case). The effect of this approach is to cause the combustion and nozzle effects which are of order $M \cdot p'$ to be of second order. This method is contrasted to Sirignano's approach (26, 27) where only the difference between the admittance functions is considered small to first order. Thus, to first order the combustion driving and nozzle damping influences are zero and the perturbations in the thermodynamic and gas dynamic properties are expressed through the simple acoustic equations in terms of a general first order function which is referred to here as the wave amplitude parameter, f. In the present work interest is primarily in the evaluation of the wave amplitude parameter at the injector (x = 0) and over the period of oscillation. At x = 0 the relationship between the dimensionless first order pressure perturbation and the wave amplitude parameter is,

$$p_1^\circ = 2\gamma M f^\circ \qquad \text{(V-2)} \qquad \text{where} \qquad p_1^\circ = \frac{\Delta p}{p_c}$$

A second order analysis is carried out in order to determine a single nonlinear ordinary differential equation governing the form of the wave amplitude parameter at the injector end over one period of oscillation. For a general combustion zone boundary condition, constant Mach number at the nozzle entrance, and the cyclic time condition[1], the equation takes the form (see Appendix A)

$$[f(\theta) - k]\frac{df}{d\theta} = \frac{\gamma-1}{\gamma+1} f(\theta) - \frac{u_2^\circ}{M^2(\gamma+1)} \qquad \text{(V-3)}$$

---

[1] It is required that all thermodynamic and gas dynamic variables be periodic (with period 2) in the "stretched" dimensionless time coordinate θ as discussed in Appendix A. For the nonlinear equations describing the combustion chamber the use of a stretched time coordinate eliminates the appearance of secular terms in the second order equations and allows the determination of periodic solution with a frequency slightly different from the acoustic frequency.

where the functional form of the perturbation in the particle velocity referenced to the injector end, U_2° , must be determined as the necessary input from the separate analysis of the combustion zone and of the response of the combustion process to to pressure oscillation. Mitchell shows that Equation V-3 can be solved directly for the nonlinear, finite amplitude form of f or linearized to determine the linear system response. In the case of shock type waves, k is interpreted as the average value of f at the shock discontinuity which is assumed to be at $x = 0$ at $\theta = 0$. In the linearized analysis k must be determined as a result of the linearization and is simply related to the first order correction in the period of oscillation.

C. Turbulent Flame Model of the Gas Rocket Combustion Process

The results from the temperature measurements and the direct photographs reported in Chapter IV support the concept of a structured finite-dimensioned turbulent flame zone. The photographs indicate that the steady-state H_2 + Air combustion process is characterized by the existence of turbulent flames - or flamelets - centered at each injection port of the choked-flow showerhead injector and extending axially into the combustion chamber. The temperature measurements confirm the presence of strong radial inhomogeneities in the local thermodynamic and gasdynamic properties within the combustion zone (defined in terms of the total chamber cross section and the axial distance from the injector to the peak in the temperature profile and the end of the luminous zone in the direct photographs) and indicate that combustion is complete within a few centimeters of the injector with the attainment of the adiabatic combustion temperature. The results with the H_2, CO, and CH_4 systems support the concept of the importance of gas phase kinetics in determining the response of the combustion process to the pressure waves. These considerations in addition to the apparent factor of two discrepancy between calculated and predicted overall activation energies suggested that the expression of the energy release rate in terms of a turbulent flame speed proportional to the square root of the Arrhenius factor, ($\sim e^{-E/2RT}$) might

be appropriate.

In addition, the direct photographic information and the axial temperature profiles provided a basis for estimating the residence time of the propellant gases in the combustion zone. Based on the injection port velocity ($\sim$ (3.6 x 10^4 cm/sec)) and the measured axial extent of the combustion zone (1 to 4 cm) this stay time was estimated at 3 x 10^{-5} to 10^{-4} seconds[1]. The ratio of this characteristic time to the measured period of oscillation is ($\sim$ (10^{-1} to 10^{-2})), (see Table II, Chapter III page 80). This comparison suggested that a quasisteady[2] treatment of the combustion zone would be appropriate.

With these considerations in mind Crocco formulated an improved model of the gas rocket combustion process. The model was refined and analyzed in the course of the present work. For reasons noted at the end of this section and in Section D, it was subsequently felt that a more physically realistic model of the combustion process could be constructed. However, insight gained in the development of the original turbulent flame model in addition to the qualitative results of that model proved invaluable in the later analysis.

As noted in Section B, the objective of the combustion modelling aspect is to obtain an expression for the perturbation in the particle velocity at the injector end (x = 0) in terms of the perturbations of the thermodynamic variables (ultimately in terms of the pressure perturbation). In the following developments all thermodynamic variables are nondimensionalized by their steady-state values at the equilibrium adiabatic burned gas state, velocities by the sound speed of the burned gases, axial position by the chamber length, and time by the wave travel time ($L_c^*/m \cdot \bar{C}_b^*$)

---

[1] It will be argued in Section D.4 that a more realistic estimate of the residence time of the combustion zone must take into account the velocity decrease due to expansion (chamber filling) in the zone.

[2] The term quasisteady used in reference to this model is not precisely accurate. An unsteadiness in the burning process was allowed due to the oscillation of the unburned gas volume. The residence time of both the unburned and burning zones was considered short compared to the period of oscillation.

in the burned gases, neglecting the influence of the mean flow.

The combustion zone was assumed to take the form of non-interacting cone-shaped turbulent flamelets as shown in Figure V-1 wherein nonsteady effects arise due to the sensitivity to the pressure oscillation of the burning rate, the injection mass flux (in the case of unchoked propellant injection), and the overall flame geometry or volume of unburned gases.

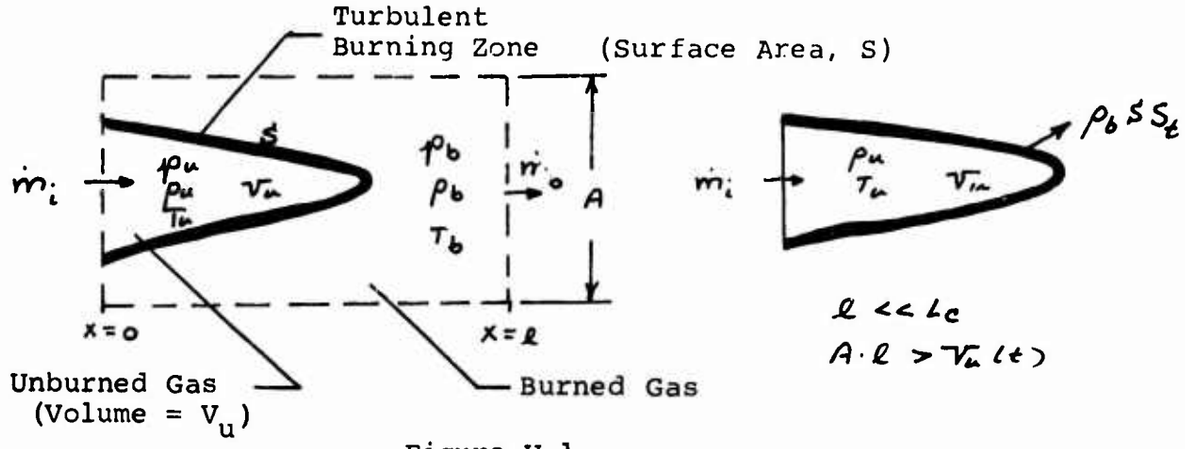

Figure V-1

With regard to the analysis based on the turbulent flame structure of Figure V-1, the following points were considered:

(1) Combustion occurs in a turbulence thickened flame zone extending from the lip of the injector port. The appropriate turbulence regime is that of high intensity small scale turbulence such that the turbulent mass burning rate can be evaluated in terms of a turbulent flame speed (S_t) and a mean burning area (S). The turbulent flame speed is in turn expressed in terms of a laminar flame speed (S_L) modified by a turbulent eddy conductivity (k_T).

(2) V_u is the finite volume of unburned propellant gases within the flame cone and is sensitive to the oscillating pressure by virtue of fluctuations in the location of the burning surface on the time scale of the pressure oscillations. However, the ratio of the unburned gas volume to the turbulent flame reference surface area, V_u/S is assumed to be time independent. For appropriate geometry the ratio is calculable in terms of the injector port

diameter, for example,

$$V_u/S = x = \frac{d_{port}}{b}$$ for conical geometry

(3) ℓ is a reference length chosen so that during non-steady burning the condition $A\cdot\ell / V_u > 1$ is preserved. Consideration of the mass conservation equation across $A\cdot\ell$ allows the derivation of the appropriate boundary condition applicable at x = 0.

(4) By virtue of the estimate of short residence time in the combustion zone compared to the wave travel time (and 6 below) the approximation of combustion at constant pressure is valid. Furthermore, the condition that $\ell/L_c << 1$ allows

$$p_u(t) = p_b(t) = p(t) \; ; \quad \bar{p}_u = \bar{p}_b = \bar{p}_c$$

(5) The negligible $\tau_{res,u}/\tau_{per}$ argument also allows the approximation that ρ_u and T_u are uniform at each instant. Furthermore, the intense level of turbulence in the volume $(A\cdot\ell - V_u)$ makes the approximation of uniform T_b and ρ_b at each instant acceptable despite the fact that $\tau_{res,b}$ in the burned gas volume may not satisfy the condition $\tau_{res,b}/\tau_{per} \ll 1$.

(6) The approximation that $\tau_{res,c}/\tau_{per} \ll 1$ and the assumption that the actual volume of the burning zone is small reduces the energy balance across the flame zone to a simple jump condition and in a sense supports the treatment of the turbulent mass burning rate in terms of an integrated steady state relationship. The hot and cold side boundary conditions remain unchanged during non-steady burning according to the model. That is,

$$\frac{dT}{dx} = 0 \quad \text{at} \quad T_u \text{ and } T_b$$

Thus, the condition $T_b = T_u + \mathcal{Q}/\bar{c}_p$ is applicable during non-steady burning.

Under these conditions the continuity equation across the control volume $A\cdot\ell$ is written as

$$\dot{m}_i = \dot{m}_b + \frac{d}{dt}\left[\rho_u V_u + \rho_b (A\cdot\ell - V_u)\right] \qquad \text{(V-4)}$$

which simplifies to

$$\dot{m}_i = \dot{m}_b^{\circ} + (1-\theta_i)\frac{d}{dt}(\rho_u v_u) - (\rho_u v_u)\frac{d\theta_i}{dp}\frac{dp}{dt} \qquad \text{(V-6)}$$

where

$$\theta_i = T_u / T_b$$

$$p_b = \rho_b T_b = \rho_u T_u$$

and $$\dot{m}_b^{\circ} = \dot{m}_b + A \cdot \ell \, d\rho_b/dt$$

The term $\dot{m}_b^{\circ}$ is interpreted as the total rate of change of burned gas mass in the combustion chamber relative to the x = 0 position. By formulating the combustion zone boundary condition in this fashion the gap is bridged between the wave dynamics analysis requirement of a boundary condition at x = 0 and the treatment of a finite dimensioned flame zone extending beyond x = 0. Perturbations in $\dot{m}_b^{\circ}$ lead directly to perturbations in u_2° .

A second continuity equation valid across the flame introduces the turbulent flame speed, S_t, as

$$\dot{m}_i = \rho_b S S_t + \frac{d}{dt}(\rho_u v_u) \quad , \quad S = \frac{v_u}{x}$$

whence

$$\frac{d}{dt}(\rho_u v_u) + \frac{S_t}{x}(\rho_u v_u) = \dot{m}_i \qquad \text{(V-7)}$$

is considered as an ordinary differential equation for the instantaneous mass ($\rho_u v_u$) within the turbulent flame cone. The equation can be integrated to yield

$$\rho_u v_u = \int_{-\infty}^{t} \dot{m}_i(t') \left[e^{-\int_{t'}^{t} \frac{S_t(t'')}{x} dt''} \right] dt' \qquad \text{(V-8)}$$

where the lower limit is set equal to $-\infty$ since ($\rho_u v_u$) is considered to vary periodically at times sufficiently long such that starting transients have become negligible. Only the limiting periodic solution is relevant. Hence,

$$\frac{d}{dt}(\rho_u v_u) = \dot{m}_i(t) - \frac{S_t}{x}(\rho_u v_u) \qquad \text{(V-9)}$$

For the case of isentropic variation of the unburned gas properties

$$\frac{d \ln T_u}{d \ln p} = \frac{\gamma_u - 1}{\gamma_u}$$

Applying the jump condition across the flame

$$\frac{d \ln T_b}{d \ln p} = \frac{\gamma_u - 1}{\gamma_u} \theta_i$$

Substituting these expressions into Equation V-6 an equation for the perturbation in mass efflux from the combustion zone extrapolated to the injector face is obtained as

$$\frac{\dot{m}_b' - \bar{\dot{m}}}{\bar{\dot{m}}} = \left\{ \theta_i \frac{\dot{m}_i'}{\bar{\dot{m}}} - 1 + [(1-\theta_i)\frac{S_t}{\alpha} + \frac{\gamma-1}{\gamma}\theta_i \frac{g}{\bar{c}_p T_b} \frac{d \ln p}{dt} \int_{-\infty}^{t} \frac{\dot{m}_i'}{\bar{\dot{m}}} e^{-\int_{t'}^{t} \frac{S_t(t'')}{\alpha} dt''} dt' \right\}$$

To determine the nonsteady combustion zone response all thermodynamic variables are expanded about their steady state values. The nonsteady flame speed is coupled to the pressure oscillation by expressing the instantaneous flame speed in terms of the steady state value plus a perturbation proportional to the oscillating pressure at the injector. There is no lag in the response of the flame speed. Thus

$$S_t = \bar{S}_t [1 + \Sigma p_i'^{\circ}] , \qquad \Sigma = \Theta(1)$$

Spalding's centroid rule is employed to relate the steady state value of the flame speed to a temperature explicit reaction rate in the following form

$$\bar{S}_t = \left[\frac{1}{\lambda} \frac{\bar{k}_T \int_0^1 \bar{R}(\bar{T}) d\bar{T}}{(\bar{T}_b - \bar{T}_u) \bar{c}_p^2 \bar{\rho}_u^2} \right]^{\frac{1}{2}}$$

where

$$\bar{R} = \bar{C}_1 g \bar{\rho}_{O_2}^{n} \bar{\rho}_f^{m} e^{-E/R\bar{T}}$$

$$\lambda = .5 - .66(1 - \tau_0) - .43(1 - \tau_0)$$

$$\tau = \frac{T - T_u}{T_b - T_u}$$

For a bimolecular, second order rate law the expression for the flame speed reduces to

$$\bar{S}_t = \frac{\bar{\theta}_i}{\bar{c}_p (1-\bar{\theta}_i)^2} \left[\frac{\bar{k}_T \bar{C}_1 g \nu_{O_2,i} \nu_{f,i}}{\Phi} \right] \left\{ \frac{[\bar{\Phi} - (\Phi - 1)\bar{\theta}_i][E_0 - E_1] - [E_1 - E_2]}{\lambda T_b} \right\}^{1/2}$$

where $E_j = E_j(H)$ = exponential integrals, $H = E/RT_b$

$\sigma_{o_2,i}, \sigma_{f,i}$ = unburned reactant mass fractions

$\bar{C}$ = pre-exponential factor

The proportionality factor or response function in the flame speed expansion is evaluated in terms of the steady state expression as

$$\Sigma = \frac{\bar{\rho}}{\bar{\xi}_t} \frac{d\bar{\xi}_t}{d\bar{\rho}}$$

The possible sensitivity of the injection mass influx to the oscillating pressure at the injector is accounted for by expressing the instantaneous mass flux in a similar Taylor series expansion about the steady state value,

$$\frac{\dot{m}_i(t)}{\bar{\dot{m}}} = 1 - \psi \rho_1'(t)$$

where the response function, ψ , is evaluated in terms of the steady state expression for isentropic flow through a convergent port. This expression is presented in Section F.2 in connection with the final model. For the case of choked propellant injection, the condition

$$\psi = 0 \;, \quad \dot{m}_i = \bar{\dot{m}}$$

is observed.

The relationship between $\frac{\dot{m}_b^\circ - \bar{\dot{m}}}{\bar{\dot{m}}}$ and u_2° is straightforward. When the mathematics are completed, a concise nonlinear, ordinary, integro-differential equation governing the form of the wave amplitude parameter is obtained as

$$\left[f - k + \frac{C}{\bar{S}}\right] = Af + B\bar{S}\int_{-\infty}^{\theta} f(t')e^{-\bar{S}(\theta - t')}\,dt' \qquad \text{(V-10)}$$

where A, B, C = Functions of $(\gamma_u, \bar{\theta}_i, \Sigma, \psi)$

and

$$\bar{S} = \frac{\bar{\xi}_t}{\chi} = \frac{L_c^*/m\bar{C}_b^*}{\tau_{comb}^*} = \frac{\text{wave travel time}}{\text{combustion time}}$$

The solution of the governing equation for the case of finite amplitude discontinuous shock-type waves required two separate analyses. The final expressions derived for $\bar{S}_t$ and Σ are algebraically complicated and depend in a rather involved fashion on the important system variables. A Fortran IV computer program was developed to evaluate these parameters and to determine the range of values for the parameters A, B, C, and S appearing in the governing ODE corresponding to realistic values of the important system variables. A second program was developed to facilitate the solution of equation V-10. An iterative technique using the method of successive approximations and based on a scheme employed by Sirignano (81) to solve a similar equation arising in the study of nonsteady burning of a solid propellant rocket motor was applied. The method of solution and the program developed were applicable with slight modifications to the solution of similar governing equations derived in the course of the evaluation of subsequent combustion models. Discussion of the numerical technique is deferred until Section F.4 where the final form of the combustion model ultimately developed is obtained.

It has been noted that this original turbulent flame model proved to be unacceptable. The decision to reject the model was based on several important considerations regarding the mechanism of turbulent combustion in the gas rocket. The inability to obtain reasonable quantitative agreement between the original model and experimentally measured stability characteristics underscored the inadequacy of the turbulent flame model.

D. General Considerations Leading to a Reformulation of the Combustion Model

For purposes of discussion the factors influencing the development of an improved analytical model of the gas rocket combustion process are conveniently categorized as follows:

(1) Questionable aspects of the original turbulent flame model and the inability to obtain satisfactory numerical results for realistic values of the important system parameters

(2) Experimental results derived from the schlieren and shadowgraph studies of the steady and nonsteady combustion zone

(3) Reconsideration of the basic nature of the combustion process in the gas rocket drawing on the available literature concerning turbulent combustion, flame stabilization, and calculations and experimental evidence for the importance in the gas rocket of strong recirculation of hot product gases

(4) Critical examination of the order of magnitude of the characteristic chemical kinetic time compared to the period of oscillation observed experimentally.

These points are elaborated upon in the following paragraphs.

D.1 Influence of the Original Turbulent Flame Model

The turbulent flame combustion model developed in Section C is similar to the earlier analyses of Merk discussed in Chapter II. The difficulties realized by Merk in obtaining predictive results from his analyses were similarly encountered in the numerical evaluation of the combustion zone response and the coupled system ODE (Equation V-10). The inability to obtain quantitative results for realistic choices of the basic system parameters[1] is not surprising in view of (a) the emphasis on the importance of the isentropic response of the thermodynamic properties of the unburned gases to the pressure oscillations, and (b) the expression of the mass burning rate in terms of a turbulent flame speed expression and the fixed volume to surface area expression. The burning rate response in the model is due explicitly to the response of the turbulent flame speed to the pressure oscillation and implicitly to the fluctuation in $(\rho_u v_u)$. The overriding importance of the specific heat ratio of the unburned gas, γ_u, in determining the nonsteady burning characteristics derives from

[1] The system parameters incorporated in the model included the propellant equivalence ratio, the overall activation energy, the heat of combustion, the thermodynamic properties of the unburned and burned gases, the chamber length and the oscillation mode order. As noted in Section C the governing nonlinear ODE was solved successfully using the iterative technique discussed in Section F.4. A well-defined range (in terms of $\tilde{A}, B, C, \Sigma, \bar{S}_t$) of discontinuous shock-type solutions was found. The appropriate numerical values of A,B,C, corresponding to discontinuous solutions could only be obtained for realistic values of E for $\gamma_u > 1.6$ or conversely for realistic choices of γ_u, $E > 60$ to 80 was required.

the assumed isentropic response of the unburned gas in the volume V_u . The response of the flame speed is zero in the absence of unburned gas response. Allowing for the possibility of a sensitive volume of unburned gases within the combustion zone the expression of the burning rate by means of a Damkohler-type turbulent flame speed expression evaluated in terms of a laminar flame speed modified by an appropriate eddy conductivity is limiting. As one quickly realizes upon recourse to the volume of literature on turbulent combustion phenomena (e.g., (130-144)), the very concept of a turbulent flame speed referenced to an appropriate surface area is nebulous and little agreement exists among various investigators in the field with regard to flame speed calculations. This is especially true for the region of high intensity small scale turbulence characterizing the gas rocket combustion process and to which the Damkohler expression is restricted. It can be argued that within certain regimes of turbulence a turbulent flame appears to propagate in a one-dimensional fashion similar to the propagation mechanism in a simple laminar flame. Considered as an in-depth 1-D reaction zone and analyzed by a simple thermal model where the turbulent diffusivity ϵ replaces $\lambda/\rho c_p$, Summerfield (132) has shown that the similarity relationship

$$\frac{S_t d_t}{\epsilon} = \frac{S_L d_L}{\nu}$$

where d_t and d_l are the respective thicknesses of the turbulent and laminar flames may be relevant.

Regardless of the formulation chosen the question of the basic validity of the turbulent flame speed concept remains, particularly (as will be shown) in view of the characteristics of the gas rocket combustion zone. In the present case introduction of the turbulent flame speed and the surface area to define the burning rate leads to the inclusion of the unknown (arbitrary) eddy conductivity and a specified V_u/S ratio. (The Summerfield similarity hypothesis would further complicate matters with the introduction of the turbulent flame thickness as a second arbitrary parameter.)

D.2 Influence of Schlieren and Shadowgraph Observations

The principal observations made on the basis of the spark and high speed schlieren and shadow photographs have been noted on pages 150 to 170 of Chapter IV. As indicated the optical work was carried out in conjunction with the analytical development of the combustion zone boundary condition. The following observations are emphasized:

(a) The assumption underlying the combustion zone response in the turbulent flame model seemed unrealistic. The assumption of a finite volume of uniform unburned premixed propellant (volume large with respect to the actual burning zone) fluctuating in size and responding isentropically to the pressure oscillations was not substantiated. There was, in fact, no evidence that the region of unburned gases which was correlated with the underexpanded portion of the choked jets plays a critical role in the combustion process. Indeed a more likely circumstance is that the unburned gases are relatively insensitive to the pressure oscillations.

(b) The postulated thinness and overall constant geometry of the burning zone was not substantiated. On the contrary and in agreement with the direct photographs and the axial temperature profiles the "combustion zone volume" was observed to be large in comparison with the zone of unburned gases. The combustion zone was observed to oscillate in overall extent in response to the pressure oscillations.

D.3 Basic Considerations on the Gas Rocket Combustion Process

With the completion of the combustion zone diagnostic experiments and the analysis of the initial turbulent flame combustion model the principal features of the combustion process in the gas rocket had been clarified. Obviously the turbulent combustion process is quite complex and there is little hope for an exact detailed analytical expression of the phenomena. At best one can only attempt to account for the gross aspects of the process.

One of the most useful early approaches to the general problem of turbulent combustion is that of Summerfield (132) who distinguished three regimes of turbulent combustion depending upon the characteristic ratio of mixing to combustion time, τ_{mix} / τ_c

A regime of weak turbulent combustion where $\tau_{mix}/\tau_c >> 1$ is amenable to analysis in terms of a wrinkled laminar flame where burning proceeds over an enlarged surface area but locally at essentially the laminar flame speed characterizing the unburned propellant. With increasing turbulent intensity a regime of stronger turbulent combustion, $\tau_{mix}/\tau_c \simeq 1$ is encountered. Turbulent burning occurs in this regime in a distributed in-depth reaction zone which can be analyzed by a simple thermal model. It is for this intermediate regime of turbulent combustion that Summerfield's similarity relationship $S_t d_t/\epsilon = S_L d_L/\nu$ was proposed. Combustion is limited in this regime by the criterion that sufficient time (eddy lifetime) exists for combustion to proceed within macroscopic eddies according to the laminar microscale laws of heat conduction and diffusion. Thus for the cases where $\tau_{mix}/\tau_c \gtrsim 1$, combustion in a turbulent stream essentially resembles laminar flame propagation. A consideration of the published studies of turbulent flames (130, 132, 134, 138) reveals that typically such flames for hydrocarbon fuels are stabilized on burners at atmospheric pressure up to mean port velocities ($\sim 10^2$ cm/sec) by the mechanism of self propagation of the flame into the unburned premixed gas by means of turbulent diffusion and heat conduction. Stabilization of turbulent flames at the lower end of the τ_{mix}/τ_c range ($\simeq$ 1) and in streams with velocities up to 3×10^3 cm/sec is only achieved by surrounding the burner port with a hot sheath of product gases from a pilot flame.

Summerfield distinguishes a third regime of turbulent combustion where $\tau_{mix}/\tau_c < 1$. For sufficiently intense levels of turbulence in the combusting stream (achieved by virtue of increased flow velocity and Reynolds number, higher pressure drop across the port, large radial and/or axial gradients of velocity at the burner port) the turbulent eddy lifetime becomes short compared to combustion times and a vigorous stirring of unburned reactants and product gases is achieved. The ideal upper limit of $\tau_{mix}/\tau_c = 0$ corresponds to the well-stirred reaction zone,

an extended zone of uniform composition and temperature where overall burning rates are high and the concept of a turbulent flame speed meaningless. Such flames are approached on open burners only in the presence of intense pilot flames. In practice turbulent combustion in high velocity, $U > 5 \times 10^3$ cm/sec, premixed streams corresponding to Summerfield's regime of $\tau_{mix} / \tau_c < 1$ has only been achieved in enclosed systems where the mechanisms of flame stabilization and propagation bear little resemblance to those characterizing the lower turbulent regime open burner flames. In the following paragraphs it will be shown that the steady combustion process in the gas rocket must properly be considered to lie in this third, $\tau_{mix} / \tau_c < 1$, regime. In Section E, a realistic model of the steady combustion process in the gas rocket is developed.

For the H_2 + Air system with showerhead injection, the unburned premixed propellant is admitted to the combustion chamber in streams having port velocities, $U_i \simeq 3.6 \times 10^4$ cm/sec and Reynolds numbers based on port diameters (Θ(6 to 8 x 10^6)). The corresponding pressure ratio across the injector, $p_{inj} = \frac{p_{mix}}{p_c}$ are (Θ(2.0 to 3.5)) with the effective area expansion ratio of

$$A_c / (n_{hole} \cdot A_{port}) \geq 150/1$$

For the range of Φ and $\dot{m}_{tot}$ considered in the experimental work and in view of the diagnostics results a conservative estimate of the "space heating rate" ($\dot{q}_{tot}$, $\frac{cal}{cm^3 sec}$) under typical near limit conditions for the H_2 + Air system can be made,

$$\dot{q}_{TOT} = \frac{\dot{m}_{TOT} \cdot \nu_{H_2} \cdot q_{H_2}}{V_{comb}}$$

For

$\Phi = 2.40$ $\quad q_{H_2} = 2.87 \times 10^4$ cal/gm H_2

$\nu_{H_2} = .0122$ $\quad \bar{p}_c = 7.8$ atm, $\dot{m}_{TOT} = 25$ gms/sec

The combustion volume is conservatively estimated on the basis of Figures IV-38, 39 which indicate an axial extent of the

combustion zone to be (Θ(2.5 cm)) for the above conditions,

$$V_c = \Theta\left[\left(\frac{A_c}{n_{holes}}\right)\cdot \ell_c\right] = \Theta\left[9.1\,cm \times 2.5\,cm\right] = \Theta(23\,cm^3)$$

$$\dot{q}_{TOT} = \Theta\left[25 \times .0182 \times 2.87 \times 10^4/23\right] = \Theta\left(400\ \frac{cal}{cm^3 sec}\right)$$

As pointed out by Longwell (113), space heating rates of this order can only be rationalized on the basis of a high intensity turbulent combustion model. In order to achieve complete combustion of this intensity a strong mixing of unburned, reacting, and product gases must occur. It is clear that the extremes of injection Reynolds No., pressure drop, and velocity must lead to large radial and axial velocity gradients near the injection port and generally to high levels of turbulence in the mixing zones of the expanding propellant jets. Within the mixing zones of the propellant jets the high intensity turbulence will naturally lead on the microscale to rapid dissipation of local fluctuations in temperature and composition. The question arises as to the mechanism by which hot product gases are supplied in sufficient quantities to the jet mixing region to sustain the steady high intensity combustion process in the high velocity streams.[1] In this regard it is helpful to consider the one-dimensional, idealized, steady-state integrated momentum equation for the control volume surrounding the expanding propellant jet. As shown in Figure V-2, the propellant jet expands from a single port to fill a tube of cross-sectional area, $A_{eff} = A_o/n_{port}$.

---

[1] The injection conditions in the gas rocket can be compared to those used by Longwell, Hottel, Blichner, and others (118, 120, 121, 122, 126) in the so-called well-stirred reactors. As in the gas rocket, injection of premixed gaseous reactants into the small volume of the stirred reactor is achieved by means of numerous underexpanded sonic jets. A steady combustion process in the stirred reactor is assured by the presence of the opposing outer wall upon which the propellant jets impinge. A vigorous stirring of products and reactants occurs in the zones between the jets.

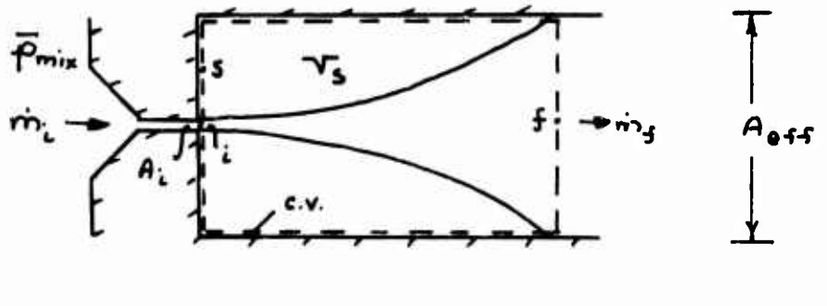

Figure V-2

For this illustrative calculation the effect of combustion is simply to influence the burned gas thermodynamic and gas dynamic properties and the fully expanded plane, f .

The momentum equation for the control volume, assuming no transverse fluid motion across the control volume boundaries, is,

$$p_i A_i + p_s (A_{eff} - A_i) + \dot{m}_i u_i = p_f A_{eff} + \dot{m}_f u_f \qquad \text{(V-11)}$$

For the case of unchoked mass injection flux the static pressure in the injection plane in the volume V_s surrounding the jet is equal to the static pressure in the injection plane (i) of the jet and Equation V-11 simplifies to,

$$p_s = p_f - \frac{\dot{m}_{eff}}{A_{eff}} (u_i - u_f)$$

where $\dot{m}_{eff} = \dot{m}_i = \dot{m}_f = \dot{m}_{tot} / n_{holes}$

In this case the momentum equation must be solved simultaneously with the remaining conservation equations for the control volume. Solutions for the local static properties in the injection plane have been obtained numerically for a range of injection conditions in connection with the experimental study of the influence of the injection Mach number on the nonsteady burning process. Typically, due to the gas rocket injection condition of $U_i > U_f$, the injection pressure is always slightly less than the steady downstream pressure, that is $p_i = p_s < p_f$.

For the typical case of choked underexpanded mass injection flux the static pressure in the jet injection plane, P_i, is determined by the upstream stagnation conditions in the mixing chamber, $p_i \neq p_s$. The momentum equation can be solved for the pressure in V_s at the injection plane,

$$p_s = \frac{p_f A_{eff} - p_i A_i - \dot{m}_{eff}(u_i - u_f)}{(A_{eff} - A_i)} \qquad \text{(V-12)}$$

For typical H_2 + Air combustion, $\Phi = 2.0$

$\dot{m}_{tot} = 25$ gms/sec, $n_{holes} = 10$, $\dot{m}_{eff} = 2.5$ gms/sec

$p_f = 7.8$ atm $= 7.90 \times 10^6$ dynes/cm^2

$u_f = 10^3$ cm/sec

$u_i = C_i = 3.6 \times 10^4$ cm/sec

$p_{mix} \simeq p_{stag} = 19.4$ atm, $p_i \simeq .52\, p_{mix} = 10.1$ atm

$A_{eff} = 0.91$ cm^2 $\qquad p_i = 1.025 \times 10^7$ dynes/cm^2

$A_i = 0.006$ cm^2

Thus, for $A_i/A_{eff} \ll 1$ which is true for all showerhead injection conditions in the gas rocket

$$p_s \simeq p_f - \underbrace{\frac{A_i}{A_{eff}} p_i}_{\Theta(6.8\times10^4 \frac{dynes}{cm^2})} - \underbrace{\frac{\dot{m}_{eff}}{A_{eff}}(u_i - u_f)}_{\Theta(9.6\times10^4 \frac{dynes}{cm^2})} \qquad \text{(V-13)}$$

and under the above conditions an estimate of the pressure difference between the injection plane and the fully expanded section in the volume V_s is obtained as,

$$p_f - p_s = 1.6 \times 10^5 \frac{dynes}{cm^2} \simeq .12\ atm \simeq 2\ psi$$

Thus, for the showerhead injection configuration of the gas rocket under both choked and unchoked injection conditions, there exists an appreciable rise in static pressure between the injector face and the fully expanded flow section. The additional term appearing in Equation indicates that this pressure recovery is larger for increased jet underexpandedness. Clearly a strong pressure driving force for recirculatory flow of combustion products from the downstream portion of the expanded jet upstream toward the injector is present during combustion with the showerhead injectors.

The contrast between the combustion process in a laminar or "conventional" turbulent burner flame and that in the gas rocket is emphasized. In the conventional system a slight pressure drop ($\mathcal{O}(10^{-5}$ atm)) and a strong ($\mathcal{O}$(6 fold)) velocity increase due to product expansion in the vicinity of the flame are typical. In the gas rocket combustion process (neglecting for a moment the effects of jet underexpandedness) a pressure rise occurs along the axis and is estimated at some 4 orders of magnitude larger than the pressure drop experienced in the conventional flame. Furthermore, due to the chamber filling expansion process in the gas rocket a velocity decrease by a factor of ($\mathcal{O}$(0.03)) occurs.

The intensity of the recirculatory flow of hot products accompanying the pressure gradient near the injector can be estimated. Considering the volume surrounding the expanding and combusting jets to be composed of product gases at the adiabatic burned gas temperature (neglecting heat losses to the injector and to the surrounding chamber), for $\Phi = 2.0$, $T_s = T_b = 1644\ ^{\circ}K$, and $\rho_f = \rho_b = 1.53 \times 10^{-3}$ gms/sec, Bernoulli's equation provides an estimate of the maximum velocity achievable in a stream tube due to the predicted pressure gradient,

$$(u_s)_{max} = 2\left(\frac{p_f - p_s}{\rho_f}\right)^{1/2} = 1.3 \times 10^{4}\ cm/sec$$

Certainly the calculation overestimates the actual velocity realized in the recirculation zone, but the point should be clear.

For the geometry of the gas rocket injection scheme the fluid dynamics serves to provide the mechanism of flame stabilization of the combusting high velocity propellant jet as well as to satisfy the macroscale mixing requirement responsible for the measured intensity of the combustion process. Reaction must be initiated in the mixing zone of the expanding jet by the forced recirculation of hot product gases to the base of the jet followed by the microscale turbulent exchange of mass and energy between hot products and the unburned gases.

In many respects the mechanism of turbulent combustion in the gas rocket resembles that in the so called "tunnel burners" where stabilization of combustion in a high velocity field is similarly achieved at a discontinuous expansion in cross-sectional areas. Ievlev (138) probed the pressure field in the vicinity of the step change in flow area and determined the extent of the finite regime of reverse flow. This measured zone of "negative pressure" was observed to enlarge with increasing injection velocity and decreasing A_{port}. For injection velocities ($\mathcal{O}(3 \times 10^3$ cm/sec)) blowoff occurred in the absence of a stabilizing tunnel surrounding and extending downstream from the burner port.

The importance of the recirculating flow of product gases in the flame stabilization process has been evidenced in several of the gas rocket experiments discussed in this work. Prior to the CO system studies a series of experiments was carried out to determine the stability characteristics of the $CH_4/O_2/N_2$ system at mean $\overline{P}_c$ = 7.8 atm with choked showerhead injection as a function of the equivalence ratio and the chamber length. Bowman reported the results of a single series of experiments with CH_4/Air and $CH_4/(.40_2 + .6N_2)$ at L_c = 54 cm. While he observed nonsteady burning of the CH_4/Air system at the stoichiometric mixture ratio at the shorter L_c, for L_c = 104 cm the stability limits were found to lie slightly off stoichiometric (see Figure V-17 in Section F of this chapter). In order to achieve combustion stabilization at the off-stoichiometric mixtures, it was necessary to increase the total propellant mass flow rate by about 20%, with an attendant increase in the injection pressure ratio, $\pi_{inj} = \frac{P_{mix}}{P_c}$ of about 8%. At the lower total mass flow the blowoff limit was found to lie

close to $\Phi = 1$ and within the system stability limits. The obvious implication is that a more favorable mixing process between hot products and unburned propellant is achieved with the higher mass flux and corresponding higher pressure ratio across the injector. It is of interest to note that Hottel (121, 126) observed precisely the same influence of mass flux and injection pressure ratio in a stirred reactor study. Shinnar (127) and Spalding (139) as well as Hottel interpreted such behavior as evidence for the improvement of mixing on both large (product recirculation) and small (local mass entrainment and turbulent exchange between products and reactants) scale.

It was noted in Chapter IV that a significant distortion in the geometry of the combustion chamber in the vicinity of the injector (achieved by removing the inner windows in the windowed combustion chamber section) prevented combustion stabilization with the H_2 + Air system. Again the principal influence of the geometry change is on the nature of the turbulent recirculation pattern associated with the injection process.

Finally it is of interest to note the effect on the system blowoff limits of decreasing the injection pressure ratio and Mach number by increasing the injection port diameter. In the series of experiments discussed in Section G of this chapter the influence on the stability characteristics of decreasing M_{inj} and P_{inj} was determined for the H_2 + Air system. A systematic decrease in the blowoff limits (Φ) of the system occurred as A_{port} increased and P_{inj}, M_{inj} decreased. The same influence of injector port area and injection Mach number was reported by Hottel (121) in the stirred reactor work.

In Section E a model of the combustion process accounting for the presence of a strong recirculation of product gases developed. For the moment note that the fluid dynamic loop is complemented as far as the recirculated product gas is concerned by virtue of the high entrainment capacity of the high velocity expanding jets.

D.4 Consideration of the Important Characteristic Times in the Gas Rocket Combustion Process

Earlier analyses of the nonsteady burning process in the gas rocket including the Sirignano-Crocco model and turbulent flame model were based upon the premise that the characteristic combustion time was negligible compared to the characteristic time of wave motion - the period of oscillation. The assumption facilitated a quasi-steady treatment of the burning process although a nonsteady effect of volume oscillation on the time scale of the pressure oscillation was included in the turbulent flame model. In addition the assumption eliminated the characteristic combustion time as an important parameter influencing the theoretically predicted nonsteady burning characteristics of the system.

In view of the correlation between the dark zone length in the direct photographs and the length of the underexpanded supersonic zone in the schlieren and shadow photographs there is justification for the statement that the residence time of particles in the unburned gas zone ($\tau_{res,u}$) is negligible compared to the period of oscillation (τ_{per}). Taking the sonic velocity ($\Theta(3.6 \times 10^4$ cm/sec)) at the injection port as an estimate of the mean velocity in the unburned gas zone and noting the measured length of the zone as ($\Theta(0.5$ cm) an estimate of $\tau_{res,u} = \Theta(10^{-5})$ sec is obtained. For reference purposes Figure V-3 shows a plot of the frequency of the experimentally observed fundamental mode oscillation as a function of the propellant equivalence ratio and chamber length for the H_2 + Air system. The equivalence ratio plotted corresponds to the lowest Φ at which the fundamental mode is observed for the chamber length noted. At $L_c \geq$ 38 cm a narrow regime of second harmonic mode oscillation is observed at the lower Φ . For the second harmonic mode oscillation the period of oscillation is nominally $\tau_{per,2} = \frac{1}{2} \tau_{per,1}$. Thus the ratio $\tau_{res,u} / \tau_{per} \leq \Theta(.02)$ is observed.

On the other hand, the approximation that the residence time of the combusting propellant gases in the burning zone ($\tau_{res,b}$) and the assumption that the characteristic chemical time due to

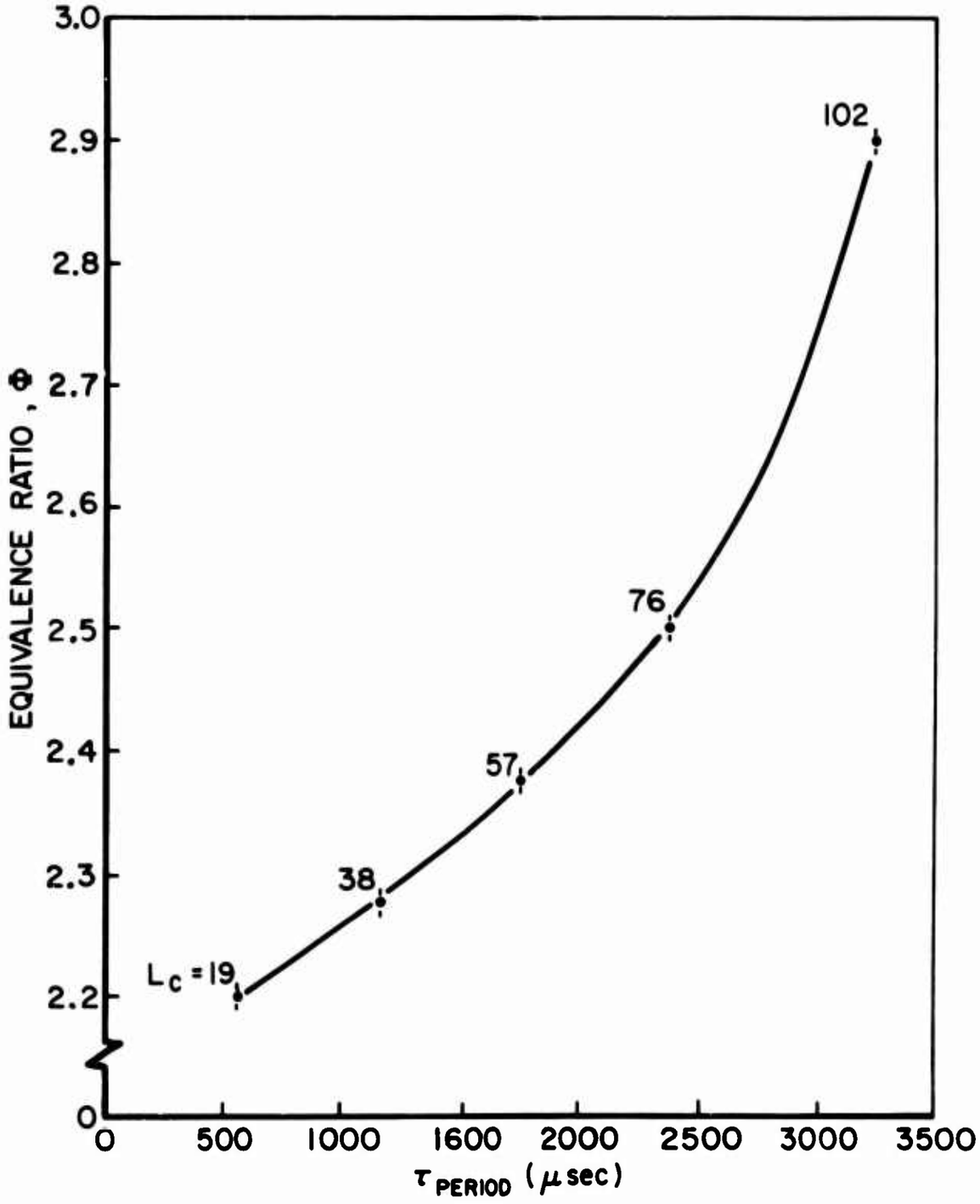

MEASURED PERIOD OF FUNDAMENTAL MODE OSCILLATION AT LIMIT AS FUNCTION OF EQUIVALENCE RATIO (Φ) AND CHAMBER LENGTH (L_C)

FOR H_2 + AIR $\bar{P}_C$ = 7.8 atm, 31 HOLE SHOWERHEAD INJECTOR NOZZLE A_C/A_t = 46

FIGURE V - 3

kinetics (τ_c) are negligible compared to τ_{per} must certainly be reconsidered. Note that τ_a does not necessarily equal $\tau_{res,b}$.

Clearly the residence time of gases in the burning zone is dependent on the aero-thermodynamic structure of the injection-mixing-combustion process as well as the chemical properties of the reacting propellants. The characteristic chemical kinetic or reaction time is likewise dependent on the local thermodynamic properties of the reacting mixture in addition to the chemical nature of the reactants. The oft-repeated statement of investigators in the liquid and solid rocket propellant fields (particularly those concerned with the nonsteady burning characteristics of these systems), that characteristic chemical times are too short (to be limiting) with respect to oscillation periods is misleading and, as will be shown, perhaps inaccurate in light of currently available reaction rate data. Culick has recognized this point in his discussion of the nonsteady burning processes in solid propellant rocket motors (24).

On the basis of the diagnostic experiments and in light of the combustion zone structure as discussed in this chapter only a limiting range on the combustion zone residence time can be specified. Unburned propellant enters the combustion chamber at sonic velocity and passes through the turbulent combustion zone surrounding and extending downstream from the underexpanded unburned gas zone. At the end of the combustion zone fully combusted and expanded product gas is emitted at a mean chamber velocity ($\mathcal{O}(0.5 \text{ to } 1.5 \times 10^3$ cm/sec)). Estimating the overall extent of the combustion zone at between 1 and 5 cm a range of possible residence times, $\mathcal{O}(3 \times 10^{-5}$ sec to 1×10^{-3} sec), is possible. In comparison with the observed oscillation periods of Figure V-3, it is likely that $\tau_{res,b}$ commensurate with τ_{per} is realized in the gas rocket combustion process.

With regard to the possibility that the characteristic chemical kinetic time appropriate to conditions existing in the combustion zone may not be negligible compared to the observed τ_{per} and may indeed be of importance in determining the non-

steady burning characteristics of the system, the following points are noted:

(1) The combustion instability data of Bowman (32) with the H_2 + Air propellant system - Figure II-9 , (showerhead injection system) and of Pelmas with the CH_4 + ($.40_2$ + $.6N_2$) system (porous plug injection) - Figure II-7 , delineate distinct regimes of harmonic mode oscillations. As noted by Bowman and in light of the observed longitudinal mode instability characteristics in liquid rocket systems, these data are suggestive of the existence and importance of a finite characteristic combustion time relative to the period of oscillation.

(2) The inference that the important characteristic time must be fundamentally related to a characteristic kinetic or reaction time (that is, the system does not appear to be mixing limited) follows from the stability limit data of Bowman with the $H_2/O_2/N_2$ system, Bowman and the present author with the $CH_4/O_2/N_2$ system, and the present author with the $CO(H_2O)/O_2/N_2$ system with and without CH_4 additive. These data have clearly demonstrated the importance of the adiabatic combustion temperature and the propellant reactivity or overall activation energy in determining the nonsteady burning characteristics of the system.

(3) The similarity between the nonsteady burning characteristics of the CH_4/Air and the $CO(H_2O)$/Air systems strongly supports the conclusion that gas phase kinetics is a limiting factor in determining the combustion zone response. Both systems support nonsteady burning at and around the stoichiometric mixture ratio with steady combustion occurring at off-stoichiometric mixtures. This experimentally observed similarity was puzzling in the context of the original Sirignano-Crocco theory and the available kinetics data. The original theory emphasized the importance of the factor E/RT. The accepted overall activation energies for the two systems are ($\sim$60 kcal/mole) for CH_4/Air and ($\sim$20 to 30 kcal/mole) for $CO(H_2O)$/Air. The S-C model predicts substantially different $T_{1_{lim}}$ for the two systems. Essentially the same $T_{1_{lim}}$ ($\sim$2430°K) is observed in the two systems. As shown in Chapter VI in the discussion of the experimental results in light of the combustion model developed in this chapter, it appears that the oxidation of CO formed as an intermediate in the CH_4 oxidation at high temperatures is the rate limiting step in the overall process. Thus in a high temperature combustion system dominated by gas phase chemical kinetic influences one would indeed expect similarity between the system response with CO and CH_4 as the fuel.

(4) Estimates of the characteristic kinetic times derived from the most relevant overall kinetics rate data for the N_2-diluted H_2/O_2, CH_4/O_2, and $CO(H_2O)/O_2$ reactions indicate that the condition of $\tau_c/\tau_{rec} \sim O(1)$ is possible for the gas rocket combustion process (see Appendix D).

(5) The radial and axial temperature profile measurements and the spark schlieren photographs indicate a systematic increase in the axial extent of the steady-state combustion volume with decreasing Φ and increasing $\dot{m}_{tot}$. These observations are consistent with the view that the combustion distribution is influenced by finite chemical reaction times.

E. High Intensity Combustion Model

In Section D certain aspects of the injection-combustion phenomena in the gas rocket were outlined. The fundamental importance of the forced recirculation of hot product gases in the annular regions surrounding the propellant jets was noted. The disparity between the combustion process in the gas rocket and a conventional turbulent burner flame was emphasized. In this section a physical and analytical expression of the steady-state high intensity turbulent combustion process is developed. The ultimate goal is to show that the distributed combustion zone may be described in terms of volume averaged thermodynamic, gasdynamic, and burning rate parameters. In Section F the combustion zone boundary condition derived on the basis of the steady state model is applied to the analysis of the wave dynamics in the combustion chamber and the coupled problem is solved to determine the nonsteady burning characteristics of the gas rocket system.

To adequately describe the combustion process associated with the high velocity, highly turbulent, underexpanded, premixed propellant jets expanding into the combustion chamber it is necessary to understand the basic properties of such jets. It has already been demonstrated that the flow field generated by such combusting jets for the injection configuration of the gas rocket leads to a steady supply of hot product gases to the volumes surrounding the jets. The works of Hottel (120, 121, 126) Abramovich (130), Spalding (139,141), and Thring and Newby (131) are particularly relevant.

The fluid and thermodynamic properties of subsonic, sonic (underexpanded), and supersonic turbulent jet flowfields have been the subject of extensive experimental and analytical work. Success in correlating theory and experimental data in the absence of combustion has been achieved principally through the application of similarity principles to describe the velocity, temperature, and composition profiles in the near mixing field for the case of jet expansion into a quiescent medium. The most significant property of such jets in terms of the present discussion is the extraordinary entrainment capacity exerted by the jets on the surrounding medium. A high velocity turbulent jet acts as an efficient ejector to aspirate gas from the surroundings into the mixing zone of the jet and thereby evidences a substantial increase in the total mass flux within the jet with axial distance from the jet port. Spalding (139,141) has treated this aspect of turbulent jets from both a theoretical and experimental standpoint. He has demonstrated the fundamental relationship between the axial decay of mean velocity in the jet and the total mass of entrained gas. An empirical expression was obtained for the functional form of the rate of mass entrainment in terms of the initial jet momentum, the density ratio of the entrained and original jet gas, and the axial displacement from the jet port. Hottel (126) reports that the near flow fields of high velocity, high Reynolds number jets (subsonic, underexpanded sonic, and supersonic) are similar and relatively insensitive to the presence of combustion in the jet mixing zone. As found by Spalding, Hottel observes that the inlet jet momentum and the density ratio[1] are of principal importance in the jet development. The principal influence of combustion according to Spalding and Hottel should be (at least to first order) to modify the density ratio. Earlier Thring and Newby (131) developed a similarity criterion for isothermal and combusting enclosed turbulent jets which is essentially equivalent to Spalding's derived entrainment law.

---

[1] The ratio of the density of the surrounding (entrained) fluid to the mean density of the fluid within the jet.

It would seem that the mechanisms by which combustion stabilization at the injector and steady combustion are achieved in the gas rocket are similar. It is apparent that the high intensity combustion process must be initiated and sustained by the entrainment of hot product gases from the surrounding recirculation zone into the mixing zone of the expanding high velocity jets. Subsequent turbulent mixing of the entrained gas and the jet flow acts to preheat and dilute the unburned premixed propellant. Only by virtue of the coupled product recirculation and entrainment phenomena can appreciable burning rates be maintained.

Acknowledging the importance of recirculation and entrainment the question arises as to the relative importance of the mixing processes (τ_{mix}) vis a vis gas phase kinetics (τ_c). Indeed the question of how to go about calculating kinetic rates given the environment of the gas rocket combustion zone must be answered. The concept of increasing overall gas phase burning rates by vigorously stirring unburned combustibles with hot products is not new. In the limit of "infinite mixing rates" (in the present context, infinite entrainment such that $\frac{\dot{m}_{recirc}}{\dot{m}_i} = \infty$ the mixing time is zero compared to the reaction time due to kinetics and the combustion zone can be analyzed as a locally well-stirred reaction volume having uniform composition, temperature, density, pressure, and burning rate (113, 117, 119). Under these conditions the characteristic time due to kinetics becomes limiting ($\tau_{mix}/\tau_c = 0$). At the opposite end of the scale ($\tau_{mix}/\tau_c \geq O(1)$) it is likely that the entrainment rate becomes of equal if not greater importance than the kinetic rates in determining the development of the combustion process. Spalding (140) analyzed the problem of the spreading rate of a confined turbulent flame behind a two-dimensional flameholder for the case when the finite entrainment rate of unburned premixed gas into the burning zone was limiting. He analyzed the case for instantaneous combustion ($\tau_{mix}/\tau_c >> 1$).

The harsh environment and small scale of the high velocity turbulent mixing-combustion zone associated with each propellant

jet in the gas rocket prevents the accurate measurement of local thermodynamic properties throughout the combustion zone. Without such information the precise determination of the relative importance of mixing and gas phase reaction is precluded. One can speculate on the degree of approach to a zone of well-stirred combustion. On the other hand, it can be argued inductively on the basis of all of the experimental stability limit data with the CO, CH_4, and $H_2/O_2/N_2$ systems that mixing effects are of secondary importance compared to chemical kinetic effects. The evidence for the primary importance of chemical kinetic factors in determining the nonsteady burning characteristics of the system has been noted. Only higher order effects, if any, due to mixing have been observed (see also Chapter VI). In any case if mixing limitations on the steady burning rate and the nonsteady characteristics do exist the effects should be more noticeable near the stoichiometric mixture ratio where characteristic chemical times are minimum. Therefore, the approximation which will be applied in the analysis, namely, that $\tau_{mix,j}/\tau_c \ll 1$, where $\tau_{mix,j}$ refers to the time to dissipate radial thermal, concentration, and velocity fluctuations in the expanding and combusting jet, is likely to be satisfied for the H_2 + Air system where nonsteady burning occurs at lower temperature off-stoichiometric mixtures. The assumption is recognized as being weaker in the case of the CH_4 and CO systems where flame stabilization is an experimentally observed problem and nonsteady burning occurs at higher temperature near $\Phi = 1$.

E.1 Well-stirred combustion zone analysis

Initially an analysis of the nonsteady burning zone was carried out for the case where a finite dimensioned well-stirred combustion zone surrounds the unburned gas zone. That is, the limiting case of $\tau_{mix}/\tau_c = 0$ over the entire burning zone was examined. Unburned gas admitted to the reaction zone was assumed to be mixed instantaneously with products with reaction occurring throughout the entire volume such that the mass burning rate could be expressed by a simple Arrhenius rate law at the uniform combustion zone conditions.

The analysis was particularly useful in suggesting a means for handling the combustion boundary condition for the case of finite combustion time (applied subsequently in the final combustion model). However, the concept of "instantaneous mixing" and "infinite recirculation" throughout the combustion zone is too extreme. While turbulent mixing rates are certainly high in the gas rocket combustion zone, the presence of a high velocity mean flow and the absence of an opposing wall as in the Longwell type stirred reactor should act to spread the finite zone of reaction. Furthermore, the necessity to consider the locally well-stirred combustion zone as one of incomplete combustion (in order to realize non-zero propellant mass fractions and thereby finite burning rates) accompanied by the experimental observation of approximately complete combustion resulted in the artificial inclusion of a thin afterburning zone wherein complete combustion to products was assured.

E.2 Recirculation-Stabilized, Distributed Combustion Zone Model

The combustion model developed in the following paragraphs accounts for the principal features of the gas rocket combustion process as considered in the preceding discussion. The basic goal as stated earlier is to show that for the envisioned high intensity combustion process there exist well-defined and mutually self consistent values for the volume-averaged properties of the combustion zone and that the steady gas phase burning rate can be expressed in terms of these spacially-averaged properties.

Consider the idealized case of the high velocity expanding and combusting jet shown in Figure V-4a . For purposes of analysis consider Figure V-4b to represent an approximation of the real jet combustion zone. In this section all quantities are considered dimensional.

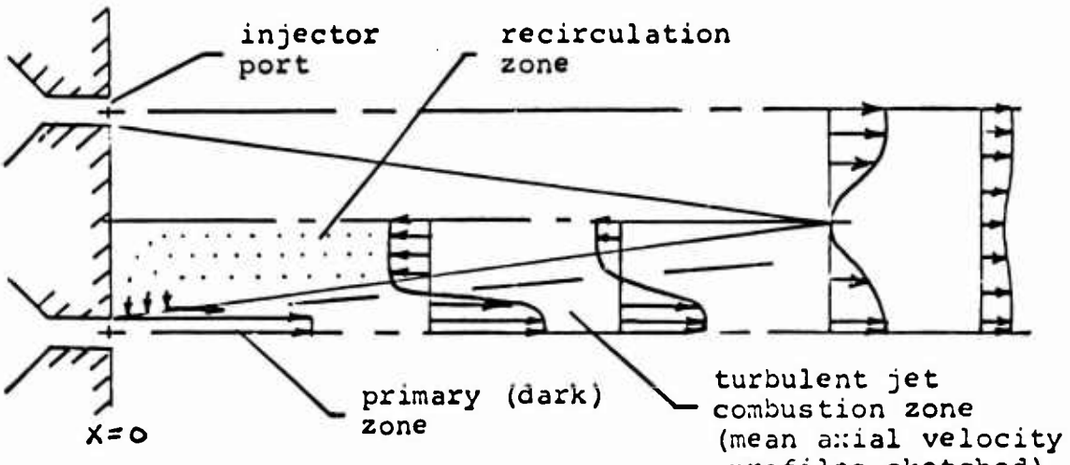

Figure V-4 a

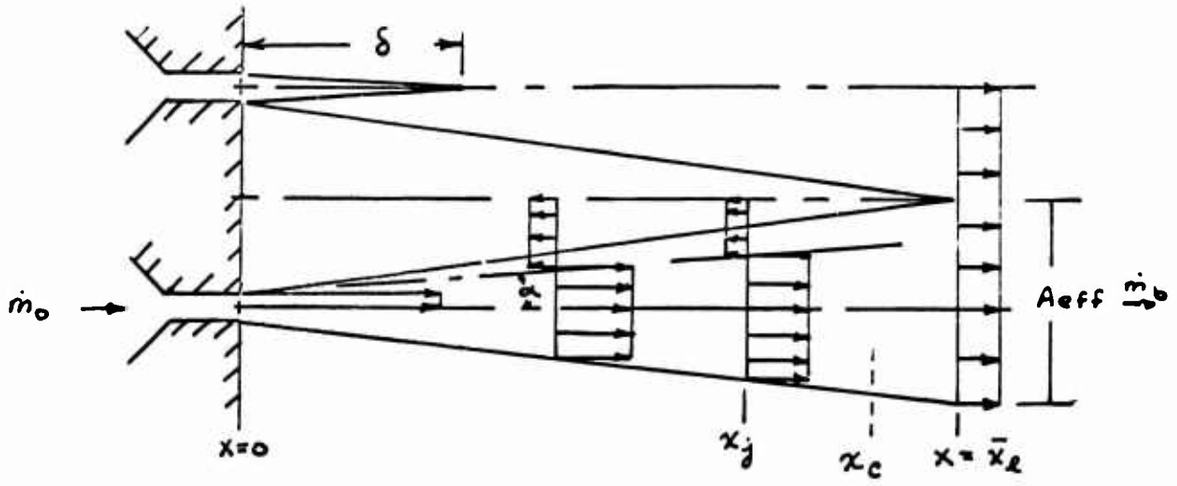

Figure V-4 b

Unburned premixed propellant enters the combustion zone at the port with inlet mass flux $\dot{m}_i = \rho_i u_i A_{port}$ where $U_i = C_i$ for choked flow. For the purposes stated here the jet is assumed to be perfectly expanded to the mean chamber pressure $p_i = p_c = p$. That is, the effect of jet underexpandedness is neglected. Gas phase combustion due to finite-rate chemical kinetics in a quasi-one-dimensional burning zone is considered. The annular region surrounding the combustion zone is assumed to be filled with burned product gases at the adiabatic combustion temperature

corresponding to the inlet mixture strength (Φ). Heat losses to the injector face[1] and the combustion chamber walls are neglected.

Combustion is stabilized at the injection port by the finite rate of recirculation and entrainment of hot product gas. Radial gradients are neglected in the mixing and combustion zone. That is, the microscale turbulence within the jet mixing zone is assumed to be sufficiently high such that $\tau_{mix,j}/\tau_c \ll 1$ where $\tau_{mix,j}$ is equivalent to the local eddy stay time within the mixing zone. Thus entrainment ($\tau_{mix} > \tau_{mix,j}$) of hot product gas leads to rapid heating of the unburned premixed propellant gases thereby stabilizing the burning zone.

The combustion zone is extended due to the mutual interaction of finite chemical kinetic rates in a high velocity field where mass entrainment and jet expansion are occurring. Axial diffusion and heat conduction are neglected. Combustion is completed and the adiabatic combustion temperature achieved within the zone length x_c and further expansion to fill the chamber is allowed. In this regard the characteristic humped shape of the axial temperature profiles measured in the recirculation zones (Figures IV-12 to IV-17 - the off-axis profiles) is recalled. The rather abrupt decay of the temperature profile following the measured zone of peak temperature can be interpreted as evidence of the completion of combustion within the turbulent mixing zone of the jet prior to the completion of jet expansion. Subsequent mixing of the expanding combusted gas with recirculating gas cooled due to heat losses to the surrounding walls could account for the temperature drop.

The principal features of the mixing process are accounted for by a Spalding-type mass entrainment law for the high velocity jet, the jet expansion angle α (alternatively the overall jet

---

[1] Not all heat transferred to the injector is lost. Due to the nonsteady temperature profile in the injector plug during an experiment there is a slowly increasing heat transfer rate to the unburned gases in the injector ports and upstream in the mixing chamber. The axial temperature profiles of Chapter IV indicate that the mean temperature of the gas in the recirculation zone is 200°K to 350°K lower than the measured peak temperature.

length, x_ℓ), and the length δ_u of the principal core zone of the jet assumed to be composed of unburned gases at the inlet temperature. The total mass of recirculated product gas is conserved. The annular recirculation regime is replenished by influx at the downstream end of the combustion zone and the mean mass of product gas in the annular region is fixed. Flow in the recirculation zone is considered incompressible.

The mass conservation equation for the axisymmetric jet is obtained in terms of the entrainment rate as follows:

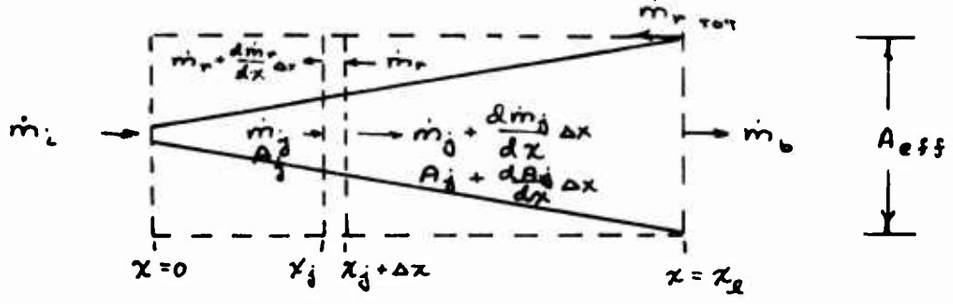

$$\frac{d\dot{m}_j}{dx} - \frac{d\dot{m}_r}{dx} = 0$$

$$\dot{m}_j = \dot{m}_i + \dot{m}_r \qquad \text{(V-14)}$$

For high intensity turbulent combusting jets, Spalding (139, 141) indicates that the mass entrainment capacity of the jet can be specified as,

$$\frac{d\dot{m}_j}{dx} = a\,(\bar{M}\rho_r)^{1/2} \qquad \text{(V-15)}$$

where $\bar{M} = \frac{\pi}{4} d_{port}^2 \rho_i u_i^2 = \dot{m}_i u_i$ = is the inlet jet momentum

ρ_r = the density of the gas being entrained

a = is an empirical constant (≈0.2 to 0.5)

Integration of Spalding's entrainment law between $\bar{x} = 0$ and $\bar{x} = \bar{x}_j$ yields,

$$\dot{m}_j(\bar{x}) = \dot{m}_i\left[1 + a\bar{x}\left(\frac{\rho_r}{\rho_i}\right)^{1/2}\right] \qquad \text{(V-16)}$$

where $\bar{x} = \frac{x_j}{d_{port}}$ and $\dot{m}_r(\bar{x}) = \dot{m}_j(\bar{x}) - \dot{m}_i$

and it is required that the recirculated mass be conserved such that

$$\dot{m}_{r\ TOTAL} = \dot{m}_j(\bar{x}_\ell) - \dot{m}_o \qquad \text{(V-17)}$$

The equation for the jet expansion is approximated according to,

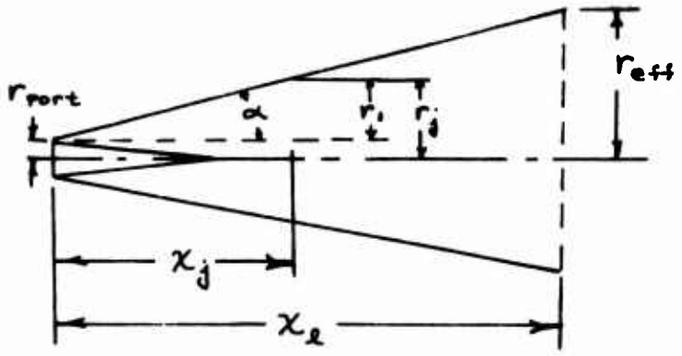

$$r_j = r_i + r_{port}$$

$$A_j = \pi(r_{port} + x_j \tan\alpha)^2$$

$$\frac{dA_j}{dx} = 2\pi \tan\alpha (r_o + x_j \tan\alpha)$$

$$r_{eff} = \left(\frac{A_c}{\pi n_{holes}}\right)^{1/2}$$

$$\tan\alpha = \frac{r_{eff} - r_{port}}{x_\ell} \qquad \text{(V-18)}$$

where the dark zone volume is neglected in approximating dA_j/dx and A_j represents the total cross section of the jet. A close examination of the direct photographs of the H_2 + Air combustion zone (e.g., Figure IV-20a) shows that,

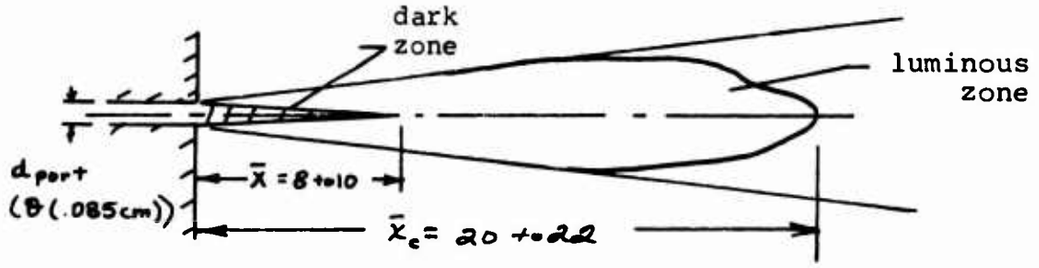

The diameter of the dark zone at the injector port is approximately one half the port diameter and the luminous zone persists up to the injector port. Thus the mixing and combustion zone extends to the injector face and the approximation that $A_j = \pi r_j^2$ becomes quite good within one to two port diameters depending on the particular value of the expansion angle α .

The momentum equation is replaced by the assumption of uniform pressure across the combustion zone. The pressure increase across the burning zone for the case of perfectly expanded injection is (~(1 to 2 psi)) and provides the driving force for the strong

recirculatory flow.

The energy equation for a slab perpendicular to the jet axis is written as,

$$\frac{d}{dx}\left[\dot{m}_j\left(c_p T_j + \frac{u_j^2}{2}\right)\right] - \frac{d}{dx}\left[\dot{m}_r\left(c_p T_r + \frac{u_r^2}{2}\right)\right] = \dot{q}\, A_j \qquad \text{(V-19)}$$

where $\dot{q}$ = the volumetric energy release rate ($\frac{\text{cal}}{\text{cm}^3\text{sec}}$) at x_j due to finite rate chemical kinetics

Integration of the energy equation between x = 0 and x = x_j yields,

$$\dot{m}_j\left(c_p T_j + \frac{u_j^2}{2}\right) - \dot{m}_i\left(c_p T_i + \frac{u_i^2}{2}\right) = \int_0^{x_j} \dot{q}(x)\cdot A_j(x)\, dx_j + \dot{m}_r\left(c_p T_r + \frac{u_r^2}{2}\right) \qquad \text{(V-20)}$$

setting $T_r = T_b$, $T_i = T_u$, $c_p = \bar{c}_p$

the energy equation becomes

$$\dot{m}_j \gamma_j + \frac{\dot{m}_j u_j^2 - \dot{m}_i u_i^2}{2\bar{c}_p(T_b - T_u)} = \frac{d_{port}}{\bar{c}_p(T_b - T_u)}\int_0^{\bar{x}_j} \dot{q}(\gamma_j)\cdot A_j(\bar{x})\, d\bar{x} + \dot{m}_r + \frac{\dot{m}_r u_r^2}{2\bar{c}_p(T_b - T_u)} \qquad \text{(V-21)}$$

where $\gamma_j = \dfrac{T_j(\bar{x}) - T_u}{T_b - T_u}$

and $\dot{q}(\gamma_j)$ = the temperature explicit energy release rate at x_j due to γ_j, ρ_j, and reactant concentration

An expression is needed for the volumetric energy release rate $\dot{q}(\gamma_j)$ due to finite rate kinetics. The fuel consumption rate is expressed in terms of an overall Arrhenius-type rate law,

$$\frac{d[F]}{dt} = -K[F]^n[O_2]^m \quad , \quad \frac{\text{moles fuel}}{\text{cm}^3\,\text{sec}}$$

where $K = k\, e^{-\frac{E}{RT}}$ is the standard rate constant involving the preexponential factor k, E the overall activation energy as discussed in Chapter IV, page 85 , and T the local temperature.

[F], $[O_2]$ are the molar concentrations of fuel and oxygen

n, m are the reaction orders for the overall rate law with respect to fuel and oxidizer

Substituting

$$[F] = \bar{\sigma}_f \cdot \rho_T \cdot {}^1/_{mw_f}$$

$$[O_2] = \sigma_{O_2} \cdot \rho_T \cdot {}^1/_{mw_{O_2}}$$

$$\dot{m}_f = -\frac{d[F]}{dt} \cdot mw_f \ , \quad \frac{\text{gms fuel}}{\text{cm}^3\,\text{sec}}$$

where

$\rho_T = \rho_j$ = density at τ_j

$\bar{\sigma}_f$, σ_{O_2} = mass fractions of fuel and oxygen

The fuel consumption rate becomes

$$\dot{m}_f = \frac{k}{mw_f^{n-1} mw_{O_2}} \rho_T^{n+m} \bar{\sigma}_f^{\,n} \sigma_{O_2}^{\,m} e^{-\frac{E}{RT}} \qquad \text{(V-22)}$$

The perfect gas law is used to express the density in terms of the local temperature and the constant mean pressure. To obtain a temperature explicit expression for $\dot{m}_f$ the mass fractions of fuel and oxidizer must be expressed in terms of the local dimensionless temperature τ_j.

For a system with no recirculation where the local temperature is simply related to the local reactant depletion (e.g., Lewis Number = 1 flames) the dimensionless temperature profile is simply related to the profile of reactant mass fraction as,

$$\tau_j = \frac{T_j - T_u}{T_b - T_u} = \frac{\bar{\sigma}_{f_i} - \bar{\sigma}_f(\tau_j)}{\bar{\sigma}_{f_i}} \quad \text{for an oxidizer rich system} \qquad \text{(V-23)}$$

$$\tau_j = \frac{\sigma_{ox_i} - \sigma_{ox}(\tau_j)}{\sigma_{ox_i}} \quad \text{for a fuel rich system}$$

such that $0 \le \tau_j \le 1$ specifies the reaction coordinate in the combustion zone.

It can easily be shown for the case where recirculation and mixing of unburned premixed reactants and of completely burned product gas at the adiabatic combustion temperature occurs that the temperature rise due to reaction and mixing (reactant depletion) can also be expressed by these simple relations.

Thus convenient temperature explicit relations for the principal species mass fractions can be written as follows for an oxidizer rich system,

$$\gamma_j = \frac{T_j - T_u}{T_b - T_u}$$

$$\nu_{f_j} = \nu_{f_i}(1 - \gamma_j)$$

$$\mu = (\nu_{ox}/\nu_f)_{STOICH}$$

$$\nu_{ox} = (1 + S)\nu_{O_2} \quad , \quad S = \frac{\text{mass diluent } (N_2)}{\text{mass oxygen}}$$

$$\Phi = \frac{(\nu_{ox}/\nu_f)_i}{\mu}$$

$$\nu_{ox_j} = \nu_{ox_i} - (\nu_{ox})_{reacted}$$

In order to determine $(\nu_{ox})_{reacted}$ (the mass fraction of oxidizer consumed at x_j) the assumption that the reaction proceeds according to the stoichiometry $\mu = (\nu_{ox}/\nu_f)_{STOICH}$ is made. The total fuel fraction consumed at $\gamma_j = 1$ is equal to ν_{f_i} for the overoxidized system. Hence, the total oxidizer consumed is $(\nu_{ox})_{reacted} = \mu\nu_{f_i} = (\nu_{ox})_r$

The total oxidizer depletion at γ_j due to reaction and mixing is therefore

$$(\nu_{ox})_r = \gamma\mu\nu_{f_i}$$

$$\nu_{ox_j} = (\Phi - \gamma_j)\mu\nu_{f_i}$$

The corresponding product mass fraction at γ_j becomes simply

$$\nu_{prod\ j} = \gamma_j(1 + \mu)\nu_{f_i}$$

where

$$\nu_{ox_j} + \nu_{f_j} + \nu_{prod\ j} = 1$$

The corresponding equations for the fuel rich system are

$$\nu_{ox_j} = \nu_{ox_i}(1 - \gamma_j)$$

$$\nu_{f_j} = \nu_{f_i} - \gamma_j\frac{\nu_{ox_i}}{\mu}$$

$$\nu_{prod\ j} = \gamma_j(1 + 1/\mu)\nu_{ox_i}$$

Defining

$$Z = \nabla_{f_j}^{n} \nabla_{ox_j}^{m}$$

$$(Z)_{\substack{ox \\ RICH}} = \nabla_{f_i}^{n+m} \mu^{n} [\Phi - \gamma_j]^{n} [1 - \gamma_j]^{m} \qquad \text{(V-24)}$$

$$(Z)_{\substack{FUEL \\ RICH}} = \mu^{n} [\Phi \nabla_{f_i}]^{n+m} [1 - \gamma_j]^{n} [1/\Phi - \gamma_j]^{m}$$

For the particular case of oxidizer rich, bimolecular, second order overall kinetics

$$(Z)_{\substack{ox \\ RICH, 2}} = \mu \nabla_{f_i}^{2} [\Phi - \gamma_j] [1 - \gamma_j] \qquad \text{(V-25)}$$

Substituting into the expression for the fuel consumption rate (m = n = 1),

$$\dot{m}_{f_j} = \frac{\hat{k} \mu}{1 + S} \left[\frac{\nabla_{f_i} \bar{\rho}}{\bar{R}}\right] \left[\frac{m w_j}{T_j}\right] [1 - \gamma_j][\Phi - \gamma_j] e^{-E/\bar{R} T_j} \qquad \text{(V-26)}$$

where

$$\rho_r = \rho_j = \frac{\bar{\rho}\, m w_j}{\bar{R}\, T_j}$$

$$E/\bar{R} T_j = H/\theta_j$$

$$H = E/\bar{R} T_b$$

$$\theta_i = T_u/T_b$$

$$\hat{k} = \frac{k}{m w_{O_2}}$$

$$\theta_j = \frac{T_j}{T_b} = \frac{T_u}{T_b} + \gamma_j \left(1 - \frac{T_u}{T_b}\right)$$

$$\theta_j = \theta_i + \gamma_j (1 - \theta_i)$$

The energy release rate due to gas phase reaction is

$$\dot{q} = \dot{m}_f \cdot q_f$$

where $q_f = q$ = the heat of combustion of the fuel which is constant for the relatively low temperatures (dissociation levels) for the gas rocket work

$$\dot{q}(\eta_j) = \rho\left[\frac{\hat{k}\mu}{1+S}\right]\left[\frac{\nu_{f_i}\bar{p}}{\bar{R}\,T_b}\right]\left[\frac{\overline{mw}_i}{\theta_j}\right][1-\eta_j][\Phi-\eta_j]\,e^{-\frac{H}{\theta_j}}\ , \frac{cal}{cm^3\,sec}$$

$$\overline{mw}_j = 1/\sum_i\left(\frac{\nu_i}{mw_i}\right) \qquad \text{(V-27)}$$

The set of equations necessary to solve for the profiles of temperature, density, species mass fraction, and the energy release rate in the quasi-one dimensional combustion zone is thus completed. The equations have been solved iteratively for the H_2 + Air system for a range of specified initial conditions ($\dot{m}_i$, d_{port}, p, T_u, Φ) with (η_{holes}, a, α , k, and E) as parameters. The calculations were carried out numerically using the IBM 360-91 computer facility. The iterative technique was straightforward with the calculation for a given set of defining conditions started at the cold boundary initial jet conditions. For dimensionless axial displacement increments of 0.002 the step size in η_j was adjusted to 0.001. The technique reduced the local error in the computed temperature profile to less than 2% for the dilute systems examined. The computer program written to carry out the calculation is listed in Appendix E.

In the course of the numerical study of the system the sensitivity of the calculated profiles, the overall reaction zone length, and the corresponding reaction (η_c) and residence ($\eta_{res,b}$) times to the important parameters was examined. Average values of the local combustion zone properties were determined as,

$$\bar{\xi}_{AVERAGE} = \frac{1}{\bar{V}_c}\int_0^{\bar{V}_c}\xi_j(A_j)\,dA_j$$

$$\bar{V}_c = \int_0^{\bar{x}_e}A_j(\bar{x})\,d\bar{x} \qquad \text{(V-28)}$$

$$\xi_j = T_j, \rho_j, \nu_{f_j}, \dot{q}_j, u_j$$

The intent here is not to belabor the numerical results. The

principal objectives of the analysis were:

(a) To demonstrate that the steady state combustion process in the gas rocket is amenable to description in terms of volume averaged combustion zone properties. As shown by Crocco (152), the concept of representing nonuniform distributions of thermodynamic and gasdynamic properties by means of spacial averaging techniques is often misapplied in practice. In terms of the gas rocket combustion process as described in the preceding paragraphs, in order for the concept of volume averaging of axial property profiles to be meaningful the averaged values of these properties should be consistent. That is, the averaged local temperature and density as determined from the spacial distributions of these properties should be consistent with the local temperature and pressure corresponding to the spacially averaged volumetric energy release rate. It can be easily shown for example, that this condition is not satisfied for a one dimensional laminar or turbulent flame zone propagating in a low velocity field by the mechansims of heat conduction and diffusion. Typically there is poor agreement between $\bar{\rho}_{AVE}$, $\bar{T}_{AVE}$, and $\bar{\dot{q}}_{AVE}$ and in general $\bar{x}_{\rho_{AVE}} < \bar{x}_{T_{AVE}} < \bar{x}_{\dot{q}_{AVE}}$ principally due to the concentration of the heat release in a relatively short zone near the burned gas temperature whereas the temperature and density profiles are primarily influenced by heat conduction and mass diffusion.

(b) To examine the consistency between experimentally measured combustion zone "dimensions", published overall reaction rate data, and the predictions of the combustion model. In this regard it is appropriate to comment on the expression of the burning rate in terms of the Arrhenius law, Equation V-22 The limitations inherent in the use of such a simple expression to express the reaction rate are well known (e.g., Fristrom & Westenberg (85) , Levy and Weinberg (112), and Sawyer (128)) and were commented on in Chapter IV. In this work the overall reaction rate data for the H_2/O_2 reaction (Sawyer and Glassman (128) and for the CH_4/O_2 reaction (Dryer and Glassman (129)) obtained in turbulent flow reactor studies are applied to evaluate the burning rate term in the gas rocket. As noted by Levy and Weinberg

such empirical Arrhenius expressions seem to offer reasonable predictions of burning rates in systems dominated by reactions occurring in the high temperature, high heat release zone. The correlation of burning rate data obtained in well-stirred reactors and the flow reactor has evidenced the utility of such overall expressions. It is felt that the combustion process in the gas rocket should also lend itself to such characterization. The use of the flow reactor results to obtain quantitative estimates of the preexponential or frequency factor and the overall activation energy to be used in the rate law is based on the observation that reaction in both systems occurs under conditions of high temperature, high diluent (N_2) concentrations, and high intensity small scale turbulence. While the use of flow reactor data to evaluate the course of reaction throughout the combustion zone in terms of evaluating local concentrations of reactants, temperature, and the burning rate may be challenged it is felt that the empirical flow reactor data provide good (certainly the best available) estimates of the overall heat release rates for the gas rocket system.

The sensitivity of the combustion distribution and the ratio of γ_{mix}/γ_c to the important parameters was examined for the H_2 + Air system at Φ = 2.0, $\bar{T}_u$ = 300°K, $\bar{P}_c$ = 4.4 atm, n_{holes} = 10, d_{port} = 0.09 cm, and $\dot{m}_i$ = 1.5 to 2.0 gms/se. The influence of the jet expansion angle (α), the mixing intensity (a), the inlet mass flux ($\dot{m}_i$), and the kinetics parameters was determined. Considering the roughness of the combustion model the numerical results were rather interesting. Agreement between calculated and measured combustion distributions (overall length) and the total heat release rate placed important restrictions on the use of realistic values for a, α , and k and E in terms of Sawyer's data. A summary of the observed influence of the various parameters on the combustion zone is included in Appendix D.

Typically a rapid increase in the jet temperature T_j with axial displacement from the injection port due to entrainment and

mixing of hot products is followed by an extended zone in which chemical reaction prevails. Essentially small expansion angles $\alpha = (\Theta(6 \text{ to } 10 \text{ degrees}))$ yield $\bar{\chi}_\ell = (\Theta(40 \text{ to } 50))$ and combustion zone ($\bar{\chi}_c$) lengths somewhat shorter for realistic a, k, and E. This is in agreement with the interpretation on page of the measured temperature profile shape. Values of a = (Θ(0.3 to 0.5)) yield mixing intensities sufficiently high to produce rapid increase of local jet temperature within 4 to 8 jet diameters of the port in a time (τ_{mix}) short compared to the overall combustion time (τ_c).

The relative lengths of the mixing and reaction zone, hence of τ_{mix} / τ_c , are sensitive to the pre-exponential factor and the activation energy used in the rate law. The accuracy of a particular choice of k and E can be tested by determining

$$\bar{Q} = \frac{\int_0^{\chi_c} \dot{q}_j \cdot A_j \cdot d\chi_j}{\dot{m}_f \cdot q}$$

$\dot{q}_j$ and A_j evaluated using Equations V-18, 27

$\dot{m}_f$ = known input fuel mass flow rate

For a rate law satisfying the gas rocket combustion conditions the total integrated heat release rate (cal/sec) must equal $\dot{m}_f \cdot q$ and $\bar{Q} = 1$. For E = 40 $\pm$ 5 kcal/mole and $\bar{k} = 10^{14}$ to 10^{15} the ratio $\bar{Q}$ is (Θ(0.97 to 1.01)). Increasingly large deviation from the nominal value $\bar{Q} = 1$ are observed for $10^{15} < k < 10^{14}$ for E = 40 kcal/mole. Sawyer's rate data for the H_2/O_2 reaction is expressed as

$$\frac{d[H_2]}{dt} = k_s [H_2] e^{-E/RT}, \left(\frac{1}{sec}\right) \qquad E = 38 \pm 2 \ \frac{kcal}{mole}$$

$$k_s = 10^{11 \pm 1.6}$$

And $k_s = \rho_{O_2} \hat{k}$

where

$$\rho_{O_2} = [O_2] \cdot mw_{O_2}$$

Sawyer's first order rate constant includes the oxygen concentration factor in the overall frequency factor k. Two means of calculating $\hat{k}$ are available. First, k_s can be interpreted as a generally valid physical constant and ρ_{O_2} appropriate to the gas rocket combustion zone conditions can be used to determine $\hat{k}_{g.r.}$. Alternatively, $\hat{k}$ can be considered the universally valid physical constant such that $\hat{k}_{g.r.} = \hat{k}_s = k_s/(\rho_{O_2})_{g.r.}$. For the gas rocket combustion zone at $\Phi = 2.0$, $\rho_{O_2} = 8(1.2\times10^{-3}\ \frac{gms}{cm^3})$ and $\hat{k}$ becomes,

$$\hat{k} = \frac{10^{11 \pm 1.6}}{1.2\times10^{-3}}$$

$$2\times10^{12} < \hat{k} < 3.3\times10^{15}$$

Using the second method, and Sawyer's experimental conditions to calculate $(\rho_{O_2})_{f.r.}$.

$$[H_2] = 1.5 \text{ to } 4.7\times10^{-7}\ \frac{moles}{cm^3}$$ = fuel concentration reported by Sawyer (128)

For the H_2/O_2 reaction and $\Phi = 2.0$, $\mu = 0.5$, $[O_2] = [H_2]$

$$\rho_{O_2} = (4.8 \text{ to } 15\times10^{-6})\ \frac{gms}{cm^3}$$

$$2\times10^{14} < \hat{k}_s < 10^{18}$$

The key point in terms of the numerical study is that regardless of the viewpoint taken with respect to extrapolating the flow reactor data to gas rocket conditions (the second method is preferred here) the values of $\hat{k}$ which yield realistic results in the combustion model are well within the "error limits" of the flow reactor data.

Figure V-5 shows typical predicted distributions of T_j, U_j, ρ_j, and $\dot{q}_j$ for the quasi-one-dimensional H_2 + Air combustion zone at $\Phi = 2.0$. The volume-averaged properties of the combustion zone are indicated. Note that combustion is complete

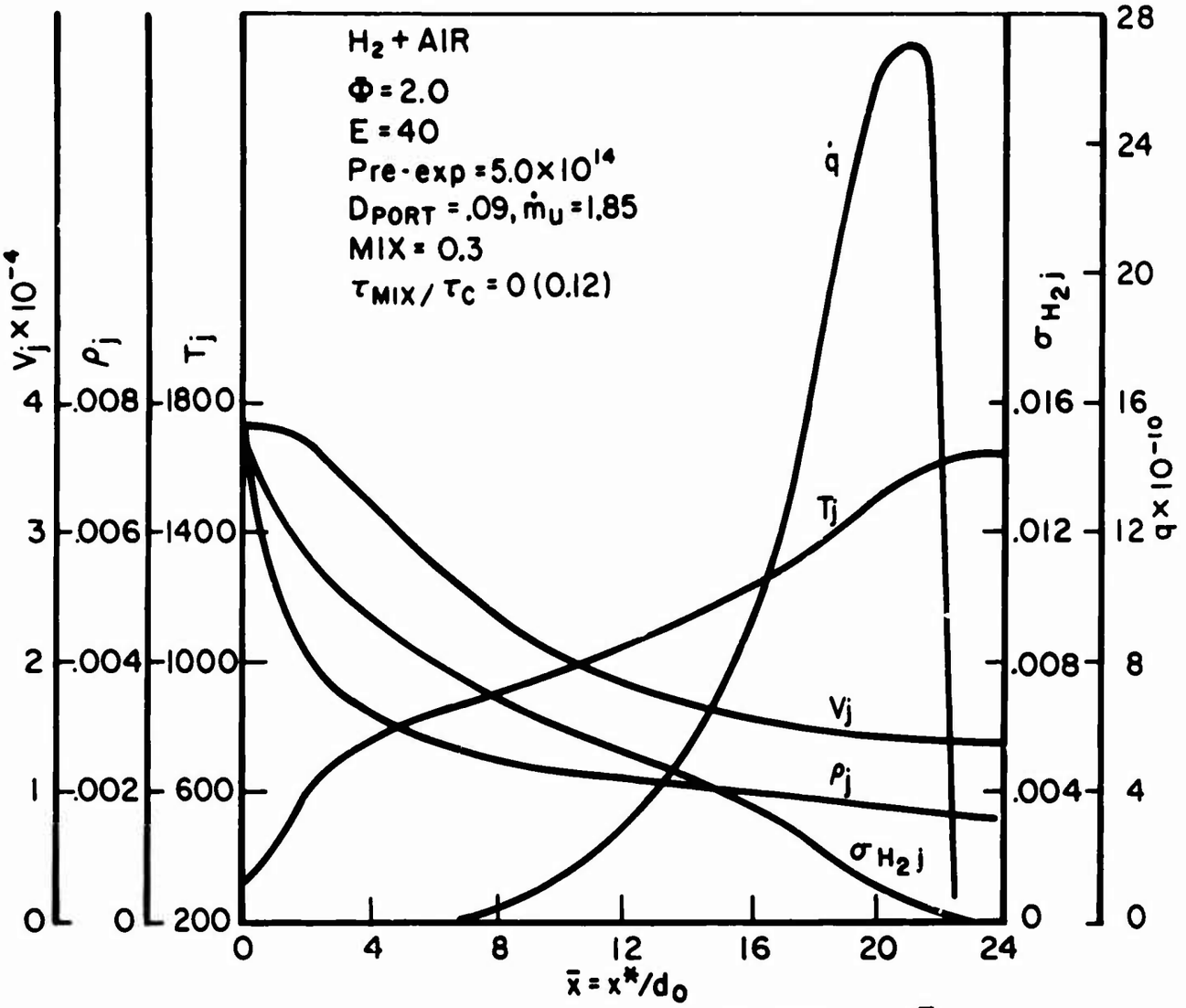

PARAMETER	VOLUME AVERAGE	CORRESP. TEMP.	$\frac{\bar{T}}{T_b}$
T_j	1356 °K	1356	0.82
ρ_j	.0019 gms/cm³	1320	0.80
V_j	1.56×10^4 cm/sec	1220	0.75
$\sigma_{H_2 j}$	.0030	1300	0.79
$\dot{q}$	1.11×10^{11} cal/cm³sec	1260	0.77

TYPICAL THEORETICAL PROFILES AND VOLUME AVERAGES FOR DISTRIBUTED COMBUSTION ZONE MODEL

FIGURE V - 5

at approximately $\bar{x}_c = 24$ where $\bar{x}_\ell = 45$ and $\alpha = 7^\circ$. For the conditions in Figure V-5 an increase in the total mass flux ($\dot{m}_{eff}$) from 1.85 to 3.0 gms/sec acts to increase the axial extent of the combustion zone from $\bar{x}_c = 24$ to 35. The consistency of the averaged properties is retained. A systematic study of the effect of combustion zone temperature (equivalence ratio) on the combustion distribution was not made. It is clear that for fixed entrainment capacity an increase in Φ implies a decrease in the mean temperature of the product gases in the recirculation zone. This must have an important nonlinear effect on the combustion zone distribution.[1] The mixing zone length should be relatively unaffected in view of the fact that the mass entrainment rate will increase $\sim (\rho_r/\rho_b)^{1/2}$. The energy entrainment rate $\sim \dot{m}_r T_r$ is thus $\sim T_r^{1/2}$ in the adiabatic model. On the other hand, the combustion zone will be extended due to the strong effect of the temperature on the reaction rate.

On the basis of the preceding discussion and in view of the calculation of the averaged combustion zone properties and $\tau_{mix}/\tau_c < .2$ in accordance with the recirculation stabilized distributed combustion zone model, justification is established for the consideration of the steady state combustion process in the gas rocket in terms of appropriate averaged values of the thermodynamic and gas dynamic properties. In particular, it is shown that the simple parametric representation

$$(\bar{\xi}_i)_c = \epsilon(\bar{\xi}_i)_b \qquad \text{where} \qquad \epsilon = \mathcal{O}(.7 \text{ to } .9)$$

and

$$\bar{\xi}_{ic} = \bar{T}_c, \bar{\rho}_c, \bar{v}_{fc}, \bar{g}_c, \bar{u}_c$$

can be used to evaluate the steady combustion process as if the combustion volume V_c were filled with burned and unburned gases at the conditions $\bar{\xi}_{ic}$.

Clearly this simplification will allow treatment of the combustion zone boundary condition in a manner similar to that applied to the well-stirred combustion zone. However, the two treatments

---

[1] The importance of the mean temperature of the gases in the recirculation zone was noted experimentally. In the optical studies with the N_2 window purge flowing the Φ_{lim} value shifted to lower Φ and higher mean T_b.

are not equivalent. The principle of the completely and instantaneously stirred combustion zone is unique. It is felt that the conditions for complete stirring of products and reactants throughout the combustion zone are not achieved in the gas rocket.

F. Development of the Combustion Zone Boundary Condition and Solution of the Nonsteady Burning Problem

In this section the nonsteady combustion process is modeled. The combustion zone boundary condition in terms of an analytical expression for U_2^o is obtained and substituted into the analysis of the wave dynamics in the combustion chamber. The nonlinear, ordinary, integro-differential equation governing the form of the wave amplitude parameter is derived. Solutions are obtained for the linearized and nonlinear forms of the equation and the principal results are summarized in terms of theoretically predicted nonsteady burning characteristics of the gas rocket system for the $H_2/O_2/N_2$ and CH_4/Air systems. Theory and experiment are compared.

F.1 Principal Approximations Invoked

(a) The finite dimensioned, distributed combustion process can be described in terms of averaged properties $p_c^*, \rho_c^*, T_c^*, \dot{g}_c^*, \gamma_c^*$ over the combustion zone volume $\forall_c^*$ (starred quantities are dimentional). The combustion zone is extended due to finite chemical kinetic reaction rates in a high velocity flow field for the case of showerhead injection. The characteristic combustion time, τ_c^*, due to reaction kinetics is equivalent to the residence time of gases in the combustion zone and serves as a measure of the mean rate of heat release in the combustion zone. That is $\tau_{mix}^*/\tau_c^* \ll 1$ and nonsteady effects due to mixing are not explicitly considered.

(b) The analysis is considered to apply to the case of porous plug injection. The model developed in the previous section explicitly considered the case of showerhead injection. In view of the racial nonuniformities of porosity in the porous injectors (manifest by hot wire velocity profiles in cold flow, temperature profiles in the combustion zone (Figure IV-10, 17), and the uneven darkening of the plug surface incurred during operation),

it is felt that a similar vigorous mixing of products and reactants characterizes the high intensity small scale (based on mean pore size) turbulent combustion zone of the porous plug. It is assumed that the distributed combustion process for the case of porous plug injection can also be characterized by averaged values of the thermodynamic and gas dynamic variables. The relative agreement between the experimentally observed nonsteady burning characteristics of the $CH_4/(.4O_2 + .6N_2)$ system using showerhead and porous plug injection and the correspondence between the effect of T_b^* on the $CO(H_2O)/O_2/N_2$ system with porous plug injection and the $H_2/O_2/N_2$ system with showerhead injection strongly support the concept that the same coupling mechanisms are active under both injection conditions. The stabilizing effect of the porous plug injector in the H_2 + Air system and the inability to sustain combustion in the $CO(H_2O)/O_2N_2$ system with showerhead injection must be explained.

(c) The combustion zone is short compared to the overall chamber length. Propellant is injected at the instantaneous mean chamber pressure which is uniform across the combustion zone,

$$p_u^* = p_b^* = p_c^* = p^*$$

$$\bar{p}_u = \bar{p}_b = \bar{p}_c = \bar{p}$$

(d) The unburned gas properties are assumed to be insensitive to the pressure oscillations. The presence and possible influence of a zone of underexpanded unburned propellant imbedded within the reaction zone disregarded. In principle, this assumption could be relaxed for the case of low velocity unchoked injection. For that case the assumption of isentropic variation of unburned gas thermodynamic properties may be appropriate.

(e) The gas in the combustion zone is calorically perfect.

(f) The mean thermodynamic and gas dynamic properties in the combustion zone and the combustion zone volume are time variant and are expressed as power series expansions about the steady state conditions. All perturbation quantities are ultimately coupled to the pressure oscillation which by virtue of (c) is uniform across the combustion zone.

(g) The burning rate term in the energy equation is expressed in terms of the overall gas phase reaction rate at the mean thermodynamic conditions and the combustion volume. The steady state value is computed as indicated in Section E on the basis of published overall chemical kinetic rate data obtained in flow reactor experiments.

(h) The possible sensitivity of the injection mass flux to oscillatory pressure at the injector is accounted for in the case of unchoked mass influx.

(i) Completely oxidized combustion products leave the combustion zone in thermodynamic equilibrium at the adiabatic combustion temperature T_b^*. In the case of quasisteady gas phase combustion (that is, the case of short characteristic combustion time relative to the wave travel time) the combustion of a parcel of unburned mixture can be considered to take place instantaneously at constant pressure. It follows that under these conditions the burned gas temperature may be assumed insensitive to the pressure oscillations. The heat of combustion (q) of the fuel may be taken as constant.

This assumption is based on the observation that the adiabatic, constant pressure, combustion temperature for mixtures of fuel and oxidizers used in the gas rocket is insensitive to combustion pressure over a wide range of pressure. Not until sufficiently high pressures to inhibit the low degree of dissociation in the product gases are encountered does $\bar{T}_b^*$ become sensitive to $\bar{p}_c^*$.

Calculations of the adiabatic equilibrium burned gas properties were carried out using the NASA Propellant Program (103) for a range of mixtures and pressures for the H_2 + Air system. Typical results are listed below. Note $[X_i]$ = mole fraction of i th species, $\bar{S}$ = entropy of product mixture.

$\Phi = 1.00$

$\bar{p}^*$ (atm)	$\bar{T}_b^*$ (^oK)	$\bar{S}$ $\frac{cal}{gm\,^oK}$	[H]	[H_2]	[H_2O]	[NO]	[N_2]	[O]	[OH]	[O_2]
2.36	2409	2.58	.0012	.0129	.3777	.0025	.6456	.0004	.0052	.0039
5.77	2431	2.50	.0008	.0106	.3314	.0028	.6469	.0002	.0047	.0031
11.2	2446	2.45	.0006	.0091	.3338	.0022	.6477	.0002	.0040	.0025

$\Phi = 2.40$

$\bar{P}^*$ (atm)	$\bar{T}_b^*$ (^oK)	$\bar{S}$ $\frac{cal}{gm\,^oF}$	$[H_2O]$	$[NO]$	$[NO_2]$	$[N_2]$	$[OH]$	$[O_2]$
2.36	1464	2.17	.1610	.0008	.00001	.7259	.00005	.1123
5.77	1464	2.10	.1610	.0008	.00001	.7259	.00004	.1123
11.2	1464	2.05	.1610	.0008	.00001	.7259	.00003	.1123

A plot of $\bar{T}_b^*$ over the complete range of Φ is shown in Figure IV-9.

Thus, for the case of short characteristic combustion time product gases are generated under isothermal conditions with respect to the combustion zone boundary. Temporal entropy variations of the product gases are simply expressed in terms of the pressure oscillations as $\frac{ds^*}{R^*} = -\frac{dp^*}{p^*}$. As indicated earlier the high level of turbulence and short entropy wavelength should lead to rapid dispersion of the entropy waves near the injector end.

With increasing combustion time relative to the wave travel time, the assumption of combustion at constant pressure becomes weaker. In particular, for $\bar{\tau}_c^* / \tau_{wave}^* \geq \Theta(1)$ fluctuations in the burned gas temperature in response to the pressure oscillations are to be expected. In the present formulation it is found (for the linearized case) that predicted oscillations in the burned gas temperature are small and have negligible influence on the theoretically predicted combustion zone mass efflux perturbation. This result is primarily a consequence of the dominant influences of the exponential factor in the burning rate law and the distinction made between the averaged combustion zone temperature (upon which the burning rate depends) and the final burned gas temperature. In other words, for purposes of numerical evaluation of the system response, the oscillation in the burned gas temperature may be neglected. Further comment on this point follows in the development of the combustion zone boundary condition.

F.2 Formulation of the Boundary Condition

Under the foregoing assumptions the simplified nonsteady combustion process is described by the equations of mass and energy conservation for the configuration shown in Figure V-6. The momentum equation is replaced by the assumption of uniform pressure across the short combustion zone. Starred quantities are considered dimensional.

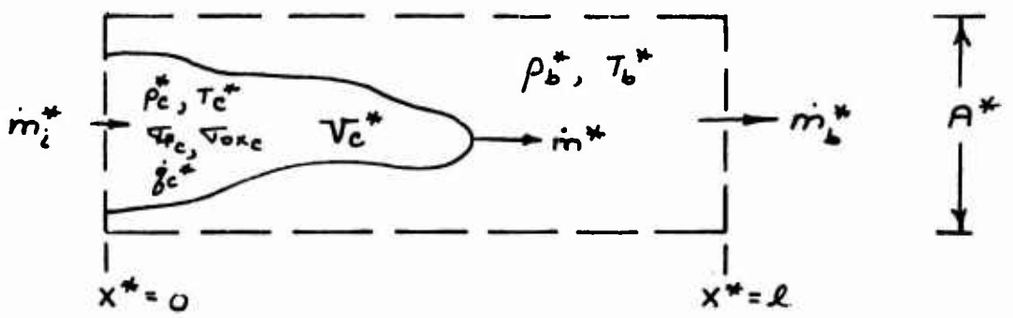

Figure V-6

To allow application of the boundary condition for the finite combustion zone at $x^* = 0$, the technique originally suggested by Crocco in the turbulent flame model is applied. The continuity equation is written for the control volume $A^* \cdot \ell^* > V_c^*$

$$\dot{m}_i^* = \dot{m}_b^* + \frac{d}{dt}\left[\rho_c^* V_c^* + \rho_b^* (A^* \cdot \ell^* - V_c^*)\right] \qquad \text{(V-30)}$$

which can be rearranged in the form

$$\dot{m}_b^{\circ *} = \dot{m}_i^* - \frac{d}{dt}\left[\left(1 - \frac{T_c^*}{T_b^*}\right)\rho_c^* V_c^*\right] \qquad \text{(V-31)}$$

where $\dot{m}_b^{o*} = \dot{m}_b^* + A^* \ell^* \frac{d\rho_b^*}{dt^*}$ = the effective instantaneous efflux of burned gas extrapolated to the injector face, $x^* = 0$

and the condition $p^* = p_u^* = p_b^* = p_c^*$ becomes

$$\rho_u^* T_u^* = \rho_b^* T_b^* = \rho_c^* T_c^*$$

where the assumption of $mw_c^* = mw_b^* = mw_u^*$ is quite good in view of the fact that the averaged combustion zone conditions are close to the burned gas properties and the gas mixtures considered are predominantly undissociated N_2.

The equations of mass and energy conservation are written for the combustion zone volume V_c^*

$$\dot{m}_i^* = \dot{m}^* + \frac{d}{dt^*}(\rho_c^* V_c^*) \tag{V-32}$$

$$\dot{m}_i^* c_{p_u}^* T_u^* + \dot{q}^* = \dot{m}^* c_{p_b}^* T_b^* + \frac{d}{dt^*}(\rho_c^* V_c^* c_{v_c}^* T_c^*) \tag{V-33}$$

The source term in the energy equation is expressed in terms of the fuel consumption rate and the constant heat of combustion of the fuel as in Section E,

$$\dot{q}^* = q^* \cdot \dot{m}_{f_c}^* \tag{V-34}$$

where $\dot{m}_{f_c}^*$ is the instantaneous averaged mass burning rate of fuel in the combustion zone volume and q* is the heat of combustion. The reaction is assumed to be represented (for purposes of calculating the heat release) sufficiently well by the stoichiometry that 1 gm of fuel burns with μ gms of oxidizer for $\Phi = 1$. For general Φ, 1 gm of fuel burns with $\Phi\mu$ gms of oxidizer. Hence,

$$\dot{m}_{b_c}^* = (1 + \Phi\mu)\dot{m}_{f_c}^* \tag{V-35}$$

where $\dot{m}_{b_c}^*$ is the total averaged mass burning rate of fuel and oxidizer in the combustion zone.

The fuel burning rate is expressed as in Section D by a bimolecular overall Arrhenius rate law in terms of the average combustion zone properties (denoted by subscript c)

$$\frac{\dot{m}_{f_c}^*}{V_c^*} = \frac{k^*}{m w_f^{*n-1} m w_{O_2}^{*m}} \rho_c^{*n+m} \nu_{f,c}^{n} \nu_{O_2,c}^{m} e^{-\frac{E^*}{\bar{R} T_c^*}} \qquad \text{(V-36)}$$

The analysis is carried out in detail for the case where the overall rate law is second order (first order with respect to fuel and oxidizer). $n = m = 1$. k^* is evaluated as discussed in Section E on the basis of flow reactor data of Sawyer (128) for the H_2/O_2 reaction and Dryer (129) for the CH_4/O_2 reaction where the "second method" is used to extrapolate flow reactor data to gas rocket conditions.

Equation V-35 is used to write

$$\dot{m}_{b,c}^* = \left[\hat{k}^* (1 + \Phi\mu) \frac{\nu_{ox,c}}{1+S} \nu_{f,c} \rho_c^* e^{-\frac{E^*}{\bar{R}^* T_c^*}} \right] \rho_c^* V_c^* \qquad \text{(V-37)}$$

where the characteristic kinetic combustion time is naturally derived as

$$\tau_c^* = \left[\hat{k}^* \frac{1+\Phi\mu}{1+S} \nu_{ox,c} \nu_{f,c} \rho_c^* e^{-\frac{E^*}{\bar{R}^* T_c^*}} \right]^{-1} \qquad \text{(V-38)}$$

According to this definition of the characteristic combustion time, the instantaneous energy release rate in the combustion volume is inversely proportional to τ_c^* according to,

$$\dot{q}^* = \frac{q^*}{(1+\Phi\mu)} \cdot \frac{\rho_c^* V_c^*}{\tau_c^*} \qquad \text{(V-39)}$$

Substituting Equation V-39 into Equation V-33 and taking $c_{p,i}^* = c_{p,b}^* = c_p^*$, the energy equation becomes,

$$\dot{m}_i^* c_p^* T_i^* + \left(\frac{q^*}{1+\Phi\mu}\right) \frac{\rho_c^* V_c^*}{\tau_c^*} = \dot{m}^* c_p^* T_b^* + \frac{d}{dt^*}\left(\rho_c^* V_c^* c_v^* T_c^*\right) \qquad \text{(V-40)}$$

The effective averaged mass fractions of fuel and oxidizer ($\nabla_{f,c}$ and $\nabla_{ox,c}$) appearing in the pre-exponential factor of the burning rate law are considered to be time dependent and are coupled to the combustion temperature and pressure. Two alternative treatments of this coupling have been considered.

In Section E, page 211, temperature-explicit expressions were derived for $\nabla_{f,c}$ and $\nabla_{ox,c}$ which are strictly valid for steady or quasi-steady combustion. In the present analysis,

$$\gamma = \frac{T_c^* - T_i^*}{T_b^* - T_i^*}$$

For the special case of second order overall kinetics, use of these relationships for $\nabla_{f,c}$ and $\nabla_{ox,c}$ yields (for $\Phi > 1$)

$$1/\gamma_c^* = \hat{k}^* \frac{\mu}{1+S} \nabla_{f,i} \frac{P^*}{\bar{R}^* T_c^*} (\Phi - \gamma)(1-\gamma) e^{-E^*/\bar{R}^* T_c^*} \qquad \text{(V-41)}$$

since $1/\nabla_{f,i} = 1 + \Phi\mu$, $\nabla_{ox} = (1+S)\nabla_{O_2}$

A simple relationship between the fuel rich and fuel lean expression is observed for the second order expression,

$$\left[1/\gamma_c^*\right]_{\substack{\text{OX RICH} \\ (\nabla_{f,i},\ \Phi)}} = \left[1/\gamma_c^*\right]_{\substack{\text{FUEL RICH} \\ (\Phi^2 \nabla_{f,i},\ 1/\Phi)}}$$

That is, to obtain $(1/\gamma_c^*)_{\Phi<1}$, $\nabla_{f,i}$ is replaced by $\Phi^2 \nabla_{f,i}$ and Φ by $1/\Phi$ in Equation V-41.

Thus, the influence on the burning rate of the fuel and oxidizer concentrations follows from the dependence of γ on T_c^* and T_b^*. For the case where fluctuations in the burned gas temperature are small, the oscillation in the fuel and oxidizer mass fractions follow the perturbations in the averaged combustion temperature.

Alternatively, for the case where $\bar{\gamma}_c^* = \Theta(\gamma_{wave}^*)$ it can be argued that the appropriate relationship between the fuel and oxidizer mass fractions and the averaged combustion zone properties should be derived directly by writing an additional conservation equation for the deficient species (e.g., fuel in an oxidizer rich initial mixture) as,

$$\dot{m}_i^* \nabla_{f,i} - \dot{m}_{fc}^* = \dot{m}^* \nabla_{f,b} + \frac{d}{dt}\left[\rho_c^* \nabla_{f,c} \bar{V}_c^*\right] \qquad \text{(V-42)}$$

Equation V-38 can be used to replace $\dot{m}_{fc}^*$ in favor of

$\nu_{f_i} \frac{\rho_c^* v_c^*}{\gamma_c^*}$. For the case of complete combination $\nu_{f,b} = 0$ and the species equation becomes,

$$\dot{m}_i^* \nu_{f_i} - \nu_{f_i} \frac{\rho_c^* v_c^*}{\gamma_c^*} = \frac{d}{dt} [\rho_c^* v_c^* \nu_{fc}] \qquad \text{(V-43)}$$

It is still necessary to make a statement about the overall reaction stoichiometry in order to eliminate $\nu_{ox,c}$ in the expression for γ_c^* . Furthermore, for the general case in which T_b^* is "allowed" to oscillate an additional expression relating T_c^*, ν_{fc}, and T_b^* is required. Since the initial mixture stoichiometry is expressed as $\nu_{ox_i} = (\Phi\mu)\nu_{f_i}$, these additional requirements are met by resorting to the steady state relationships, (see Appendix B).

$$\nu_{ox,c} = \mu \nu_{f_i} [\Phi - 1] + \mu \nu_{f,c}$$

$$c_p^* T_c^* + q \nu_{f,c} = c_p^* T_b^* \qquad \text{(V-44)}$$

In other words, use of a more precise expression for $\nu_{f,c}$ which allows for the additional storage or capacitance term in the species equation and allowance for a variable burned gas temperature nevertheless necessitates the use of steady state approximations to complete the system.

Initially, the system response was evaluated for the case where Equation V-23 and V-24 were used to solve for the species mass fractions in terms of the temperature-explicit formulations. The particular case where oscillations in T_b^* are neglected was considered.

A second determination of the linearized system response has been completed for the case where the species conservation equation (V-43) together with the stated approximations (V-44) are solved simultaneously with the mass and energy conservation equations to determine an explicit relationship between the fuel mass fraction, $\nu_{f,c}$ and T_c^* and p_c^*. Details of that analysis are summarized in Appendix B. It is appropriate here to merely emphasize the principal results of that calculation by way of comparison of the system response for the two approaches.

As expected the two methods yield identical results for the case where $\bar{\gamma}_c = \bar{\gamma}_c^* / \gamma_{wave}^* \ll 1$. (Equivalence is also found at

$\bar{\gamma}_c >> 1.0$.) For $\bar{\gamma}_c = \Theta(1)$, the perturbation in the burned gas temperature is found to be Θ (.05 to .15) times the perturbation in the averaged combustion temperature. Significantly, the influence of such a small burned gas temperature perturbation on the combustion zone mass efflux or velocity oscillation is found to be entirely negligible. Similarly, the calculated system responses for the two treatments of the species mass fractions showed that the quasi-steady treatment is sufficiently accurate. For $\bar{\gamma}_c = \Theta(1)$ the magnitude of the perturbation in the fuel mass fraction as determined by the simultaneous solution of the conservation equations is larger by some (0 to 12%, depending on Φ) than the value determined from the single quasi-steady relation. Since the species mass fraction perturbation is predicted to lag slightly, the combustion temperature perturbation for $\bar{\gamma}_c = \Theta(1)$ the real component of the species perturbation is even closer to the (real) value calculated from the quasi-steady equation. As noted earlier, these results are not particularly surprising in view of the strong exponential temperature dependence of the burning rate for combustion systems characterized by high overall activation energies.

In view of these results for the linearized case a detailed examination of the linear and nonlinear system response is carried out for the particular case where the influence of perturbations in the burned gas temperature is neglected (T_b^* is taken as a constant to first order) and where the simplified temperature-explicit relationships for $\bar{\nu}_{f,c}$ and $\bar{\nu}_{ox,c}$ (Equation V-41) are used. It should be noted that a considerable mathematical simplification follows and allows a direct evaluation of the full nonlinear system stability characteristics.

All thermodynamic variables are nondimensionalized by their steady state burned gas values, length by L_c^*/m where m = 1, 2, 3, 4, for fundamental, second, third, fourth, etc., harmonic modes and L_c^* is the chamber length, velocity by the steady state sound speed $\bar{C}_b^*$ of the burned gas, time by $L_c^*/m\bar{C}_b^*$, volume by $L_c^* \cdot A_{eff}^*$ where $A_{eff}^* = A_{CH}/n_{holes}$ and energy release rate by $\bar{h}_b^* \bar{\rho}_b^* \bar{C}_b^*$ where $\bar{h}_b^*$ is the steady state enthalpy of the combustion products.

Nondimensionalizing all variables as above and in light of the foregoing comments, the equations of mass and energy conservation become

$$\dot{m} = \dot{m}_i - \frac{d}{dt}(\rho_c V_c) \tag{V-45}$$

$$\dot{m}_i T_i + \bar{q}\,\frac{\rho_c V_c}{\gamma_c} = \dot{m} + \frac{1}{\gamma} T_c \frac{d}{dt}(\rho_c V_c) + \frac{1}{\gamma}(\rho_c V_c)\frac{dT_c}{dt} \tag{V-46}$$

where $\bar{q} = (1 - \bar{T}_i)$ since $\nabla_{f_i} q^* = \bar{C}_p^* (\bar{T}_b^* - \bar{T}_i^*)$

and $\frac{1}{\gamma_c} = \frac{\tau^*_{wave}}{\tau_c^*}$ = ratio of wave travel time (½ period of oscillation) to the characteristic combustion time.

Eliminating $\dot{m}$ from Equations V-45 and V-46 an equation for ($\rho_c V_c$) is obtained as,

$$\frac{d}{dt}(\rho_c V_c) + \frac{\beta}{\gamma_c}(\rho_c V_c) = \xi \dot{m}_i \tag{V-47}$$

where

$$\beta = \frac{\bar{q} - \frac{1}{\gamma}\gamma_c \frac{dT_c}{dt}}{1 - T_c/\gamma} \tag{V-48}$$

$$\xi = \frac{1 - T_i}{1 - T_c/\gamma} \tag{V-49}$$

which can be solved explicitly for ($\rho_c V_c$) as,

$$\rho_c V_c = \int_{-\infty}^{t} \xi(t')\,\dot{m}_i(t') \left[e^{-\int_{t'}^{t} \frac{\beta(t'')}{\gamma_c(t'')} dt''} \right] dt' \tag{V-50}$$

where the lower limit is set equal to $-\infty$ since ($\rho_c V_c$) is considered to vary periodically at times sufficiently long such that starting transients have become negligible. Only the limiting periodic solution is relevant. Subsequently, the periodicity condition is used to eliminate the infinite range of integration in the numerical analysis.

Equation V-31 is written in dimensionless terms

$$\dot{m}_b^\circ = \dot{m}_i - (1-\tau_c)\frac{d}{dt}(\rho_c v_c) + (\rho_c v_c)\frac{d\tau_c}{dt} \qquad \text{(V-51)}$$

Substituting for $\frac{d}{dt}(\rho_c v_c)$ and $(\rho_c v_c)$ from Equations V-47 and V-50,

$$\dot{m}_b^\circ = \alpha \dot{m}_i + \delta \int_{-\infty}^{t} \xi(t')\dot{m}_i(t')\left[e^{-\int_{t'}^{t} \frac{\beta(t'')}{\tau_0(t'')}dt'}\right]dt' \qquad \text{(V-52)}$$

$$\alpha = 1 - (1-\tau_c)\xi$$

$$\delta = (1-\tau_c)\frac{\beta}{\tau_c} + \frac{d\tau_c}{dt}$$

All variables in Equation V-52 are time dependent in general. Pressure oscillations in the gas rocket, both linear and nonlinear shock-type waveforms, are characteristically low amplitude, $0 < \frac{\Delta p}{\bar{p}} < 0.2$. It is appropriate to consider all time dependent variables as the sum of a steady state value and a time dependent perturbation. In accordance with the Mitchell-Crocco analysis of the chamber wave dynamics all perturbation quantities are ordered in terms of powers of the steady state Mach number of the burned gases. Denoting steady state values by the superposed bar, $\bar{\dot{m}}_b^\circ = \bar{\dot{m}}_i = \bar{\dot{m}}$

The instantaneous perturbation in the mass efflux from the combustion zone, extrapolated to the injector face is

$$\dot{m}_b^\circ - \bar{\dot{m}} = \bar{\dot{m}}\left\{\alpha\frac{\dot{m}_i}{\bar{\dot{m}}} - 1 + \delta\int_{-\infty}^{t}\xi(t')\frac{\dot{m}_i(t')}{\bar{\dot{m}}}\left[e^{-\int_{t'}^{t}\frac{\beta(t'')}{\tau_c(t'')}dt''}\right]dt'\right. \qquad \text{(V-53)}$$

The combustion zone variables are written as linear expansions about the steady state values. In general, $\epsilon = \bar{\epsilon} + \epsilon_1 + \epsilon_2$ where $\epsilon_1 = \Theta(M)$, $\epsilon_2 = \Theta(M^2)$

$$\rho_c = 1 + \rho_1 + \rho_2 + \cdots \qquad \rho_b = 1 + \rho_1 + \rho_2 + \cdots$$

$$\rho_c = \bar{\rho}_c + \rho_{c_1} + \rho_{c_2} + \cdots \qquad T_b = 1 + T_{b_1} + T_{b_2} + \cdots$$

$$T_c = \bar{T}_c + T_{c_1} + T_{c_2} + \cdots \qquad T_i = \bar{T}_i \qquad \text{(V-54)}$$

$$u_b = \bar{u} + u_1 + u_2 + \cdots$$

All lowest order terms are of order 1 with exception of $\bar{u}$ which is nondimensionalized by the steady state burned gas sound speed, such that $\bar{u} = M$.

The burned gas mass flux per unit area extrapolated to the injector is,

$$\dot{m}_b^\circ = \rho_b^\circ u_b^\circ = (1+\rho_1^\circ+\rho_2^\circ+\cdots)(M + u_1^\circ + u_2^\circ + \cdots)$$

$$\dot{m}_b^\circ - \bar{\dot{m}} = u_1^\circ(1+\rho_1^\circ) + M\rho_1^\circ + u_2^\circ + \theta(M^3) \qquad \text{(V-55)}$$

$$\text{since } \bar{\dot{m}}_b^\circ = \bar{\dot{m}} = \bar{u} = M$$

The possible sensitivity of the injection mass flux to the oscillatory pressure at the injector is accounted for by expressing the instantaneous mass influx in a power series expansion about the steady state value,

$$\dot{m}_i = \bar{\dot{m}}_i + \dot{m}_{i_1} + \dot{m}_{i_2} + \cdots \qquad \text{(V-56)}$$

For the case of choked mass injection flux $\dot{m}_{i_{1,2,\ldots}} = 0$ and $\dot{m}_i = \bar{\dot{m}}$ is equal to a constant. For the case of unchoked mass injection $\dot{m}_{i_1}$ is related to the pressure oscillation at the injector face p_1° by means of a "response function" determined from the steady state isentropic laws coupling the pressure ratio across the injector to the mass flow. The original formulation by Crocco in the turbulent flame model is utilized. For isentropic flow, the mass flux per unit area is

$$\dot{m}_i^* = \sqrt{\frac{\gamma}{R^*}}\,\frac{p^*}{\sqrt{T^*_{stag}}}\,M_i\left[1 + \left(\frac{\gamma-1}{2}\right)M_i^2\right]^{\frac{1}{2}}$$

where

$$\frac{p^*_{stag}}{p_c^*} \simeq \frac{p^*_{mix}}{p_c^*} = \left(1 + \frac{\gamma_i - 1}{2}M_i^2\right)^{\frac{\gamma_i}{\gamma_i - 1}}$$

$$\dot{m}_i^* = (\text{constant})\cdot\left(\frac{p_c^*}{p^*_{mix}}\right)^{\frac{1}{\gamma_i}}\left[1 - \left(\frac{p_c^*}{p^*_{mix}}\right)^{\frac{\gamma_i - 1}{\gamma_i}}\right]^{\frac{1}{2}}$$

The response function is determined as

$$\frac{p_c^*}{\dot{m}_i^*}\frac{d\dot{m}_i^*}{dp_c^*} = -\frac{\gamma_i - 1}{2\gamma_i}\frac{1}{\left(\frac{p_{mix}^*}{p_c^*}\right)^{\frac{\gamma_i-1}{\gamma_i}} - 1} + \frac{1}{\gamma_i}$$

and Equation V-56 becomes

$$\dot{m}_i/\bar{\dot{m}} = 1 - \psi p_i^\circ + \theta(M^2) = 1 + \mu_i + \cdots \qquad \text{(V-57)}$$

$$\psi = +\frac{\gamma_i - 1}{2\gamma_i}\frac{1}{\left(p_{mix}^*/p_c^*\right)^{\frac{\gamma_i-1}{\gamma_i}} - 1} - \frac{1}{\gamma_i} \qquad \text{(V-58)}$$

The condition of choked injection flux is defined by,

$$\psi = 0 \quad , \quad p_{inj} = \frac{p_{mix}^*}{p_c^*} \geq \left(\frac{\gamma_i + 1}{2}\right)^{\frac{\gamma_i}{\gamma_i - 1}}$$

$$\dot{m}_i = \bar{\dot{m}}$$

For the case of unchoked injection the mass influx is coupled to the pressure oscillation, $\psi > 0$. Due to the low inertia of the gaseous flow system (the injector and the mixing chamber), the response time required for the injection mass influx to adjust to a change in the pressure drop across the injector due to a change in p_c is short compared to the wave travel time in the combustion chamber. The mass influx therefore responds with negligible lag to the p_c fluctuations and is essentially 180° out of phase with the pressure oscillations[1]. An estimate of the lag can be made on the basis of the wave propagation time in the injection ports. For injectors 0.6 cm thick and an unburned gas sound speed of 3×10^4 cm/sec, the lag is ($\theta(2 \times 10^{-5}$ sec)) or 1 to 2 orders of magnitude less than the period of oscillation.

The strength (magnitude of ψ) of the coupling is increased with decreasing steady state pressure drop (decreasing M_{inj}) across the injector. In the incompressible flow limit of low pressure drop,

$$p_{inj} = 1 + \Delta p \; , \quad \lim_{\Delta p \to 0} \psi = \frac{1}{2\Delta p}$$

F.2a Sensitivity of the Characteristic Combustion Time to the Pressure Oscillations

The experimental observations have demonstrated the important

[1]Denoted by the minus sign in Equation V-57 .

influence of chemical kinetic factors on the nonsteady burning characteristics of the system. It is logical to suspect that such an influence derives from a coupled response of the gas phase burning rate to the pressure oscillation. In terms of the present model this implies a response of the characteristic combustion time τ_c to the pressure oscillations principally through the temperature sensitivity of the burning rate. The important nonsteady effect of the variation in ($\rho_e v_e$) is already included in terms of Equation V-50 and is implicitly coupled to the characteristic combustion time through the exponential term. As will be apparent, insensitivity of the characteristic combustion time to pressure oscillations naturally precludes the support of combustion oscillations.

The instantaneous value of τ_c is expressed in terms of the steady state value plus a time dependent perturbation proportional to the perturbations in the averaged combustion temperature and pressure. This formulation can be justified in view of the low amplitude of the experimentally observed sustained oscillations and the schlieren and shadowgraph observations indicating the absence of extraordinary nonlinear chemico-fluid dynamic coupling (such as observed by Tsuji and Takeno (76)) between the combustion process and the pressure waves during nonsteady burning. That is, to $\theta(M^2)$

$$\frac{1}{\tau_c^*} = \frac{1}{\bar{\tau}_c^*} + \Sigma_1^*$$

In nondimensional form,

$$\frac{1}{\tau_c} = \frac{1}{\bar{\tau}_c}\left[1 + \Sigma_1 + \theta(M^2)\right] \qquad \text{(V-59)}$$

where

$$\Sigma_1 = \Sigma_T T_{c_1} + \Sigma_p p_1^{\circ}$$

and

$$\Sigma_T = \frac{1}{\bar{\tau}_c}\frac{\partial \ln 1/\bar{\tau}_c^*}{\partial \ln \bar{T}_c^*}$$

$$\Sigma_p = \frac{\partial \ln 1/\bar{\tau}_c^*}{\partial \ln \bar{p}_c^*}$$

For the second order overall rate law, oxidizer rich expression of Equation V-41,

$$\Sigma_T = \frac{1}{\bar{T}_c^2}\frac{E^*}{R^* T_b^*} - \frac{1}{\bar{T}_c} - \frac{1}{1-\bar{T}_c}\left[\frac{1}{\Phi-\bar{T}} + \frac{1}{1-\bar{T}}\right] \qquad \text{(V-60)}$$

$$\Sigma_p = 1$$

For an initially fuel rich mixture, $1/\Phi$ replaces Φ in the expression for Σ_T. The steady state characteristic combustion time may be determined from Equation V-41 in terms of the properties of the unburned propellant mixture and the steady state mean thermodynamic conditions within the combustion zone.

The expression for $(\dot{m}_b^\circ - \bar{\dot{m}})$ can be developed in general in terms of T_{c_1} and p_1°. Equation V-53 is written in the form

$$\dot{m}_b^\circ - \bar{\dot{m}} = \bar{\dot{m}}\left[\left(\alpha\frac{\dot{m}_i}{\bar{\dot{m}}} - 1\right) + \delta\frac{\rho_c v_c}{\bar{m}}\right] \qquad \text{(V-61)}$$

where

$$\frac{\rho_c v_c}{\bar{m}} = \int_{-\infty}^{t} \xi(t')\frac{\dot{m}_i(t')}{\bar{\dot{m}}}\left[e^{-\int_{t'}^{t}\beta(t'')/\tau_c(t'')\,dt''}\right]dt'$$

Equations V-54 to V-60 are used to simplify $\alpha, \delta, \xi, \beta, 1/\tau_c$

$$\xi(t) = \bar{\xi} + \xi_1 + \theta(M^2), \qquad \bar{\xi} = \frac{1-\bar{T}_i}{1-\bar{T}_c/\gamma}, \qquad \xi_1 = \frac{\bar{\xi}}{\gamma-\bar{T}_c}T_{c_1}$$

$$\alpha(t) = \bar{\alpha} + \alpha_1 + \theta(M^2), \qquad \bar{\alpha} = 1 - \bar{\xi}(1-\bar{T}_c), \qquad \alpha_1 = \frac{\gamma-1}{\gamma-\bar{T}_c}\bar{\xi}\,T_{c_1}$$

$$\beta(t) = \bar{\beta} + \beta_1 + \theta(M^2), \qquad \bar{\beta} = \bar{\xi}, \qquad \beta_1 = \frac{\bar{\beta}}{\gamma-\bar{T}_c}T_{c_1} - \frac{\bar{\gamma}_c}{\gamma-\bar{T}_c}\frac{dT_{c_1}}{dt}$$

$$\delta(t) = \bar{\delta} + \delta_1 + \theta(M^2), \qquad \bar{\delta} = \frac{\bar{\beta}}{\bar{\gamma}_c}(1-\bar{T}_c)$$

$$\delta_1 = \frac{\bar{\delta}}{1-\bar{T}_c}\left\{\left[(1-\bar{T}_c)\Sigma_T - \frac{\gamma-1}{\gamma-\bar{T}_c}\right]T_{c_1} + (1-\bar{T}_c)\Sigma_p p_1^\circ\right\} + \frac{\gamma-1}{\gamma-\bar{T}_c}\frac{dT_{c_1}}{dt}$$

$$\frac{\beta(t)}{\gamma_c(t)} = \frac{\bar{\beta}}{\bar{\gamma}_c} + \frac{1}{\bar{\gamma}_c}\left[\beta_1 + \bar{\beta}\left(\Sigma_T T_{c_1} + \Sigma_p p_1^\circ\right)\right] \qquad \text{(V-62)}$$

The first term in Equation V-61 is

$$\alpha \frac{\dot{m}_1}{\bar{\dot{m}}} - 1 = -\bar{\xi}(1-\bar{\tau}_c) + \frac{\gamma-1}{\gamma-\bar{\tau}_c}\bar{\xi}\,\tau_{c_1} + \left[1-\bar{\xi}(1-\bar{\tau}_c)\right]\mu_1$$

The second term is

$$\delta \frac{\rho_c v_c}{\bar{\dot{m}}} = \bar{\delta}\frac{\overline{\rho_c v_c}}{\bar{\dot{m}}} + \delta_1 \frac{\overline{\rho_c v_c}}{\bar{\dot{m}}} + \bar{\delta}\left(\frac{\rho_c v_c}{\bar{\dot{m}}}\right)_1$$

since

$$\frac{\rho_c v_c}{\bar{\dot{m}}} = \frac{\overline{\rho_c v_c}}{\bar{\dot{m}}} + \left(\frac{\rho_c v_c}{\bar{\dot{m}}}\right)_1$$

Substitution of these expressions into Equation V-50 and retaining only terms to $\Theta(M)$, the steady state relationship is obtained as,

$$\frac{\overline{\rho_c v_c}}{\bar{\dot{m}}} = \bar{\gamma}_c \tag{V-63}$$

and the first order equation becomes

$$\left(\frac{\rho_c v_c}{\bar{\dot{m}}}\right)_1 = \frac{\bar{\gamma}_c}{\gamma-\bar{\tau}_c}\tau_{c_1} - \bar{\beta}\left[\Sigma_T + \frac{1}{\gamma-\bar{\tau}_c}\right]\int_{-\infty}^{t}\tau_{c_1} e^{-\frac{\bar{\beta}}{\bar{\gamma}_c}(t-t')}dt' - \bar{\beta}\left[\Sigma_p+\Psi\right]\int_{-\infty}^{t}\rho_1^{\circ} e^{-\frac{\bar{\beta}}{\bar{\gamma}_c}(t-t')}dt' \tag{V-64}$$

Considering the lowest order terms within the brackets in Equation V-61 to order M (since $\bar{\dot{m}} = M$)

$$\dot{m}_b^{\circ} - \bar{\dot{m}} = \bar{\dot{m}}\left[\alpha\frac{\overline{\dot{m}_1}}{\bar{\dot{m}}} - 1 + \bar{\delta}\frac{\overline{\rho_c v_c}}{\bar{\dot{m}}}\right] = \bar{\dot{m}}\left[-\bar{\xi}(1-\bar{\tau}_c) + \frac{\bar{\beta}}{\bar{\gamma}_c}(1-\bar{\tau}_c)\bar{\tau}_c\right] \equiv 0$$

That is $\dot{m}_b^{\circ} - \bar{\dot{m}} = \Theta(M^2)$. Hence in Equation V-55 where

$\dot{m}_b^{\circ} - \bar{\dot{m}} = u_1^{\circ}(1+\rho_1^{\circ}) + u_2^{\circ} + M\rho_1^{\circ} + \Theta(M^3)$

the boundary condition on the first order perturbation in the particle velocity is

$$u_1^{\circ} = 0 \tag{V-65}$$

and

$$u_2^{\circ} = (\dot{m}_b^{\circ} - \bar{\dot{m}}) - M\rho_1^{\circ} \tag{V-66}$$

where, in the present model $\tau_{b_1}^{\circ} \simeq 0$

$$p_b = \rho_b \tau_b$$

$$p_1^{\circ} \cong \rho_1^{\circ}$$

An expression for $\frac{\dot{m}_b^{\circ} - \bar{\dot{m}}}{\bar{\dot{m}}}$ is obtained as,

$$\frac{\dot{m}_b^{\circ} - \bar{\dot{m}}}{\bar{\dot{m}}} = \bar{\beta}(1-\bar{\tau}_c)\left[\Sigma_T + \frac{1}{\gamma-\bar{\tau}_c}\right]\tau_{c_1} + \left\{\bar{\beta}(1-\bar{\tau}_c)\Sigma_p - \Psi\left[1-\bar{\beta}(1-\bar{\tau}_c)\right]\right\}\rho_1^{\circ} + \bar{\gamma}_c\frac{\gamma-1}{\gamma-\bar{\tau}_c}\frac{d\tau_{c_1}}{dt}$$

$$- \frac{\bar{\beta}^2}{\bar{\gamma}_c}(1-\bar{\tau}_c)\left\{\left[\Sigma_T + \frac{1}{\gamma-\bar{\tau}_c}\right]\int_{-\infty}^{t}\tau_{c_1} e^{-\frac{\bar{\beta}}{\bar{\gamma}_c}(t-t')}dt' + \left[\Sigma_p+\Psi\right]\int_{-\infty}^{t}\rho_1^{\circ} e^{-\frac{\bar{\beta}}{\bar{\gamma}_c}(t-t')}dt'\right\} \tag{V-67}$$

From Appendix A the result of the Mitchell-Crocco analysis of the wave dynamics in the combustion chamber is simply,

$$u_2^\circ = M^2 \left\{ (\gamma-1) f(\theta) - (\gamma+1)[f(\theta) - k] \frac{df}{d\theta} \right\} \qquad \text{(V-68)}$$

where $0 \leq \theta \leq 2$ = is the dimensionless stretched time

$$f(\theta) = \theta(1)$$

$$p_1^\circ = 2\gamma M f(\theta) \quad \text{at } x = 0$$

and where $k = \dfrac{f(0)+f(2)}{2}$ = for nonlinear shock-type waves with discontinuity, k is the average value of f at the discontinuity which is assumed to be at $\theta = 0$.

For linear waves k must be determined as the correction on the period of oscillation ($\theta = 2$) from the linearized analysis. Rearranging terms

$$(f - k)\frac{df}{d\theta} = \frac{\gamma-1}{\gamma+1} f - \frac{u_2^\circ}{M^2(\gamma+1)} \qquad \text{(V-69)}$$

where

$$\frac{u_2^\circ}{M^2(\gamma+1)} = \frac{\dot{m}_b^\circ - \bar{\dot{m}}}{M^2(\gamma+1)} - \frac{M p_1^\circ}{M^2(\gamma+1)} = \frac{1}{\gamma+1}\left[\frac{\dot{m}_b^\circ - \bar{\dot{m}}}{M^2} - 2\gamma f \right] \qquad \text{(V-70)}$$

In order to reduce Equation V-69 to a form which can be solved for f, an additional relationship is required which will allow the specification of the functional relationship between the averaged combustion temperature and pressure. In previous investigations of nonsteady burning in solid, liquid, and gaseous systems (e.g., 27, 80), the isentropic relationship has been applied to couple an "averaged" combustion temperature to the pressure. In the original turbulent flame model, the actual burning process was considered to be quasi-steady ($\bar{\tau}_c \ll 1$) and the condition of isentropic variation of the unburned gas properties together with the quasi-steady flame jump condition, $T_b^* = T_u^* + q^*/c_p^*$, pro-

vided the important additional bit of information to close the analysis. In the present formulation, the necessity to consider the complex gas phase combustion process in terms of approximate time-dependent averaged thermodynamic variables coupled with the experimental result that the combustion volume must also be considered as time dependent, precludes the exact determination of the relationship between the combustion temperature and pressure. The difficulty appears to lowest order if we write the steady state relationship as

$$\bar{\tau}_c = \frac{\dot{m}\,\bar{\tau}_c}{\bar{\rho}_c} = \dot{\bar{m}}\,\bar{\tau}_c\,\bar{T}_c$$

where the right hand side is a function of the known steady state mass flux and pressure and the averaged combustion temperature. In lieu of an exact integration of the governing partial differential equations relating local thermodynamic properties throughout the turbulent combustion zone, the averaged combustion temperature and, hence, the mean steady state combustion volume appear as parameters. It is precisely because of this difficulty that the analysis in Section E·2 was carried out. In that section, the appropriateness of considering the burning process in terms of self-consistent volume-averaged thermodynamic properties was verified. Typical averaged values ($\bar{T}_c = \mathcal{O}(.75$ to $.9$) were calculated and the overall combustion volume determined. These results are used here to specify values of the steady state averaged combustion zone properties ($\bar{T}_c$, $\bar{\rho}_c$, $\bar{\tau}_c$, $\bar{\tau}_c$).

In the absence of information about the x-dependence or time history (in the Lagrangian sense) of the combustion process the non-steady combustion volume, pressure, and temperature are implicitly coupled to first order. In the following paragraphs the nature of this coupling is explored. It is suggested that precise experimental information regarding two nonsteady parameters (e.g., the phase relative to the pressure oscillation and magnitude of the volume oscillation, or the relative (to p_i°) phases of the volume and mean temperature oscillations) over the range of equivalence ratios would be required to completely define the system. Lacking such detailed information, the consequences (with respect to the linear overall system response) of several alternative relationships

between the volume, temperature, and pressure oscillations are discussed. A detailed examination of the linear and nonlinear system response for a particularly simple form of the coupling relationship is carried out.

In the present model Equation V-64 represents an implicit relationship between the perturbations in the mass, temperature, T_{c_1}, and pressure oscillations (p_1°). A second equation relating these variables and introducing the time dependent combustion volume follows from the perfect gas law. The combustion zone volume is nondimensionalized by dividing V_c^* by $\frac{L_c^*}{m} \cdot A_{eff}^*$ where V_c^* can be approximated as $\ell_c^* \cdot A_{eff}^*$ where $\ell_c^* = (1/A_{eff}^*)\int_0^{\bar{x}_c} A_j^*(\bar{x})\, d\bar{x}$. Hence, $\bar{V}_c = \Theta(\ell_c^*/(L_c^*/m)) = \Theta(1/40) = \Theta(M)$. The nonsteady dimensionless combustion volume is expressed as the sum of the steady state value and a time dependent perturbation,

$$V_c = \underset{\Theta(M)}{\bar{V}_c} + \underset{\Theta(M)}{V_{c_1}} + \underset{\Theta(M^2)}{V_{c_2}} + \Theta(M^3)$$

From Equation V-64 , $(\rho_c V_c)_1 = \Theta(M^2)$, and

$$\rho_c V_c = (\bar{\rho}_c + \rho_{c_1} + \cdots)(\bar{V}_c + V_{c_1} + V_{c_2} + \cdots)$$

$$(\rho_c V_c)_1 = \rho_c V_c - \overline{\rho_c V_c} = \bar{V}_c \rho_{c_1} + \bar{\rho}_c V_{c_2} + V_{c_1}\bar{\rho}_c + V_{c_1}\rho_{c_1} = \Theta(M^2)$$

Therefore, $V_{c_1} = 0$ and

$$(\rho_c V_c)_1 = \bar{V}_c \rho_{c_1} + \bar{\rho}_c V_{c_2} \qquad \text{(V-71)}$$

The perfect gas relationship is combined with Equation V-71 to obtain a second expression for $\frac{(\rho_c V_c)_1}{\dot{m}}$ as,

$$\left(\frac{\rho_c V_c}{\dot{m}}\right)_1 = \bar{\tau}_c \left[p_1^\circ - \frac{T_{c_1}}{\bar{T}_c} + \frac{V_{c_2}}{\bar{V}_c} \right] \qquad \text{(V-72)}$$

Equations V-64 and V-72 can be solved simultaneously to obtain

$$T_{c_1} = \mathcal{T}(p_1^\circ, V_{c_2}) \qquad \text{(V-73)}$$

Equation V-64, 72, and 73 can be considered as equations coupling T_{c_1} and p_1° once the nonsteady volume contribution $(V_{c_2}/\bar{V}_c)$ is known.

Case 1: $\bar{V}_c = \bar{V}_c \neq V_c(t)$ This case is contradicted by the experimental observations (see Chapter IV) but can be considered as an approximation to the subcase of $V_{c_2}/\bar{V}_c \ll p_1^\circ, T_{c_1}$

Neglecting $V_{c_2}/\bar{V}_c$ in Equation V-72 an implicit relationship is obtained between T_{c_1} and p_1° as,

$$T_{c_1} - \frac{\gamma-\bar{T}_c}{\gamma}\bar{T}_c\frac{\bar{\beta}}{\bar{\tau}_c}\left[\Sigma_T + \frac{1}{\gamma-\bar{T}_c}\right]\int_{-\infty}^{t} T_{c_1}(t')\, e^{-\frac{\bar{\beta}}{\bar{\tau}_c}(t-t')}\, dt'$$
$$= \frac{\gamma-\bar{T}_c}{\gamma}\bar{T}_c\, p_1^\circ + \frac{\bar{\beta}}{\bar{\tau}_c}(\Sigma_p + \psi)\int_{-\infty}^{t} p_1^\circ(t')\, e^{-\frac{\bar{\beta}}{\bar{\tau}_c}(t-t')}\, dt' \qquad \text{(V-74)}$$

A general solution for the combustion zone boundary condition requires for this case a simultaneous solution of Equations V-67 and V-74 . In the limit of short combustion time ($\bar{\tau}_c \ll 1$) Equation V-74 yields

$$T_{c_1} = \frac{\bar{T}_c(\Sigma_p + \psi + 1)}{1 - \Sigma_T \bar{T}_c} p_1^\circ \qquad \text{(V-75)}$$

where the coefficient is in general less than zero for $\bar{T}_c \lesssim \Theta(1)$ and high overall activation energy systems. $T_{c_1} \sim -p_1^\circ$ describes a circumstance where the temperature oscillation is essentially out of phase (by 180°) with the pressure oscillation and as will be seen, nonsteady burning is precluded. In the limit of long combustion time, Equation V-74 gives

$$T_{c_1} = \eta_0 p_1^\circ \quad , \quad \eta_0 = \frac{\gamma-\bar{T}_c}{\gamma}\bar{T}_c \qquad \text{(V-76)}$$

That is, the temperature oscillation is in phase and somewhat smaller than the pressure oscillation. It is of interest to consider the approximate relationship between T_{c_1} and p_1° for arbitrary $\bar{\tau}_c$, which is valid for the near limit linearized case of continuous harmonic oscillations, where,

$$p_1^\circ = p_1 e^{i\pi t}$$
$$T_{c_1} = T_1 e^{i(\pi t - \epsilon_{Tp})} \qquad \text{(V-77)}$$

---

[1] Crocco (154) suggests another way of considering this formulation is to consider $\bar{V}_c$ as a fixed zone equal in extent to the minimum of the nonsteady volume. The approximate averaging procedure would then be considered to apply to this constant minimum portion of the overall combustion volume.

The perturbation quantities are considered to be 2π periodic in the dimensionless time, t and $\epsilon_{\tau p}$ is considered as the finite phase angle of the oscillation in the mean combustion temperature relative to the pressure oscillation. p_1 and T_1 are defined as (real) positive amplitude factors. Substituting Equations V-77 into V-74 and carrying out the integration yields,

$$\frac{T_1}{p_1} = \left[\frac{\bar{a}_4^2 + \bar{a}_2^2}{a_1^2 + a_2^2} \right]^{\frac{1}{2}} = \bar{G}\,\eta_0 \qquad \text{(V-78)}$$

$$\epsilon_{\tau p} = \tan^{-1}\left[\frac{\bar{a}_4 a_1 + \bar{a}_2 a_2}{\bar{a}_2 a_1 - \bar{a}_4 a_2} \right] \qquad \text{(V-79)}$$

where

$$a_1 = 1/\eta_0 - \frac{b^2}{b^2+\pi^2}\Sigma_0 \qquad b = \frac{\bar{\beta}}{\bar{\tau}_c}\,,\ \Sigma_0 = \Sigma_T + \frac{1}{\gamma - \bar{\tau}_c}$$

$$a_2 = \frac{b\pi}{b^2+\pi^2}\Sigma_0 \qquad a_3 = \frac{b}{b^2+\pi^2}(\Sigma_p + \psi)$$

$$\bar{a}_2 = b a_3 + 1$$

$$\bar{a}_4 = \pi a_3 \qquad \text{(V-79a)}$$

A summary of the results of calculations of G and $\epsilon_{\tau p}$ for the typical case of H_2 + Air combustion is listed below. The calculated results correspond to $\bar{p}_c^*$ = 7.8 atm, $\bar{T}_i^*$ = 300°K, E* = 38 kcal/mole, $\hat{k}^*$ = 5 x 10^{14}, γ = 1.25, $\bar{T}_c$ = .80, η_0 = .288, $\psi = 0$ L_c^*/m = 80.

Φ	1.0	1.5	1.9	2.0	2.1	2.2	2.3	2.4	2.5	2.6	3.0	3.1	4.0
G	22.0	1.1	1.03	.75	.70	.65	.62	.59	.58	.69	.78	.92	1.0
$\epsilon_{\tau p}$	180	180	176	175	173	169	164	150	127	97	52	8	0

Table VI

The condition for positive coupling of the burning rate and the pressure oscillations will be seen to require that the real component of T_{c_1} be positive[1], that is, that $|\epsilon_{\tau p}| < \frac{\pi}{2}$. For this special case, the system is observed to be damped for $\Phi \leq 2.6$ ($\bar{\tau}_c \leq .75$).

[1] A necessary but not sufficient condition for unstable system operation.

With increasing Φ and $\bar{\tau}_c$, G rapidly approaches unity and $\epsilon_{\tau p}$ approaches 0. That is for the special case where the influence of volume oscillations is neglected in the calculation of the temperature-pressure coupling, conditions favoring positive driving ($\tau_1 \simeq \gamma_0 p_1$ and $\epsilon_{\tau p} \gtrsim 0$) are rapidly approached with increasing Φ (for $\bar{\tau}_c > 1$) due to the strong dependence of the mean combustion time on the combustion temperature.

Case 2: $\bar{V}_c = \bar{V}_c(t)$ The condition of unsteady overall combustion volume is consistent with the experimental schlieren observations discussed in Chapter IV. It is recalled that an oscillation in the axial extent of the burning zone was observed to accompany the appearance of small amplitude shock-type instability for the H_2 + Air system, $\Phi \simeq 2.6$. The shock wave passage was observed to follow the maximum in the volume oscillation by 1/3 to 1/2 the period. Significantly, the observed dimensionless fluctuation in the burning zone does not appear to be negligible compared to the dimensionless pressure oscillation. Scaling the axial dimension of the burning zone directly from Figures IV-31 and IV-32, a crude estimate of $|\bar{V}_{c_2}|_{max}/\bar{V}_c = \Theta(.25 \text{ to } .3)$ is obtained. The sustained dimensionless shock wave amplitude was measured as $\frac{\Delta p}{\bar{p}_c} \simeq .06$

Again, restricting attention to the near limit case of continuous harmonic oscillations, the perturbation quantities are written as

$$p_1^\circ = p_1 e^{i\pi t}$$
$$\tau_{c_1} = \tau_1 e^{i(\pi t - \epsilon_{\tau p})}$$
$$\bar{V}_{c_2} = \bar{V}_2 e^{i(\pi t - \epsilon_{vp})} \qquad \text{(V-80)}$$

$p_1, \tau_1, \bar{V}_2$ are defined as positive real amplitude factors and $\epsilon_{\tau p}$ and ϵ_{vp} are finite phase angles of the temperature and volume oscillations with respect to the pressure oscillations. p_1°, τ_{c_1}, and $\bar{V}_{c_2}$ are considered to be 2π periodic in the dimensionless time, t . Substitution of Equations V-80 into Equations V-64 and V-72 and integration of V-64 , gives

$$\frac{(\rho_c \bar{V}_c)_1}{\bar{m}} = \left[C_1 - C_2 \frac{b - i\pi}{b^2 + \pi^2}\right] \frac{e^{i(\pi t - \epsilon_{\tau p})}}{\tau_1} - C_3 \frac{b - i\pi}{b^2 + \pi^2} e^{i\pi t} p_1 \qquad \text{(V-81)}$$

$$\frac{(\rho_c \bar{V}_c)_1}{\bar{m}} = \bar{\gamma}_c \left[p_1 e^{i\pi t} - \frac{\tau_1}{\bar{\tau}_c} e^{i(\pi t - \epsilon_{\tau p})} + \frac{\bar{V}_{c_2}}{\bar{V}_c} e^{i(\pi t - \epsilon_{\tau p})} \right] \qquad \text{(V-82)}$$

where $C_1 = \frac{\bar{\gamma}_c}{\gamma - \bar{\gamma}_c}$, $\bar{\beta} = \frac{\gamma}{\gamma - \bar{\gamma}_c}(1 - \bar{\theta}_i)$, $\bar{\theta}_i = \frac{\bar{T}_i}{T_b}$

$$C_2 = +\bar{\beta}\left[\Sigma_T + \frac{1}{\gamma - \bar{\gamma}_c}\right] = \beta \Sigma_0$$

$$C_3 = +\bar{\beta}\left[\Sigma_p + \psi\right]$$

Eliminating $\frac{(\rho_c \bar{V}_c)_1}{\bar{m}}$ from Equations V-81 and V-82 and equating the real terms of the result and expression gives

$$\left[C_1 T_1 \cos\epsilon_{Tp} - \frac{C_2 T_1}{b^2+\pi^2}(b\cos\epsilon_{Tp} - \pi\sin\epsilon_{Tp}) - \frac{C_3 b p_1}{b^2+\pi^2}\right]\cos\pi t$$

$$+\left[C_1 T_1 \sin\epsilon_{Tp} - \frac{C_2 T_1}{b^2+\pi^2}(\pi\cos\epsilon_{Tp} + b\sin\epsilon_{Tp}) - \frac{C_3 \pi p_1}{b^2+\pi^2}\right]\sin\pi t$$

$$= \bar{\gamma}_c\left[p_1 - \frac{T_1}{\bar{T}_c}\cos\epsilon_{Tp} + \frac{V_2}{\bar{V}_c}\cos\epsilon_{Vp}\right]\cos\pi t$$

$$- \bar{\gamma}_c\left[\frac{T_1}{\bar{T}_c}\sin\epsilon_{Tp} - \frac{V_2}{\bar{V}_c}\sin\epsilon_{Vp}\right]\sin\pi t \qquad \text{(V-83)}$$

Equating the coefficients of $\cos\pi t$ and $\sin\pi t$ yields

$$C_1 T_1 \cos\epsilon_{Tp} - \frac{C_2 T_1}{b^2+\pi^2}(b\cos\epsilon_{Tp} - \pi\sin\epsilon_{Tp}) - \frac{C_3 b}{b^2+\pi^2} p_1 = \bar{\gamma}_c\left[p_1 - \frac{T_1}{\bar{T}_c}\cos\epsilon_{Tp} + \frac{V_2}{\bar{V}_c}\cos\epsilon_{Vp}\right] \qquad \text{(V-84)}$$

$$C_1 T_1 \sin\epsilon_{Tp} - \frac{C_2 T_1}{b^2+\pi^2}(\pi\cos\epsilon_{Tp} + b\sin\epsilon_{Tp}) - \frac{C_3 \pi}{b^2+\pi^2} p_1 = -\bar{\gamma}_c\left[\frac{T_1}{\bar{T}_c}\sin\epsilon_{Tp} - \frac{V_2}{\bar{V}_c}\sin\epsilon_{Vp}\right] \qquad \text{(V-85)}$$

It can be immediately seen that the combustion model implies that either or both ϵ_{Tp} and ϵ_{Vp} are non zero. For $\epsilon_{Tp} = \epsilon_{Vp} = 0$, equation V-85 gives,

$$\frac{T_1}{p_1} = -\frac{C_3}{C_2}$$

Both C_3 and C_2 are >0 and $\frac{T_1}{p_1} > 0$ by definition. Hence, $\epsilon_{Tp} = \epsilon_{Vp} = 0$ leads to a contradiction. The combustion model applies to the case where the oscillations in the averaged combustion zone temperature and/or the combustion zone volume are out of phase with the pressure oscillation.

Equations V-84 and V-85 are reformulated as

$$\bar{a}_1 T_1 - \bar{a}_2 p_1 = V_1 \cos \epsilon_{vp} \qquad \text{(V-86)}$$

$$\bar{a}_3 T_1 - \bar{a}_4 p_1 = V_1 \sin \epsilon_{vp} \qquad \text{(V-87)}$$

where

$$V_1 = V_2 / V_c$$

$$\bar{a}_1 = a_1 \cos \epsilon_{Tp} + a_2 \sin \epsilon_{Tp}$$

$$\bar{a}_3 = -a_2 \cos \epsilon_{Tp} + a_1 \sin \epsilon_{Tp}$$

and

$a_1, a_2, \bar{a}_2, \bar{a}_4$ are given in (V-79a)

Equations V-86 and V-87 are solved to obtain T_1/p_1 and ϵ_{Tp} in terms of the volume oscillation amplitude and phase angle. Dividing V-87 by V-86 gives

$$\frac{T_1}{p_1} = \frac{\bar{a}_4 - \bar{a}_2 \tan \epsilon_{vp}}{\bar{a}_3 - \bar{a}_1 \tan \epsilon_{vp}} \qquad \text{(V-88)}$$

Eliminating T_1 from V-86 and V-87 yields

$$\frac{V_1}{p_1} = \frac{\bar{a}_1 \bar{a}_4 - \bar{a}_2 \bar{a}_3}{\bar{a}_3 \cos \epsilon_{vp} - \bar{a}_1 \sin \epsilon_{vp}} \qquad \text{(V-89)}$$

An expression for ϵ_{Tp} is obtained from Equation V-89 as

$$\epsilon_{Tp} = \tan^{-1} \chi \qquad \text{(V-90)}$$

$$\chi = \frac{K_N}{K_D} = \frac{(\bar{a}_4 a_1 + \bar{a}_2 a_2) + \frac{V_1}{p_1}(a_2 \cos \epsilon_{vp} + a_1 \sin \epsilon_{vp})}{(\bar{a}_2 a_1 - \bar{a}_4 a_2) + \frac{V_1}{p_1}(a_1 \cos \epsilon_{vp} - a_2 \sin \epsilon_{vp})}$$

whence

$$\cos \epsilon_{Tp} = \frac{\chi_D}{(\chi_N^2 + \chi_D^2)^{1/2}}, \quad \sin \epsilon_{Tp} = \frac{\chi_N}{(\chi_N^2 + \chi_D^2)^{1/2}}$$

Substitution of these expressions for $\cos \epsilon_{Tp}$ and $\sin \epsilon_{Tp}$ into Equation V-88 yields a simplified relationship for T_1/p_1,

$$\frac{T_1}{p_1} = \eta = \frac{N}{D} \qquad \text{(V-91)}$$

$$N = \left[\left(\frac{V_1}{p_1} \right)^2 + 2 \left(\frac{V_1}{p_1} \right) \left(\bar{a}_4 \sin \epsilon_{vp} + \bar{a}_2 \cos \epsilon_{vp} \right) + \bar{a}_4^2 + \bar{a}_2^2 \right]^{\frac{1}{2}}$$

$$D = (a_1^2 + a_2^2)^{1/2}$$

Equations V-88 to V-91 are considered as generalized expressions for the amplitude and phase of the temperature oscillation in terms of the pressure oscillation with the amplitude and phase of the volume oscillation appearing as parameters. Equations V-90 and V-91 reduce to V-79, and V-78 obtained previously if V_1/P_1 is set equal to zero. As noted earlier, a precise experimental determination of V_1/P_1 and ϵ_{vp} as functions of Φ would suffice to allow a complete solution to the system. Alternatively, the temperature-pressure coupling and the system response can be evaluated in detail for several choices of V_1/P_1 and ϵ_{vp} .

Figures V-7 and V-8 summarize the results of calculations of the amplitude ratio, η, and phase angle, ϵ_{Tp}, for the case of oxidizer-rich H_2 + Air combustion ($\bar{P}_c^* = 7.8$ atm, $T_i^* = 300^\circ K$, $E^* = 38$ kcal/mole, $\hat{k}^* = 5\times10^{14}$, $\gamma = 1.25$, $\bar{T}_c = .80$, $\psi = 0$, $\eta_0 = .288$ $L_c^*/m = 80$). With respect to these results the following points are noted:

(i) For small values of the volume amplitude ratio ($V_1/P_1 = 0.1$) the calculated η and ϵ_{Tp} are in close agreement with values obtained earlier for $V_{c2} = 0$. ϵ_{vp} has only a minor influence. Favorable coupling ($|\epsilon_{Tp}| \leq \pi/2$) of the temperature and pressure oscillations occurs only for $\Phi \geq 2.7$ with η rapidly approaching η_0 and ϵ_{Tp} approaching zero as Φ and $\bar{\tau}_c$ increase.

(ii) The important influence of allowing $V_c(t)$ is clearly shown. For fixed Φ and $\bar{\tau}_c$, larger values of V_1/P_1 eventually lead to larger η and, for $\bar{\tau}_c \leq \Theta(4)$, to a regime of positive coupling for $\alpha_1(\bar{\tau}_c) < \epsilon_{vp} < \alpha_2(\bar{\tau}_c)$

(iii) For $V_1/P_1 = 5$, $\alpha_1 = \Theta(3\pi/4)$, $\alpha_2 = \Theta(3\pi/2)$ for $\Phi = 2.0$, $\bar{\tau}_c = .056$. α_1 and α_2 increase with increasing $\Phi, \bar{\tau}_c$. For $\Phi = 2.6$, $\bar{\tau}_c = .75$, $\alpha_1 = \Theta(\pi)$ $\alpha_2 = \Theta(7\pi/4)$.

(iv) For fixed V_1/P_1 and $\bar{\tau}_c \leq \Theta(4)$, η exhibits a weak dependence on Φ, $\bar{\tau}_c$, and ϵ_{vp} over the range (ϵ_{vp}) of positive coupling. Whereas $\bar{\tau}_c$ undergoes a systematic increase of several orders of magnitude as Φ increases from 2.0 to 3.0, $\eta = \Theta(.3 \text{ to } .6)$, for $V_1/P_1 = 5.0$.

(v) For $\bar{\tau}_c \gg 1$ large V_1/P_1 leads to values of $\eta > 1$ and a shift in the regime of positive coupling to $\alpha_1 = \Theta(7\pi/4)$, $\alpha_2 = \Theta(\pi/2)$.

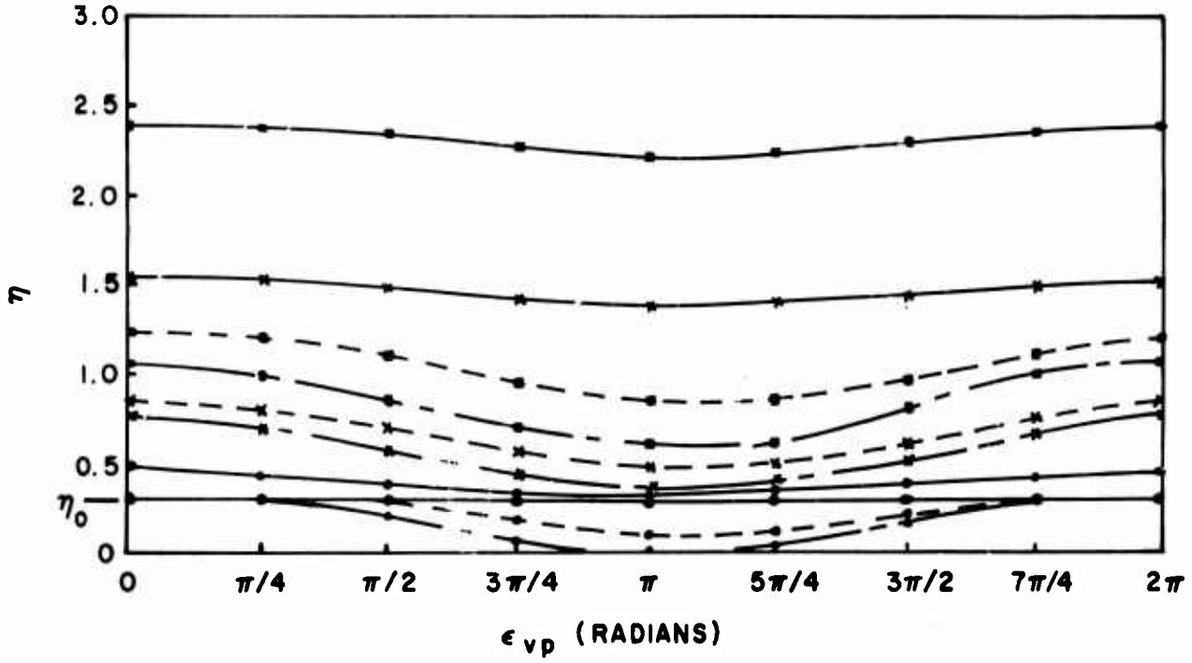

FIGURE V - 7: η vs. ϵ_{vp} WITH Φ AND V_1/p_1 AS PARAMETERS
H_2 + AIR, $\bar{T}_c = .8$

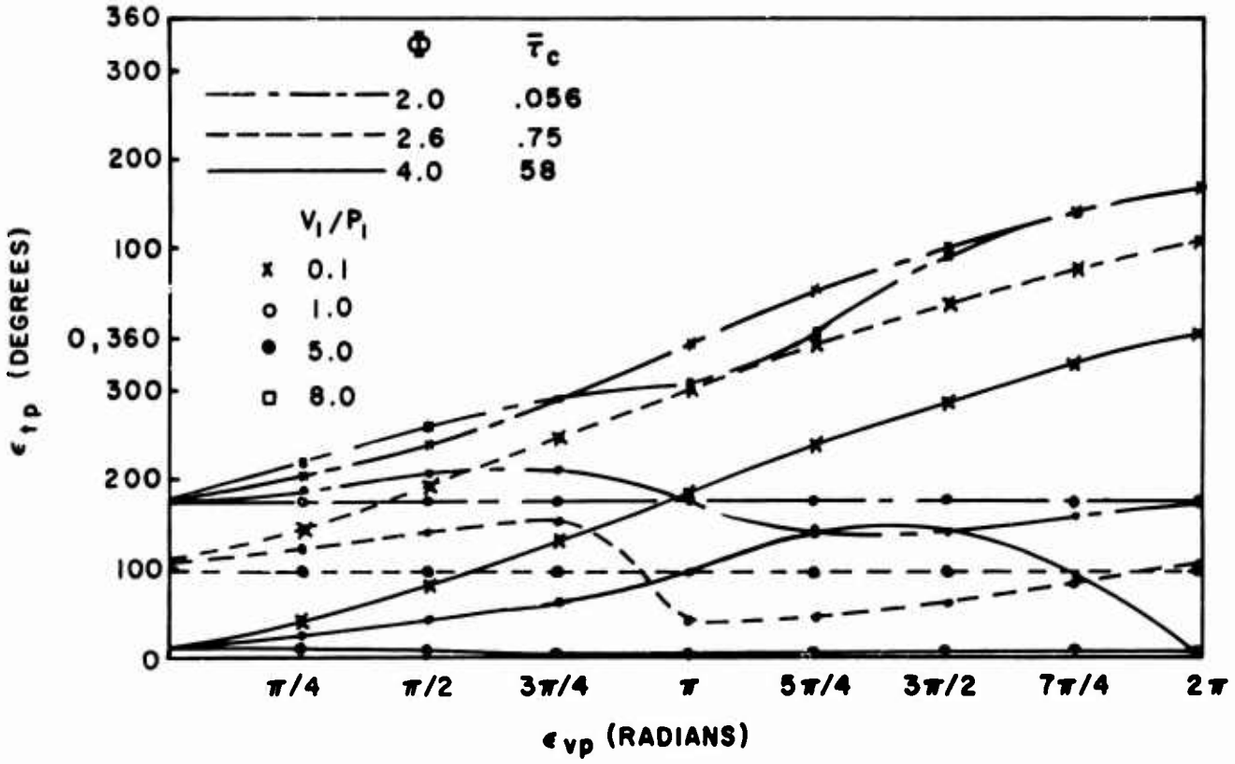

FIGURE V - 8: ϵ_{tp} vs. ϵ_{vp} WITH Φ AND V_1/P_1 AS PARAMETERS
H_2 + AIR, $\bar{T}_c = .8$

Therefore, for the physically realistic case in which the effect of the nonsteady combustion volume is accounted for, the linear system admits the possibility of positive coupling of the temperature and pressure oscillations. In general, for harmonic oscillations,

$$T_{c_1} = \eta e^{-i\epsilon_{\tau p}} p_1^\circ \qquad \text{(V-92)}$$

where both the amplitude ratio, η , and the phase angle, $\epsilon_{\tau p}$, are dependent upon the amplitude and phase of the volume oscillation. For the limiting case of negligible volume oscillation (or alternatively the case where the boundary condition is formulated according to Crocco's suggestion, see footnote page 240), $T_{c1} \sim - P_1^\circ$ at short $\bar{\tau}_c$ and $T_{c1} \simeq \eta_0 P_1^\circ$ ($\eta_0 = \frac{\gamma - \bar{\tau}_c}{\gamma} \bar{\tau}_c$) for $\bar{\tau}_c \geq 3$. For $\bar{\tau}_c$ = Θ(.5to 3), $\frac{\eta}{\eta_0} \simeq 1$ and $\epsilon_{\tau p}$ decreases rapidly from π to 0.

From the schlieren observations of the H_2 + Air combustion zone during sustained nonlinear oscillations, an estimate can be made of the volume oscillation amplitude ratio, V_1/P_1. From Figures IV-31,32 and page 242, $V_1/P_1 = \frac{V_{c_2}}{\bar{V}_c} \Big/ \frac{\Delta p}{\bar{p}_c} = \Theta(5 \text{ to } 10)$. The phase angle was estimated as $\pi \leq \epsilon_{vp} \leq \frac{5\pi}{3}$. Although certainly not conclusive evidence, the experimental results do offer direct support for the stated conclusions regarding the temperature-pressure coupling for Φ = 2.6, $V_1/P_1 = \Theta(5)$.

In order to calculate the overall system response for the H_2+Air and CH_4+Air systems, the weak dependence of η ($\frac{\eta}{\eta_0}$ = 1 to 2) on Φ, $\bar{\tau}_c$ and ϵ_{vp} for the regime of positive coupling is used to set $\eta = \eta_0$. In principle, calculation of the response for various parametric values of $\epsilon_{\tau p}$ could be carried out. At this point $\epsilon_{\tau p}$ is retained in the coupling expression. For the analysis of the linear system response, the influence of finite $\epsilon_{\tau p}$ is noted. Results of detailed calculations of the linear and nonlinear system response for a particular choice of $\epsilon_{\tau p}$, namely $\epsilon_{\tau p}$ sufficiently small such that $\cos\epsilon_{\tau p} \simeq 1$ and $\sin\epsilon_{\tau p} \simeq 0$ (within the regime of positive coupling) are presented.

Using Equation V-92 to replace T_{c1} in Equation V-67, the expression for the perturbation in the mass efflux from the combustion zone becomes

$$\frac{\dot{m}_b^\circ - \bar{\dot{m}}}{\bar{\dot{m}}} = \bar{\beta}(1-\bar{\tau}_c)\left[\left(\Sigma_\tau + \frac{1}{\gamma - \bar{\tau}_c}\right)\eta e^{-i\epsilon_{\tau p}} + \Sigma_p\right] p_1^\circ + \bar{\tau}_c \frac{\gamma - 1}{\gamma - \bar{\tau}_c} \eta e^{-i\epsilon_{\tau p}} \frac{dp_1^\circ}{dt}$$
$$- \Psi\left[1 - \bar{\beta}(1-\bar{\tau}_c)\right] p_1^\circ$$
$$- \frac{\bar{\beta}^2}{\bar{\tau}_c^2}(1-\bar{\tau}_c)\left[\left(\Sigma_\tau + \frac{1}{\gamma - \bar{\tau}_c}\right)\eta e^{-i\epsilon_{\tau p}} + (\Sigma_p + \Psi)\right] \int_{-\infty}^{t} p_1^\circ(t') e^{-\frac{\bar{\beta}}{\bar{\tau}_c}(t-t')} dt' \qquad \text{(V-93)}$$

which is substituted into Equation V-70 to obtain $\frac{u_2^\circ}{M^2(\gamma+1)}$ which is used in Equation V-69 to obtain a single nonlinear ordinary integro-differential equation governing the form of the wave amplitude parameter, f,

$$\left(f - k + C\bar{\tau}_c\right)\frac{df}{d\theta} = Af + B\bar{\tau}_c^{-1}\int_{-\infty}^{\theta} f(t')\, e^{-\frac{\bar{\beta}}{\bar{\tau}_c}(\theta - t')}\, dt' \qquad \text{(V-94)}$$

where

$$A = \frac{3\gamma - 1}{\gamma + 1} - \frac{2\gamma}{\gamma+1}\cdot\bar{\beta}(1-\bar{\tau}_c)\left[\left(\Sigma_\tau + \frac{1}{\gamma - \bar{\tau}_c}\right)\eta e^{-i\epsilon_{\tau p}} + \Sigma_p\right] + \frac{2\gamma}{\gamma+1}\left[1 - \bar{\beta}(1-\bar{\tau}_c)\right]\psi$$

$$B = \frac{2\gamma}{\gamma+1}\,\bar{\beta}^2(1-\bar{\tau}_c)\left[\left(\Sigma_\tau + \frac{1}{\gamma-\bar{\tau}_c}\right)\eta e^{-i\epsilon_{\tau p}} + \Sigma_p + \psi\right]$$

$$C = \frac{2\gamma}{\gamma+1}\,\frac{\gamma-1}{\gamma-\bar{\tau}_c}\,\eta\, e^{-i\epsilon_{\tau p}}$$

Similar equations have been obtained by Mitchell (34) and Sirignano (81) governing the wave amplitude parameter in theoretical studies of nonsteady burning in liquid and solid propellant rockets with concentrated combustion. As shown by Mitchell, Equation V-94 can be simultaneously solved for the linear stability characteristics (stability limits) as well as the nonlinear stability characteristics (finite wave amplitude and waveform) of the system.

F.3 Linearized Analysis of Equation V-94

Considering η and $\epsilon_{\tau p}$ as fixed parameters, the time dependent variables in Equation V-94 are f and k. The equation can be linearized by considering f and k as power series expansions in a small amplitude parameter ϵ. That is, for

$$f = \epsilon f_1 + \epsilon^2 f_2 + \cdots$$

$$k = k_0 + \epsilon k_1 + \cdots$$

Equation V- becomes

$$\left[-k_0 + C\bar{\tau}_c\right]\frac{df_1}{d\theta} = Af_1 + B\bar{\tau}_c^{-1}\int_{-\infty}^{\theta} f_1(t')\, e^{-\frac{\bar{\beta}}{\bar{\tau}_c}(\theta - t')}\, dt' \qquad \text{(V-95)}$$

For continuous linear waves, 2π periodic in θ, $f_1 = e^{\lambda + i\pi\theta} = \bar{f}_1 e^{i\pi\theta}$ and $\lambda = 0$, $\bar{f}_1 = 1$ describes stability boundary. Making this substitution for f_1 in Equation V-95 an equation valid at the stability

limit is obtained as

$$i\pi\left(-k_o - C\bar{\tau}_c\right) = A + \frac{B\bar{\tau}_c^{-1}}{\left(\bar{\beta}/\bar{\tau}_c\right)^2+\pi^2}\left(\frac{\bar{\beta}}{\bar{\tau}_c} - i\pi\right) \qquad \text{(V-96)}$$

where, in general A and B are complex through the appearance of the factor $e^{-i\epsilon_{\tau p}} = \cos\epsilon_{\tau p} - i\sin\epsilon_{\tau p}$. A and B are written as

$$A = A_r + iA_i$$

$$A_r = \frac{3\gamma-1}{\gamma+1} - \frac{2\gamma}{\gamma+1}\bar{\beta}(1-\bar{\tau}_c)\left[\left(\Sigma_\tau + \frac{1}{\gamma-\bar{\tau}_c}\right)\eta\cos\epsilon_{\tau p} + \Sigma_p\right] + \frac{2\gamma}{\gamma+1}\left[1-\bar{\beta}(1-\bar{\tau}_c)\right]\psi$$

$$A_i = +\frac{2\gamma}{\gamma+1}\bar{\beta}(1-\bar{\tau}_c)\left(\Sigma_\tau + \frac{1}{\gamma-\bar{\tau}_c}\right)\sin\epsilon_{\tau p}$$

$$B = B_r + iB_i$$

$$B_r = \frac{2\gamma}{\gamma+1}\bar{\beta}^2(1-\bar{\tau}_c)\left[\left(\Sigma_\tau + \frac{1}{\gamma-\bar{\tau}_c}\right)\eta\cos\epsilon_{\tau p} + \Sigma_p + \psi\right]$$

$$B_i = -\frac{2\gamma}{\gamma+1}\bar{\beta}^2(1-\bar{\tau}_c)\left[\left(\Sigma_\tau + \frac{1}{\gamma-\bar{\tau}_c}\right)\eta\sin\epsilon_{\tau p}\right]$$

Substituting for A and B in Equation V-96 and equating real and imaginary terms, two equations valid at the stability limit are obtained

$$A_r + \frac{\bar{\tau}_c^{-1}}{\left(\bar{\beta}/\bar{\tau}_c\right)^2+\pi^2}\left[B_r\frac{\bar{\beta}}{\bar{\tau}_c} + B_i\pi\right] = 0 \qquad \text{(V-97)}$$

$$k_o = \frac{\bar{\tau}_c^{-1}}{\left(\bar{\beta}/\bar{\tau}_c\right)^2+\pi^2}\left[B_r - B_i\frac{\bar{\beta}}{\pi\bar{\tau}_c}\right] - \frac{A_i}{\pi} + \bar{\tau}_c C \qquad \text{(V-98)}$$

In terms of the Mitchell-Crocco analysis, T_1 is the first order correction on the period of oscillation T defined by

$$T = T_o + M T_1 \quad , \quad T_o = 2$$

$$T_1 = -k$$

$$T_1 = -\bar{\tau}_c C - \frac{\bar{\tau}_c}{\left(\bar{\beta}/\bar{\tau}_c\right)^2+\pi^2}\left[B_r - B_i\frac{\bar{\beta}}{\pi\bar{\tau}_c}\right] + \frac{A_i}{\pi} \qquad \text{(V-99)}$$

The linear stability limit is defined in terms of the important system (steady state) parameters by Equation V-97. Substituting for A_r, A_i, B_r, B_i, and $\bar{\beta}$, the stability limit condition can be written as,

$$(1-\bar{T}_i)\left\{\left[\left(\Sigma_T+\frac{1}{\gamma-\bar{T}_c}\right)\eta\left(\cos\epsilon_{Tp}+\frac{\bar{\beta}}{\pi\bar{T}_c}\sin\epsilon_{Tp}\right)+\Sigma_p\right\}\right.$$

$$=\frac{\gamma-\bar{T}_c}{\gamma(1-\bar{T}_c)}\left[\frac{3\gamma-1}{2\gamma}+\psi\right]\left[1+\left(\frac{\bar{\beta}}{\pi\bar{T}_c}\right)^2\right]-(1-\bar{T}_i)\psi \qquad \text{(V-100)}$$

Setting L = left-hand side of Equation V-100

R = right-hand side of Equation V-100

the stability condition is

L > R unstable

L = R limit

L < R stable

Σ_T and Σ_p are defined for the second order overall rate law, oxidizer-rich initial mixture by Equations V-60 with the condition that $1/\Phi$ replaces Φ for fuel rich combustion. Substitution for Σ_T and Σ_p gives the limit condition as

$$(1-\bar{\theta}_i)\left\{\left[\frac{H}{\bar{T}_c^2}-\frac{1}{\bar{T}_c}-\frac{1}{1-\bar{\theta}_i}\left(\frac{1}{\Phi-\gamma}+\frac{1}{1-\gamma}\right)+\frac{1}{\gamma-\bar{T}_c}\right]\eta\left(\cos\epsilon_{Tp}+\frac{\bar{\beta}}{\pi\bar{T}_c}\sin\epsilon_{Tp}\right)+1\right\}$$

$$=\frac{\gamma-\bar{T}_c}{\gamma(1-\bar{T}_c)}\left(\frac{3\gamma-1}{2\gamma}+\psi\right)\left\{1+\left[\frac{\gamma(1-\bar{\theta}_i)}{\gamma-\bar{T}_c}\right]^2\frac{1}{(\pi\bar{T}_c)^2}\right\}-(1-\bar{\theta}_i)\psi \qquad \text{(V-101)}$$

where

$$H=\frac{E^*}{\bar{R}^*\bar{T}_b^*}\quad,\quad \bar{\theta}_i=\bar{T}_i=\frac{T_i^*}{T_b^*}$$

The influence of the various steady state combustion parameters on the system stability are clearly shown in Equation V-101. In particular it is apparent that regardless of the amplitude ratio (η) and the phase angle (ϵ_{Tp}) of the temperature oscillation nonsteady burning is precluded for the case where $\bar{T}_c$ is sufficiently small ($1/\bar{T}_c^2$ sufficiently large) such that R > L. This condition is in fact realized for the H_2 + Air system (see Appendix D) as Φ approaches unity and stable combustion at and around the stoichiometric mixture ratio is predicted.

It has been noted earlier that under conditions of favorable coupling, $\eta = \Theta(\eta_0)$ independent of ϵ_{Tp} In any case the calculated stability limits are quite insensitive to moderate changes in η as long as $\eta = \Theta(\eta_0)$. The influence of finite ϵ_{Tp} on the predicted

linear stability characteristics is readily seen from Equation V-101. Depending upon the relative magnitudes and signs of $\cos \epsilon_{\tau p}$ and $\frac{\bar{\beta}}{\pi \bar{\tau}_c} \sin \epsilon_{\tau p}$ finite $\epsilon_{\tau p}$ can produce a significant damping for $\bar{\tau}_c \simeq \Theta(1)$. For example, as $\epsilon_{\tau p} \to \frac{\pi}{2}$ the sine term becomes important relative to the cosine term and, as $\bar{\tau}_c$ becomes large, a significant decrease in L occurs.

In light of the discussion (pages 242 to 247) of the temperature-pressure coupling and the comparison with the schlieren observations it is considered relevant to examine the theoretically predicted stability limit conditions for the $H_2/O_2/N_2$ and CH_4/Air systems for the particular case where η is set equal to η_0 and $\epsilon_{\tau p}$ is considered sufficiently small such that $\cos \epsilon_{\tau p} \simeq 1$, $\sin \epsilon_{\tau p} \simeq \epsilon_{\tau p} \simeq 0$. Note that for small $\bar{\tau}_c$, $\frac{\epsilon_{\tau p}}{\bar{\tau}_c} > 1$ may be realized. Neglecting this term essentially removes an additional destabilizing factor at small $\bar{\tau}_c$. However for small $\bar{\tau}_c$ the $1/\bar{\tau}_c^2$ dependence of R dominates and the results are unchanged. For $\bar{\tau}_c = \Theta(1)$, $\frac{\bar{\beta}}{\pi \bar{\tau}_c} \epsilon_{\tau p} = \Theta(.7) \epsilon_{\tau p} \ll 1$, for $\gamma = 1.25$, $\bar{T}_c = .8$. It is also noted that for $\epsilon_{\tau p} = 0$ the linearized results can be compared to results for the full nonlinear system governed by Equation V-94.

From Equation V-99 for the case of small $\epsilon_{\tau p}$ the first order correction to the period of oscillation is simply,

$$\pi_1 = -\bar{\tau}_c \left[C + \frac{B_r}{\bar{\beta}^2 + \pi^2 \bar{\tau}_c^2} \right]$$

Since the bracketed terms are positive, at the limit the period of oscillation is predicted to be less than the acoustic period.

The influence of the following parameters on the theoretically predicted stability limit conditions for the above conditions has been examined: Φ, δ (% DILUTION), $\bar{\theta}_i$, $\bar{\rho}_c$, E, $\hat{k}$, $\bar{T}_c$, L_c, m, Ψ, η

The IBM 360-91 computer facility was utilized to perform the computations. In view of the important dependence of many of the steady-state variables on the equivalence ratio and $\bar{\theta}_i$, Appendix D summarizes the numerical data appropriate to the calculations. Recall that

$$1/\bar{\tau}_c = (L_c^*/m \bar{c}_b^*) \cdot 1/\bar{\tau}_c^*$$

Figures V-9 to V-16 summarize the principal theoretical results of the linearized analysis for $\epsilon_{\tau p} = 0$ for:

H_2 + Air

$\bar{P}_c^*$ = 7.8 atm

$\bar{T}^*$ = 300°K

E^* = 38 kcal/mole

$\hat{k}^*$ = 5×10^{14}

$\bar{T}_c$ = 0.80

γ = 1.25

η_o = 0.288

In Figure V-9 the terms L and R in Equation V-101 are plotted as a function of $\bar{\Phi}$, with L_c^*/m (in centimeters) as a parameter (stars indicating dimensional quantities are deleted in the figures). Solutions to the equation, that is the limit conditions ($\bar{\Phi}_{lim}$) are denoted by the curve intersections, with the unstable regime located at $R \leq L$. Characteristically the L curve has a minimum at $\bar{\Phi} = 1$ and increases monotonically away from $\bar{\Phi} = 1$ due to the decrease of the combustion temperature and the influence of the Arrhenius factor The influence of η is noted. For stronger temperature response the L curve is shifted to larger values and essentially unchanged in shape. The R curves are principally influenced by the ratio of the wave travel time to the combustion time , $1/\bar{\tau}_c$. Primarily due to the dependence of $1/\bar{\tau}_c$ on the combustion temperature, R attains a maximum at $\bar{\Phi} = 1$ where $\bar{\tau}_c$ is small and monotonically decreases away from $\bar{\Phi} = 1$. The steepness of the decay of the R curves for off-stoichiometric mixtures is due to the exponential dependence of $1/\bar{\tau}_c$ on the combustion temperature. The order of magnitude of R at a given $\bar{\Phi}$ is of course influenced by the kinetic constants k and E which appear in the burning rate law. Schematically the influence of these parameters is shown in Figure V-10 .

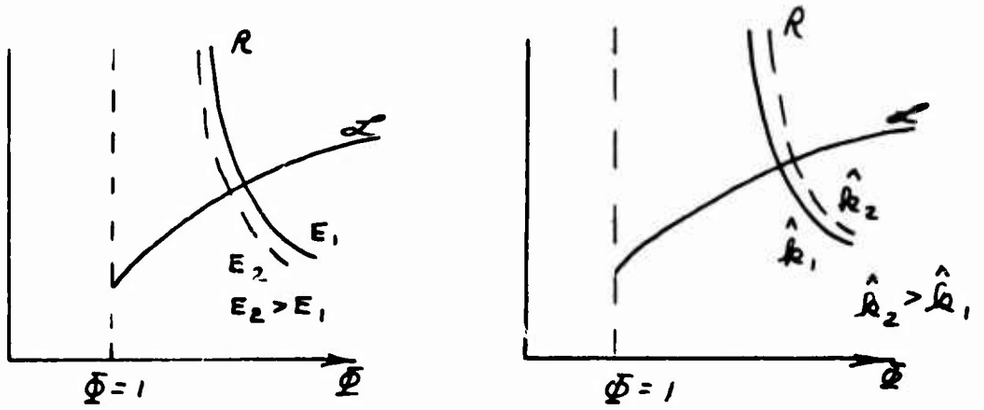

Figure V-9

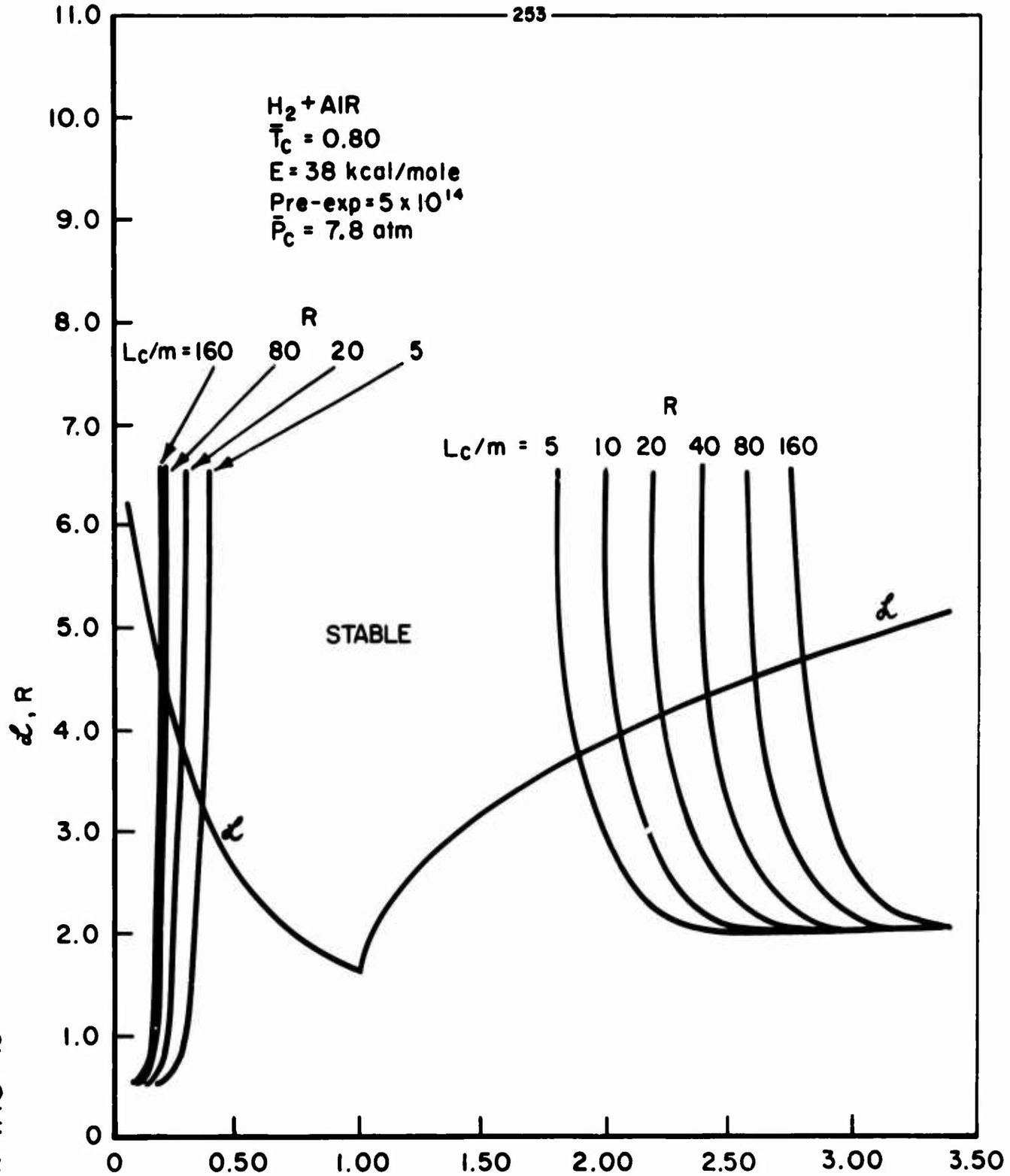

JP 13 R 4176 70

THEORETICAL STABILITY CHARACTERISTICS
SOLUTIONS TO LINEARIZED EQUATION
FOR STABILITY LIMIT

FIGURE V-10

The important point to note is that the numerical values chosen for k and E are based on the overall kinetics data obtained in an environment resembling the gas rocket combustion zone. The use of turbulent flow reactor data to compute k and E has been discussed. The data used in this analysis satisfy the condition $\int_0^{V_c} \dot{q}\, dV_c / \dot{m}_{f_i} \cdot q \simeq 1$ [1] That is, the integrated heat release rate over the combustion zone for the particular choice of k and E is consistent with the total heat release rate based on fuel mass flow rate. Finally it is noted that an order of magnitude change in the pre-exponential factor, k, produces only a modest shift in the value of R for a particular O.

In Figure V-11 the ratio of $\bar{\tau}_c^*$ to $\tau_{per}^* = 2 \cdot \tau_{wave}^*$ is plotted as a function of Φ for L_c^*/m as a parameter. $\tau_{per}^* = \tau_{per}^*(\Phi, L_c^*/m)$ and $\bar{\tau}_c^*$ are calculated in Appendix D. The ratios of $\bar{\tau}_c^*/\tau_{per}^*$ corresponding to the stability limits as determined in Figure V-9 are noted. Three observations with regard to the data of Figures V-9 and V-11 are made: First, the steepness of the R curves at the stability limit due to the extreme sensitivity of the burning rate ($\sim 1/\bar{\tau}_c$) to the combustion temperature is suggestive of the experimentally observed strong sensitivity of the onset of nonsteady burning to slight changes in the mixture strength near the stability limit. For the H_2 + Air system a condition of stable combustion with constant propellant flow rates and mean $\bar{P}_c^*$ can be established with Φ just below the oxidizer rich limit. A small increase in the air mass flow rate sufficient to change Φ by 0.05 produces an abrupt appearance of sustained shock-type instability which can in turn be suppressed by a small increase in the H_2 flow rate. Second, the influence of larger values of η on the value of $(\tau_c^*/\tau_{per}^*)_{lim}$ is relatively small. This result is somewhat reassuring in view of the uncertainty in η. An order of magnitude increase in η would produce a relatively small shift in the limit conditions and no change in the qualitative nature of the results. On the other hand, precludes nonsteady burning while small would allow nonsteady burning only for $(\tau_c^*/\tau_{per}^*) \geq O(1)$. Third, the predicted important influence of (τ_c^*/τ_{per}) on the limit conditions and the indication that $(\tau_c^*/\tau_{per}^*)_{lim} = O(.2 \text{ to } .3)$ suggested the investigation

[1] See discussion page 216 .

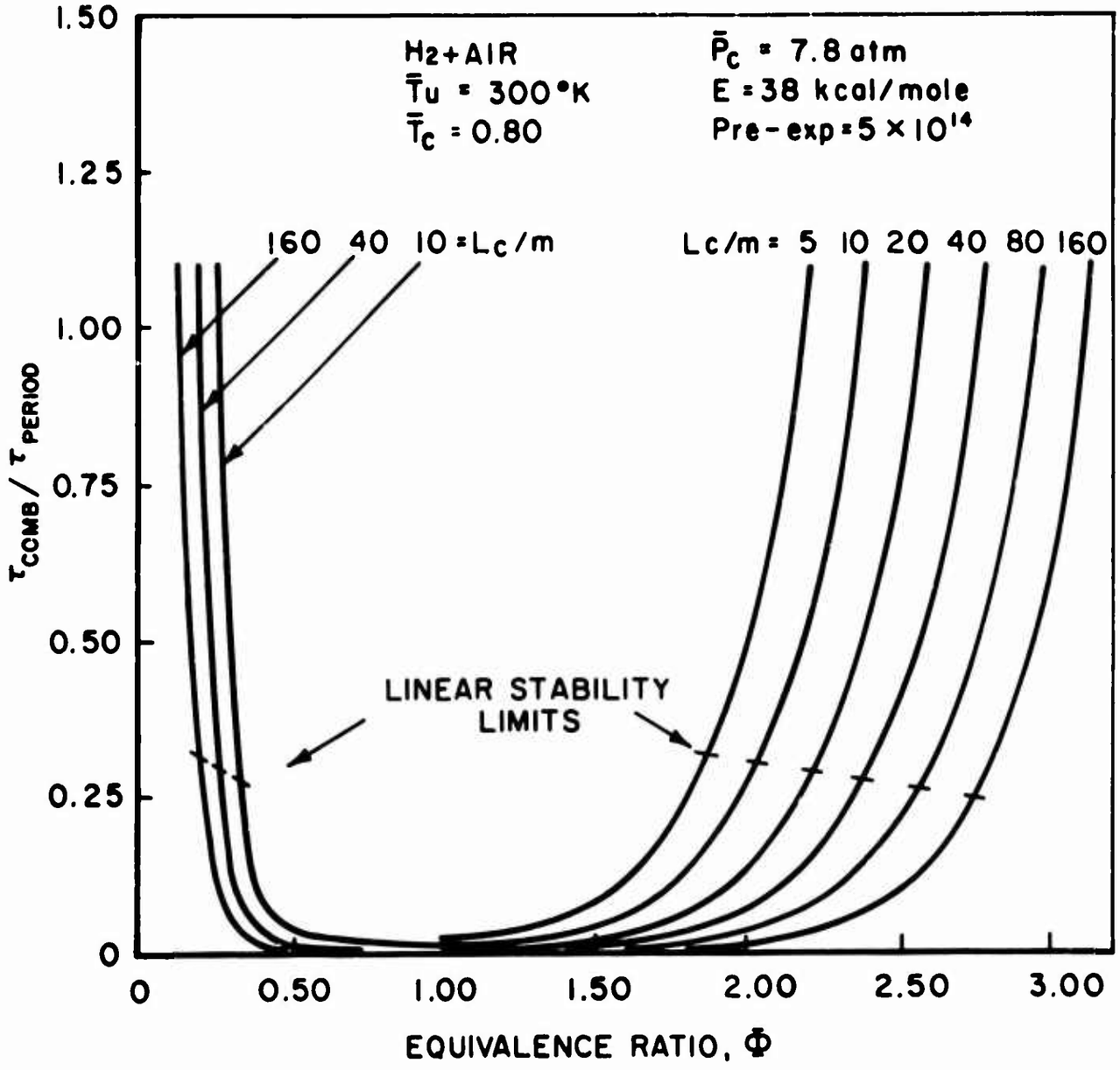

RATIO OF CHARACTERISTIC COMBUSTION TIME TO PERIOD OF OSCILLATION (2×τ WAVE)

FIGURE V-11

summarized in Appendix C of the influence of the alternative heuristic expression for γ_{c_1} on the predicted stability characteristics of the system. In the present case a factor of 2 increase in η would lead to $(\gamma_c^*/\gamma_{p\bar{n}}^*)_{lim} = \Theta(.1 \text{ to } .15)$. In view of the simplifications already included in the model the results for the present case where $\gamma_{c_1} \sim -\Sigma \bar{r}_c \rho_i^b$ are considered to provide a valid approximation of the lower[1] stability limit conditions. The analysis in Appendix C supports this conclusion. The interesting result of that analysis is that with further increase of $\bar{\Omega}$ beyond the lower linear limit a strong damping influence is encountered as $(\gamma_c^*/\gamma_{wave}^*)$ approaches unity. Due to these additional damping factors the R curves are observed to undergo minimums in the regime of nonsteady combustion with a second upper stability limit predicted. That is for the case where the instantaneous burning rate is determined by the integrated effect (see Appendix C) of the nonsteady pressure and temperature over the total combustion time, as $(\gamma_c^*/\gamma_{p\bar{n}}^*) \to 1$ the behavior of the R curves is as shown in Figure V-12 .

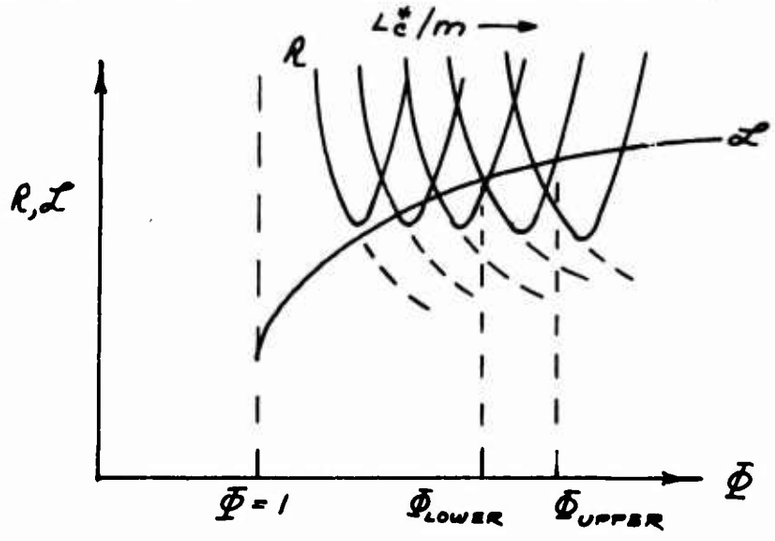

Figure V-12

As will be pointed out in the discussion of the theoretically predicted nonlinear stability characteristics, the present formulation for small ϵ_{TP} correctly predicts (qualitatively and quantitatively) all of the nonsteady burning characteristics observed in

[1]The lower stability limit refers to $\bar{\Omega}_{lim}$ closest to $\bar{\Omega} = 1$ for both fuel rich and fuel lean mixtures.

the H_2 and CH_4 systems with the single exception of the "upper stability limit".

As noted on page 251 a strong stabilizing influence at higher $\bar{\gamma}_c$ is experienced for finite values of the phase angle of the temperature oscillation with respect to p_1^o . For larger values of $\epsilon_{\tau p}$, the second term in $\mathcal{L} \sim \frac{1}{\bar{\gamma}_c} \sin \epsilon_{\tau p}$ becomes important. A family of L curves corresponding to different values of L_c^*/m must be considered. As $\bar{\gamma}_c$ increases with increasing Φ the behavior of the L and R curves is as shown in Figure V-13 .

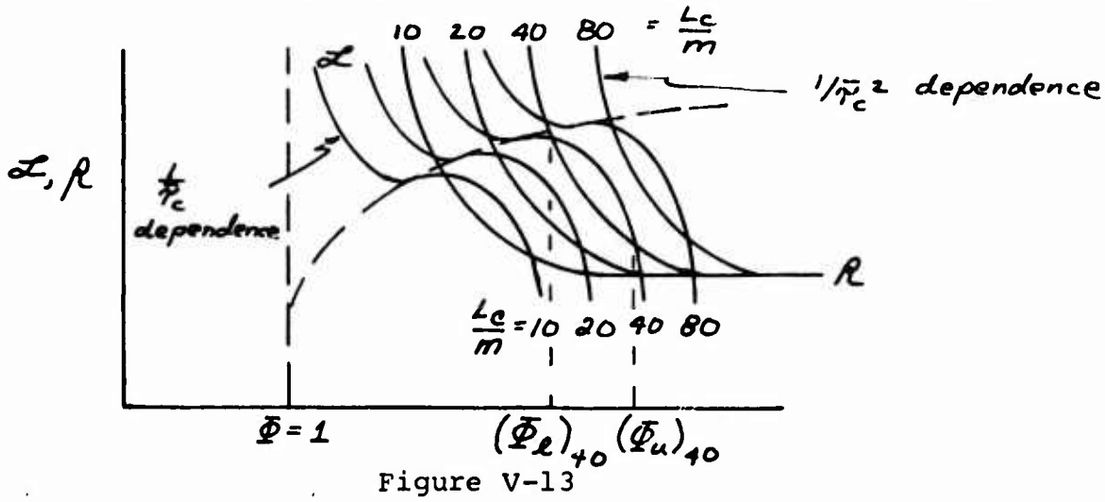

Figure V-13

Therefore, qualitatively the predicted stability characteristics for the case of finite $\epsilon_{\tau p}$ $(\leq \frac{\pi}{2})$ are seen to be in complete agreement with the experimental observations. Nonsteady burning is predicted to occur for the H_2 + Air system at off-stoichiometric mixture ratios. Harmonic mode oscillations are predicted to occur for $\Phi_\ell \leq \Phi \leq \Phi_u$ or alternatively for $\gamma_\ell \leq \gamma \leq \gamma_u$ with higher mode regimes located closer to the stoichiometric ratio. In general some overlap between regions of harmonic mode oscillations is predicted. In the absence of such stabilizing factors, the linear analysis for small $\epsilon_{\tau p}$ is really insufficient to determine which mode is supported in the regime between (for example) the fundamental mode limit and the second harmonic mode limit - the regime designated in Figure V-14 by "second harmonic". With no limitation on $\gamma_a^*/\gamma_{p_{en}}^*$ this region is accessible to 2nd, 3rd, etc. harmonic mode oscillation.

[1] This behavior is essentially identical to that shown in Figure V-12. In V-13 the additional stabilizing factor (at large $\bar{\gamma}_c$) is retained in the L terms.

The stability limit data of Figure V-9 is plotted in Figure V-14 in the conventional Φ - L_c^* plane to allow comparison with the experimental results of Bowman (Figure II-9) and Schob in Figure V-15 below[1].

The theoretically predicted lower stability limits show excellent agreement with the experimental data. Considering the oxidizer rich characteristics it is observed that the theoretical model correctly predicts:

(a) The progression to lower harmonic mode order for fixed L_c^* and increasing Φ. In principle an infinite series of harmonic mode limits is predicted for $m = 1,2,3,4,\ldots$ each falling closer to $\Phi = 1$. $m \to \infty$ is equivalent to $1/\tau_c \to \infty$. In practice (Figure II-9) the higher harmonic modes are damped at lower L_c and lower Φ.

(b) The progression toward higher harmonic modes at fixed Φ and increasing L_c.

(c) The collapse of the stability limits toward $\Phi = 1$ as L_c^* is decreased. The slow approach of the limits toward $\Phi = 1$ observed by Bowman is predicted as well as the rapid decrease of Φ_{lim} for $L_c^* < 20$ cm observed by Schob.

The curve corresponding to $\tau_c / \tau_{pos} = 1$ for the fundamental mode oscillation is shown.

Figure V-16 indicates that a slight difference in the adiabatic combustion temperature at the fuel rich and fuel lean stability limits is to be expected due to the difference between the burned gas sound speed for fuel rich and fuel lean systems at the same combustion temperature (see Figures D-2 and D-3). This is precisely the behavior observed by Pelmas (29) with the H_2 + Air system.

Figure V-17 shows the systematic shift of the predicted stability limits towards $\Phi = 1$ with increasing dilution[2] of the H_2 + Air system. It has already been noted that a similar stability limit shift has been observed experimentally by Bowman (Figure II-9). The important influence of the increased dilution at each Φ in depressing the mean combustion temperature is responsible for the predicted behavior. With increasing dilution the L curve is shifted upward due to the increase of the Arrhenius factor. However,

---

[1] Bowman did not extend his experimental measurements to $L_c^* < 10$ inches. Schob's data is shown to illustrate the experimentally observed short length stability characteristics of the H_2 + Air system

[2] Percent dilution of air mixture as defined page 98 .

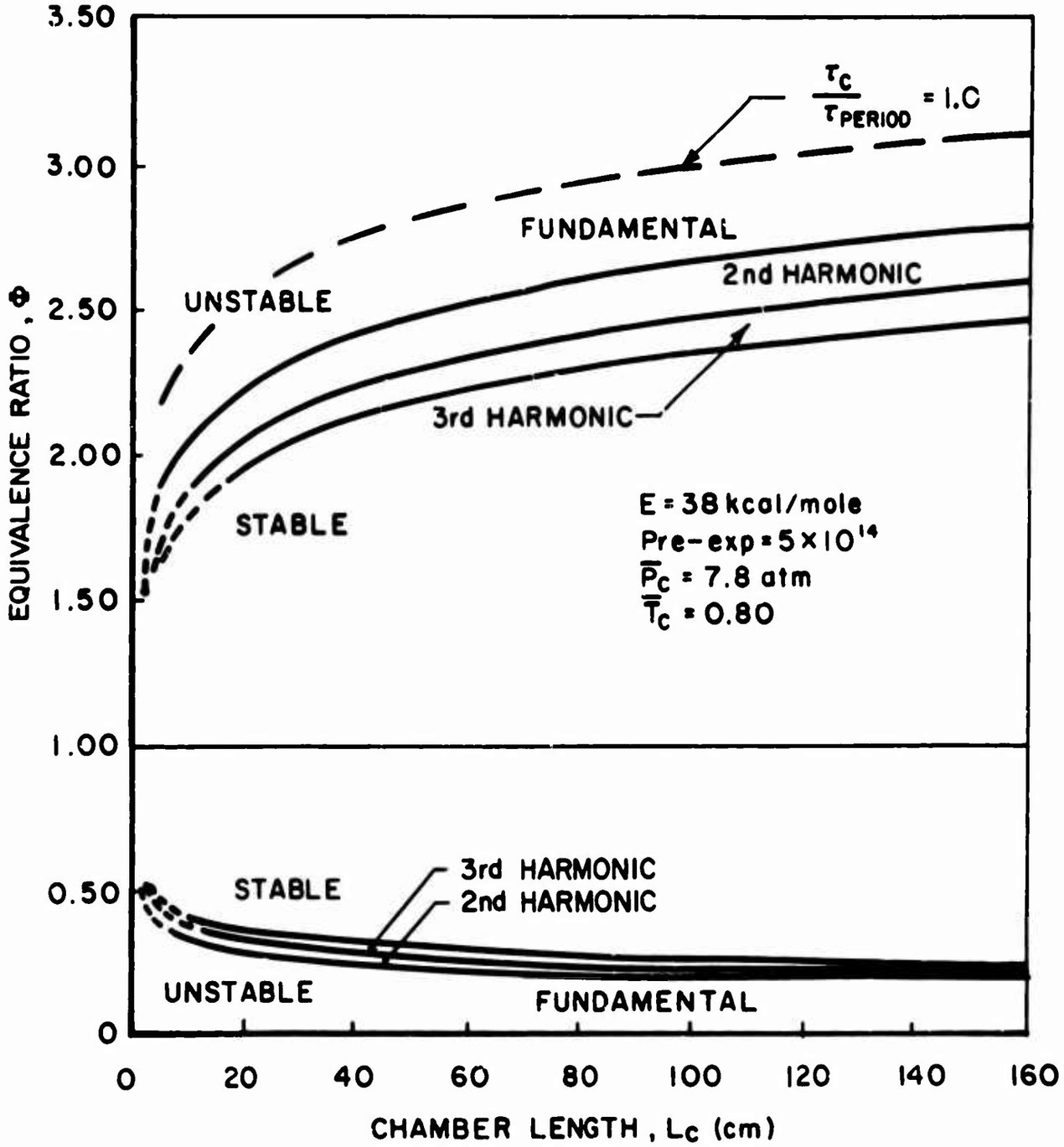

THEORETICALLY PREDICTED LINEAR STABILITY LIMITS FOR H_2 + AIR IN $\Phi - L_C$ PLANE

FIGURE V - 14

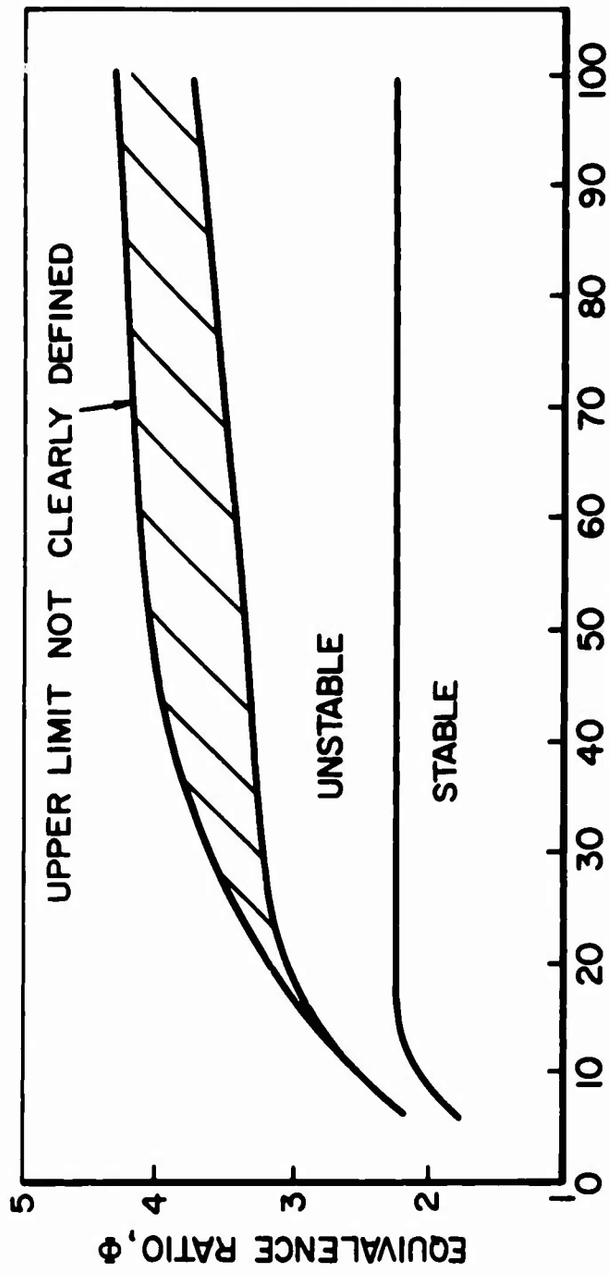

EXPERIMENTALLY OBSERVED REGIME OF UNSTABLE COMBUSTION FOR H_2 + AIR, P_c = 4.4 atm, 6 PORT DOUBLE TRIPLET INJECTOR

(SCHOB, W., MSE THESIS, PRINCETON UNIV, 1963)

FIGURE V - 15

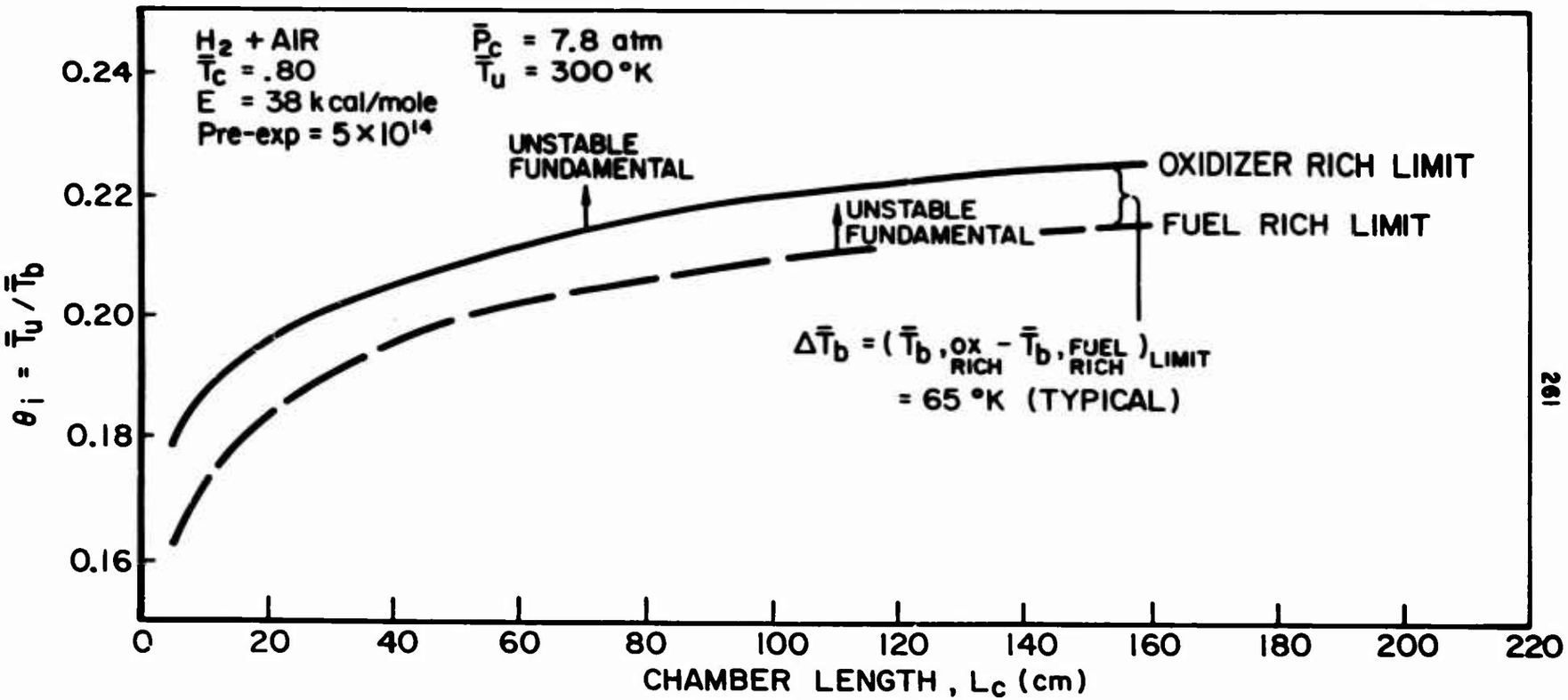

FIGURE IV-16

THEORETICALLY PREDICTED LINEAR STABILITY LIMIT FOR FUNDAMENTAL MODE OSCILLATIONS IN $\theta_i - L_c$ PLANE

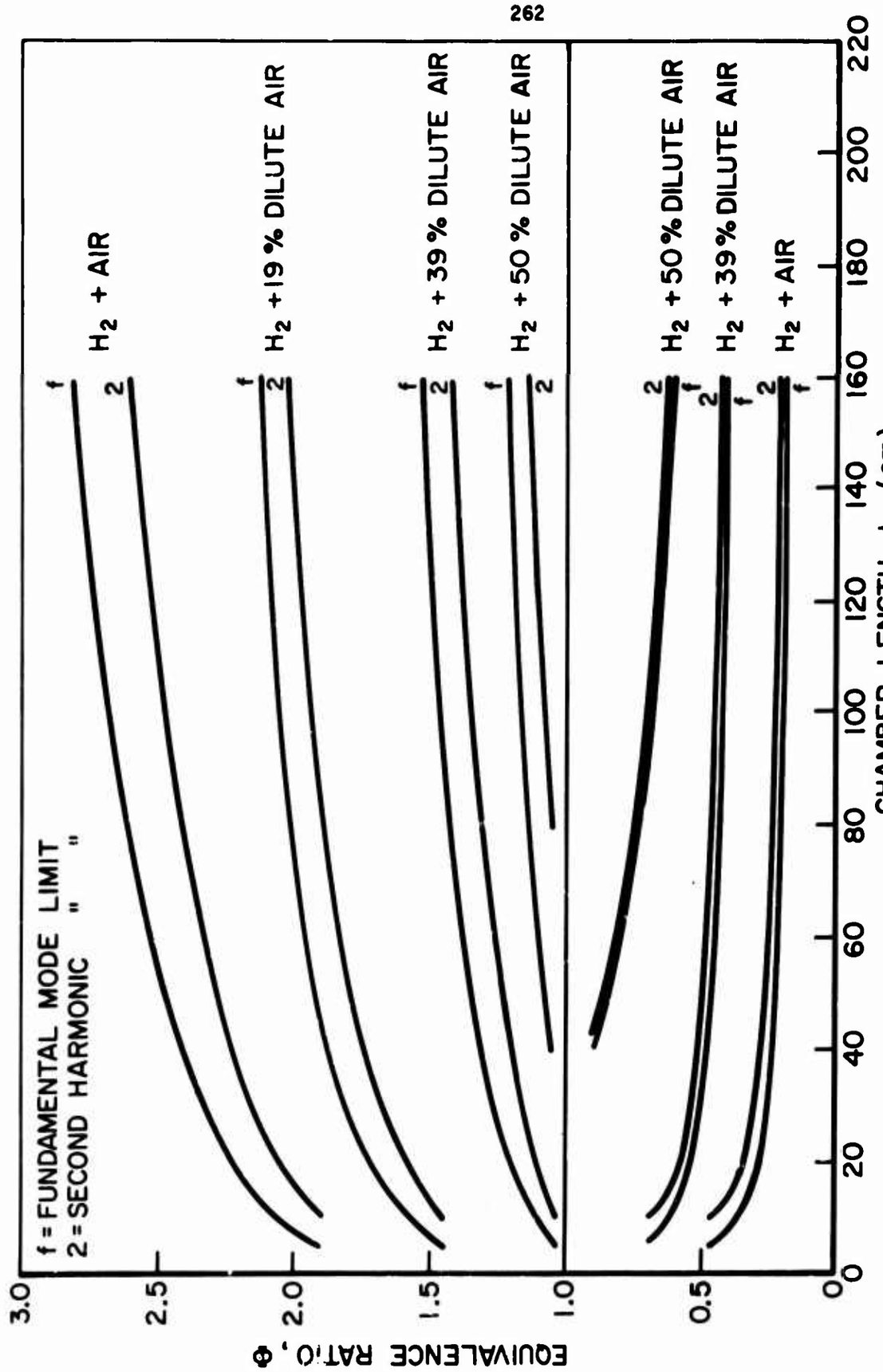
f = FUNDAMENTAL MODE LIMIT
2 = SECOND HARMONIC " "
H2 + AIR
H2 +19 % DILUTE AIR
H2 + 39 % DILUTE AIR
H2 + 50 % DILUTE AIR
H2 + 50 % DILUTE AIR
H2 + 39 % DILUTE AIR
H2 + AIR
EQUIVALENCE RATIO, Φ
CHAMBER LENGTH, Lc (cm)
THEORETICALLY PREDICTED LINEAR STABILITY LIMITS
FOR H2 + AIR AND H2 + DILUTE AIR
E = 38 k cal/mole , T̄c = 0.8 , Pre-exp = 5 x 10^14 , P̄c=7.8 atm

FIGURE V - 17

this effect is relatively small compared to the shift of the R curve in the vicinity of the L curve toward $\bar{\Phi} = 1$ due to the strong influence of the combustion temperature on the combustion time.

Figures V-18 and V-19 summarize the principal theoretical predictions for:

CH_4 + Air
$\bar{P}_c^* = 7.8$ atm
$\bar{T}_u^* = 300^\circ K$
$\bar{T}_c = 0.80$
$E^* = 62.5$ kcal/mole
$\hat{K}^* = 5 \times 10^{15}$
$\gamma = 1.25$

In Figure V-18 the terms L and R in Equation V-100 are plotted corresponding to the curves in Figure V-9 for the H_2 + Air system. The wave travel time was assumed to be the same for the fuel rich and fuel lean mixtures (hence, the horizontal asymptote). In Figure V-19 the stability limit data of Figure V-18 are plotted in the conventional $\bar{\Phi}$, L_c plane. Note the expanded $\bar{\Phi}$ scale.

The contrast between the results for the H_2 and CH_4 systems is important. The CH_4 results evidence the same basic trends with regard to the appearance of harmonic modes and the approach of the predicted limits to $\bar{\Phi} = 1$ at shorter chamber lengths. In the case of the CH_4 + Air system the lower harmonic mode limits collapse to $\bar{\Phi} = 1$ such that over the range of practical L_c nonsteady burning is predicted at all $\bar{\Phi}$.

This behavior is directly attributed to the slower overall kinetics of the CH_4/O_2 system in comparison to the H_2/O_2 system (Appendix D). In terms of the combustion model nonsteady burning arises only for

$$\tau_c^*/\tau_{per}^* > (\tau_c^*/\tau_{per}^*)_{lim}$$

For the H_2 + Air system $(\tau_c^*/\tau_{per}^*)_{lim} = \Theta(.2 \text{ to } .3)$, $\bar{T}_c = .8$
For the CH_4 + Air system $(\tau_c^*/\tau_{per}^*)_{lim} = \Theta(.15 \text{ to } .25)$, $\bar{T}_c = .8$
Due to the inherently slower kinetics of the CH_4/O_2 system this condition is satisfied at higher combustion temperatures, that is closer to $\bar{\Phi} = 1$.

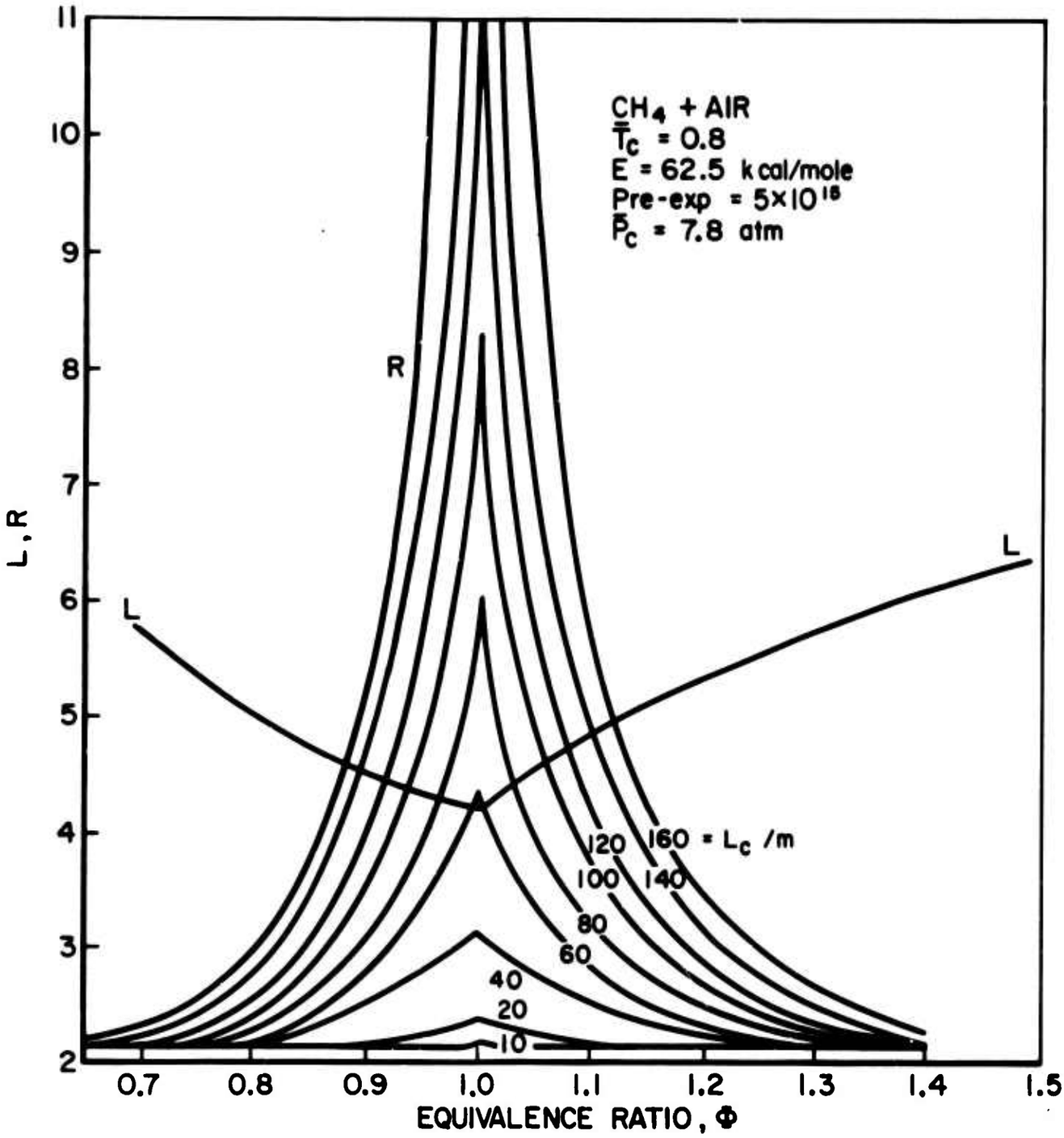

THEORETICAL STABILITY CHARACTERISTICS
SOLUTIONS TO LINEARIZED EQUATION
FOR STABILITY LIMIT

FIGURE V - 18

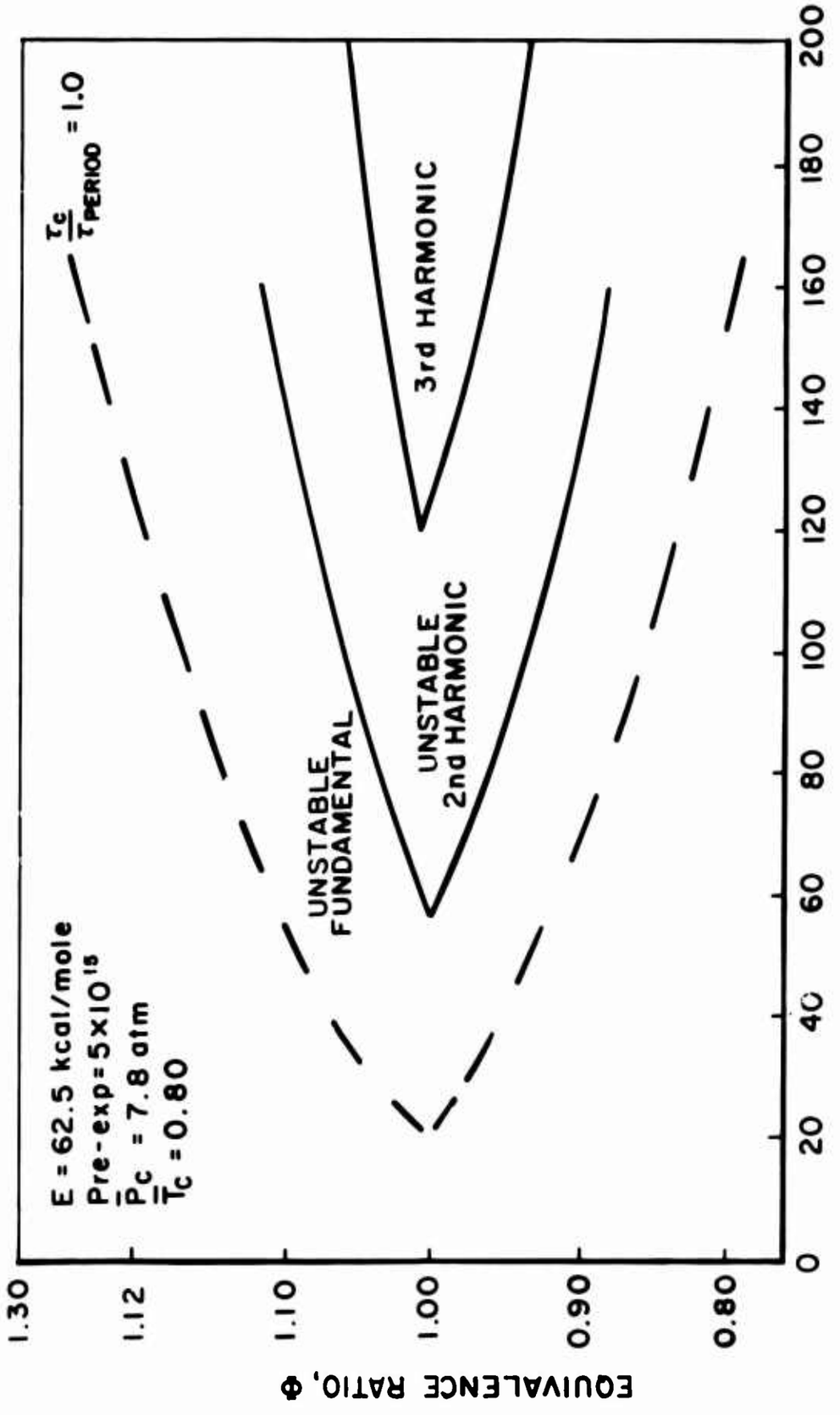

THEORETICALLY PREDICTED LINEAR STABILITY LIMITS FOR CH_4 + AIR IN Φ - Lc PLANE (EXPANDED Φ SCALE)

FIGURE V-19

The prediction of nonsteady burning near $\Phi = 1$ agrees with the experimental observations of Bowman at short L_c^* and of this author at higher L_c^*. Figure V-20 presents the experimental results for the CH_4 + Air and CH_4 + ($.40_2$ + $.6N_2$) systems. Note that Bowman observed the fundamental mode to be sustained at $\Phi = 1$ while the experiments at longer L_c^* carried out in the course of the present work evidence nonsteady combustion at slightly off-stoichiometric mixtures. The theoretical results suggest a reasonable explanation for this previously unexplained length effect. Theory predicts the fundamental mode to be sustained at $\Phi = 1$ up to $L_c^* = 50$. For $L_c^* > 50$ cm due to the necessity to satisfy the criterion $(\gamma_c^*/\gamma_{per}^*)_{lim} = 0.2$) and the increase in γ_{per}^* of the fundamental mode with increasing L_c^*, the fundamental mode limit shifts monotonically to off-stoichiometric mixtures with increasing L_c^* in agreement with the experimental result.

Experimentally the failure to observe the predicted regimes of higher harmonic mode oscillations must be due to the same type of (unaccounted for) damping factors which limit the appearance of higher harmonic modes in the H_2 + Air system. It is noted that combustion with the CH_4 + Air system is significantly rougher than with the H_2 + Air system. The level of random noise is higher in the CH_4 system. Such random pressure fluctuations inhibit the smooth input of energy to the wave system and lead to dissipation of power $(pu)_1 = (pu - \overline{pu})$ which otherwise would be available to drive the oscillations. Second harmonic mode oscillation implies the sustained oscillation of two shock waves at the fundamental frequency. It is expected that such damping influences would be increasingly more severe as the number of sustained waves increases. Finally it is noted that the experimental work always is limited by the finite sensitivity of the transducers. Near-limit experiments suffer from the inability to resolve low amplitude pressure oscillations. High random noise levels of the combustion process and the lower S/N ratio further restrict the ability to discern 2nd and 3rd harmonic modes.

As was evidenced in the analysis for the $H_2/O_2/N_2$ system, the affect of finite ϵ_{rp} on the predicted linear stability characteristic for the CH_4/Air system is to introduce a stabilizing influence at larger $\bar{\gamma}_c$ or off-stoichiometric mixtures. Stable combustion for the CH_4/Air system would be predicted for $\bar{\gamma}_c > (\bar{\gamma}_c)_{upper}$.

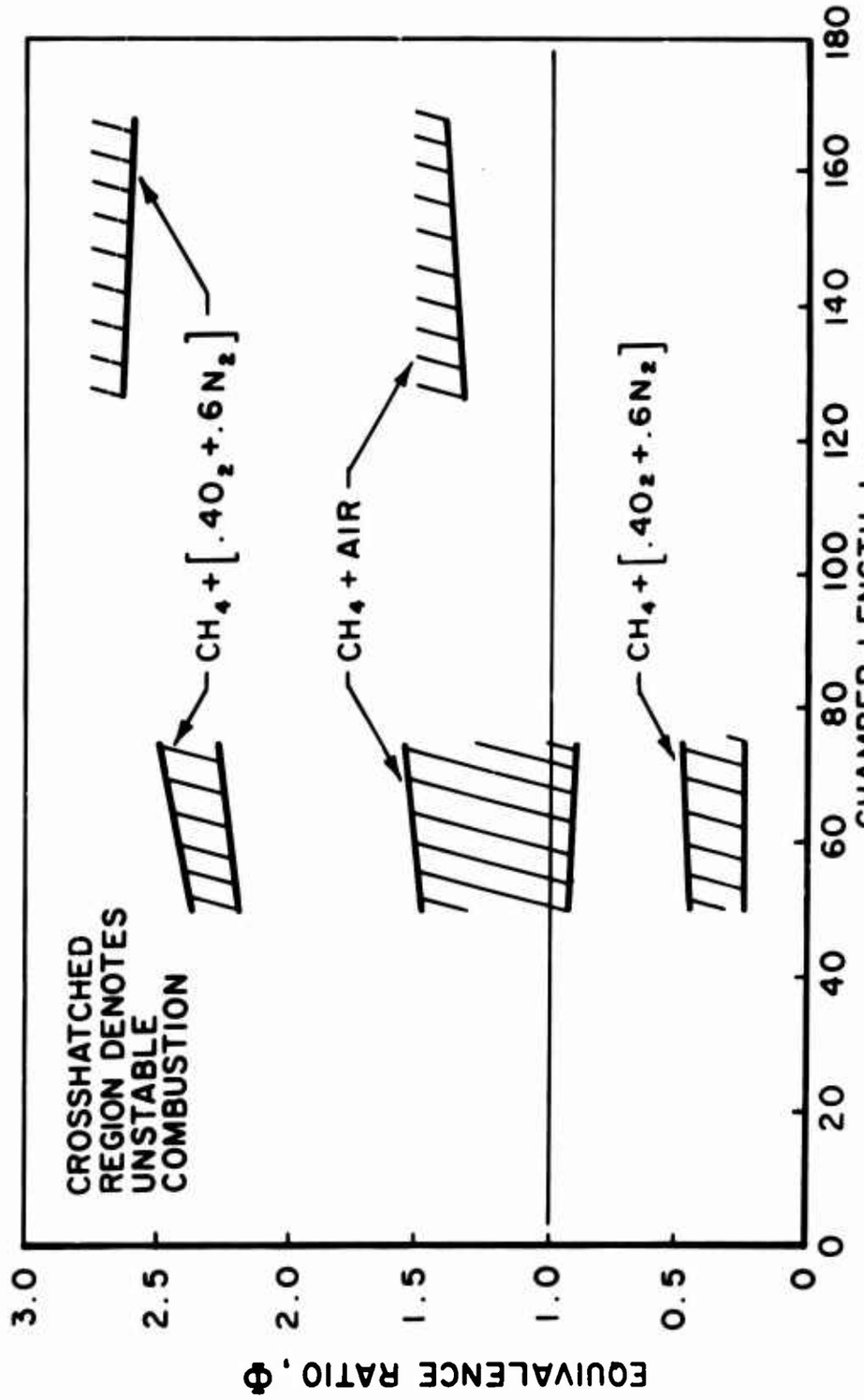

EXPERIMENTALLY OBSERVED REGIMES OF UNSTABLE COMBUSTION FOR CH_4-O_2-N_2 MIXTURES, $\bar{P}_c$ = 4.4 atm, 31 HOLE SHOWERHEAD, 4 HOLE NOZZLE

FIGURE V-20

F.4 Discontinuous, shock-type solutions to Equation V-94

Discontinuous shock-type solutions to Equation V-94 for the wave amplitude parameter f have been obtained for the H_2 + Air system under the conditions noted on page 252 ($\epsilon_{TP}=0$). The method of solution is based on an iterative technique employing the method of successive approximations originally developed by Sirignano (81) to obtain discontinuous solutions to a similar equation arising in the study of unstable combustion in a solid propellant rocket motor.

The iterative technique relies on certain properties of the governing equation. Equation V-94 can be written as,

$$\left(f - k + C\bar{\tau}_c\right)\frac{df}{d\theta} = g(\theta) \qquad \text{(V-102)}$$

where

$$g(\theta) = Af + B\bar{\tau}_c^{-1}\int_{-\infty}^{\theta} f(t')\, e^{-\frac{\beta}{\bar{\tau}_c}(\theta - t')}\, dt' \qquad \text{(V-103)}$$

Solutions ($f(\theta)$) to the equation are sought which are periodic in $\theta = 2$ with discontinuities only at the end points of the integral $0 \le \theta \le 2$, as shown in Figure V-21.

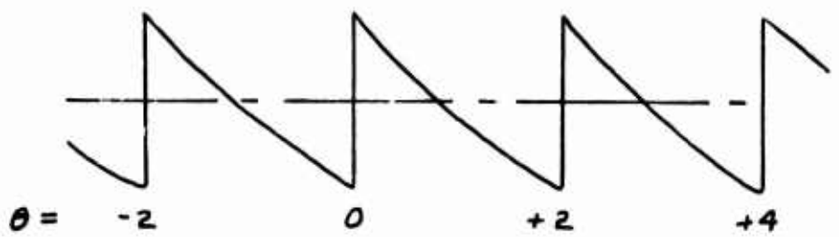

Figure V-21

Equation V-102 can be written as

$$\frac{df}{d\theta} = \frac{g(\theta)}{[f - k + C\bar{\tau}_c]} \qquad \text{(V-104)}$$

where $C = \frac{2\gamma}{\gamma+1}\,\frac{\gamma-1}{\gamma-\eta_c}\,\eta = \mathcal{O}(.2)$, in the present case.

For small $\bar{\tau}_c$, $C\bar{\tau}_c$ is small compared to f and k which are of order 1. It has been noted that for the case of shock-type solutions $k = \frac{f(0) + f(2)}{2}$ the average value of $f(\theta)$ at the shock

which is assumed to be at $\theta = 0$. Hence, at some $\theta = \theta_j$, $f(\theta_j) = k$ Since $c\bar{\tau}_c$ is small but finite, there is likewise a value of $\theta = \theta^*$ where $f(\theta^*) = k - c\bar{\tau}_c$. In order that $\frac{df}{d\theta}$ be continuous at θ^* a condition on $g(\theta)$ is,

$$g(\theta^*) = 0$$
$$\text{where} \quad f(\theta^*) = k - c\bar{\tau}_c \tag{V-105}$$

Equation V-102 can be integrated formally between $\theta = 0$ and θ to obtain a quadratic expression for $f(\theta)$,

$$[f(\theta) - k + c\bar{\tau}_c]^2 - [f(0) - k + c\bar{\tau}_c]^2 = 2\int_0^\theta g(\theta')\,d\theta'$$

which gives

$$f(\theta) = (k - c\bar{\tau}_c) \pm \sqrt{[f(0) - k + c\bar{\tau}_c]^2 + 2\int_0^\theta g(\theta')\,d\theta'} \tag{V-106}$$

Equation V-106 defines $f(\theta)$ over the interval $0 \le \theta \le 2$ Since $f(\theta)$ passes through $k - c\bar{\tau}_c$ at θ^*, $f(\theta)$ must be expressed as,

$$f(\theta) = (k - c\bar{\tau}_c) + \sqrt{[f(0) - k + c\bar{\tau}_c]^2 + 2\int_0^\theta g(\theta')\,d\theta'} \quad , \quad 0 \le \theta \le \theta^* \tag{V-107}$$

$$f(\theta) = (k - c\bar{\tau}_c) - \sqrt{[f(0) - k + c\bar{\tau}_c]^2 + 2\int_0^\theta g(\theta')\,d\theta'} \quad , \quad \theta^* \le \theta \le 2 \tag{V-108}$$

A second condition can be obtained by integrating Equation V-102 over the period,

$$\int_0^2 g(\theta')\,d\theta' = -c\bar{\tau}_c[f(0) - f(2)]$$

$$\int_0^2 g(\theta')\,d\theta' = \left[A + \frac{B}{\beta}\right]\int_0^2 f(\theta')\,d\theta' \tag{V-109}$$

The second condition is simply

$$\left[A + \frac{B}{\beta}\right]\int_0^2 f(\theta')\,d\theta' = -c\bar{\tau}_c[f(0) - f(2)] \tag{V-110}$$

It is of interest to note parenthetically that Equation V-110 can be obtained by considering the integral over the period of the instantaneous power input to the wave system.

Defining the net power input to the wave at any instant as $\hat{P}$

$\hat{P} = (pu)^1_{\text{combustion zone}} - (pu)^1_{\text{nozzle}}$ since energy addition and removal occur only at the concentrated boundary conditions

$$(\rho u)'_{\text{combustion zone}} = M\rho_1^\circ + u_2^\circ \quad \text{(for case where } \rho_1^\circ \approx \rho_1^\circ\text{)}$$
$$= \dot{m}_b^\circ - \bar{\dot{m}}$$

$$(\rho u)'_{\text{nozzle}} = M\frac{3\gamma-1}{2\gamma}\rho_1' \quad \text{(isentropic oscillation at nozzle)}$$

and $$\rho_1^\circ = \rho_1'$$

$$\hat{P} = \frac{\dot{m}_b^\circ - \bar{\dot{m}}}{\bar{\dot{m}}} - \frac{3\gamma-1}{2\gamma}\rho_1^\circ \qquad \text{(V-111)}$$

Equation V-67 is used to express $\frac{\dot{m}_b^\circ - \bar{\dot{m}}}{\bar{\dot{m}}}$

For constant amplitude oscillations, $\int_0^2 \frac{\hat{P}}{M}\,d\theta = 0$

Substituting for $\frac{\dot{m}_b^\circ - \bar{\dot{m}}}{\bar{\dot{m}}}$ in Equation V-111 and integrating over the period, it can be shown that (for $\psi = 0$)

$$\int_0^2 \rho_1^\circ(\theta')\,d\theta' = -\frac{2\gamma}{3\gamma-1}\,\frac{\gamma-1}{\gamma-\bar{\tau}_c}\,\eta\,\bar{\tau}_c\left[\rho_1^\circ(0) - \rho_1^\circ(2)\right] \qquad \text{(V-112)}$$

which is the same result obtained in Equation V-110 when the appropriate terms are inserted $\left(A + B/\bar{\beta} = \frac{3\gamma-1}{\gamma+1} \text{ for } \psi = 0\right)$

Since $\rho_1^\circ(0) - \rho_1^\circ(2) = \Delta\rho_1^\circ$, for continuous waves, the condition $\int_0^2 \rho_1^\circ(\theta')\,d\theta' = 0$

is observed.

For discontinuous oscillations the nonlinear system requires

$$\int_0^2 p_1^\circ(\theta')\,d\theta' < 0 \qquad \text{(V-113)}$$

That is 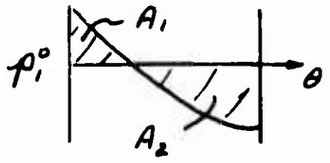

$|A_2| > |A_1|$

To obtain a solution $f(\theta)$ satisfying these conditions, an initial approximation for $f(\theta)$ is made, by choosing $\xi(\theta)$

$$f(\theta) = f(0) + \xi(\theta) \quad , \quad \text{e.g.,} \quad \xi(\theta) = -\theta$$

where $\xi(0) = 0$. Equation V-110 is used to obtain a first approximation to $f(\,)$ as,

$$f(0) = \frac{\gamma}{3\gamma-1}\,\frac{\gamma-1}{\gamma-\bar{\tau}_c}\,\eta\,\bar{\tau}_c\,\xi(2) - \frac{1}{2}\int_0^2 \xi(\theta')\,d\theta' \qquad \text{(V-114)}$$

A new $f(\theta)$ is defined as,

$$f(\theta) = f(0) + \xi(\theta) \qquad \text{(V-115)}$$

which is substituted into Equation V-103 to obtain $g(\theta)$. To eliminate the infinite range of integration, the periodicity condition on $f(\theta)$, namely, $f(\theta') = f(\theta' + 2j)$ where j is an integer, can be used to simplify the integral term. It can be shown that,

$$\int_{-\infty}^{\theta} f(t')\,e^{-\frac{\bar{\beta}}{\bar{\tau}_c}(\theta-t')}\,dt' = e^{-\frac{\bar{\beta}}{\bar{\tau}_c}\theta}\left[\int_0^{\theta} f(t')\,e^{+\frac{\bar{\beta}}{\bar{\tau}_c}t'}\,dt' + \frac{1}{e^{+2\bar{\beta}/\bar{\tau}_c}-1}\int_0^2 f(t')\,e^{+\frac{\bar{\beta}}{\bar{\tau}_c}t'}\,dt'\right] \qquad \text{(V-116)}$$

Equations V-115 and V-116 are used to evaluate $g(\theta)$.

A third condition which must be satisfied and which can be used to determine k is obtained from the observation $f(\theta^*) = k - c\bar{\tau}_c$ and Equation V-106 , that is,

$$\left[f(0) - k + c\bar{\tau}_c\right]^2 + 2\int_0^{\theta^*} g(\theta')\,d\theta' = 0 \qquad \text{(V-117)}$$

Since the term in the radical must everywhere be non-negative to prevent imaginary values of $f(\theta)$ it is clear that $[f(0)-k+c\bar{\tau}_c]^2+2\int_0^{\theta} g(\theta')d\theta'$ attains a minimum value equal to zero at θ^* . Since,

$$[f(0)-k+c\bar{\tau}_c]^2 > 0$$

and defining $\bar{g}(\theta) = \int_0^{\theta} g(\theta')d\theta'$

it is clear that $\bar{g}(\theta^*)$ must reach a minimum at θ^* where $g(\theta^*) = 0$.

With $g(\theta)$ defined, θ^* is determined from the consideration that at θ^* , $df/d\theta < 0$ for acceptable wave shapes. For $\theta < \theta^*$ $f(\theta) > k - c\bar{\tau}_c$ hence $g(\theta) < 0$ from Equation V-104 . For $\theta > \theta^*$, $g(\theta) > 0$ Therefore, near θ^* the curve for $g(\theta)$ must have a positive slope. Having determined θ^* satisfying these conditions a new value for k is calculated from Equation V-117

$$k = f(0) - c\bar{\tau}_c - \sqrt{-2\int_0^{\theta^*} g(\theta')d\theta'} \qquad \text{(V-118)}$$

where the minus sign is consistent with the observation that for small $\bar{\tau}_c$, $c\bar{\tau}_c$ is small relative to $f(0)$, and $k < f(0)$ The value of k from Equation V-118 is substituted into Equations V-107 and V-108 to evaluate a new $f_2(\theta)$ which is used to define a new $\xi_2(\theta)$

$$\xi_2(\theta) = f_2(\theta) - f(0)$$

The iteration is continued until convergence is achieved.

A digital computer program using the above iterative scheme was written to obtain shock-type solutions to Equation V-94. Initially solutions to Equation V-94 were examined for arbitrary values of the parameters A, B, C, $\bar{\tau}_c$ For certain ranges of the parameters discontinuous shock-type solutions are obtained. Convergence is generally fairly rapid except near the boundaries of regimes of (A, B, C, $\bar{\tau}_c$) where shock-type solutions exist. Figure V-22 shows a typical iteration sequence for $f(\theta)$ away from the boundary. Essentially the wave-form is well defined after two iterations.

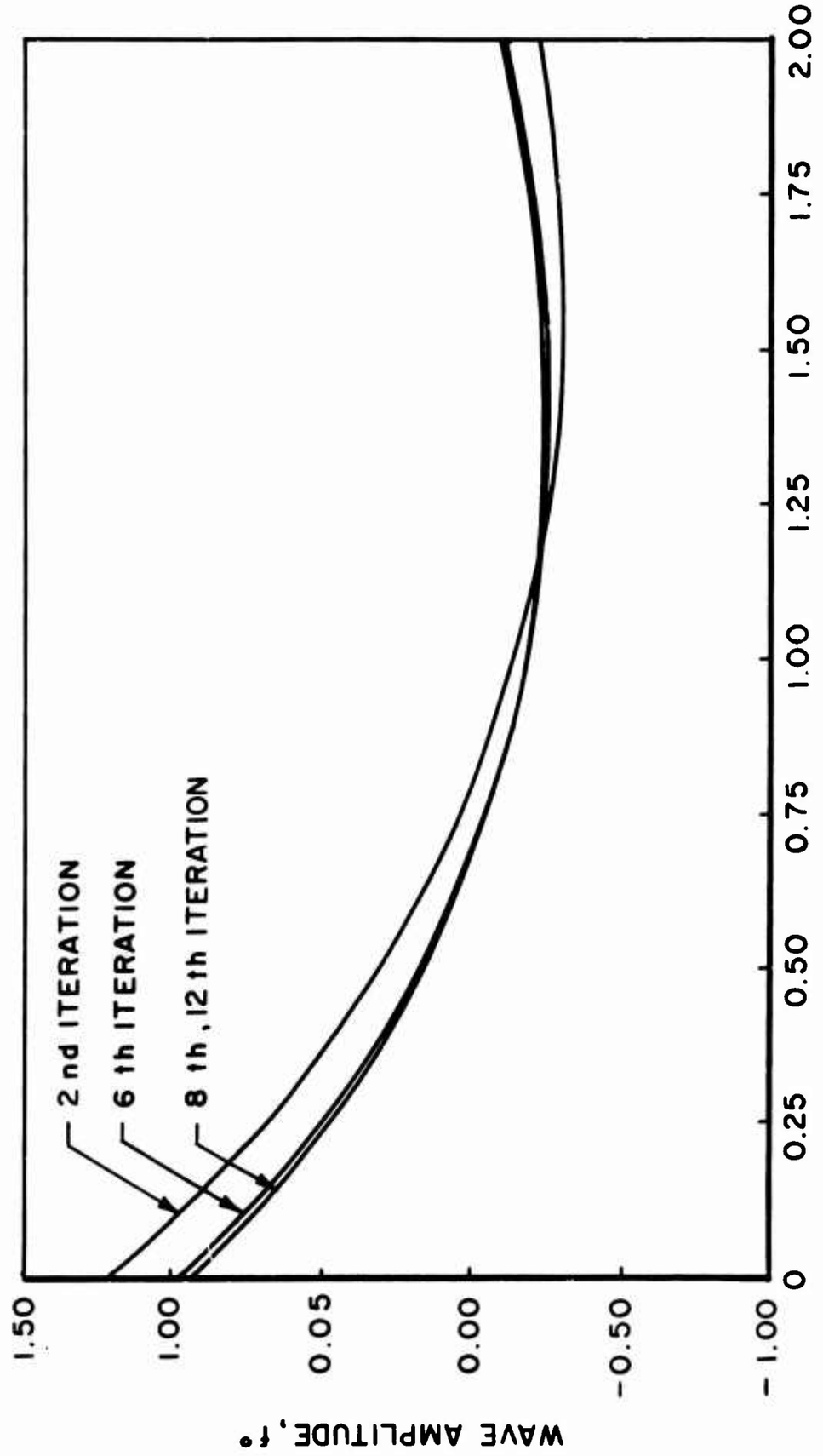

TYPICAL CONVERGENCE OF ITERATIONS TO DISCONTINUOUS SHOCK TYPE SOLUTIONS OF EQUATION V-94

FIGURE V - 22

Discontinuous shock type solutions are obtained only for $A<0$. For choked mass injection flux $\psi=0$ and $\mathcal{B} = \left[\frac{3\gamma-1}{\gamma+1} - A\right]\bar{\beta} > 0$ for shock-type solutions. For A sufficiently negative ($A < -.5$) shock type solutions are found only for values of $\bar{\tau}_c = \tau_c^*/\tau^*_{wave} > .1$ in agreement with the results of the linearized analysis. Assuming $\bar{\tau}_c$ is in the appropriate range, the condition for shock-type solutions is $A \overset{S}{<} 0$ ($\overset{S}{<}$ = "sufficiently less than"). That is

$$(1-\bar{\theta}_c)\left[\Sigma_T + \frac{1}{\gamma-\bar{\tau}_c}\right]\eta + \Sigma_p \overset{S}{>} \frac{\gamma-\bar{\tau}_c}{\gamma(1-\bar{\tau}_c)}\left\{\frac{3\gamma-1}{2\gamma} + \left[1-\bar{\beta}(1-\bar{\tau}_c)\right]\psi\right\}$$

This condition is equivalent to Equation V-101 for the linear limit where $(\bar{\beta}/\pi\bar{\tau}_c)^2$ is small compared to 1 .

Figures V-23 to V-26 summarize the principal results of the nonlinear analysis for $\Phi > 1$ for the H_2 + Air system under the conditions n ted on page 252 . In Figure V-23 the parameters A and B are shown as a function of Φ for $\bar{T}_c$ = 0.80 and 0.75. Figure V-24 shows the predicted shock wave amplitude where,

$$\Delta f^\circ = \frac{1}{2\gamma M}\Delta p_1^\circ$$

as a function of Φ with L_c^*/m and $1/\bar{\tau}_c$ as parameters. The linear stability limits determined from Figure V-24 are denoted for $\Delta f^\circ = 0$ by the black squares. Figure V-25 shows the ratio τ^*_{wave}/τ_c^* as a function of Φ near the stability limits defined by Figure V-24. Figure V-26 shows the typical discontinuous fundamental mode shock type solutions obtained for near limit mixtures for L_c^* = 80 cm.

On the basis of these results the following points are noted: (a) The nonlinear stability limits fall at lower Φ and larger $1/\bar{\tau}_c$ than the corresponding linear limits. The linear and nonlinear analyses thus define two regimes of solutions to Equation V-94 which are designated here as regimes I and II. In regime I the solutions to the nonlinear equation and the linearized form

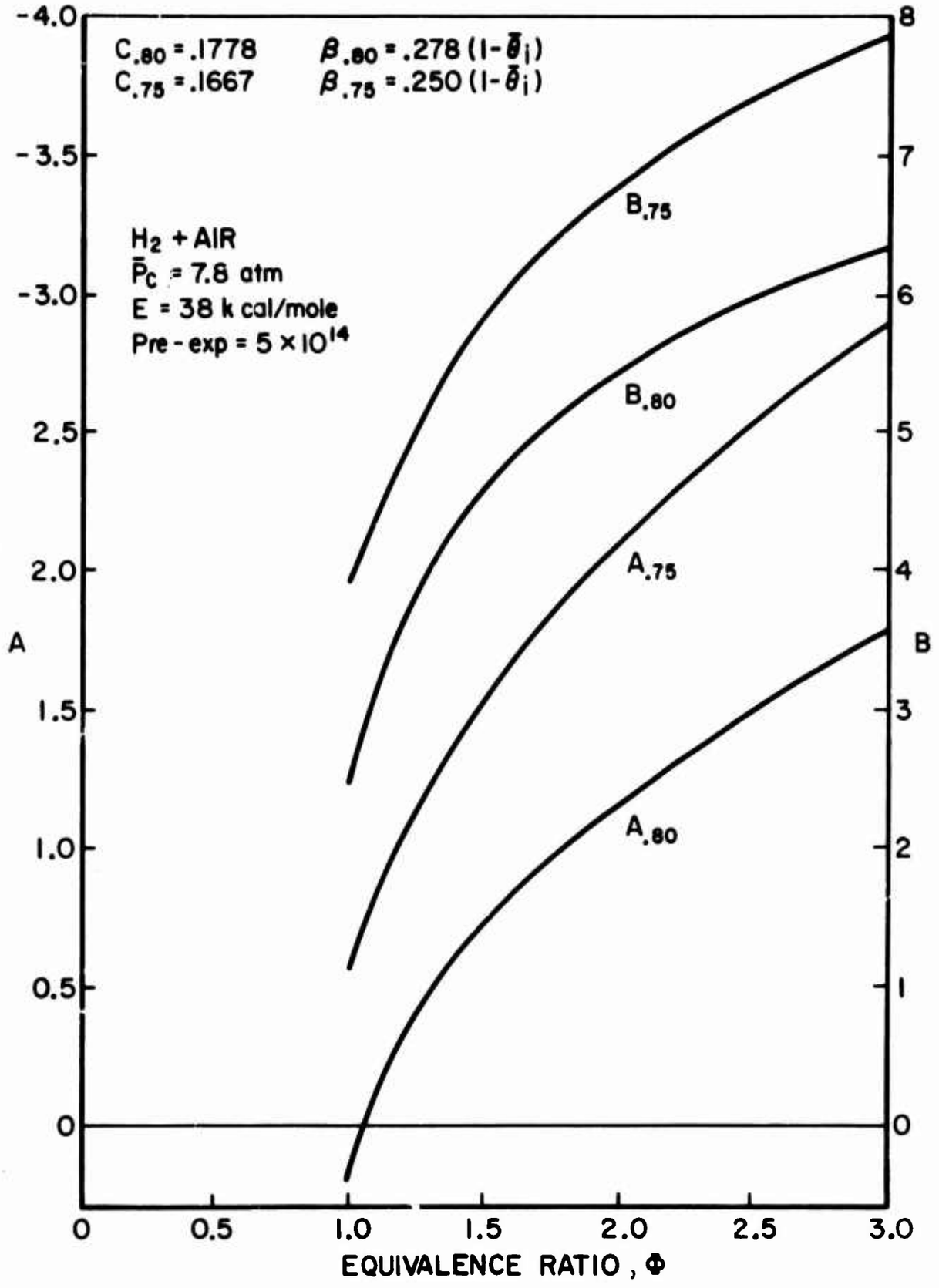

COEFFICIENTS A, B, C, $\bar{\beta}$ APPEARING IN EQUATION V-94
AS A FUNCTION OF EQUIVALENCE RATIO FOR $\bar{T}_c$ = 0.75, 0.80

FIGURE V- 23

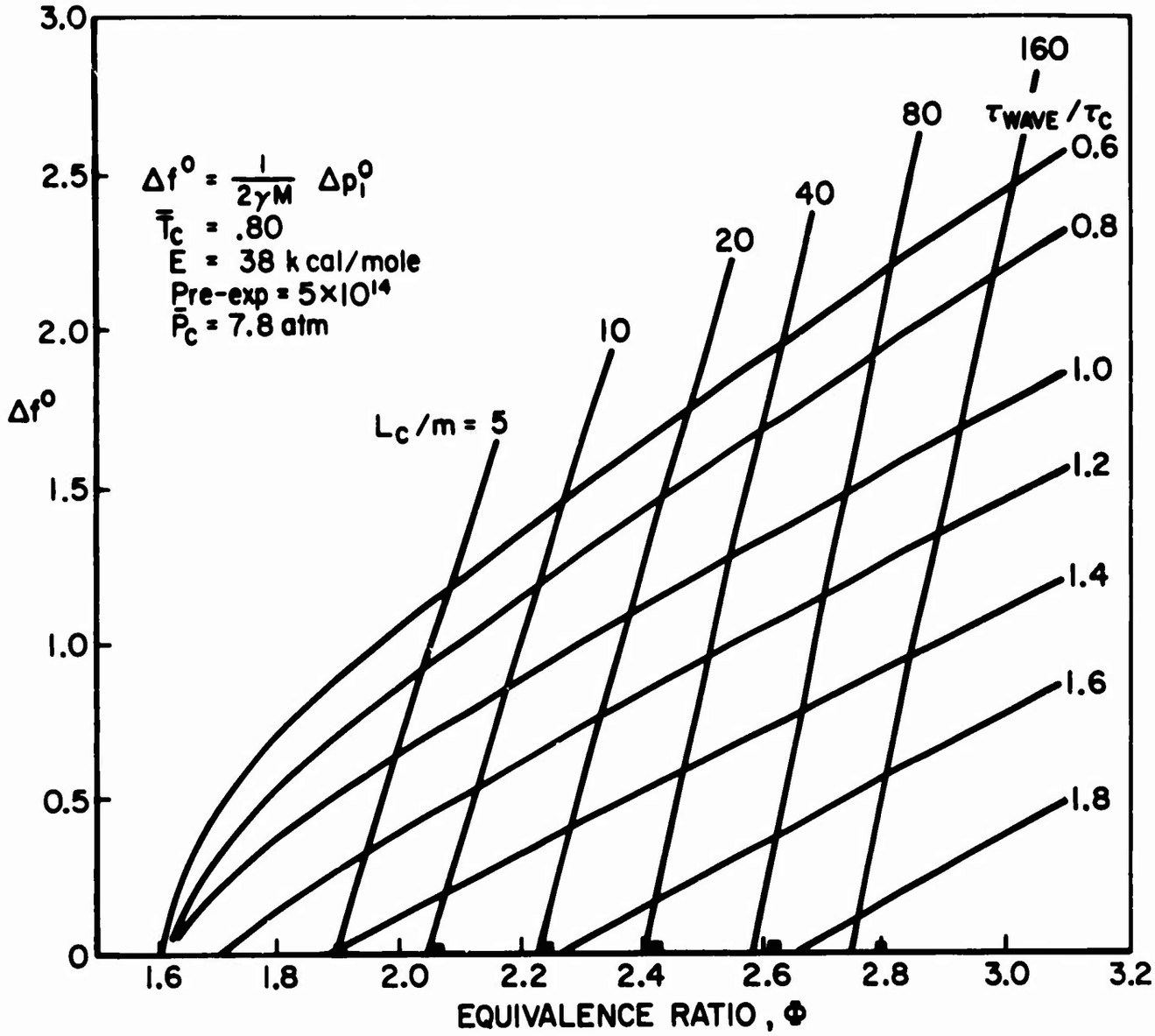

PREDICTED WAVEFORM FUNCTION AMPLITUDE (Δf^0)
AT X=0, θ=0 AS A FUNCTION OF EQUIVALENCE RATIO FOR H_2 +AIR
WITH L_c AND τ_{WAVE}/τ_c AS PARAMETERS

FIGURE V- 24

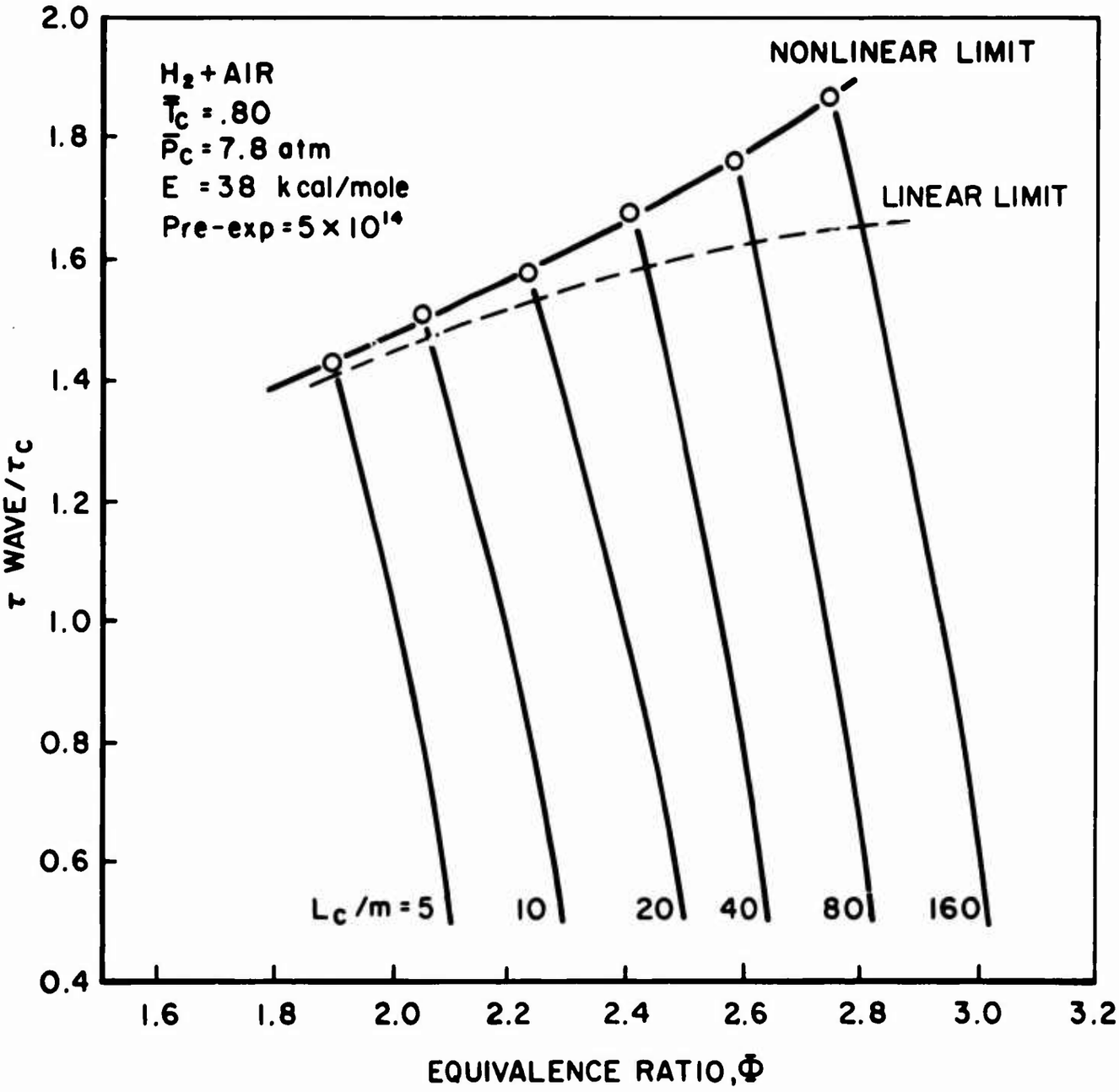

RATIO OF WAVE TRAVEL TIME (1/2 PERIOD) TO CHARACTERISTIC COMBUSTION TIME VS EQUIVALENCE RATIO NEAR STABILITY LIMIT

FIGURE V-25

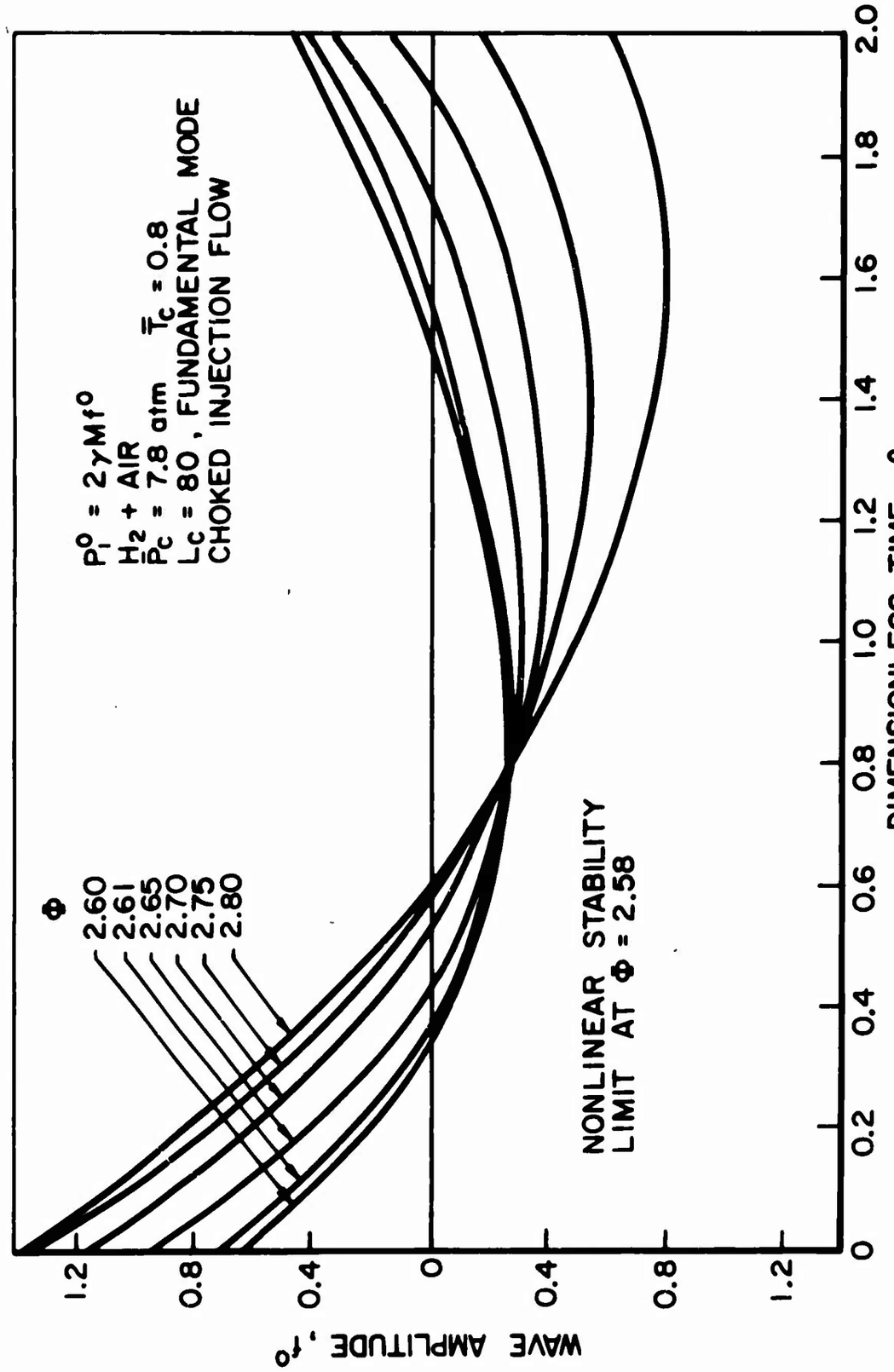

DISCONTINUOUS SOLUTIONS FOR WAVE FUNCTION f^0
AS FUNCTION OF DIMENSIONLESS TIME, θ

FIGURE V - 26

of the equation overlap. The linear stability limit defines the regime I as a zone wherein small perturbations are linearly unstable. Small disturbances are amplified and grow in regime I. The nonlinear analysis indicates that in regime I finite amplitude discontinuous solutions to the equation exist. The inference drawn is that in regime I small disturbances are amplified with the final form of the sustained pressure oscillation being the discontinuous solution obtained in the nonlinear treatment.

No proofs of the uniqueness or stability of the final form of the nonlinear periodic solutions have been offered. The numerical iterative technique used to obtain nonlinear solutions suggests the uniqueness and stability of the solutions found. Convergence to the solution is rapid away from the nonlinear limit and is independent of the initial form of $\xi(\theta)$ chosen to begin the iteration. Convergence rates differed at most by 1 or 2 iterations for,

$$\xi(\theta) = -b\theta \quad , \quad b = .5, 1, 2, 5$$

$$\xi(\theta) = 1 - (\theta - 1)^b, \quad b = 2, 4$$

Following Mitchell's reasoning (34), the discontinuous solutions obtained in regime I represent unique stable limit cycles for Equation V-94 . Disturbances in regime I with amplitudes exceeding the predicted finite amplitude of the discontinuous solution are damped until the disturbance matches the predicted solution, while infinitesimal disturbances must grow to attain the final wave form.

In regime II the nonlinear analysis shows that finite amplitude discontinuous solutions are possible while the linear analysis indicates the regime to be linearly stable. That is, infinitesimal perturbations in regime II are damped according to the linearized results. Mitchell has observed a similar behavior of the linear and nonlinear stability limits. In the present case the same apparent contradiction in terms arises as observed by Mitchell. That is, a regime of finite amplitude discontinuous periodic solutions is found to exist in a regime predicted to be linearly stable. The finite amplitude oscillations are therefore

not the result of a systematic growth of small perturbations from the steady state which in fact must be damped in this region. Mitchell interpreted this phenomenon as indicating that the discontinuous oscillations result from the growth of finite amplitude oscillations which appear spontaneously. It would seem that a kind of triggering must exist near the linear limit in regime II where a sufficiently strong random oscillation is driven rather then damped and eventually assumes the predicted discontinuous shock type oscillation.

If indeed this interpretation is applicable to the present situation, in order that the linear limit stability criterion remain valid as well as the criterion that small perturbations away from the discontinuous solutions in regime II always lead to the return to the predicted waveform, an unstable limit cycle must lie between the nonlinear limit and the linear limit. That is one should be able to find a second set of finite small amplitude solutions to the nonlinear equation which decay to zero amplitude at the nonlinear limit. This analysis has not been carried out in the present case. Mitchell succeeded in finding such finite amplitude solutions which are continuous and which by comparison with Sirignano's results (26) were interpreted as the required unstable solutions.

From Figure V-26 the predicted waveform of the shock-type solution is observed to approach the ramp-type waveform as the displacement from the nonlinear limit (beyond the linear limit) increases. As the nonlinear limit is approached the waveform becomes concave upward such that the peak-to-peak wave amplitude exceeds the amplitude of the shock type discontinuity. At the nonlinear limit the predicted shock amplitude is zero while the peak-to-peak amplitude remains finite. A cusp at $\theta = 0$ and 2 which is physically unrealistic is predicted. It is expected that continuous finite amplitude oscillations exist having peak-to-peak wave amplitudes which increase from zero near the nonlinear limit and which match the peak to peak wave amplitude predicted for the discontinuous oscillation at some small displacement

from the nonlinear limit. Finite disturbances with amplitudes above the continuous solution amplitude are sustained and eventually assume the predicted discontinuous waveform. Smaller amplitude oscillations are damped.

(c) The rapid (nearly linear with Φ increase in shock amplitude Δf° and the approach to ramp-type pressure waveform with slight departures from the nonlinear stability limit is observed. This effect is principally due to the rapid decrease in $1/\bar{\tau}_c$ as Φ is increased near the limit. Typically A changes by only about 3% for $L_c^*/m = 80$ and $2.6 \leq \Phi \leq 2.8$, while the dimensionless shock amplitude increases from 0 to 2.5. For $M = \Theta(0.02)$, $\gamma = 1.25$ the predicted dimensionless shock amplitudes at x = 0 are

$$\frac{\Delta p^*}{\bar{p}_c^*} = \Delta p_i^\circ = 2\gamma M \Delta f^\circ = \Theta(0 \text{ to } .15)$$

(d) The theoretically predicted sharp increase in shock amplitude with increasing Φ near the stability limit, the order of magnitude of the shock amplitude, and the waveform over the period of oscillation are observed to be in excellent agreement with the experimental results of Bowman for the H_2 + Air system (Figures II-8, 10). Typically the experimentally observed increase in Δp_i° from 0 to Θ(0.1 to .15) occurs for an increase in Φ of $\Theta(0.15)$.

(e) Significantly the present analysis offers no insight into the experimentally observed maximum of the sustained shock amplitude with increasing Φ and decrease in wave amplitude thereafter for further increase in Φ with the eventual encounter of an upper stability boundary at higher Φ. An explanation for this strong damping influence has been suggested earlier and the strong stabilizing influence encountered at $\bar{\tau}_c > 1$ for the case of finite ϵ_{TP} and for the heuristic model where $\tau_c' \sim \int_{t-\bar{\tau}_c}^{t} p_i^\circ \, dt'$ (Appendix C) was noted.

(f) Equations V-101 and V-119 show the important influence of the distribution of the combustion process on the nonsteady combustion characteristics. $\bar{\tau}_c \to 1$ leads to large values of the right hand sides of Equations V-101and V-119 and precludes the possi-

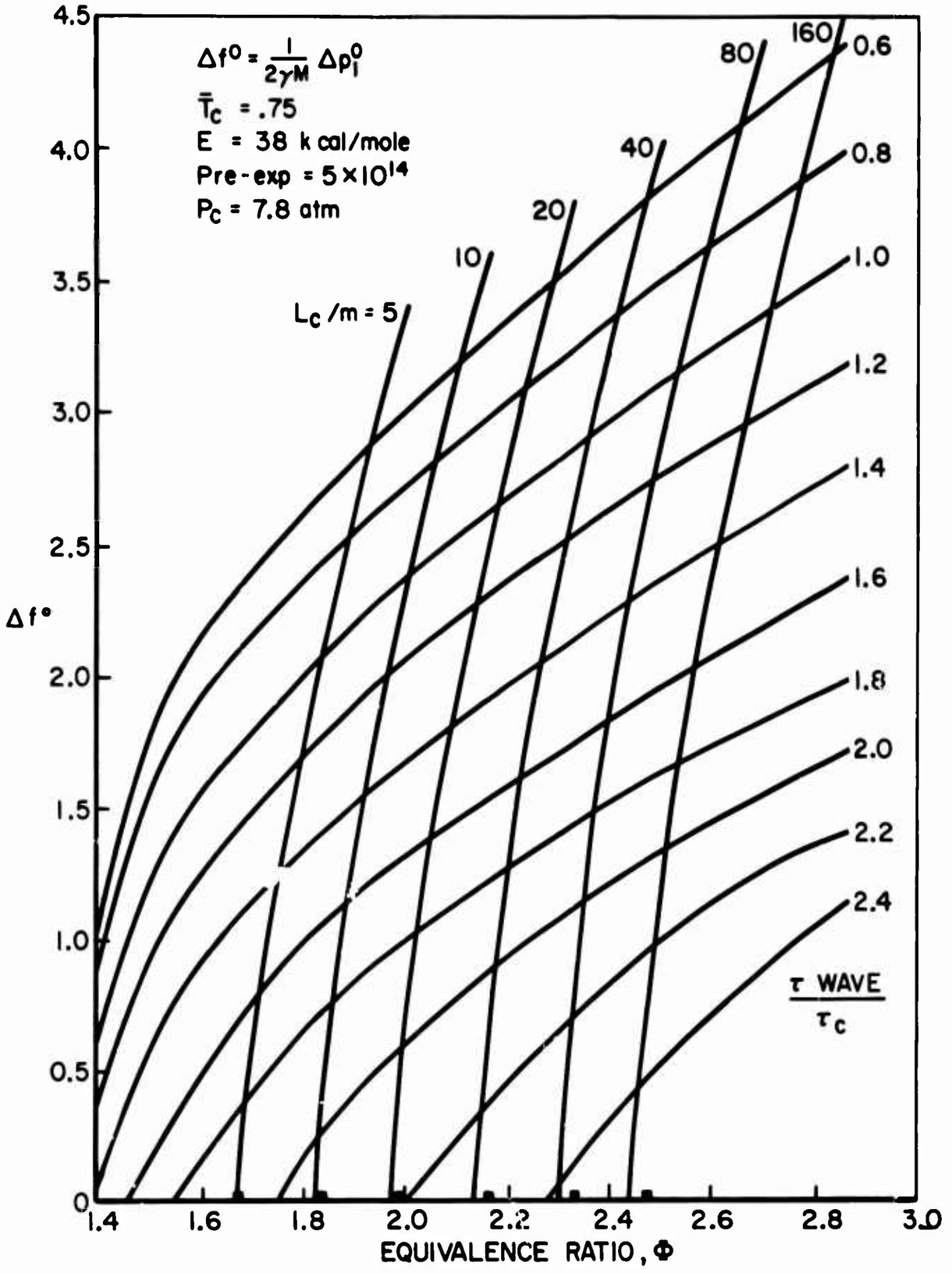

PREDICTED WAVE FORM FUNCTION AMPLITUDE (Δf°) AT X=0, θ=0, AS A FUNCTION OF EQUIVALENCE RATIO FOR H_2 + AIR WITH L_c/m AND $\frac{\tau \text{WAVE}}{\tau_c}$ AS PARAMETERS

FIGURE V- 27

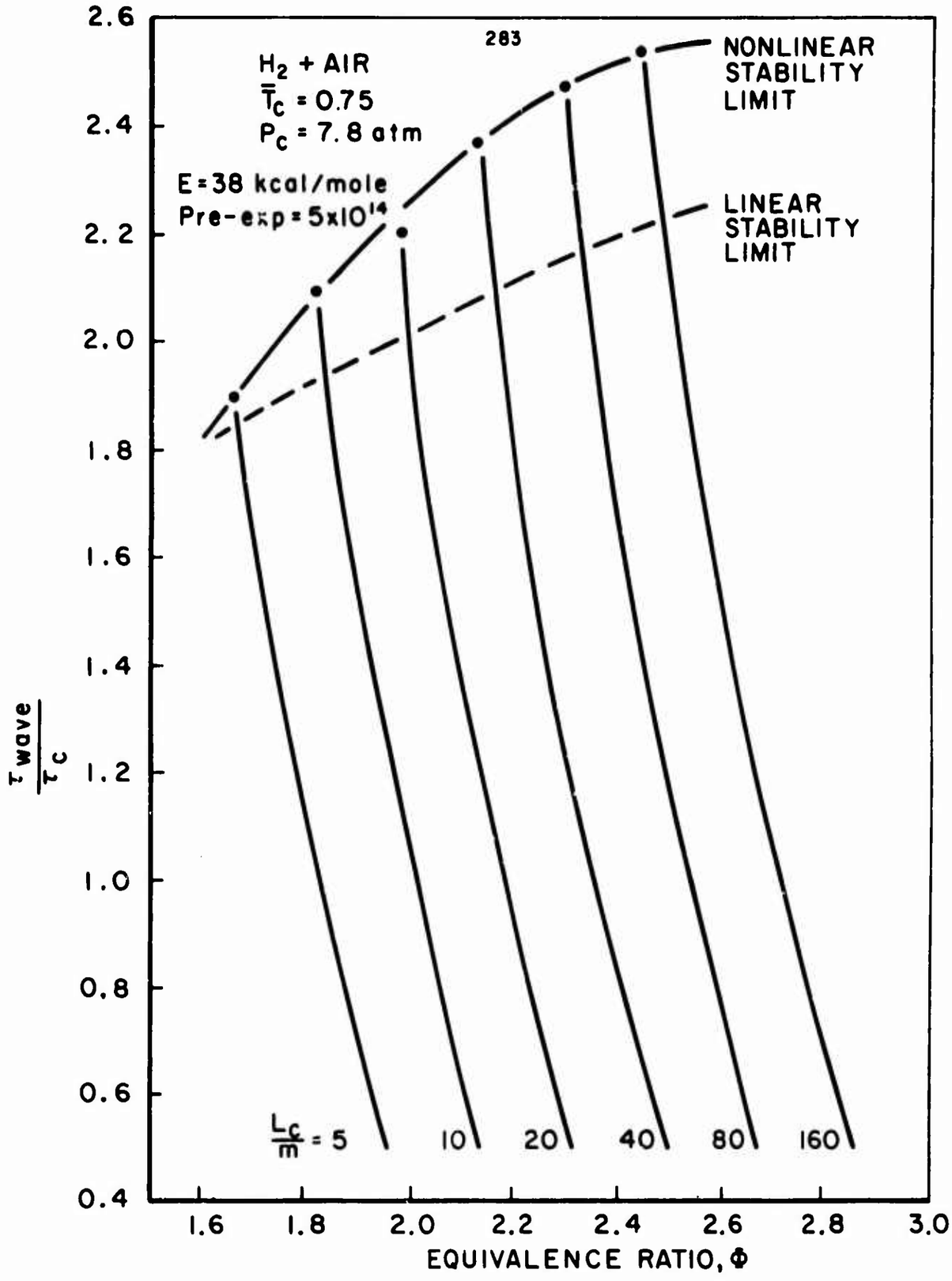

RATIO OF WAVE TRAVEL TIME (1/2 PERIOD) TO CHARACTERISTIC COMBUSTION TIME VS. EQUIVALENCE RATIO NEAR STABILITY BOUNDARY

FIGURE V- 28

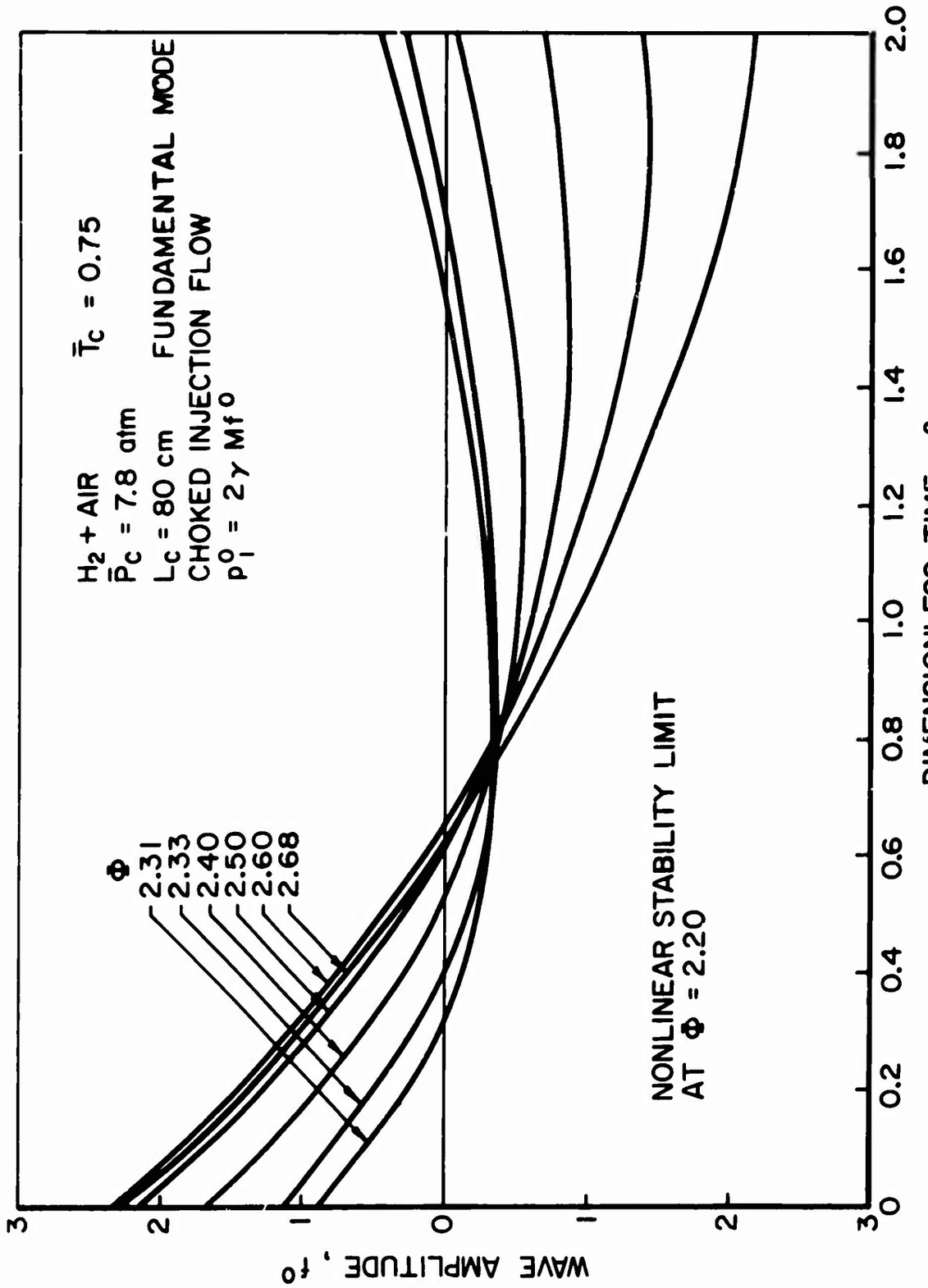
H_2 + AIR
$\bar{P}_c$ = 7.8 atm
L_c = 80 cm
CHOKED INJECTION FLOW
$p_1^o = 2\gamma M f^o$
$\bar{T}_c$ = 0.75
FUNDAMENTAL MODE
Φ
2.31
2.33
2.40
2.50
2.60
2.68
NONLINEAR STABILITY LIMIT
AT Φ = 2.20
WAVE AMPLITUDE , f^o
DIMENSIONLESS TIME , θ
DISCONTINUOUS, SHOCK TYPE, SOLUTION FOR WAVE FUNCTION,
f^o, AS FUNCTION OF DIMENSIONLESS TIME, θ

FIGURE V - 29

bility of linear and nonlinear instability. The calculations for the linearized stability characteristics were carried out for $\bar{T}_c = 0.80$ which is consistent with the numerical study of the distributed combustion zone. Calculations have been carried out to obtain the linear and nonlinear stability characteristics of the H_2 + Air system under the conditions on page but with $\bar{T}_c = 0.75$. The same trends of the linearized limits are observed for $\bar{T}_c = 0.80$ and 0.75. The increase "driving" for the system with $\bar{T}_c = 0.75$ is evidenced by the shift in the linear and nonlinear stability limits toward $\bar{\Phi} = 1$, an increase in the ratio $(\tau_{wave}^* / \bar{\tau}_c^*)_{lim}$, and a more rapid increase in shock amplitude with linear displacement (in $\bar{\Phi}$) away from the nonlinear limit. Figures V-26 to 30 summarize the principal results of the nonlinear analysis for $\bar{T}_c = 0.75$.

G. The influence of unchoked injection mass flux and of preheating the unburned premixed propellants -- Theory and Experiment

The original turbulent flame model had suggested that the presence of unchoked mass injection flux ($M_{inj} < 1$) may have an important influence on the nonsteady combustion characteristics of the system. An indication of the possible influence of the ratio of the unburned to burned gas temperatures ($\bar{\theta}_i$) was also derived. These two predictions led to two separate experimental investigations the results of which are in complete agreement with the predictions of the present distributed combustion model. Rather than devote a separate chapter to these experimental results obtained during the course of the diagnostic work the experimental data are presented here as further confirmation of the new theoretical predictions.

G.1 Unchoked Mass Injection

The case of unchoked mass injection flux is defined by $M_{inj} < 1$ and $\psi > 0$. The important influence of $\psi > 0$ on the linear and nonlinear response is easily seen from Equation V-101 for the linear limit and the condition V-119. For $\psi > 0$ additional

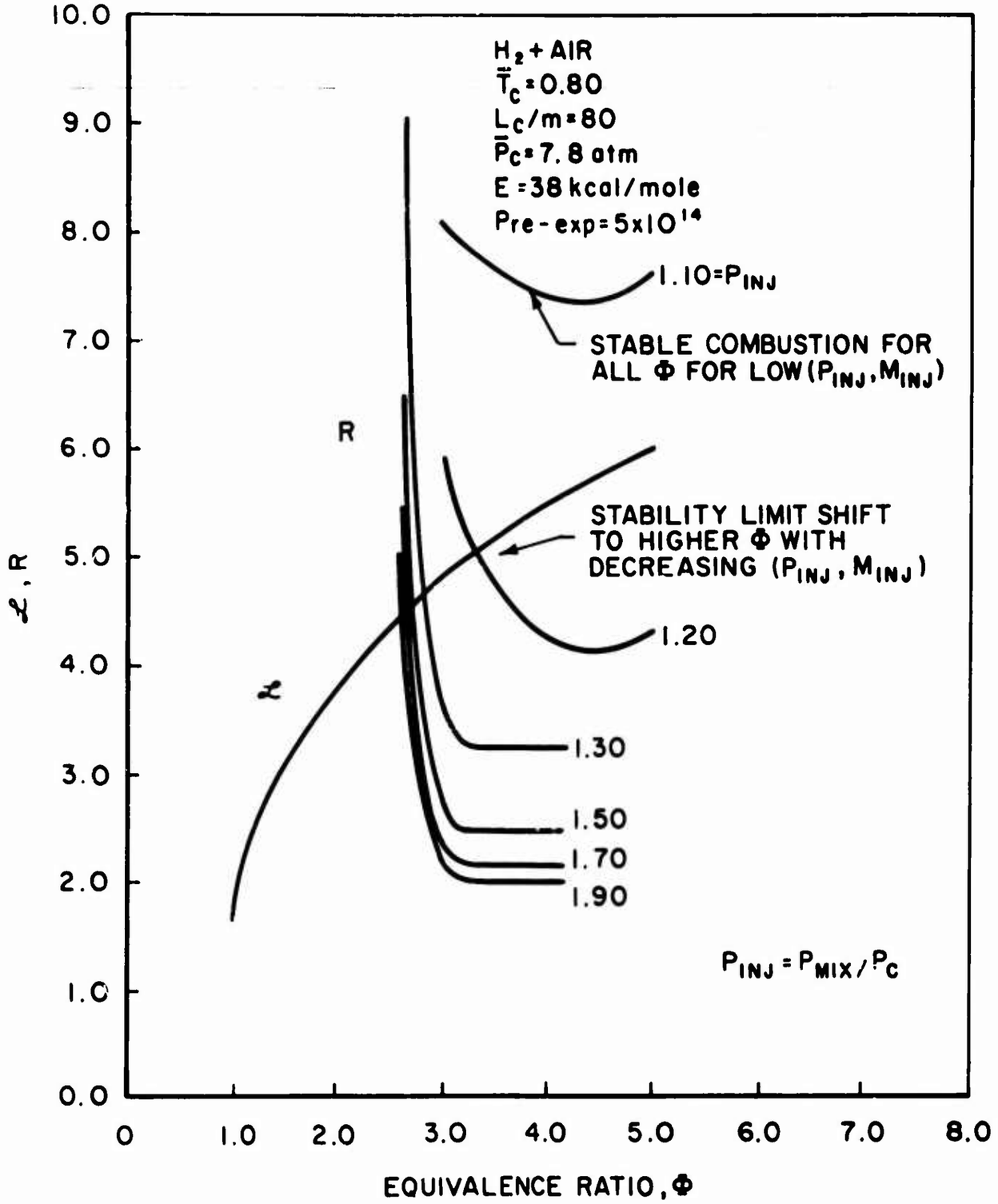

THEORETICAL PREDICTION OF STABILIZING INFLUENCE OF DECREASING INJECTION PRESSURE RATIO AND MACH NUMBER (P_{INJ}, M_{INJ})

FIGURE V - 30

positive stabilizing terms appear on the right hand sides of these equations. In Figure V-30 the predicted influence of decreasing the steady state pressure drop (ratio, $\rho_{inj} = \frac{\bar{p}^*_{mix}}{\bar{p}^*_c}$) across the injector on the linear response of the previously studied H_2 + Air system is shown. As (M_{inj}, ρ_{inj}) are decreased, all other parameters remaining fixed, a systematic progression of the linear limit to higher Φ is observed. Eventually for sufficient decrease in (M_{inj}, ρ_{inj}) a condition of stable combustion over the entire range of Φ is predicted. In terms of Equation V-119 an increase in ψ leads to an increase in the value of A for fixed Φ which has the effect of decreasing the predicted shock amplitude.

To test the prediction of the strong stabilizing influence of decreasing (M_{inj}, ρ_{inj}) a series of experiments were carried out with the H_2 + Air system at $\bar{P}_c^*$ = 4.4 atm, L_c^* = 104 cm, using the 10 hole showerhead injector. (M_{inj}, ρ_{inj}) were decreased systematically by simply enlarging the injection port diameters for a sequence of experiments (d_{port} = 0.07 cm to 0.19 cm). The stability limits and the sustained shock amplitudes were determined as a function of Φ over the range of $1 \geq M_{inj} \geq 0.30$ and injection pressure drops of 16 atm $> \Delta p_{inj} >$ 0.5 atm. Figures V-31 and V-32 summarize the principal experimental results. The value of P_{inj} recorded in Figure V-32 is the static pressure at the inlet of the injection port to the combustion chamber. The values of M_{inj} and P_{inj} noted were determined by the simultaneous solution of the equations of conservation of mass, momentum, and energy for the gas rocket injection configuration using the measured values of $\bar{p}^*_{mix}$ and $\bar{p}_c^*$. For the case of unchoked injection there is always a slight increase in pressure along the jet axis as noted earlier.

The possibility of a dynamic coupling of the acoustic fields in the mixing chamber and combustion chamber for the case of unchoked injection was recognized. As pointed out in Chapter II, Tsuji and Takeno observed low amplitude oscillations upstream of the primary injector during sustained nonsteady burning in the combustion chamber. In order to ascertain the degree of steadiness

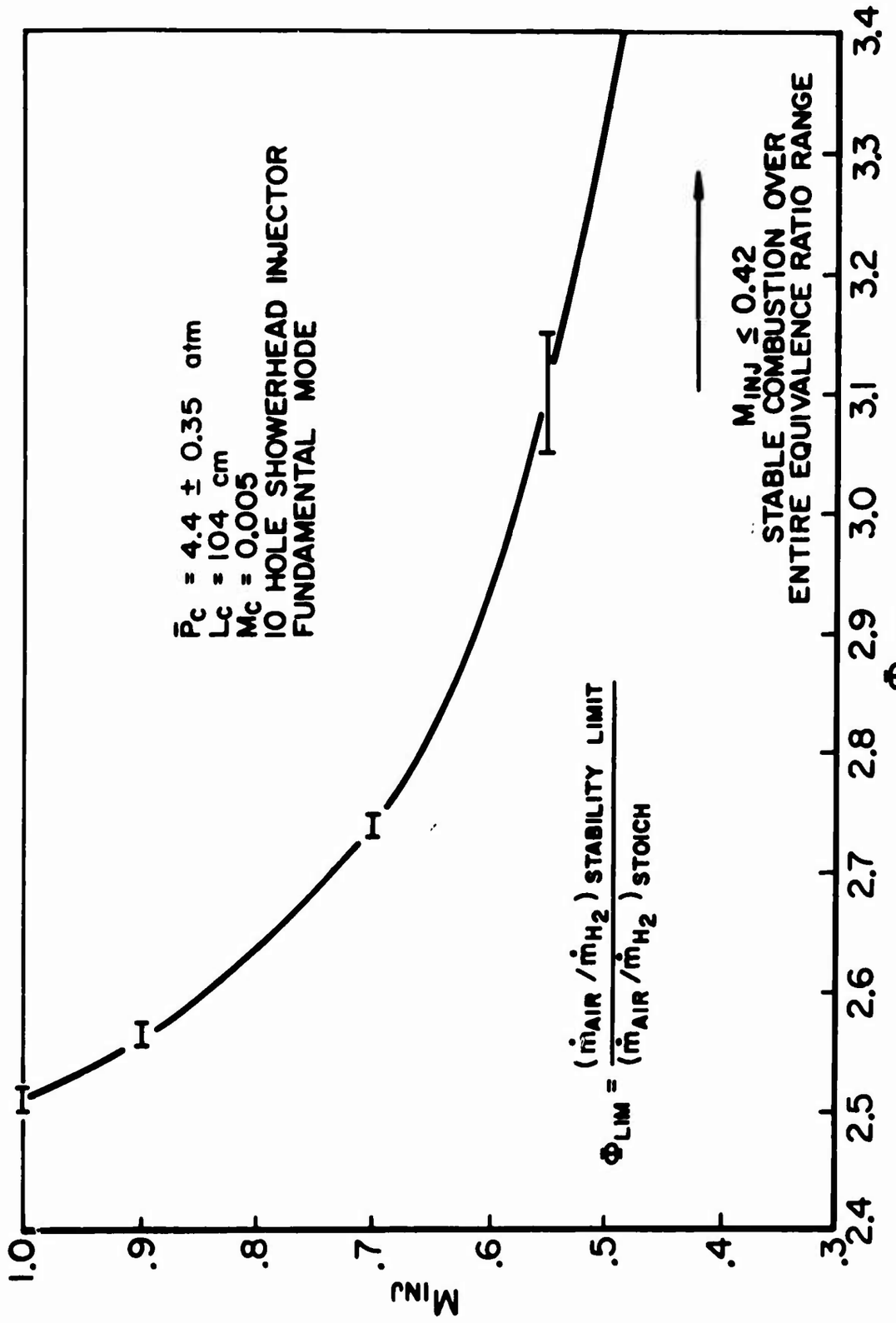

EQUIVALENCE RATIO AT THE STABILITY LIMIT, Φ_{LIM}, AS FUNCTION OF INJECTION MACH NUMBER FOR H_2+AIR

JP 13 R 4130 69

FIGURE V-31

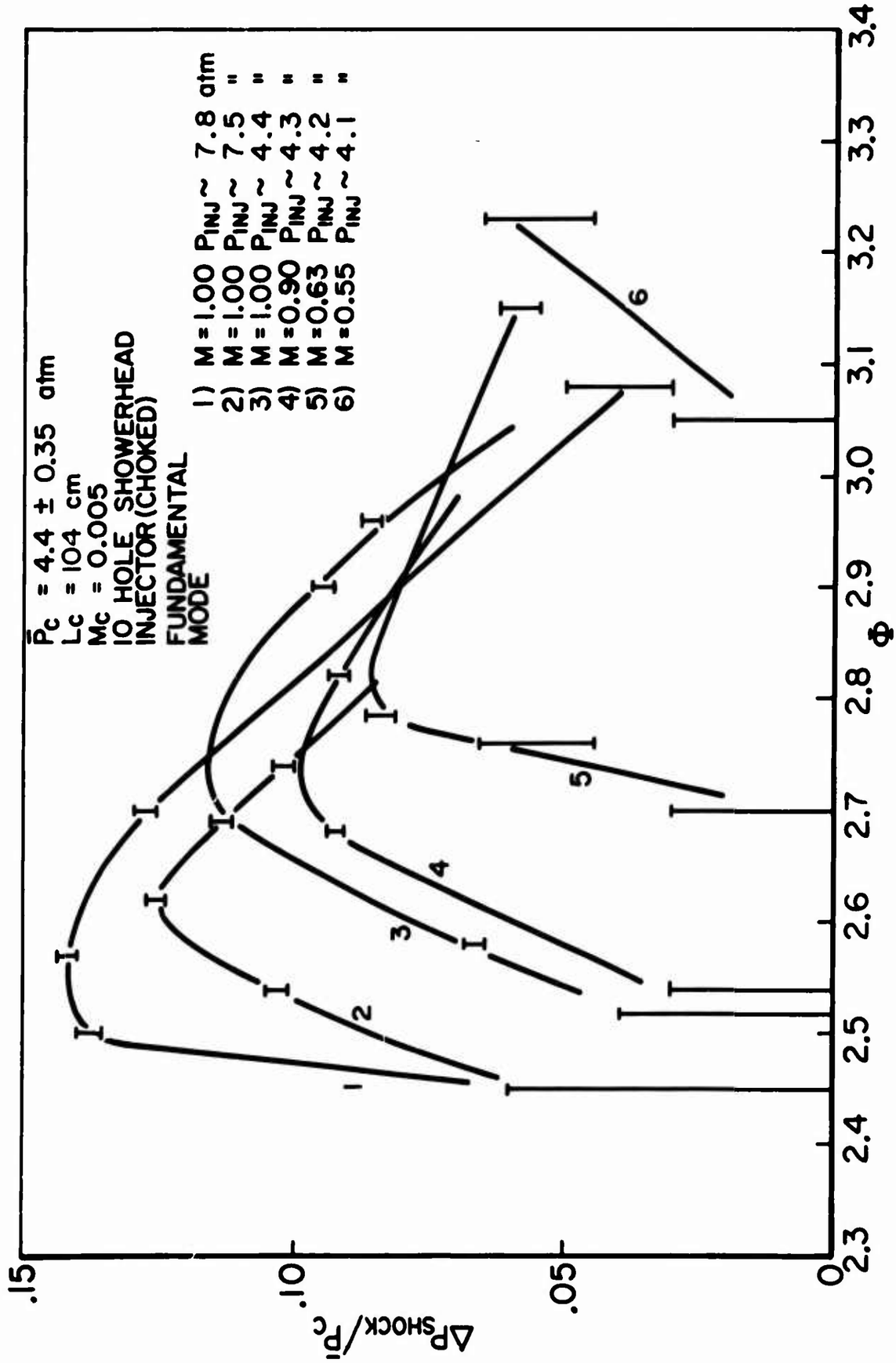

VARIATION OF SHOCK AMPLITUDE $\Delta P/\bar{P}_c$ v EQUIVALENCE RATIO Φ, AS A FUNCTION OF INJECTION MACH NUMBER FOR H_2+AIR

FIGURE V-32

of $\bar{p}^*_{mix}$ with unchoked injection the mixing chamber section was modified to allow placement of a Dynisco pressure transducer just upstream of the primary injector. No systematic oscillation in $\bar{p}^*_{mix}$ was observed in the course of the above experiments for both stable and unstable system operation. The absence of oscillations in $\bar{p}^*_{mix}$ was verified for choked and unchoked propellant injection.

The experimental results confirm the theoretically predicted stabilizing influence of decreasing (M_{inj}, p_{inj}). For $M_{inj} \leq 0.42$ corresponding to $\Delta p_{inj} = 0.5$ atm and $p_{inj} = 1.10$ stable combustion is observed over the entire range of Φ . For $M_{inj} < 1$ the amplitude of the sustained shock waves is markedly damped and decreases systematically with decreasing M_{inj}.

G.2 Preheated unburned propellant

The predicted influence of the ratio $\bar{\theta}_i = \bar{T}_i^*/\bar{T}_b^*$ on the system response can best be seen from Equation V-101 for the linearized stability limit. For the case of choked injection flux the factor $(1 - \bar{\theta}_i)$ appears explicitly in L and .
For the dilute mixtures near the H_2 + Air stability limits preheating the unburned gas essentially increases the burned gas temperature by an amount equal to the increment in $\bar{T}_u^*$. Figure V-33 shows the predicted ratio of $\bar{\theta}_i^*$ as a function of Φ for oxidizer rich mixtures of H_2 + Air at $\bar{P}_c^* = 7.8$ atm with the initial unburned gas temperature as a parameter. In view of the strong dependence of the predicted linear and nonlinear system response on the ratio $(1/\bar{T}_c)$, an increase in $\bar{T}_i^*$ accompanied by an increase in $\bar{T}_b^*$ leads to shorter $\bar{\tau}_c^*$ for fixed $\bar{T}_c$. Thus at each Φ an increase in $\bar{T}_i^*$ decreases both L and R. Figure V-34 shows the typical predicted influence on the oxidizer rich linear stability limit for the H_2 + Air system of preheating the unburned gas mixture. The shift of the stability limit to higher Φ with increasing preheat is observed. From Equation V-119 an increase in $\bar{T}_i^*$ is likewise seen to have a stabilizing influence on the nonlinear response in the sense that at fixed Φ, A becomes less negative with increasing $\bar{T}_i^*$.

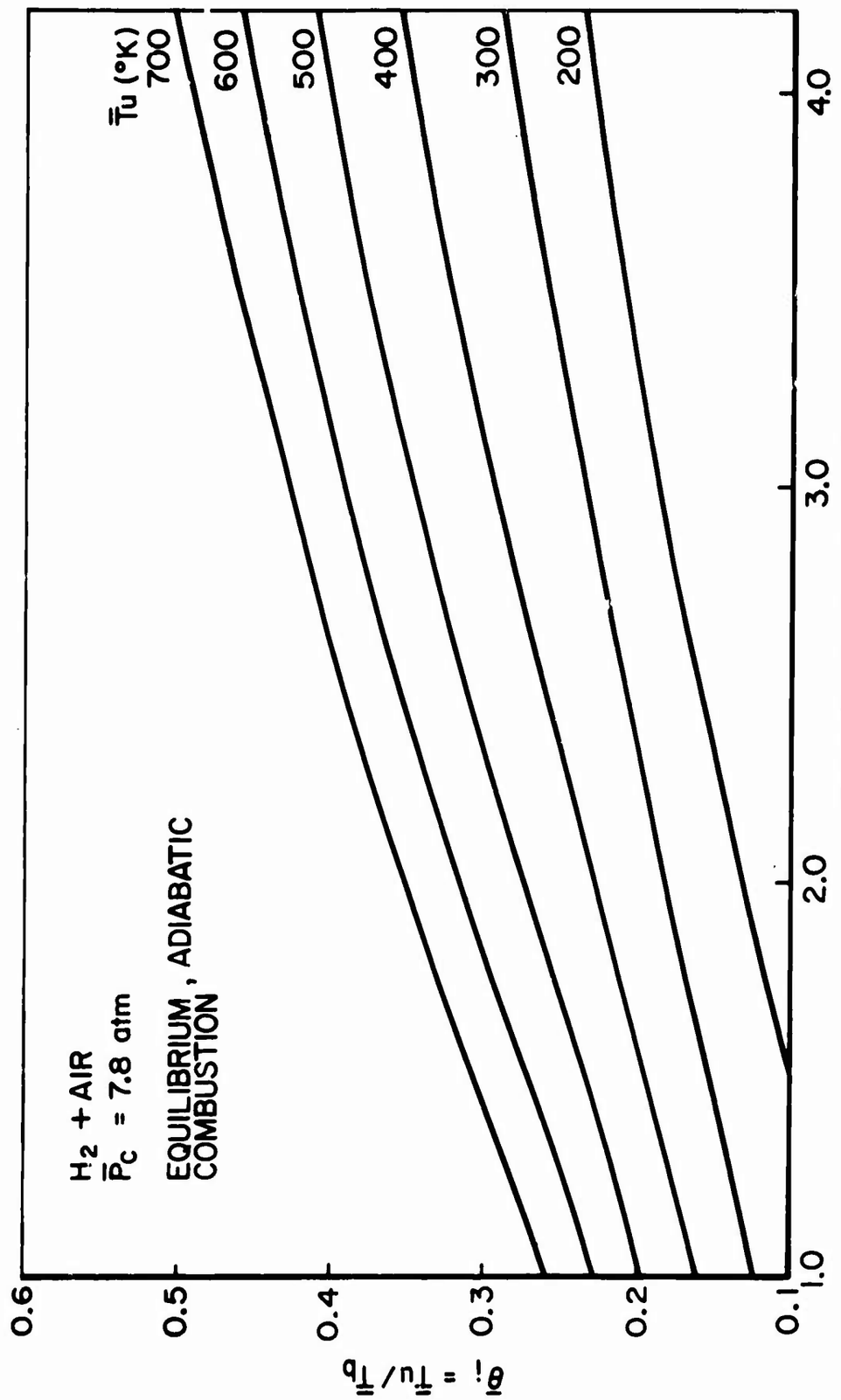

RATIO OF UNBURNED TO BURNED GAS TEMPERATURE ($\bar{\theta}_i$)
AS A FUNCTION OF EQUIVALENCE RATIO, Φ WITH $\bar{T}_u$ AS PARAMETER

FIGURE V-33

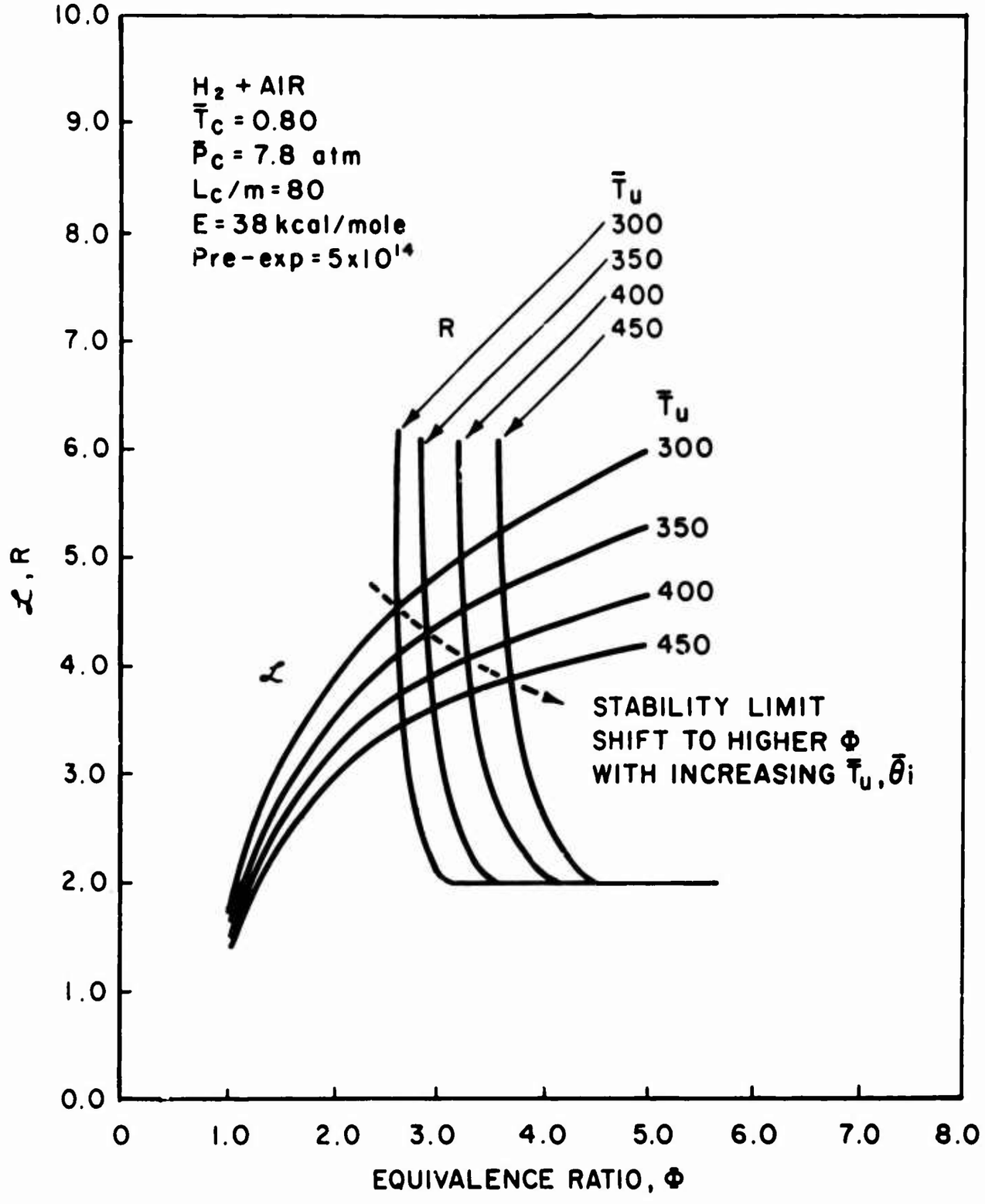

THEORETICAL PREDICTION OF STABILIZING INFLUENCE OF PREHEATING UNBURNED PROPELLANT MIXTURE

FIGURE V-34

In order to test the theoretical prediction of the stabilizing influence of preheating the unburned gas mixture a heat exchanger was installed in the air line of the propellant flow system upstream of the mixing chamber. The heat exchanger and the mixing chamber were electrically insulated, wrapped with resistance wire, and thermally insulated. In view of the long residence time of the gas in the mixing chamber (θ(0.2 sec)) and the previously verified homogeneity of the unburned gases at the downstream and of the mixing chamber it was felt that thermal equilibration should also be achieved between the preheated air and unheated H_2 propellant. A copper-constantan thermocouple placed 0.6 cm upstream of the primary injector allowed the unburned gas temperature to be monitored continuously during the experiments.

The system allowed the determination at fixed Φ of the effect of a systematic increase in $\overline{T}_i{}^*$ and $\overline{\theta}_i$. Figure V-35 summarizes the principal results of this investigation. For a typical case, at Φ = 2.6, a 30% increase in the unburned gas temperature from 300°K to 400°K results in a 25% increase in temperature ratio. The fundamental mode shock type oscillation sustained in the absence of preheat is completely suppressed with preheating of the unburned mixture. The experimental results are seen to confirm the theoretically predicted decrease in shock amplitude at fixed Φ and the accompanying strong shift in the stability limit to higher Φ with increasing preheat.

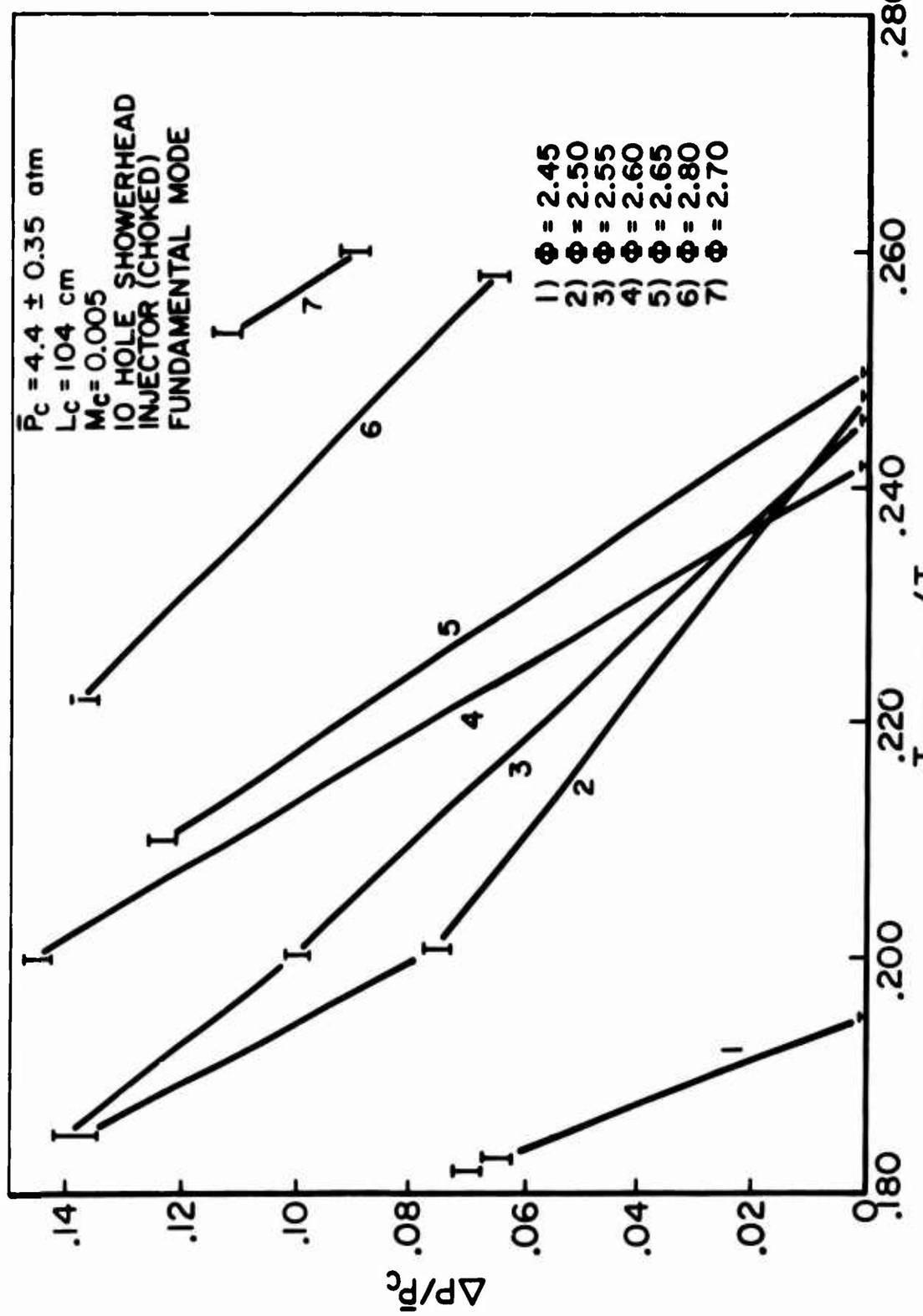

VARIATION OF SHOCK AMPLITUDE, $\Delta P/\bar{P}_c$, WITH RATIO OF TEMPERATURES OF UNBURNED AND BURNED GASES, T_U/T_B, AT 7 EQUIVALENCE RATIOS FOR H_2 + AIR

FIGURE V-35

CHAPTER VI: Discussion and Conclusions

A. General Summary

To summarize, this research effort has been directed toward the goal of developing a consistent experimental and theoretical description of the phenomenon of intrinsic unstable combustion in a gaseous propellant rocket motor. A determination was sought of the contribution of gas phase rate processes (in particular chemical kinetics) to the coupling of a finite dimensioned turbulent combustion zone and finite amplitude longitudinal mode pressure oscillations. The inadequacy of the original Sirignano-Crocco theory in effecting an explanation for the stability characteristics of the system observed experimentally by Pelmas (29) and Bowman (32) provided the immediate background for the present work.

Initial investigations with the $CO(H_2O)/O_2/N_2$ propellant system have confirmed the critical importance of the mean combustion temperature in determining the onset of nonsteady burning. As previously observed in the $H_2/O_2/N_2$ and $CH_4/O_2/N_2$ systems, the spontaneous transition from a region of stable system operation located about the stoichiometric mixture ratio for the $CO(H_2O)/O_2/N_2$ system to a regime of nonsteady combustion characterized by finite amplitude, constant frequency, longitudinal mode pressure oscillations occur at approximately fixed combustion temperature independent of the relative dilution of the combustible mixture. Subsequent experiments in which trace amounts of CH_4 (known to have an inhibiting effect on the overall rate of reaction in the $CO(H_2O)/O_2$ system) were added to the $CO(H_2O)/O_2/N_2$ mixtures have shown conclusively the dominant influence of the propellant chemistry on the linear and nonlinear system response.

The results of the work with the CO system underscored the necessity to develop a suitable model of the nonsteady combustion process. Parallel experimental and theoretical investigations

have culminated in the development of an analytical model which successfully predicts the observed stability characteristics of the gas rocket. The results of the theoretical model correctly reflect the dependence of the linear and nonlinear system response on (a) the propellant chemistry including the characteristic (chemical kinetic) combustion time and the mean combustion temperature or equivalence ratio; (b) the harmonic mode order; (c) the chamber length, mean chamber Mach number, and combustion pressure; and (d) the propellant injection Mach number

B. Discussion of Theoretical Model

It is appropriate to briefly review the principal ingredients and results of the analytical model developed in Chapter V and to point out the influence of the diagnostic experiments which were carried out in support of the analytical work.

Three distinct aspects of the nonsteady gas rocket operation were treated analytically. These include descriptions of (a) the wave dynamics in the high aspect ratio combustion chamber; (b) the nonsteady nozzle behavior; and (c) the steady combustion process and the coupling of the burning rate and the pressure waves. The results of a series of diagnostic experiments served to justify the treatment of the wave dynamics according to techniques developed by Mitchell and Crocco [34]. The analysis applies to the case of longitudinal mode instability in a rocket combustor where the mean chamber Mach number is small. In particular the analysis is restricted to the case where the mean chamber Mach number serves as a measure of the steady state level of combustion as well as the mean nozzle outflow. Under these circumstances the interaction between the combustion zone processes and the pressure oscillation is of second order such that to lowest order the acoustic equations describe the flow field. The analysis was simplified further for the case where the combustion zone and nozzle effects are (spacially) concentrated at the chamber extremities thereby allowing the combustion and nozzle influences to be applied as boundary conditions on

the acoustic equations in the homentropic flow field. Consideration of the steady state operating characteristics of the gas rocket combined with the measurement of radial and axial steady state temperature distribution within the combustion zone and direct, schlieren, and shadow photographs of the steady and nonsteady combustion of H_2 + Air have shown that the combustion process in t' - gas rocket satisfies these requirements of the Mitchell-Crocco analysis. The mean chamber Mach number is of the order of .02. For fixed Φ a doubling of the Mach number by means of halving the nozzle contraction ratio requires a doubling of the total mass throughput (energy release) in order to maintain fixed chamber pressure. Similarly a 70% increase in total mass flow is required to increase the mean chamber pressure by 75%. The temperature profiles and photographs established that while a systematic increase in the axial extent of the combustion zone occurs as the adiabatic combustion temperature of the propellant mixture is decreased, the mean mass throughput increased, and the number of injection holes decreased, the overall length of the combustion zone remains short compared to the total chamber length. Use of a four-holed plug nozzle served as a practical approximation to the short nozzle (constant Mach number at the nozzle entrance) assumed analytically.

Closure of the analytical problem was achieved by the development of an expression for the instantaneous perturbation in the mass efflux from the finite-dimensioned combustion zone in terms of the pressure perturbation. The mass efflux perturbation which is simply related to the effective velocity perturbation at the injector, supplied the appropriate combustion zone boundary condition required in the Mitchell-Crocco analyses. The derivation of the combustion zone boundary condition relies upon the characterization of the (finite volume) combustion zone in terms of mean thermodynamic and gas dynamic properties which represent averages of the distributed quasi one-dimensional turbulent combustion zone.

In view of the preponderance of experimental instability data having been obtained with choked showerhead injection for the H_2 + Air propellant system, a major experimental and analytical effort was devoted to (a) experimentally characterizing the principal aspects of steady and nonsteady combustion of H_2 + Air with showerhead injection; and (b) combining the results of the experimental diagnostics with current knowledge of high intensity turbulent jets and combustors, and overall chemical kinetic rate laws in order to provide a rational basis for considering the process in terms of volume averaged mean properties.

The diagnostic experiments collectively showed that, for the case of choked showerhead injection, the combustion zone is characterized by the existence of distributed high intensity turbulent reaction zones centered at each injection port and extending from the port axially 1 to 4 cm into the combustion chamber. From the temperature measurements and the direct photographs it appeared that reaction is completed with the attainment of the equilibrium adiabatic combustion temperature within the mixing zone of the high velocity expanding jet. The region surrounding the turbulent burning zone is filled with recirculating combustion products slightly cooled by contact with the chamber walls. The central underexpanded, supersonic zone of cool, unburned premixed propellants was observed to extend 0.5 to 1 cm into the surrounding combustion zone. On the basis of the instantaneous and high speed shadow and schlieren photographs there appeared to be no intrinsic fluid dynamic jet unsteadiness associated with this underexpanded unburned gas zone during conditions of stable and unstable operation. Axial temperature profiles and spark schlieren photographs of steady combustion revealed a systematic lengthening of the overall burning zone as the unburned propellant mixture was leaned for initially oxidizer rich mixtures. High speed 16 mm schlieren photographs of the nonsteady combustion of oxidizer rich mixtures of H_2 + Air have shown that the finite dimensioned com-

bustion zone volume is itself nonsteady in the presence of sustained shock type instabilities and oscillates in size at precisely the same frequency of the pressure oscillation. The magnitude of the volume oscillation diminishes with decreasing shock wave amplitude and is absent during steady combustion. The shock wave passage very nearly corresponds to the observed minimum in the volume oscillation.

These data plus several basic considerations regarding the steady combustion process in the gas rocket provided sufficient insight for the formulation of a model of the overall burning process. For the typical case of choked high velocity ($\Theta(2\times10^4$ cm/sec)), high Reynolds number ($\Theta(10^6$ to $10^7)$) propellant injection where the ratio of combustion chamber cross-section to total injector port area is $\geq \Theta(150/1)$ it was shown that:

(a) The estimated space heating rate for the gas rocket approaches the level predicted for the so-called well stirred combustors where a vigorous mixing of hot combusted products and fresh unburned reactants sustains the combustion process

(b) Simple one-dimensional momentum considerations of the injection-combustion geometry indicate a strong pressure driving force for recirculation of product gases to the injector face

(c) The high velocity propellant jet has a high entrainment capacity and rapidly ingests recirculated product gas into the developing mixing zone

An analysis was completed for the case where the combustion zone is treated as a quasi one-dimensional distributed turbulent combustion zone stabilized at the injector by the recirculation of hot product gases and the intense mixing of products and reactants. A Spalding-type mass entrainment law where the rate of mass entrainment by a high velocity expanding jet is proportional to the inlet jet momentum and the density of the gas being entrained was used to provide a reasonable expression of the axial jet development. Overall reaction rate data from turbulent flow reactor studies was used to calculate the local

energy release rate due to chemical kinetics in terms of local temperature, species concentration, and density. For moderate entrainment of burned gases (assumed to be at the adiabatic combustion temperature) the jet is rapidly heated and the distribution of reaction arises primarily due to the action of finite kinetic rates in the high velocity field. The validity of considering the combustion process in terms of mean properties of the distributed zone for the described system was shown. The process of high intensity combustion in the gas rocket was shown to be analogous to that occurring in the so-called tunnel burners and well-stirred combustors and was distinguished from "conventional" turbulent burner flames stabilized due to heat and mass transfer from the combustion zone by the processes of turbulent conduction and diffusion. Numerous examples were cited (from the experimental work) of the importance of the properties of the recirculation zone in determining the steady and nonsteady operating characteristics of the gas rocket. Finally, the consideration of the turbulent combustion process in the case of unchoked porous plug injection in terms of mean thermodynamic and gas dynamic properties was justified on the basis of the observed nonuniformity of plug porosity, the fine scale of the pore mesh, and the observed similarity between the stability characteristics of the $CH_4/O_2/N_2$ system with showerhead and porous plug injection.

The combustion zone boundary condition was formulated for the case when the finite combustion zone volume is characterized by mean thermodynamic properties. By virtue of the short extension of the combustion zone relative to the chamber length the approximation of spacially uniform pressure across the combustion zone is valid. The experimentally observed steadiness of the axial extent of the unburned gas zone was incorporated as an assumption in the model. The unburned gas temperature (T_i) was assumed to be insensitive to the pressure oscillations. Entropy waves due to the nonsteady combustion process were assumed to be rapidly dispersed near the injector end. The mean combustion zone properties and the combustion

zone volume were assumed to be time variant and were expressed as linear power series expansions about the steady state mean values. The possible sensitivity of the injection mass flux of unburned propellant to the nonsteady pressure at the injector in the case of unchoked flow was accounted for by expressing the instantaneous flux in a Taylor series expansion about the steady state value. For choked propellant injection the mass influx is insensitive to the pressure oscillations. For the case of unchoked injection the mass influx is strongly coupled to the pressure oscillations and, due to the low inertia of the gas system, always oscillates 180^{o} out of phase with the pressure oscillation.

The equations of mass and energy conservation for the finite combustion volume, V_c, were combined to eliminate the mass efflux $\dot{m}$ and to obtain an expression for $\rho_c V_c$ which in turn was used in the mass conservation equation written for an arbitrary control volume $A \cdot \ell$ where the condition $A \cdot \ell > V_c(t)$ is observed. This latter equation resulted in an explicit relationship between the effective mass efflux from the combustion zone extrapolated to the injection (x = o) face and the important combustion zone variables.

In order to perform the above operations the source term in the energy equation was expressed in terms of the (assumed constant) heat of combustion per unit mass of mixture and the "mixture" mass reaction rate. Under the approximation that the mixing time (between products and reactants) is short compared to the characteristic reaction time, the residence time of gases in the combustion zone is equivalent to the characteristic combustion time due to finite rate kinetics. Hence, $\dot{q} = q\dot{m}_b = q(\rho_c A_c \cdot U_c) = q \cdot \frac{\rho_c V_c}{\tau_c}$ where τ_c was identified as the characteristic combustion time. τ_c is essentially a measure of the mean rate of energy release due to combustion. An expression for $\frac{\rho_c V_c}{\tau_c}$ was derived from an approximation of the burning rate by means of a second order overall Arrhenius rate law in terms of the average combustion zone properties. A simple formulation for τ_c followed naturally and facilitated the use of the most relevant overall chemical kinetic rate data obtained in turbulent flow reactor

studies in order to calculate the steady state value of $\bar{\tau}_c$. The validity of this approach, in particular the recourse to flow reactor data to obtain the empirical constants necessary for the calculation of numerical values of $\bar{\tau}_c$ should be reemphasized. It was noted that overall chemical kinetic rate data is generally correlated by expressing the mass consumption rate of "fuel" (e.g., H_2, CO, CH_4) per unit volume in terms of empirical data fit parameters including (1) the pre-exponential factor; (2) reaction orders with respect to fuel and oxidizer concentrations; and (3) an overall activation energy. The fundamental parameter arising from such overall rate experiments is the overall rate of consumption of fuel species as a function of the mean temperature. Taken out of context a "measured" overall activation energy for a given reaction is of no fundamental significance in determining the overall mean burning rate or mean characteristic kinetic time. (The overall activation energy is, however, of independent significance in determining the response of a combustion system to changes in the mean reaction temperature). It was shown for the $CH_4/O_2/N_2$ system that the measured overall rate data extracted from the turbulent flow reactor studies is in good agreement with data obtained in other systems.

Fluctuations in the characteristic combustion time were coupled to oscillations in the combustion pressure and the mean combustion zone temperature. Insensitivity of the combustion time to oscillations in the thermodynamic properties of the combustion zone was shown to preclude the support of combustion chamber oscillations. The instantaneous value of $1/\tau_c$ was expressed by a linear expansion about the steady state value with perturbations of order M, that is

$$\frac{1}{\tau_c} = \frac{1}{\bar{\tau}_c}\left[1 + \Sigma_1\right] \qquad \text{where} \qquad \Sigma_1 = \Theta(M)$$

$$\text{or} \quad \tau_c = \bar{\tau}_c + \tau_{c_1} \qquad \text{where} \qquad \tau_{c_1} = -\bar{\tau}_c \Sigma_1 \qquad \text{(V-59)}$$

$$\text{where} \quad \tau_{c_1} = -\bar{\tau}_c\left[\Sigma_T T_{c_1}(t) + \Sigma_\rho \rho_1^\circ(t)\right] \quad \text{and} \quad \Sigma_T = \frac{1}{\bar{\tau}_c}\frac{\partial \ln 1/\bar{\tau}_c}{\partial \ln \bar{T}_c}$$

$$\Sigma_\rho = \frac{\partial \ln 1/\bar{\tau}_c}{\partial \ln \bar{\rho}_c}$$

The influence of perturbations in the species mass fractions and the burned gas temperature was examined for two alternative formulations. The use of quasi-steady temperature explicit formulations for $\sigma_{f,c}$ and $\sigma_{ox,c}$ together with the neglect of perturbations in T_b was found (Appendix B) to be sufficiently accurate for the determination of the linear system response. Considerable simplification results from these approximations. The fact that results obtained using the quasi-steady formulation differ only slightly from results obtained using more exact expressions (including a statement of species conservation) is a consequence of the overriding importance of the exponential term in the Arrhenius factor in the overall burning rate law. That oscillations in $T_b(t)$ are small and of minor importance follows from the distinction made between the averaged (time dependent) combustion zone temperature $T_c(t)$ upon which the burning rate depends and the fact that $\bar{T}_c \simeq \bar{T}_b$.

In order to complete the model a relationship was needed to couple oscillations in the combustion temperature and pressure. It was pointed out that a penalty is exacted for treating the combustion process in terms of approximate averaged values; namely, that information about the time history in the Lagrangian sense of following a parcel of gas through the finite-dimensioned combustion zone is lost. A consequence of the method is that the combustion temperature, pressure, and volume remain implicitly coupled to all orders. To lowest order $\bar{T}_c = \bar{T}_c^*/\bar{T}_b^*$ appeared as a parameter. The system was analyzed for several choices of $\bar{T}_c$. To first order the implicit relationship between T_{c_1}, p_1° and v_{c_2} (perturbations in temperature, pressure, and volume) was obtained. The functional relationship between T_{c_1} and p_1° was expressed in terms of amplitude and phase of the volume oscillation for the case of linear oscillations, 2π periodic in time. In principle, experimental measurement of the phase and amplitude of the volume oscillations as a function of Φ (i.e., $\bar{\tau}_c$) would be sufficient to allow a calculation of $T_{c_1}[p_1^\circ, \bar{\tau}_c]$. Several specific

cases were examined in detail for the H_2 + Air system. The experimental observation of large dimensionless oscillations in the combustion zone "extent" where the amplitude peaked at π to $\frac{2\pi}{3}$ radians prior to passage of the low amplitude shock wave was shown to be consistent wit' theoretically predicted regime of strong temperature response.

The combustion zone boundary condition was derived in general form for the case where $\tau_{c_1}(t) = \eta e^{-i\epsilon_{\tau p}} p_1^{\circ}(t)$ where η is a real amplitude factor and $\epsilon_{\tau p}$ a finite phase angle. The important consequence of a lag $\epsilon_{\tau p}$ in the combustion temperature oscillation relative to the pressure oscillation was indicated.

A second alternative heuristic formulation of τ_{c_1} according to

$$\tau_{c_1} = -\Sigma_\tau \int_{t-\bar{\tau}_c}^{-t} \tau_{c_1}(t')dt' - \Sigma_p \int_{t-\bar{\tau}_c}^{t} p_1^{\circ}(t')dt' \qquad \text{(C-4)}$$

was discussed in Appendix C. .The results of that analysis are essentially equivalent to the analysis of Chapter V for the case of finite

Application of the combustion zone boundary condition derived for both expressions of τ_{c_1} to the analyses of the wave dynamics led to the formulation of a nonlinear ordinary integro-differential equation governing the form of the wave amplitude parameter f which is proportional to the dimensionless pressure perturbation at the injector according to

C. Principal Results of the Theoretical Analysis

For the case where τ_{c_1} is coupled to the oscillations in temperature and pressure by Equation V-59, the linearized form of the final governing equation for the wave amplitude parameter was solved to obtain the linear system response. The full non-linear form of the equation was solved by a numerical iterative technique based on the method of successive approximation to obtain the non-linear response.

For the $H_2/O_2/N_2$ system a determination of the system linear response in terms of the predicted linear stability limits as well as the nonlinear response in terms of the predicted shock-type wave amplitude and waveforms within the regime of nonlinear instability was achieved. In addition the linear stability characteristics of the CH_4/Air system were determined. These analyses were carried out for the case of choked injection.

Detailed numerical results for the linear and nonlinear system response were presented for the particular case where $\epsilon_{\tau f} = 0$. The influence of finite $\epsilon_{\tau p}$ (e.g., $\epsilon_{\tau p} = 0\,(\frac{\pi}{4} + 0\,\frac{\pi}{2})$) on the predicted linear stability characteristics was emphasized. Finally, an examination of the predicted linear stability characteristics for the H_2/Air system for the case where γ_c, is specified by equation C-4 was completed. It is appropriate to review the important aspects of these theoretical results in light of the accumulated experimental data.

A significant aspect of the theoretical results is the dominant influence on the linear and nonlinear response of the ratio of the characteristic combustion time $\bar{\gamma}_c^*$ to the wave travel time (defined as $L_c^*/m\bar{C}_b^*$ or ½ the period of oscillation where L_c^* is the chamber length, $\bar{C}_b^*$ the burned gas sound speed, and m the harmonic mode order). The rather remarkable quantitative and qualitative agreement between theory and experiment is attributed to the influence of the important system variables (including the propellant equivalence ratio and combustion temperature, the % dilution of the unburned gas mixture and the unburned gas temperature, the overall activation energy for the fuel-oxygen mixture, the chamber length and the harmonic mode order) on this ratio of characteristic times.

For the case where γ_c, was expressed by equation V-59 and $\epsilon_{\tau p} = 0$ a single linear stability limit was found to correspond to an approximately fixed critical ratio of ($\bar{\gamma}_c^* / \gamma^*_{wave}$), independently of the propellant equivalence ratio, % dilution, chamber length, and mode order. The system was predicted to be linearly unstable for ($\bar{\gamma}_c^* / \gamma^*_{wave}$) $\geq$ ($\bar{\gamma}_c^* / \gamma^*_{wave})_{lim}$. For the $H_2/O_2/N_2$ system and a mean combustion temperature of 0.8 $\bar{T}_b^*$, this

critical factor was found to be σ (0.2 to 0.3) while the CH_4/Air system showed a critical ratio σ (0.15 to 0.25). It is of interest to note that experimentally (see Figure V-3) the measured period of the fundamental mode oscillation at the stability limit for the H_2/Air system increases from 5.5×10^{-4} sec to 2.37×10^{-3} sec as the chamber length is increased from 19 cm to 76 cm. Concurrently a shift in the equivalence ratio at the measured stability limit (Φ_{lim}) from 2.2 to 2.5 occurs. From measured overall kinetics rate data for the H_2/Air system (see Figures D-1 and 5) for $\bar{T}_c = 0.80$ the shift in Φ_{lim} corresponds to a calculated increase in the characteristic combustion time from 1.1×10^{-4} sec to 4.4×10^{-4} sec. Thus, at L_c = 19 cm, $\Phi_{lim,1} = 2.2$, and $\bar{\tau}_c^*/\tau_{wave}^* = 0.40$ while at L_c = 76 cm, $\Phi_{lim,1} = 2.5$, and $\bar{\tau}_c^*/\tau_{wave}^* = 0.37$. In other words, comparison of experiment and theory shows excellent agreement with respect to the theoretical prediction of a constant ratio of $\bar{\tau}_c^*/\tau_{wave}^*$ at the stability limit. An additional inference drawn from the linearized analysis was the conclusion that the stability limit should be sharply defined in terms of Φ_{lim} due to the strong sensitivity of the characteristic combustion time to the equivalence ratio through the mean combustion temperature. It was pointed out that experimentally a marked sensitivity to small changes in Φ near the stability limit is observed.

The results of the linearized analysis were translated into theoretical predictions of the stability limits for the $H_2/O_2/N_2$ and CH_4/Air systems in the conventional Φ-L_c plane. Comparison of theory and experiment showed excellent quantitative and qualitative agreement for the H_2/Air system with respect to:

(1) The existence of two regimes of nonsteady burning located about the stoichiometric mixture ratio

(2) The progression to lower harmonic mode order for fixed L_c and increasing Φ and the progress to higher harmonic mode order at fixed Φ and increasing L_c

(3) The absence of an "upper length (L_c) limit" and the collapse of the stability limits toward the stoichiometric mixture ratio at short chamber lengths

(4) The prediction of a slight difference in the adiabatic combustion temperature at the fuel rich and fuel lean limits

(5) The marked shift of the stability limits toward the stoichiometric mixture ratio with increasing dilution of the unburned gas mixture.

Comparison of theory and experiment showed good agreement for the CH_4/Air system with respect to:

(1) The existence at short chamber lengths of a single regime of nonsteady burning located at and around the stoichiometric mixture ratio and the shift of the limits away from the stoichiometric mixture ratio at longer chamber lengths.

(2) The ordering of harmonic modes and the absence of an upper length limit (see Figures II-7 and V-17)

The unique behavior of the H_2/Air and CH_4/Air systems was attributed to the inherently slower overall chemical kinetics of the CH_4/O_2 system. The condition of $(\bar{\tau}_c/\tau_{per}) \geq (\bar{\tau}_c/\tau_{per})_{lim} = \mathcal{O}(0.1 \text{ to } 0.3)$ is satisfied at higher combustion temperatures (closer to the stoichiometric mixture ratio) for systems characterized by slower overall reaction rates (e.g., the CH_4/Air system as compared to the H_2/Air system).

An additional rather interesting observation follows from a consideration of the experimental results with the $CO(H_2O)/O_2/N_2$ and $CH_4/O_2/N_2$ systems in light of the analytical results and the available overall reaction rate data for the two systems (see Table IV, Figure IV-1, and Appendix D). Experimentally the the stability limits for both systems were found to lie at off-stoichiometric mixture ratios for oxygen enriched combustion $[O_2]/[N_2] > 0.2$. With increasing dilution the stability limits were observed to shift toward $\Phi = 1$ with nonsteady combustion at $\Phi = 1$ in the case where air served as the oxidizer. It was concluded from a review of the literature on the kinetics of CO and CH_4 oxidation at high temperatures that the overall consumption of CH_4 is dominated by the reaction kinetics associated with the oxidation of CO formed as a long-lived intermediate in the CH_4/O_2 reaction scheme. In agreement with this observation, extrapolation of rate data for CO/O_2 and CH_4/O_2 systems to high temperatures

(Figure D-6) indicates that at temperatures in excess of 1600°K to 1800°K the overall oxidation of CO should be rate limiting. While calculations for the linear stability characteristics of the $CO/O_2/N_2$ system were not carried out, it is clear that the similarity between the experimentally observed stability characteristics of the $CO/O_2/N_2$ and $CH_4/O_2/N_2$ systems is precisely what would be expected on the basis of present knowledge of the overall kinetics of these systems and the theoretical prediction of the critical importance of the characteristic combustion time due to kinetics (in determining the nonsteady burning characteristics). The experimentally observed shift of the stability limit for the $CO/O_2/N_2$ system toward the stoichiometric mixture ratio upon the addition of trace amounts of CH_4 to the unburned gas mixture is likewise in agreement with the (kinetically predicted) inhibiting influence of small amounts of CH_4 to slow the overall oxidation rate of CO. If the inhibiting effect of CH_4 is interpreted as an increase in the overall activation energy the observed shift in the limits is consistent with the theoretical prediction of the linearized stability limit shift arising from an increase in the activation energy.

The nonlinear stability characteristics of the system were analyzed for the H_2/Air system for the case where was given by V-59 and $\epsilon_{TP} = 0$. An iterative technique originally due to Sirignano (81) was adapted with some modification to the numerical solution of the nonlinear ordinary differential equation governing the wave amplitude parameter (f). The criteria for the existence of discontinuous shock-type solutions for (f) were determined. The nonlinear stability limit and the predicted discontinuous shock-wave amplitude and wave form at the injector end were determined in terms of the ratio of characteristic times ($\bar{\tau}_c^* / \tau_{wave}^*$), the propellant equivalence ratio, and the ratio of chamber length to mode order, (L_c^*/m). The results showed the important influence of the ratio $\bar{\tau}_c^* / \tau_{wave}^*$ on the predicted nonlinear system

response. The nonlinear stability limit was found to be at somewhat lower values of $\bar{\tau}_c^*/\tau_{wave}^*$, $(\bar{\tau}_c^*/\tau_{wave}^*)_{lim}$ = $\sim$(.19 to .25) where a slightly larger decrease in $(\bar{\tau}_c^*/\tau_{wave}^*)_{lim}$ was observed at the nonlinear limit with increasing Φ and L_c^*/m. In agreement with the experimental results and as suggested by the linearized analysis, the nonlinear limit was sharply defined in the sense that a rapid increase in shock amplitude was predicted for increasing Φ (increasing $\bar{\tau}_c^*/\tau_{wave}^*$) near the limit. Predicted shock-wave amplitudes at the injector and were found to be in good agreement with experimental observations. As observed experimentally the predicted shock-type wave form approached the ramp-type waveform as displacement for the nonlinear limit increased. Near the nonlinear limit the waveform was found to be concave upward also in agreement with experimental data. From the discovery that nonlinear solutions for the pressure waveform were found to exist in a region near the linear limit predicted to be linearly stable and that the solutions converged to waveforms having zero amplitude shocks or cusps at the nonlinear limit, it was argued that one should be able to find continuous finite amplitude solutions to the nonlinear equation. It was inferred that these low amplitude continuous solutions must arise due to a weak triggering of the nominally steady system near the nonlinear limit. Practically, such triggering influences could be attributed to random pressure fluctuations within the intense turbulent combustion zone.

The influence on the linear and nonlinear system response of the combustion distribution was suggested to follow from the effect of $\bar{T}_c$ on the predicted results. Implicit in the aforementioned analytical results was the assumption that $\bar{T}_c$ was a constant over the range of variables examined. Larger values of $\bar{T}_c$ lead to a shift of the linear and nonlinear stability limits away from the stoichiometric mixture ratio.

The theoretical prediction of the existence of a regime of nonsteady burning for $\bar{\tau}_c^*/\tau_{wave}^* \geq \Theta(.15 \text{ to } .3)$ and the failure to predict a maximum of the dimensionless shock strength with increasing displacement ($> \bar{\tau}_c^*$) from the stability limit suggested the consideration of the heuristic expression for τ_{c_1} (Equation C-4) and, in addition, the examination of the influence on the linear stability characteristics of finite ϵ_{Tp} according to the original formulation.

For the integral expression of τ_{c_1}, it was shown that the form of the governing equation for the stability limit was identical to that of the "linear" τ_{c_1} formulation with the exception that additional terms which are small for small $\bar{\tau}_c$ exerted a strong stabilizing influence at larger $\bar{\tau}_c = \Theta(1)$. That is, the accumulated linear and nonlinear results obtained from the linear τ_{c_1} analysis remained essentially valid at the "lower" stability limit. However, an additional upper (equivalence ratio) limit was predicted at each L_c^*/m. The system was predicted to be linearly unstable within a narrow range of the characteristic time ratio such that,

$$\left(\bar{\tau}_c^*/\tau_{wave}^*\right)_{lower} \leq \left(\bar{\tau}_c^*/\tau_{wave}^*\right) \leq \left(\bar{\tau}_c^*/\tau_{wave}^*\right)_{upper}$$

The results allowed a definite statement of which harmonic mode is sustained at each Φ. A distinct separation of harmonic mode regimes followed. In addition, the linearized results predicted the existence of a lower length limit or equivalently a minimum Φ (for the H_2/Air system) at which nonsteady burning is possible. Although a nonlinear analysis was not carried out a simple extension of the numerical technique to allow solution of the more complicated governing nonlinear ODE is possible. This extra effort is probably not warranted since the linear analysis clearly implies the existence of a shock amplitude maximum for $\bar{\tau}_c^*/\tau_{wave}^*$ intermediate between the limit values with a decay to zero amplitude at the limits.

Entirely equivalent results were obtained for the case of finite phase angle of the temperature oscillation with respect

to the pressure oscillation (ϵ_{TP}) according to the analysis of Chapter V. The linear system was found to admit a similar resonance for $\bar{\tau}_c = \Theta(1)$ with stable operation for H_2/Air at very short and at long $\bar{\tau}_c$.

The analytical work was completed with an investigation of the influence of unchoked propellant injection and preheating of the unburned gas mixture on the predicted linear stability characteristics.

Theoretically, the linear stability limit was found to shift systematically to higher equivalence ratio with decreasing injection Mach number or decreasing injection pressure ratio ($\bar{P}_{inj} = \bar{P}_{mix}/\bar{P}_c$). For sufficient decrease of $\bar{P}_{inj}$ a condition of stable combustion for all $\bar{\Phi}$ was predicted. It is important to note that this prediction runs counter to what one might infer on the basis of experience with liquid propellant rocket motors where it is found that decreasing the injection pressure drop tends to be destabilizing. That is, low frequency longitudinal modes in liquid motors can be suppressed by increasing the pressure drop across the injector. The basic difference between the gaseous and liquid propellant systems in this regard lies in the fact that the gaseous system (in the case of unchoked injection) should respond rapidly to fluctuations in the injection pressure drop whereas the massive liquid flow system responds slowly with important time lag effects.

The prediction that the coupling of the mass influx and the pressure waves exerts a strong stabilizing influence on the system was completely confirmed by a series of experiments with the H_2/Air system in which the injection Mach number was decreased by enlarging the total port flow area of a showerhead injector. With decreasing M_{inj} a shift of the limit to higher $\bar{\Phi}$ and a decrease in shock amplitude at fixed $\bar{\Phi}$ was observed. For $M_{inj} \leq 0.4$ stable combustion was observed over the entire range of equivalence ratio.

The excellent agreement between theory and experiment on the influence of M_{inj} provides an explanation for the otherwise anomalous behavior of the H_2/Air system with porous plug injection . The failure of the H_2/Air system with porous plug injection to support unstable combustion over the entire range of Φ is directly attributed to the pronounced damping influence active in the case of low M_{inj}, P_{inj} injection. Clearly the ability of a premixed gaseous propellant system to support unstable combustion must depend upon the relative balance of destabilizing factors arising from the response of the combustion process to the pressure waves and the inherently stabilizing factors of mean outflow through the nozzle and the response of the injection system in the case of unchoked injection.

Theory and experiment were also found to be in agreement with respect to the predicted influence of preheating the premixed gases on the stability characteristics. Experiments were carried out to determine the stability limit and wave amplitude (within the regime of nonsteady burning) as functions of Φ for the H_2/Air system for increasing amounts of preheat (increasing $\bar{T}_i^*$). The predicted stabilizing influence of increasing $\bar{T}_i^*$, hence the ratio $\bar{T}_i^*/\bar{T}_b^*$, primarily due to the accompanying decrease in $\bar{\pi}_c^*/\tilde{\pi}_{wave}^*$ at each Φ was found to be in agreement with the experimental results

It is of interest to comment upon the influence of the mean chamber Mach number, the combustion pressure, and the chamber length on the system stability characteristics. According to Bowman ((32), see Figure II-10), an increase in M or L_c was observed to have an equivalent effect on the nonlinear system response. According to the analytical model, the dimensionless shock amplitude at the injector is directly proportional to M in agreement with Bowman's results. Physically this dependence is precisely what one would expect when it is recalled that experimentally the Mach number increase was achieved by decreasing the nozzle contraction ratio and doubling

the total propellant flow (burning) rate. Ideally the linear limit is independent of M. The observed shift in the linear limit to lower combustion temperature with increasing L_c was shown to be in good agreement with the theoretical results. The analysis in Appendix C suggested a possible explanation for the observed influence of L_c on the wave amplitude. A more likely explanation may follow simply from the observation that (due to the nonadiabaticity of the gas rocket) $\bar{P}_c$ was maintained constant with increasing L_c by increasing $\dot{m}_{tot}$ (see Table III), hence by increasing M (at the injector). As noted the increase in M should contribute to the observed increase in wave amplitude with increasing L_c.

The predicted stability characteristics are sensitive to $\bar{P}_c$ principally through the influence of the mean density of the combustion zone ($\bar{\tau}_c^* \sim 1/\bar{\rho}_c^*$ for second order overall rate law). Bowman observed (Figure 33 of reference (32)) a shift at fixed Φ, fixed L_c to higher harmonic modes as $\bar{P}_c$ was increased. Theory and experiment are thus in qualitative agreement on this point. A decrease in $\bar{\tau}_c^*$ leads to a stabilizing decrease in $\bar{\tau}_c^*/\tau_{wave}^*$ for the fundamental mode and the criterion that $\bar{\tau}_c > (\bar{\tau}_c)_{lim}$ would eventually be satisfied only for a higher mode. The experimental observation that larger wave amplitude is achieved for higher $\bar{P}_c$ and the linear limit shift toward the stoichiometric mixture with larger $\bar{P}_c$ are clouded by the fact that the total mass flux was increased substantially in order to increase $\bar{P}_c$. Consequently, comparison of wave amplitude data for gas rocket experiments carried out at substantially different mean combustion pressures is perhaps a poor procedure. For fixed Φ, $M \sim \dot{m}_{tot}/\bar{P}_c$ and an estimated increase in M of 10 to 20 % at the combustion zone boundary accompanied the increase in $\bar{P}_c$ from 4.4 to 11.2 atm. According to the analytical model one would predict an increase in shock wave amplitude with the Mach number increase.

D. General Comments

It is recognized that rather drastic simplifications of the nonsteady combustion process in the gas rocket have been considered. The relatively good agreement between results of the theoretical model and the experimentally observed linear and nonlinear stability characteristics of the $H_2/O_2/N_2$, $CH_4/O_2/N_2$, and $CO(H_2O)/O_2/N_2$ systems supports the conclusion that the principal factors have been correctly accounted for. The consideration of the nonsteady gas phase combustion zone in terms of mean thermodynamic and gas dynamic variables and a mean volume was shown to be consistent with results of experimental diagnostics, overall chemical kinetic rate data, and fundamental considerations of the physics of the combustion process in the gas rocket. The dramatic influence of the mean characteristic combustion time (calculated on the basis of the mose relevant overall kinetic rate data and consistent with the measured mean burning rate in the gas rocket) relative to the wave travel time in the combustion chamber on the theoretically predicted system response offers strong support for the inference of the overriding importance of chemical kinetic factors in determining the nonsteady burning characteristics of the gas rocket for the case where the mass injection flux is positively decoupled form the pressure oscillations.

Comparison of theory and experiment have clearly demonstrated that finite chemical kinetic burning rates can lead to combustion-driven pressure oscillation for (a) reactants such as H_2/O_2 governed by "fast" overall kinetics but combusting at low temperatures (due to mixture dilution with N_2, heat losses, mixing with cooler recirculating product gases, incomplete combustion), or (b) reactants such as CH_4/O_2 governed by "slow" overall kinetics but combusting at high temperatures.

In light of these investigations and considering the results of Putnam and Tsuji and Takeno (Chapter II), it is

concluded that a rocket-type combustor employing energetic premixed gaseous propellants naturally offers two possible mechanisms for sustaining longitudinal mode combustion oscillations. For the case of propellant injection with a large pressure drop across the primary injector a regime of chemical-kinetically driven oscillations is encountered. With decreasing injection pressure drop and Mach number the increasing sensitivity of the injection mass flux to the pressure oscillations acts to stabilize the combustion driven oscillations. The second regime of nonsteady burning is encountered at low propellant injection pressure drops and is associated with a highly nonlinear chemico-fluid dynamic interaction between the nonsteady injection mass flow, the combustion zone, and the pressure waves. Essentially the instability in this case is a fluid dynamically driven phenomenon where the importance of the gas phase chemistry is associated with the ignition delay factors (77) of the unburned gas mixture. In view of the fact that the gas rocket systems used by Zucrow, Osborn et al. at Purdue and by Tsuji and Takeno in Japan were operated with extremely low primary injection pressure drops, it is speculated that oscillations of the second category were observed by those investigators. It would seem to be inappropriate to compare the results obtained with the system at Princeton to the results of the Purdue and Japanese investigators.

Obviously the results of the present investigation may be of practical utility to designers of gaseous fueled combustors. The criticality of the ratio of the characteristic combustion time to the period of oscillation, for sustained oscillations, suggests the use of this ratio as a fundamental design parameter. The ratio incorporates the basic system parameters associated with the reactants, geometry of the combustion chamber, and mode of oscillation.

Depending upon the desireability[1] of system operation with low amplitude sustained combustion (pressure) oscillations one can eliminate by suitable injection design the fluid dynamically driven mode of operation and apply the above criterion for sustained combustion driven oscillations.

The question remains of the fundamental relevance of the results obtained in this and in previous investigations of nonsteady combustion in the Princeton gas rocket to the phenomena of unstable combustion in practical liquid and solid propellant systems. A great deal of research effort has been devoted to the analysis of mechanisms of coupling of the energy (or mass) release due to combustion and finite amplitude pressure oscillations. As Culick has pointed out (24), one of the weakest arguments in the current theories of nonsteady combustion in solid propellant systems is that of quasisteady response of the gas phase. It would seem that a similar statement applies to analyses of liquid rocket instabilities. In support of the application of such quasisteady assumptions investigators have relied on the simple statement that the characteristic times due to finite rate gas phase chemical kinetics are (too) short relative to characteristic wave travel times. This statement simply cannot be supported in the case of acoustic oscillations on the basis of currently available kinetic rate data. To be sure, the characteristic time for the molecular scale interaction of (for example) the CO molecule and the OH radical to yield CO_2 and H may well be $\Theta(10^{-6}$ to 10^{-8} sec). However, for the high intensity combustion processes typical of solid and liquid rockets it is suggested that the relevant characteristic kinetic time should be calculated on the basis of well-stirred or turbulent

1. One can envision numerous applications where low amplitude oscillations of a particular character are desireable. for example, the substantial increase in the heat transfer load to the surrounding chamber walls during oscillatory combustion may be advantagous in the design of a heat exchanger. Recently, combustion oscillations in a simple premixed gaseous combustor have been used (153) with KOH seeding to increase the mean ionization level, local particle velocity, and power density in an MHD system.

flow reactor studies of overall reaction rates. For liquid and solid propellant rocket gas phase combustion zones composed of hydrocarbon species, active H, OH, and O radicals as well as CO, CO_2, H_2O, O_2 etc. it would seem presumptuous to exclude overall reaction kinetics from the list of potential sources for driving combustion oscillations or as a potential source of triggering large amplitude oscillations.

In view of these comments it is appropriate to second Cuiick's motion (24) for a relaxation of the quasisteady treatment of the gas phase combustion process in treatments of nonsteady combustion in liquid and solid propellant rocket combustion models. It would also seem worthwhile to carry out fundamental studies using flow or well-stirred reactors to obtain overall reaction rate data for (initial) mixtures of species felt to be typical of gas phase combustion zones in liquid and solid rockets.

BLANK PAGE

REFERENCES

1. Crocco, L., "Aspects of Combustion Instability in Liquid Propellant Rockets," ARS Journal, Part I: Vol. 21, No. 6, Nov.-Dec. 1951, pp. 163-170; Part II: Vol. 22, No. 1, Jan.-Feb. 1952, pp. 7-16.

2. Summerfield, M., "A Theory of Unstable Combustion in Liquid Propellant Rocket Systems," ARS Journal, Vol. 21, No. 5, Sept.-Oct. 1951, pp. 108-114.

3. Crocco, L. and Cheng, S. I., Theory of Combustion Instability In Liquid Propellant Rocket Motors, AGARDograph 8, Butterworths, London, 1950.

4. Barrere, M., "Rocket Propulsion," Elsevier, Amsterdam, 1960, pp. 646-680.

5. Berman, K. and Logan, S. E., "Combustion Studies with a Rocket Motor having a Full Length Observation Window," ARS Journal, Vol. 22, No. 2, Mar.-Apr. 1952, pp. 78-85.

6. Berman, K. and Cheney, S. H., "Combustion Studies in Rocket Motors," ARS Journal, Vol. 23, No. 2, Mar.-Apr. 1953, pp. 89-95.

7. Berman, K. and Cheney, S. H., "Rocket Motor Instability Studies," Jet Propulsion, Vol. 25, No. 10, Oct. 1955, pp. 513-518.

8. Gunder, D. F. and Friant, D. R., "Stability of Flow in a Rocket Motor," Journal of Applied Mathematics, Vol. 17, 1950, pp. 327-333.

9. Lee, Y. C., Pickles, A. M. and Miesse, C. C., "Experimental Aspects of Rocket System Stability," Jet Propulsion, Vol. 26, No. 1, Jan. 1956, pp. 34-38.

10. Barrere, M. and Montet, A., "Low Frequency Combustion Instability in Rocket Motors - Experimental Study," Jet Propulsion, Vol. 26, No. 1, Jan. 1956, pp. 9-19.

11. Osborne, J. R. and Zucrow, M. J., "An Unclassified Literature Survey on Combustion Pressure Oscillations in Liquid Propellant Rocket Motors, June 1957, TM57-1, Purdue University.

12. Krier, H., T'ien, J. S., Sirignano, W. A. and Summerfield, M., "Nonsteady Burning Phenomena of Solid Propellants: Theory and Experiments," AIAA Journal, Vol. 6, No. 2, Feb. 1968, pp. 278-285.

13. Krier, H., Summerfield, M., Mathes, H. B. and Price, E. W., "Entropy Waves Produced in Oscillatory Combustion of Solid Propellants," AIAA Journal, Vol. 7, No. 11, Nov. 1969, pp.2079-2086.

14. T'ien, J. S., Sirignano, W. A. and Summerfield, M., "Theory of L-Star Combustion Instability with Temperature Oscillations," AIAA Journal, Vol. 8, No. 1, Jan. 1970, pp. 120-126.

15. Crocco, L. and Harrje, D. T., "Combustion Instability in Liquid Propellant Rocket Motors," Experimental Methods in Combustion Research, AGARD, New York, 1961.

16. Elias, I. and Gordon, R., "Longitudinal Vibrations of Gas at Ambient Pressure in a Rocket Thrust Chamber," ARS Journal, Vol. 22, No. 5, Sept.-Oct. 1952, pp. 263-268.

17. Rogers, D. E. and Marble, F., "A Mechanism for High-Frequency Oscillation in Ramjet Combustors and After Burners," Jet Propulsion, Vol. 26, No. 6, June 1956, pp. 456-462.

18. Crocco, L., Grey, J. and Harrje, D. T., "On the Importance of the Sensitive Time Lag in Longitudinal Mode High-Frequency Rocket Combustion Instability," Jet Propulsion, Vol. 28, No. 12, Dec. 1958, pp. 841-843.

19. Crocco, L., Grey, J. and Harrje, D. T., "Theory of Liquid Propellant Rocket Combustion Instability and Its Experimental Verification," ARS Journal, Vol 30, No. 2, Feb. 1960, pp. 159-168.

20. Levine, R. S., "Experimental Status of High Frequency Liquid Rocket Combustion Instability," Tenth Symposium (International) on Combustion, The Combustion Institute, 1965, pp. 1083-1099.

21. Crocco, L., "Theoretical Studies on Liquid Propellant Rocket Instability," Tenth Symposium (International) on Combustion, The Combustion Institute, 1965, pp. 1101-1128.

22. Price, E. W., "Experimental Solid Rocket Instability," Tenth Symposium (International) on Combustion, The Combustion Institute, 1965, pp. 1067-1082.

23. Summerfield, M. and Krier, H., "Errors in Nonsteady Combustion Theory in the Past Decade (A Review)," AIAA Paper No. 69-178, New York, Jan. 1969.

24. Culick, F. E. C., "A Review of Calculations for Unsteady Burning of a Solid Propellant," AIAA Journal, Vol. 6, No. 12, Dec. 1968, pp. 2241-2255.

25. Smith, R. P. and Sprenger, D. F., "Combustion Instability in Solid Propellant Rockets," Fourth Symposium (International) On Combustion, Williams and Wilkens, Baltimore, 1953, pp. 893-906.

26. Sirignano, W. A., "A Theoretical Study of Nonlinear Combustion Instability: Longitudinal Mode," Technical Report No. 677, April 1964, Princeton University, Department of Aerospace and Mechanical Sciences.

27. Sirignano, W. A. and Crocco, L., "A Shock Wave Model of Unstable Rocket Combustors," AIAA Journal, Vol. 2, No. 7, July 1964, pp. 1285-1296.

28. Bortzmeyer, H. G. and Crocco, L., "Analysis of Longitudinal Mode High Frequency Combustion Instability in a Gas Fueled Rocket Motor," Aeronautical Engineering Laboratory, Report No. 587, Dec. 1961, Princeton.

29. Pelmas, R., Glassman, I. and Webb, M., "An Experimental Investigation of Longitudinal Mode Combustion Instability in a Rocket Motor Using Premixed Gaseous Propellants, Aeronautical Engineering Laboratory, Report No. 589, Dec. 1961, Princeton.

30. Bertrand, J., Glassman, I. and Crocco, L., "Theoretical and Experimental Investigations in a Gas Fueled Rocket Motor," Aeronautical Engineering Laboratory, Report No. 624, Sept. 1962, Princeton.

31. Schob, W., "An Experimental Investigation of Heat Transfer and Pressure Effects on Longitudinal Mode Combustion Instability in a Rocket Motor Using Premixed Gaseous Propellants," M.S.E. Thesis, 1963, Princeton.

32. Bowman, C. T., "Experimental Investigation of High Frequency Longitudinal Combustion Instability in Gaseous Propellant Rocket Motors, Technical Report No. 784, Jan. 1967, Princeton University, Department of Aerospace and Mechanical Sciences.

33. Bowman, C. T., Glassman, I. and Crocco, L., "Combustion Instability in Gas Rockets," AIAA Journal, Vol. 3, No. 10, Oct. 1965, pp. 1981-1982.

34. Mitchell, C. E., "Axial Mode Shock Wave Combustion Instability in Liquid Propellant Rocket Engines," Technical Report No. 798, July 1967, Princeton University, Department of Aerospace and Mechanical Sciences.

35. Mitchell, C. E., Crocco, L. and Sirignano, W., "Nonlinear Longitudinal Instability in Rocket Motors with Concentrated Combustion," Combustion Science and Technology, Vol. 1, No. 1, July 1969, pp. 35-63.

36. Rayleigh, L., The Theory of Sound, Vol. II, Dover, New York, 1945.

37. Markstein, G. H., "Interaction of Flame Propagation and Flow Disturbances," Third Symposium (International) On Combustion, Williams and Wilkens, Baltimore, 1949, pp. 162-167.

38. Kaskan, W. E., "An Investigation of Vibrating Flames," Fourth Symposium (International) On Combustion, Williams and Wilkens, Baltimore, 1953, pp. 575-591.

39. Markstein, G. H., "Instability Phenomena in Combustion Waves," Fourth Symposium (International) On Combustion, Williams and Wilkens, Baltimore, 1953, pp. 44-59.

40. Kaskan, W. E. and Noreen, A. E., "High Frequency Oscillations of a Flame Held by a Bluff Body," Transactions ASME, 77, 885, 1955.

41. Markstein, G. H., "A Shock Tube Study of Flame Front Pressure Wave Interaction," Sixth Symposium (International) On Combustion, The Combustion Institute, 1957, pp. 387-398.

42. Markstein, G. H., ed., Nonsteady Flame Propagation, Pergamon Press, New York, 1964.

43. Kahane, A. and Lees, L., "Unsteady One-Dimensional Flow with Heat Addition or Entropy Gradients," Third Symposium (International) On Combustion, Williams and Wilkens, Baltimore, 1949, pp. 222-229.

44. Chu, B. T., "Generation of Pressure Waves at a Flame Front," Fourth Symposium (International) On Combustion, Williams and Wilkens, Baltimore, 1953, pp. 603-612.

45. Blackshear, P. L., "Driving Standing Waves by Heat Addition," NACA TN2772, Aug. 1952.

46. Blackshear, P. L., "Growth of Disturbances in a Flame Generated Shear Region," Sixth Symposium (International) On Combustion, The Combustion Institute, 1957, pp. 512-522.

47. Putnam, A. and Dennis, W., "A Study of Burner Oscillations of the Organ-Pipe Type," Transactions ASME, 75, 15, 1953.

48. Putnam, A. and Dennis, W., "The Suppression of Burner Oscillations by Acoustical Dampers," Transactions ASME, Vol. 77, 1955, pp. 875-883.

49. Putnam, A. and Dennis, W., "Survey of Organ-Pipe Oscillations in Combustion Systems, Journal of Acoustical Society, Vol. 28, No. 2, March 1956, pp. 246-259.

50. Putnam, A. and Dennis, W., "Organ-Pipe Oscillations in a Burner with Deep Ports," Journal of Acoustical Society, Vol. 28, No. 2, March 1956, pp. 260-269.

51. Putnam, A. and Dennis, W., "Organ-Pipe Oscillations in a Flame Filled Tube," Fourth Symposium (International) on Combustion, Williams and Wilkens, Baltimore, 1953, pp. 566-575.

52. Merk, H. J., "An Analysis of Unstable Combustion of Premixed Gases," Sixth Symposium (International) on Combustion, The Combustion Institute, 1957, pp. 500-512.

53. Merk, H. J., "Analysis of Heat-Driven Oscillations of Gas Flows, I: General Considerations," Applied Science Research, A6, 1956-57, pp. 317-336.

54. Merk, H. J., "Analysis of Heat-Driven Oscillations of Gas Flows, II: On the Mechanisim of Rijke-Tube Phenomenon," Applied Science Research, A6, 1956-57, pp. 402-420.

55. Merk, H. J., "Analysis of Heat Driven Oscillations of Gas Flows, III: Characteristic Equation for Flame-Driven Oscillations of the Organ-Pipe Type," Applied Science Research, A7, 1957-58, pp. 175-191.

56. Merk, H. J., "Analysis of Heat Driven Oscillations of Gas Flows, IV: Discussion of Theoretical Results Concerning Flame-Driven Oscillations," Applied Science Research, A7, 1957-58, pp. 192-204.

57. Merk, H. J., "Analysis of Heat Driven Oscillations of Gas Flows, V: Influence of Heat Transfer in the Burner Port on the Stability of Combustion of Premixed Gases," Applied Science Research, A8, 1958-59, pp. 1-27.

58. Zucrow, M. J. and Osborn, J. R., "An Experimental Study of High Frequency Combustion Pressure Oscillations," Jet Propulsion, Vol. 28, No. 10, Oct. 1958, pp. 654-659.

59. Crocco, L., "Comments on the Zucrow-Osborn Paper on Combustion Oscillations," Jet Propulsion, Vol. 28, No. 12, Dec. 1958, pp. 843-844.

60. Zucrow, M. J. and Osborn, J. R., "Reply to Crocco's Criticism of the Zucrow-Osborn Paper," Jet Propulsion, Vol. 29, No. 3, March 1959, pp. 221-222.

61. Zucrow, M. J., Osborn, J. R. and Pinchak, A. C., "Luminosity and Pressure Oscillations Observed with Longitudinal and Transverse Modes of Combustion Instability," ARS Journal, Vol. 30, No. 8, Aug. 1960, pp. 758-761.

62. Osborn, J. R. and Davis, L. R., "Effects of Injection Location on Combustion Instability in Premixed Gaseous Bipropellant Rocket Motors," Report No. I-61-1, Jan. 1961, Purdue University, Jet Propulsion Center.

63. Osborn, J. R. and Bonnell, J. M., "Importance of Combustion Chamber Geometry in High Frequency Oscillations in Rocket Motors," ARS Journal, Vol. 34, No. 4, April 1961, pp. 482-485.

64. Osborn, J. R. and Bonnell, J. M., "Effect of Fuel Composition on High Frequency Oscillations in Rocket Motors Burning Premixed Hydrocarbon Gases and Air," ARS Journal, Vol. 31, No. 10, Oct. 1961, pp. 1397-1401.

65. Osborn, J. R. and Rahon, J. R., "Effects of Radial Energy Release Variations on Transverse Combustion Pressure Oscillations," Report No. I-62-3, March 1962, Purdue University, Jet Propulsion Center.

66. Osborn, J. R. and Derr, R. L., "An Experimental Investigation of Longitudinal Combustion Pressure Oscillations," Report No. I-62-8, Aug. 1962, Purdue University, Jet Propulsion Center.

67. Osborn, J. R., "Longitudinal Mode Instability," AIAA Journal, Vol. 2, No. 12, Dec. 1964, pp. 2237-2238.

68. Crocco, L., "Reply by Author to J. R. Osborn," AIAA Journal, Vol. 2, No. 12, Dec. 1964, pp. 2238-2239.

69. Goede, P. J., "Small Amplitude Combustion Pressure Oscillations in the Gas Rocket," Report No. 777-66-4, June 1966, Purdue University, Jet Propulsion Center.

70. Zucrow, M. J., Osborn, J. R. and Bonnell, J. M., "High Frequency Combustion Pressure Oscillations in Motors Burning Gaseous Propellants," TM-65-5, Aug. 1965, Purdue University, Jet Propulsion Center.

71. Bonnell, J. M., "High Frequency Combustion Pressure Oscillations in Gaseous Propellant Rockets: Design Considerations," ASME Paper 67-VIBR-34, March 1967.

72. Bonnell, J. M., "Combustion Stability in an Annular Gas Combustors," AIAA Journal, Vol. 6, No. 10, Oct. 1968, pp. 1941-1945.

73. Tsuji, H. and Takeno, T., "Studies of High Frequency Combustion Oscillations in a Gaseous Propellant Rocket Motor," Report No. 391, March 1964, University of Tokyo, Aeronautical Research Institute.

74. Tsuji, H. and Takeno, T., "An Experimental Investigation on High-Frequency Combustion Oscillations," Tenth Symposium (International) on Combustion, The Combustion Institute, 1965, pp. 1327-1335.

75. Tsiji, H. and Takeno, T., "Propagation of Pressure Waves in High-Frequency Combustion Oscillations," AIAA Journal, Vol. 6, No. 4, April 1968, pp. 730-732.

76. Takeno, T., "Experimental Studies on Driving Mechanism of the High Frequency Combustion Oscillation in a Premixed Gas Rocket," ISAS Report No. 420, Vol. 33, No. 2, Jan. 1968, University of Tokyo.

77. Takeno, T., "A Theoretical Study for Initiation of High-Frequency Combustion Oscillation in Premixed Gas Rocket," ISAS Report No. 430, Vol. 33, No. 12, Nov. 1968, University of Tokyo.

78. Pickford, R. and Peoples, R., "Inherent Stability of the Combustion Process," ARS Paper No. 1490-60, Dec. 1960, Washington.

79. Culick, F. E. C., "Stability of High Frequency Pressure Oscillation in Gas and Liquid Rocket Combustion Chambers," Technical Report No. 480, June 1961, M. I. T., Aerophysics Laboratory.

80. Culick, F. E. C., "Stability of High Frequency Pressure Oscillations in Rocket Combustion Chambers," AIAA Journal, Vol. 1, No. 5, May 1963, pp. 1097-1104.

81. Sirignano, W. A., "A Theory of Axial-Mode Shock Wave Oscillations in a Solid Rocket Combustor," Twelfth Symposium (International) on Combustion, The Combustion Institute, 1969, pp. 129-137.

82. Mitchell, C. E., "The Effect of Entropy Waves on High Frequency Pressure Oscillations in Liquid Rocket Motors," Combustion Science and Technology, Vol. 1, No. 4, Feb. 1970, pp. 269-274.

83. Knauer, R. C. and Webb, M. J., "Prevention of Flashback Damage in Combustors," Astronautics, Dec. 1960, pp. 84.

84. Thomas, J. and Layton, J. P., "Final Summary Technical Report on Transient Pressure Measuring Methods Research," Technical Report No. 595t, March 1967, Princeton University, Department of Aerospace and Mechanical Sciences.

85. Fristrom, R. M. and Westernberg, A. A., Flame Structure, McGraw-Hill, New York, 1965, pp. 323-377.

86. Kaskan, W. E. and Browne, W. G., "Kinetics of the $H_2/CO/O_2$ System," Report No. 63SD848, Feb. 1964, General Electric Co., Missiles and Space Division.

87. Friedman, R. and Nugent, R. G., "Flame Structure Studies IV. Premixed Carbon Monoxide Combustion," Project-Squid Technical Report ARC-3-P, April 1958, Atlantic Research Corporation.

88. Shuler, K. E., "On the Kinetics of Elementary Gas Phase Reactions at High Temperatures," Fifth Symposium (International) on Combustion, 1955, pp. 56-75.

89. Sobolev, G. K., "High Temperature Oxidation and Burning of Carbon Monoxide," Seventh Symposium (International) on Combustion, The Combustion Institute, 1959, pp. 386-390.

90. Hoare, D. E. and Walsh, A. D., "The Oxidation of Carbon Monoxide," Transactions of Faraday Society, Vol. 50, Part 1, Jan. 1954, pp. 37-50.

91. Brokaw, R. S., "Ignition Kinetics of the Carbon Monoxide-Oxygen Reaction," Tenth Symposium (International) on Combustion, The Combustion Institute, 1965, pp. 1063-1073.

92. Friedman, R. and Cyphers, J. A., "On the Burning Rate of Carbon Monoxide," Journal of Chemical Physics, Vol. 25, No. 3, Sept. 1956, pp. 448-547.

93. Laffitte, P., Cusin, F. and James, H., "Kinetic Study of the Carbon Monoxide-Oxygen Reaction Through the Inhibition Mechanism of this Reaction," Combustion and Flame, Vol. 6, No. 8, Sept. 1962, pp. 163-171.

94. Kaskan, W. E., "The Dependence of Flame Temperature on the Mass Burning Velocity," Sixth Symposium (International) on Combustion, The Combustion Institute, 1957, pp. 134-143.

95. Hottel, H. C., Williams, G. C., Nerheim, N. M. and Schneider, G. R., "Kinetic Studies in Stirred Reactors: Combustion of Carbon Monoxide and Propane," Tenth Symposium (International) on Combustion, The Combustion Institute, 1965, pp. 111-121.

96. Burgoyne, J. H. and Hirsch, H., "The Combustion of Methane at High Temperatures," Proceedings of the Royal Society, 227A, 1954-55, pp. 73-93.

97. Hoare, D. E. and Walsh, A. D., "The Oxidation of Methane, Parts I and II," Fifth Symposium (International) on Combustion, The Combustion Institute, 1955, pp. 467-483.

98. Enikolopyan, N. S., "The Kinetics and Mechanism of Methane Oxidation," Seventh Symposium (International) on Combustion, The Combustion Institute, 1959, pp. 157-164.

99. Fenimore, C. P. and Jones, G. W., "The Water-Catalyzed Oxidation of Carbon Monoxide by Oxygen at High Temperature," Journal of Physical Chemistry, Vol. 61, No. 5, May 1957, pp. 651-654.

100. Kozlov, G. I., "On High Temperature Oxidation of Methane," Seventh Symposium (International) on Combustion, The Combustion Institute, 1959, pp. 142-149.

101. Friedman, R., "Measurement of the Temperature Profile in a Laminar Flame," Fourth Symposium (International) on Combustion, Williams and Wilkens, Baltimore, 1953, pp. 259-263.

102. Cookson, R. A., Dunham, P. G. and Kilham, J. K., "Non Catalytic Coatings for Thermocouples," Combustion and Flame, Vol. 8, No. 2, June 1964, pp. 168-170.

103. Zeleznik, F. J. and Gordon, S., "A General IBM 704 or 7090 Computer Program for Computation of Chemical Equilibrium Compositions, Rocket Performance, and Chapman-Jouget Detonations," NASA TN D-1454, Oct. 1962.

104. Scheer, M. D., "Kinetics of the Gas Phase Oxidation of Formaldehyde," Fifth Symposium (International) on Combustion, The Combustion Institute, 1955, pp. 435-446.

105. Grard, F. and Vanpee, M., "The Kinetics of the Slow Combustion of Methane at High Temperature," Fifth Symposium (International) on Combustion, The Combustion Institute, 1955, pp. 484-490.

106. Nemeth, A. and Sawyer, R. F., "CO After Burning in Methane and Methane/Hydrogen Flames," WSCI Paper #68-17, Aoril 1968, Los Angeles.

107. Nemeth, A. and Sawyer, R. F., "The Overall Kinetics of High Temperature Oxidation in a Flow Reactor," Report TS-68-2,1968, University of California, Department of Mechanical Engineering, Thermal Systems Division.

108. Kydd, P. H. and Foss, W., "Combustion of Fuel-Lean Mixtures in Adiabatic Well-Stirred Reactors," Tenth Symposium (International) on Combustion, The Combustion Institute, 1965, pp. 101-110.

109. Longwell, J. P. and Weiss, M. A., "High Temperature Reaction Rates in Hydrocarbon Combustion," Industrial and Engineering Chemistry, Vol. 47, No. 8, 1955, pp. 1634-1643.

110. Williams, G. C., Hottel, H. C. and Morgan, A. C., "The Combustion of Methane in a Jet-Mixed Reactor," Twelfth Symposium (International) on Combustion, The Combustion Institute, 1969, pp. 913-925.

111. Bittker, D. A. and Browkaw, R. S., "Estimate of Chemical Space Heating Rates in Gas-Phase Combustion with Application to Rocket Propellants," ARS Journal, Vol. 30, No. 2, Feb. 1960. pp. 179-185.

112. Weinberg, F. J. and Levy, A., "Optical Flame Structure Studies: Examination of Reaction Rate Laws in Ethylene-Air Flames," Combustion and Flame, Vol. 3, No. 2, June 1959, pp. 229-253.

113. Longwell, J. P., Frost, E. E. and Weiss, M. A., "Flame Stability in Bluff Body Recirculation Zones," Industrial and Engineering Chemistry, Vol. 45, No. 8, Aug. 1953, pp. 1629-1634.

114. Longwell, J. P., "Flame Stabilization by Bluff Bodies and Turbulent Flames in Ducts," Fourth Symposium (International) on Combustion, Williams and Wilkens, Baltimore, 1954, pp. 90-97.

115. Hottel, H., Williams, G. C., Scurlock, A. C., "Flame Stabilization and Propagation in High Velocity Streams," Third Symposium on Combustion, Williams and Wilkens, Baltimore, 1949, pp. 21-40.

116. Zukowski, E. E. and Marble, F. E., "Experiments Concerning the Mechanism of Flame Blowoff from Bluff Bodies," Proceedings of Gas Dynamics Symposium on Aerothermochemical Phenomena, Aug. 1955, pp. 205-208.

117. Avery, W. H. and Hart, R. W., "Combustor Performance with Instantaneous Mixing," Industrial and Engineering Chemistry, Vol. 45, No. 8, Aug. 1953, pp. 1634-1637.

118. Longwell, J. P., Weiss, M. A., and Lang, R. J., "Combustion Rates in Spherical Reactors," Industrial and Engineering Chemistry, Vol. 50, No. 2, Feb. 1958, pp. 257-264.

119. Avery, W. H., "Space Heating Rates and High Temperature Kinetics," Fifth Symposium (International) on Combustion, The Combustion Institute, 1955, pp. 86-91.

120. Hottel, H. C., Williams, G. C., and Bonnell, A. H., "Application of Well-Stirred Reaction Theory to the Prediction of Combustor Performance," Combustion and Flame, Vol. 2, No. 1, March 1958,

121. Hottel, H. C., Williams, G. C., and Baker, M. L., "Combustion Studies in a Stirred Reactor," Sixth Symposium (International) on Combustion, The Combustion Institute, 1957, pp. 398-411.

122. Blichner, O., "A Fluid Dynamic Study of a Spherical and a Cylindrical Reactor," Eighth Symposium (International) on Combustion, The Combustion Institute, 1961, pp. 995-1002.

123. Jain, V. K. and Spalding, D. B., "The Effects of Finite Recirculation in a Stirred Reactor," Combustion and Flame, Vol. 10, No. 3, March 1966, pp. 37-43.

124. Jenkins, D. B., Yumlu, V. S., and Spalding, D. B., "Combustion of Hydrogen and Oxygen in a Steady-Flow Adiabatic Stirred Reactor," Eleventh Symposium (International) on Combustion, The Combustion Institute, 1967, pp. 779-790.

125. Jones, A. and Prothero, A., "Solution of the Steady-State Equations for an Adiabatic Stirred Reactor," Combustion and Flame, Vol. 12, No. 5, Oct. 1968, pp. 457-464.

126. Hottel, H. C., Williams, G. C., and Miles, G. A., "Mixedness in the Well-Stirred Reactor," Eleventh Symposium (International) on Combustion, The Combustion Institute, 1967, pp. 771-778.

127. Evangelista, J. J., Shinnar, R., and Katz, S., "The Effect of Imperfect Mixing on Stirred Combustion Reactors," Twelfth Symposium (International) on Combustion, The Combustion Institute, 1969, pp. 901-912.

128. Sawyer, R. F., "The Homogeneous Gas Phase Kinetics of Reactions in the Hydrazine-Nitrogen Tetroxide Propellant System," Technical Report 761, 1965, Princeton University, Department of Aerospace and Mechanical Sciences.

129. Dryer, F. and Glassman, I., "Overall Reaction Rates of Paraffin Hydrocarbons," Paper presented at 10th AFOSR Contractors' Conference on Chemical Kinetics of Propulsion, University of California, Berkeley, California, 1969.

130. Abramovich, G. N., The Theory of Turbulent Jets, M. I. T. Press, Cambridge, 1963.

131. Thring, M. W. and Newby, M. P., "Combustion Length of Enclosed Turbulent Jet Flames," Fourth Symposium (International) on Combustion, Williams and Wilkens, Baltimore, 1953, pp. 789-796.

132. Summerfield, M., Reiter, S. H., Kebely, V., and Mascolo, R. W., "The Structure and Propagation Mechanism of Turbulent Flames in High Speed Flow," Jet Propulsion, Vol. 25, No. 8, August 1955, pp. 377-384.

133. Weinberg, F. J. and Fox, M. D., "An Experimental Study of Burner-Stabilized Turbulent Flames in Premixed Reactants," Proceedings of Royal Society, A268, 1962, pp. 222-239.

134. Hottel, H. C., "Burning in Laminar and Turbulent Fuel Jets," Fourth Symposium (International) on Combustion, Williams and Wilkens, Baltimore, 1953, pp. 97-113.

135. Grover, J. H., Fales, E. N., and Scurlock, A. C., "Turbulent Flame Studies in Two-Dimensional Open Burners," Ninth Symposium (International) on Combustion, The Combustion Institute, 1963, pp. 21-35.

136. Spalding, D. B., "Ends and Means in Flame Theory," Sixth Symposium (International) on Combustion, The Combustion Institute, 1957, pp. 12-20.

137. Spalding, D. B., "I. Predicting the Laminar Flame Speed in Gases with Temperature-Explicit Reaction Rates," pp. 287-295, "II. One-Dimensional Laminar Flame Theory for Temperature-Explicit Reaction Rates," pp. 296-307, Combustion and Flame, Vol. 1, 1957.

138. Ievlev, V. N., "Combustion of a Turbulent Jet in Burners with Preliminary Mixing," Sixth Symposium (International) on Combustion, The Combustion Institute, 1957, pp. 317-325.

139. Spalding, D. B., "Theoretical Relationships Between Combustion Intensity and Pressure Drop for One-Stream Combustion Chambers, Report No. 19, 181, C. F. 393, April 1957, British Aeronautical Research Council.

140. Spalding, D. B., "Theory of Rate of Spread of Confined Turbulent Pre-Mixed Flames," Seventh Symposium (International) on Combustion, The Combustion Institute, 1959, pp. 595-603.

141. Ricou, F. P. and Spalding, D. B., "Measurements of Entertainment by Axisymmetrical Turbulent Jets," Journal of Fluid Mechanics, Vol. 11, Part I, Aug. 1961, pp. 21-32.

142. Spalding, D. B., "The Spread of Turbulent Flames Confined in Ducts," Eleventh Symposium (International) on Combustion, The Combustion Institute, 1967, pp. 207-815.

143. Spalding, D. B., Some Fundamentals of Combustion, Butterworths, London, 1955.

144. Lefebvre, A. H. and Reid, R., "The Influence of Turbulence on the Structure and Propagation of Enclosed Flames," Combustion and Flame, Vol. 10, No. 4, Dec. 1966, pp. 355-366.

145. Hammitt, A. G., "The Oscillation and Noise of an Over Pressure Jet," Journal of Acoustical Society, Vol. 28, No. 9, Sept. 1961, pp. 673-680.

146. Westley, R. and Woolley, J. H., "Investigation of the Near Noise Fields of a Choked Axisymmetric Air Jet," Proceedings AFOSR-UTIAS Symposium, 1968, Toronto, pp. 147-153.

147. Powell, A., "On the Mechanism of Choked Jet Noise," Proceedings of Physical Society, Sect. B., Vol. 66, 1953, pp. 1039.

148. Weinberg, F., Optics of Flames, Butterworths, Washington, 1963.

149. Hyzer, W. G., Engineering and Scientific High-Speed Photography, MacMillan, New York, 1962.

150. Gaydon, A. G., The Spectroscopy of Flames, Chapman and Hall, London, 1957.

151. Gaydon, A. G. and Wolfhard, H. G., Flames: Their Structure, Radiation and Temperature, MacMillan, New York, 1960.

152. Crocco, L., "One-Dimensional Treatment of Steady Gas Dynamics," Fundamentals of Gas Dynamics, Princeton University Press, Princeton, 1953, pp. 272-309.

153. Ibberson, V.J., et al., "A Combustion Oscillator for MHD Energy Conversion," Paper presented at Thirteenth International Symposium on Combustion, Salt Lake City, Utah, August 1970.

154. Crocco, private communication

APPENDIX A: Mitchell-Crocco Analysis of Combustion Chamber Wave Dynamics

The principal assumptions invoked by Mitchell are summarized in Chapter V, pages 172 to 177. For complete details of the theoretical analysis refer to Mitchell [34]. Under the conditions noted Mitchell writes the conservation of mass and momentum for an elemental volume in the combustion chamber in dimensional form,

$$\frac{\partial \rho^*}{\partial t^*} + \frac{\partial}{\partial x^*}(\rho^* u^*) = 0 \tag{A-1}$$

$$\frac{\partial u^*}{\partial t^*} + u^* \frac{\partial u^*}{\partial x^*} = -\frac{1}{\rho^*} \frac{\partial p^*}{\partial x^*} \tag{A-2}$$

Nondimensionalizing all variables as discussed in Chapter V, page 229, equations A-1, 2 become

$$\frac{\partial \rho}{\partial t} + \frac{\partial}{\partial x}(\rho u) = 0 \tag{A-3}$$

$$\frac{\partial u}{\partial t} + u \frac{\partial u}{\partial x} = -\frac{1}{\gamma \rho} \frac{\partial p}{\partial x} \tag{A-4}$$

The homentropic condition, the definition of the sound speed, and the perfect gas relationship are used to obtain the relations,

$$\frac{2}{\gamma-1} \frac{\partial a}{\partial t} + \frac{2u}{\gamma-1} \frac{\partial a}{\partial x} + a \frac{\partial u}{\partial x} = 0 \tag{A-5}$$

$$\frac{\partial u}{\partial t} + u \frac{\partial u}{\partial x} + \frac{2a}{\gamma-1} \frac{\partial a}{\partial x} = 0 \tag{A-6}$$

Adding and subtracting equations A-5, 6 the Riemann form of the equations is obtained,

$$\frac{\partial}{\partial t}\left(u + \frac{2}{\gamma-1} a\right) + (u+a) \frac{\partial}{\partial x}\left(u + \frac{2}{\gamma-1} a\right) = 0 \tag{A-7}$$

$$\frac{\partial}{\partial t}\left(u - \frac{2}{\gamma-1} a\right) + (u-a) \frac{\partial}{\partial x}\left(u - \frac{2}{\gamma-1} a\right) = 0 \tag{A-8}$$

In order to solve A-7, 8 the combustion zone and nozzle boundary conditions and the time condition are specified. The nozzle boundary condition is simply,

$$u = Ma \qquad \text{at} \quad x = 1 \tag{A-9}$$

The combustion zone boundary condition valid at x = 0 follows from the analysis of Chapter V, pages 224 to 251 . Expanding all variables in power series about the steady state values where the mean flow Mach number is used as the expansion parameter (refer to the discussion in Chapter V, pages 172 to 177),

$$u = M + u_1 + u_2 + \cdots \tag{A-10}$$

$$a = 1 + a_1 + a_2 + \cdots \tag{A-11}$$

where $(\epsilon_i)_1 = \theta(M)$, $(\epsilon_i)_2 = \theta(M^2)$

Substituting A-10, 11 into A-7, 8 and ordering terms, the first order equations are,

$$\frac{\partial}{\partial t}\left(u_1 + \frac{2}{\gamma-1}a_1\right) + \frac{\partial}{\partial x}\left(u_1 + \frac{2}{\gamma-1}a_1\right) = 0 \tag{A-12}$$

$$\frac{\partial}{\partial t}\left(u_1 - \frac{2}{\gamma-1}a_1\right) - \frac{\partial}{\partial x}\left(u_1 - \frac{2}{\gamma-1}a_1\right) = 0 \tag{A-13}$$

The second order equations are similarly obtained as,

$$\frac{\partial}{\partial t}\left(u_2 + \frac{2}{\gamma-1}a_2\right) + \frac{\partial}{\partial x}\left(u_2 + \frac{2}{\gamma-1}a_2\right) = -\left(M + u_1 + a_1\right)\frac{\partial}{\partial x}\left(u_1 + \frac{2}{\gamma-1}a_1\right) \tag{A-14}$$

$$\frac{\partial}{\partial t}\left(u_2 - \frac{2}{\gamma-1}a_2\right) - \frac{\partial}{\partial x}\left(u_2 - \frac{2}{\gamma-1}a_2\right) = -\left(M + u_1 - a_1\right)\frac{\partial}{\partial x}\left(u_1 - \frac{2}{\gamma-1}a_1\right) \tag{A-15}$$

The first and second order nozzle boundary conditions are simply,

$$M + u_1 + u_2 = M(1 + a_1 + a_2) \tag{A-16}$$

$$u_1 = 0 \qquad \text{at} \quad x = 1 \tag{A-17}$$

$$u_2 = Ma_1 \qquad \text{at} \quad x = 1 \tag{A-18}$$

The combustion zone boundary conditions determined in Chapter V are,

$$u_1 = 0 \qquad \text{at} \quad x = 0 \tag{A-19}$$

$$u_2 = u_2^{\circ} \qquad \text{at} \quad x = 0 \tag{A-20}$$

The inhomogeneous terms appearing in the second order equations depend on the solutions for the first order functions. Since the second order homogeneous equations are functionally identical to the first order equations, particular solutions to the second order equations in terms of time (t) will generally involve aperiodic terms proportional to (t) which grow with time. The point is that while periodic solutions in (t) to first order may be found, the second order solutions are not necessarily periodic with the same period. To alleviate this situation and to restrict the search to solutions periodic with the same period to all orders such that,

$$a_1(t) + a_2(t) + \cdots = a_1(t + \mathcal{P}) + a_2(t + \mathcal{P}) + \cdots$$

$$a_i(t) = a_i(t + \mathcal{P}) \tag{A-21}$$

Mitchell defines the stretched time coordinate, θ, where

$$\theta = \frac{\mathcal{T}_0}{\mathcal{T}} t = \frac{\mathcal{T}_0}{\mathcal{P}} t \quad , \qquad \mathcal{T}_0 = 2 \tag{A-22}$$

and $\theta = 0$ to 2 defines the period of oscillation for all orders,

$$t = \left(1 + \frac{\mathcal{T}_1}{2} + \cdots\right)\theta \tag{A-23}$$

Equations A-12, 13 are written in terms of x and θ and solutions are obtained in straightforward fashion for U_1 and a_1 with the homogeneous boundary conditions, $U_1 = 0$ at $x = 0$ and 1 and the cyclic condition $f(\theta) = f(\theta + 2)$,

$$u_1 = f(\theta - x) - f(\theta + x) \tag{A-24}$$

$$a_1 = \frac{\gamma - 1}{2}\left[f(\theta - x) + f(\theta + x)\right] \tag{A-25}$$

$$\rho_1 = \gamma\left[f(\theta - x) + f(\theta + x)\right] \tag{A-26}$$

The wave amplitude parameter (f) must be determined from the second order analysis and the second order boundary conditions.

The second order equations are written in terms of (x, Θ),

$$\frac{\partial}{\partial\theta}\left(u_2+\frac{2}{\gamma-1}a_2\right)+\frac{\partial}{\partial x}\left(u_2+\frac{2}{\gamma-1}a_2\right)=\frac{T_1}{2}\frac{\partial}{\partial\theta}\left(u_1+\frac{2}{\gamma-1}a_1\right)-(M+u_1+a_1)\frac{\partial}{\partial x}\left(u_1+\frac{2}{\gamma-1}a_1\right) \tag{A-27}$$

$$\frac{\partial}{\partial\theta}\left(u_2-\frac{2}{\gamma-1}a_2\right)-\frac{\partial}{\partial x}\left(u_2-\frac{2}{\gamma-1}a_2\right)=\frac{T_1}{2}\frac{\partial}{\partial\theta}\left(u_1-\frac{2}{\gamma-1}a_1\right)-(M+u_1-a_1)\frac{\partial}{\partial x}\left(u_1-\frac{2}{\gamma-1}a_1\right) \tag{A-28}$$

Substituting for U_1 and a_1 from equations A-24, 25, Mitchell obtains particular solutions to these equations by inspection,

$$u_2+\frac{2}{\gamma-1}a_2=2\frac{\partial f(\theta-x)}{\partial\theta}\left[x\left(\frac{\gamma+1}{2}f(\theta-x)+M+\frac{T_1}{2}\right)+\frac{\gamma-3}{4}\int_{\theta-x}^{\theta+x}f(\eta)d\eta\right] \tag{A-29}$$

$$u_2-\frac{2}{\gamma-1}a_2=2\frac{\partial f(\theta+x)}{\partial\theta}\left[x\left(\frac{\gamma+1}{2}f(\theta+x)-M+\frac{T_1}{2}\right)-\frac{\gamma-3}{4}\int_{\theta+x}^{\theta-x}f(\eta)d\eta\right] \tag{A-30}$$

Adding these particular solutions to the homogeneous solutions for the second order functions and applying the boundary and cyclic conditions, the general nonlinear ordinary differential equation governing the first order wave amplitude parameter is obtained,

$$\left[(\gamma+1)f(\theta)+T_1-\frac{3-\gamma}{2}\int_0^2 f(\eta)d\eta\right]\frac{df}{d\theta}=-u_2^o+(\gamma-1)Mf(\theta) \tag{A-31}$$

where $f(\theta)=\Theta(M)=M\hat{f}$, $\hat{f}=\Theta(1)$, $u_2^o=\Theta(M^2)$

An expression for T_1, the first order perturbation in the period of oscillation, is derived for shock type solutions by considering the conditions for the propagation of weak shock waves in a flow field where the mean particle velocity is of $\Theta(M)$. For weak shock waves the shock velocity is simply the average velocity of sound waves upstream and downstream of the shock. Mitchell thus obtains,

$$T_1=-\frac{\gamma+1}{2}\left[f(0)+f(2)\right]+\frac{3-\gamma}{2}\int_0^2 f(\theta')d\theta' \tag{A-32}$$

where f(0) = the value of f immediately following the shock
f(2) = the value of f immediately before the shock

APPENDIX B: General Combustion Zone Boundary Condition

In Chapter V, the combustion zone boundary condition was developed by combining the equations of mass and energy conservation. The burning rate term in the energy equation was expressed in terms of an overall rate law where the influence of finite species (fuel and oxidizer) mass fractions appeared in the pre-exponential factor. The equations were linearized for the case where,

$$\sigma_{f,c} = \sigma_{f_i}(1-\gamma) \tag{B-1}$$

$$\sigma_{ox,c} = \sigma_{ox_i}(1-\mu\sigma_{f_i}\gamma) \tag{B-2}$$

where $\sigma_{f,c}, \sigma_{ox,c}$ =averaged mass fractions of fuel and oxidizer in the combustion zone

$$\left(\frac{\sigma_{ox_i}}{\sigma_{f_i}}\right)/\mu = \Phi$$

$$\mu = (\sigma_{ox}/\sigma_f)_{STOICH}$$

$$\gamma = \frac{T_c - \bar{T}_i}{T_b - \bar{T}_i}, \qquad T_c = T_c(t) \tag{B-3}$$

The burning rate is sensitive to the pressure oscillations through the (weak) pressure and temperature dependence of the pre-exponential factor and the (strong) temperature dependence of the exponential factor. It is the purpose of this discussion to show that the use of the quasi-steady relationships B-1 to B-3 to express the influence of variations in the species mass fractions (explicitly in terms of the perturbations in the mean temperature), together with the neglection of the influence of perturbations in the final burned gas temperature are sufficiently accurate approximations. That is, it will be shown for typical H_2 + Air mixtures, that the difference in terms of the combustion zone admittance coefficient between the above treatment and a "more exact" formulation using a species conservation and accounting for variable $T_b(t)$ is small.

Allowing for storage of deficient species in accordance with Equation V-42, the combustion zone boundary condition can be obtained from the conservation equations, which are written here in dimensional form as:

mass: $$\dot{m}_i^* = \dot{m}^* + \frac{d}{dt^*}(\rho_c^* V_c^*) \qquad \text{(B-4)}$$

energy: $$\dot{m}_i^* c_{p_i}^* T_i^* + \dot{q}^* = \dot{m}^* c_{p_b}^* T_b^* + \frac{d}{dt^*}(\rho_c^* V_c^* c_{v_c}^* T_c^*) \qquad \text{(B-5)}$$

species: $$\dot{m}_i^* \nu_{f_i} - \dot{m}_{f_c}^* = \dot{m}^* \nu_{f,b} + \frac{d}{dt^*}(\rho_c^* V_c^* \nu_{f,c}) \qquad \text{(B-6)}$$

$$\nu_{f,b} = 0 \text{ for complete combustion}$$

In addition

state: $$p^* = \rho^* R^* T^*$$

burning rate: $$\dot{q}^* = q^* \cdot \dot{m}_{f_c}^*$$

where q^* = heat of combustion per unit mass of fuel.

$$\frac{\dot{m}_{f_c}^*}{V_c^*} = -mw_f^* \frac{d[X_f^*]_c}{dt^*} = mw_f^* \chi^* [X_f^*]_c^n [X_{O_2}^*]_c^m, \quad \frac{\text{gms fuel reacting}}{\text{cm}^3 \text{ sec}}$$

$$[X_f^*]_c = \frac{\text{moles fuel}}{\text{cm}^3} = \frac{\nu_{f,c}}{mw_f^*} \rho_c^*$$

$$[X_{O_2}^*]_c = \frac{\text{moles } O_2}{\text{cm}^3} = \frac{\nu_{O_2,c}}{mw_{O_2}} \cdot \rho_c^*$$

$n = m = 1$ (overall 2nd order reaction)

$$\hat{k}^* = k^*/mw_{O_2}, \qquad \nu_{Ox} = (1+S)\nu_{O_2}$$

Since $\dot{m}_{b,c}^*$ = total mass burning rate = $\dot{m}_{f_c}^*/\nu_{f_i} = (1+\Phi\mu)\dot{m}_{f_c}^*$

$$\dot{m}_{b,c}^* = \left[\frac{\hat{k}^*}{\nu_{f_i}(1+S)} (\nu_{ox,c})^1 (\nu_{f,c})^1 \rho_c^* e^{-\frac{E^*}{R^* T_c^*}}\right] \rho_c^* V_c^*$$

Defining $1/\tau_c^* = \left[\frac{\hat{k}^*}{\nu_{f_i}(1+S)} \rho_c^* \nu_{ox,c} \nu_{f,c} e^{-E^*/R^* T_c^*}\right]$ where the factor ν_{f_i} is incorporated in the denominator, the energy release rate term becomes,

$$\dot{q}^* = \nu_{f_i} q^* \frac{\rho_c^* V_c^*}{\tau_c^*}$$

$$\dot{m}_{f_c}^* = \nu_{f_i} \frac{\rho_c^* V_c^*}{\tau_c^*}$$

Nondimensionalizing all variables (page 229), the conservation equations become,

$$\dot{m}_i = \dot{m} + \frac{d}{dt}(\rho_c v_c) \tag{B-7}$$

$$\dot{m}_i \bar{T}_i + (1-\bar{T}_i)\frac{\rho_c v_c}{r_c} = \dot{m} T_b + \frac{1}{\gamma}\frac{d}{dt}(\rho_c v_c T_c) \tag{B-8}$$

$$\dot{m}_i \bar{v}_{fi} - \bar{v}_{fi}\frac{\rho_c v_c}{r_c} = \frac{d}{dt}(\rho_c v_c \bar{v}_{f,c}) \tag{B-9}$$

state

$$p = \rho T = \rho_i T_i = \rho_b T_b = \rho_c T_c \tag{B-10}$$

where the relationships

$$\frac{q^* \bar{v}_{fi}}{\bar{c}_p^* \bar{T}_b^*} = \frac{c_p^*(\bar{T}_b^* - \bar{T}^*)}{c_p^* T_b^*} = (1-\bar{T}_i)$$

burning rate

$$1/r_c = \bar{c}\rho_c \bar{v}_{ox,c} \bar{v}_{f,c} e^{-\frac{E^*}{\bar{R}^* T_b^*}} \tag{B-11}$$

Equations B-7 to B-11 now contain the new dependent variables ($\bar{v}_{ox,c}$), ($\bar{v}_{f,c}$), and T_b where previously Equations B-1, 2, 3 were used to replace ($\bar{v}_{ox,c}$) and ($\bar{v}_{f,c}$), in favor of T_c (through γ) and perturbations in T_b were effectively neglected ($T_b \simeq \bar{T}_b = 1$). Hence, two additional equations are needed. This requirement can be satisfied by resorting to two approximate conditions.

Consistent with the use of an overall rate expression it is assumed that the reaction obeys an overall stoichiometry defined by $(\bar{v}_{ox}/\bar{v}_f)_{st} = \mu$. Letting the subscript r denote species fraction reacted,

$$\bar{v}_{ox,r} = \mu \bar{v}_{f,r} \tag{B-12}$$

and, since

$$\Phi = (\bar{v}_{oxi}/\bar{v}_{fi})\mu$$

$$\bar{v}_{f,c} = \bar{v}_{fi} - \bar{v}_{f,r}$$

$$\bar{v}_{ox,c} = \bar{v}_{oxi} - \bar{v}_{ox,r}$$

$$= \Phi\mu\bar{v}_{fi} - \mu\bar{v}_{f,r} = \mu\left[\Phi\bar{v}_{fi} + \bar{v}_{fi} - \bar{v}_{fi} - \bar{v}_{f,r}\right.$$

$$\therefore \bar{v}_{ox,c} = \mu\bar{v}_{fi}(\Phi - 1) + \mu\bar{v}_{f,c} \tag{B-13}$$

The factor in $1/r_c^*$, equivalent to Z (Equation V-24) becomes

$$z = \sigma_{ox,c}\,\sigma_{f,c} = \mu\left[\bar{\sigma}_{f,i}(\bar{\Phi}-1) + \sigma_{f,c}\right]\sigma_{f,c}$$

$$z = \mu\bar{\sigma}_{f,i}^{2}\left[(\bar{\Phi}-1) + \left(\frac{\bar{\sigma}_{f,c}}{\bar{\sigma}_{f,i}}\right)\left(\frac{\sigma_{f,c}}{\bar{\sigma}_{f,c}}\right)\right]\left[\frac{\bar{\sigma}_{f,c}}{\bar{\sigma}_{f,i}}\,\frac{\sigma_{f,c}}{\bar{\sigma}_{f,c}}\right] \qquad \text{(B-14)}$$

An expression coupling T_c, T_b, and $\sigma_{f,c}$ valid in steady state is,

$$c_{p_c}^{*}\,T_c^{*} + \sigma_{fc}\,q^{*} = c_{p_b}^{*}\,T_b^{*} \qquad \text{(B-15)}$$

In the nonsteady case, the equation remains approximately valid since T_c^{*} is close to T_b^{*} and the effective capacitance term which is missing in (B-15) must be small. In dimensionless form

$$T_c + \frac{1-\bar{T}_i}{\bar{\sigma}_{f,i}}\,\sigma_{f,c} = T_b \qquad \text{(B-16)}$$

Equations B-7 to B-16 complete the system. As discussed in Chapter V, the system is still missing one equation due to the approximate averaging procedure. T_c, $\bar{v}_c$, and ρ remain implicitly coupled. However, the difference between the two systems (B-1 to 3, vs B-9 to 16) can be examined without solving the complete problem. Linearizing Equations B-7 to 16 according to

$$\dot{m} = \bar{\dot{m}} + \dot{m}_1 + \dot{m}_2 \qquad \rho = 1 + \rho_1$$

$$\dot{m}_i = \bar{\dot{m}}_i\,(1 - \psi\rho_i^{\circ}) \qquad T_c = \bar{T}_c + T_{c_1}$$

$$u_b = \bar{u} + u_1 + u_2 \qquad \rho_c = \bar{\rho}_c + \rho_{c_1}$$

$$\sigma_{f,c} = \bar{\sigma}_{f,c}\,(1 + \alpha_{c_1} + \alpha_{c_2}) \qquad T_b = 1 + T_{b_1}$$

$$\frac{1}{T_c} = \frac{1}{\bar{T}_c}\,(1 + \Sigma_1) \qquad \rho_b = 1 + \rho_{b_1}$$

$$\rho_c v_c = \overline{\rho_c v_c} + (\rho_c v_c)_1 \qquad \text{(B-17)}$$

The steady state equations become

$$\bar{\dot{m}}_i = \bar{\dot{m}} = \bar{u} = M \qquad \text{(B-18)}$$

$$\bar{\dot{m}} = \frac{\overline{\rho_c v_c}}{\bar{T}_c}\,, \qquad \overline{\rho_c v_c} = \bar{T}_c\,\bar{\dot{m}} = \Theta(M) \qquad \text{(B-19)}$$

$$\frac{\bar{\sigma}_{f,c}}{\bar{\sigma}_{f,i}} = \frac{1-\bar{T}_c}{1-\bar{T}_i} \qquad \text{(B-20)}$$

$$\overline{\rho_c T_c} = \overline{\rho_i T_i} = \overline{\rho_b T_b} = 1 \qquad \text{(B-21)}$$

The perturbation equations are,

$$\dot{m}_{i_1} = \dot{m}_1 = \overline{v_c}_1 = 0$$

continuity: $$\dot{m}_{i_2} = \dot{m}_2 + \frac{d}{dt}(\rho_c v_c)_1 \qquad \text{(B-22)}$$

energy: $$\dot{m}_{i_2}\bar{T}_i + (1-\bar{T}_i)\left[\bar{\dot{m}}\,\Sigma_1 + \frac{1}{\bar{\rho}_c}(\rho_c v_c)_1\right] = \bar{\dot{m}}\,T_{b_1} + \dot{m}_2 + \frac{1}{\gamma}\frac{d}{dt}\left[(\rho_c v_c)_1\bar{T}_c + (\overline{\rho_c v_c})T_{c_1}\right] \qquad \text{(B-23)}$$

species: $$\dot{m}_{i_2} = \bar{\dot{m}}\,\Sigma_1 + \frac{(\rho_c v_c)_1}{\bar{T}_c} + \frac{\bar{v}_{f,c}}{\bar{v}_{f_i}}(\overline{\rho_c v_c})\frac{d\alpha_{c_1}}{dt} + \frac{\bar{v}_{f,c}}{\bar{v}_{f_i}}\frac{d}{dt}(\rho_c v_c)_1 \qquad \text{(B-24)}$$

matching: $$T_{b_1} = T_{c_1} + \frac{\bar{v}_{f,c}}{\bar{v}_{f_i}}(1-\bar{T}_i)\alpha_{c_1} = T_{c_1} + (1-\bar{T}_c)\alpha_{c_1} \qquad \text{(B-25)}$$

state: $$p_1^0 = \frac{T_{c_1}}{\bar{T}_c} + \frac{\rho_{c_1}}{\bar{\rho}_c} = \rho_{b_1} + T_{b_1} \qquad \text{(B-26)}$$

And Σ_1, follows from the definition of $1/\bar{T}_c^*$, where

$$\frac{E^*}{\bar{R}^*T_c^*} = \frac{E^*}{\bar{R}^*\bar{T}_b^*}\frac{1}{T_c} = \frac{E^*}{\bar{R}^*\bar{T}_b^*}\frac{1}{T_c}\left(1 - \frac{T_{c_1}}{T_c}\right)$$

$$e^{-\frac{E^*}{\bar{R}^*\bar{T}_b^*}\frac{1}{T_c}\left(1-\frac{T_{c_1}}{T_c}\right)} \simeq e^{-\frac{E^*}{\bar{R}^*\bar{T}_c^*}}\left[1 + \frac{E^*}{\bar{R}^*\bar{T}_b^*}\frac{T_{c_1}}{\bar{T}_c^2}\right]$$

$$\rho_c^*(v_{ox,c})(v_{f,c}) = \bar{\rho}_c^*\left(1+\frac{\rho_{c_1}}{\bar{\rho}_c}\right)\mu v_{f_i}^2\left[(\Phi-1) + \frac{1-\bar{T}_c}{1-\bar{T}_i}(H\alpha_{c_1})\right]\left[\frac{1-\bar{T}_c}{1-\bar{T}_i}(1+\alpha_{c_1})\right]$$

$$= \bar{\rho}_c^*\mu v_{f_i}^2\frac{1-\bar{T}_c}{1-\bar{T}_i}\left[(\Phi-1) + \frac{1-\bar{T}_c}{1-\bar{T}_i}\right] + \mathcal{O}(M) \text{ terms}$$

And Σ_1, becomes

$$\Sigma_1 = \frac{1}{\bar{T}_c^2}\frac{E^*}{\bar{R}^*\bar{T}_b^*}T_{c_1} + \frac{\rho_{c_1}}{\bar{\rho}_c} + \left[1 + \frac{1}{1 + \frac{1-\bar{T}_i}{1-\bar{T}_c}(\Phi-1)}\right]\alpha_{c_1} \qquad \text{(B-27)}$$

$$\Sigma_1 = \left(\frac{H}{\bar{T}_c^2} - \frac{1}{\bar{T}_c}\right)T_{c_1} + \rho_1^0 + \chi\alpha_{c_1}$$

$$H = \frac{E^*}{\bar{R}^*\bar{T}_b^*}, \qquad \chi = 1 + \frac{1}{1 + \frac{1-\bar{T}_i}{1-\bar{T}_c}(\Phi-1)}$$

Eliminating $\dot{m}_2$ from the continuity (B-23) and energy (B-24) equations, an ordinary differential equation is obtained for $(\rho_c v_c)_1$ as

$$\frac{d}{dt}(\rho_c v_c)_1 + \frac{\bar{\beta}}{\bar{T}_c}(\rho_c v_c)_1 = \bar{\dot{m}}\,\xi(t) \qquad \text{(B-28)}$$

$$\bar{\beta} = \frac{1-\bar{T}_i}{1-\bar{T}_c/\gamma} = \frac{\gamma}{\gamma-\bar{T}_c}(1-\bar{T}_i)$$

$$\xi(t) = -\bar{\beta}(\psi \rho_1^\circ + \Sigma_1) + \frac{\gamma}{\gamma - \bar{\tau}_c}\left[T_{b_1} + \frac{\bar{\nu}_c}{\gamma}\frac{dT_{c_1}}{dt}\right] \tag{B-29}$$

which has the solution

$$(\rho_c v_c)_1 = \int_{-\infty}^{t} \bar{m}\, \xi(t) e^{-\frac{\bar{\beta}}{\bar{\tau}_c}(t-t')} dt' \tag{B-30}$$

Similarly the species equation (B-24) can be written as

$$\frac{d}{dt}(\rho_c v_c)_1 + \frac{\hat{\beta}}{\bar{\tau}_c}(\rho_c v_c)_1 = \bar{m}\,\psi(t) \tag{B-31}$$

$$\hat{\beta} = \frac{1-\bar{\tau}_i}{1-\bar{\tau}_c}$$

$$\psi(t) = -\hat{\beta}\left[\psi \rho_1^\circ + \Sigma_1\right] - \bar{\nu}_c \frac{d\alpha_{c_1}}{dt} \tag{B-32}$$

which has the solution

$$(\rho_c v_c)_1 = \int_{-\infty}^{t} \bar{m}\, \psi(t) e^{-\frac{\hat{\beta}}{\bar{\tau}_c}(t-t')} dt' \tag{B-33}$$

Eliminating $(\rho_c \bar{v_c})_1$, from Equations (B-30) and (B-33) an implicit relationship between T_{c_1}, α_{c_1}, ρ_1° and T_{b_1}, is obtained as

$$\int_{-\infty}^{t} \xi(t) e^{-\frac{\bar{\beta}}{\bar{\tau}_c}(t-t')} dt' = \int_{-\infty}^{t} \psi(t) e^{-\frac{\hat{\beta}}{\bar{\tau}_c}(t-t')} dt' \tag{B-34}$$

In order to investigate the dependence of α_{c_1}, on T_{c_1}, and ρ_1° to understand the influence of finite T_{b_1}, all perturbation quantities are assumed 2π periodic in t and are written as $\epsilon = \epsilon_1 e^{i\pi t}$ where ϵ_1 = complex amplitude.

$$\rho_1^\circ = \rho_1 e^{i\pi t}$$

$$T_{c_1} = T_1 e^{i\pi t}$$

$$\alpha_{c_1} = \alpha_1 e^{i\pi t}$$

$$T_{b_1} = T_{b_1} e^{i\pi t} = \left[T_1 + (1-\bar{\tau}_c)\alpha_1\right] e^{i\pi t} \tag{B-35}$$

Terms arising from the influence of finite T_{b_1}, will be underscored as $\underline{(\,)}$. Substituting (B-35) into (B-30) and (B-33)

$$(\rho_c v_c)_1 = \bar{m}\left\{\frac{\bar{\tau}_c}{\gamma-\bar{\tau}_c}T_1 + \frac{\gamma}{\gamma-\bar{\tau}_c}\frac{\bar{\beta}/\bar{\tau}_c - i\pi}{(\frac{\bar{\beta}}{\bar{\tau}_c})^2+\pi^2}\left[\frac{1}{=} - (1-\bar{\tau}_i)\left(\frac{\bar{H}}{\bar{\tau}_c^2} - \frac{1}{\bar{\tau}_c} + \frac{1}{\gamma-\bar{\tau}_c}\right)\right]T_1\right.$$
$$\left. - (\psi+1)\rho_1 + \left[(1-\bar{\tau}_c) - (1-\bar{\tau}_i)\chi\right]\alpha_1\right\} e^{i\pi t} \quad \text{(B-36)}$$

$$(\rho_c v_c)_1 = -\bar{m}\left\{\bar{\tau}_c\alpha_1 + \hat{\beta}\frac{\frac{\hat{\beta}}{\bar{\tau}_c} - i\pi}{(\frac{\hat{\beta}}{\bar{\tau}_c})^2+\pi^2}\left[(\psi+1)\rho_1 + \left(\frac{\bar{H}}{\bar{\tau}_c^2} - \frac{1}{\bar{\tau}_c}\right)T_1 + (\chi-1)\alpha_1\right]\right\} e^{i\pi t} \quad \text{(B-37)}$$

Eliminating $(\rho_c v_c)_1$, from (B-36) and (B-37)

$$\alpha_1 = \frac{\left[\hat{H}(\bar{B}-\hat{B}) - \bar{B}\left(\frac{1}{1-\bar{\tau}_i} - \frac{1}{\gamma-\bar{\tau}_c}\right) - \frac{1}{\gamma-\bar{\tau}_c}\right]T_1 + \left[(\psi+1)(\bar{B}-\hat{B})\right]\rho_1}{1 - \hat{B} + \bar{B}/\hat{\beta} - \chi(\bar{B}-\hat{B})} \quad \text{(B-38)}$$

where

$$\hat{H} = \frac{\bar{H}}{\bar{\tau}_c^2} - \frac{1}{\bar{\tau}_c} \quad \text{(B-39)}$$

$$\bar{\beta} = \frac{\gamma}{\gamma-\bar{\tau}_c}(1-\bar{\tau}_i), \quad \hat{\beta} = \frac{1-\bar{\tau}_i}{1-\bar{\tau}_c}$$

$$\bar{B} = \frac{\bar{\beta}^2 - i\pi\bar{\beta}\bar{\tau}_c}{\bar{\beta}^2 + (\pi\bar{\tau}_c)^2} \quad \text{(B-40)}$$

$$\hat{B} = \frac{\hat{\beta}^2 - i\pi\hat{\beta}\bar{\tau}_c}{\hat{\beta}^2 + (\pi\bar{\tau}_c)^2} \quad \text{(B-41)}$$

Equation (B-38) is written as

$$\alpha_1 = \alpha_T T_1 + \alpha_\rho \rho_1 \quad \text{(B-42)}$$

where

$$\alpha_T = \frac{\hat{H}(\bar{B}-\hat{B}) - \bar{B}\left(\frac{1}{1-\bar{\tau}_i} - \frac{1}{\gamma-\bar{\tau}_c}\right) - \frac{1}{\gamma-\bar{\tau}_c}}{1-\hat{B} + \bar{B}/\hat{\beta} - \chi(\bar{B}-\hat{B})} \quad \text{(B-43)}$$

$$\alpha_\rho = \frac{(\psi+1)(\bar{B}-\hat{B})}{1-\hat{B} + \bar{B}/\hat{\beta} - \chi(\bar{B}-\hat{B})} \quad \text{(B-44)}$$

The expression for Σ_1 becomes

$$\Sigma_1 = \Sigma_T T_1 + \Sigma_\rho \rho_1$$

$$\Sigma_T = \hat{H} + \chi\alpha_T \quad \text{(B-45)}$$

$$\Sigma_\rho = 1 + \chi\alpha_\rho \quad \text{(B-46)}$$

In order to make a comparison of the two treatments of the un-

steady species mass fraction, Σ_T and Σ_p as defined by (B-45) and (B-46) and by Equation V-60, (denoted by superposed bar)

$$\bar{\Sigma}_T = \hat{H} - \frac{1}{1-\bar{T}_c}\left[\frac{1}{\bar{\Phi}-\bar{T}} + \frac{1}{1-\bar{T}}\right]$$

$$\bar{\Sigma}_p = 1 \qquad \text{(V-60)}$$

must be compared. Thus

$$\Delta\Sigma_T = \frac{\Sigma_T - \bar{\Sigma}_T}{\bar{\Sigma}_T} = \frac{\chi\alpha_T + \frac{1}{1-\bar{T}_c}\left[\frac{1}{\bar{\Phi}-\bar{T}} + \frac{1}{1-\bar{T}}\right]}{\bar{\Sigma}_T} \qquad \text{(B-47)}$$

and

$$\Delta\Sigma_p = \frac{\Sigma_p - \bar{\Sigma}_p}{\bar{\Sigma}_p} = \chi\alpha_p \qquad \text{(B-48)}$$

serve as accurate measures of the difference between the two analyses in terms of the influence of the treatment of the species mass fraction. The actual values of α_T and α_p are important in determining the influence of T_{b_1} as compared to T_{c_1}, since

$$T_{b_1} = T_1 + (1-\bar{T}_c)\alpha_1$$

$$T_{b_1} = [1 + (1-\bar{T}_c)\alpha_T]T_1 + [(1-\bar{T}_c)\alpha_p]p_1 \qquad \text{(B-49)}$$

Calculations of the terms $\Delta\Sigma_T, \Delta\Sigma_p, T_{b_1}$ and α_T, α_p have been carried out for the typical case of H_2+Air combustion, oxidizer rich mixtures, $\bar{T}_i^* = 300^\circ K$, $\bar{p}_c^* = 7.8$ atm, $\gamma = 1.25$, $E = 38$ kcal/gm mole, $\hat{k}^* = 5 \times 10^{14}$, $\bar{T}_c = 0.80$, and choked injection ($\psi = 0$). The particular case of $L_c^*/m = 80$ was examined in detail but the results apply to all L_c^*/m with an appropriate shift of the $\bar{\nu}_c$ vs $\bar{\Phi}$ curve.

First, defining

$$\bar{\alpha}_T = -\frac{1}{1-\bar{T}_c}\left[\frac{1}{\bar{\Phi}-\bar{T}} + \frac{1}{1-\bar{T}}\right] \qquad \text{(B-50)}$$

$$\bar{\Sigma}_T = \hat{H} + \bar{\alpha}_T \qquad \text{(B-51)}$$

it can be shown that

$$\chi = -(1-\bar{T}_c)\bar{\alpha}_T \qquad (= .2\bar{\alpha}_T \text{ for } \bar{T}_c = 0.8) \qquad \text{(B-52)}$$

Hence

$$\Delta\Sigma_T = -\frac{\bar{\alpha}_T}{\bar{\Sigma}_T}\left[(1-\bar{T}_c)\alpha_T + 1\right] \qquad \text{(B-53)}$$

$$\Delta\Sigma_p = -(1-\bar{T}_c)\bar{\alpha}_T\alpha_p \qquad \text{(B-54)}$$

It is of interest to note the asymptotic behavior of α_T, α_p, $\Delta\Sigma_T$, and $\Delta\Sigma_p$ in the limits of $\bar{\nu}_c \simeq 0$ and $\bar{\nu}_c \to \infty$ (for $\bar{T}_c = 0.8$)

$$\bar{\nu}_c \simeq 0 \longrightarrow \bar{B} = \hat{B} = 1$$

$$(\alpha_p)_{\bar{\nu}_c=0} = 0 \qquad (\Delta\Sigma_T)_{\bar{\nu}_c=0} = 0$$

$$(\alpha_T)_{\bar{\nu}_c=0} = -5 \qquad (\Delta\Sigma_p)_{\bar{\nu}_c=0} = 0$$

$$(T_{b_1})_{\bar{\nu}_c=0} = 0$$

That is, in the quasi-steady limit of short combustion time relative to the wave travel time the isothermal response is appropriate.

$$\bar{\gamma}_c \to \infty \qquad \bar{\mathcal{B}} = \hat{\mathcal{B}} = 0$$

$$(\alpha_p)_{\bar{\gamma}_c \to \infty} = 0 \qquad (\Delta\Sigma_p)_{\bar{\gamma}_c \to \infty} = 0$$

$$(\alpha_T)_{\bar{\gamma}_c \to \infty} = -\frac{1}{\gamma - \bar{T}_c} = -2.2 \qquad T_{b_1} = .56\, T_{c_1}$$

$$(\Delta\Sigma_T)_{\bar{\gamma}_c \to \infty} = -\frac{\bar{\alpha}_T}{\bar{\Sigma}_T}(.56) \to 0 \text{ with } \downarrow T_{b_1}$$

For values of $\bar{\gamma}_c$ intermediate (ie. between $\bar{\gamma}_c = 3 \times 10^{-3}$ for $\Phi = 1.0$ and $\bar{\gamma}_c = 58$ for $\Phi = 4.0$ for the parameters noted on page B-8), Equations (B-43) and (B-44) must be solved for the real and imaginary components of α_T and α_p (since $\bar{B}$ and $\hat{B}$ are complex according to Equations (B-41)). The results of these calculations are summarized in Figure B-1a, b.

On the basis of these calculations it is concluded for the H_2 + Air system: first, that the influence of α_p is entirely negligible; second, that within the regime of $\bar{\gamma}_c = \Theta(1)$ where strong coupling is possible in accordance with the discussions of Chapter V, the approximation of the species mass fraction perturbation in terms of the quasi-steady temperature explicit relations (B-1,2) under the condition that perturbations in T_b are neglected is quite good. The predicted perturbation in the burned gas temperature within the regime of strong coupling is in general $\leq \Theta(0.1 \times T_{c1})$ and increases to $\Theta(0.5 \times T_{c1})$ as $\bar{\gamma}_c \to \infty$.

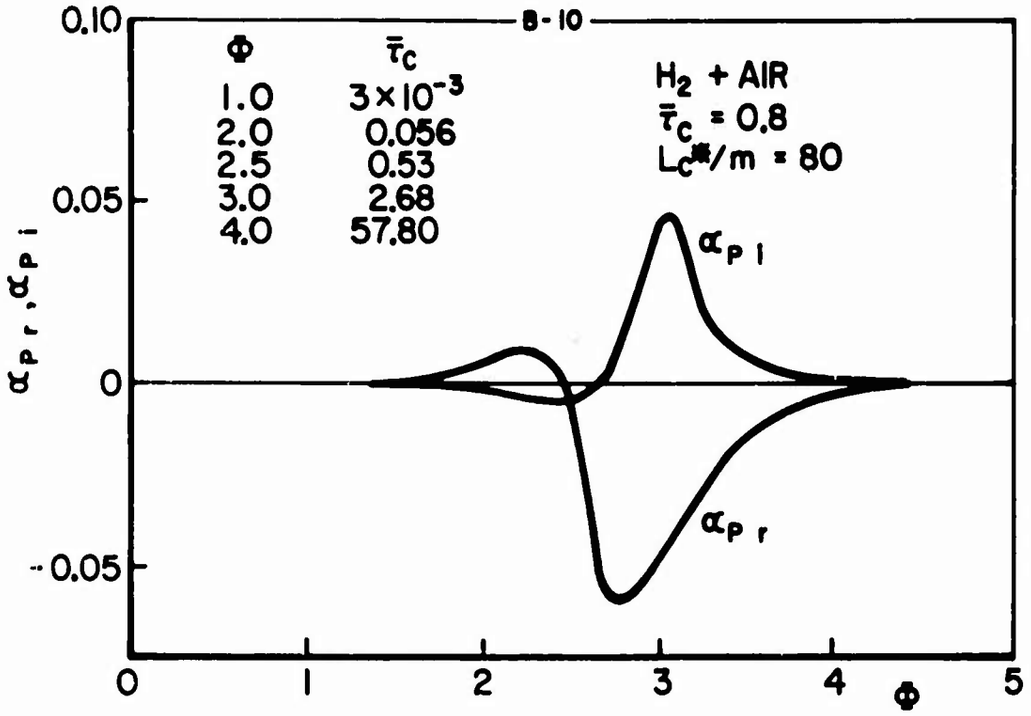

a) PRESSURE COEFFICIENT (α_P) vs Φ

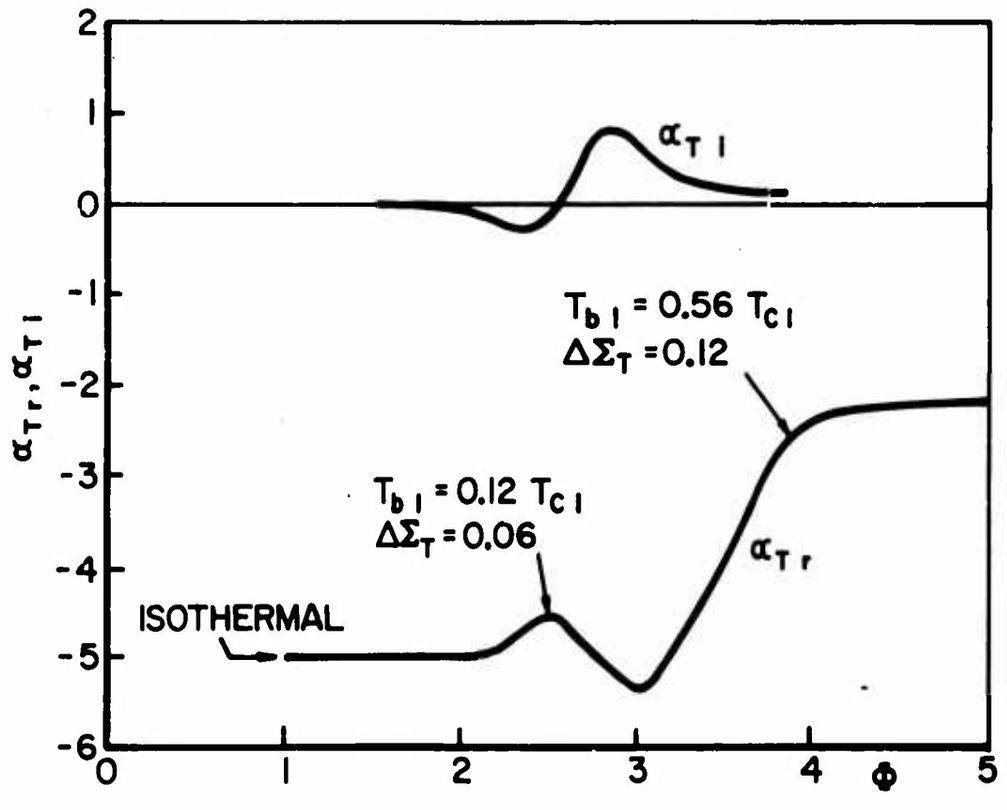

b) TEMPERATURE COEFFICIENT (α_T) vs Φ

PRESSURE AND TEMPERATURE COEFFICIENTS
OF SPECIES PERTURBATION

FIGURE B-1

APPENDIX C: Comparison of Nonsteady Combustion Model To Original Crocco Time Lag Model. Suggestion of Improved Formulation of Σ_1

The final form of the nonsteady combustion model applied in Chapter V to the gas rocket system considers all time dependent combustion zone variables to be linearly related to the pressure at each instant. In particular the instantaneous gas phase fuel burning rate in the finite dimensioned combustion zone volume is expressed as

$$\dot{m}_{fc}^{*} = \frac{\rho_c^{*} v_c^{*}}{\tau_c^{*}} \tag{C-1}$$

The discussions of pages 220 - 222 and 224 - 229 of Chapter V review these points. In dimensionless terms the mean mass burning rate is simply

$$\bar{\dot{m}} = \frac{\overline{\rho_c v_c}}{\bar{\tau}_c} \tag{C-2}$$

One of the principal results of the analysis and calculations is the dominant influence of the dimensionless ratio $\bar{\tau}_c = \bar{\tau}_c^{*} / \tau_{wave}^{*}$ on the theoretically predicted nonsteady burning characteristics of the gas rocket system. For the particular case examined ($T_{c_1} = \eta_0 p_1^{\circ}$) the linear and nonlinear stability limits are found to correspond to $\bar{\tau}_c \simeq .5$ to .6 for $\bar{T}_c = 0.8$, $\eta_0 = 0.288$ and $\bar{\tau}_c = .3$ to .5 for $\bar{T}_c = 0.75$, $\eta_0 = 0.3$. There is no a priori reasoning available to exclude the possibility of nonsteady burning at $\bar{\tau}_c \leq 0.1$ since small $\bar{\tau}_c$ merely implies small combustion volume or small $\rho_c v_c$. However, the discovery that, while indeed the predicted appearance of nonsteady burning is associated with short $\bar{\tau}_c$, $\bar{\tau}_c^{*}$ at the limit should be 0.15 to 0.30 of the period of oscillation (τ^{*}_{per}) suggested that perhaps the approximation applied in the analysis of Chapter V,

$$\tau_{c_1} = -\Sigma_T \bar{\tau}_c T_{c_1} - \Sigma_p \bar{\tau}_c p_1^{\circ} \tag{C-3}$$

could be generalized (for the case where T_{c_1} and p_1° are considered real) as

$$\tau_{c_1} = -\Sigma_T \int_{t-\bar{\tau}_c}^{t} T_{c_1}(t')\,dt' - \Sigma_p \int_{t-\bar{\tau}_c}^{t} p_1^{\circ}(t')\,dt' \tag{C-4}$$

Note that Equation C-3 follows from Equation V-59 which gives

$$\frac{1}{\tau_c} = \frac{1}{\bar{\tau}_c}\left[1 + \Sigma_T T_{c_1} + \Sigma_p p_1^{\circ}\right]$$
$$\tau_c = \bar{\tau}_c + \tau_{c_1} = \bar{\tau}_c\left[1 - \Sigma_T T_{c_1} - \Sigma_p p_1^{\circ}\right] \qquad \text{(C-5)}$$

from which Equation C-3 follows. Also it is noted that C-3 follows directly from Equation C-4 in the event that $T_{c1}(t)$ and $p_1^{\circ}(t)$ are constant over the combustion time $\bar{\tau}_c$. This is of course the case for short $\bar{\tau}_c$. Alternatively, Equations C-3 and C-4 can be differentiated with respect to time. Equivalence of the derivatives $\frac{d\tau_{c_1}}{dt}$ or $\frac{d\tau_c}{dt}$ as determined from Equations C-3 and C-4 requires

$$\frac{dT_{c_1}}{dt} = \frac{T_{c_1}(t) - T_{c_1}(t-\bar{\tau}_c)}{\bar{\tau}_c} \qquad \text{(C-6)}$$

and

$$\frac{dp_1^{\circ}}{dt} = \frac{p_1^{\circ}(t) - p_1^{\circ}(t-\bar{\tau}_c)}{\bar{\tau}_c} \qquad \text{(C-7)}$$

Clearly the right hand sides of Equations C-6 and C-7 approximate[1] (in general) the derivatives only in the limit of short $\bar{\tau}_c$ or in the particular case of larger $\bar{\tau}_c$ where $p_1^{\circ}(t)$ and $T_{c1}(t)$ vary linearly with time.

It is of interest to compare the formulation of the combustion model in Chapter V with Crocco's original so-called "time lag" model (3) of unstable combustion in a liquid propellant rocket motor. For the case of fixed mass injection flux (choked flow, $\psi = 0$ in the gas rocket model), Crocco designates the time between injection and (assumed instantaneous) combustion of a propellant element as the "time lag", a portion of which is time variant. During this "sensitive" time lag there is a complex feedback loop between the varying pressure field and the combustion process such that the sensitive time lag is influenced by the pressure. Furthermore, the rate processes characterizing the

---

[1] This argument applies to the case where all perturbation quantities are considered real. As shown in Chapter V, for the case where $T_{c1}(t)$ and τ_{c1} are complex Equation C-3 is valid for all $\bar{\tau}_c$.

total combustion process must be influenced by the local thermodynamic conditions within the combustion zone. Under the postulate that all such rate processes (in particular that rate process dominating the overall coupling) can ultimately be expressed as

$$f(t) \sim p^n \tag{C-8}$$

where

$$f(t) \sim \frac{\partial E}{\partial t} \qquad \left(\text{e.g., } \frac{\text{moles, gms, ergs}}{\text{sec}}\right)$$

Crocco suggests that transformation of unburned propellant to products at time t occurs only after an amount E_a of some quantity E is accumulated during the time $(t - \bar{\tau})$ by virtue of the pressure sensitive rate process f(t) such that

$$\int_{t-\bar{\tau}}^{t} f(t')dt' = E_a \tag{C-9}$$

In the steady state,

$$\bar{f} \cdot \bar{\tau} = E_a \tag{C-10}$$

Linearizing the system by setting

$$p = \bar{p} + p'$$
$$T = \bar{T} + T'$$
$$\tau = \bar{\tau} + \tau'$$
$$f = \bar{f}\left[1 + n\frac{p'}{\bar{p}}\right] \qquad \text{which follows from equation C-8}$$

Crocco obtains

$$\tau' = -n\int_{t-\bar{\tau}}^{t} \frac{p'}{\bar{p}}\,dt' \tag{C-11}$$

which can be differentiated to obtain

$$\frac{d\tau'}{dt} = \frac{d\tau}{dt} = -n\,\frac{p'(t) - p'(t-\bar{\tau})}{\bar{p}} \tag{C-12}$$

$d\tau/dt$ can be simply related to the perturbation in the burning rate under the condition that the amount of propellant injected during the interval dt must burn between $(t + \tau)$ and $(t + dt + \tau + d\tau)$, i.e., that

$$\dot{m}_i(t)dt = \dot{m}_b(t+\tau)(dt + d\tau) \tag{C-13}$$

Hence, for $\bar{m}_i = \bar{m}_b$

$$\frac{m_b(t) - \bar{m}_b}{\bar{m}_b} = -\frac{d\tau}{dt} = +\eta \frac{p'(t) - p'(t-\tau)}{\bar{p}} \tag{C-14}$$

or

$$m_b(t) = \bar{m}_i - \bar{m}_i \frac{d\tau}{dt} \tag{C-15}$$

The combustion model of Chapter V bears some formal resemblance to this original development where from Equation C-2 one identifies $\bar{m}$ with $\bar{f}$, $\overline{\rho_c v_c}$ with E_a, and $\bar{\tau}_c$ with $\bar{\tau}$ and from Equation C-3 and C-4, τ_c, with τ_i. In particular the integral formulation for τ' in Equation C-11 follows naturally from the consideration of instantaneous combustion at t after an interval τ following injection. In the present model the concept of instantaneous combustion after a time delay is <u>not</u> applicable. Rather, the combustion time $\bar{\tau}_c$ appearing in the analysis represents the kinetic time corresponding to the time required to effect conversion from unburned reactants to products. However, in light of (a) the rather remarkable agreement between theory and experiment with regard to the near limit linear and nonlinear stability characteristics and the correspondence of these near limit results to relatively short $\bar{\tau}_c$, (b) the failure of the model to predict the experimentally observed strong stabilizing effect (the upper stability limit) of increasing Φ (and $\bar{\tau}_c$) at off-limit mixtures[1], and (c) the similarity between the present model and Crocco's time lag model and the success of the original time lag model in predicting a finite regime of characteristic times in which oscillations are sustained and beyond which oscillations are damped, it was decided to examine the predicted system behavior for the case where Equation C-4 is assumed to represent the response of the characteristic combustion time to oscillations in pressure and temperature. The definitions of parameters and variables appearing in Equation C-4 are unchanged from the original expressions used in Chapter V. The only other modification in the analysis is the expression of $\dot{m}_i(t)$ as

$$\dot{m}_i(t) = \bar{\dot{m}}_i \left[1 - \frac{\psi}{\bar{\tau}_c} \int_{t-\bar{\tau}_c}^{t} p_i^{\circ}(t')\,dt'\right] \tag{C-16}$$

---

[1] As noted in Chapter V the limitation $\epsilon_{rp} = 0$ is probably unrealistic. An upper limit follows for the case of finite $\epsilon_{rp} = \theta(\pi/4 \text{ to } \pi/2)$

by analogy to Equation C-4. Actually only the case of choked injection ($\psi = 0$) flux is treated numerically.

The analysis of the combustion zone boundary condition is otherwise unchanged up to Equation V-50 for $\left(\frac{\rho_c v_c}{\bar{\dot{m}}}\right)$ which is simply

$$\frac{\rho_c v_c}{\bar{\dot{m}}} = \int_{-\infty}^{t} \xi(t') \frac{\dot{m}_i(t')}{\bar{\dot{m}}} \left[e^{-\int_{t'}^{t} \frac{\beta(t'')}{\tau_c(t'')} dt''} \right] dt' \qquad \text{(C-17)}$$

The algebra leading to an expression for $\left(\frac{\rho_c v_c}{\bar{\dot{m}}}\right)_1$ corresponding to Equation V-64 is involved and is complicated by the additional integral term appearing in the exponential due to γ_c, from Equation C-4. Carrying out the integrations and noting that $\frac{\overline{\rho_c v_c}}{\bar{\dot{m}}} = \bar{\gamma}_c$ a new expression for $\left(\frac{\rho_c v_c}{\bar{\dot{m}}}\right)_1$ is obtained as

$$\left(\frac{\rho_c v_c}{\bar{\dot{m}}}\right)_1 = \frac{\bar{\gamma}_c}{\gamma - \bar{\tau}_c} \tau_{c_1} - \frac{\bar{\beta}}{\gamma - \bar{\tau}_c} \int_{-\infty}^{t} \tau_{c_1}(t') e^{-\frac{\bar{\beta}}{\bar{\tau}_c}(t-t')} dt' - \frac{\bar{\beta}}{\bar{\gamma}_c} [\Sigma_p + \psi] \int_{-\infty}^{t} e^{-\frac{\bar{\beta}}{\bar{\tau}_c}(t-t')} \left[\int_{t'-\bar{\tau}_c}^{t'} \rho_1^{\circ} dt'' \right] dt' \qquad \text{(C-18)}$$

where

$$\Sigma = \Sigma_T + \eta \Sigma_p$$

$$\gamma_{c_1} = \frac{\Sigma}{\bar{\tau}_c} \int_{t-\bar{\tau}_c}^{t} \rho_1^{\circ}(t') dt' \qquad \text{(C-19)}$$

Similarly an expression for the perturbation in the mass efflux from the combustion zone extrapolated to the injector face is obtained as

$$\frac{\dot{m}_b^{\circ} - \bar{\dot{m}}}{\bar{\dot{m}}} = \frac{\bar{\beta}(1-\bar{\tau}_c)}{\gamma - \bar{\tau}_c} \eta \rho_1^{\circ} + \bar{\gamma}_c \frac{\gamma - 1}{\gamma - \bar{\tau}_c} \eta \frac{d\rho_1^{\circ}}{dt} - \frac{\bar{\beta}^2}{\bar{\tau}_c} \frac{1-\bar{\tau}_c}{\gamma - \bar{\tau}_c} \eta \int_{-\infty}^{t} \rho_1^{\circ} e^{-\frac{\bar{\beta}}{\bar{\tau}_c}(t-t')} dt'$$

$$+ \bar{\beta}(1-\bar{\tau}_c) \frac{\Sigma}{\bar{\tau}_c} \int_{t-\bar{\tau}_c}^{t} \rho_1^{\circ}(t') dt' - \frac{\psi}{\bar{\tau}_c} [1 - \bar{\beta}(1-\bar{\tau}_c)] \int_{t-\bar{\tau}_c}^{t} \rho_1^{\circ}(t') dt'$$

$$- \left(\frac{\bar{\beta}}{\bar{\tau}_c}\right)^2 (1-\bar{\tau}_c)(\Sigma + \psi) \int_{-\infty}^{t} e^{-\frac{\bar{\beta}}{\bar{\tau}_c}(t-t')} \left[\int_{t'-\bar{\tau}_c}^{t'} \rho_1^{\circ}(t'') dt'' \right] dt' \qquad \text{(C-20)}$$

Equation C-20 reduces to Equation V-67 for $\int_{t-\bar{\tau}_c}^{t} p_1^{\circ}(t')dt' = \bar{\tau}_c p_1^{\circ}(t)$

Applying the condition $\frac{\dot{m}_b^{\circ} - \bar{m}}{\bar{m}}$ to the Mitchell-Crocco analysis of the combustion chamber wave dynamics, the nonlinear ordinary integro-differential equation governing the wave amplitude parameter becomes

$$[f - k + C\bar{\tau}_c]\frac{df}{d\theta} = Af + B\bar{\tau}_c^{-2}\int_{-\infty}^{\theta} e^{-\frac{\bar{\beta}}{\bar{\tau}_c}(\theta - t')}\left[\int_{t'-\bar{\tau}_c}^{t'} f(t'')dt''\right]dt' + D\bar{\tau}_c^{-1}\int_{-\infty}^{\theta} f(t')e^{-\frac{\bar{\beta}}{\bar{\tau}_c}(\theta-t')}dt' + E\bar{\tau}_c^{-1}\int_{\theta-\bar{\tau}_c}^{\theta} f(t')dt' \qquad \text{(C-21)}$$

where

$$A = \frac{3\gamma - 1}{\gamma + 1} - \frac{2\gamma}{\gamma+1}\left[\frac{\bar{\beta}(1-\bar{\tau}_c)}{\gamma - \bar{\tau}_c}\right]\eta$$

$$B = \frac{2\gamma}{\gamma+1}\bar{\beta}^2(1-\bar{\tau}_c)(\Sigma + \Psi)$$

$$C = \frac{2\gamma}{\gamma+1}\frac{\gamma-1}{\gamma-\bar{\tau}_c}\eta$$

$$D = \frac{2\gamma}{\gamma+1}\bar{\beta}^2\frac{1-\bar{\tau}_c}{\gamma-\bar{\tau}_c}\eta$$

$$E = -\frac{2\gamma}{\gamma+1}\bar{\beta}(1-\bar{\tau}_c)\Sigma + \frac{2\gamma}{\gamma+1}\left[1 - \bar{\beta}(1-\bar{\tau}_c)\right]\Psi$$

Equation C-21 is of the same form as Equation V-94 but is complicated by the new terms involving $\int_{t-\bar{\tau}_c}^{t}$. Equation C-21 reduces to Equation V-94 for the particular case where $\int_{t-\bar{\tau}}^{t} f(t')dt' = \bar{\tau}_c f(t)$

As in Chapter V a linearized analysis of Equation C-21 allows a determination of the linear stability characteristics of the system. Substituting

$$f = \bar{f}e^{i\pi\theta} \qquad \text{(C-22)}$$

into quation C-21 and defining the limit condition by $\bar{f} = 0$, an equation valid at the stability limit is obtained as

$$A + \frac{E\bar{\tau}_c^{-1}}{\pi}\sin\pi\bar{\tau}_c + \frac{D\bar{\tau}_c^{-1}\frac{\bar{\beta}}{\bar{\tau}_c}}{\left(\frac{\bar{\beta}}{\bar{\tau}_c}\right)^2 + \pi^2} + \frac{B\bar{\tau}_c^{-2}}{\pi}\frac{\frac{\bar{\beta}}{\bar{\tau}_c}\sin\pi\bar{\tau}_c}{\left(\frac{\bar{\beta}}{\bar{\tau}_c}\right)^2 + \pi^2}$$

$$- \frac{B\bar{\tau}_c^{-2}}{\left(\frac{\bar{\beta}}{\bar{\tau}_c}\right)^2 + \pi^2}(1 - \cos\pi\bar{\tau}_c) = 0 \qquad \text{(C-23)}$$

which can be reformulated as

$$\left[\bar{A} + \frac{\bar{B}/\bar{\beta}}{1+\left(\frac{\pi\bar{\tau}_c}{\bar{\beta}}\right)^2}\right] + \left[\frac{B/\bar{\beta}}{1+\left(\frac{\pi\bar{\tau}_c}{\bar{\beta}}\right)^2} + E\right]\left[\frac{\sin\pi\bar{\tau}_c}{\pi\bar{\tau}_c} - 1\right] - \frac{B/\bar{\beta}^2}{1+\left(\frac{\pi\bar{\tau}_c}{\bar{\beta}}\right)^2}\left(1-\cos\pi\bar{\tau}_c\right) = 0 \qquad \text{(C-24)}$$

where $\bar{A} = A + E$

$\bar{B} = B + D$

Equation C-24 is to be compared to Equation V-100 ($\epsilon_{Tp} = 0$). The first term in Equation C-24 is the only term obtained in the original analysis. The two additional terms contain both stabilizing and destabilizing factors and are small for small $\bar{\tau}_c$. A measure of the divergence between the two analyses is simply the degree to which the conditions $\frac{\sin\pi\bar{\tau}_c}{\pi\bar{\tau}_c} = 1$ and $\cos\pi\bar{\tau}_c = 1$ are satisfied. Note that

$\bar{\tau}_c$	$\pi\bar{\tau}_c$	$\frac{\sin\pi\bar{\tau}_c}{\pi\bar{\tau}_c}$	$\cos\pi\bar{\tau}_c$
0.01	.0314	1.000	0.9995
0.10	.314	0.985	0.951
0.20	.628	0.942	0.807
0.40	1.256	0.760	0.296

The two additional terms become increasingly important with increasing $\bar{\tau}_c$. It is useful to obtain the stability limit condition in a form analagous to Equation V-101. The limit condition becomes

$$(1-\bar{\tau}_i)\left[\Sigma + \frac{\eta}{\gamma-\bar{\tau}_c}\right] + (1-\bar{\tau}_i)\bar{\beta}\Sigma\left[\frac{1-\cos\pi\bar{\tau}_c}{(\pi\bar{\tau}_c)^2}\right] =$$

$$\frac{\gamma-\bar{\tau}_c}{\gamma(1-\bar{\tau}_c)}\,\frac{3\gamma-1}{2\gamma}\left[1+\left(\frac{\bar{\beta}}{\pi\bar{\tau}_c}\right)^2\right] + (1-\bar{\tau}_i)\Sigma\left[1-\frac{\sin\pi\bar{\tau}_c}{\pi\bar{\tau}_c}\right] + F(\psi) \qquad \text{(C-25)}$$

where

$$F(\psi) = -(1-\bar{\tau}_i)\psi - \bar{\beta}(1-\bar{\tau}_i)\psi\left[\frac{1-\cos\pi\bar{\tau}_c}{(\pi\bar{\tau}_c)^2}\right]$$

$$+ \psi\left\{1-\bar{\tau}_i - \frac{\gamma-\bar{\tau}_c}{\gamma(1-\bar{\tau}_c)}\left[1+\left(\frac{\bar{\beta}}{\pi\bar{\tau}_c}\right)^2\right]\left[1-\frac{\sin\pi\bar{\tau}_c}{\pi\bar{\tau}_c}\right]\right\} \qquad \text{(C-26)}$$

For the case of $\psi = 0$, Equation C-25 reduces to

$$L = R + R_2 = \bar{R} \qquad \text{(C-26)}$$

where

$$L = (1-\bar{T}_i)\left(\Sigma + \frac{\eta}{\gamma-\bar{T}_c}\right)$$

$$R = \frac{\gamma-\bar{T}_c}{\gamma(1-\bar{T}_c)} \frac{3\gamma-1}{2\gamma}\left[1+\left(\frac{\bar{\beta}}{\pi\bar{T}_c}\right)^2\right]$$

$$R_2 = (1-\bar{T}_i)\,\Sigma\,(\delta_1-\delta_2)$$

$$\delta_1 = 1 - \frac{\sin\pi\bar{T}_c}{\pi\bar{T}_c} \qquad \delta_2 = \frac{1-\cos\pi\bar{T}_c}{\pi\bar{T}_c}\,\frac{\bar{\beta}}{\pi\bar{T}_c}$$

A detailed numerical investigation of the linear and nonlinear system response as determined by Equations C-25 and C-26 has not been carried out. In view of the somewhat arbitrary specifications of the perturbation of the combustion time in terms of the perturbations in temperature and pressure by the integral expressions in Equations C-4 and C-19, only general comments are offered here. Essentially the influence of the various system parameters such as Φ, L_c^*/m, $\bar{T}_c$, E^*, $\bar{k}^*$, and ψ remains unchanged with respect to the location of the "lower" stability limit. From the new equations it is seen that L and R are identical to the original terms in Equation V-101 defining the stability limit for $\psi = 0$. The term R_2 is new. R_2 is small and negative relative to R for $\bar{\gamma}_c \ll 1$ and becomes less negative and finally positive with increasing $\bar{\gamma}_c$. Eventually the term exerts a strong stabilizing influence on the predicted system response for $\bar{\gamma}_c \cong \Theta(1)$. This effect can clearly be seen from Equations C-26 and C-27. Note that the principal influence of R_2 arises through the factors $\Sigma\,[\delta_1-\delta_2]$. For the H_2 + Air system with $\bar{T}_i^* = 300^\circ K$ and $2.0 \le \Phi \le 3.0$, $.818 \ge 1-\bar{T}_i \ge .764$. For $\bar{T}_c = 0.80$ and $\gamma = 1.25$, $2.26 \ge \bar{\beta} \ge 2.12$.

Figures C-1 and C-2 show the theoretically predicted stability characteristics according to the linearized analysis of Equation C-26 for the same system analyzed in Chapter V (see Figures V - 9, 11, 14). Only the oxidizer rich system is considered here.

Recall that nonsteady burning is implied for $\bar{R} \geq L$. Comparison of Figures C-1, 2 and V-9,14 shows that the influence of the additional term R_2 is manifest in (a) the slight shift of the lower stability limit $(\bar{\Phi}_{lim})_{lower}$ toward the stoichiometric mixture ratio at fixed L_c^*/m, e.g., for $L_c^*/m = 80$, $(\bar{\Phi}_{lim})_{lower}$ shifts from 2.6 to 2.52, (b) the existence of a minimum $(\bar{R}_{min})$ in the $\bar{R}$ vs $\bar{\Phi}$ curves, and (c) the existence of a second linear limit designated as the "upper" stability limit $(\bar{\Phi}_{lim})_{upper}$ at each L_c^*/m such that stable combustion is predicted at $\bar{\Phi} > (\bar{\Phi}_{lim})_{upper}$. Thus a finite regime with respect to $\bar{\Phi}$ and $\bar{\tau}_c$ of nonsteady combustion is predicted by this present heuristic model. That is, unstable combustion is predicted for a given L_c^*/m for

$$(\bar{\Phi}_{lim})_{lower} \leq \bar{\Phi} \leq (\bar{\Phi}_{lim})_{upper} \qquad \text{(C-28)}$$

or, alternatively, for a finite range of $\bar{\tau}_c$

$$(\bar{\tau}_{c\ lim})_{lower} \leq \bar{\tau}_c \leq (\bar{\tau}_{c\ lim})_{upper} \qquad \text{(C-29)}$$

This prediction is inagreement with the experimental results and represents an improvement over the analysis of Chapter V in this respect.

Several additional points are noted from the results of Figures C-1 and C-2. The analysis predicts a closure of the finite $\bar{\Phi}$ regime of nonsteady burning at lower chamber lengths (L_{min}) for each mode of oscillation. L_{min} increases for increasing mode order. This prediction of an L_{min} is in agreement with the experimental results of Schob and Pelmas who investigated the experimental stability characteristics of the H_2 + Air system at short L_c. Pelmas (29) reports L_{min} = 10 to 12 cm for H_2 + Air, 10 hole showerhead injection, and $\bar{P}_c^*$ = 7.8 atm. Significantly no upper length limit is predicted in the present analysis which also is consistent with all experimental data on the gas rocket system. On the contrary, the locus of the minima of the R curves shows that $\frac{d\bar{R}_{min}}{d\bar{\Phi}} < 0$ while $\frac{d\bar{\alpha}}{d\bar{\Phi}} > 0$, that is, that

$$\frac{d\left[\mathcal{L}(\bar{\Phi}_i) - \bar{\mathcal{R}}_{min}(\bar{\Phi}_i)\right]}{d\,\bar{\Phi}} > 0$$

The numerical results of Chapter V show that a nearly linear increase in dimensionless shock amplitude occurs with increasing $\bar{\Phi}$ displacement from the nonlinear limit (and, hence, the linear limit as well). From Figure V-24 , it is noted that this corresponds to an increase in shock amplitude at $\bar{\Phi}_i$ with increasing $L(\bar{\Phi}_i) - R(\bar{\Phi}_i)$. From the steepness of the $\bar{R}$ curves at the linear limit in Figure C-1 it is concluded that a similar rapid increase in shock strength accompanies displacement from $(\bar{\Phi}_{lim})_{lower}$ into the regime of nonsteady burning. The existence at each L_c^*/m of an $\bar{R}_{min}$ suggests that a dimensionless shock amplitude maximum must exist intermediate between $(\bar{\Phi}_{lim})_{lower}$ and $(\bar{\Phi}_{lim})_{upper}$ with a decay of shock amplitude to zero near $(\bar{\Phi}_{lim})_{upper}$. The relation in C-30 indicates that as L_c^*/m increases larger dimensionless shock amplitude maxima are possible. In other words, for fixed mode order the theory predicts that larger dimensionless amplitude shock waves should be sustained at longer chamber lengths. Consider the fundamental mode (m=1) $L_c^* = 40$ and 80 cm curves of Figure C-1. For $L_c^* = 40$ cm, $(\bar{\Phi}_{lim})_{lower} = 2.36$ and at $\bar{R}_{min}$, $\bar{R}_{min} = 2.42$ or $\Delta\bar{\Phi}_{40} = \bar{\Phi}_{min} - (\bar{\Phi}_{lim})_{lower} = 0.06$. For $L_c^* = 80$ cm $(\bar{\Phi}_{lim})_{lower} = 2.62$ and at $\bar{R}_{min}$, $\bar{\Phi}_{min} = 2.52$ or $\Delta\bar{\Phi}_{80} = 0.10$. Using Figure V-24 as a means of estimating the sustained wave amplitude at $\bar{R}_{min}$ for $L_c = 40$ and 80 cm, $\Delta f^o = 0.6$ and 1.5 respectively at $\bar{\Phi}_{min}$. That is for a factor of two increase in the chamber length the theory suggests that a factor of two increase in maximum sustained dimensionless shock amplitude. As noted in Figure II-10 this is precisely the order of magnitude increase in peak fundamental mode dimensionless shock strength observed by Bowman in the H_2 + Air system with a doubling of L_c.

A second point is the implication (following the above reasoning of extrapolating nonlinear results from the analysis of Chapter V to the present analysis) that at fixed chamber length

the maximum possible shock wave amplitude decreases as the mode order increases. Bowman's experimental results with the H_2 + Air system show the same dependence.

From Figure C-1 it is noted that for $L_c^* \leq 20$, $(\Phi_{lim})_{upper,i}$ for $(L_c^*/m)_i = \frac{1}{2} (L_c^*/m)_j$ is less than $(\Phi_{lim})_{lower,j}$. In the conventional Φ vs L_c stability limit plot of Figure C-2 this translates into a short length separation of the regimes of harmonic mode oscillations. This effect is not observed experimentally. As noted in Figure C-1 the separation in terms of is small and must be dependent upon the particular values of the numerous parameters used in the analysis, hence, upon the shape of the $\bar{R}$ curves in the vicinity of the L curve. In general, the upper stability limit for the (m + 1)st mode overlaps the lower stability limit of the mth mode. For example, at $L_c^* = 80$ cm the theory predicts the appearance at $\Phi \simeq 2.36$ of the second harmonic mode. Following the previous discussion, a sharp increase in the dimensionless second harmonic shock strength with increasing Φ up to $\Phi \simeq 2.42$ occurs followed by a decrease in shock amplitude out to $\Phi \simeq 2.52$ whereupon the fundamental mode oscillation is sustained with increasing strength out to $\Phi \simeq 2.62$. Decrease in fundamental mode oscillation amplitude is predicted at larger Φ with completely stable combustion for $\Phi \gtrsim 2.$. These trends are precisely those observed experimentally by Bowman (Figure II-10).

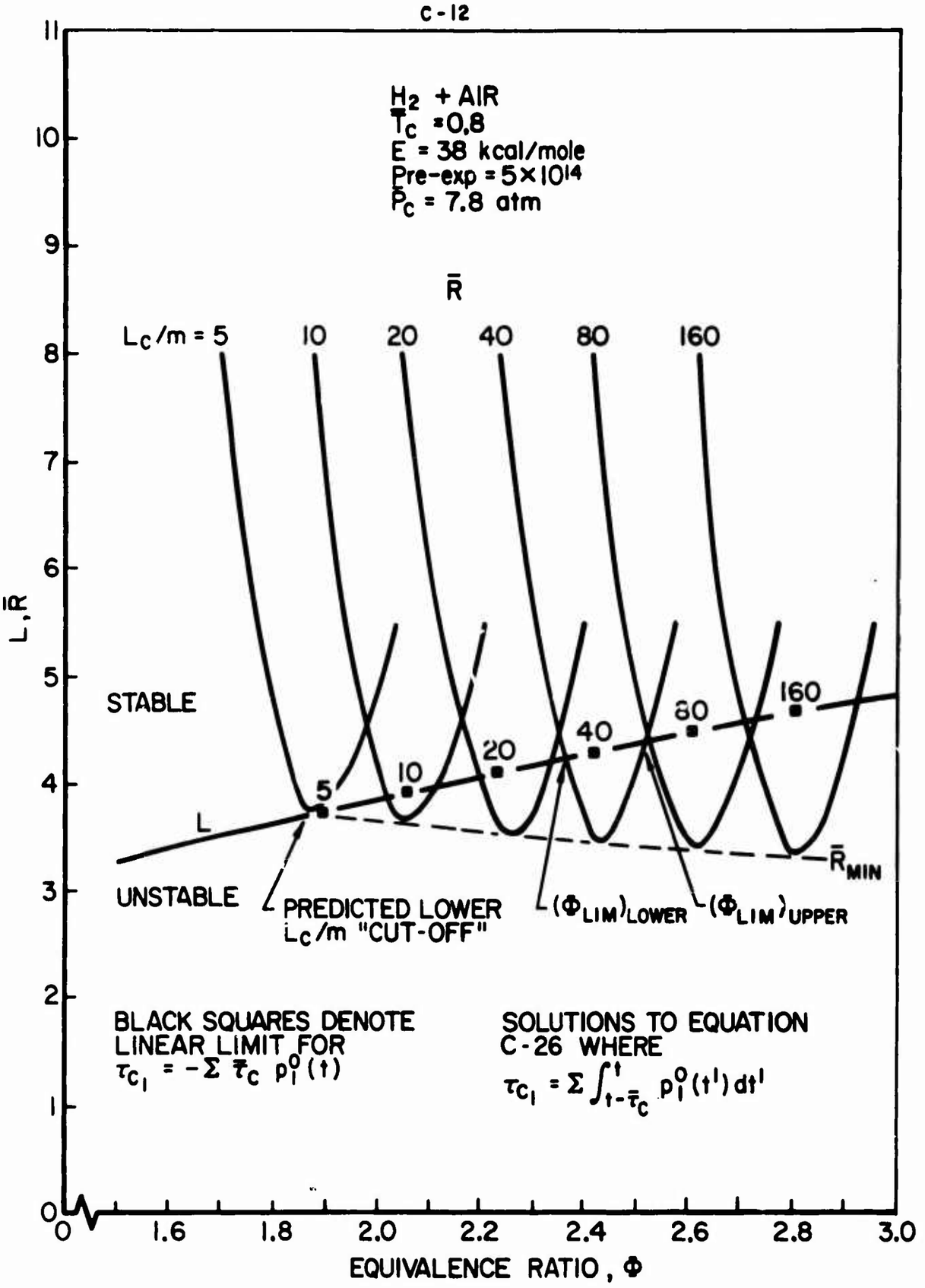

SOLUTIONS TO LINEARIZED EQUATION
FOR STABILITY LIMITS

FIGURE C-1

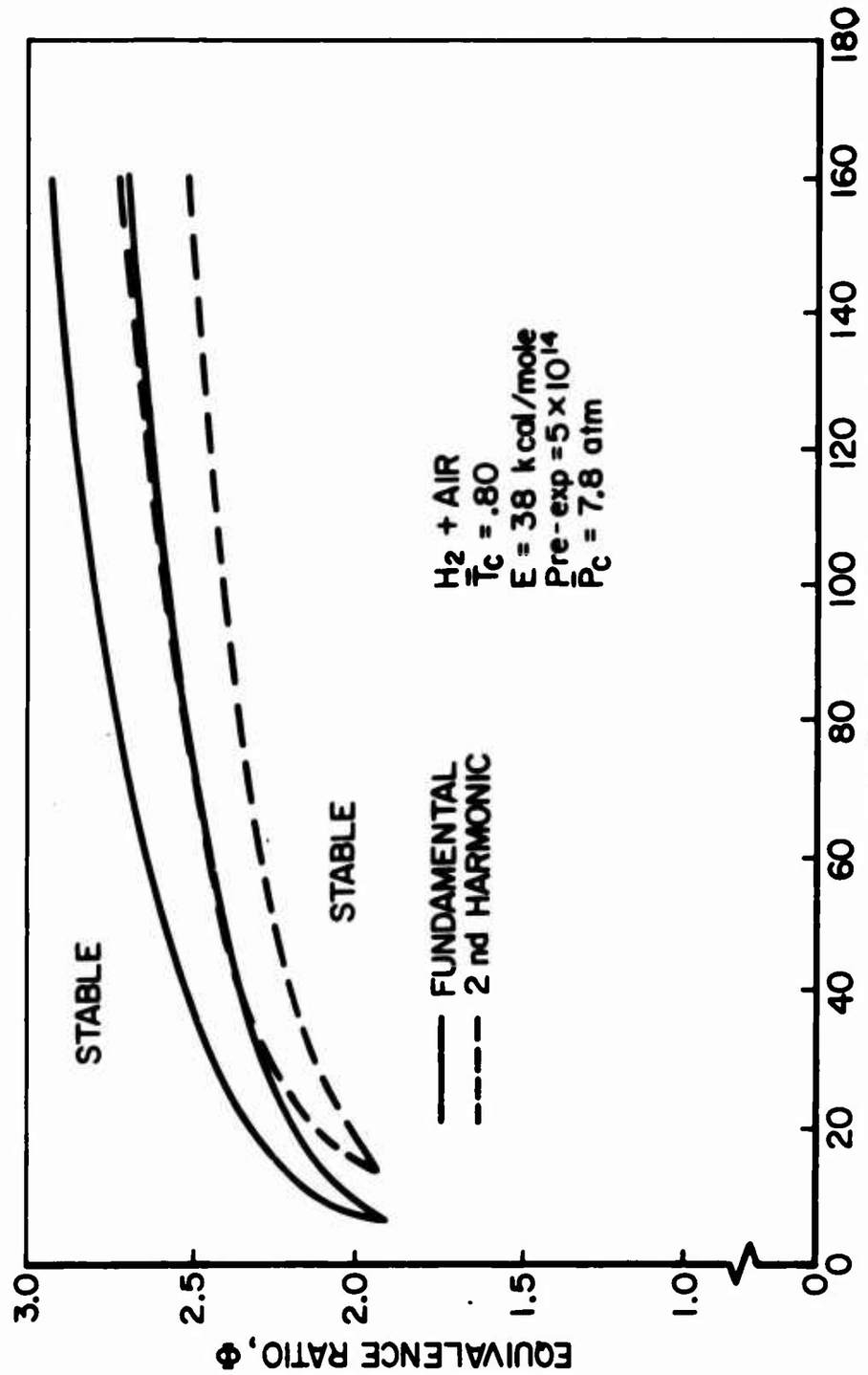

THEORETICALLY PREDICTED LINEAR STABILITY LIMITS FROM EQUATION C-26

FIGURE C - 2

APPENDIX D: Numerical Data Used In Theoretical Analysis

This section summarizes the important numerical information required in the analysis and calculations. As shown by the results of the theoretical analysis the stability characteristics depend principally upon the dimensionless ratio $1/\bar{P}_c = \tau^*_{wave}/\tau_c^*$ and the overall activation energy $E^* = \frac{kcal}{mole}$ Other factors influencing the system response are $\bar{\theta}_i = T_i^*/T_b^*$, $\gamma = \gamma_c = \bar{c}_p^*/\bar{c}_v^*$ and $\gamma_i = (\bar{c}_p^*/\bar{c}_v^*)_i$

The calculations have been carried out for $\gamma_i = 1.4$ and $\gamma = \gamma_c = 1.25$. γ_i influences ψ and the results are independent of γ_i for choked mass injection flux. The theoretical predictions are insensitive to $\gamma_c = 1.25 \pm .10$. The choice of $\gamma_c = 1.25$ is consistent with the fact that the mean properties of the combustion zone correspond to dilute mixtures predominantly composed of product gases. Likewise the theoretical predictions show only a second order influence of $\bar{\theta}_i$. Since $\bar{\theta}_i$ is primarily a function of the equivalence ratio Φ, changes in $\bar{\theta}_i$ for fixed $\bar{T}_i^*$ can be related directly to Φ. Figure D-1 depicts the relationship between the ratio $\bar{\theta}_i$ and Φ for the H_2 + Air and CH_4 + Air systems for $\bar{T}_i^* = 300^oK$ and $\bar{P}_c^* = 7.8$ atm.

Calculation of $1/\bar{P}_c$ requires the independent calculation of τ^*_{wave} and τ_c^*.

(a) Calculation of τ^*_{wave}

$\tau^*_{wave} = \frac{1}{2}\tau^*_{per}$ where τ^*_{per} is the dimensional period of oscillation. τ^*_{per} is defined as, $\tau^*_{per} = 2L_c^*/m\bar{c}_b^*$

where L_c^* = chamber length in cm

m = harmonic mode order = $\begin{cases} 1 & \text{fundamental mode} \\ 2 & \text{second harmonic mode} \\ 3 & \text{third harmonic mode, etc.} \end{cases}$

$\bar{c}_b^* = \left[\bar{R}^*\gamma\bar{T}_b^*/mw_b^*\right]^{\frac{1}{2}}$ = sound speed in burned gas

τ^*_{per} calculated in this manner does not correspond precisely to the measured period of sustained oscillations due to the influence of heat loss and mean flow in the chamber. For the case

of low mean flow Mach number τ^*_{per} differs from the measured period principally due to the nonadiabatic effects and

$$\tau^*_{per} < (\tau^*_{per})_{measured}$$

Typically the difference between the ideal τ^*_{per} and the actual measured $(\tau^*_{per})_m$ is of the order of 15%. This corresponds to an effective combustion chamber temperature of 75% of $\bar{T}^*_b$. For example at L^*_c = 76.2 cm, the measured frequency of the fundamental mode oscillation is 410 cps at $\bar{\Phi}$ = 2.80 ($\bar{T}^*_b$ = 1328 °K). Since the shock velocity is approximately the mean sound speed in the chamber gases

$$c^*_{eff} = \lambda^* \cdot f^* = \frac{2L^*_c}{m} \cdot f^* = \frac{2(76.2)}{1} \cdot 410 = 6.25 \times 10^4 \frac{cm}{sec}$$

$$T^*_{eff} = \frac{c_{eff}\, MW^*_b}{\gamma \bar{R}^*} \simeq 1000°K$$

$$T^*_{eff} / \bar{T}_b{}^* \simeq 0.75, \quad \tau^*_{per} / (\tau^*_{per})_{meas} = \frac{1}{.75^{1/2}} = 1.15$$

In Figure D-2 the molecular weight of the burned gases for the adiabatic combustion of H_2 + Air and CH_4 + Air at $\bar{P}_c{}^*$ = 7.8 atm is shown as a function of Φ. Figure IV-9 shows the adiabatic combustion temperature for the H_2 + Air system as a function of Φ. These data are combined to determine for the H_2 + Air system $\tau^*_{wave} = \frac{1}{2} \cdot \tau^*_{per}$ shown in Figure D-3 as a function of Φ with L^*_c/m as a parameter. The asymmetry of τ^*_{wave} about Φ = 1 is due to the monotonic increase in MW^*_b with increasing Φ. For the same combustion temperature the acoustic period is shorter for fuel rich mixtures due to the lower MW^*_b of the product gases.

(b) Calculation of $\bar{\tau}_c{}^*$

In Chapter V an expression is derived (Equation V-41) for the dimensional characteristic combustion time, $\bar{\tau}_c{}^*$, as

$$\bar{\tau}_c{}^* = \left\{ \hat{k} \frac{\mu}{1+\delta} \sigma_{f_i} \left[\frac{\bar{P}^* MW^*}{\bar{R}^* \bar{T}_c{}^*} \right] [\Phi - \bar{\tau}][1 - \bar{\tau}]\, e^{-\frac{E^*}{\bar{R}^* \bar{T}_c{}^*}} \right\}^{-1}$$

The equation applies to the case of a second order (first order with respect to fuel and oxidizer) overall reaction rate law and $\bar{\Phi} > 1$. For fuel rich initial mixtures ν_{fi} is replaced by $\nu_{f_i} \bar{\Phi}^2$ and $\bar{\Phi}$ by $1/\bar{\Phi}$. $\bar{\tau}_c^*$ is a strong function of the $\bar{\Phi}$ by virtue of the strong variation in $\bar{T}_b^*$ with $\bar{\Phi}$ and the important sensitivity of $\bar{\tau}_c^*$ to $\bar{T}_c^* = \epsilon \bar{T}_b^*$ in the exponential factor. The important variables in Equation V-41 are determined as follows (the discussion of Chapter V, pages 209 to 213 is pertinent):

$\nu_{O_2}, \nu_{ox}, \nu_f$ = mass fractions of O_2, oxidizer ($O_2 + N_2$), and fuel

$\nu_{O_2 i}, \nu_{ox_i}, \nu_{f_i}$ = mass fractions of O_2, oxidizer, and fuel in the initial mixture

$\nu_{ox} = (1+\delta)\nu_{O_2}$, $\delta = \dfrac{\text{mass of } N_2 \text{ diluent}}{\text{mass of } O_2}$ in the initial mixture

$\mu = \left(\dfrac{\nu_{ox}}{\nu_f}\right)_{STOICH}$ = the stoichiometric mixture ratio of oxidizer to fuel

$\mu_{H_2 + AIR} = 34.07$ gms air / gm H_2

$\mu_{CH_4 + AIR} = 17.34$ gms air / gm CH_4

$\delta_{AIR} = 3.29$ gms N_2 / gm O_2

$\nu_{ox} = 4.29 \nu_{O_2}$ for air

$[\mu/(1+\delta)]_{H_2+AIR} = 7.94$ gms O_2 / gm H_2

$[\mu/(1+\delta)]_{CH_4+AIR} = 4.04$ gms O_2 / gm CH_4

$\bar{\Phi} = \dfrac{(\nu_{ox}/\nu_f)_i}{\mu}$ = initial propellant mixture equivalence ratio

$\bar{p}^*$ = mean combustion chamber pressure

$$\bar{R}^* = 8.32 \times 10^7 \text{ erg/mole}^\circ\text{K} = 1.986 \frac{\text{cal}}{\text{mole}^\circ\text{K}}$$

$$\gamma^* = \frac{\bar{T}_c^* - \bar{T}_i^*}{\bar{T}_b^* - \bar{T}_i^*}$$

$\bar{T}_i^*$ = specified unburned gas temperature

$\bar{T}_b^*$ = adiabatic combustion temperature known as a function of Φ and is essentially independent of pressure at the combustion temperatures and pressures typical of gas rocket operation

Figure IV - 32 shows $\bar{T}_b^*$ as a function of Φ for H_2 + Air

Figure D - 4 shows $\bar{T}_b^*$ as a function of Φ for $CH_4/O_2/N_2$ mixtures

Table D - 1 summarizes $\nu_{H_2,i}$, $\bar{T}_b^*$, and MW_b^* as a function of Φ for the H_2 + Air and H_2 + dilute Air systems. For the dilute mixtures $\nu_{H_2,i}$ is dependent upon the percent dilution defined as

$$\% \text{ dilution } (N_2) = \frac{\text{gms } N_2 \text{ diluent added}}{\text{gms air + gms } N_2 \text{ added}} \times 100$$

and $$\Phi = \frac{(\nu_{ox}/\nu_f)_i}{\mu} = \frac{(\nu_{O_2}/\nu_f)_i}{\left(\frac{\mu}{1+\delta}\right)}$$ = constant independent of % dilution

Also $\bar{T}_c^* = \epsilon \cdot \bar{T}_b^*$, where ϵ = 0.75, 0.80 have been examined

The only remaining terms are k^* and E^*, the pre-exponential constant and the overall activation energy appearing in the overall reaction rate law. The calculations have been restricted to rate laws having first order dependence on the O_2 and fuel concentrations such that

$$\frac{d[F]}{dt} = k^* [F][O_2] e^{-\frac{E^*}{\bar{R}^* T^*}}, \quad \frac{\text{moles}}{\text{cm}^3 \text{sec}}$$

k^* = standard bimolecular 2nd order overall rate constant, $\frac{\text{cm}^3}{\text{mole sec}}$

$[X_i]$ = molar concentration of species X_i $\frac{\text{moles}}{\text{cm}^3}$

The rate law can be written as

$$mw_f^* \frac{d[F]}{dt} = \hat{k}^* \rho_{TOT}^{*2} v_f v_{O_2} e^{-\frac{E^*}{\bar{R}^* T^*}} \qquad \frac{gms}{cm^3 sec}$$

$$\hat{k}^* = \frac{k^*}{mw_{O_2}^*}, \quad \frac{cm^3}{gm\,sec}$$

Following the discussion of Chapter V pages 209 - 213 and 216-218, the relevant kinetic constants k^* and E^* are assumed equal to the preexponential factor and the overall activation energy obtained from flow reactor measurements of the rate of oxidation of H_2 and CH_4 in dilute O_2/N_2 mixtures at high temperatures.

H_2/O_2 Rate Constants

Sawyer and Glassman [128] studied the H_2/O_2 reaction rate in very dilute mixtures for near stoichiometric mixtures of H_2 and O_2. Sawyer defines,

$$\frac{d[H_2]}{dt} = k_s^* [H_2] e^{-\frac{E^*}{\bar{R}^* T^*}}$$

$$k_s^* = 10^A \quad (1/sec)$$

The range of experimental variables in Sawyer's experiments is defined by,

$T^* = 880$ to $980^\circ K$

$\Phi = 0.77$ to 4.0

$[H_2]_i = (1.1 \text{ to } 4.7) \times 10^{-7}$ moles/cm^3

$\bar{p}_c^* = 1$ atm

and Sawyer defines

$E^* = 38 \pm 5$ kcal/mole

$A = 11.0 \pm 2$

As indicated in Chapter V, page 217, since the oxidizer concentration is incorporated in Sawyer's pre-exponential factor,

$$\hat{k}^* = k_s^* / [O_2]^* \times MW_{O_2}^*$$

As noted in Chapter V, page 216-218, the best means of extrapolating the flow reactor data to other ranges of temperature and pressure is to take,

$$\hat{k}^* = k_s^* / [\rho_{O_2}]^* \text{ flow reactor}$$

where $\rho_{O_2}^* = [O_2]^*_{\text{flow reactor}} \times MW_{O_2}^*$

On a molar basis,

$$\mu_{H_2} + \text{Air} = 0.5$$

$$[O_2]^* = \Phi \mu \cdot [H_2]^* = 0.5 \cdot \Phi \cdot [H_2]^*$$

Sawyer does not report $[O_2]^*$ explicitly in terms of $[H_2]^*$. Assuming that high Φ corresponds to the lower range of $[H_2]^*$,

$$[O_2]^* = \Theta(2 \times 10^{-7} \text{ moles/cm}^3)$$

$$\rho_{O_2}^* = \Theta(6.4 \times 10^{-6} \text{ gms/cm}^3)$$

and,

$$\hat{k}^* = \frac{\Theta(10^{11 \pm 2})}{\Theta(10^{-5})} \quad \frac{\text{cm}^3}{\text{gmsec}}$$

$$\hat{k}^* = \Theta(10^{14} \text{ to } 10^{18}) \text{ cm}^3/\text{gmsec}$$

The stability characteristics of the H_2 + Air system are determined theoretically in Chapter V for,

$$\hat{k}^* = 5 \times 10^{14} \text{ cm}^3/\text{gm sec}$$

$$E^* = 38 \text{ kcal/gm mole}$$

This is consistent with the observation that the higher end of the $\hat{k}^*$ scale corresponds to the higher end of the E* scale such that the measured rate $(d[H_2]^*/dt)_{MW_{H_2}}$ at T* is a constant.

Figure D-5 shows the calculated characteristic combustion time for $\bar{T}_c = 0.75$ and 0.80 as a function of $\bar{\Theta}_i$ for the H_2 + Air system for $\bar{T}_i^* = 300^\circ$K and $\bar{p}_c^* = 7.8$ atm.

CH_4/O_2 Rate Constants

Dryer and Glassman [129] have studied the CH_4/O_2 reaction rate in very dilute systems for oxidizer rich mixtures of CH_4 and O_2. Dryer defines $\frac{d[CH_4]}{dt} = k_D^* [CH_4]^n [O_2]^m e^{-\frac{E^*}{\bar{R}^* T^*}} \frac{moles}{cm^3 sec}$

The ranges of experimental variables pertaining to Dryer's experiments are,

$T^* = 1200^\circ K$ to $1400^\circ K$

Φ = oxidizer rich

$\bar{p}_c^* = 1$ atm

$[\nabla CH_4]_{molar}^i$ = initial molefraction of $CH_4 = 0.005$

and Dryer obtains

$E^* = 62.5 \pm 1.0$ kcal/gm-mole

$k_D^* = 10^{15.3 \pm 0.2}$

$n = 0.7 \pm 0.05$

$m = 0.8$ to 1.0 rate is insensitive to O_2 order in this range

Calculating the density of the N_2 dilute mixture at $T^* = 1300^\circ K$ as,

$$\rho_T = 8.29 \times \frac{\bar{p}_c^* mw^*}{T^*} \times 10^{-4} \quad (\bar{p}_c^* \text{ in psi}) \quad \frac{gms}{cm^3}$$

$$\rho_T = 2.5 \times 10^{-4} \text{ gms/cm}^3$$

$$n_T = 9.6 \times 10^{-6} \text{ moles/cm}^3$$

Therefore $[CH_4] \sim 5 \times 10^{-8}$ moles/cm^3 the rate expression is written as,

$$\frac{d[CH_4]}{dt} = k_D^* [CH_4]^{-\epsilon} [CH_4]' [O_2]' e^{-\frac{E^*}{\bar{R}^* T^*}} \quad \frac{moles}{cm^3 sec}$$

$$\hat{k}^* = \left\{ k_D [CH_4]^{-\epsilon} \right\} / mw_{O_2}^* \qquad \epsilon = 0.3 \pm 0.05$$

$$2.0 \times 10^{15} \leq \hat{k}^* \leq 3.5 \times 10^{16}$$

The stability characteristics of the CH_4 + Air system are determined theoretically in Chapter V for,

$\hat{k}^* = 5 \times 10^{15}$ cm^3/gm sec

$E^* = 62.5$ kcal/gm mole

TABLE D - 1: DATA FOR H_2-O_2-N_2 MIXTURES [T_b(^oK), MW_b (gms/mole)]

Tu = 300^oK, $\overline{P}_c$ = 7.8 atm

	AIR			+ 19% DIL			+ 39% DIL			+ 50% DIL		
Φ	$\nabla_{H_{2i}}$	T_b	MW_b	$\nabla_{H_{2i}}$	T_b	MW_b	$\nabla_{H_{2i}}$	T_b	MW_b	$\nabla_{H_{2i}}$	T_b	MW_b
0.2	.128	1396	11.52	.106	1318	12.82	.0824	1206	14.62	.0618	1133	15.78
0.4	.0683	1895	16.91	.0562	1733	18.22	.0430	1521	19.86	.0318	1392	20.82
0.6	.0466	2175	20.35	.0382	1958	21.44	.0291	1680	22.72	.0214	1518	23.43
0.8	.0356	2352	22.76	.0289	2100	23.61	.0220	1777	24.55	.0162	1593	25.05
1.0	.0285	2410	24.39	.0238	2175	25.11	.0176	1838	25.79	.0130	1641	26.13
1.2	.0239	2209	22.36	.0194	1953	25.68	.0147	1634	26.22	.0108	1457	26.49
1.4	.0205	2020	20.46	.0167	1774	26.07	.0126	1480	26.52	.0093	1318	26.75
1.6	.0180	1871	18.88	.0146	1637	26.35	.0111	1364	26.74	.00814	1216	26.94
1.8	.0161	1741	17.56	.0130	1520	26.59	.00985	1266	26.93	.00725	1129	27.10
2.0	.0145	1629	16.44	.0119	1421	26.78	.00890	1184	27.08	.00653	1057	27.23
2.22	.0131	1524	15.48	.0107	1329	26.96	.00810	1108	27.21	.00594	990	27.34
2.38	.0121	1458	14.65	.0098	1272	27.07	.00740	1061	27.29	.00545	950	27.41
2.62	.0111	1369	13.92	.00905	1194	27.21	.00685	998	27.41	.00503	894	27.50
2.78	.0104	1322	13.28	.00845	1154	27.29	.00635	965	27.46	.00468	866	27.55
3.0	.0097	1258	12.71	.00785	1098	27.38	.00594	921	27.54	.00437	828	27.61

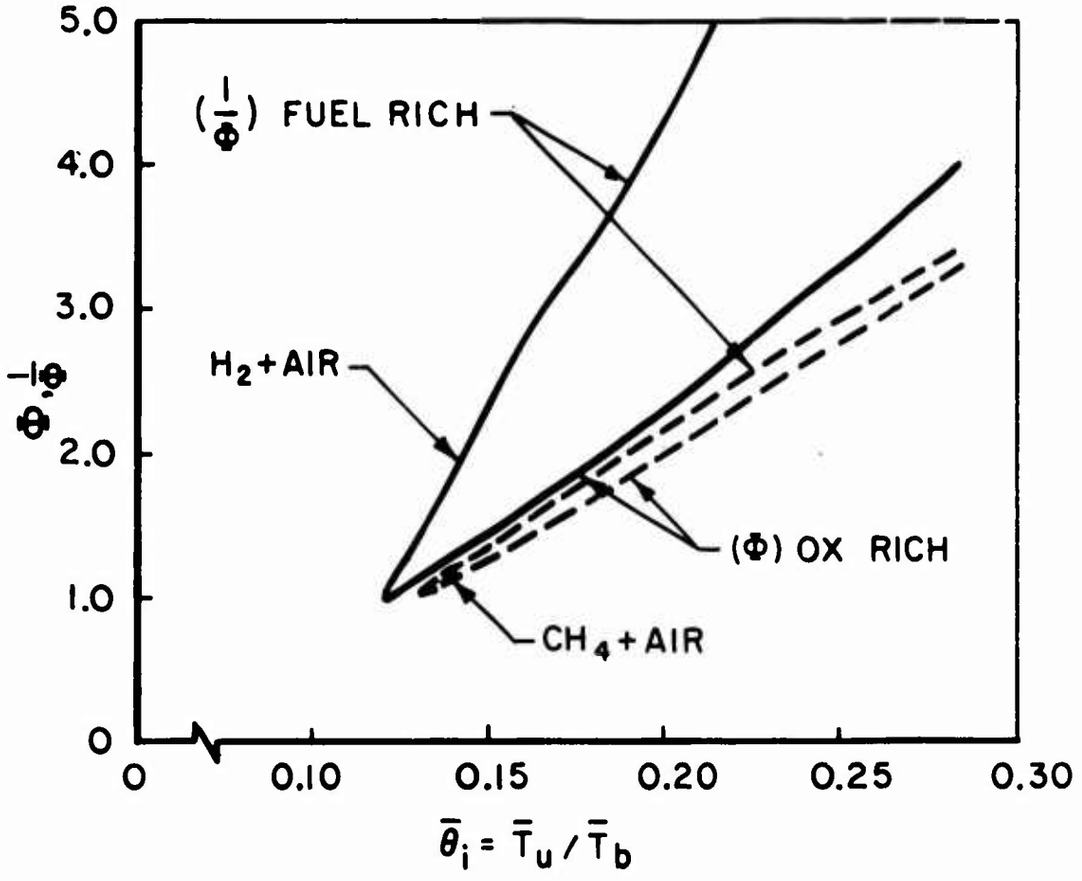

RATIO OF UNBURNED TO BURNED GAS TEMPERATURE, $\bar{\theta}_i$
AS A FUNCTION OF PROPELLANT EQUIVALENCE RATIO
$\bar{T}_u$ = 300 °K , $\bar{P}_c$ = 7.8 atm

FIGURE D-1

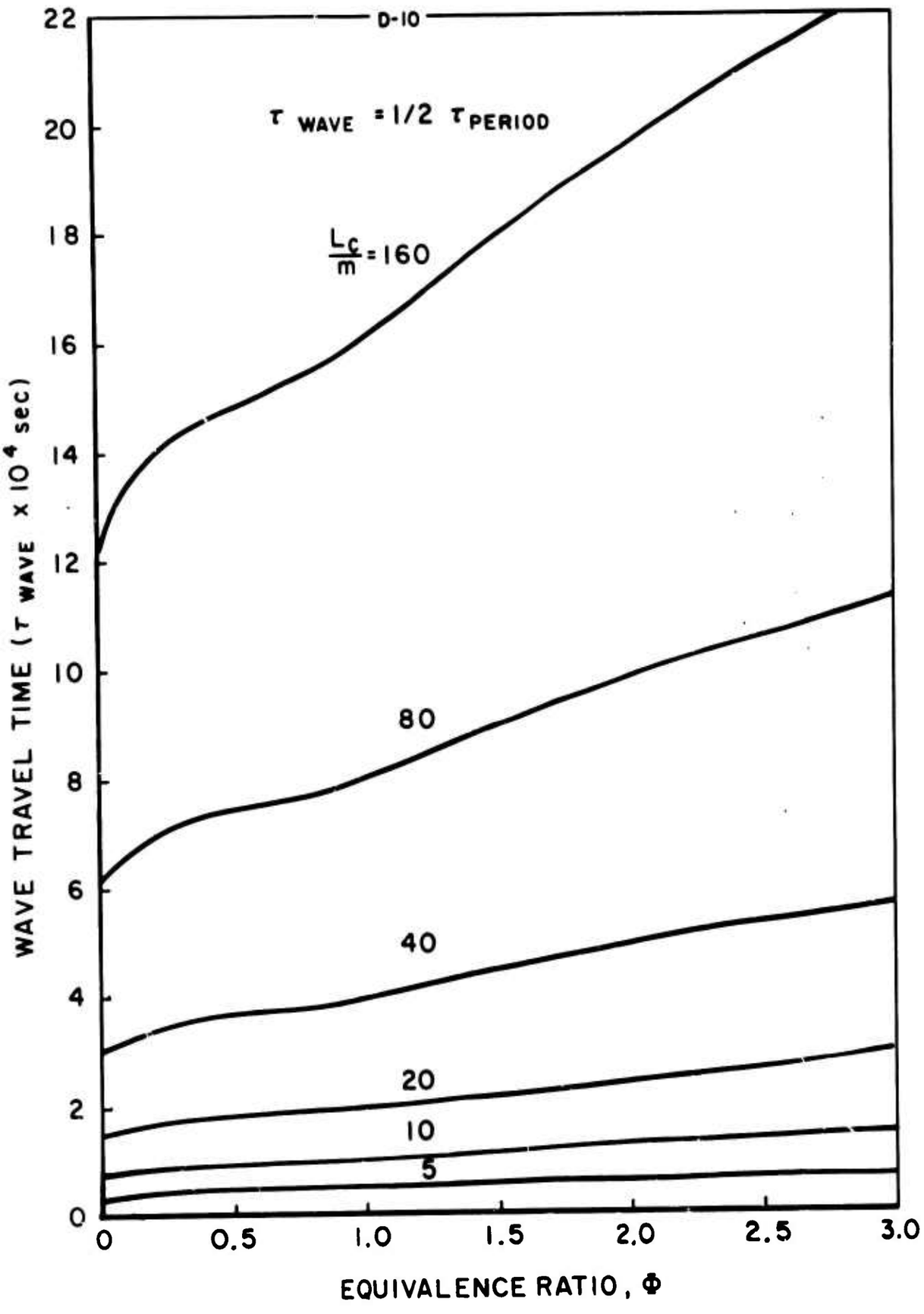

WAVE TRAVEL TIME AS FUNCTION OF EQUIVALENCE RATIO FOR H_2 + AIR, $\bar{T}u = 300°K$, $\bar{P}_c = 4.4$ TO 7.8 atm

FIGURE D - 3

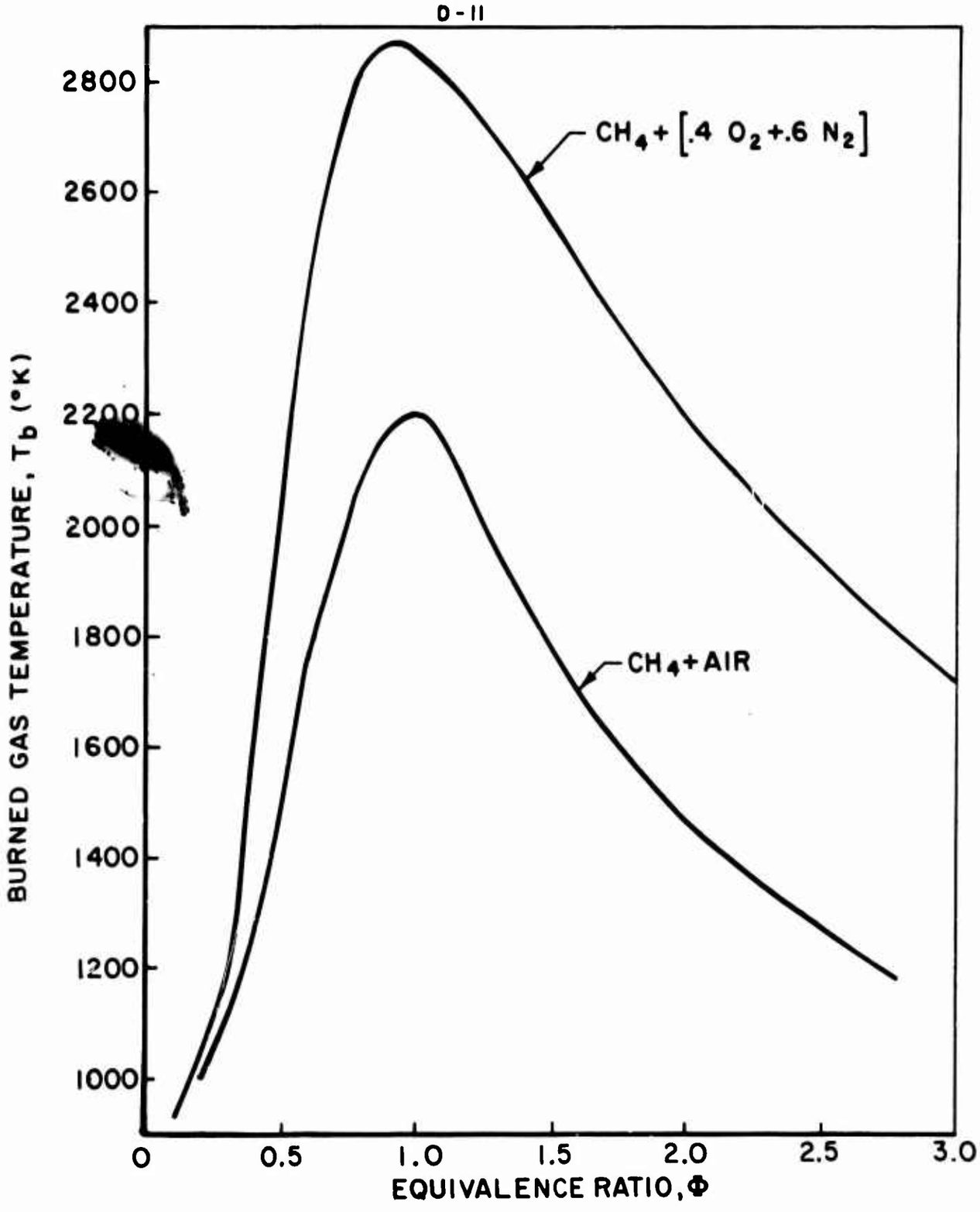

THEORETICAL ADIABATIC COMBUSTION TEMPERATURE AS A FUNCTION OF EQUIVALENCE RATIO FOR $CH_4 - O_2 - N_2$, $P_c = 7.8$ atm, $\bar{T}_u = 298°$ K

FIGURE D-4

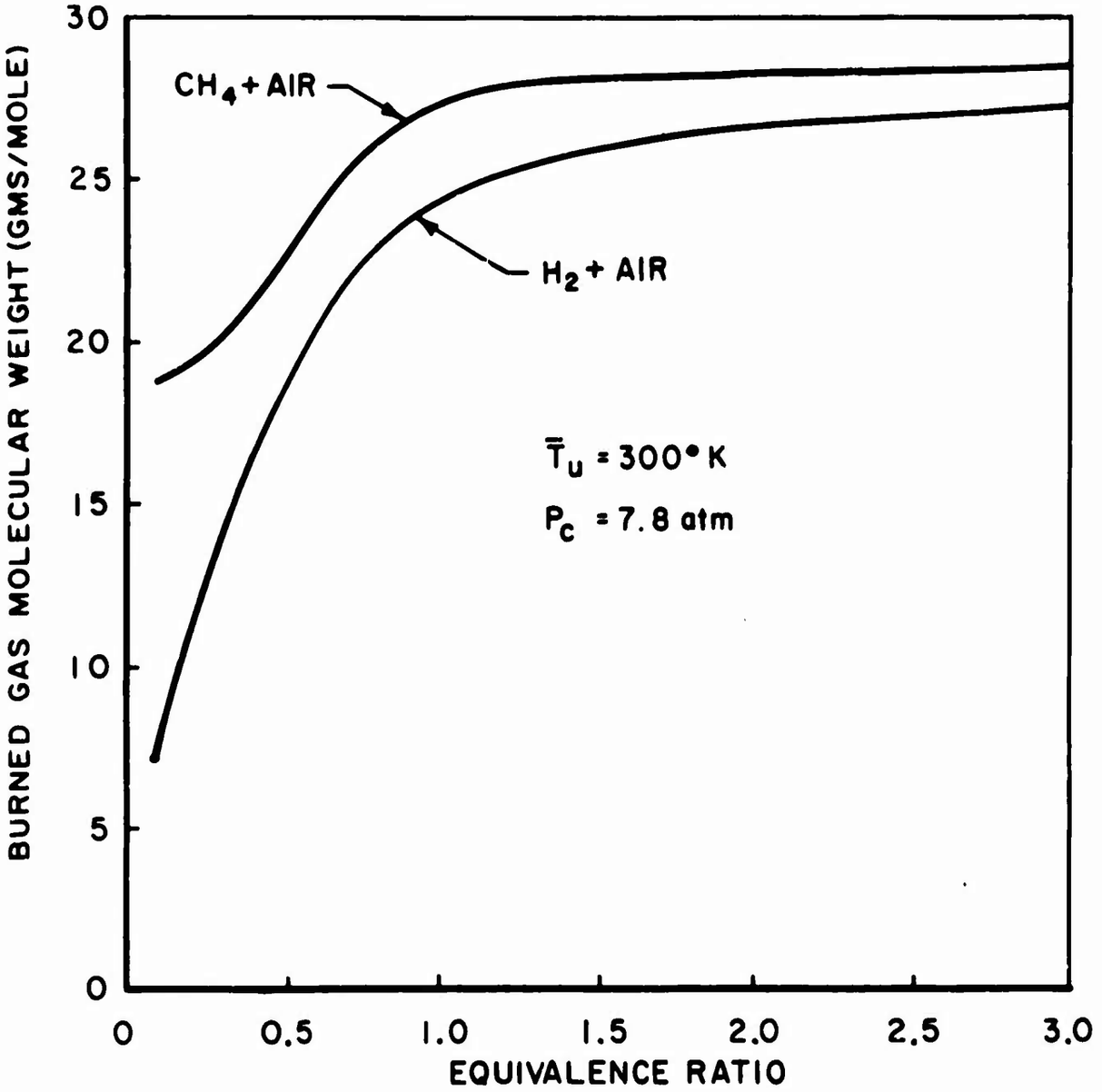

MOLECULAR WEIGHT OF BURNED GAS (MW_b) AS A FUNCTION OF EQUIVALENCE RATIO

FIGURE D-2

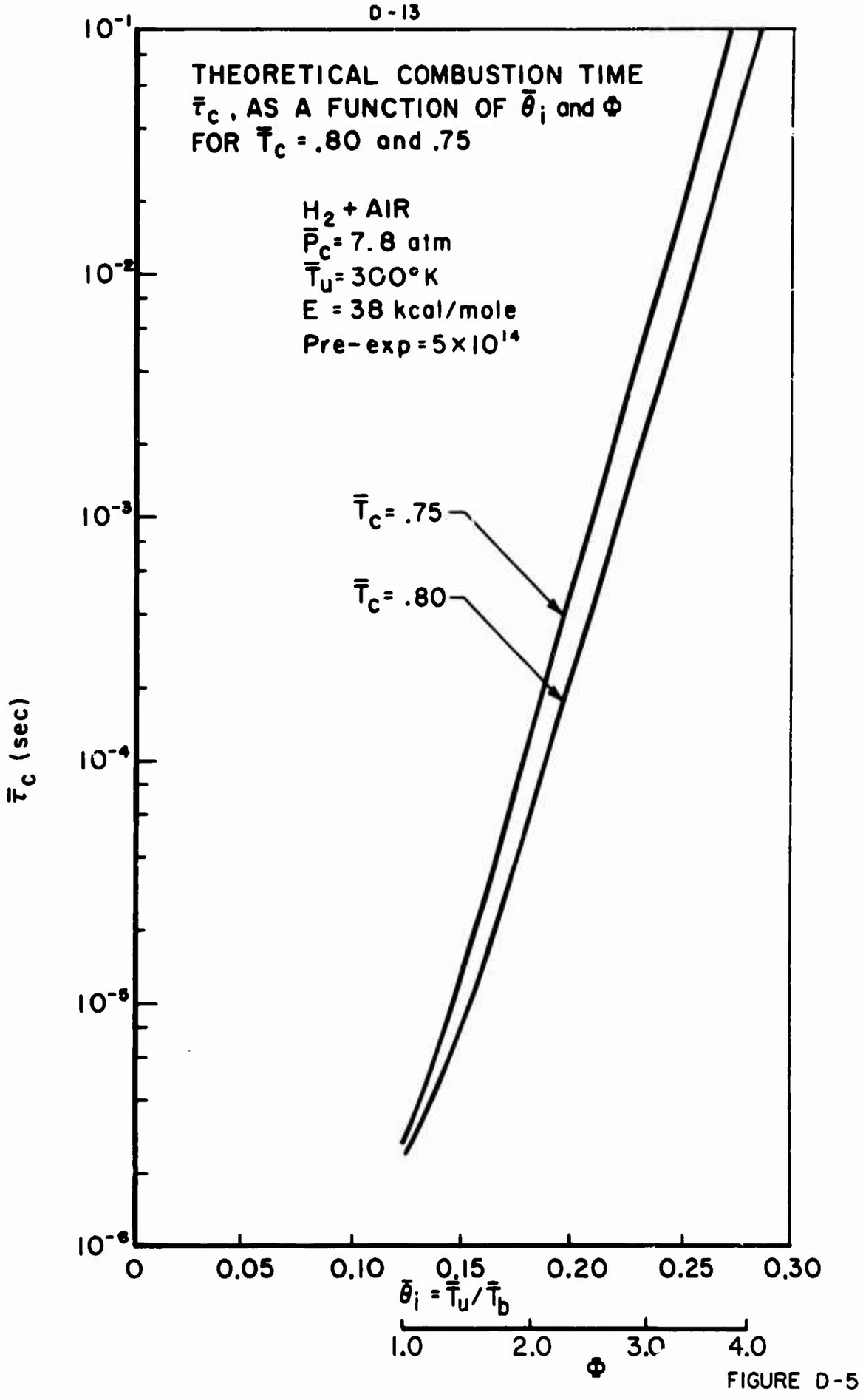
THEORETICAL COMBUSTION TIME
$\bar{\tau}_c$, AS A FUNCTION OF $\bar{\theta}_i$ and Φ
FOR $\bar{T}_c$ = .80 and .75
H_2 + AIR
$\bar{P}_c$ = 7.8 atm
$\bar{T}_u$ = 300°K
E = 38 kcal/mole
Pre-exp = 5×10^{14}
$\bar{T}_c$ = .75
$\bar{T}_c$ = .80
$\bar{\tau}_c$ (sec)
10^{-1}
10^{-2}
10^{-3}
10^{-4}
10^{-5}
10^{-6}
0
0.05
0.10
0.15
0.20
0.25
0.30
$\bar{\theta}_i = \bar{T}_u / \bar{T}_b$
1.0
2.0
3.0
4.0
Φ

FIGURE D-5

Summary of Overall Reaction Rate Data For CH_4/O_2 Combustion

Table D-2 summarizes experimentally measured overall reaction rate expressions for the CH_4/O_2 combustion system. The experimental techniques used by the various investigators have been noted in Table IV, page 88. These data have been combined with the reported experimental conditions in each investigation to obtain a numerical evaluation of $\frac{d f_{CH_4}}{dt}$ as a function of $1/T$ where f_{CH_4} = the mole fraction of CH_4. This dependency is plotted in Figure D-6. The vertical bars bracket the temperature regime experimentally investigated.

As noted in Chapter IV (pages 92-95) the overall oxidation rate of CO is felt to play a key (perhaps rate limiting) role in the overall oxidation rate of CH_4. For comparison purposes overall data for CO combustion (Figure IV-1) have been included in Figure D-6. While extrapolation of overall rate data outside the experimental temperature range may be questionable, one may conclude from these data that in the lower temperature regime ($1000^{\circ}K$ to $1350^{\circ}K$) the overall oxidation rate of CH_4 is limiting while at temperatures above $1650^{\circ}K$ to $1850^{\circ}K$ the overall oxidation rate of CO is limiting. In other words the stoichiometric mixture ratio for the CO/O_2 and CH_4/O_2 systems (with equivalent dilution) is approached. It is expected that one should observe a close similarity between the overall oxidation rates for the two systems.

Table D-2

Summary of Overall Reaction Rate Data For CH_4 Combustion

Overall Consumption Rate of CH_4 Expressed As:

$$\frac{d[CH_4]}{dt} = k[CH_4]^a[O_2]^b[H_2O]^c e^{-E/\bar{R}T} \quad \frac{\text{moles}}{\text{cm}^3 \text{ sec}}$$

where $[A] = \frac{\text{moles A}}{\text{cm}^3 \text{ sec}}$, $E = \frac{\text{kcal}}{\text{mole}}$

*	INVESTIGATOR	REF	TEMP(°K)	P(ATM)	k	a	b	c	E
J	Sawyer & Nemeth	106	1180-1282	1	6×10^{10}	-.4	1.4	0	57
K	Dryer & Glassman (1)	129	1200-1300	1	2×10^{15}	.7	.8	0	62.5
L	Kozlov (2)	100	1173-1373	1	$\frac{7\times10^{8}}{T}$	-.5	1.5	0	60
M	Williams & Hottel	110	1450-1750	.6	5×10^{18}	1	.5	.5	57
	Burgoyne & Hirsch	96	1273-1373	1	3×10^{10}	-.6	1.0	0	64
	Kydd & Foss	108	1200-1450	1	2×10^{10}	1	0	0	57

* Capital letters refer to curve designations in Figure D-6

(1) Turbulent flow-reactor technique

(2) Kozlov expresses rate law in terms of mole fractions of CH_4, O_2. Hence, the T^{-1} factor appears in k .

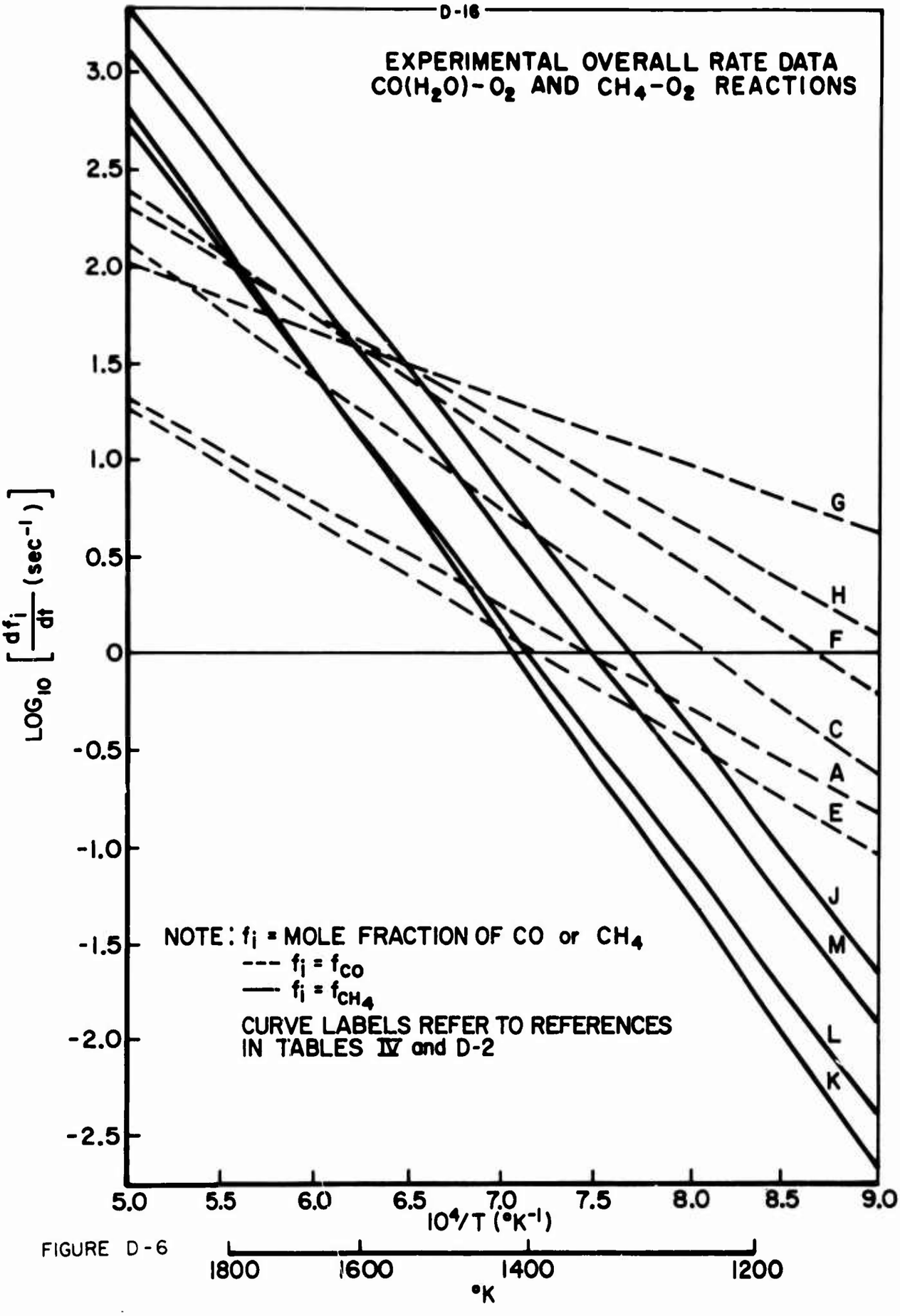
EXPERIMENTAL OVERALL RATE DATA
CO(H2O)-O2 AND CH4-O2 REACTIONS
LOG10 [dfi/dt (sec-1)]
3.0
2.5
2.0
1.5
1.0
0.5
0
-0.5
-1.0
-1.5
-2.0
-2.5
G
H
F
C
A
E
J
M
L
K
NOTE: fi = MOLE FRACTION OF CO or CH4
--- fi = fCO
—— fi = fCH4
CURVE LABELS REFER TO REFERENCES
IN TABLES IV and D-2
5.0
5.5
6.0
6.5
7.0
7.5
8.0
8.5
9.0
10⁴/T (°K⁻¹)
1800
1600
1400
1200
°K

FIGURE D-6